

LEWIS GRANT  
IN-20-CR  
101095  
P. 509

# **DYNAMIC MODELING OF SOLAR DYNAMIC COMPONENTS AND SYSTEMS**

**Final report: NASA Grant NAG3-817**

**J. I. Hochstein and T. Korakianitis**

(NASA-CR-190838) DYNAMIC MODELING  
OF SOLAR DYNAMIC COMPONENTS AND  
SYSTEMS Final Report (Memphis  
State Univ.) ~~509 p~~

N92-34198

Unclass

G3/20 0121095

523225p 522p

1-B.

---

## ***Dynamic Modeling of Solar Dynamic Power Components and Systems***

---

Final Report: NASA Grant NAG3-817

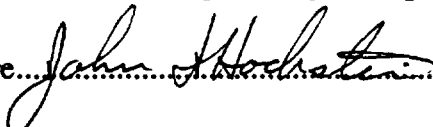
### **ABSTRACT**

A summary of the research efforts supported by the subject grant is presented. The bulk of funds provided by the grant was expended in supporting four graduate students, (Messrs. McTavish, Iqbal, Ali, Zou), and the report is logically organized according to their contributions. The summary highlights key accomplishments of the study and refers the reader to the appropriate Magisterial theses, (provided as appendices to this report), for technical details. In addition, a copy of the view-foils used for the final oral report has been included as an appendix to serve as an intermediate level review of the study.

---

J. I. Hochstein, Principal Investigator

Dept. of Mechanical Engineering, Memphis State University, Memphis, TN 38152

Signature.......... Date 14 SEP 1992

T. Korakianitis, Co-Principal Investigator

Dept. of Mechanical Engineering, Washington University, St. Louis, MO 63130

Signature.......... Date 1992-Sep-14

---

The purpose of this grant was to support NASA in modeling efforts to predict the transient dynamic and thermodynamic response of the space station solar dynamic power generation system. In order to meet the initial schedule requirement of providing results in time to support installation of the system as part of the initial phase of space station, early efforts were executed with alacrity and often in parallel. Initially, methods to predict the transient response of a Rankine as well as a Brayton cycle were developed. Review of preliminary design concepts led NASA to select a regenerative gas-turbine cycle using a Helium-Xenon mixture as the working fluid and, from that point forward, the modeling effort focused exclusively on that system. Although initial project planning called for a three year period of performance, revised NASA schedules moved system installation to later and later phases of station deployment. Eventually NASA elected to halt development of the solar dynamic power generation system for space station and to reduce support for this project to two-thirds of the original level. The research in-progress was pursued to reasonable conclusions and culminated in the three Magisterial theses attached as appendices to this report.

During the first two years there was a concerted effort to use EASY-5 (as directed by NASA), a commercial software package for predicting the dynamic response of multi-component systems. Compressible-flow turbomachinery-cycle calculations require numerous iterations to converge to an operating condition for steady-state as well as transient operation. The development cycle was to write component models using standard FORTRAN 77 and then convert the code into EASY-5 macros. After the expenditure of considerable effort, it became apparent that the EASY-5 modeling paradigm would not support the iterative computations required by the demands of this study. The component models were reassembled into a subroutine structure controlled by a FORTRAN 77 executive (main) program.

A review of existing literature on modeling of transient turbomachinery performance revealed a surprising dearth of component-level models for compressible flow machinery. Various published component-level models used incompressible-flow assumptions, no-density-variation assumptions, no-mass-storage through the transient assumptions, and other similar simplifications without significant mathematical or theoretical justification. At the other

extreme, transient fully-compressible three-dimensional CFD tools have been used to study flow in turbomachinery blade passages. These tools require significant execution times on today's fastest supercomputers to model only a part of the turbomachine and therefore are not suitable for the present study.

A detailed presentation of all the models developed, simulations performed, and conclusions reached, is available in the three Magisterial theses produced by students supported by this research effort. These theses, in their entirety, are included as appendices to this report. The following paragraphs present a brief summary of the contents of these theses.

Iqbal (1990) modeled the heat exchangers and radial turbomachinery components using multi-segmented EASY-5 macros. The heat exchangers were discretized using length-wise elements for which the transient conservation-laws were enforced using fully-implicit finite-difference schemes. The models employed typical compressor and turbine performance maps and assumed instantaneous response of turbomachinery to inlet transients. The resulting system model was used to examine transient performance during several transients of interest: maximum and minimum insolation orbits; radiator panel loss; and coolant-pump loss.

Ali (1990) developed several radial turbomachinery models employing nodes at the inlet, middle, and outlet of the impeller. The models enforced the fully-compressible transient conservation-laws to predict the transient response of these components. The models were implemented as FORTRAN 77 subroutines and tested to identify the most stable algorithm. This model was then used to predict the transient thermodynamic response of radial impellers to step, ramp and sinusoidal variations of properties at impeller inlet. Sample computations for a constant-speed variable rate-of-work machine, and for a constant-work variable-speed machine, are included in the thesis.

Zou (1991) improved the transient thermodynamic models for the heat exchangers, the ducts, and the radial turbomachines. He assembled the various models into a FORTRAN 77 program for modeling the transient thermodynamic response of the complete power generation system. Transient conservation-law equations were enforced for each component. The mass-flow rate at a critical point in the cycle (between recuperator outlet and receiver inlet) was iteratively



adjusted during the solution for each time step until the transient conservation laws were satisfied in each component as well as for the system as a whole, (conservation of mass, matching of mass-flow rate, pressure and temperature at each thermodynamic point throughout the transients). Transient simulations were executed to compare predictions from different system models: an all instantaneous-response components system model; a transient heat exchanger with instantaneous-response turbomachinery system model; and a fully transient model. It was concluded that, although the instantaneous-response turbomachinery transient-heat-exchanger models were sufficiently accurate for most transients, the predictions might become suspect for the very high-speed transients associated control signals required maintain synchronous speed in the alternator.

A fourth appendix has been attached to this report which contains copies of the view-foils used during the final oral presentation to NASA personnel. Review of this appendix will provide an intermediate level introduction to the history and accomplishments of this study. In particular, it should highlight for the reader the most significant results and conclusions generated by the study.

## Appendix A

### Transient Model of Space Station Solar Dynamic Power Generating System

WASHINGTON UNIVERSITY  
SEVER INSTITUTE OF TECHNOLOGY

---

TRANSIENT MODEL OF SPACE STATION SOLAR DYNAMIC POWER GENERATING SYSTEM

by Ahsan Iqbal

Prepared under the direction of

Professor John I. Hochstein  
and  
Professor Theodosios P. Korakianitis

---

A thesis presented to the Sever Institute of  
Washington University in partial fulfillment  
of the requirements for the degree of

MASTER OF SCIENCE

May, 1990

Saint Louis, Missouri

WASHINGTON UNIVERSITY  
SEVER INSTITUTE OF TECHNOLOGY

---

ABSTRACT

---

TRANSIENT MODEL OF SPACE STATION SOLAR DYNAMIC POWER GENERATING SYSTEM

by Ahsan Iqbal

---

ADVISORS: Professor J. I. Hochstein  
Professor T. P. Korakianitis

---

May, 1990 .

Saint Louis, Missouri

---

A transient model of the Space Station Closed Brayton Cycle Power Generating System was developed using EASY5, a commercially available dynamic analysis code. Heat exchangers and radiators were modelled as multi-segmented Macro components that use a fully-implicit finite difference scheme. A constant speed, variable-power compressor and turbine were modelled as instant response machines. System simulations including maximum and minimum insolation orbits, radiator panel loss and coolant pump loss were analyzed.

TABLE OF CONTENTS

1. INTRODUCTION.....	1
1.1 Literature search .....	3
1.2 Space Station .....	4
1.2.1 Design and Power Requirements.....	4
1.2.2 Solar Dynamic Power Generating System.....	6
1.2.2.1 Concentrator and Receiver .....	9
1.2.2.2 Power Conversion Unit .....	9
1.2.2.3 Radiator .....	11
1.2.3 Control Schemes.....	11
1.2.4 Orbital Control Characteristics.....	13
2. EASY5.....	16
2.1 EASY5 Model .....	16
2.1.1 Model File.....	17
2.1.1.1 FORTRAN Blocks .....	17
2.1.1.2 Macro Components .....	18
2.1.2 Analysis File.....	18
2.1.3 EASY5 Output.....	19
3. COMPONENT MODELLING.....	20
3.1 Heat Exchanger .....	20
3.1.1 Closed Brayton Cycle Gas Cooler, Bleed Cooler and Recuperator .....	20
3.1.2 Analytical Model.....	22
3.1.3 Component Tests and Results.....	29
3.1.3.1 Transient Performance .....	29
3.1.3.2 Number of Segments Convergence Study .....	33
3.1.3.3 Time and Spatial Variation with Temperature .....	33
3.2 Radiator .....	37
3.2.1 Closed Brayton Cycle Radiator.....	37
3.2.2 Analytical Model.....	39
3.2.3 Component Tests and Results.....	43
3.2.3.1 Number of Segments Convergence Study .....	43
3.2.3.2 Spatial Temperature Variation with Time .....	43

3.2.3.3 Transient Performance .....	47
3.3 Receiver .....	47
3.3.1 Closed Brayton Cycle Receiver .....	47
3.3.2 Analytical Model .....	50
3.4 Pipes .....	52
3.4.1 Pipes - Hardware .....	52
3.4.2 Pipes - Analytical Model .....	52
3.5 Manifolds .....	53
3.5.1 Manifolds - Hardware and Analytical Model .....	53
3.6 Pump .....	54
3.6.1 Pump - Hardware and Analytical Model .....	54
3.7 Combined Rotating Unit .....	54
3.7.1 Turboalternator .....	54
3.7.2 Turboalternator - Analytical Model .....	56
3.7.2.1 Constant Speed Machine .....	56
3.7.2.2 Variable Speed Machine .....	58
4. TRANSIENT SYSTEM PERFORMANCE .....	62
4.1 Coolant Loop .....	62
4.1.1 Response to a Step .....	65
4.1.2 Response to a Double Step .....	70
4.1.3 Response to a Sinusoid .....	74
4.2 Gas Loop .....	74
4.2.1 Response to a Step .....	81
4.2.2 Response to a Double Step .....	81
4.2.3 Response to a Sinusoid .....	88
4.3 System Transients .....	88
4.3.1 Maximum Insolation Orbit .....	88
4.3.2 Minimum Insolation Orbit .....	97
4.3.3 Minimum Insolation Peaking Orbit .....	97
4.3.4 Loss of One Radiator Panel .....	100
4.3.5 Loss of Pump .....	100

5. SUMMARY AND CONCLUSIONS.....	110
6. RECOMMENDATIONS FOR FURTHER STUDY.....	112
7. ACKNOWLEDGEMENTS.....	113
8. APPENDICES.....	115
Appendix 8.1 EASY5 System Model File .....	115
Appendix 8.2 Film Coefficient Calculation .....	132
Appendix 8.3 CBC Subsystem Performance Over One Orbit .....	133
9. BIBLIOGRAPHY.....	134
10. VITA.....	136

LIST OF TABLES

No.		Page
1.	Coolant Loop Convention.....	64
2.	Gas Loop Convention.....	80
3.	System Convention.....	94



LIST OF FIGURES

No.		Page
1.	Power Generation/Energy Storage Efficiency Comparison.....	5
2.	Photovoltaic and Solar Dynamic System Size Comparison.....	5
3.	Closed Brayton Cycle (CBC) Subsystem Block Diagram.....	7
4.	CBC Subsystem Schematic.....	8
5.	CBC Temperature-Entropy Diagram.....	10
6.	Space Station Orbit Parameters.....	14
7.	Space Station Orbit Characteristics.....	15
8.	CBC Gas Cooler/Recuperator Design.....	21
9.	CBC Bleed Cooler Design.....	23
10.	Heat Exchanger Finite Difference Scheme.....	25
11.	Heat Exchanger Model Flowchart.....	30
12.	Gas Cooler - Fluid A Transient Performance.....	31
13.	Gas Cooler - Fluid B Transient Performance.....	32
14.	Gas Cooler - Number of Segments Convergence Study.....	34
15.	Gas Cooler - Combined Time Step and Segment Study.....	35

16. Gas Cooler - Spatial Temperature Variation with Time.....	36
17. CBC Radiator Panel Design.....	38
18. Radiator Finite Difference Scheme.....	40
19. Radiator Model Flowchart.....	44
20. Radiator Transient Performance.....	45
21. Radiator - Spatial Temperature Variation with Time.....	46
22. Radiator - Number of Segments Convergence Study.....	48
23. CBC Receiver Design.....	49
24. Receiver Finite Difference Scheme.....	51
25. CBC Turboalternator Design.....	55
26. Variable Speed Turbine Model Flowchart.....	59
27. Variable Speed Compressor Model Flowchart.....	60
28. Coolant Loop Schematic.....	63
29. Coolant Loop - Response to a Step.....	66
30. Coolant Loop - Response to a Step.....	67
31. Coolant Loop - Response to a Step.....	68
32. Coolant Loop - Response to a Step.....	69

33. Coolant Loop - Response to a Double Step.....	71
34. Coolant Loop - Response to a Double Step.....	72
35. Coolant Loop - Response to a Double Step.....	73
36. Coolant Loop - Response to a Sinusoid.....	75
37. Coolant Loop - Response to a Sinusoid.....	76
38. Coolant Loop - Response to a Sinusoid.....	77
39. Coolant Loop - Response to a Sinusoid.....	78
40. Gas Loop Schematic.....	79
41. Gas Loop - Response to a Step in Salt Temperature.....	82
42. Gas Loop - Response to a Step in Salt Temperature.....	83
43. Gas Loop - Response to a Step in Salt Temperature.....	84
44. Gas Loop - Response to a Double Step in Salt Temperature....	85
45. Gas Loop - Response to a Double Step in Salt Temperature....	86
46. Gas Loop - Response to a Double Step in Salt Temperature....	87
47. Gas Loop - Response to Sinusoidal Salt Temperature.....	89
48. Gas Loop - Response to Sinusoidal Salt Temperature.....	90
49. Gas Loop - Response to Sinusoidal Salt Temperature.....	91

50. Full System Schematic (Coolant Loop).....	92
51. Full System Schematic (Gas Loop).....	93
52. Maximum Insolation Orbit Transient.....	95
53. Maximum Insolation Orbit Transient.....	96
54. Minimum Insolation Orbit Transient.....	98
55. Minimum Insolation Peaking Orbit Transient.....	99
56. Loss of One Radiator Panel Transient.....	101
57. Loss of One Radiator Panel Transient.....	102
58. Loss of One Radiator Panel Transient.....	103
59. Loss of One Radiator Panel Transient.....	104
60. Loss of Pump Transient.....	105
61. Loss of Pump Transient.....	106
62. Loss of Pump Transient.....	107
63. Loss of Pump Transient.....	108

NOMENCLATURE

- $\dot{m}$  - Mass Flow Rate (kg/s)
- $c$  - Specific Heat (J/Kg.K)
- $T$  - Temperature (K)
- $h$  - Film Coefficient (W/m<sup>2</sup>.K)
- $A$  - Area (m<sup>2</sup>)
- $t$  - Time (s)
- $x$  - Longitudinal Distance (m)
- $m$  - Mass (Kg)
- $g$  - Acceleration (m/s<sup>2</sup>)
- $h_L$  - Head Loss (N/m<sup>2</sup>)
- $v$  - Velocity (m/s)
- $L/D$  - Length/Diameter
- $q$  - Energy (J)
- $W$  - Work (J)
- $\sigma$  - Stefan-Boltzman Constant
- $\rho$  - Density (Kg/m<sup>3</sup>)
- $\eta$  - Efficiency

SUBSCRIPTS

- $a$  - Fluid A
- $b$  - Fluid B
- $w$  - Wall
- $i$  - ith segment
- $p$  - Constant pressure (specific heat)

v - Constant volume (specific heat)

p - polytropic (efficiency)

i - isentropic (efficiency)

SUPERSCRIPT

n - Time step

# TRANSIENT MODEL OF SPACE STATION SOLAR DYNAMIC POWER GENERATING SYSTEM

## 1. INTRODUCTION

NASA has selected a Solar Dynamic Power Generating System (SDPGS) based on the Closed Brayton Cycle (CBC) to provide electrical power for the proposed Space Station's power requirements. The SDPGS, along with the photovoltaic power conversion systems, will produce the 75 kW necessary for Space Station Phase I operation<sup>1</sup>. The development of a transient model of the SDPGS thermal system is the focus of the research effort documented by this thesis.

The SDPGS thermal systems transient model is a part of the overall NASA plan to combine a thermal performance model with an electrical system model, developed by the Rocketdyne Division of Rockwell International Corporation, to produce a complete system simulation. This tool will be used to demonstrate the reliable and safe operation, not simply at design point, but at all points in the entire operating envelope. Specifically, these models separately or combined will be used to:

- investigate transient behavior during orbital fluctuations;
- investigate worst-case scenarios;
- verify the control system architecture;

- identify potential problem areas;
- evaluate design solutions; and
- optimize system performance.

To facilitate NASA's objective of model integration and to provide a framework for the various groups modelling the system, NASA specified that all model components be written and connected using EASY5<sup>2</sup>, a dynamic analysis code produced by Boeing Computer Services, a division of the Boeing Company. EASY5 is a general purpose computer code which provides extensive standard simulation and analysis capabilities as well as the option to write unique component models as FORTRAN blocks.

The objectives of the thermal system simulation are to:

- produce detailed models of the system components suitable for studying their time-dependent thermodynamics in response to various inputs;
- integrate these component models into EASY5; and
- investigate the response of the system to specified inputs representative of real conditions the system might encounter.

The methodology used in writing the CBC thermal model has been the following:

- produce a system fabric that defines each component, its function, and rules for nomenclature and passing of variables around the system loop;
- prepare a model of the component based on first-principles applied to a finite size control volume (standard FORTRAN was used for the initial model.);



- test the model using various inputs such as step, double step or sinusoidal functions, and verify realistic response;
- install the FORTRAN model of each component in the system fabric with appropriate transformations to adapt to EASY5;
- study the response of the system;
- convert the FORTRAN model to an EASY5 Macro (or model that can be used repeatedly) and install it in the system;
- continue the building-block approach until the system model is complete; and
- run transients to study system performance.

The remainder of this document discusses in detail the steps followed in building a full thermodynamic systems model and in analyzing various system transients.

## 1.1 LITERATURE SEARCH

An extensive literature search produced little information on dynamic system modelling of power conversion systems. A few papers focused more on components<sup>3,4,5</sup> than on systems and were tied directly to the computational hardware of the time, such as analog computers. The Electrical Power Research Institute funded Babcock and Wilcox to model large power generation plants, but their research was tailored to very large machines, and unfortunately access to this research was restricted. The literature search concluded that there was no open literature available on modelling the dynamics of a thermodynamic power system starting from first principles and employing zero-dimensional or one-dimensional component models.

Although formulation of the heat transfer equations for the different components could be easily derived from the various papers, solutions to these relations were not found<sup>3,4,5</sup>. Solutions of equations using nonlinear terms like the fourth order radiation term were not found.

## 1.2 SPACE STATION

The peak power requirement for the proposed NASA Space Station is estimated at 75 kW for the Initial Operating Capability. This requirement is expected to grow as the Station expands. These design parameters forced a new look at power generating options.

### 1.2.1 Design and Power Requirements

A key design requirement of the Space Station is the Initial Operating Capability requirement of 75 kW for peak demand, which is expected to grow to 300 kW as the Station evolves. Traditional photovoltaic power generating systems are at a substantial disadvantage at these power levels. As Figure 1 indicates, photovoltaic systems operate at roughly one-third the efficiency of a solar dynamic power conversion system<sup>6</sup>.

For vehicles in Low Earth Orbit, solar dynamic systems offer the additional advantage of a low frontal area. Since solar dynamic systems use concentrators as an energy source for the cycle, they have a lower energy collection or frontal area and consequently lower propellant penalties for reboosting to compensate for drag-induced orbital decay. This is graphically shown in Figure 2 comparing the frontal areas of

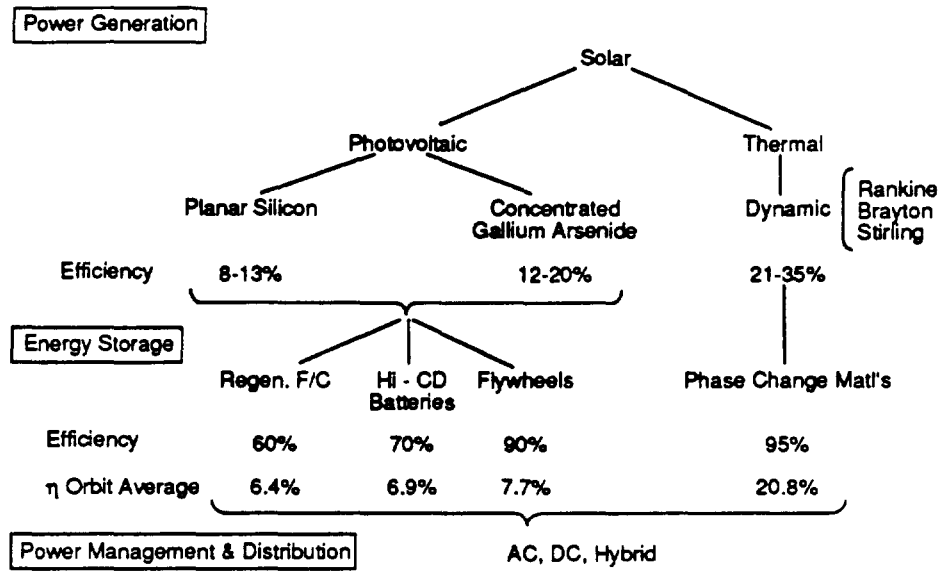


Figure 1. Power Generation/Energy Storage Efficiency Comparison.  
(Reprinted from AIAA-85-1480<sup>1</sup>)

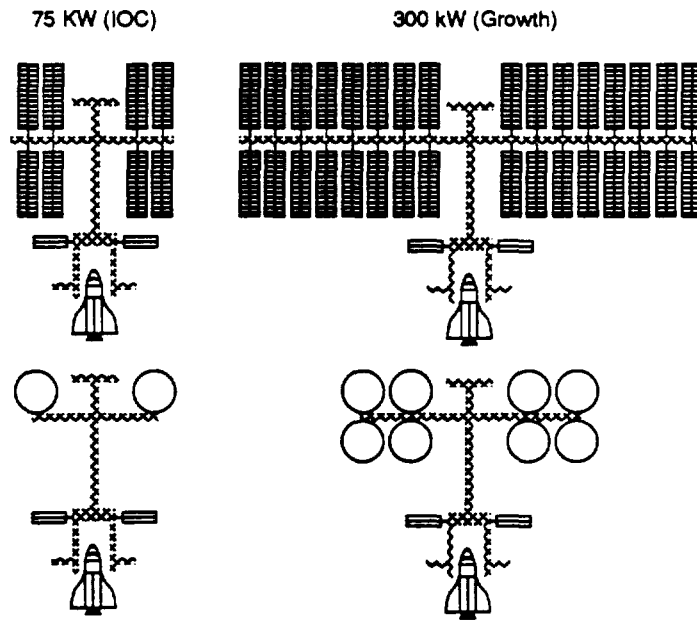


Figure 2. Photovoltaic and Solar Dynamic System Size Comparison.  
(Reprinted from AIAA-85-1480<sup>1</sup>)

photovoltaic and SDPGS systems. As a compromise between efficiency and the risk of unproven technology, NASA chose a hybrid power generating system for Initial Operating Capability consisting of a photovoltaic subsystem and a solar dynamic subsystem. The photovoltaic subsystem consists of:

- four solar arrays providing a net average power of 25 kW;
- nickel-hydrogen batteries for energy storage; and
- thermal control of batteries and Power Management and Delivery equipment using a capillary-pumped cooling system with a heat-pipe radiator.

The solar dynamic subsystem, the subject of this project, will consist of two 25 kW modules. The details of the solar dynamic subsystem are described below.

#### 1.2.2 Solar Dynamic Power Generating System

The solar dynamic subsystem uses solar radiation as its energy source, and space for an energy sink, to run a power conversion system based on the Closed Brayton Cycle (CBC)<sup>7</sup>. The cycle working fluid is a helium/xenon mixture. Heat is rejected via a cooling loop using liquid FC-75 as the coolant. Each module consists of three major assemblies (Figure 3): concentrator and receiver (with phase change salt), Power Conversion Unit, and radiator. Figure 4 depicts the energy conversions in each of these major assemblies and their interfaces.

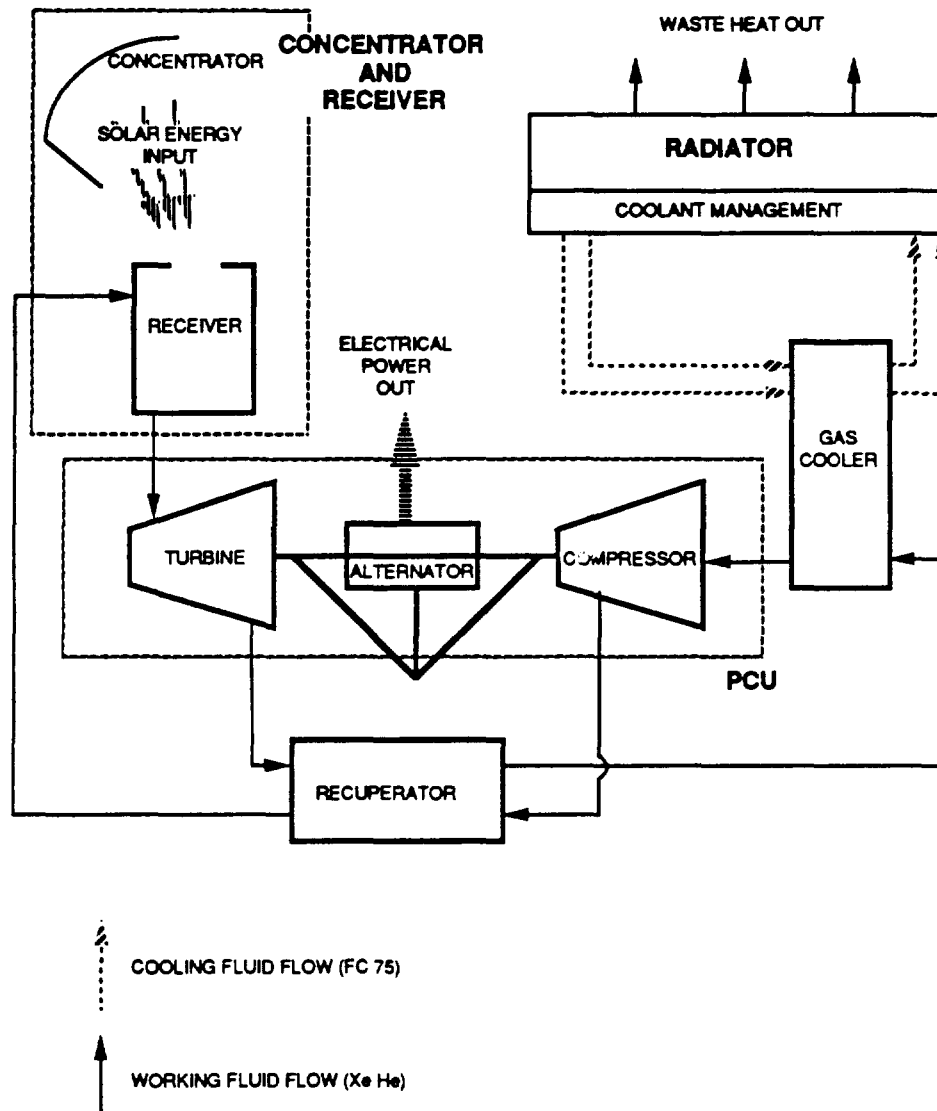
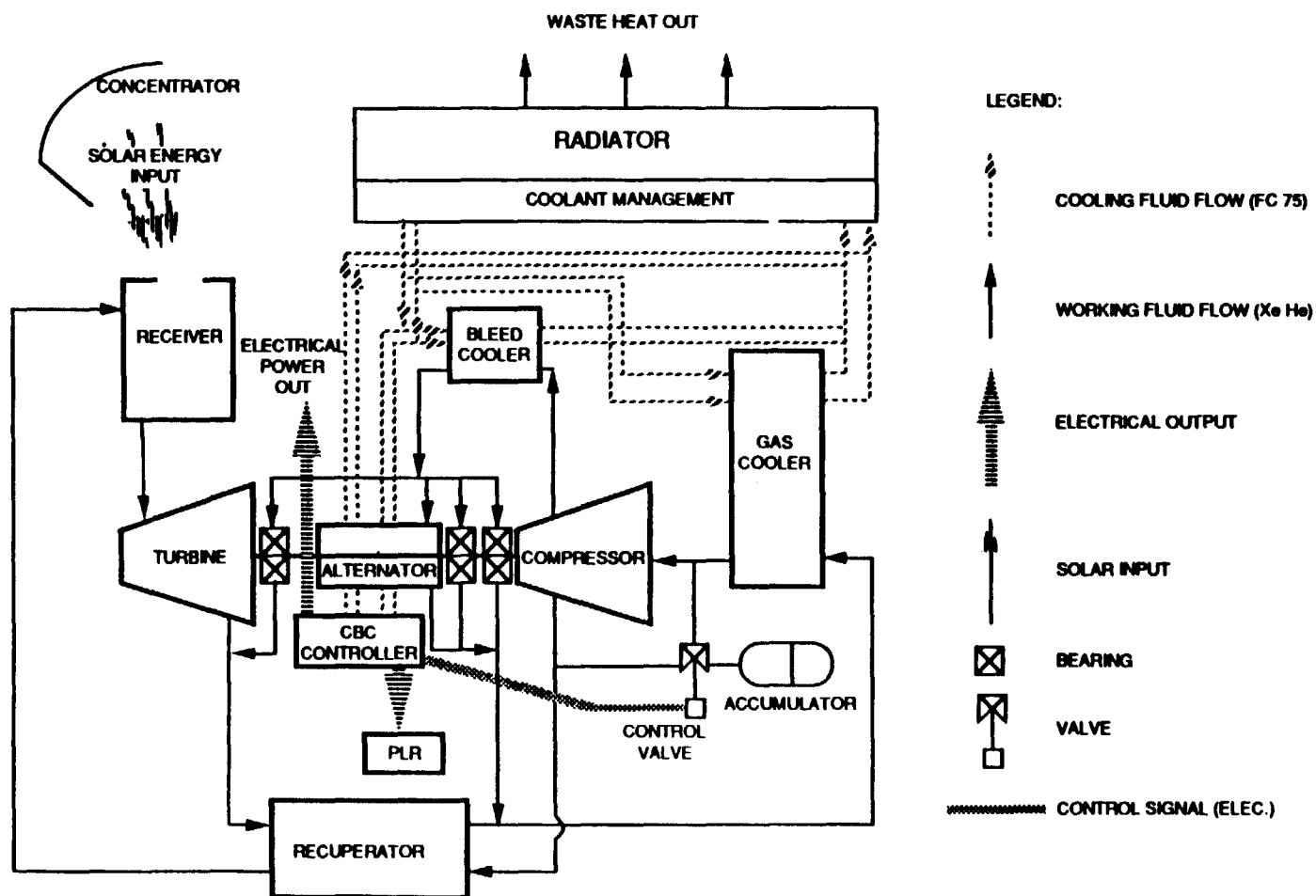


Figure 3. Closed Brayton Cycle (CBC) Subsystem Block Diagram.  
(Reprinted from DR02-RI/RD 85-320-2<sup>7</sup>)

Figure 4. CBC Subsystem Schematic.  
(Reprinted from DR02-RI/RD 85-320-27)



#### 1.2.2.1 Concentrator and Receiver

The concentrator is a concave reflective system that collects and focuses the solar flux into the receiver cavity. As the Station passes behind the Earth during its orbit, the solar flux is periodically interrupted by the Earth's shadow. The receiver's function is to convert this intermittent energy into a steady energy flux to drive the CBC engine. This is achieved using a phase changing lithium fluoride calcium difluoride eutectic salt sealed in canisters lining the receiver walls. When the concentrator is in direct sunlight, these salts absorb part of the incident flux and change to liquid phase. The remainder of the incoming energy is used to heat the cycle working fluid. When the Station is in the Earth's shadow, the eutectic salts return from the liquid to a solid state and release energy into the helium/xenon flowing through the receiver.

The control scheme for these assemblies involves various tracking and pointing devices that can change the receiver temperature and hence the thermodynamic conditions in the Closed Brayton Cycle.

#### 1.2.2.2 Power Conversion Unit

This unit is designed to convert the thermal energy collected by the receiver into electrical energy. High pressure helium/xenon gas enters the receiver and is heated. On the T-S diagram<sup>8</sup> in Figure 5, this is represented by path 3-4. Expansion through the turbine drives the shaft which produces useful power in the alternator and also runs the compressor. The thermodynamic process in the turbine is shown as path 4-5. The low temperature, low pressure gas leaving the turbine is

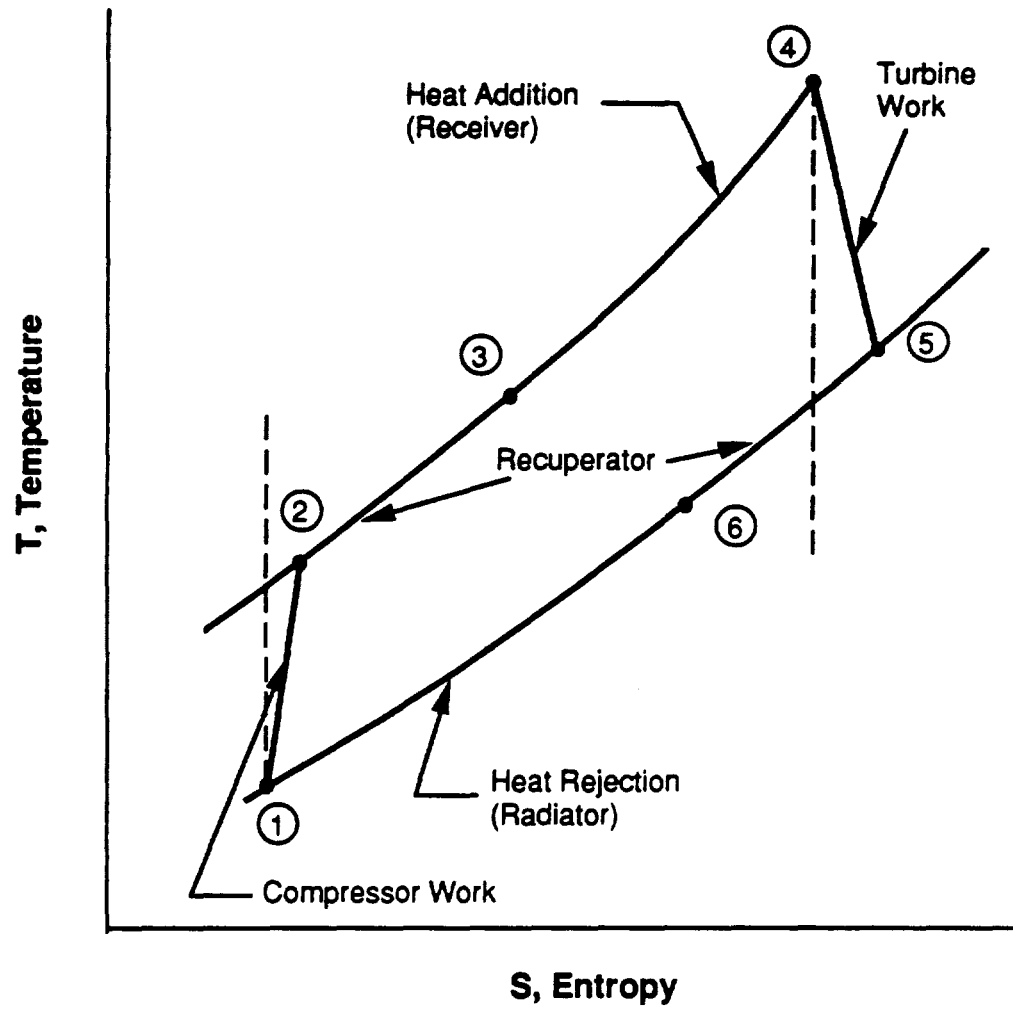


Figure 5. CBC Temperature-Entropy Diagram.



further cooled by passage through the recuperator (5-6) and the gas cooler (6-1). Path 1-2 represents the compressor, powered by part of the turbine work, which compresses the gas in preparation for the receiver. The Power Conversion Unit performance is controlled by the accumulator, the alternator load, and the receiver and gas cooler conditions.

#### 1.2.2.3 Radiator

The purpose of this assembly is to reject energy from the system to space. This energy flow is accomplished using large surface area radiators through which FC-75 liquid coolant is pumped. FC-75 transports energy extracted from the helium/xenon gas in the gas cooler to the Radiator. The control scheme for this loop uses the FC-75 inventory control valves and electric pumps.

#### 1.2.3 Control Schemes

A number of control schemes have been designed for various conditions likely to be encountered during the operating life of the energy conversion system. All of these involve a few control mechanisms.

- The concentrator tracking and pointing mechanism -  
this system controls the flow of energy into the working fluid,  
and can be used as a switch to shut the system down.
- The accumulator and inventory control valves -

the valves in the helium/xenon loop regulate the mass of gas in the loop and hence the mass flow rate. This in turn controls the performance of the turbine and the compressor.

- The parasitic load controller -

this control system passes unused alternator energy through resistors. This energy is then radiated to space, thus maintaining the shaft at a constant speed.

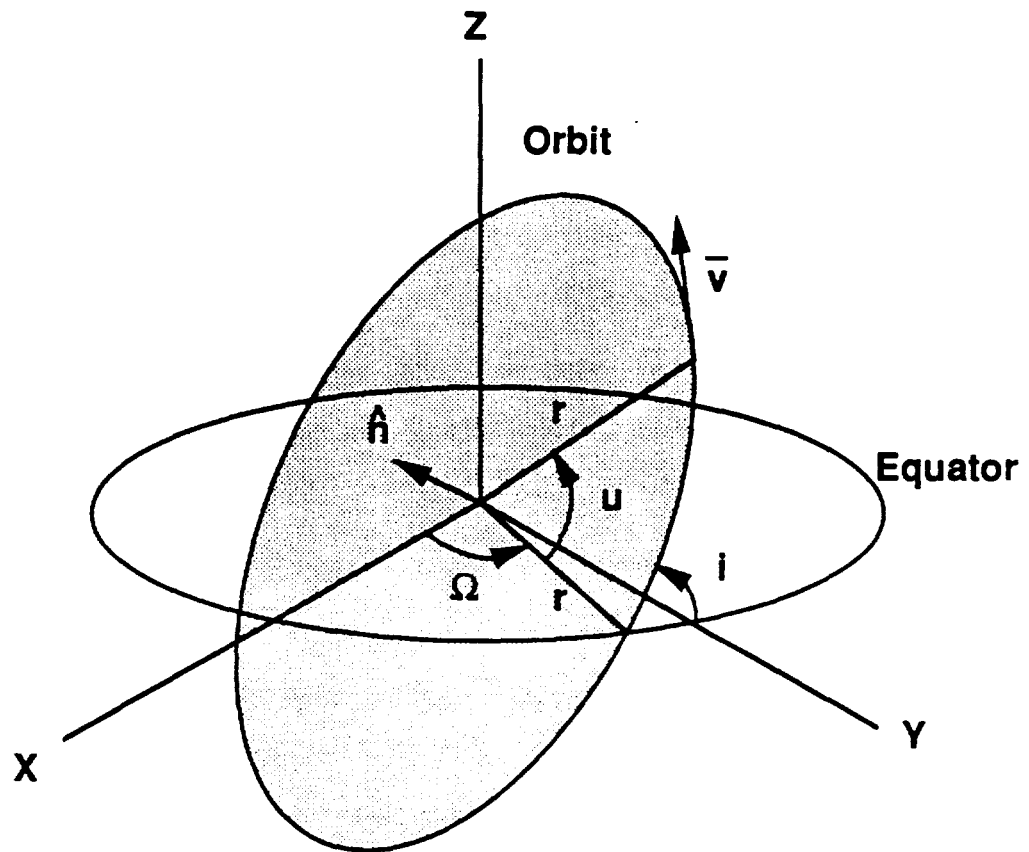
For steady-state operation the inventory control mechanism coupled with the parasitic load controller is sufficient. The objective is to keep the shaft at a constant 1067 Hz. The parasitic load controller maintains a steady load on the alternator. Small control inputs required to correct for orbital fluctuations can be managed using the solenoid control valves on the accumulator.

Start up and shut down transients also require control of concentrator tracking and focusing. In start up, for example, the concentrator is focused on the receiver. The alternator is used as a motor to turn the Power Conversion Unit shaft until the helium/xenon has accumulated enough energy for steady state operation. All through this process the parasitic load controller maintains constant shaft speed once 32,000 rpm has been reached.

Shut down is accomplished in approximately the same manner but the sequence is reversed. The concentrator is first off-pointed, then the alternator load is decreased gradually to zero. At this point half routine power is drawn by the parasitic load controller and the rotor brought to a quick halt.

#### 1.2.4 Orbital Control Characteristics

The thermodynamic transients of the SDPGS are a function of the orbital characteristics of the Space Station (Figures 6-7). The Space Station's orbit varies from a minimum insolation orbit to a maximum insolation orbit. Insolation is defined as the time spent by the Freedom Space Station in direct sunlight. The eclipse phase, on the other hand is the time spent in the Earth's shadow. The conversion system's performance depends on variables such as eclipse time, insolation time, orbital period, and sink temperature. The orbital altitude varies from 250 nautical miles to 180 nmi. The lower altitude orbit (180 nmi) is the minimum insolation orbit while the higher 250 nmi orbit is the maximum insolation orbit. The orbit inclination is fixed at  $28.5^{\circ}$ . The rate of precession is  $-7.3$  deg/day which produces a period of 49.3 days. The eclipse periods are 36.4 and 28.2 minutes for the maximum and minimum insolation orbits respectively. These conditions are used to bound the normal operating environment for the SDPGS.



**Equatorial plane & orbit plane with  
orbit elements and parameters**

- $r$  Orbit Radius
- $i$  Orbit Inclination
- $\Omega$  Longitude of Ascending Node
- $u$  Argument of latitude
- $\bar{v}$  Velocity Vector
- $\hat{n}$  Normal to Orbit Plane

(Staiger, P.J., Space power and Propulsion System Analyses, January, 1988, Rocketdyne Division)

Figure 6. Space Station Orbit Parameters.

### **ORBIT CHARACTERISTICS:**

- Orbit Inclination: 28.5 deg
- Orbit Altitude 180-250 nmi.
- Orbit Precession
  - Rate: -7.3 deg/day
  - Period: 49.3 days

### **MINIMUM INSOLATION ORBIT**

- Orbital period = 91.06 minutes (180 nmi)
- Insolation =  $1.323 \text{ kW/m}^2$
- Concentration Reflectivity = 0.9
- Eclipse Period = 36.36 min

### **MAXIMUM INSOLATION ORBIT**

- Orbital period = 93.71 minutes (250 nmi)
- Insolation =  $1.419 \text{ kW/m}^2$
- Concentration Reflectivity = 0.93
- Eclipse Period = 28.15 min

Figure 7. Space Station Orbit Characteristics.

## 2. EASY5

"The EASY5 Engineering Analysis SYstem from Boeing is a computer program used to model, analyze, and design large, complex, dynamic systems"<sup>2</sup> . This proprietary simulation and control language can be used to simulate dynamic responses and to perform control system analyses on systems described by non-linear differential or difference equations.

The program uses English-like language to define commands. It has FORTRAN compatibility, allowing any user or system library to be accessed. It has the capability to integrate component modules in FORTRAN and permits the user to define new components. Output from EASY5 can be requested in the form of system schematics, time histories, and Bode or Nyquist plots, among other options. EASY5 was installed on a VAXstation 2000. This machine uses the VMS operating system.

### 2.1 EASY5 MODEL

Two input files are required for an EASY5 simulation. The first is the model file containing the component models with their respective descriptive differential equations, as well as specification of intercomponent connectivity. The second is the analysis file which provides parameters required by the component models as well as information for output format. The executable file is at least 740 blocks in size since it must provide all the EASY5 utilities which a user may select.

EASY5 post-processing can be in a batch or interactive mode. Output spans a wide range of plotting and printing possibilities including time history plots, Nyquist and Bode plots, eigenvalue lists, and data tables.

#### 2.1.1 Model File

Component description can be accomplished in several ways in the model file. Standard blocks residing in the EASY5 component library can be used. Special components (Macro or FORTRAN components) can be created to suit the user's needs.

The standard blocks model many common dynamic input-output relationships and can be grouped together to represent a set of differential equations. Included in the library are transfer functions, function generators, tabular functions and integrators. The inlet and outlet port definitions facilitate interconnections between components. The user-defined components are of two types, FORTRAN or Macro, and are used to model special components or processes which are not amenable to assembly from standard blocks.

##### 2.1.1.1 FORTRAN Blocks

FORTRAN blocks are components that contain FORTRAN statements. These components cannot be stored and must be redefined each time they are used. The advantages of FORTRAN components are that they are relatively easy to build, use the versatility of the FORTRAN language, and can be easily debugged in the VAX environment.

All inputs and outputs must be clearly specified for a particular block. If the same FORTRAN block is to be used in another part of the system model, its inputs and outputs must be redefined and the code modified. This can prove cumbersome and time-consuming for components used more than once. In such a case, a Macro component is desirable.

#### 2.1.1.2 Macro Components

Macro components are user defined and can be stored in the user's permanent file for subsequent use. The user defines the Macro's inputs, outputs, and logic using a FORTRAN-like code. Thus, without too much difficulty, FORTRAN components can be converted into Macro components using the Macro guidelines. These components then become generic and can have multiple occurrences in the system model without redefinition.

#### 2.1.2 Analysis File

The control of model execution resides in the analysis file. Every component (standard, FORTRAN, or Macro) may have parameters associated with it. This provides an easy way of executing multiple analyses without having to create another executable file. The analysis file also contains simulation and output controls. Variables such as integration time step, maximum simulation time, and print frequency are all defined in this file. Options such as time history output and Nyquist or Bode plots may be specified. EASY5 output facilities are very extensive and versatile.



### 2.1.3 EASY5 Output

EASY5 output can be processed in a batch or interactive mode. The output can consist of print files or plot files containing the output of the analysis performed. For instance, a time history of certain variables at various time steps or a plot of different variables with respect to time can be requested. In the interactive mode, these plots can be modified; they can be rescaled, the subtitles can be changed, and the plots can be displayed in different formats.

### 3. COMPONENT MODELLING

The modeling methodology was the following:

- study the physics of the component;
- write differential equations to describe the transient response of the component;
- write FORTRAN code to approximate and solve the equations; and
- test the component model with various inputs and study the response.

The development of each component in the SDPGS will be described using the above sequence.

#### 3.1 HEAT EXCHANGER

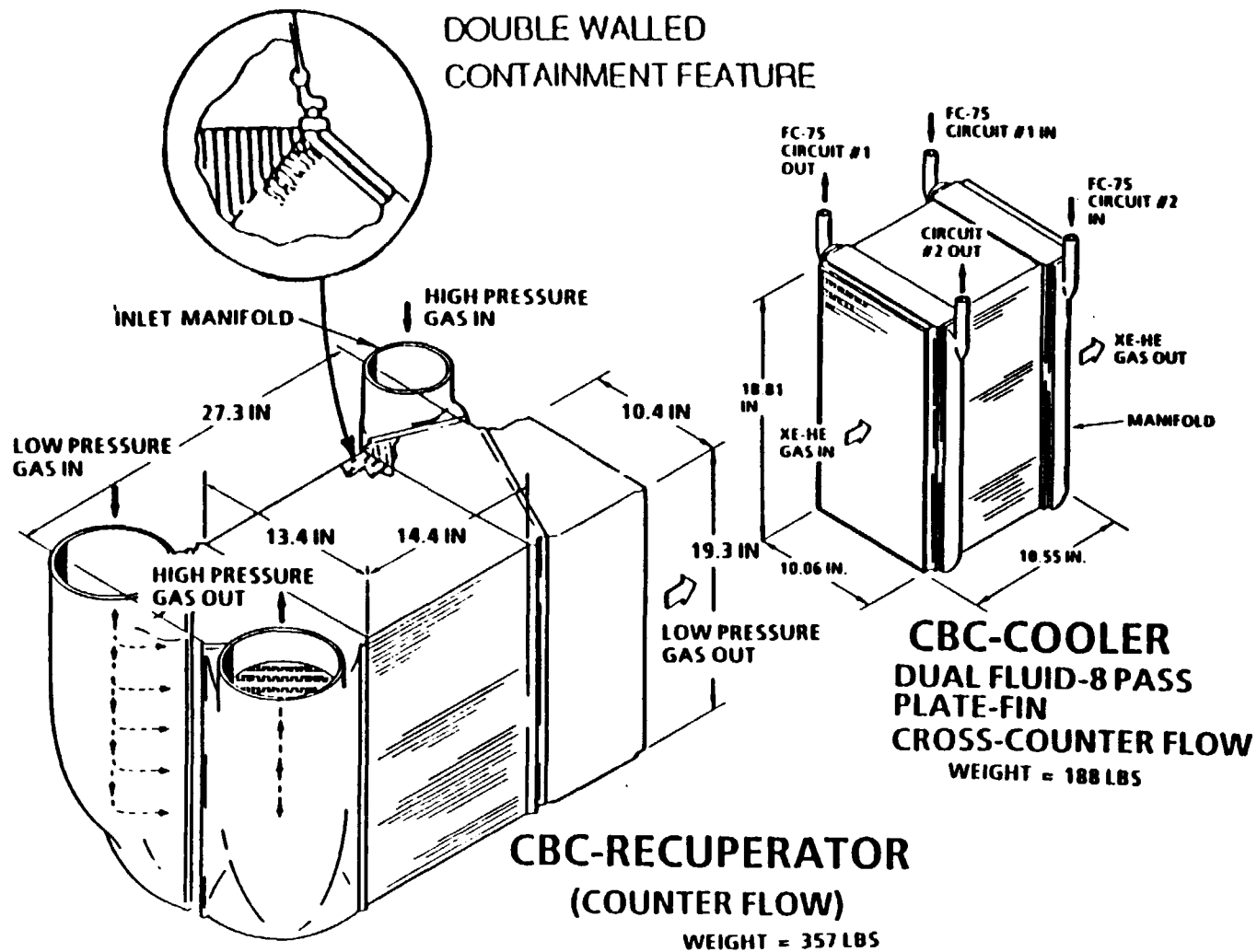
The heat exchanger component model describes a number of heat exchangers in the CBC-PGS that share approximately the same physical description. Each heat exchanger is denoted by HXnn in EASY5, where nn is a two digit number identifying the particular heat exchanger unit.

##### 3.1.1 Closed Brayton Cycle Gas Cooler, Bleed Cooler, Recuperator

The gas cooler, bleed cooler and recuperator share the same physics of heat transfer in that they are all counter-flow heat exchangers described by surface areas, heat transfer coefficients, fluid densities and thermal masses.

The gas cooler (Figure 8) is an eight pass, cross-counter-flow, plate-fin heat exchanger. It is a redundant alternating sandwich design

Figure 8. CBC Gas Cooler/Recuperator Design.  
(Reprinted from DR02-R1/RD 85-320-27)



that connects to independent fluid loops and results in double sandwich gas side passages. The helium/xenon gas mixture enters the cooler after passing through the recuperator. The cold-side fluid, FC-75, transports energy to the radiator.

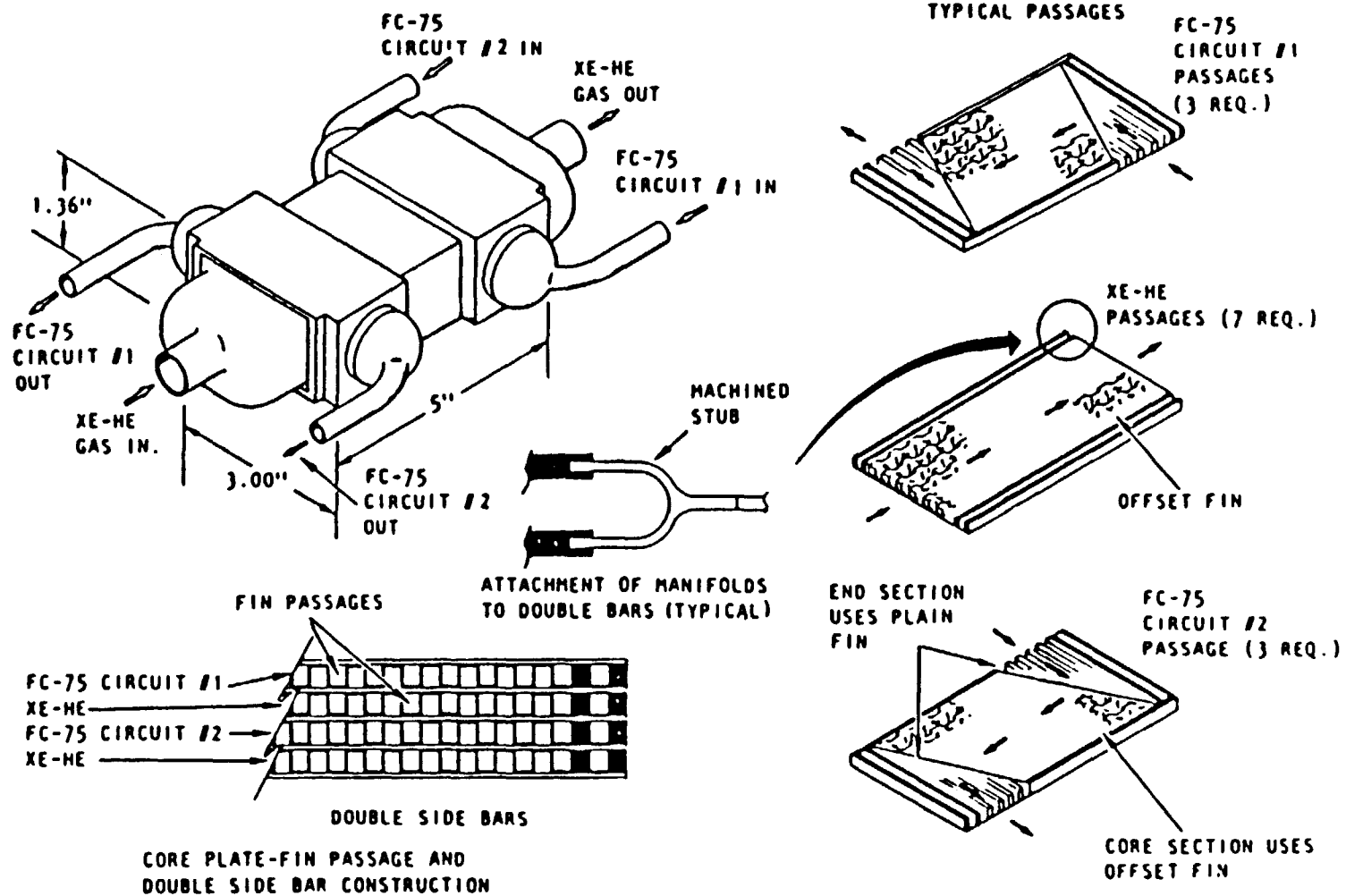
The recuperator (Figure 8) is a pure counter-flow plate-fin unit designed for 94% thermal effectiveness. The two fluids are high and low pressure helium/xenon gas. The high pressure gas comes from the compressor while the low pressure, hotter gas enters after expansion through the turbine. All fins in the recuperator are 0.006 inches thick and constructed from CRES 304L, a stainless steel. The tube plate thickness is 0.01 inches, and the unit is designed for a maximum temperature of 1017 °F.

The bleed cooler (Figure 9) is a small counter-flow, plate-fin heat exchanger similar to the gas cooler. The fin sandwiches are 0.077 inches high on the gas side and 0.1 inch high on the liquid side. The bleed cooler serves to cool the gas used in the turboalternator gas bearing. This unit is made entirely of 304L stainless steel.

### 3.1.2 Analytical Model

The idealized heat exchanger for developing the analysis is presumed to be a single-pass pure counter-flow heat exchanger with an equivalent heat transfer surface and wall mass. Boundary conditions between the component and the surroundings are assumed to be adiabatic. An energy balance is used to develop the differential equations, and temperatures are calculated for an n-segment model using a fully implicit backward differencing in time and central difference in space

Figure 9. CBC Bleed Cooler Design.  
(from DR02-RI/RD 85-320-27)



(BDT-CDS) finite difference scheme.<sup>9</sup> A Gaussian elimination method with scaling and partial pivoting is used to solve the system of  $3n$  simultaneous equations.

The heat exchanger is represented by dividing the control volume into  $n$  sections as shown in Figure 10. Each section consists of three elements. Consider the  $i$ -th section that has been cross-hatched. Element (i) is fluid A flowing in the indicated direction. Element (ii) is a wall element in contact with fluid A on one side and fluid B on the other. Element (iii) is the counter-flowing fluid B. No energy flow is assumed between adjoining wall elements although adjoining fluid elements have a net energy transfer.

For the  $i$ -th section, an energy balance can be performed on each section:

$$\left[ \begin{array}{c} \text{RATE OF CHANGE} \\ \text{OF ENERGY IN} \\ \text{C.V.} \end{array} \right] - \left[ \begin{array}{c} \text{NET CONVECTION} \\ \text{INTO C.V.} \end{array} \right] + \left[ \begin{array}{c} \text{NET DIFFUSION} \\ \text{INTO C.V.} \end{array} \right]$$

Conduction in the fluid was assumed to be negligible. Subsequent calculations showed the magnitude of conduction to be approximately 0.03% of convection and diffusion, validating the initial assumption. Radiation heat transfer between adjacent walls of the heat exchanger is also assumed negligible since an alternating sandwich type construction would maintain the walls at approximately the same temperature.

Assuming the temperatures in each element are given by an average temperature  $T_{xi}$ , where  $x$  is the fluid A, fluid B or wall  $w$  and  $i$  is the  $i$ -th section of the heat exchanger, then for an infinitesimal volume in element (i),

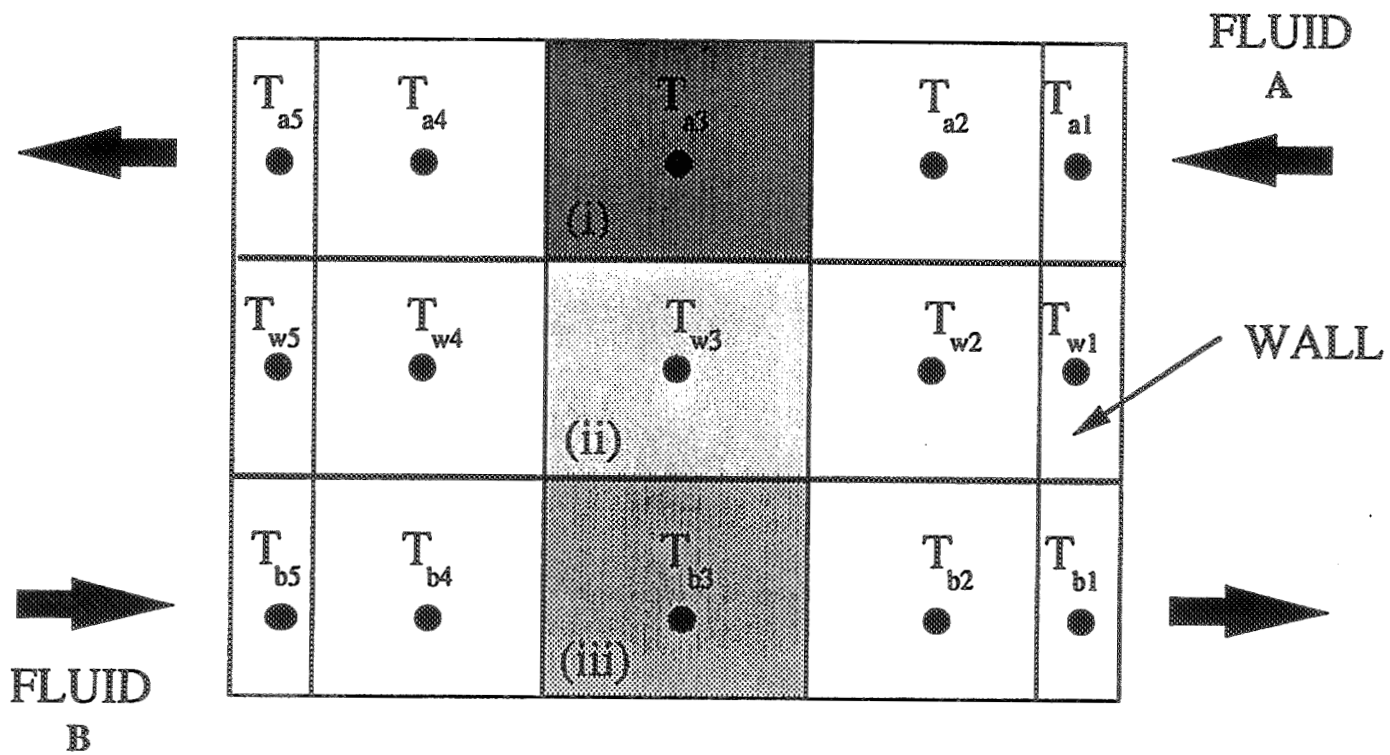


Figure 10. Heat Exchanger Finite Difference Scheme.

$$\frac{\partial (mc_v T)_a}{\partial t} = (hA)_a (T_w - T_a) + (\dot{m}c_p)_a \frac{\partial T_a}{\partial x} dx \quad (1)$$

It is assumed that there is no temperature gradient along the wall of element (ii), so the equation may be written as:

$$\frac{\partial (mcT)_w}{\partial t} = (hA)_a (T_a - T_w) + (hA)_b (T_b - T_w) \quad (2)$$

And similar to (1), the energy balance for element (ii) yields

$$\frac{\partial (mcT)_b}{\partial t} = (hA)_b (T_w - T_b) + (\dot{m}c)_b \frac{\partial T_b}{\partial x} dx \quad (3)$$

Using the subscript i for the node location, the above three equations may be written as:

$$(\dot{m}c_v)_{ai} \left[ \frac{\partial T_a}{\partial t} \right]_i = (hA)_{ai} (T_{wi} - T_{ai}) + (\dot{m}c_p)_a [T_{a(i-1)} - T_{a(i+1)}] \quad (4)$$

$$(\dot{m}c)_{wi} \left[ \frac{\partial T_w}{\partial t} \right]_i = (hA)_{ai} (T_{ai} - T_{wi}) + (hA)_{bi} [T_{bi} - T_{wi}] \quad (5)$$

$$(\dot{m}c)_{bi} \left[ \frac{\partial T_b}{\partial t} \right]_i = (hA)_{bi} (T_{wi} - T_b) + (\dot{m}c)_b [T_{b(i-1)} - T_{b(i+1)}] \quad (6)$$



Applying the simple Euler method of integration to the control volume for the time derivative produces the following equations. These are written with an n superscript representing the time step

$$(\dot{m}c_v)_{ai} \left[ \frac{T_{ai}^n - T_{ai}^{n-1}}{\Delta t} \right] = (hA)_{ai} (T_{wi}^n - T_{ai}^n) + (\dot{m}c_p)_a [T_{a(i-1)}^n - T_{a(i+1)}^n] \quad (7)$$

$$(\dot{m}c)_{wi} \left[ \frac{T_{wi}^n - T_{wi}^{n-1}}{\Delta t} \right] = (hA)_{ai} (T_{ai}^n - T_{wi}^n) + (hA)_{bi} [T_{bi}^n - T_{wi}^n] \quad (8)$$

$$(\dot{m}c)_{bi} \left[ \frac{T_{bi}^n - T_{bi}^{n-1}}{\Delta t} \right] = (hA)_{bi} (T_{wi}^n - T_{bi}^n) + (\dot{m}c)_b [T_{b(i+1)}^n - T_{a(i-1)}^n] \quad (9)$$

In this fully implicit scheme, all temperatures at time step n are unknowns. The above equations are rearranged to give a system of equations of the form

$$[A]\{T\} = \{B\} \quad (10)$$

where A is an (n x n) matrix of coefficients, T is a (1 x n) vector of unknowns and B is a (1 x n) vector of known quantities. Equation 7, for example, can be rearranged following form.

$$\left[ \frac{(\dot{m}c_v)_{ai}}{\Delta t} + (hA)_{ai} \right] T_{ai}^n + \left[ -(\dot{m}c_p)_a \right] T_{a(i-1)}^n + \left[ (\dot{m}c_p)_a \right] T_{a(i+1)}^n + \left[ (-hA)_{ai} \right] T_{wi}^n - \left[ \frac{(\dot{m}c_v)_{ai}}{\Delta t} \right] T_{ai}^{n-1} \quad (11)$$

The right hand side constitutes one element of the B matrix, while the left hand side coefficients appear as elements in the the A matrix. The temperatures at time step n are the unknowns in the T-vector.

Several other steps were taken to simplify the solution. It is assumed that

$$T_{an} = (T_a)_{outlet} \quad (12)$$

$$T_{bn} = (T_b)_{outlet} \quad (13)$$

$$T_{a1} = \text{Inlet Temperature for A} \quad (14)$$

$$T_{bn} = \text{Inlet Temperature for B} \quad (15)$$

The end sections have been modified to provide an accurate answer using few nodes. Sections 1 and n represent 1% each of the volume of the heat exchanger while the remaining 98% is divided among the rest of the n-2 sections. Therefore the minimum number of nodes used in a model is 3. Heat transfer coefficients were computed for each component and fluid<sup>10,11</sup> and are specified in the analysis file. The film coefficients are assumed constant through a transient since they change by less than 3% over 100 K.

The set of simultaneous equations (10) is solved using a Gaussian elimination method with scaling and partial pivoting. This solution method is written as a subroutine. A flowchart showing the programming logic used in implementing the finite difference scheme is presented in Figure 11.

### 3.1.3 Component Tests and Results

The following sections describe the tests performed on the component model to verify the code and the mathematical logic.

#### 3.1.3.1 Transient Performance

The typical response of the gas cooler to a step change in inlet temperature of fluid A is shown in Figure 12. The corresponding response for fluid B is shown in Figure 13. Several curves for different integration time steps illustrate the effect of varying time-step size. The model size was set at 5 nodes as optimum for maximum accuracy without exorbitant run times. This choice will be explained in succeeding tests. At time zero, a step in the inlet temperature of fluid A of 100 K was introduced, producing a change in outlet temperatures in fluid A and fluid B until both achieved a steady state after approximately 200 seconds. The transients indicate that a time step of 10 seconds provides a reasonable compromise between accuracy and CPU usage. The final steady-state temperatures are close to those found in the DR02 steady state calculations.

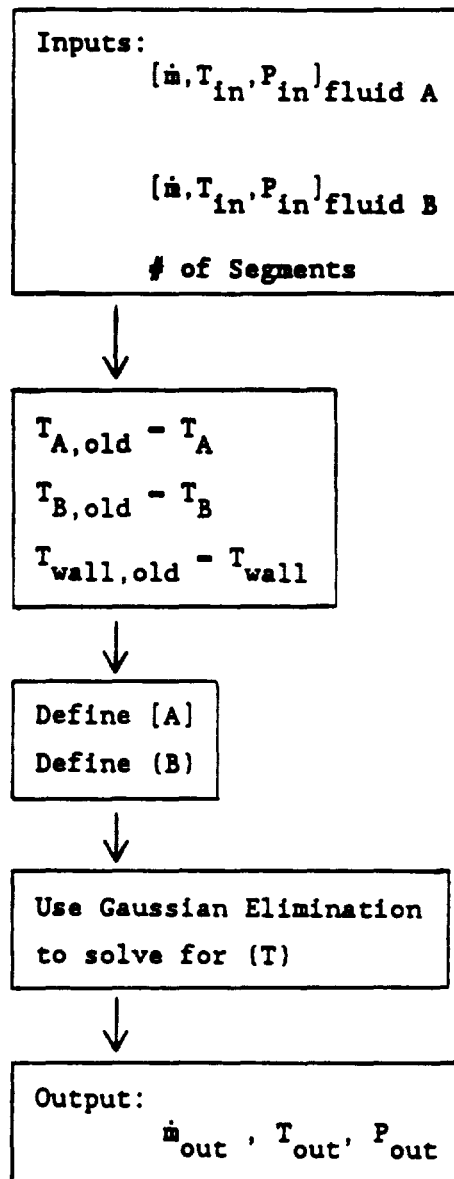
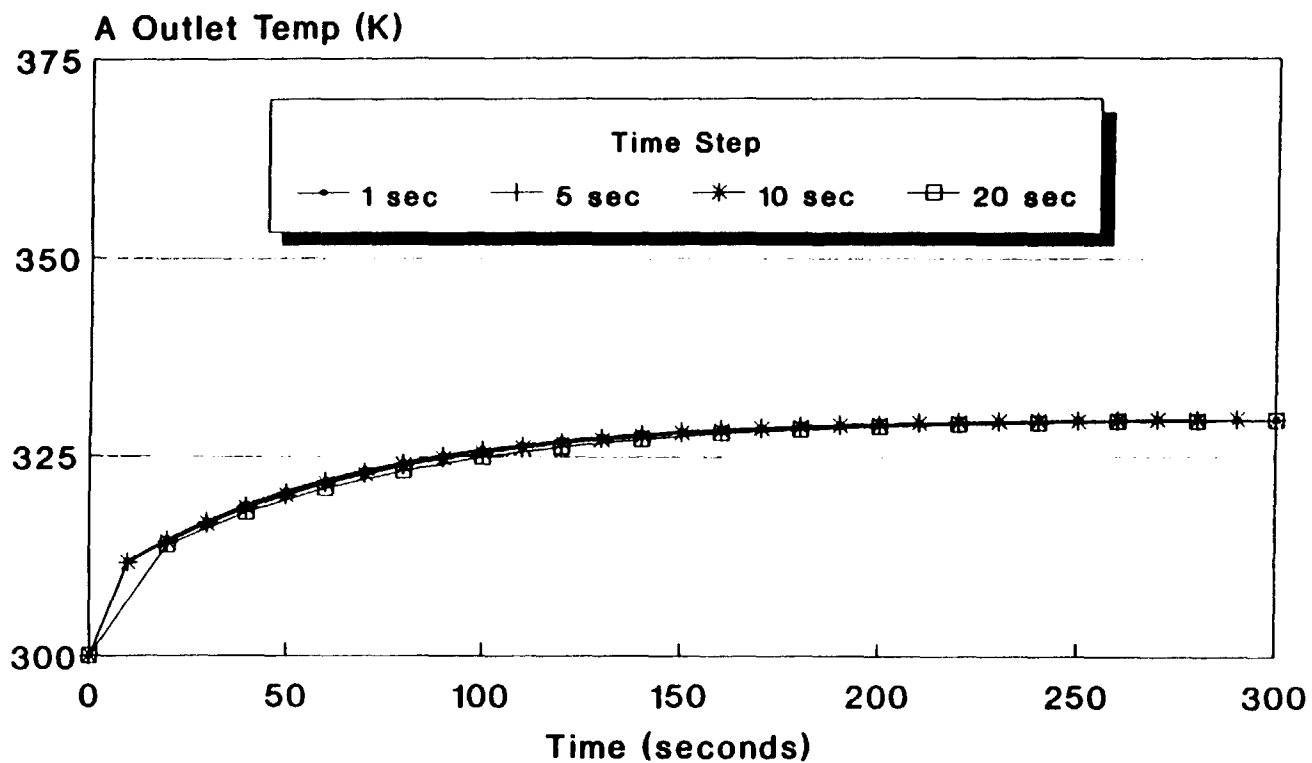


Figure 11. Heat Exchanger Model Flowchart.

Figure 12. Gas Cooler - Fluid A Transient Performance.

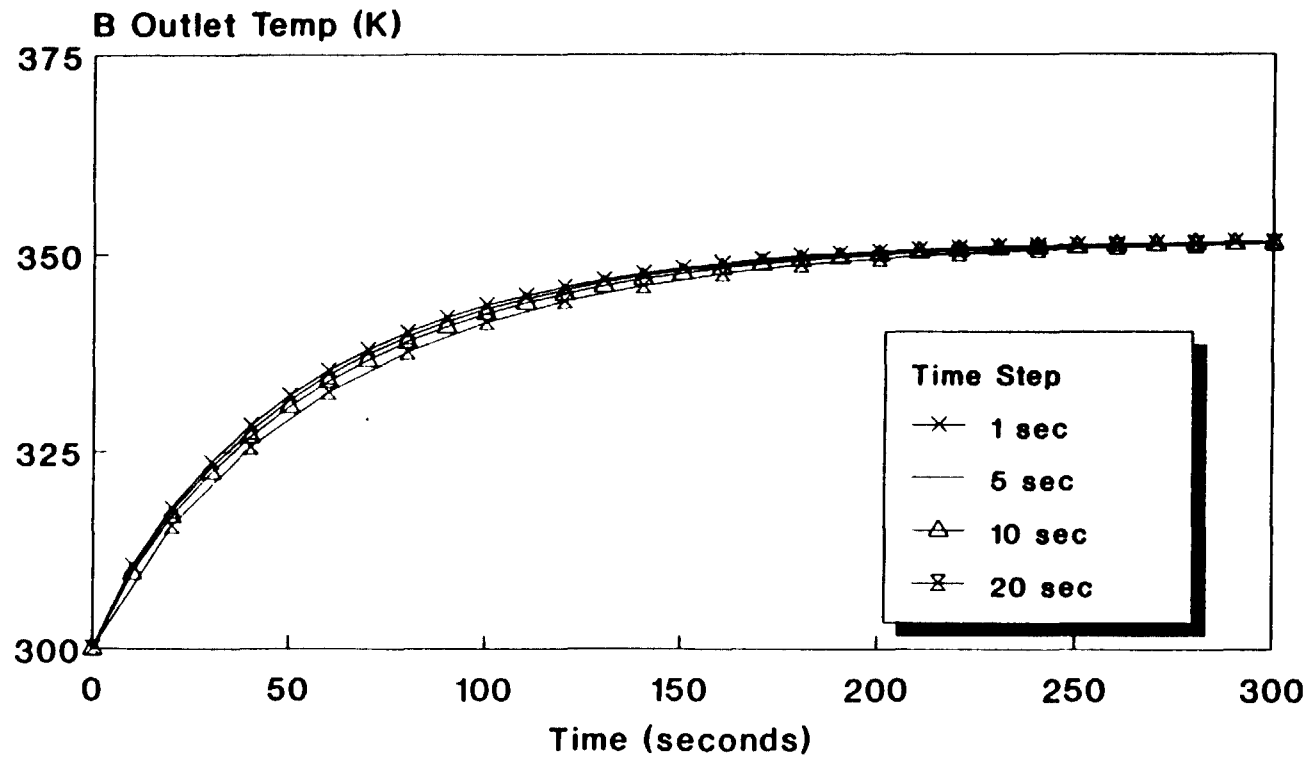
## Gas Cooler Fluid A Transient Performance



A Intemp=400 K, B Intemp=300 K  
# of segments=5,  
A. Iqbal 11/8/89 SMALL.FOR

Figure 13. Gas Cooler - Fluid B Transient Performance.

## Gas Cooler Fluid B Transient Performance



A Intemp=400 K, B Intemp=300 K  
# of segments=5,  
A. Iqbal 11/8/89 SMALL.FOR

### 3.1.3.2 Number of Segments Convergence Study

The dependence of fluid outlet temperature on the number of segments used in the model of the gas cooler is shown in Figure 14. This plot shows the increasing accuracy of the model as more and more segments are used in a simulation. However, past a certain point, a marginal increase in accuracy requires a much larger number of segments and correspondingly more CPU time.

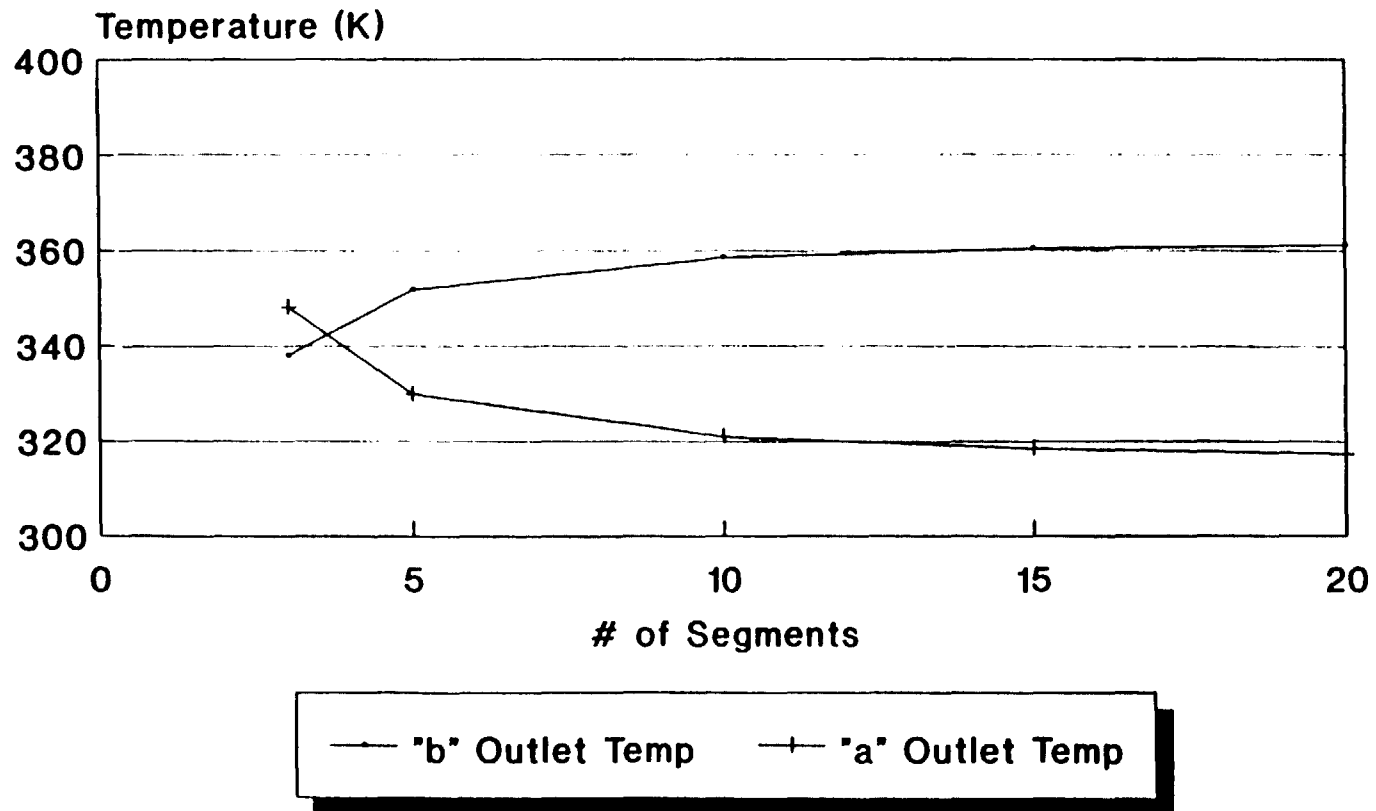
The analysis was produced by running the response to a step input of 100 K in fluid A of the gas cooler while the fluid B inlet temperature is held constant at 300 K. By varying the number of segments and recording the corresponding steady state outlet temperatures, the plot shown in Figure 14 was produced. It indicates that using five segments for such models should be adequate for most analyses. Further transients were run using 5 and 10 segment heat exchangers using both 10 and 20 second time steps as shown in Figure 15. It is clear from these results that a 10 second step is sufficiently small for the present study. Further, a 5 segment model was judged to provide sufficient accuracy for the purposes of this investigation.

### 3.1.3.3 Time and Spatial Variation with Temperature

Figure 16 shows the spatial temperature profile in the heat exchanger at different times during a transient. For these computations a 5 segment model was used. This figure shows the segment temperatures at various times during the transient. The transient is the response to a 100 K step in fluid A while the fluid B inlet temperature is held constant at 300 K. An integration time step of 10 seconds was chosen to

# Gas Cooler

## Number of Segments Convergence Study

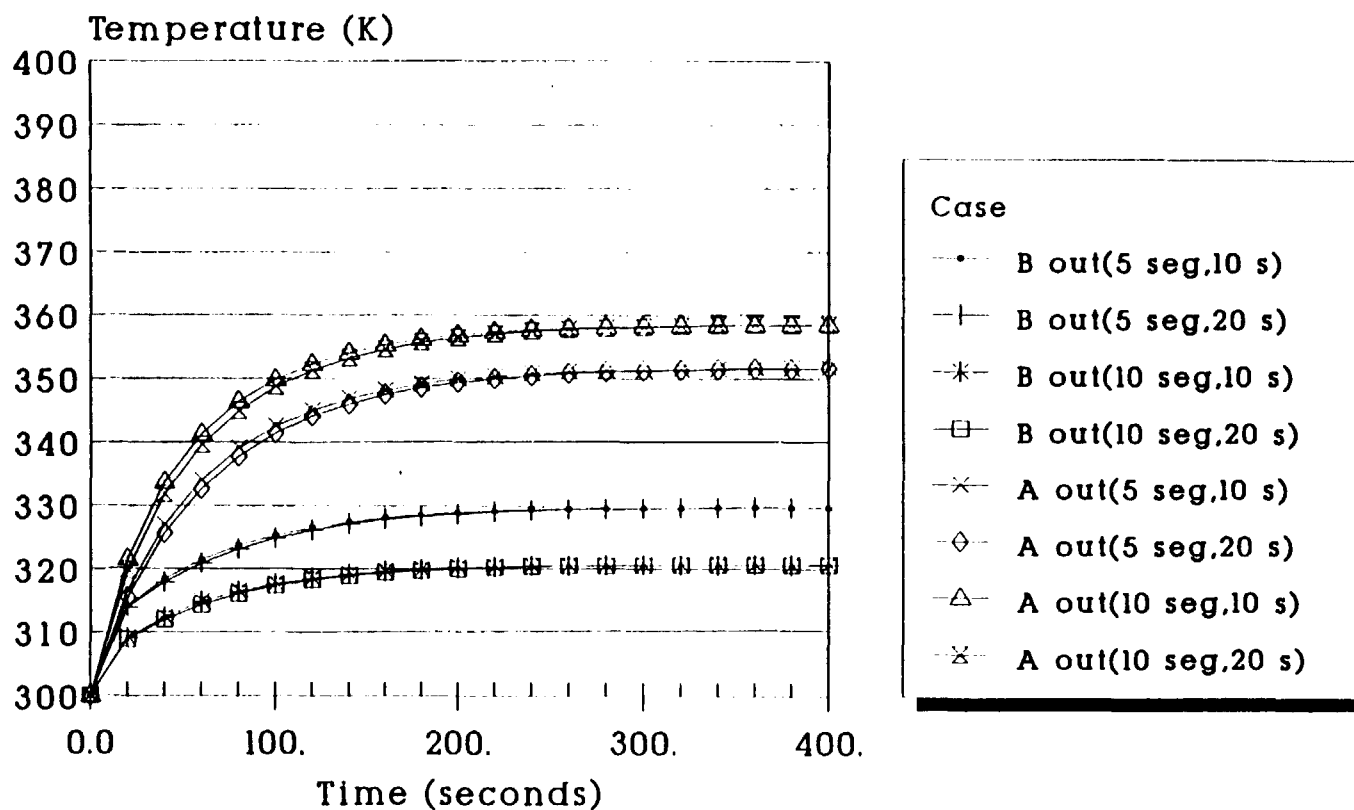


"a" Intemp=400 K, "b" Intemp=300K  
 Delta T=10 s,  
 A. Iqbal 11/9/89 SMALL.FOR



Figure 15. Gas Cooler - Combined Time Step and Segment Study.

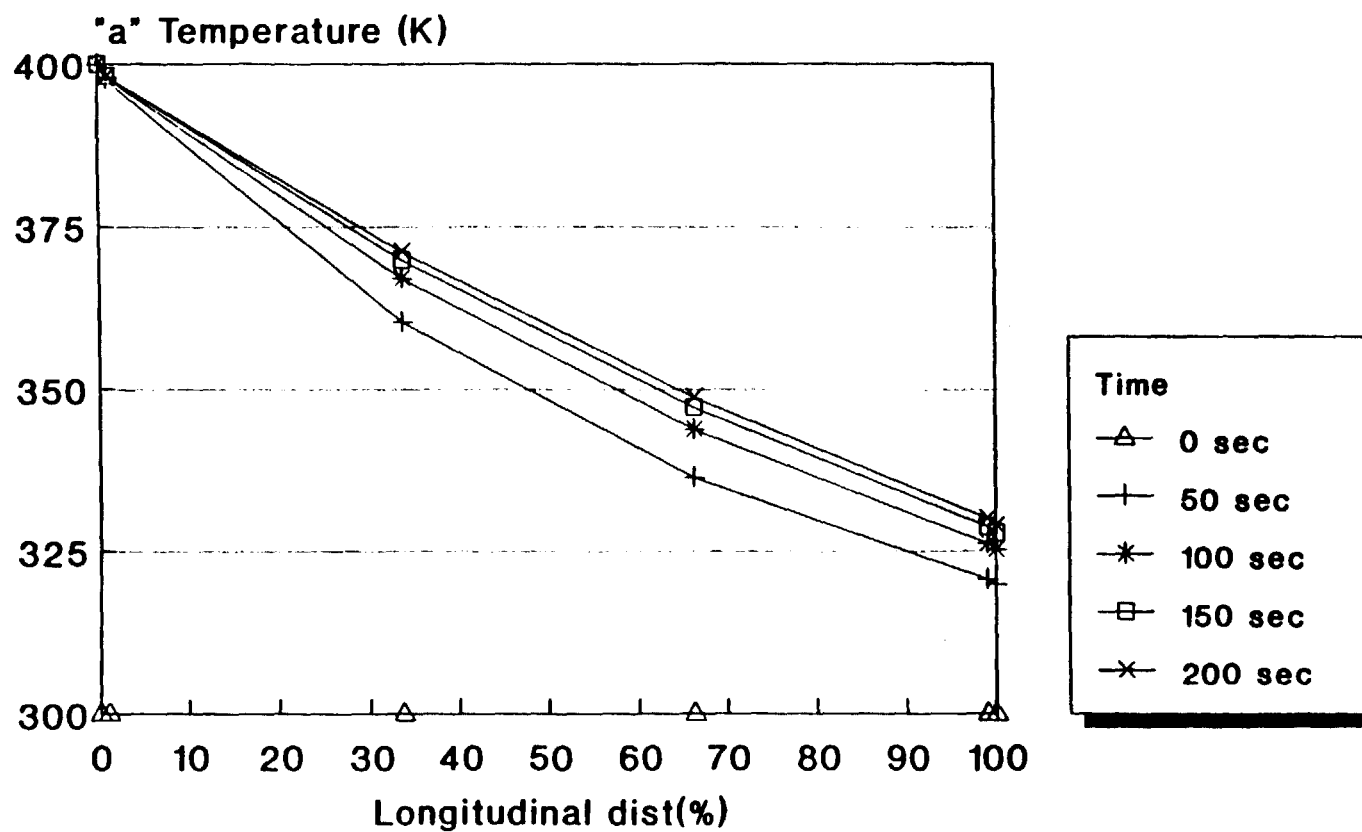
## Gas Cooler Combined Time Step and Segment Study



"a" Intemp=400 K, "b" Intemp=300 K  
 seg = # of segments  
 A. Iqbal 4/28/90 SMALLV.FOR

Figure 16. Gas Cooler - Spatial Temperature Variation with Time.

## Gas Cooler Spatial Temperature Variation with Time



"a" Intemp=400 K, "b" Intemp=300 K  
 #Seg=5, Delta T=10 s,  
 A. Iqbal, 11/9/89 SMALL.FOR

provide adequate accuracy while conserving CPU time (as demonstrated in section 3.1.3.1). Since the segments are not of the same size, the spatial variation is the distance along the length of the heat exchanger.

### 3.2 RADIATOR

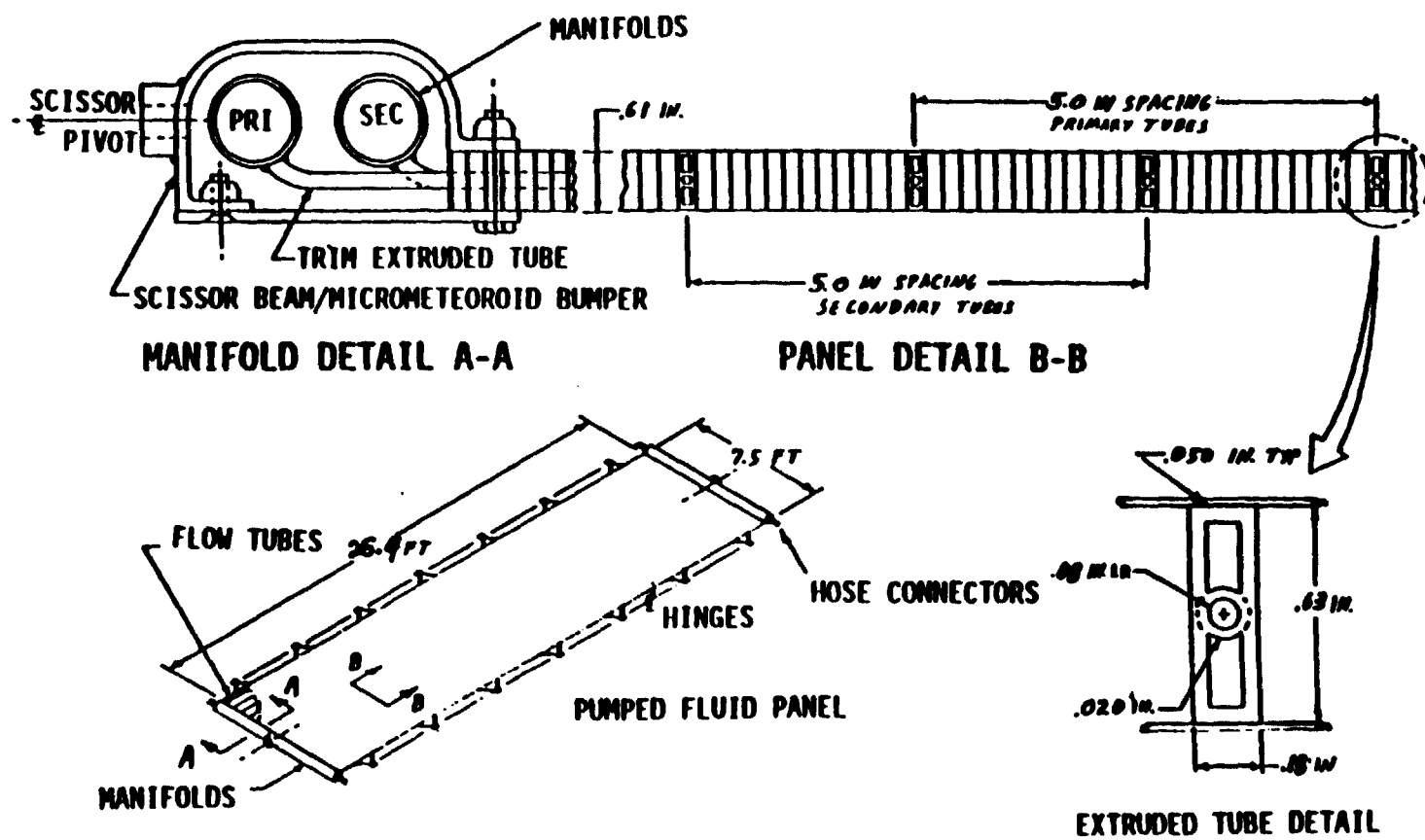
The energy sink for the CBC is deep space. The coolant loop carries thermal energy from the heat exchangers (gas cooler, bleed cooler, alternator cooler) to the radiator where it is radiated to space using large panels.

#### 3.2.1 Closed Brayton Cycle Radiator

The CBC radiator is of the pumped-fluid loop type. Two redundant fluid loops are passed through aluminum panels. These deployable hinged panels (see Figure 17) contain aluminum coolant channels which are attached to aluminum face-sheets which act as heat transfer fins. Aluminum honeycomb is used to stiffen the panels.

The six radiator panels are constructed by bonding the extruded aluminum channels to the honeycomb which is sandwiched between aluminum face-sheets. The adhesive is Hysol EA 9649. Tube inner diameter is 2 mm with a 0.5 mm wall. The primary and secondary lines alternate through the panel and are connected to the primary and secondary manifolds respectively. The scissors deployment mechanism extends the panels from stowed to operational position. Flexible metal hoses are used to transport fluid across the rotating joints. The primary and secondary loops are connected to separate pumps capable of providing a full backup

Figure 17. CBC Radiator Panel Design.  
(Reprinted from DR02-R1/RD 85-320-27)



in case one of the systems fails. Since the two loops are completely independent and sealed from one another for redundancy, only one loop is operational at one time.

### 3.2.2 Analytical Model

The idealized radiator is considered to be a tube attached to a radiating skin. The energy transfer from the tube to the skin is assumed to be uniform across the length and breadth of the panel. Coolant flow and temperature is considered uniform across the cross-section of the tube. The panel size is considered to be one-fourth the total radiator size since four radiator components are used in parallel to simulate the entire radiator. The sink temperature is a function of the power-generating-system orientation and the orbit, and is thus considered a known variable in the algorithm. An energy balance is used to develop the governing differential equations, and temperatures are calculated for an n-section model using a fully-implicit backward-differencing finite difference scheme similar to the one used in the heat exchanger. The same Gaussian elimination method that was used for the heat exchanger is also used to solve the system of  $2n$  simultaneous equations.

The radiator is represented by dividing the control volume into  $n$  sections as shown in Figure 18. Each section consists of two elements. The sink temperature is assumed to be a function of time but spatially constant across the panel. Consider the generalized section that has been crosshatched. Element (i) is the fluid A flowing in the direction indicated. Element (ii) is the wall element in contact with fluid A on one side and radiating to space on the other. No energy

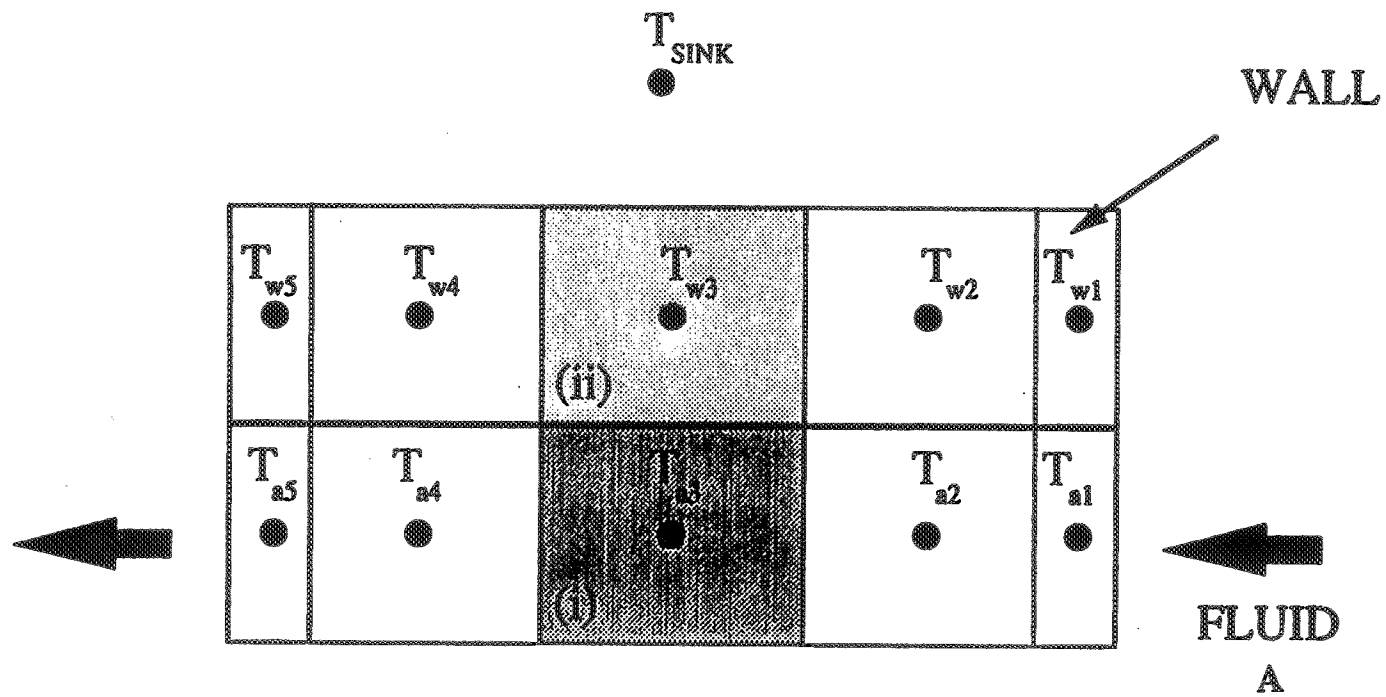


Figure 18. Radiator Finite Difference Scheme.

flow is assumed between adjoining wall elements, unlike the fluid elements.

For each element an energy balance is enforced:

$$\left[ \begin{array}{c} \text{RATE OF} \\ \text{CHANGE OF} \\ \text{ENERGY IN} \\ \text{C.V.} \end{array} \right] = \left[ \begin{array}{c} \text{NET} \\ \text{CONVECTION} \\ \text{INTO C.V.} \end{array} \right] + \left[ \begin{array}{c} \text{NET} \\ \text{RADIATION} \\ \text{INTO C.V.} \end{array} \right] + \left[ \begin{array}{c} \text{NET} \\ \text{DIFFUSION} \\ \text{INTO C.V.} \end{array} \right]$$

If the temperatures in each element are given by  $T_a$  or  $T_w$ , representing fluid A and the wall respectively, then for an infinitesimal volume in element (i),

$$\frac{\partial (mcT)_a}{\partial t} = (hA)_a (T_w - T_a) + (\dot{m}c_p)_a \frac{\partial T_a}{\partial x} dx \quad (16)$$

For element (ii), assuming no temperature gradient, the equation may be written as:

$$\frac{\partial (mcT)_w}{\partial t} = (hA)_a (T_a - T_w) + \sigma A (T_{\text{sink}}^4 - T_w^4) \quad (17)$$

Using the i subscript for the node location, the above equations may be written as

$$(\dot{m}c)_{ai} \left[ \frac{\partial T_a}{\partial t} \right] = (hA)_{ai} (T_{wi} - T_{ai}) + (\dot{m}c_p)_a [T_{a(i-1)} - T_{a(i+1)}] \quad (18)$$

$$(mc)_{wi} \left[ \frac{\partial T_w}{\partial t} \right]_i = (hA)_{ai} (T_{ai} - T_{wi}) + \sigma A (T_{sink}^4 - T_w^4) \quad (19)$$

Since equation (19) is non-linear, and a linear equation solver is to be used, the equation was linearized by substituting for the  $T_{wi}^4$  term with  $(T_{wi})(T_{wi}^3)$ . The set of equations was solved for  $T_{wi}$  while the previous value of wall temperature was used for  $T_{wi}^3$ . If these new and old values did not match within an acceptable tolerance after solving the linear algebra problem, the procedure was repeated using a modified relaxation method where:

$$T_{old} = [(T_{old}^4 + T_{new}^4)/2]^{1/4} \quad (20)$$

This method provided a stable solution for this finite difference scheme. Applying the simple Euler method of integration for the time term produces the following equations:

$$(mc)_{ai} \left[ \frac{T_{ai}^n - T_{ai}^{n-1}}{\Delta t} \right] = (hA)_{ai} (T_{wi}^n - T_{ai}^n) + (\dot{m}c_p)_a [T_{a(i-1)}^n - T_{a(i+1)}^n] \quad (21)$$

$$(mc)_{wi} \left[ \frac{T_{wi}^n - T_{wi}^{n-1}}{\Delta t} \right] = (hA)_{ai} (T_{ai}^n - T_{wi}^n) + \sigma A [T_{sink}^4 - T_{wi}^n (\bar{T}_{wi}^n)^3] \quad (22)$$

where  $\bar{T}_{wi}$  is derived using the relaxation scheme described above.

The end-sections are modified in a manner similar to the heat exchanger model. Each end-section represents 1% of the volume of the component while the remaining 98% is shared amongst the rest of the n-2



sections. The flowchart for this scheme is shown in Figure 19. Heat transfer coefficient calculations are shown in the appendix.<sup>10,11,12</sup>

### 3.2.3 Component Tests and Results

The radiator model was tested to determine the response to typical inputs such as steps, and to determine the sensitivity of the result to parameters such as time-step size and the number of segments in the model.

#### 3.2.3.1 Number of Nodes Convergence Study

The effect of time step size on the outlet temperature response is shown in Figure 20. The response is to a step of magnitude 100 K in the inlet temperature, from 300 K to 400 K. The initial conditions for the radiator wall, liquid, and sink temperatures are 300 K for the initial condition. This plot shows the radiator achieving steady state after approximately 150 seconds. It also demonstrates that, given the coarseness of the model, a time step of 10 seconds is adequate.

#### 3.2.3.2 Spatial Temperature Variation with Time

The temperature profile in the radiator at various times in response to a step is shown in Figure 21. The usual 100 K step input in inlet temperature was chosen to excite the system. An integration time step of 10 seconds was used based on the previous test. This test helps expose any gross inconsistencies in the finite-difference scheme or the implementation. The results show the model to be functioning correctly.

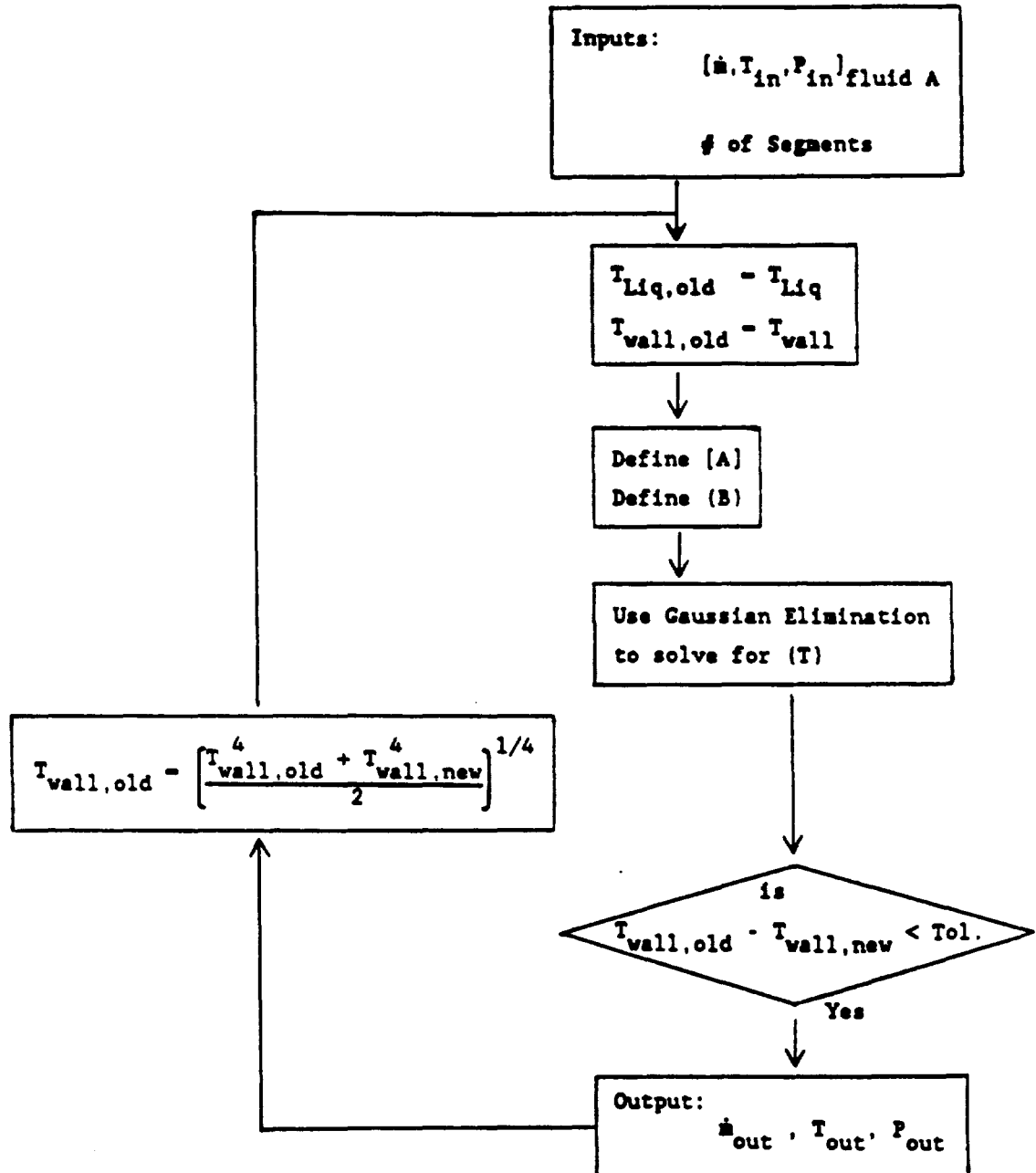
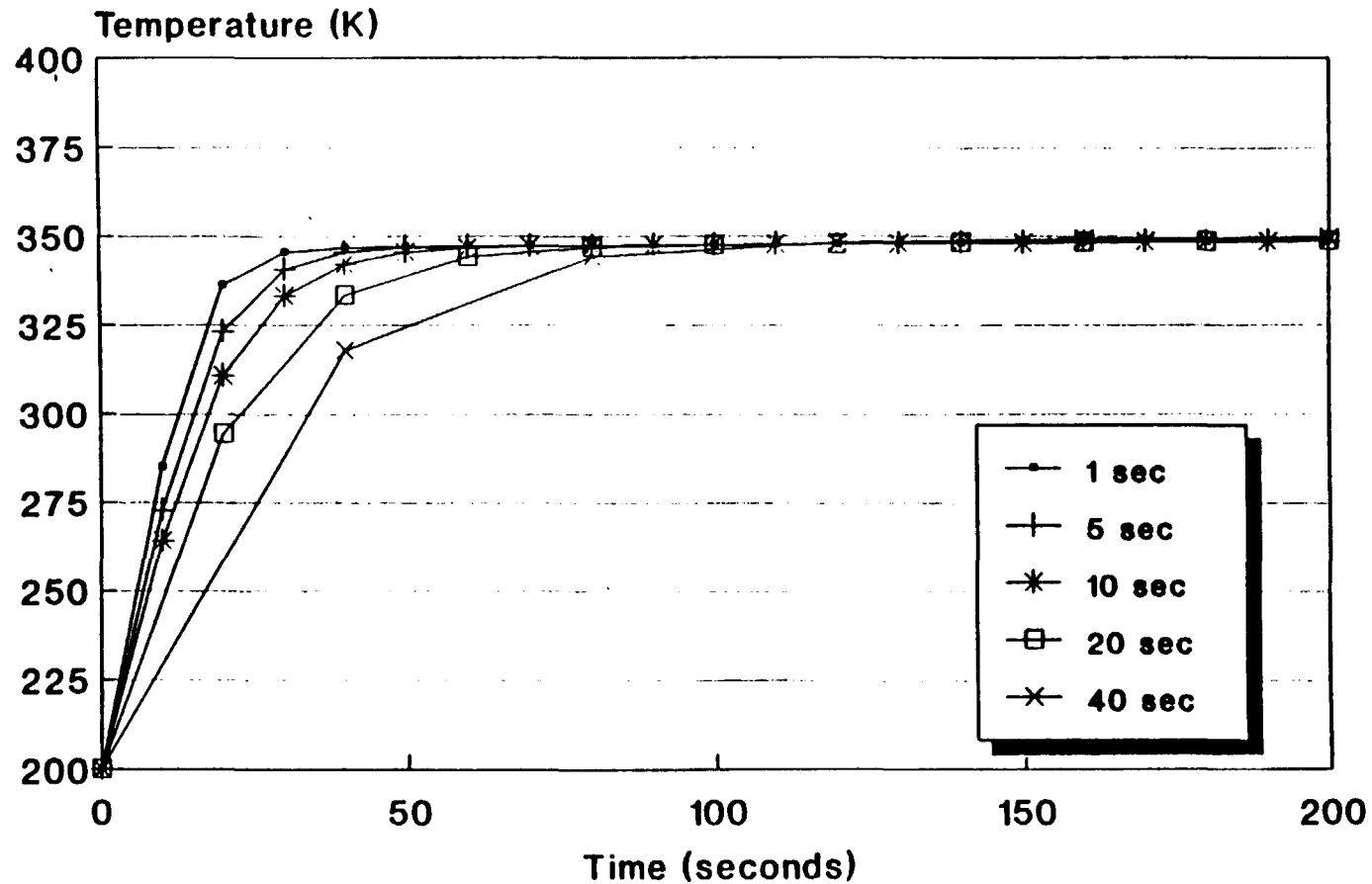


Figure 19. Radiator Model Flowchart.

# Radiator Transient Performance

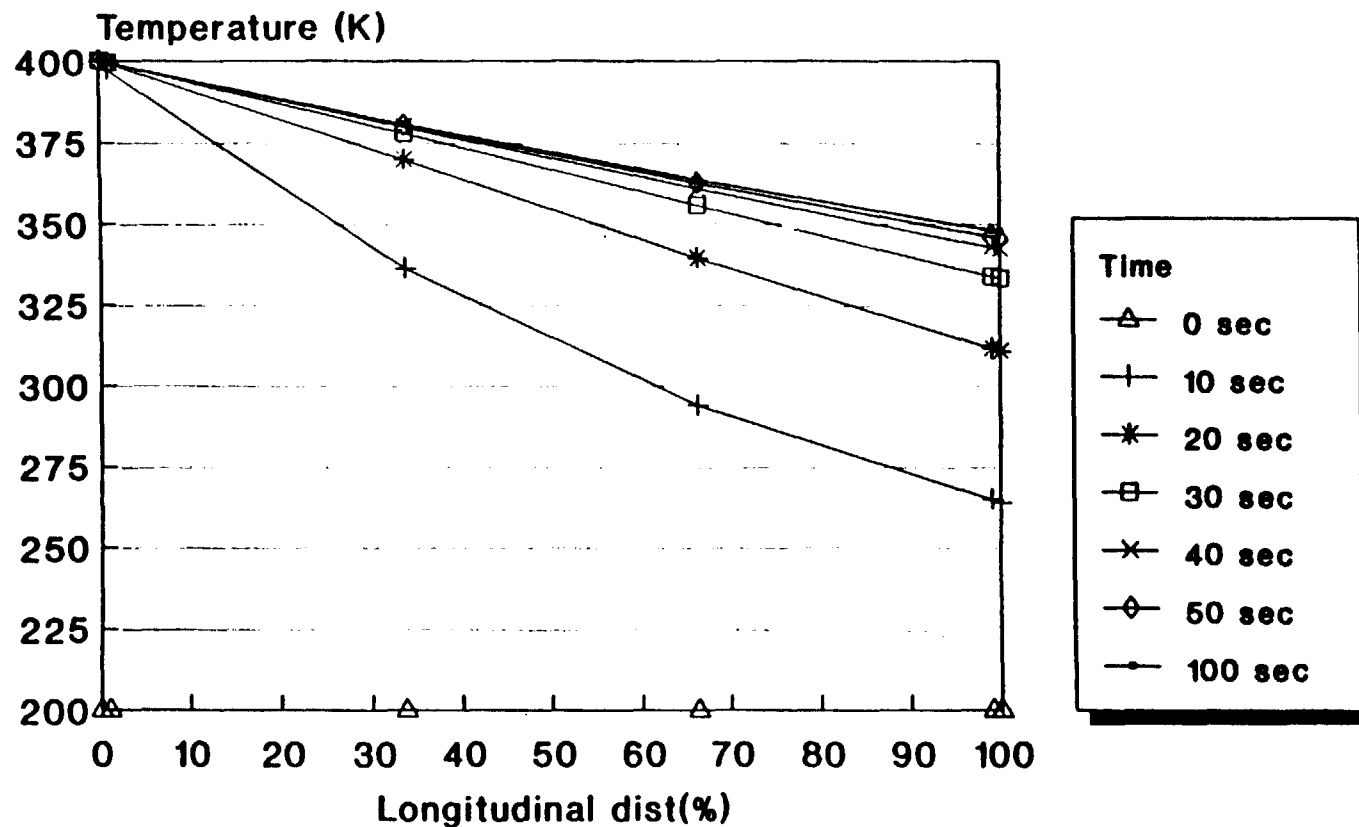
Figure 20. Radiator Transient Performance.



\*a\* Intemp=400 K, Sink temp=200 K  
 # of segments=5, Conv=1%  
 A. Iqbal 11/8/89 SMSEGRAD.FOR

Figure 21. Radiator - Spatial Temperature Variation with Time.

## Radiator Spatial Temperature Variation with Time



"a" Tempin=400 K, Sink Temp=200 K  
 #Seg=5, Delta T=10 s, Conv = 1%  
 A. Iqbal, 11/9/89 SMSEGRAD.FOR

### 3.2.3.3 Transient Performance

A sequence of analyses were performed using the same boundary conditions but with different numbers of segments in the radiator model. The functional dependence revealed by these analyses is shown in Figure 22. As seen in the heat exchanger model, accuracy is improved as more segments are used, but by a smaller and smaller margin with each additional segment.

## 3.3 RECEIVER

The energy source for the Closed Brayton Cycle is solar energy which is channelled through the receiver.

### 3.3.1 Closed Brayton Cycle Receiver

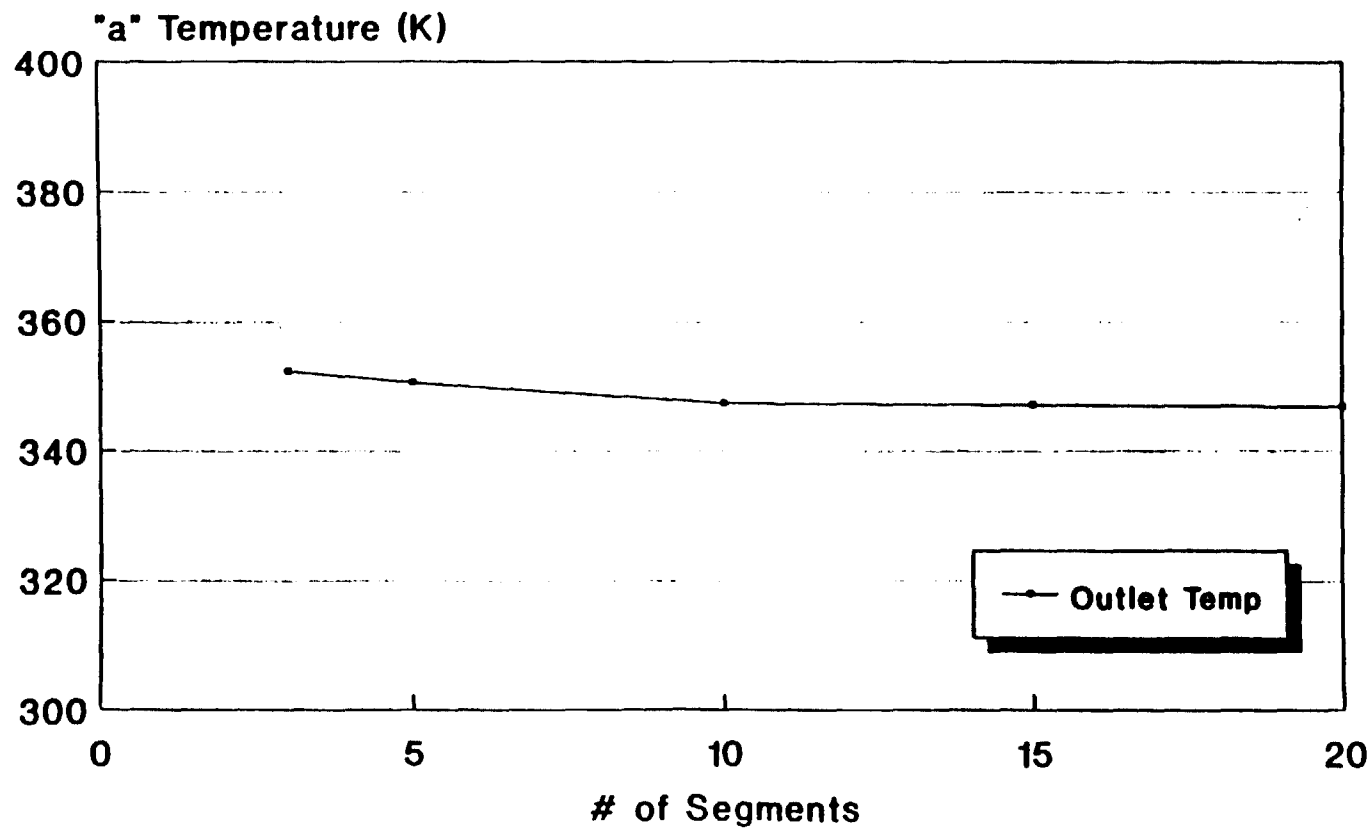
The CBC receiver consists of a cylindrical cavity which is lined with tubes carrying helium-xenon gas (Figure 23). The tubes themselves are encased by salt canisters through which the solar energy must pass. The tubes are brazed to the canisters to provide good thermal contact.

The salts provide the mechanism for achieving near constant energy flux into the CBC working fluid. The salts melt during insolation, absorbing some of the incident energy flux, and solidify during eclipse, releasing the stored energy to the helium-xenon. The melting point of the  $\text{LiF-CaF}_2$  mixture is 1042 K.

The gas tubes that run the length of the cavity are connected to manifolds at either end. There are 82 tubes, each being 0.875 inches in

Figure 22. Radiator - Number of Segments Convergence Study.

## Radiator Number of Segments Convergence Study



'a' Tempin=400 K, Sink Temp=200 K  
Delta T=10 s, Conv=1%  
A. Iqbal 11/9/89 SMSEGRAD.FOR

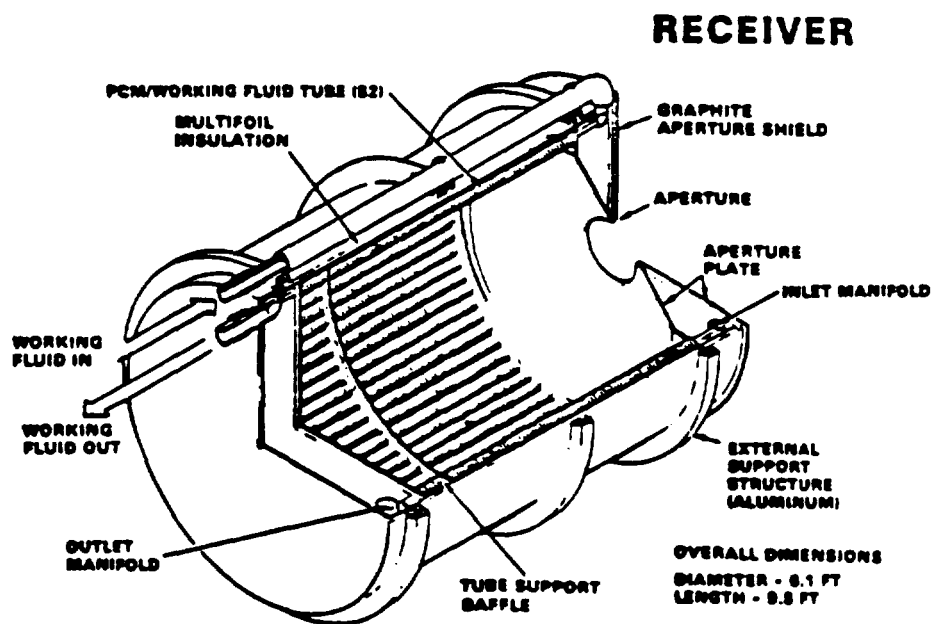
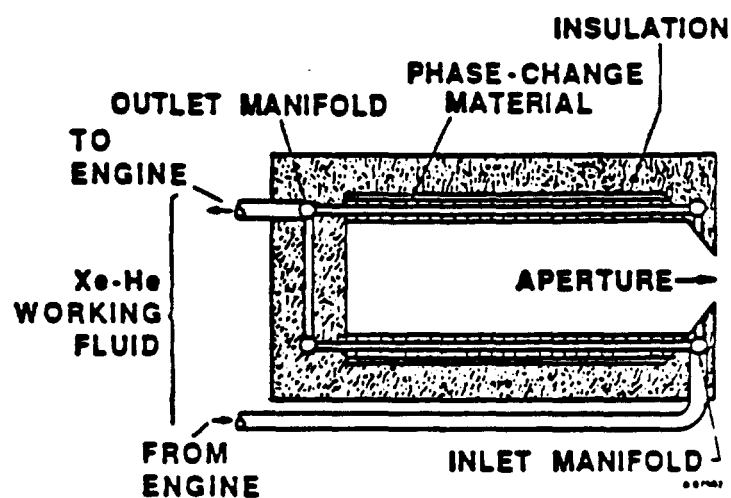


Figure 23. CBC Receiver Design.  
(Reprinted from DR02-R1/RD 85-320-2<sup>7</sup>)

diameter. Each tube has a length of 9.8 feet. The tubes, and phase-change material containment, are made of Haynes +188, a cobalt-based alloy known for its high strength and resistance to creep rupture.

### 3.3.2 Analytical Model

The receiver is modelled as a tube with a uniform temperature wall boundary representing the salt. It is assumed that the salt temperature is specified, and is uniform along the length of the tube. The salt temperature is specified in EASY5 as a function of time to drive the transient analyses.

Aside from the uniform boundary temperature, the receiver model uses the same governing equations as the other heat exchangers. It is represented by dividing the control volume into  $n$  segments (Figure 24). Each segment consists of three elements: (i) containing the fluid A, (ii) representing the wall of the tube and canister, and (iii) representing the salt. Element (iii) uses the same temperature throughout the length of the receiver.

An energy balance is performed on each element:

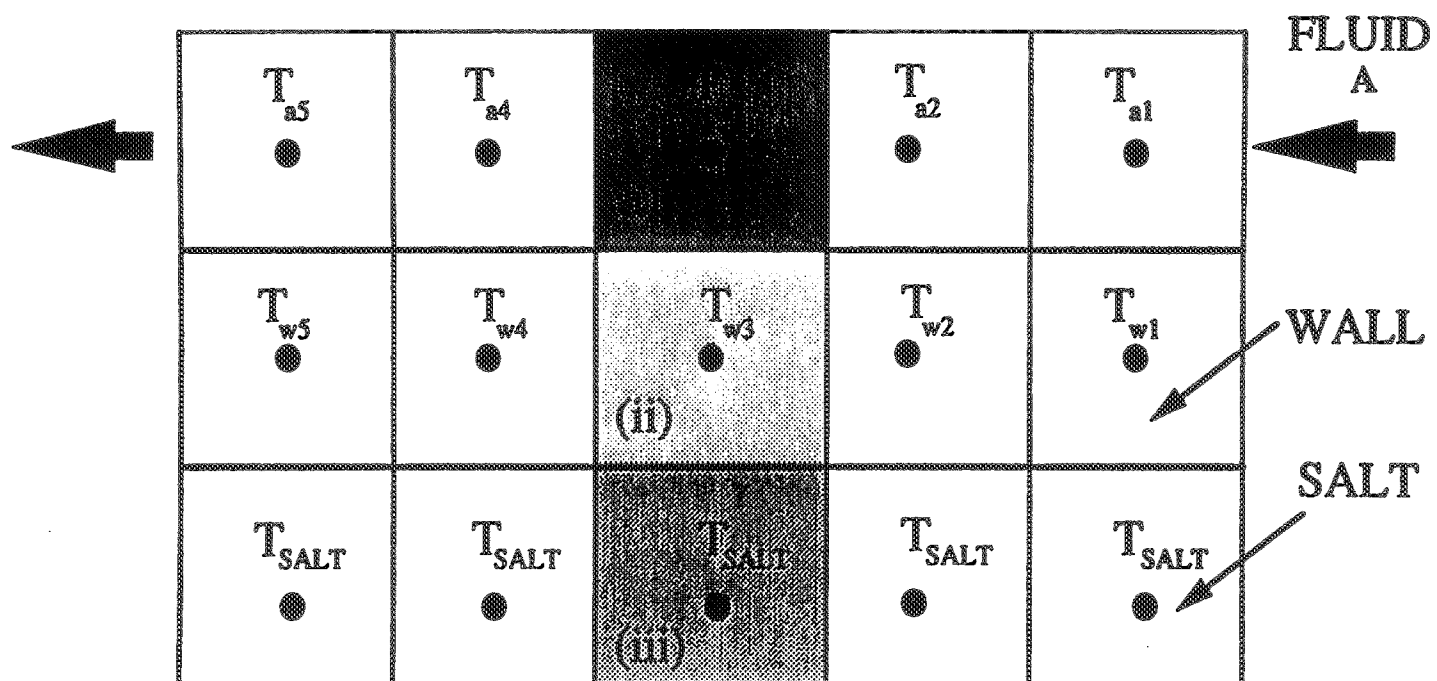
$$\left[ \begin{array}{c} \text{RATE OF CHANGE} \\ \text{OF ENERGY} \end{array} \right] = \left[ \begin{array}{c} \text{NET CONVECTION} \\ \text{IN} \end{array} \right] + \left[ \begin{array}{c} \text{NET DIFFUSION} \\ \text{IN} \end{array} \right]$$

For element (i), equation (1) holds true and equation (2) is modified to reflect the salt temperature  $T_S$ .

$$\frac{\partial (mcT)_w}{\partial T} = (hA)_a (T_a - T_w) + (hA)_s (T_S - T_w) \quad (23)$$



Figure 24. Receiver Finite Difference Scheme.



Applying the Euler method of integration and using the subscript i for the node location as before, equation (23) becomes:

$$(mc)_{wi} \left[ \frac{T_{wi}^n - T_{wi}^{n-1}}{\Delta t} \right] = (hA)_{ai} (T_{ai}^n - T_{wi}^n) + (hA)_{si} [T_S^n - T_{wi}^n] \quad (24)$$

where  $T_S$  is a known variable. As with the heat exchanger, equations (12) and (14) hold true for the receiver. The set of simultaneous equations is solved in a manner similar to that used for the heat exchanger model.

### 3.4 PIPES

#### 3.4.1 Pipes - Hardware

Fluid transfer between components is accomplished using pipes or ducts. The ducts are fabricated using two different stainless steel alloys, Hastelloy X for high temperature applications and 347 stainless steel for lower temperature applications. Multi-ply bellows are used throughout the ducting system.

#### 3.4.2 Pipes - Analytical Model

Assuming a constant thermal energy loss from the pipe, and a pressure loss due to friction, an outlet pressure and temperature are calculated. The temperature drop is simply calculated:

$$q = \dot{m}c(T_{in} - T_{out}) \quad (25)$$

where  $q$  is the energy loss in the pipe.

The pressure drop is calculated assuming incompressible fully-developed flow:

$$\Delta P_L = \rho g h_L \quad (26)$$

where  $h_L$  is the head loss, which can be determined from the Darcy-Weisbach equation:

$$\Delta P_L = f \left[ \frac{L}{D} \right] \left[ \frac{\rho V^2}{2} \right] \quad (27)$$

where  $f$  is the Darcy friction factor, a function of the Reynolds number,  $R$ , and  $\epsilon/D$  for the pipe. For laminar flow where  $R < 2100$  then

$$f = \frac{64}{R}, \quad (28)$$

and for turbulent flow (assuming a smooth pipe),

$$f = 0.316 R^{-1/4} \quad (29)$$

from the Nikuradse equation<sup>13</sup>.

### 3.5 MANIFOLDS

#### 3.5.1 Manifolds - Hardware and Analytical Model

Flow through the gas and liquid loop is split and rejoined at a number of places. It is assumed that the splitting of flow is in a fixed ratio as indicated in the DR02 document. Splitting manifolds divide the mass flow in the dictated ratios, keeping the temperatures and pressures unchanged. Merging manifolds compute an exit temperature

based on a simple energy balance using the mass fraction, specific heat, and temperature of each stream entering the manifold component.

### 3.6 PUMP

#### 3.6.1 Pump - Hardware and Analytical Model

The coolant flow is maintained by the CBC coolant pump/accumulator package. Since the cooling system has two redundant loops, two independent pump/accumulator combinations are provided, each capable of providing for the head/flow needs of the energy-rejection system. The pump/accumulator is assumed to deliver fluid at a constant pressure and mass flow rate. The mass flow can be varied as function of time to observe the dynamics of loss of coolant flow.

### 3.7 COMBINED ROTATING UNIT

The largest part of the Power Conversion Unit is the combined rotating unit. This assembly consists of a single-stage, radial-outflow compressor, a single-stage radial-inflow turbine and a straddle-mounted Rice alternator.

#### 3.7.1 Turboalternator

The assembly features radial aerodynamic components integrated with a high-speed, solid-rotor Rice alternator supported by foil gas bearing as shown in Figure 25. Cooling is provided to the alternator stator by FC-75 coolant and to the alternator rotor and gas bearing by cooled bleed helium-xenon gas. At design point, the rotating speed is

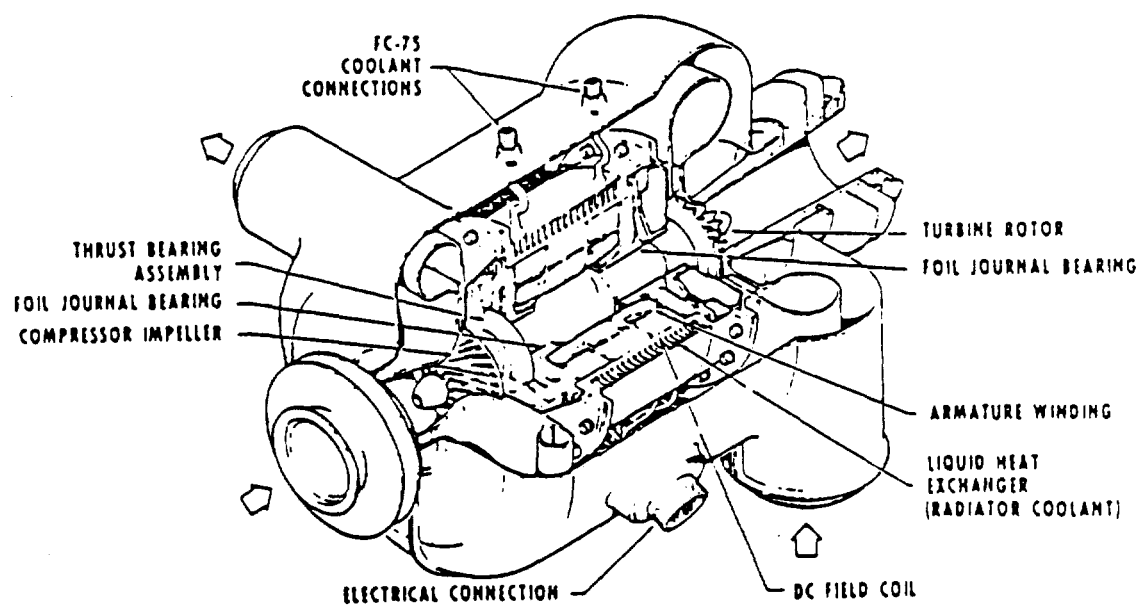


Figure 25. CBC Turboalternator Design

(from DR02-RI/RD 85-320-2<sup>7</sup>)

maintained at 32,000 rpm. The compressor and turbine diameters are 6.42 and 7.66 inches respectively.

### 3.7.2 Turboalternator - Analytical model

The turboalternator can be modelled using two separate control schemes. The first is a constant-speed machine, which would represent the design point of the combined rotating unit, and the second is a constant-work machine, which is more representative of the combined rotating unit in the startup and shut-down modes.

#### 3.7.2.1 Constant Speed Machine

The constant-speed model of the compressor and turbine assumes instantaneous response and a constant shaft speed. The instantaneous response has been shown by M. Samad Ali<sup>14</sup> to be a good assumption for studying the cooling system performance since response times for the alternator and compressor are many orders of magnitude smaller than the heat exchangers.

Compressor and turbine response is based on the performance maps for similar machines as actual data for the SDPGS turbomachinery is not available<sup>15</sup>. Isentropic efficiencies were converted to polytropic efficiencies using

$$\eta_{p,c} = \frac{\ln(P_{out}/P_{in})^{R/C_p}}{\ln\left[\frac{(P_{out}/P_{in})^{R/C_p}}{\eta_{i,c}} + 1\right]} \quad (30)$$

for the compressor and

$$\eta_{p,e} = \frac{\ln \left[ 1 - \eta_{i,e} \left( 1 - (P_{in}/P_{out})^{R/C_p} \right) \right]}{\ln(P_{in}/P_{out})^{R/C_p}} \quad (31)$$

for the Turbine<sup>16</sup>. Since the shaft speed is constant, the turbomachinery is essentially locked into one operating point with a given  $\eta_{tur}$ ,  $\eta_{com}$  and pressure ratio.

The turbine model uses the following polytropic relations to calculate the outlet temperature:

$$\left[ \frac{T_{in}}{T_{out}} \right] = \left[ \frac{P_{in}}{P_{out}} \right]^{(\eta_{tur} * R/C_p)} \quad (32)$$

and for the compressor

$$\left[ \frac{T_{out}}{T_{in}} \right] = \left[ \frac{P_{out}}{P_{in}} \right]^{(R/C_p * \eta_{com})} \quad (33)$$

The rate of turbine and compressor work output is calculated using

$$\dot{W}_{tur} = \dot{m} c_p (T_{in}^{total} - T_{out}^{total}) \quad (34)$$

and similarly, the rate of compressor work required is calculated using the results of equation 33. Alternator work available is then given by:

$$\dot{W}_{alt} = \dot{W}_{tur} + \dot{W}_{com} \quad (35)$$

EASY5 solves the system model by tracing a path around the system using the system schematic. The initial component chosen for a solution is arbitrary. Once the outlet conditions of the component are calculated, EASY5 marches to the next component in the system flowchart for a solution. Once around the loop constitutes a single call to the model for that particular time. This process is repeated at the next time level.

#### 3.7.2.2 Variable Speed Machine

The variable speed model of the turbine and compressor assumes constant alternator work and calculates the new operating point of the turbomachinery using performance maps.

The objective of the variable speed model was to simulate situations where the constant speed assumption is not valid, for example in startup or shutdown conditions, as well as conditions close to the boundary of the operating envelope. The turbine and compressor operation is modelled using performance maps shown in Appendix B. These non-dimensional maps were adapted for this model since actual performance data is not available. Given the speed, efficiency, and mass flow rate, the pressure ratio across the turbine or compressor can be calculated using this data.

The turbine and compressor model flowcharts are shown in Figure 26 and 27 respectively. The turbine model uses the inlet mass flow rate, pressure and temperature, as well as the shaft speed calculated from the compressor model to determine the turbine's operating point using performance maps. Since both pressure ratio and the efficiency are



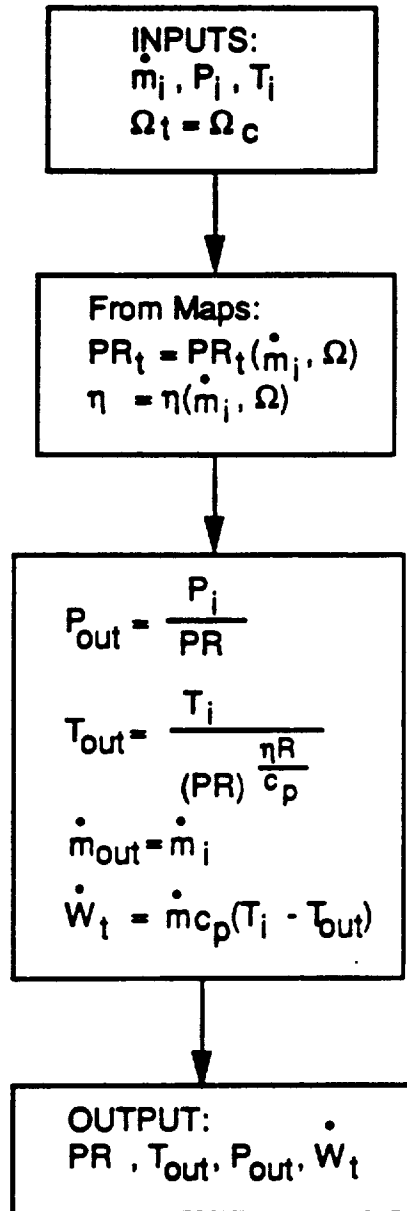


Figure 26. Variable Speed Turbine Model Flowchart

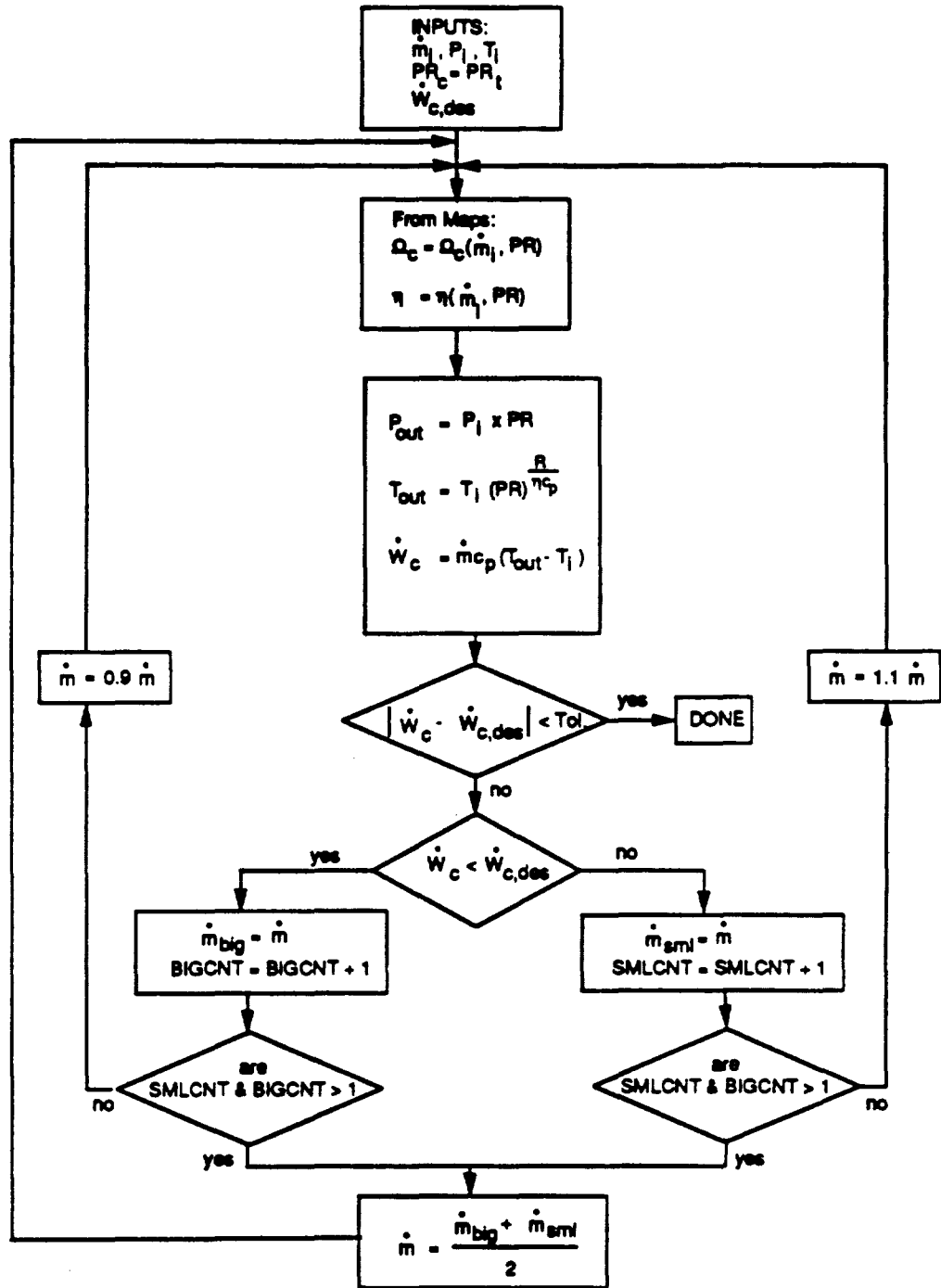


Figure 27. Variable Speed Compressor Model Flowchart

functions of two variables, namely speed and mass flow rate, linear interpolation is used to determine the operating point. The model outputs are the turbine output power, the outlet pressure, temperature and pressure ratio.

The compressor model shown in Figure 27 uses as input the inlet mass flow rate, the temperature and pressure. The model assumes the same pressure ratio as the turbine, and a desired compressor work. The desired work is calculated by subtracting the constant alternator work from the energy provided by the turbine.

The model iteration is started by assuming a mass flow rate through the compressor. This quantity is adjusted until the calculated compressor work equals the desired compressor work. A bisection method is used to converge to the correct mass flow rate, which results in a correct energy balance for the entire system.

In the gas loop, the turbine, compressor and other models work in a sequential fashion, where the output of one component is taken as the input to the next. Thus at each time step, EASY5 marches once around the gas loop and thus computes the state of each component at that time. For a variable speed machine several passes around the system loop are required to converge to the correct mass flow rate. This capability of repeated calls to the system model at one time step is not available in EASY5. Therefore, a fully functioning variable speed model could not be implemented.

#### 4. TRANSIENT SYSTEM PERFORMANCE

Individual component models were originally written in FORTRAN. They were subsequently transferred to EASY5 as FORTRAN blocks and then converted to EASY5 Macros if appropriate. These building blocks were then combined to simulate the two subsystems of the Closed Brayton Cycle: the gas loop and the liquid loop. Finally the subsystems were integrated to assemble the full system.

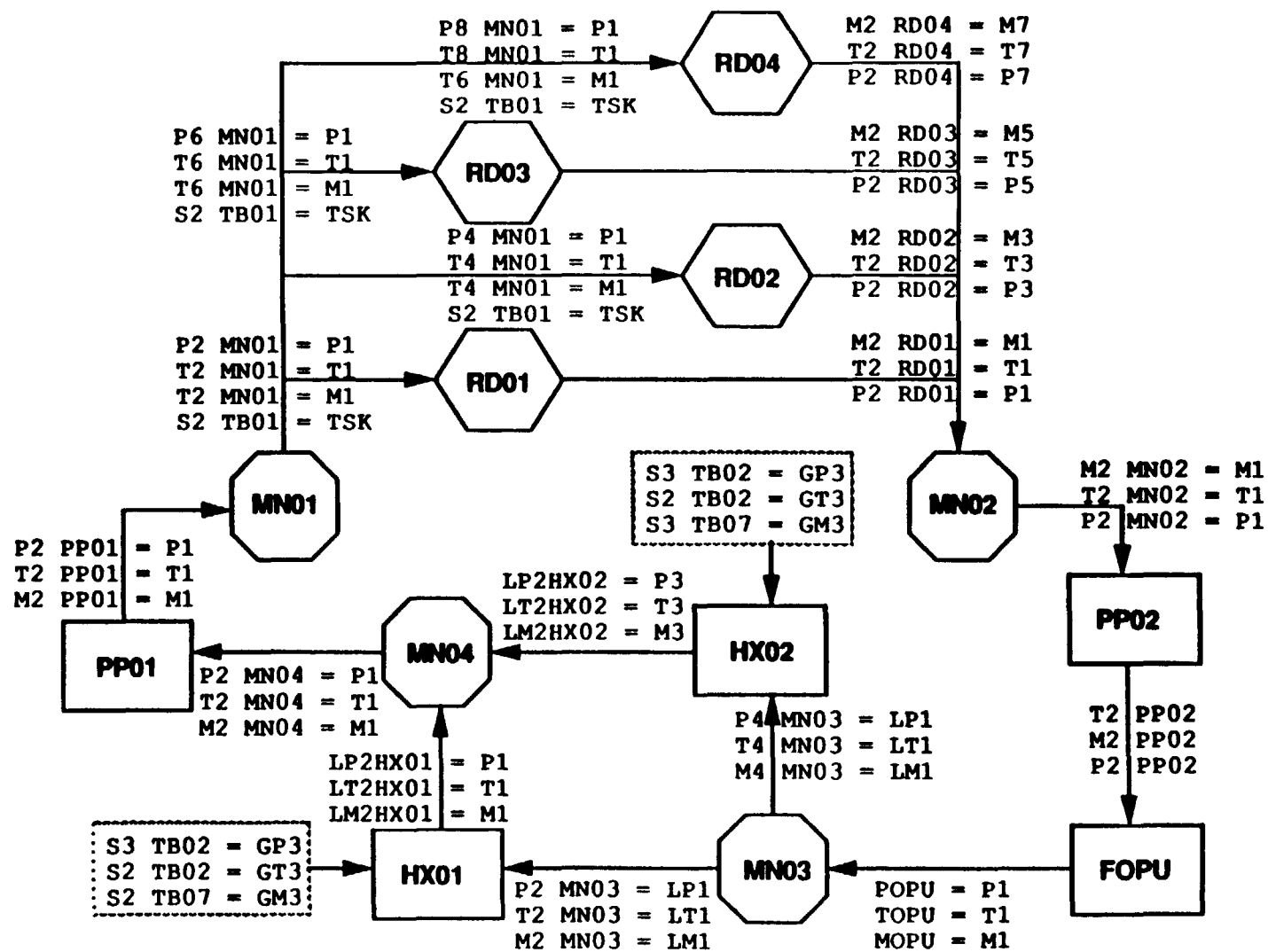
After assembly, each subsystem was subject to a number of tests to verify the transient response and to debug the model. These tests included a step input, a double step input where the second step returned the system to its initial state, and a sinusoidal input.

The response of the fully integrated system to several possible scenarios culminated the study of transients in the power generating system. These included an orbital fluctuation transient for a maximum insolation orbit, a loss of radiator panel transient, and a loss of coolant pump transient.

##### 4.1 COOLANT LOOP

The coolant loop schematic is shown in Figure 28. This subsystem consists of two heat exchangers (the gas cooler and the bleed cooler), four radiator panels connected in parallel, a pump, several pipe components, and four manifolds. The naming convention used for components and variables is given in Table 1 and is used throughout the rest of the analysis.

Figure 28. Coolant Loop Schematic.



CBC Coolant Loop Schematic

Table 1. Coolant Loop Convention

Variable Name (Example) - P2 MN01  
Variable ID      Component ID

<u>IDENTIFICATION</u>	<u>COMPONENT</u>
MNnn	Manifold
RDnn	Radiator
PPnn	Pipe
HX01	Heat Exchanger (Gas Cooler)
HX02	Heat Exchanger (Bleed Cooler)
FOPU	Pump

<u>IDENTIFICATION</u>	<u>VARIABLE</u>
S3 TB02	Inlet Gas Pressure
S2 TB02	Inlet Gas Temperature
S2 TB07	Inlet Gas Mass Flow Rate
P1, M1, T1	Inlet Pressure, Mass Flow and Temp.
LP1, LM1, LT1	Inlet Liquid Pressure, Mass Flow, Temp.
GP1, GM1, GT1	Inlet Gas Pressure, Mass Flow, Temp.
TSK	Sink Temperature

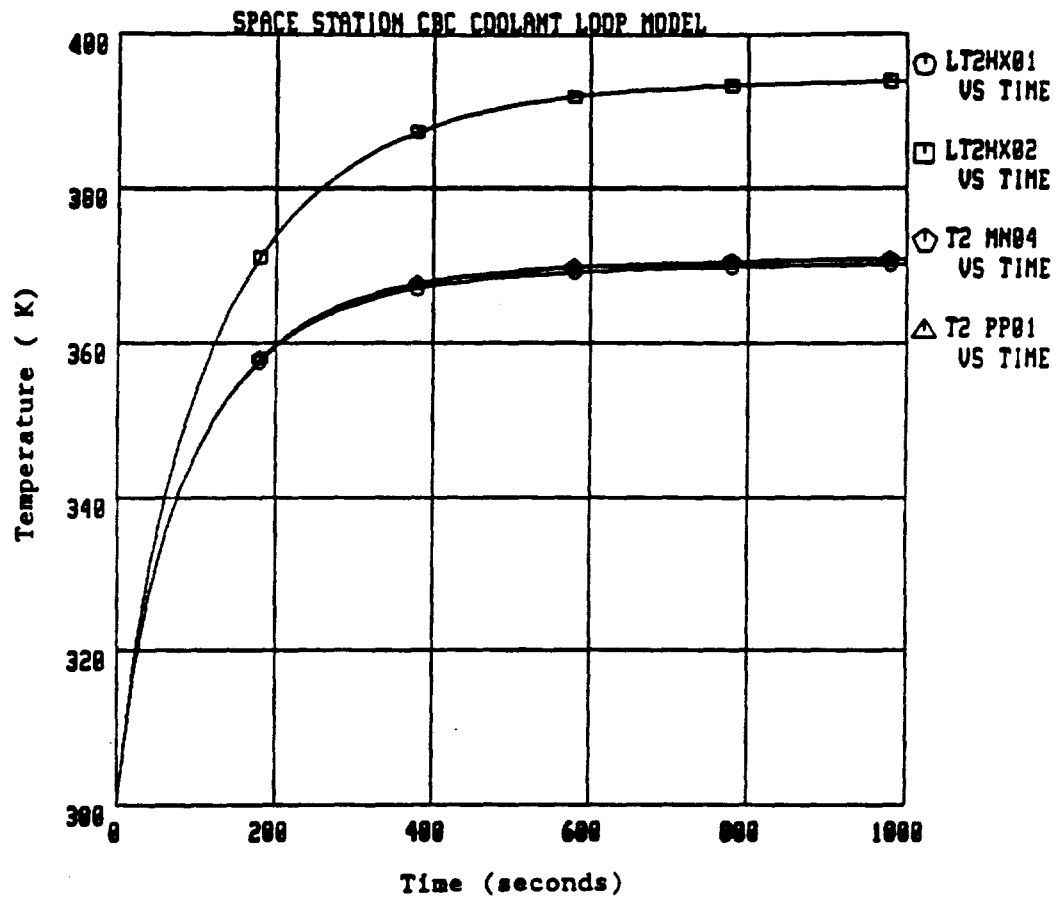
- Odd-numbered variables are inlet variables
- Even-numbered variables are outlet variables
- FOxx denotes FORTRAN component

The gas cooler (HX01) is the primary driver in the Coolant Loop transients, since it carries the majority of the FC-75 massflow, while the bleed cooler carries the remainder of the flow. The manifolds, MN03 and MN04, control the fraction of flow into each heat exchanger and combine those flows at their exit. Manifolds MN01 and MN02 split and combine the flow four ways for the four radiator panels. Each radiator panel (RD--) represents 1/4 of the total radiator area.

The input used to test the coolant loop is the gas cooler gas inlet temperature. This input (S2 TB02) is table driven. Another user-specified variable is the Sink Temperature (S2 TB01), but it is held constant at 200 K for all subsystem tests.

#### 4.1.1 Response to a Step

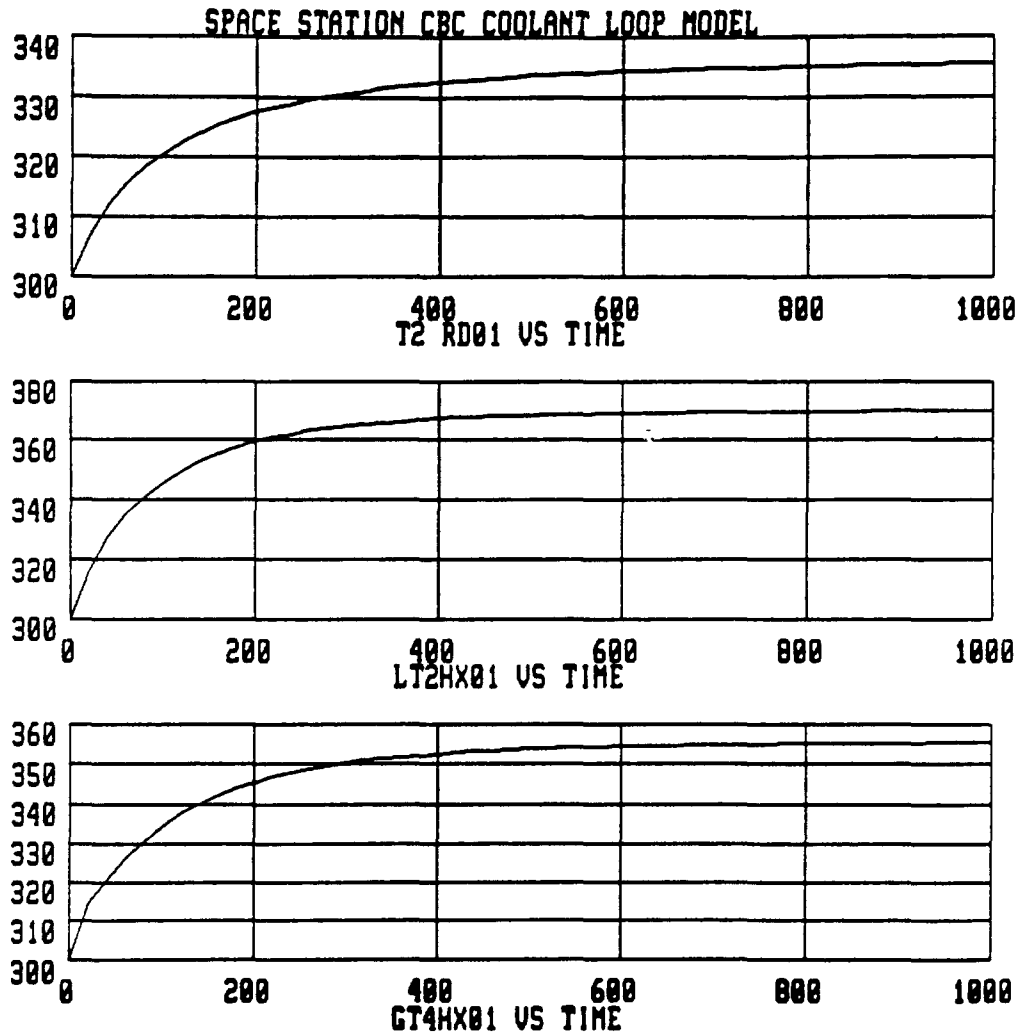
A step of 100 K in the gas inlet temperature of the gas cooler produces the response shown in Figures 29-32. These figures show the temperature in various parts of the coolant loop. Notably, the transient shows a time constant of approximately 200 seconds, which is much greater than the time constants for the individual components, 30 seconds for the Radiator and 70 seconds for the Heat Exchanger. These numbers can be compared to time constants in the compressor and turbine<sup>9</sup>, almost 5 orders of magnitude less, as shown by M.Samad Ali<sup>14</sup>. It can then be concluded that for investigating the thermodynamic transients of the system, an instantaneous-response turbine and compressor model is adequate. On the other hand, development of the control schemes for the Power Conversion Unit requires a transient model



LT2HX01 - COOLANT OUTLET TEMP., GAS COOLER  
LT2HX02 - COOLANT OUTLET TEMP., BLEED COOLER  
T2 MN04 - COOLANT OUTLET TEMP., MANIFOLD 4  
T2 PP01 - COOLANT OUTLET TEMP., PIPE 1

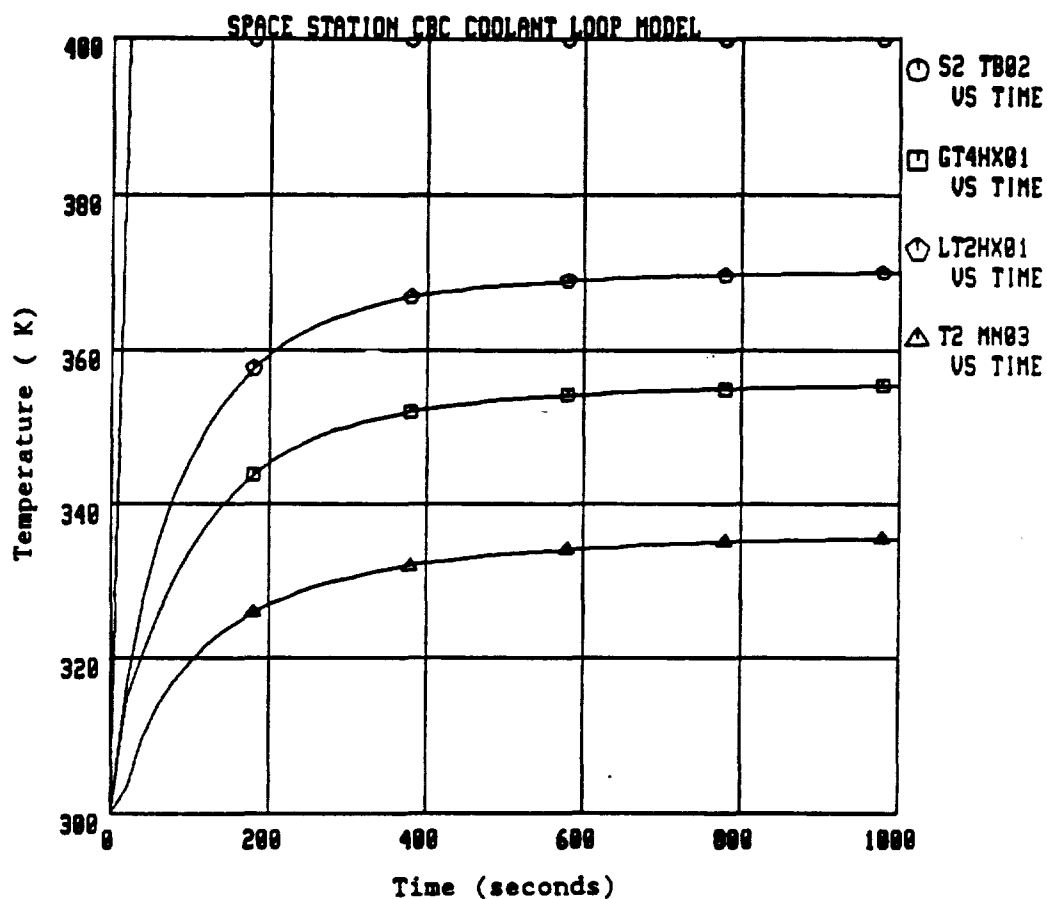
Figure 29. Coolant Loop - Response to a Step.





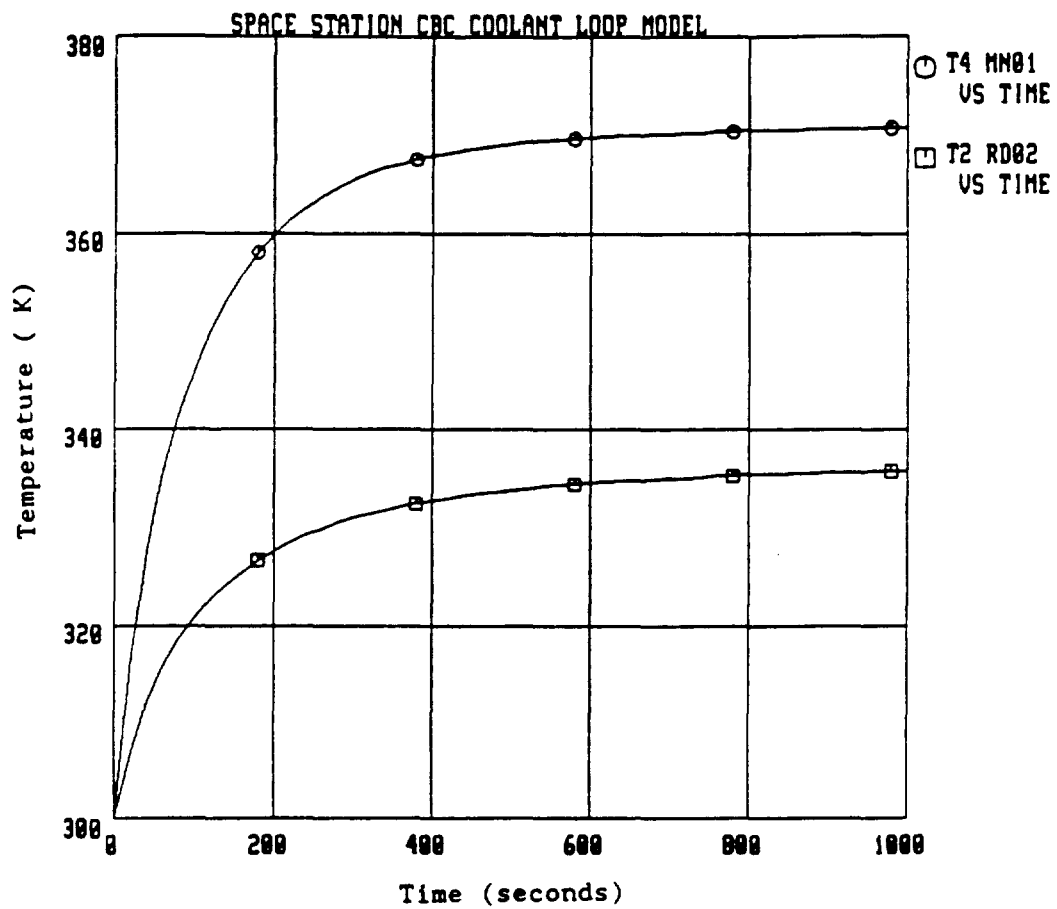
T2 RD01 - COOLANT OUTLET TEMP., RADIATOR 1  
LT2HX01 - COOLANT OUTLET TEMP., GAS COOLER  
GT4HX01 - GAS OUTLET TEMP., GAS COOLER

Figure 30. Coolant Loop - Response to a Step.



S2 TB02 - GAS INLET TEMP., GAS COOLER  
 GT4HX01 - GAS OUTLET TEMP., GAS COOLER  
 LT2HX01 - COOLANT OUTLET TEMP., GAS COOLER  
 T2 MN03 - COOLANT OUTLET TEMP., MANIFOLD 3

Figure 31. Coolant Loop - Response to a Step.



T4 MN01 - COOLANT OUTLET TEMP., MANIFOLD 1  
T2 RD02 - COOLANT OUTLET TEMP., RADIATOR 2

Figure 32. Coolant Loop - Response to a Step.

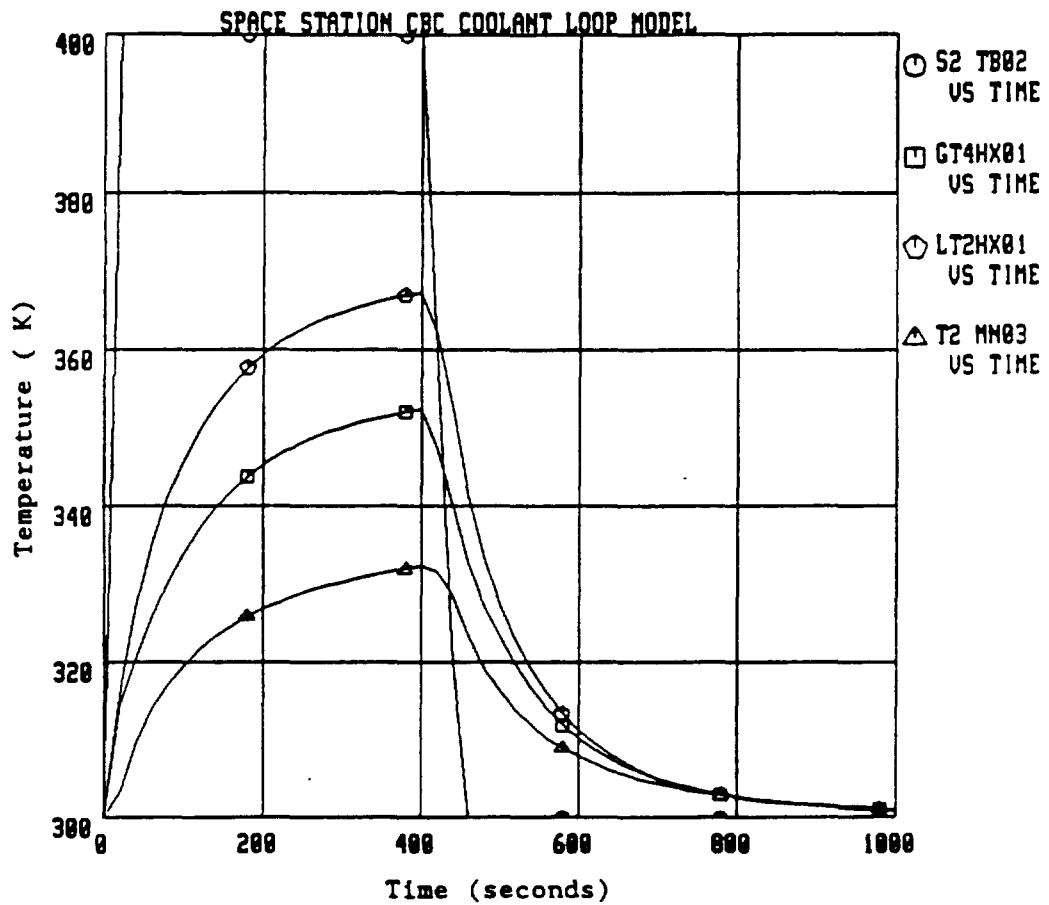
of the turboalternator, since times for the electronics to respond to changes in turbine or compressor operation may become important.

The influence of the larger gas cooler (compared to the bleed cooler) on the FC-75 temperature is shown in Figure 31. The temperature of the fluid after mixing of the gas cooler and bleed cooler streams is slightly higher than that of the gas cooler (LT2HX01). This shows that the influence of hot bleed gas (which cools the alternator bearings) on coolant temperatures is relatively small due to the small mass of gas involved.

#### 4.1.2 Response to a Double Step

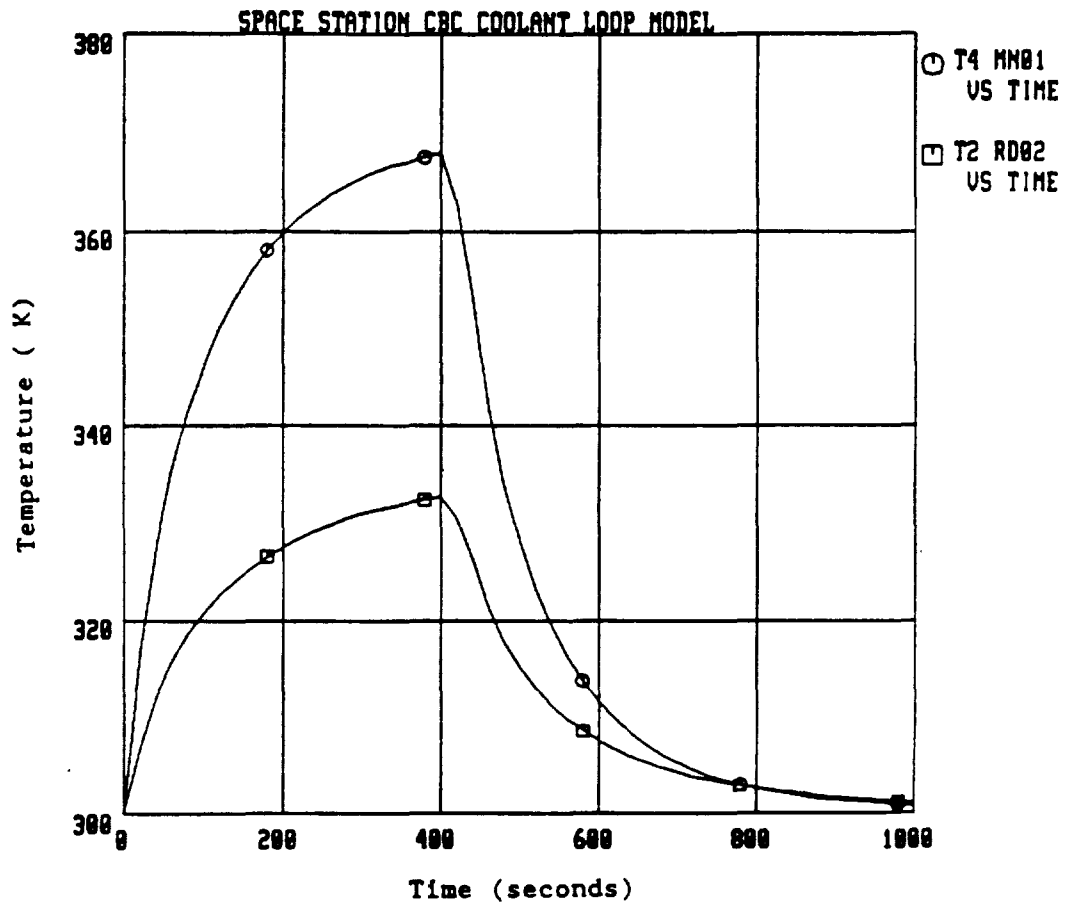
This test resembled the previous one, except that the gas inlet temperature was stepped down to the original 300 K after 400 seconds. The response to this double step is shown in Figures 33-35. All temperatures return to their initial condition as the system approaches steady state. The double step input is plotted in Figure 33, as well as the gas and coolant exit temperatures for the gas cooler.

This test was important in proving the validity of the logic and software used in the model. If the system had not returned to its original state, either a coding error was present or a serious flaw in model formulation would be exposed. Review of the predicted response demonstrates correct functioning of the model.



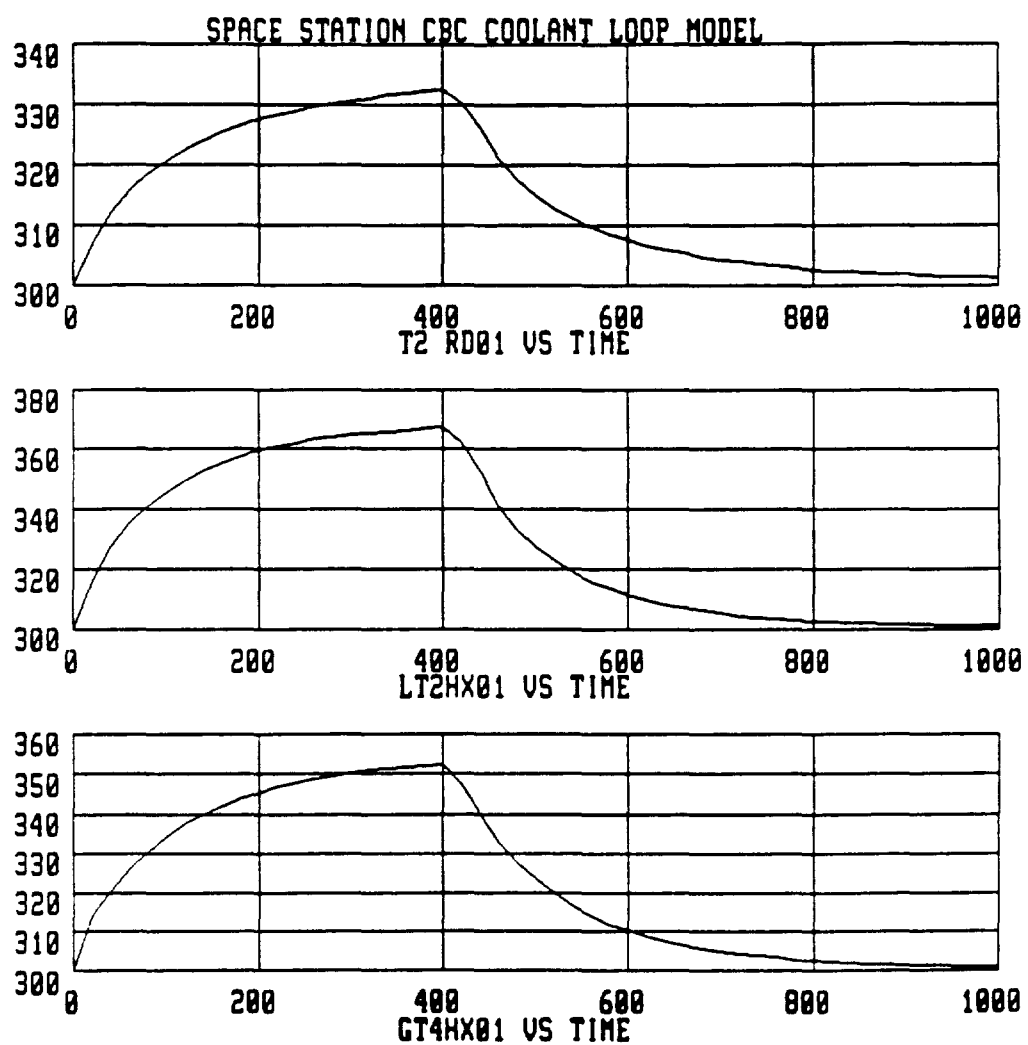
S2 TB02 - GAS INLET TEMP., GAS COOLER  
GT4HX01 - GAS OUTLET TEMP., GAS COOLER  
LT2HX01 - COOLANT OUTLET TEMP., GAS COOLER  
T2 MN03 - COOLANT OUTLET TEMP., MANIFOLD 3

Figure 33. Coolant Loop - Response to a Double Step.



T4 MN01 - COOLANT OUTLET TEMP., MANIFOLD 1  
T2 RD02 - COOLANT OUTLET TEMP., RADIATOR 2

Figure 34. Coolant Loop - Response to a Double Step.



T2 RD01 - COOLANT OUTLET TEMP., RADIATOR 1  
LT2HX01 - COOLANT OUTLET TEMP., GAS COOLER  
GT4HX01 - GAS OUTLET TEMP., GAS COOLER

Figure 35. Coolant Loop - Response to a Double Step.

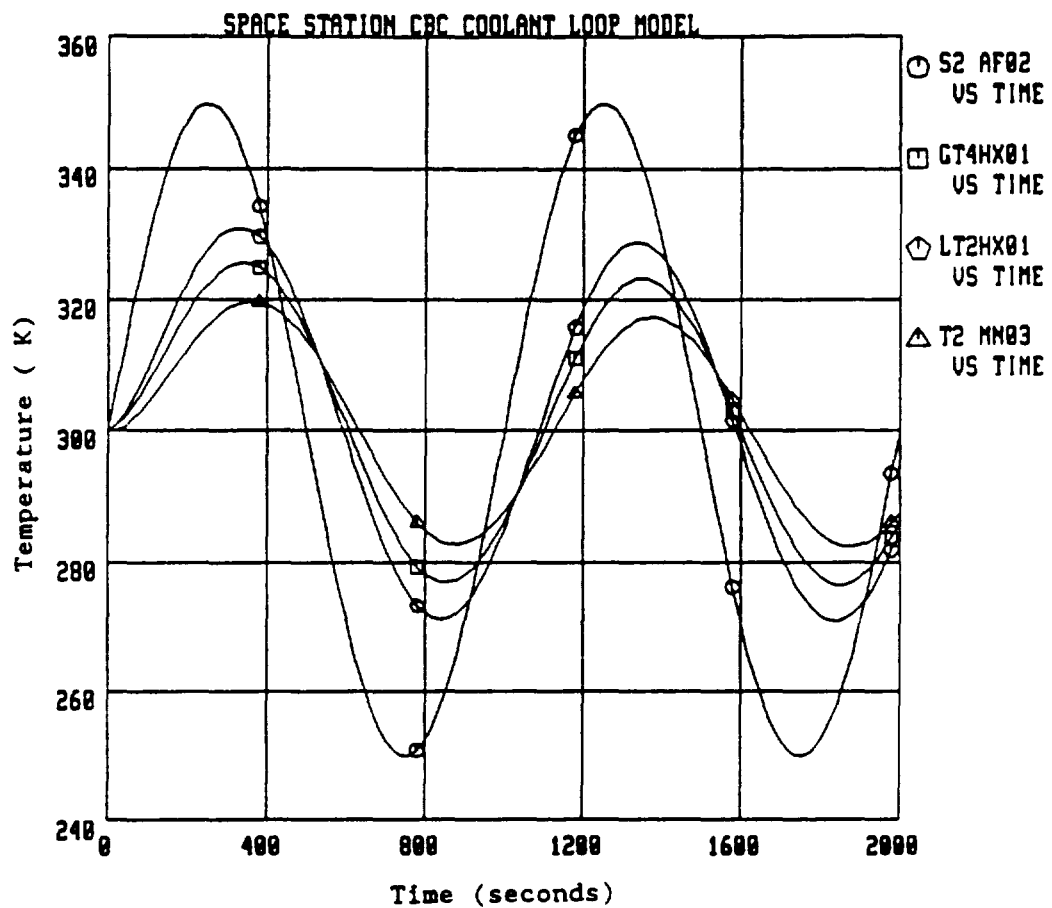
#### 4.1.3 Response to a Sinusoid

A sinusoidal temperature input for the gas inlet temperature (HX01) produced the plots shown in Figure 36-39. The sinusoidal amplitude was 50 K and the period was 1000 seconds. This transient shows response phase lag for the various components. Figure 36 shows the gas cooler gas inlet (S2 AF02), gas outlet (GT4HX01) and coolant outlet (LT2HX01) temperatures as a function of time. All exit temperatures lag the inlet temperatures as expected.

#### 4.2 GAS LOOP

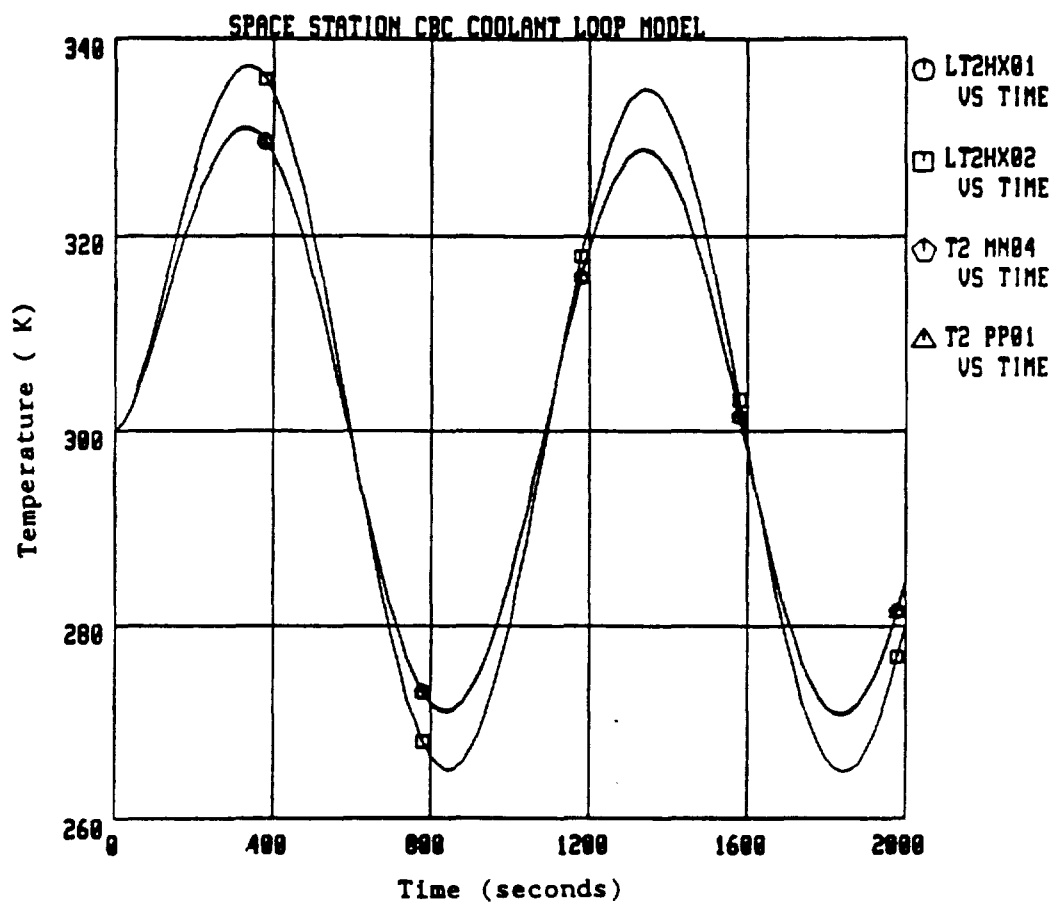
The gas loop subsystem schematic is shown in Figure 40, and the loop naming convention is presented in Table 2. The loop consists of a receiver (RX01), turbine (FOTR), recuperator (HX01), gas cooler (HX02), compressor (FOCR), and an alternator (FOAL). No ducts were included in this model. A constant energy loss model or pressure drop duct model would only shift the transient but not alter its trend. The primary time-dependent inputs to the subsystem are the receiver salt temperature and the coolant inlet temperature for the gas cooler. For these series of transients, the coolant inlet temperature was held constant at 300 K (steady state), while the salt temperature was changed. The turboalternator is assumed to be a constant-speed machine with design-point operation as its initial condition.





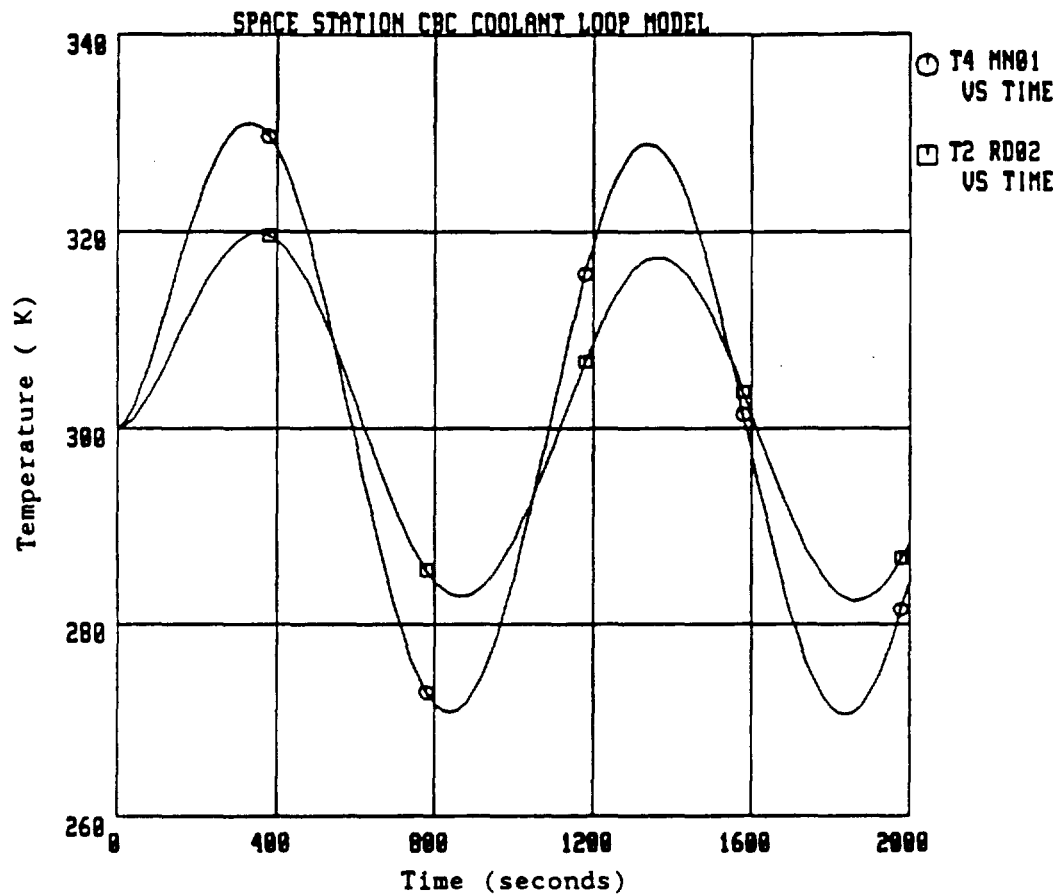
S2 AF02 - GAS INLET TEMP., GAS COOLER  
GT4HX01 - GAS OUTLET TEMP., GAS COOLER  
LT2HX01 - COOLANT OUTLET TEMP., GAS COOLER  
T2 MN03 - COOLANT OUTLET TEMP., MANIFOLD 3

Figure 36. Coolant Loop - Response to a Sinusoid.



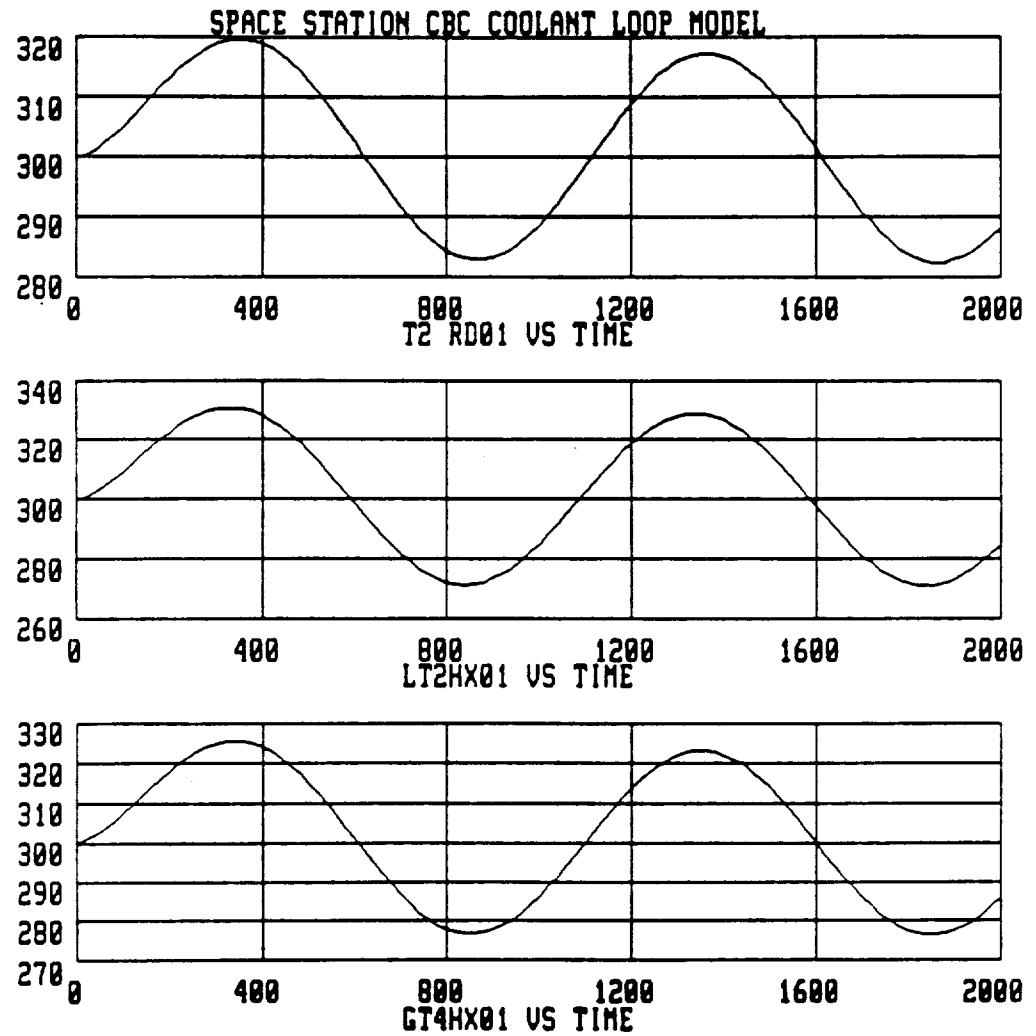
LT2HX01 - COOLANT OUTLET TEMP., GAS COOLER  
 LT2HX02 - COOLANT OUTLET TEMP., BLEED COOLER  
 T2 MN04 - COOLANT OUTLET TEMP., MANIFOLD 4  
 T2 PP01 - COOLANT OUTLET TEMP., PIPE 1

Figure 37. Coolant Loop - Response to a Sinusoid.



T4 MN01 - COOLANT OUTLET TEMP., MANIFOLD 1  
T2 RD02 - COOLANT OUTLET TEMP., RADIATOR 2

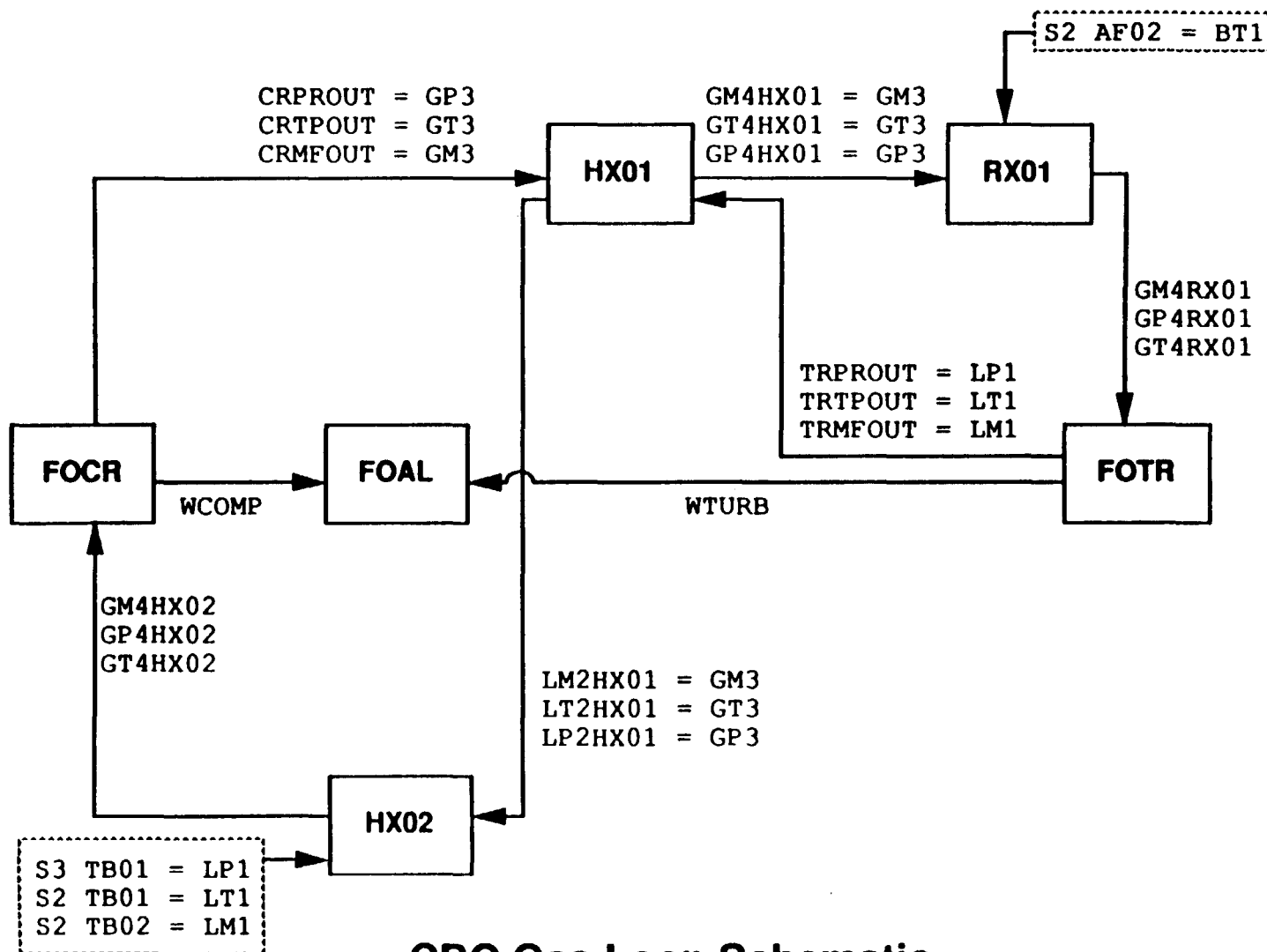
Figure 38. Coolant Loop - Response to a Sinusoid.



T2 RD01 - COOLANT OUTLET TEMP., RADIATOR 1  
LT2HX01 - COOLANT OUTLET TEMP., GAS COOLER  
GT4HX01 - GAS OUTLET TEMP., GAS COOLER

Figure 39. Coolant Loop - Response to a Sinusoid.

Figure 40. Gas Loop Schematic.



**CBC Gas Loop Schematic**

Table 2. Gas Loop Convention

Variable Name (Example) - GT4HX01  
                                     Variable ID      Component ID

<u>IDENTIFICATION</u>	<u>COMPONENT</u>
FOCR	Compressor
FOTR	Turbine
FOAL	Alternator
RXnn	Receiver
TBnn	Look-up Table
AFnn	Analytical Function
HX01	Heat Exchanger (Recuperator)
HX02	Heat Exchanger (Gas Cooler)

<u>IDENTIFICATION</u>	<u>VARIABLE</u>
S3 TB01	Inlet Coolant Pressure
S2 TB02	Inlet Coolant Temperature
S2 TB02	Inlet Coolant Mass Flow Rate
P1, M1, T1	Inlet Pressure, Mass Flow and Temp.
LP1, LM1, LT1	Inlet Liquid Pressure, Mass Flow, Temp.
GP1, GM1, GT1	Inlet Gas Pressure, Mass Flow, Temp.
TRPROUT	Turbine Outlet Pressure
TRTPOUT	Turbine Outlet Temperature
TRMFOUT	Turbine Outlet Mass Flow
CRPROUT	Compressor Outlet Pressure
CRTPOUT	Compressor Outlet Temperature
CRMFOUT	Compressor Outlet Mass Flow
WCOMP	Compressor Work
WTURB	Turbine Work

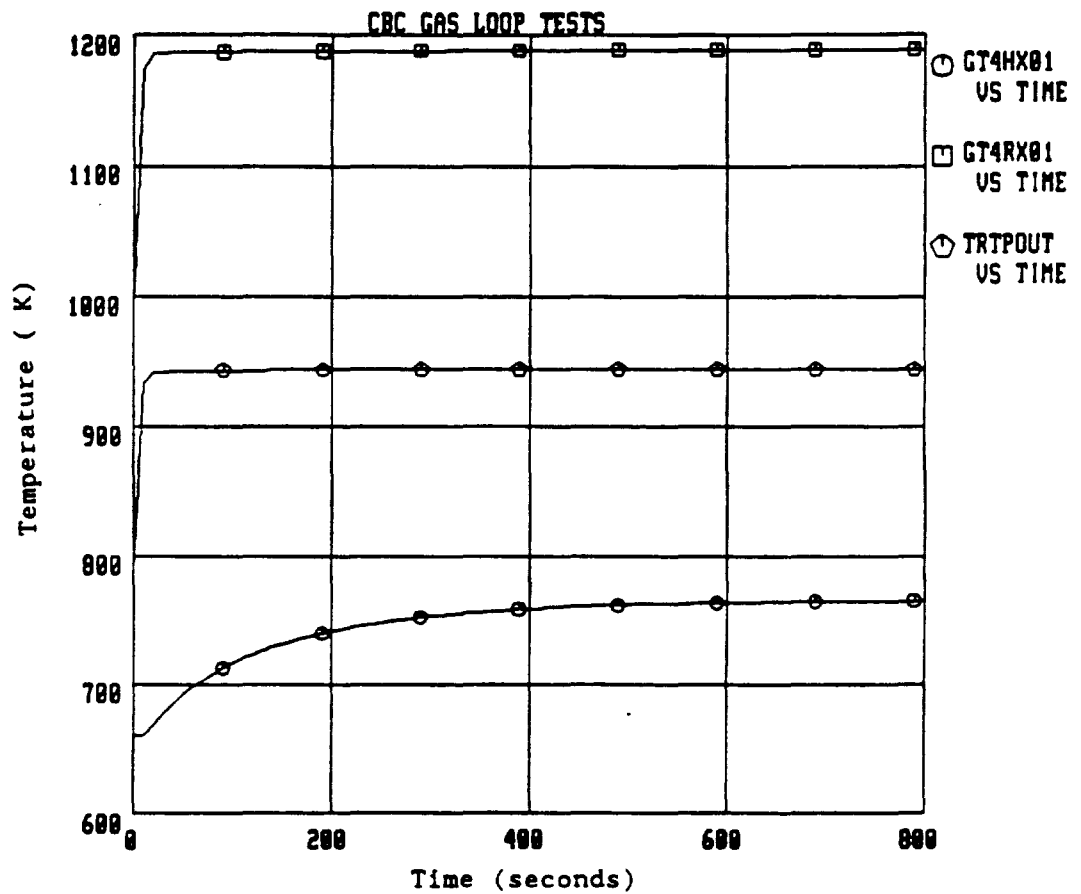
- Odd-numbered variables are inlet variables
- Even-numbered variables are outlet variables
- FOxx denotes FORTRAN component

#### 4.2.1 Response to a Step

When receiver salt temperature was stepped from 1000 K to 1200 K, the gas loop subsystem responded as shown in Figures 41-43. The turbine outlet temperature (TRTPOUT - Figure 41) responds almost instantly to the step (GT4RX01 - Figure 41). Since the recuperator and the gas cooler separate the flow from the turbine to the compressor, the compressor outlet temperature transient (CRTPOUT - Figure 42) does not reach steady state until 500 seconds, since that is the time it takes the heat exchanger transients to reach steady state. The power output from the alternator (Figure 43) shows an initial overshoot. This is due to the Turbine response being much faster to a change in Receiver temperature than the Compressor.

#### 4.2.2 Response to a Double Step

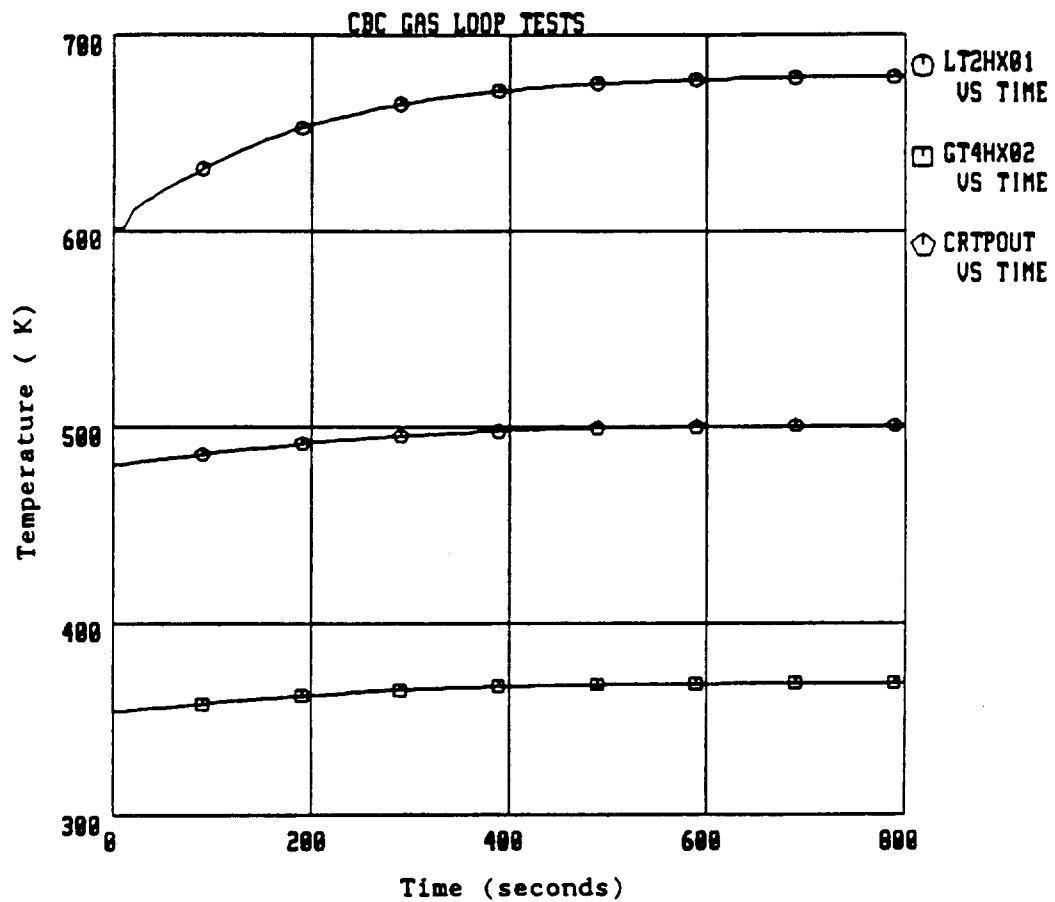
The double step in salt temperature consists of an initial step of 200 K from 1000 K to 1200 K, and a second step back to the initial condition of 1000 K. The response to this input is shown in Figures 44-46. All component variables return to the initial condition after 800 seconds.



GT4HX01 - GAS OUTLET TEMP., RECUPERATOR  
GT4RX01 - GAS OUTLET TEMP., RECEIVER  
TRTPOUT - GAS OUTLET TEMP., TURBINE

Figure 41. Gas Loop - Response to a Step in Salt Temperature.





LT2HX01 - GAS OUTLET TEMP., RECUPERATOR  
GT4HX02 - GAS OUTLET TEMP., GAS COOLER  
CRTPOUT - GAS OUTLET TEMP., COMPRESSOR

Figure 42. Gas Loop - Response to a Step in Salt Temperature.

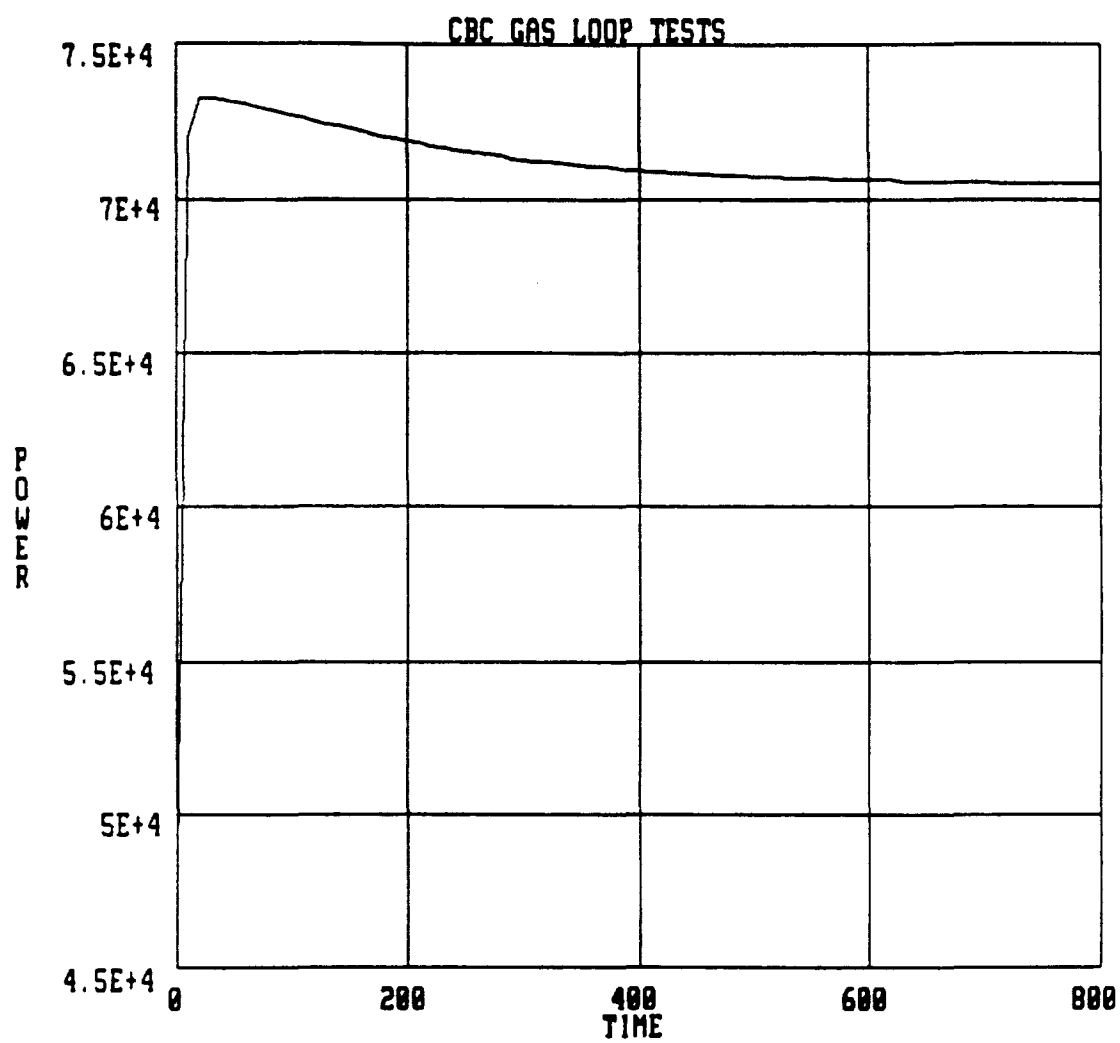
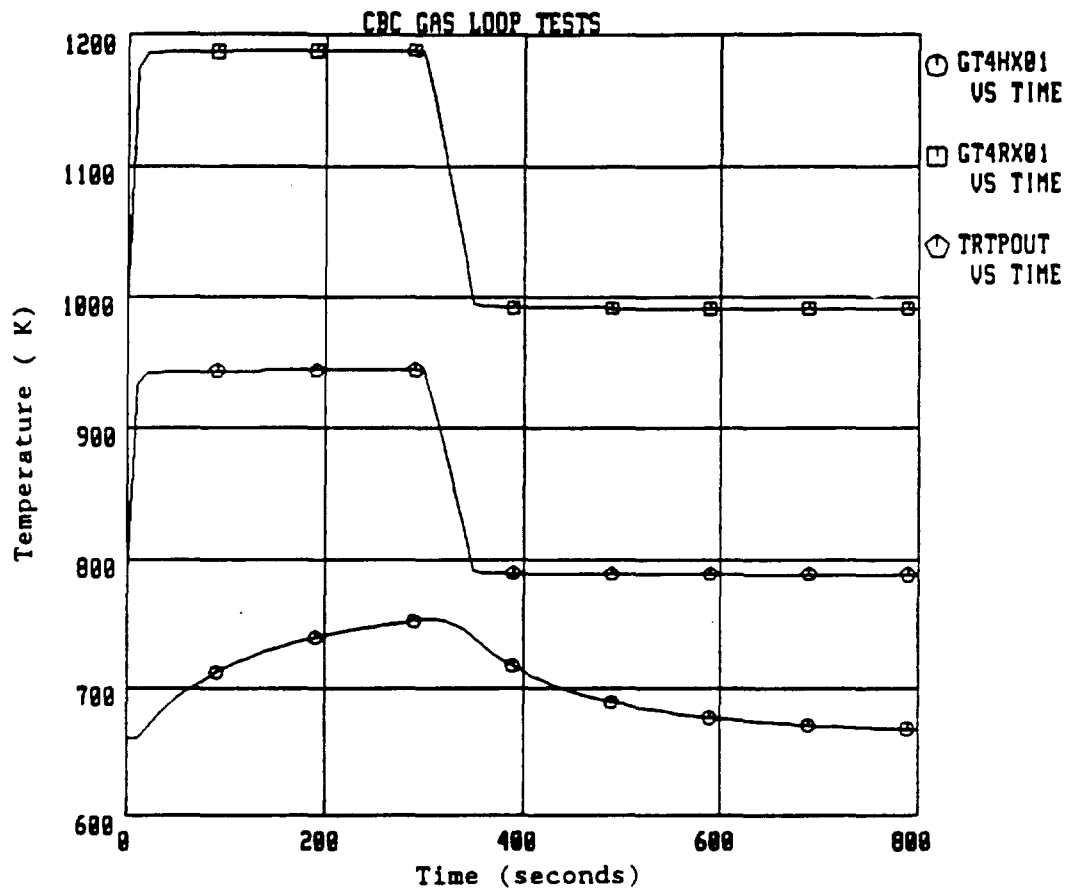
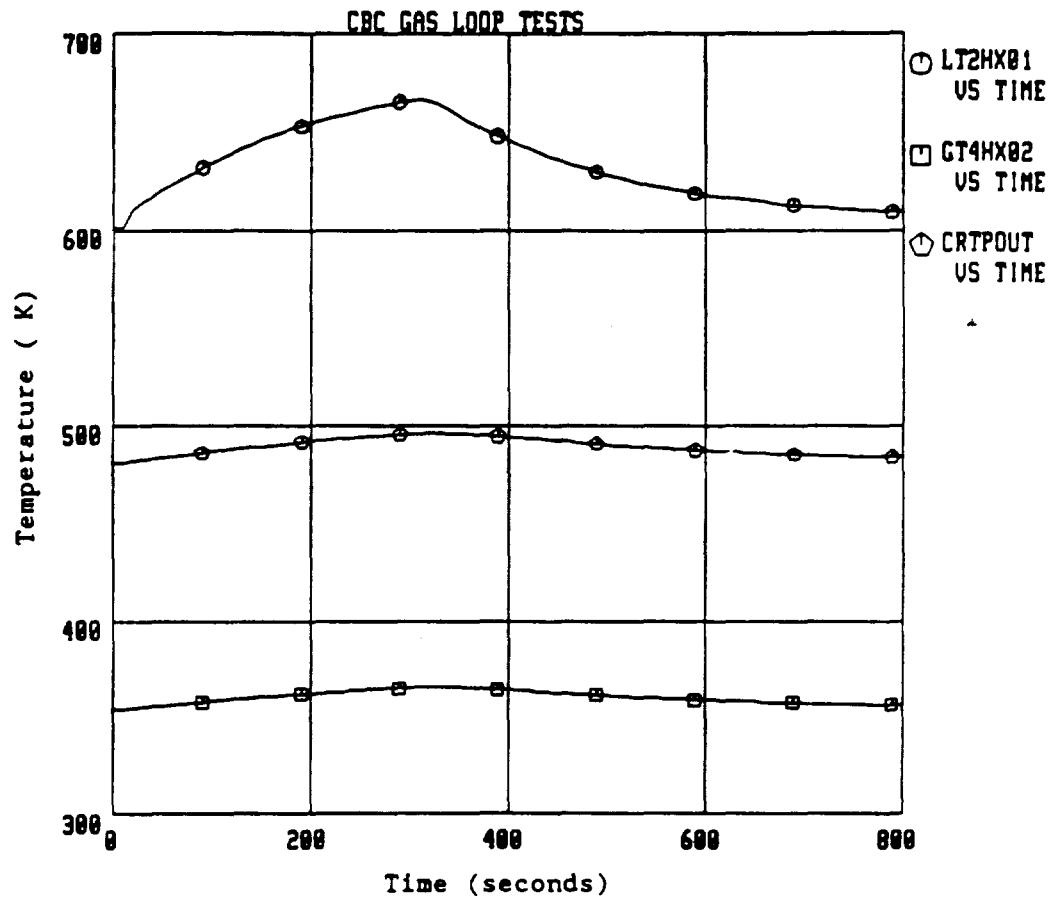


Figure 43. Gas Loop - Response to a Step in Salt Temperature.



GT4HX01 - GAS OUTLET TEMP., RECUPERATOR  
GT4RX01 - GAS OUTLET TEMP., RECEIVER  
TRTPOUT - GAS OUTLET TEMP., TURBINE

Figure 44. Gas Loop - Response to a Double Step in Salt Temperature



LT2HX01 - GAS OUTLET TEMP., RECUPERATOR  
GT4HX02 - GAS OUTLET TEMP., GAS COOLER  
CRTPOUT - GAS OUTLET TEMP., COMPRESSOR

Figure 45. Gas Loop - Response to a Double Step in Salt Temperature

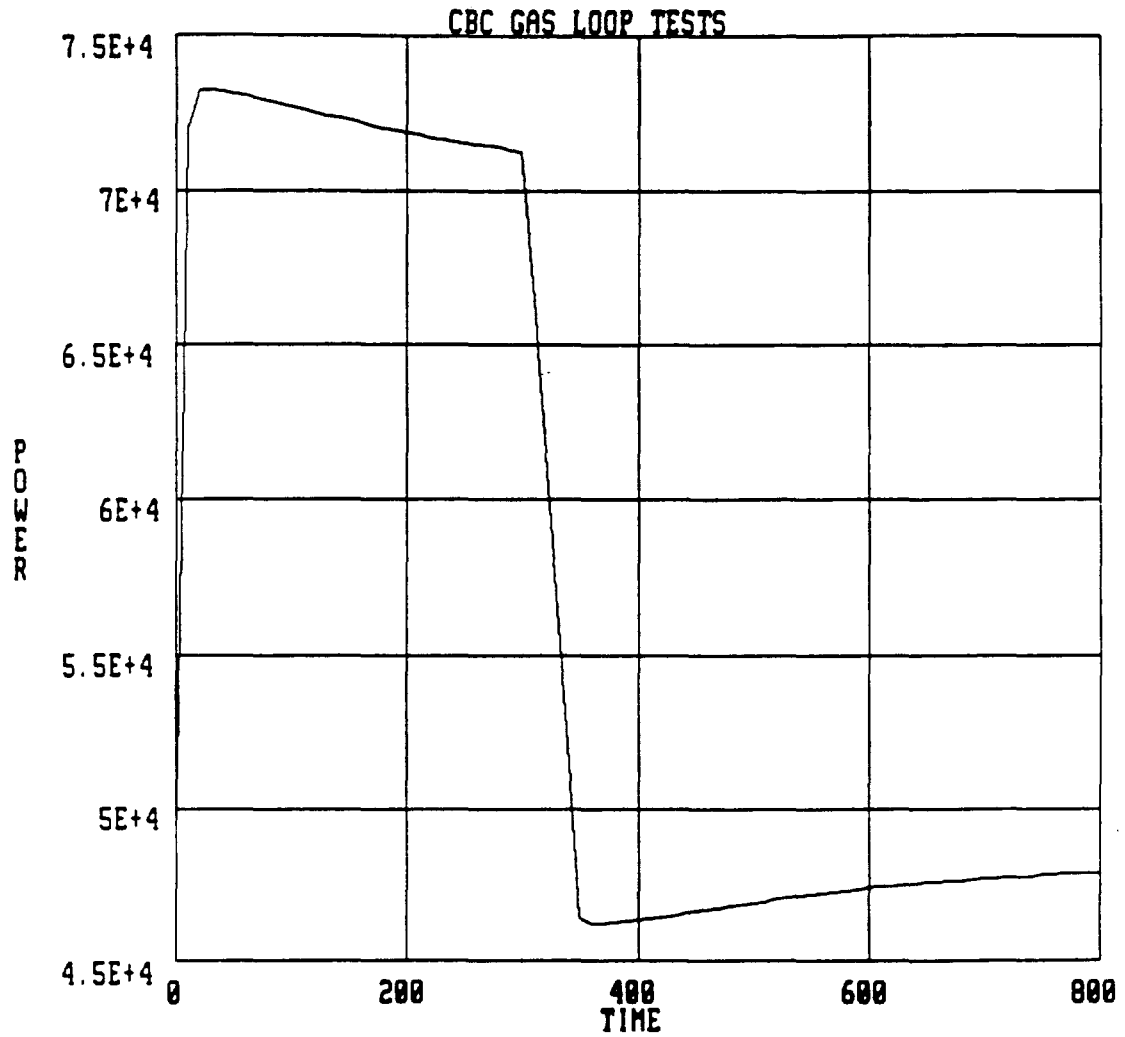


Figure 46. Gas Loop - Response to a Double Step in Salt Temperature

#### 4.2.3 Response to a Sinusoid

A sinusoidal variation of receiver salt temperature produces the transients shown in Figures 47-49. The amplitude of the variation is 1000 K and the period is 400 seconds. Recuperator exit temperature (GT4HX01 - Figure 47) lags the Receiver exit temperature (GT4RX01 - Figure 47) which in turn lags the salt temperature (S2 AF02 - Figure 47). This result gives added confidence in the validity of the model.

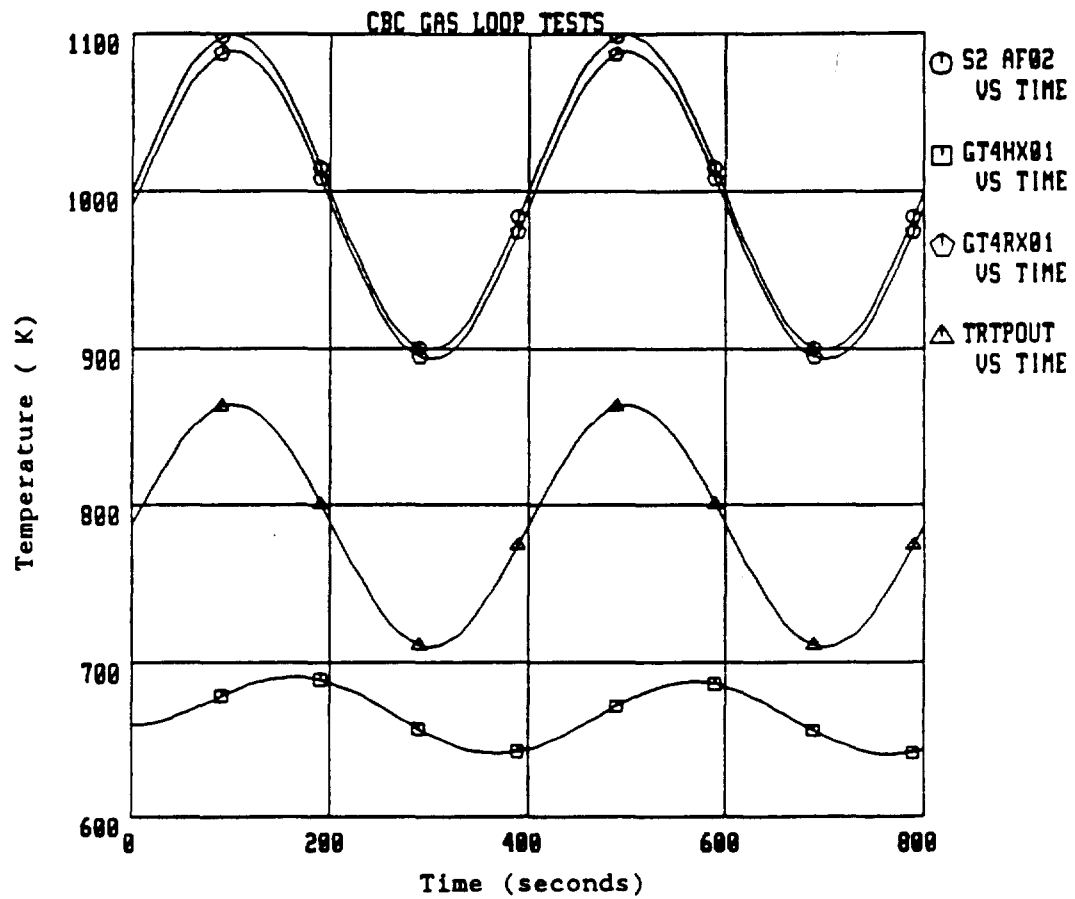
#### 4.3 SYSTEM TRANSIENTS

The gas loop and the coolant loop subsystems were integrated into a full system model by connecting them at the gas cooler. The integrated system is capable of modelling a number of the transients of interest to NASA. These include orbital transients and component-loss scenarios for the coolant pump and a radiator panel.

The schematic for the integrated system is shown in Figures 50-51, where Figure 50 shows the coolant loop while Figure 51 shows the gas loop with the interfaces indicated.

##### 4.3.1 Maximum Insolation Orbit

The 250 nautical mile orbit or the maximum insolation orbit defines one end of the operating envelope of the Space Station. Using data published in DR02 for receiver outlet temperature and the sink temperature (which varies due to the affect of the Earth on the view factor), an analysis file was constructed. The transient for a complete orbit with fixed gas inventory is plotted in Figures 52-53.



S2 AF02 - SALT TEMP., RECEIVER  
 GT4HX01 - GAS OUTLET TEMP., RECUPERATOR  
 GT4RX01 - GAS OUTLET TEMP., RECEIVER  
 TRTPOUT - GAS OUTLET TEMP., TURBINE

Figure 47. Gas Loop - Response to Sinusoidal Salt Temperature

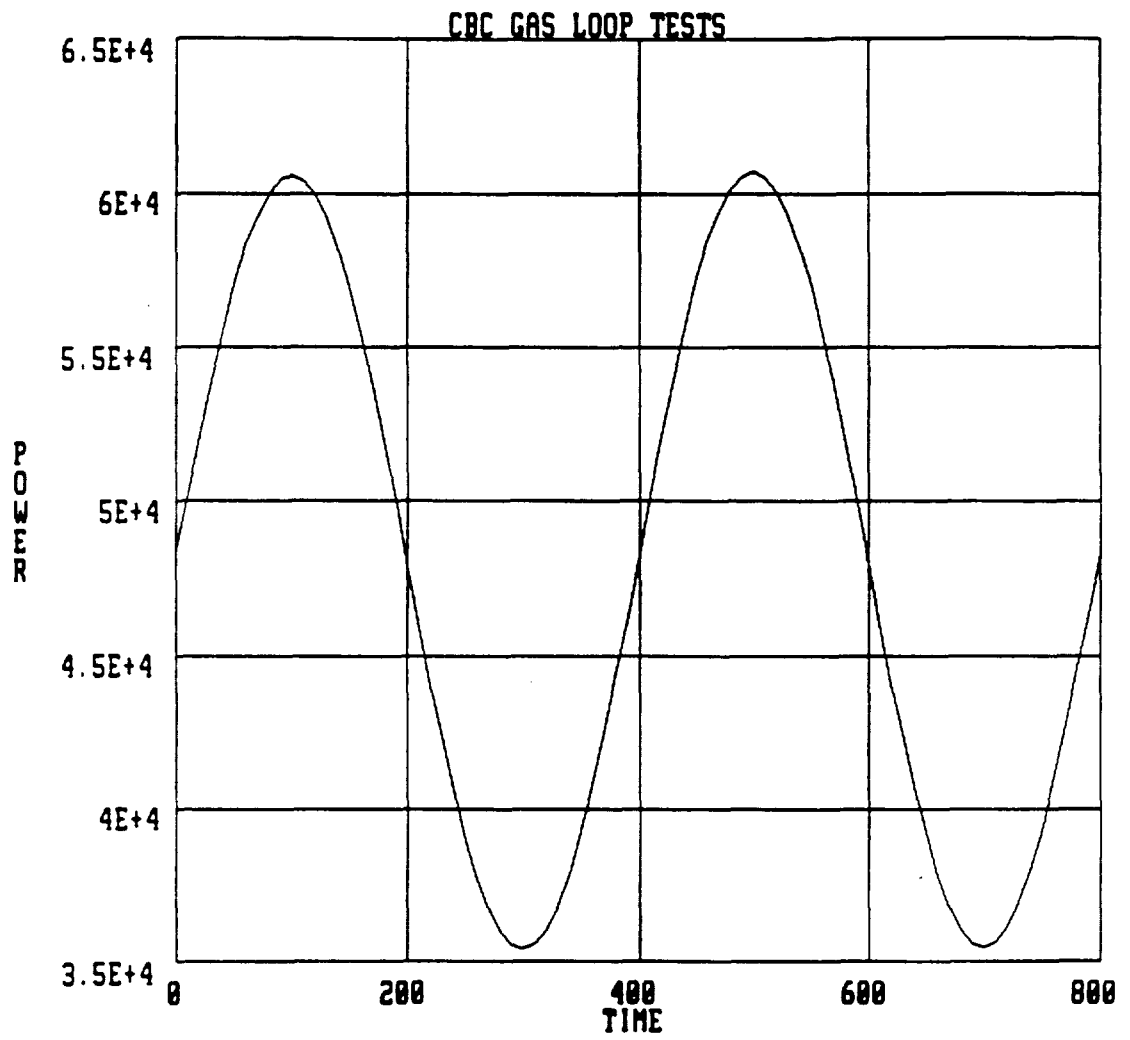
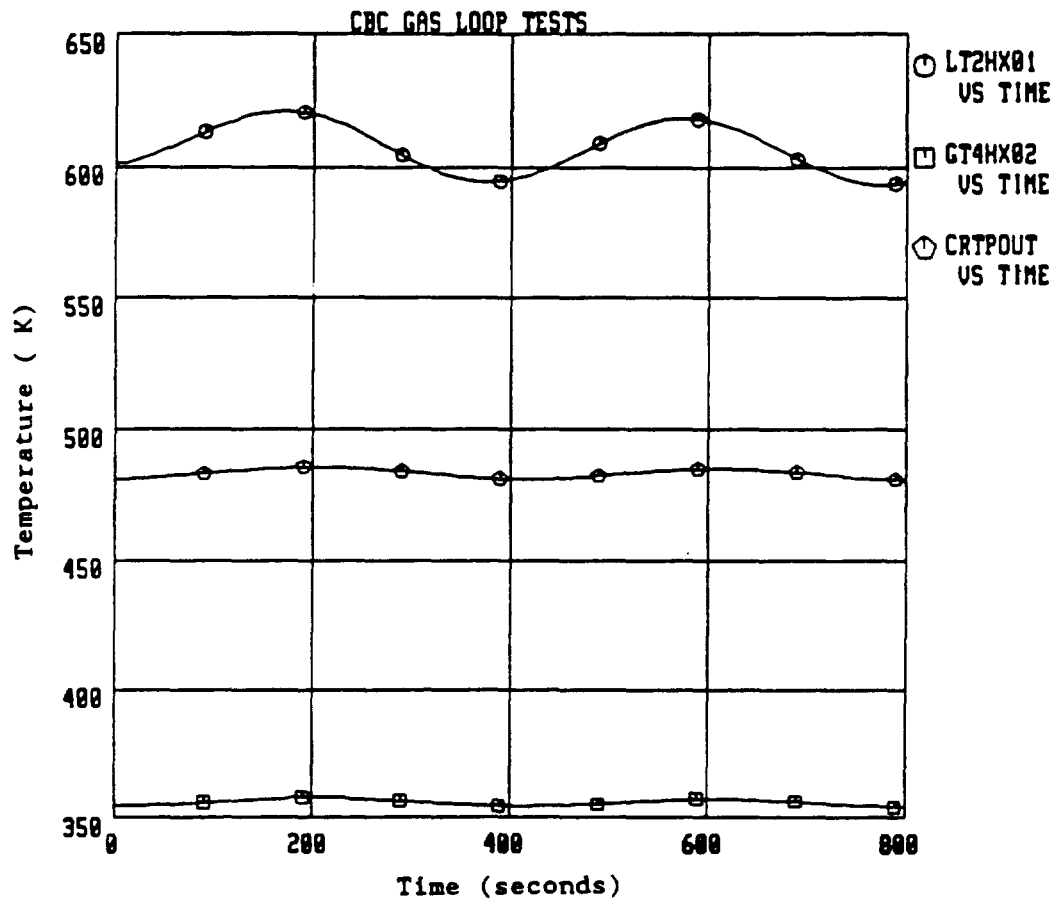


Figure 48. Gas Loop - Response to Sinusoidal Salt Temperature

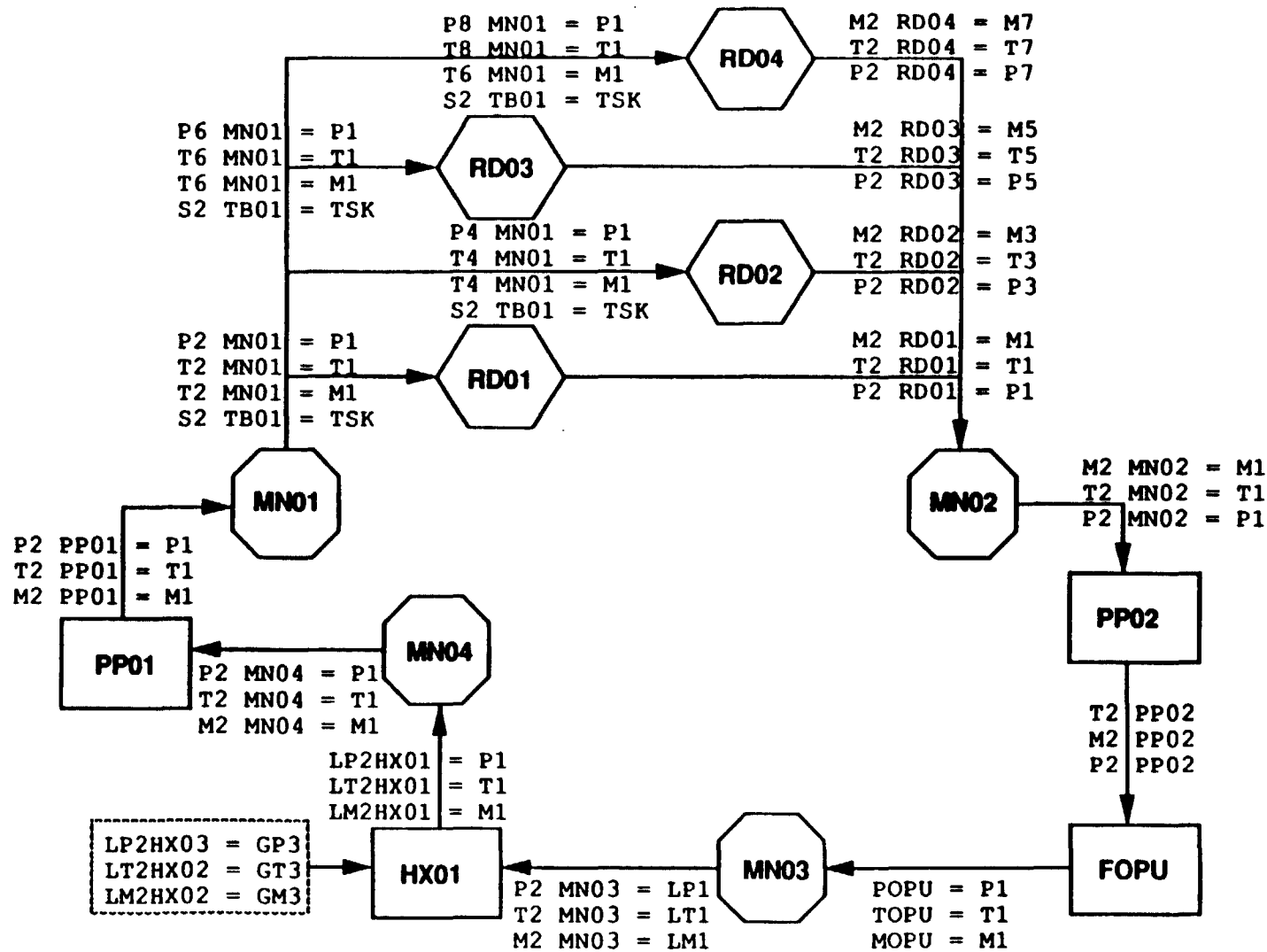




LT2HX01 - GAS OUTLET TEMP., RECUPERATOR  
GT4HX02 - GAS OUTLET TEMP., GAS COOLER  
CRTPOUT - GAS OUTLET TEMP., COMPRESSOR

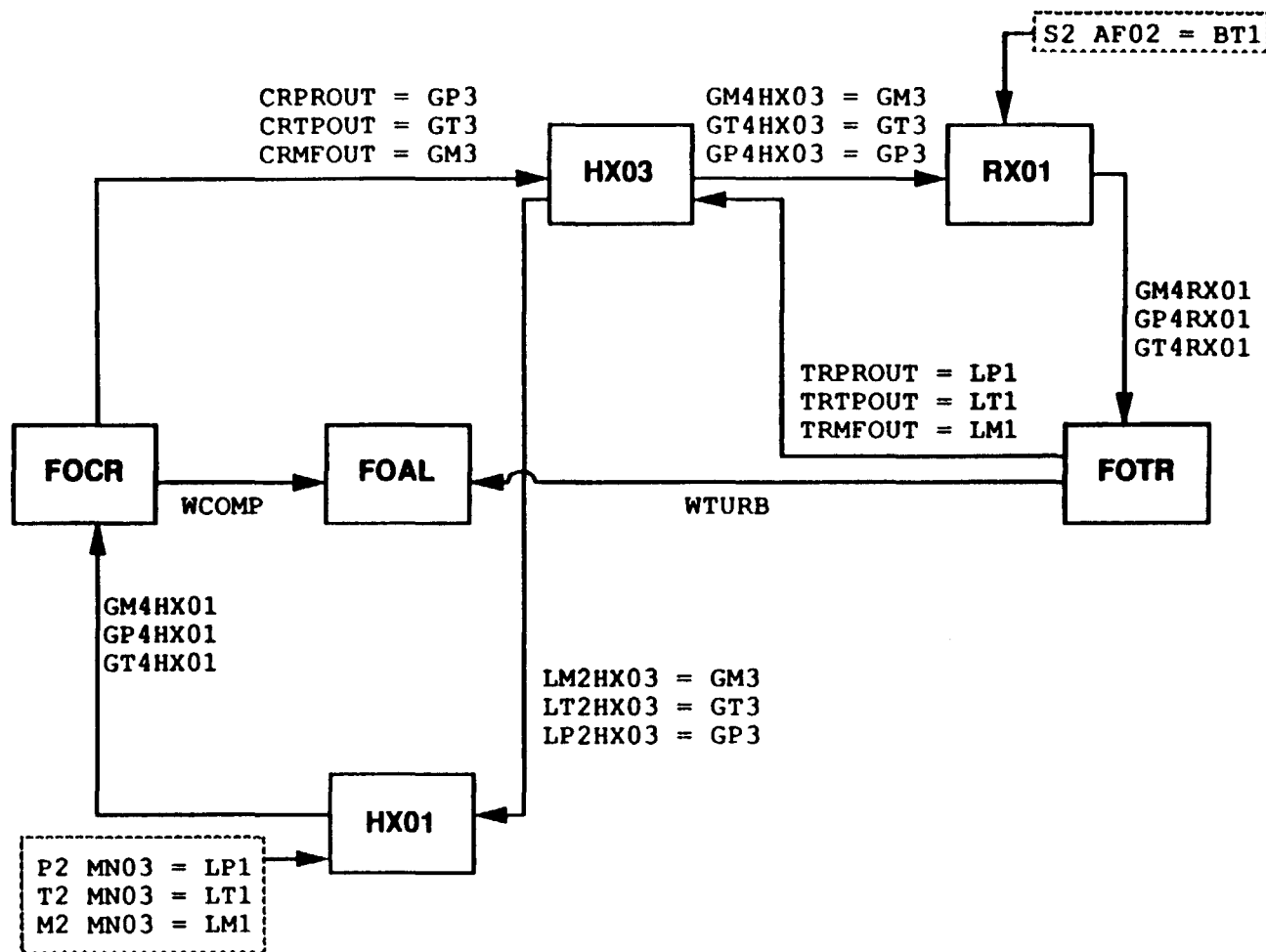
Figure 49. Gas Loop - Response to Sinusoidal Salt Temperature

Figure 50. Full System Schematic (Coolant Loop)



CBC Full System Schematic (Coolant Loop)

Figure 51. Full System Schematic (Gas Loop)



CBC Full System Schematic (Gas Loop)

Table 3. System Convention

Variable Name (Example) - GT4HX01  
                                     Variable ID      Component ID

<u>IDENTIFICATION</u>	<u>COMPONENT</u>
FOCR	Compressor
FOTR	Turbine
FOAL	Alternator
RXnn	Receiver
TBnn	Look-up Table
AFnn	Analytical Function
HX01	Heat Exchanger (Gas Cooler)
HX02	Heat Exchanger (Recuperator)
MNnn	Manifold
RDnn	Radiator
PPnn	Pipe
FOPU	Pump

<u>IDENTIFICATION</u>	<u>VARIABLE</u>
S2 TB01	Sink Temperature Variation
S2 AF02	Receiver Salt Temp. Variation
P1, M1, T1	Inlet Pressure, Mass Flow and Temp.
LP1, LM1, LT1	Inlet Liquid Pressure, Mass Flow, Temp.
GP1, GM1, GT1	Inlet Gas Pressure, Mass Flow, Temp.
TRPROUT	Turbine Outlet Pressure
TRTPOUT	Turbine Outlet Temperature
TRMFOUT	Turbine Outlet Mass Flow
CRPROUT	Compressor Outlet Pressure
CRTPOUT	Compressor Outlet Temperature
CRMFOUT	Compressor Outlet Mass Flow
WCOMP	Compressor Work
WTURB	Turbine Work
TSK	Sink Temperature
BT1	Receiver Salt Temperature

- Odd-numbered variables are inlet variables
- Even-numbered variables are outlet variables
- FOxx denotes FORTRAN component

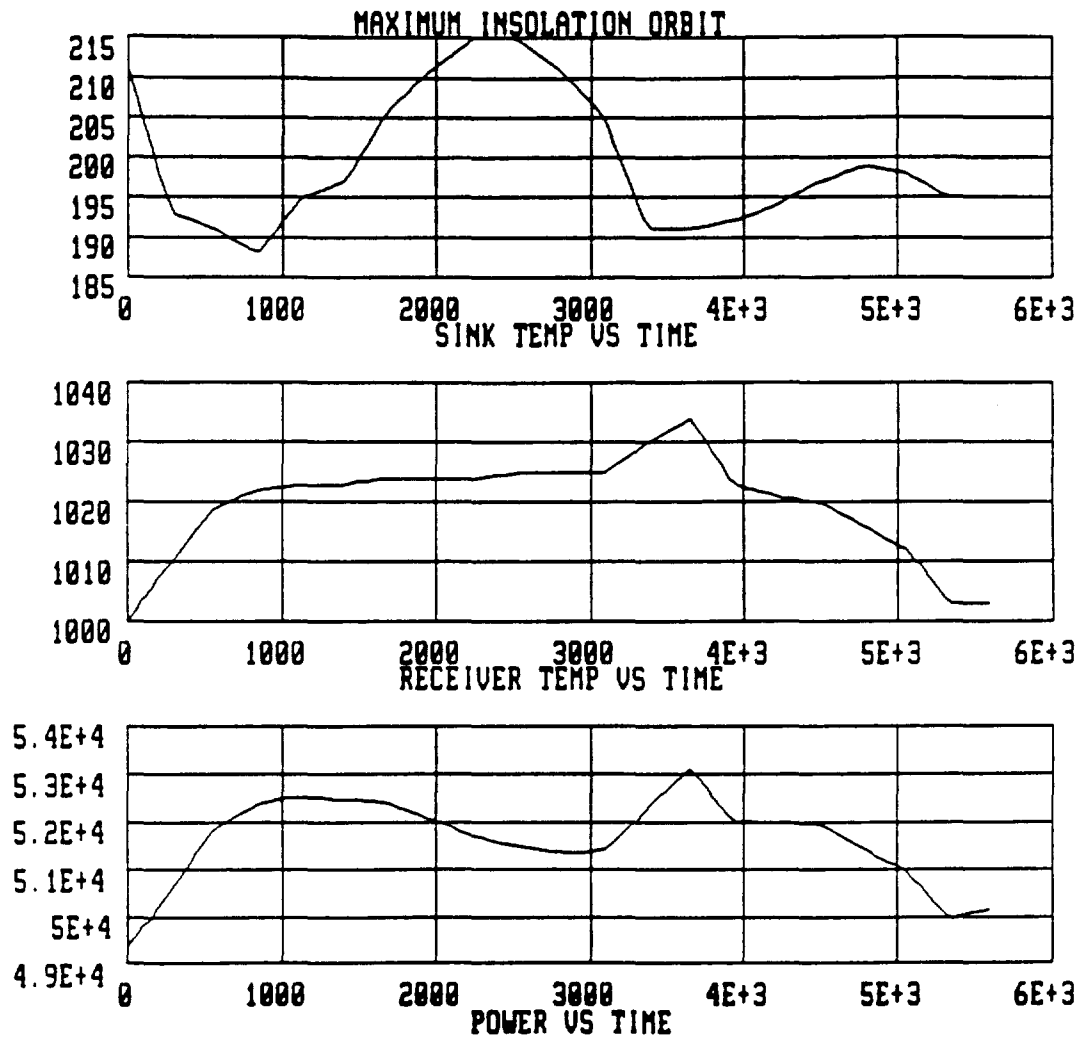
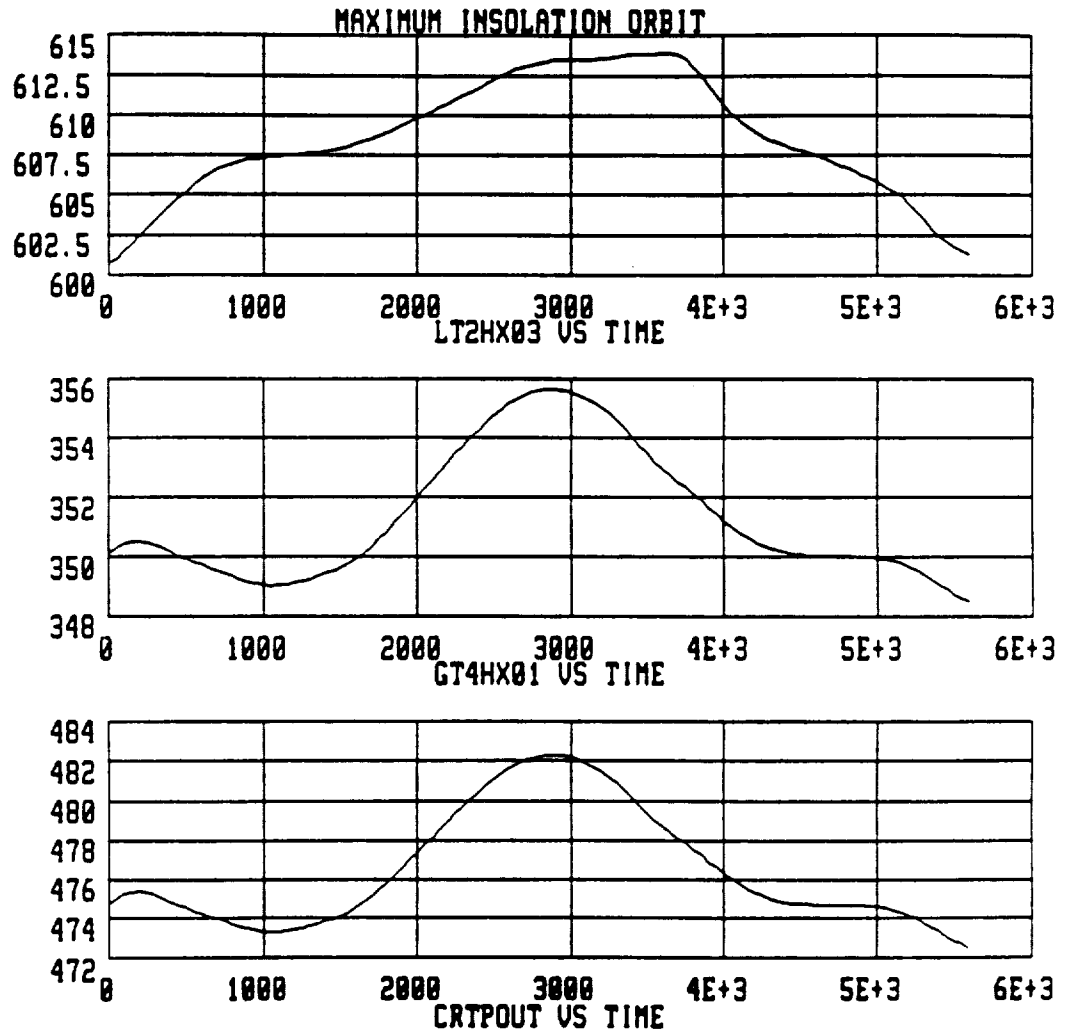


Figure 52. Maximum Insolation Orbit Transient



LT2HX03 - GAS OUTLET TEMP., RECUPERATOR  
GT4HX01 - GAS OUTLET TEMP., GAS COOLER  
CRTPOUT - GAS OUTLET TEMP., COMPRESSOR

Figure 53. Maximum Insolation Orbit Transient

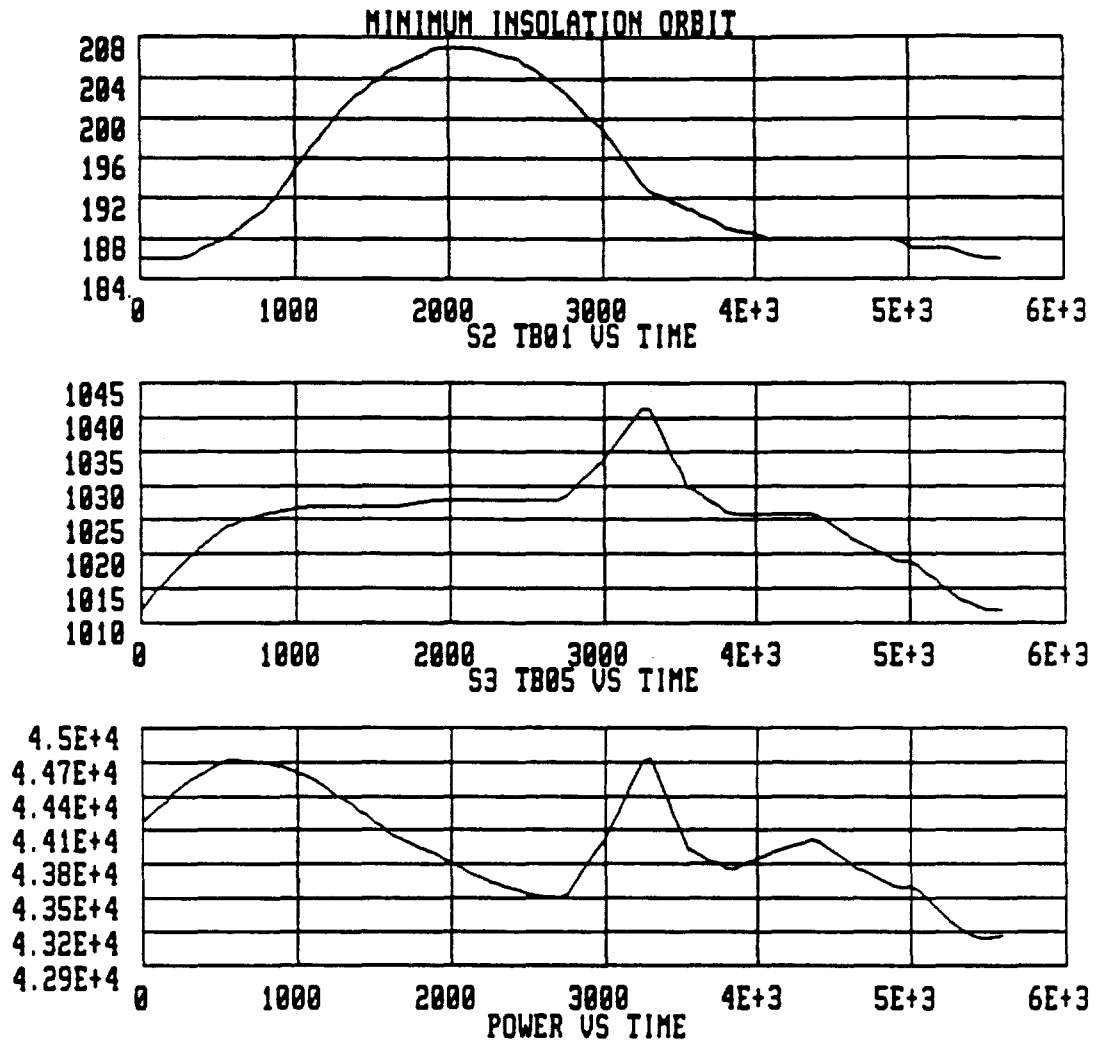
The results show a qualitative similarity of power (Figure 52) with alternator power computed by NASA for a maximum insolation orbit shown in Appendix 8.3. This increases confidence in using this model to predict system dynamic performance.

#### 4.3.2 Minimum Insolation Orbit

The minimum insolation or 180 nautical mile orbit system transient is shown in Figure 54. NASA supplied data was used to vary the sink and receiver temperature during the orbit. This and other orbital data might have been abridged in the DR02, since the sink temperature does not return to original value at the start of the orbit. Consequently all system variables do not return to their initial value. A fixed gas inventory was assumed with the mass flow rate at 0.8528 Kg/s. The power fluctuations are similar to the maximum insolation orbit and can easily be compensated for by using the parasitic load resistor.

#### 4.3.3 Minimum Insolation Peaking Orbit

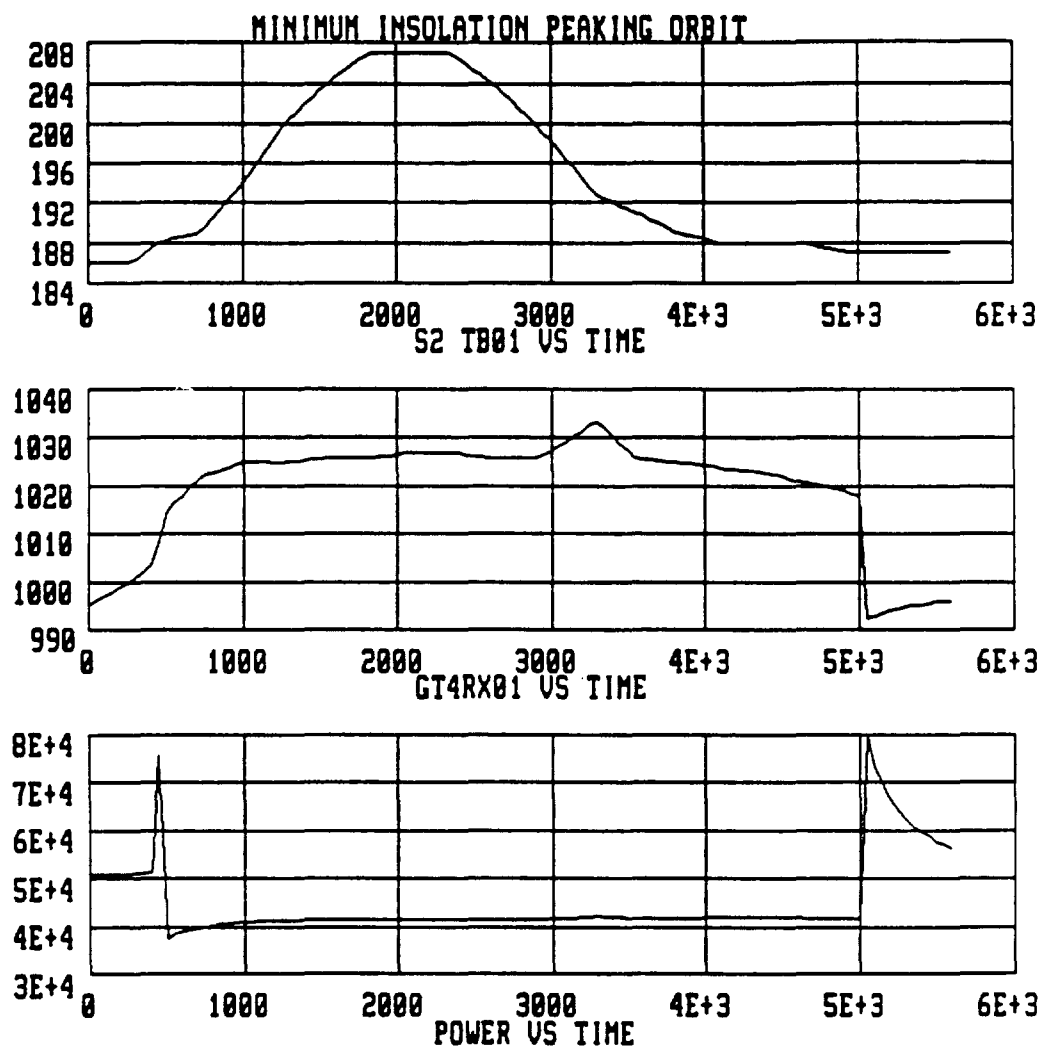
This system transient models a situation of maximum power demand during a minimum insolation (180 nmi) orbit. The system inputs, the sink temperature, the receiver temperature and the power output are shown in Figure 55. A peaking orbit is one in which the electrical power system is called upon to provide 15% more power than the nominal for a continuous period of 7 and a half minutes. By decreasing the gas inventory from 1.19 Kg/s to 0.79 Kg/s after 7.5 minutes into the orbit, the alternator power is decreased to adjust to normal power



S2 TB01 - SINK TEMPERATURE  
S3 TB05 - SALT TEMP., RECEIVER  
POWER - ALTERNATOR POWER

Figure 54. Minimum Insolation Orbit Transient





S2 TB01 - SINK TEMPERATURE  
 GT4RX01 - SALT TEMP., RECEIVER  
 POWER - ALTERNATOR POWER

Figure 55. Minimum Insolation Peaking Orbit Transient

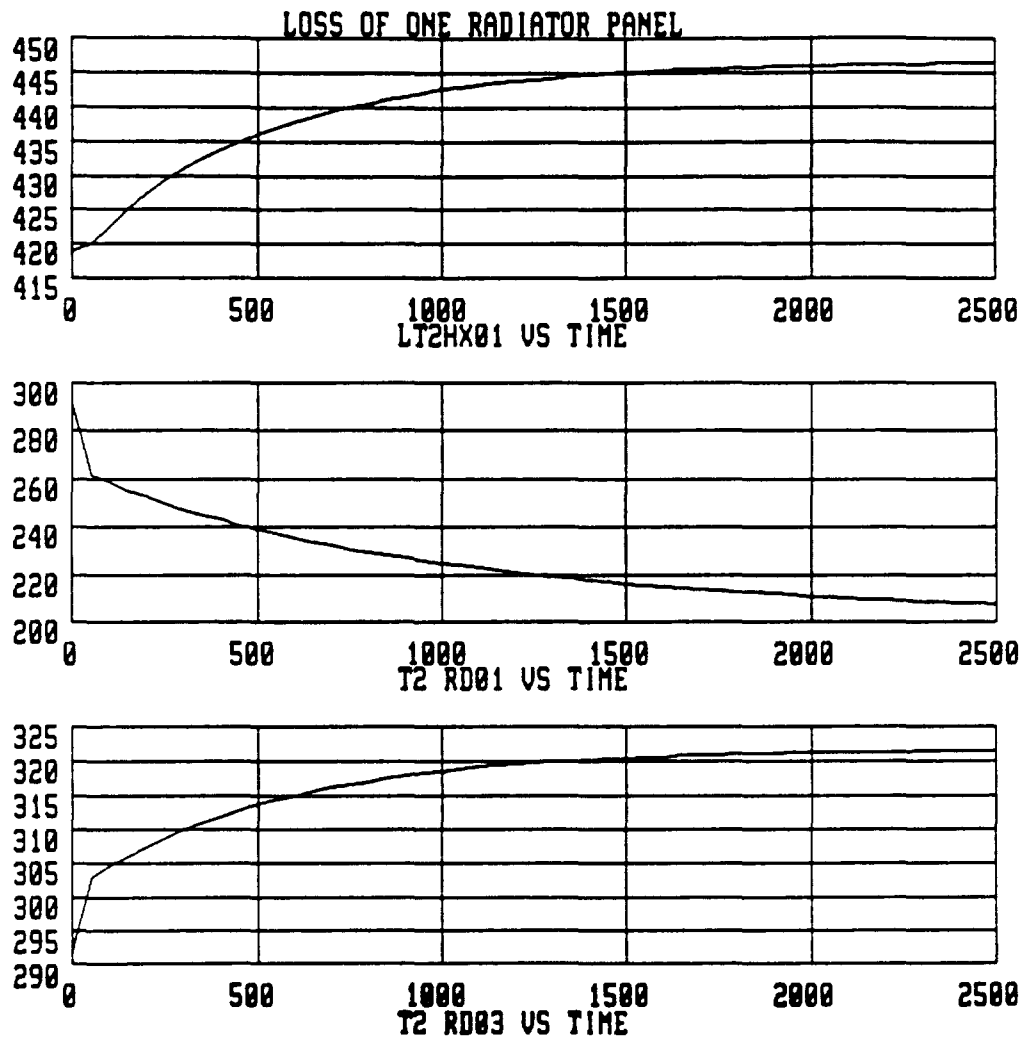
requirements. At 85.5 minutes into the orbit, the mass flow rate is increased to 1.19 kg/s, and the power output once more increased.

#### 4.3.4 Loss of One Radiator Panel

This scenario presumes the loss of one radiator panel due to manifold blockage or damage, and predicts the effect on system performance. The transient analysis is shown in Figures 56-59. These results indicate that the system will achieve a new steady state with a lower power output than before but still within the limits of turbomachinery performance. Figure 56 shows temperature in panel 1 (T2 RD01) dropping as flow is choked off, while panel 3 temperature rises to compensate. Figure 58 shows a 13 % drop in power after the system again achieves steady state in approximately 42 minutes.

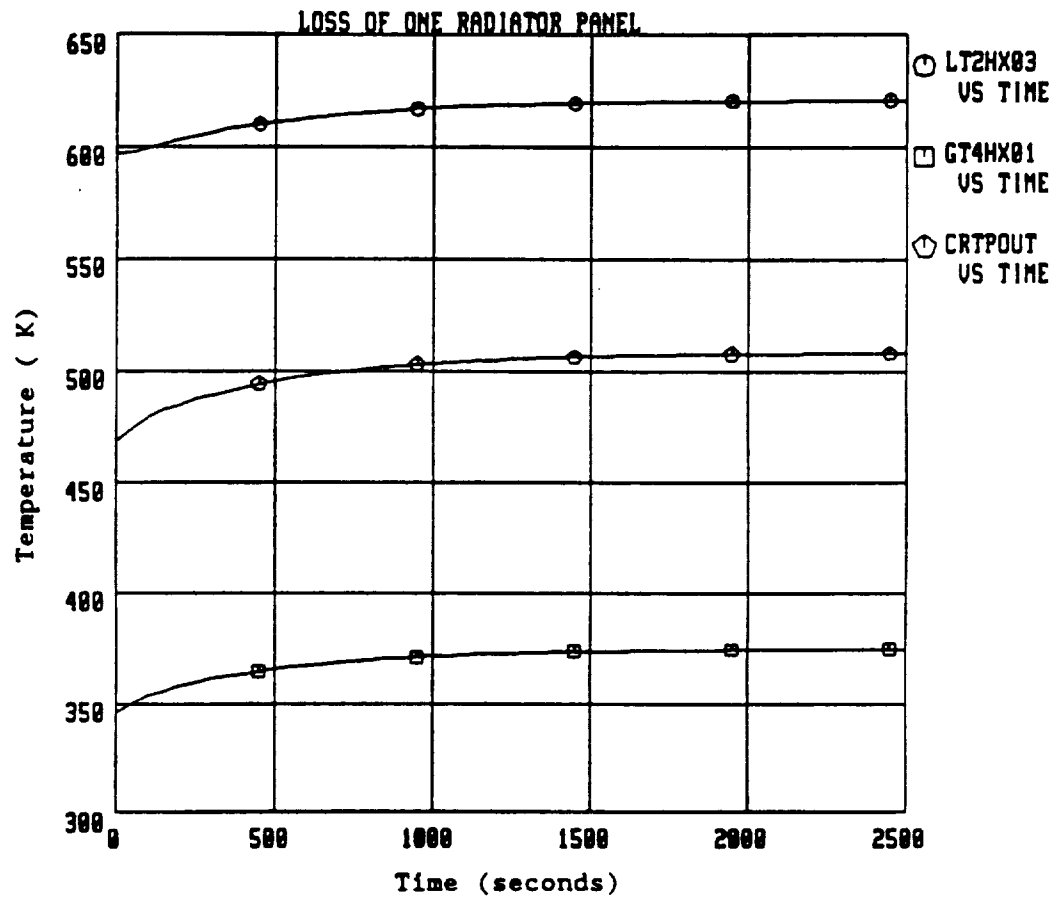
#### 4.3.5 Loss of Pump

The catastrophic scenario of losing a coolant pump is presented in Figures 60-63. These transients show that as the CBC engine loses the ability to reject heat, it quickly reaches a state where power output is zero, accompanied with an uncontrolled rise in all component temperatures. The time to reach zero power output (Figure 62) is about 5 minutes. The CBC power generating system is equipped with a redundant coolant loop, but the results indicate that response to such a catastrophic loss will have to be within 5 minutes if damage is to be controlled.



LT2HX01 - COOLANT OUTLET TEMP., GAS COOLER  
T2 RD01 - COOLANT OUTLET TEMP., RADIATOR 1  
T2 RD03 - COOLANT OUTLET TEMP., RADIATOR 3

Figure 56. Loss of One Radiator Panel Transient



LT2HX03 - GAS OUTLET TEMP., RECUPERATOR  
GT4HX01 - GAS OUTLET TEMP., GAS COOLER  
CRTPOUT - GAS OUTLET TEMP., COMPRESSOR

Figure 57. Loss of One Radiator Panel Transient

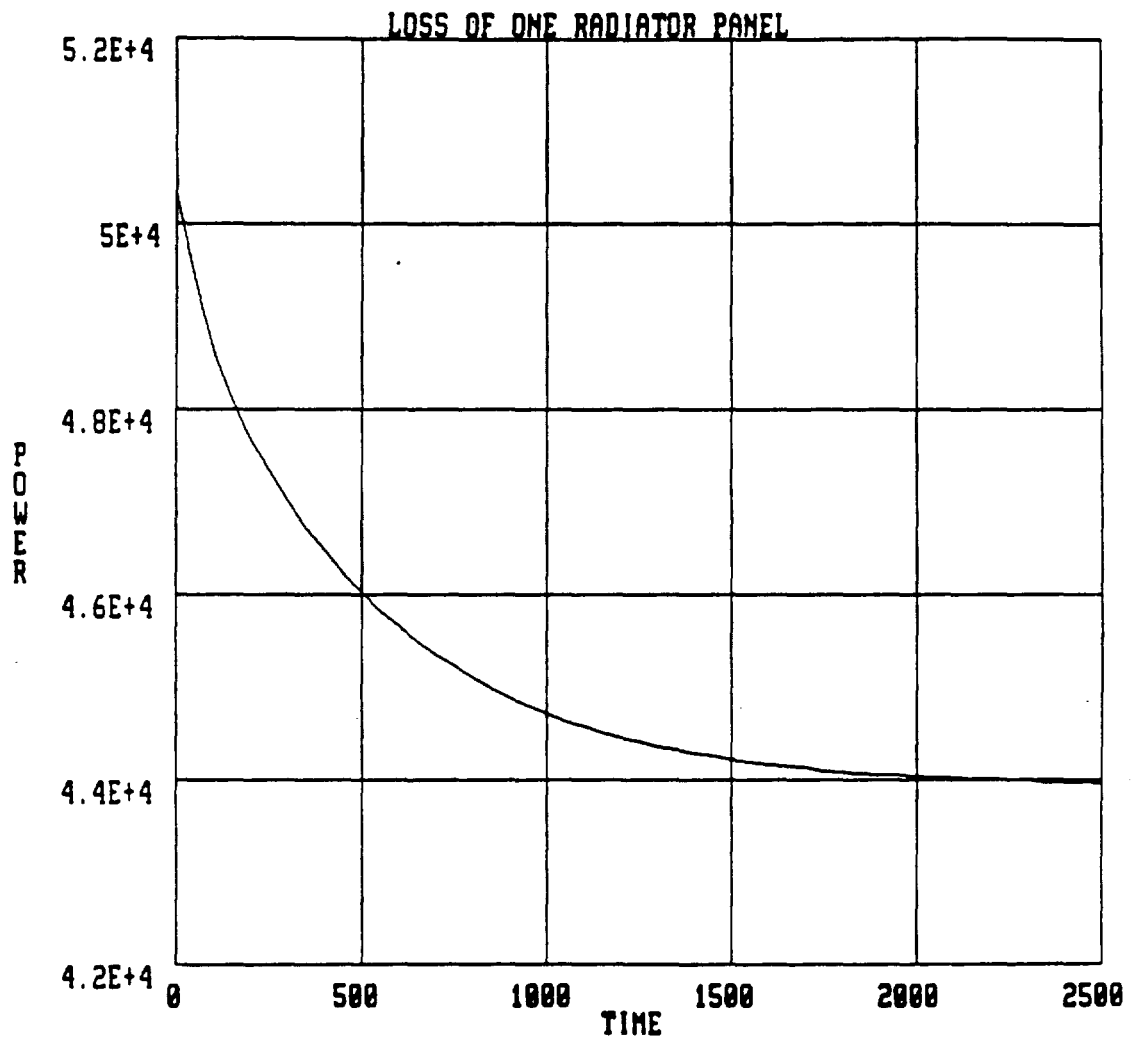
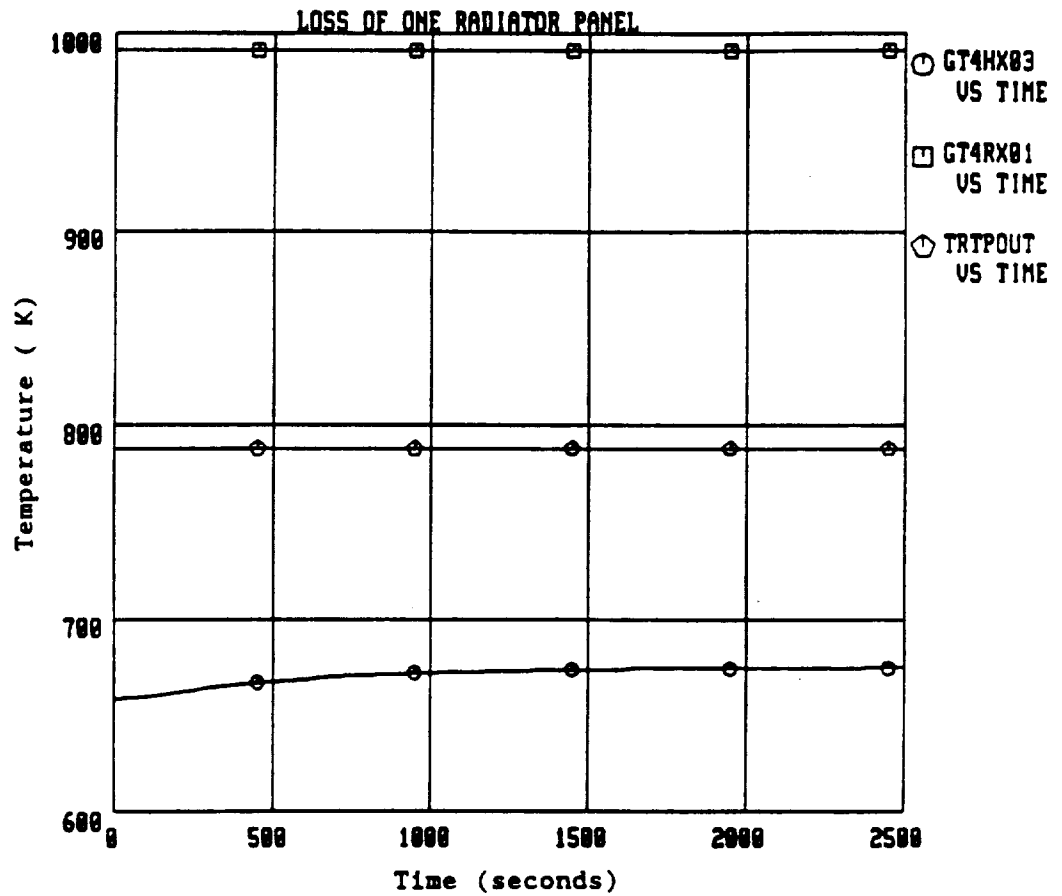
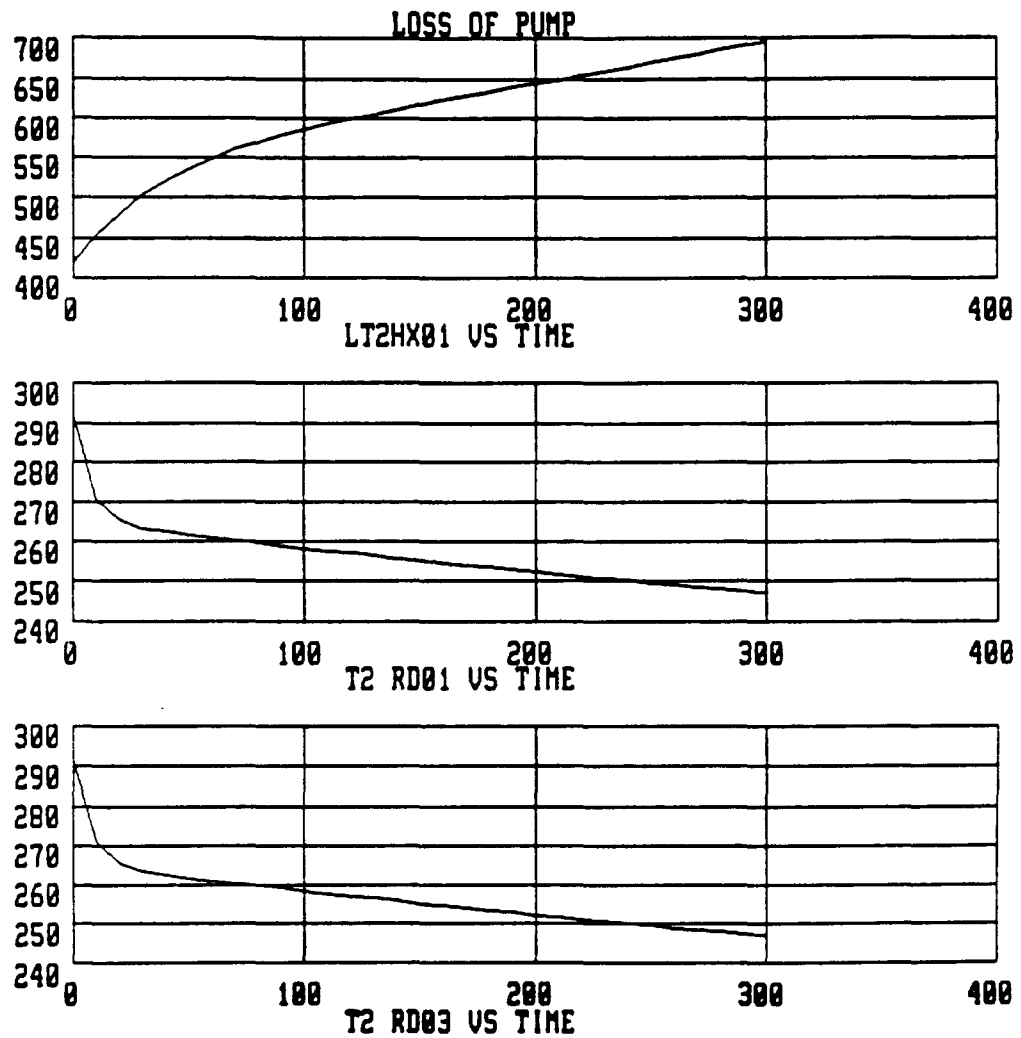


Figure 58. Loss of One Radiator Panel Transient



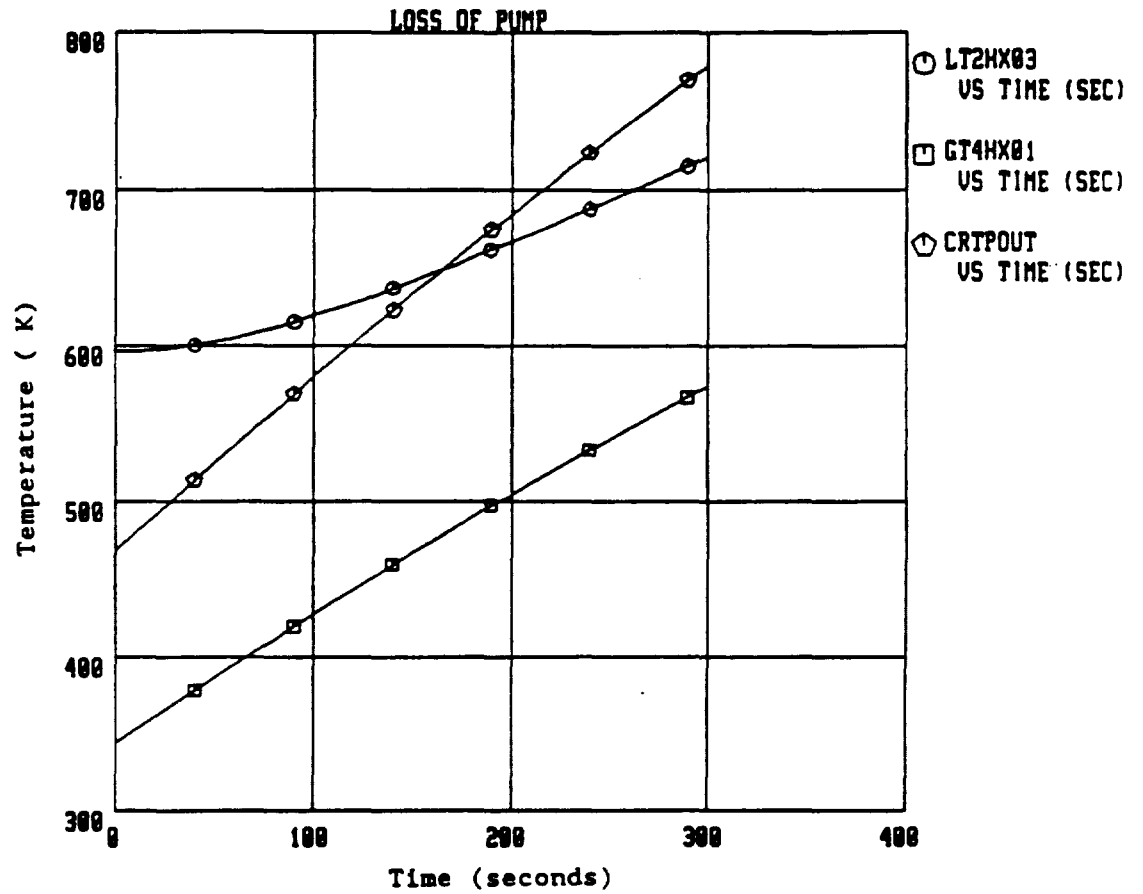
GT4HX03 - GAS OUTLET TEMP., RECUPERATOR  
GT4RX01 - GAS OUTLET TEMP., RECEIVER  
TRTPOUT - GAS OUTLET TEMP., TURBINE

Figure 59. Loss of One Radiator Panel Transient



LT2HX01 - COOLANT OUTLET TEMP., GAS COOLER  
T2 RD01 - COOLANT OUTLET TEMP., RADIATOR 1  
T2 RD03 - COOLANT OUTLET TEMP., RADIATOR 3

Figure 60. Loss of Pump Transient



GT4HX03 - GAS OUTLET TEMP., RECUPERATOR  
GT4RX01 - GAS OUTLET TEMP., RECEIVER  
TRTPOUT - GAS OUTLET TEMP., TURBINE

Figure 61. Loss of Pump Transient



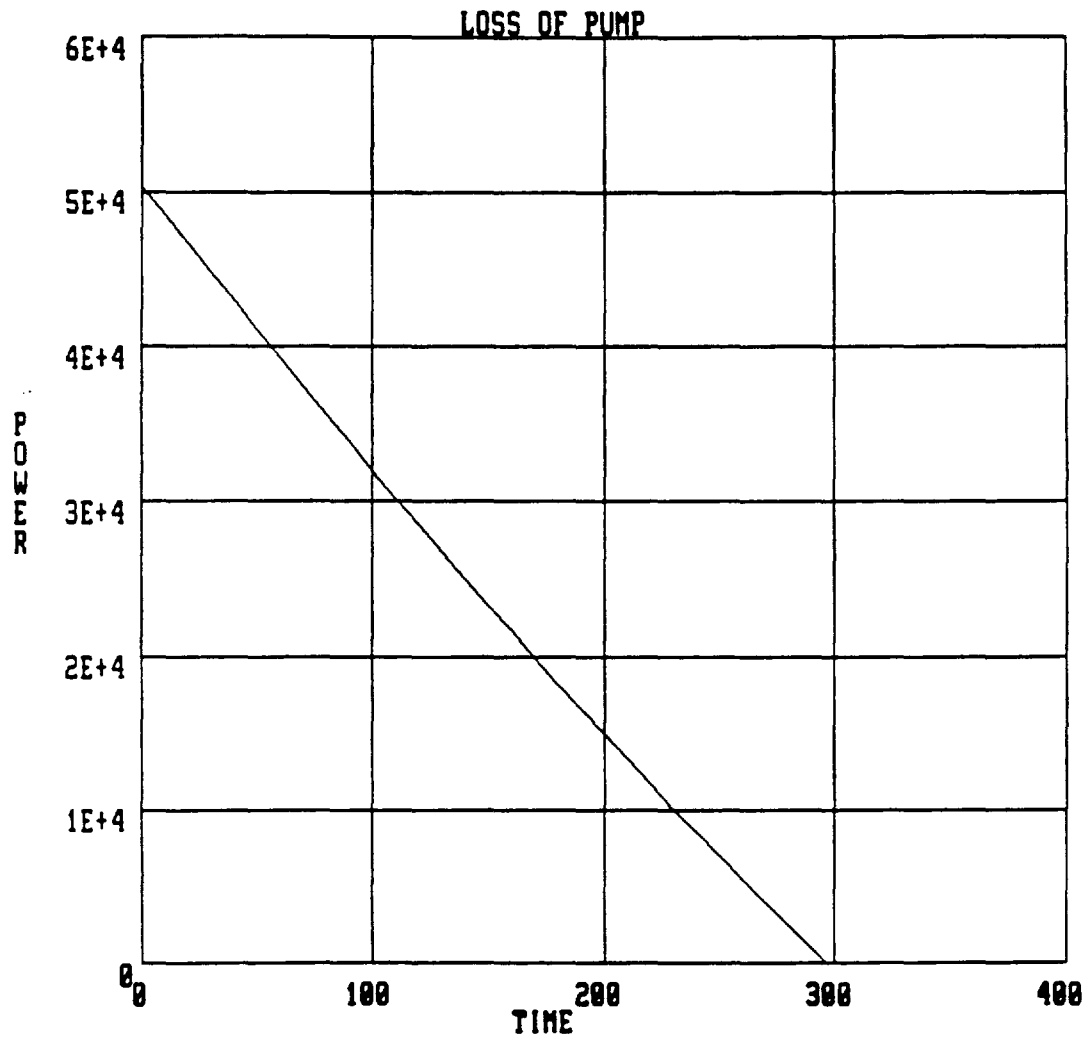
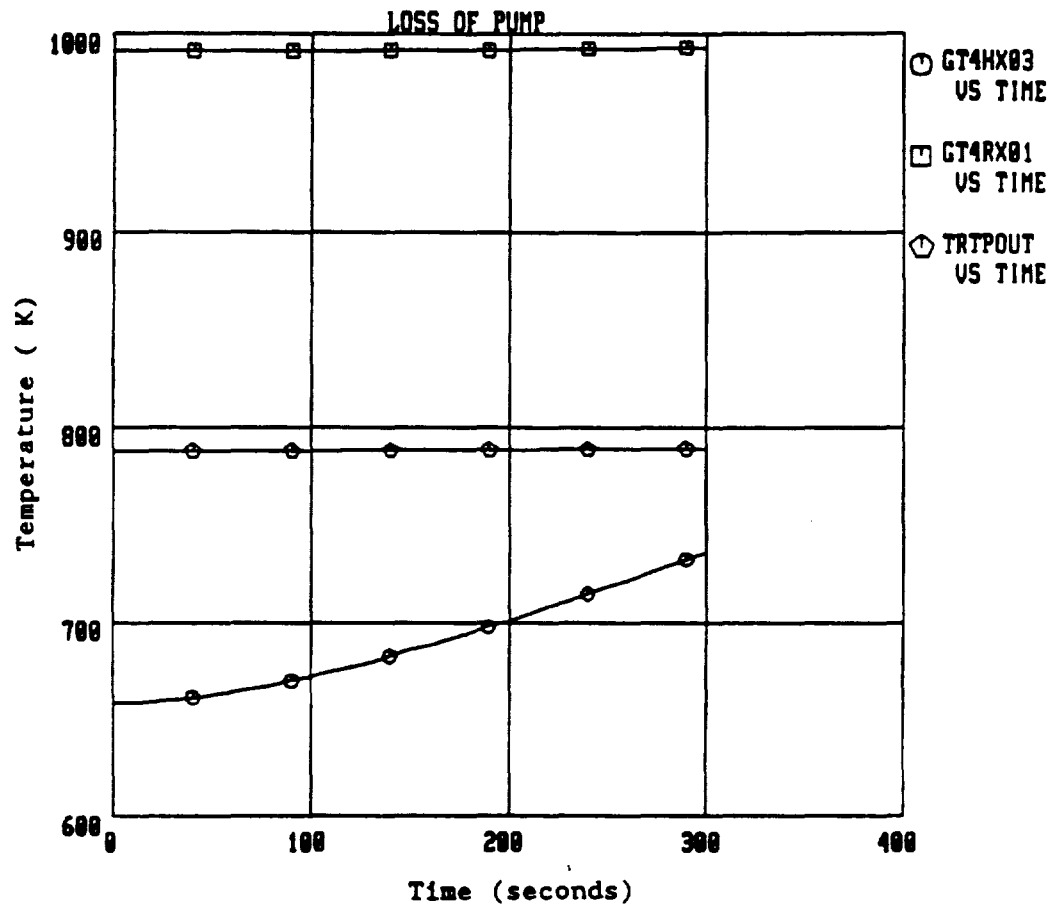


Figure 62. Loss of Pump Transient



LT2HX03 - GAS OUTLET TEMP., RECUPERATOR  
GT4HX01 - GAS OUTLET TEMP., GAS COOLER  
CRIPOUT - GAS OUTLET TEMP., COMPRESSOR

Figure 63. Loss of Pump Transient

Since a constant speed machine was assumed for this case, it is difficult to predict machine behavior when operation has moved substantially from design point. For this purpose the machine's behavior over a wide operating condition would have to be charted. In addition, for a real situation, the ideal constant speed would have to be sacrificed once temperature conditions are substantially outside normal operating temperatures.

## 5. SUMMARY AND CONCLUSIONS

Heat exchanger, radiator, and one fluid heat exchanger transient models were written in FORTRAN using a backward-difference finite-difference scheme to represent components proposed for use in the Solar Dynamic Power Generation System for Space Station Freedom. These models were later translated into EASY5, a dynamic analysis code, as EASY5 Macro components. The alternator, turbine and compressor were modelled as fixed-speed machines. Time-dependent models of other small components, such as manifolds, pipes, and pumps which make up the remainder of the CBC Power Generating System were also modelled. A model of a variable-speed, constant-work machine was attempted, but was recognised to be beyond the EASY5 operating environment.

Transient analyses were performed using the component models to examine the effect of the number of segments and integration time-step size on the transient response predicted by the model.

Tests were run on EASY5 models of the gas and liquid subsystems separately in EASY5 to verify model performance. Subsequently the subsystems were integrated into the complete SDPGS.

System simulations showed the response time of the power system to be greater than 30 minutes. This provided evidence to support the instantaneous-thermodynamic-response turbomachinery model used in this analysis, since the response time of the combined rotating unit was many orders of magnitude less than that of the remainder of the system. The steady-state temperatures provided by the DR02<sup>7</sup> were in close agreement

with the EASY5 model used, increasing confidence in the accuracy of the model.

Orbital simulation of a maximum insolation orbit, the minimum insolation orbit and the minimum insolation peaking orbit showed qualitatively similar results as NASA studies using HOT TUBE, which calculated temperatures in the system on various stages of the orbit.

Failure scenarios indicate that in some situations, such as the loss of a coolant pump and backup with a simultaneous loss of concentrator off pointing ability, total loss of power will occur in under five minutes. This provides a design goal for the emergency system response time.

## 6. RECOMMENDATION FOR FURTHER STUDY

This research can be continued by focusing on two areas: greater model refinement and expanded system description. Model refinement refers to inclusion of component details as they become known in the course of designing and building actual hardware. Expanded system description would entail including some components that hitherto were not considered in the present model.

Future refinement can be made in the turbomachinery, heat exchangers, and receiver models. Actual performance maps can be incorporated into the compressor/turbine model to more accurately represent the machines. Similarly, as more details of the receiver become known, and the behavior of the phase change material is quantified, the model should be altered to include these refinements. Heat exchanger models could also be improved as details of interior construction are available.

The system can be expanded by including the accumulator and hence the effect of variable mass flow in the gas loop. This would serve to verify shaft speed control using this technique. This expansion is not possible using EASY5 since it does not permit iteration inside the system loop at a single time level. It therefore may be necessary to build the variable speed model in FORTRAN.

Finally the electrical model should be integrated into the existing thermodynamic model to produce a complete model of the CBC power generating system. This model could then also be used to simulate control system response.

7. ACKNOWLEDGEMENTS

My wife, and my best friend, Linda. In the towering Hindu Kush mountains, there is an azure placid lake, Saif-ul-maluk. Legend has it that its depth cannot be measured. It makes me think of Linda, and how immeasurable her contribution is to anything I do.

My four year old son Jaffar. Just thinking of him makes me smile.

My advisor Prof. Hochstein. Undoubtedly one of the most intelligent and gracious persons I have had the privilege to know. I thank him for his patience, and his kindness.

My advisor Prof. Korakianitis. He gave me impetus to finish when I faltered.

My family that has always stood behind me.

The Washington University Rowing Team. They might have made it harder for me to graduate, but it was fun.

8. APPENDICES



# APPENDIX 8.1

## EASYS CBC System Model File

```

*****
*****
* COMSYS is the model file for the CBC complete system.
* It utilizes Macro's for several components including the
* Heat Exchanger, the receiver and the Radiator. Both the
* Radiator, and HX incorporate small end segments to provide
* a more accurate result.
* Author: A. Iqbal
* -----
*   DATE | VERSION | PROGRAMMER | ACTION
* -----
*   2/03/90   1.2      Iqbal   Originally written
*   11/14/89   1.3      Iqbal   Changed Radiator and Heat
*                               Exchanger to include small
*                               segments.
*   11/20/89   1.4      Iqbal   Changed compressor and turbine
*                               models to include performance
*                               bounds.
*****
*****
*-----
*   R A D I A T O R   P A N E L   M A C R O
*-----
DEFINE MACRO = RD , SYMBOL=200
DESCRIPTION = RADIATOR PANEL
MACRO INPUTS = P1 T1 M1 TSK, RSG, SSC, DYC, CPL, MLQ,
HLQ, ALQ, MWL, CPW, BOL
MACRO OUTPUTS = P2 T2 M2
MACRO CODE
STOP SORT
*-----
*   Defining of States, Variables, and Parameters. States have
*   time derivatives, Variables are any quantity that may be
*   plotted or used as an input to another component, and
*   Parameters are values that can be set in the analysis file
*   to save compilation.
*-----
*   All FORTRAN statements have to follow the "FORTRAN STATEMENTS"
*   command. Any FORTRAN statement is valid except SUBROUTINE,
*   PROGRAM, ENTRY, RETURN, STOP or END. Statements have to be
*   between columns 7-72.
*-----
*   All non-executable FORTRAN statements have to be preceded by
*   the "DECLARATION," command.
*-----
C234567890123456789012345678901234567890123456789012345678901234567890
DECLARATION, REAL*8 AMTRD--(99,99), BMTD--(99), TEMD--(99),
$ TLORD--(50), TWORD--(50), TWNRD--(50), MCWRD--
$ SCWRD-- , MCLRD-- , SCLRD-- , HALRD-- , SHLRD-- ,
$ LDRD-- , FCLRD-- , BTZRD-- , SBZRD-- , LITRD-- ,
$ CONRD-- , MDLRD-- , TLQRD--(50), TWLRD--(50)
DECLARATION, INTEGER WLBRD-- , WLRD-- , LQBRD-- , LQERD-- ,
$ SEGRD-- , I RD-- , K RD-- , L RD-- , N RD-- ,
$ SIZRD-- , DIMRD-- , CODRD-- , ITRD--
C-----
C List of constants and variables used in the program:
C AMT = A Matrix in finite difference scheme.
C BMT = B Matrix in finite difference scheme.
C TEM = Solution matrix to Ax=B.
C TLO = Old liquid temperature matrix.
C TWO = Old Wall Temperature matrix.
C TWN = New Wall Temperature matrix.
C LDT = Derivative of Liquid temperature. (Dummy)
C LIT = Liquid Inlet Temperature at each time step.
C CON = Convergence parameter (in %).
C MDL = Massflow for liquid.

```

```

C   CPL = Cp for liquid.
C   TLQ = Liquid Temperature Matrix.
C   TWL = Wall temperature matrix.
C   MCW = (Mass)x(Cp) for the wall.
C   SCW = Same as MCW but for small segment.
C   MCL = (Mass)x(Cp) for the liquid.
C   SCL = Same as MCL, but for small segment.
C   HAL = (h)x(Area) for the liquid.
C   SHL = Same as HAL but for small segment.
C   FCL = (Massflow)x(Cp) for the liquid.
C   BTZ = (Stefan-Boltzmann constant)x(Surface Area)
C   SBZ = Same as BTZ but for small segment
C   SEG = Number of nodes used for computation in Radiator.
C   TSK = Sink Temperature (In-Orbit Shade)
C   WLB = Beginning element # for Wall temperatures in TEM
C   WLE = Ending element # for Wall temperatures in TEM
C   LQB = Beginning element # for Liquid temperatures in TEM
C   LQE = Ending element # for Liquid temperatures in TEM
C   SI2 = # of element used in TEM matrix.
C   DIM = Dimension of AMT matrix
C   COD = Return code from GAUSS indicating zero pivot.
C   ITR = Iterations in a time step to converge to a solution.
C   LIQ = Liquid inlet temperature used to compute Steady State
C         and temperatures w/ time.

```

C-----

```

      print*, 'in radiator'
      MDLRD-- = M1 RD--
      FCLRD-- = MDLRD--*CPLRD--
      SEGRD-- = NINT(RSGRD--)
      MCLRD-- = (MLQRD-- * CPLRD--) * 0.98/(SEGRD-- - 2)
      SCLRD-- = (MLQRD-- * CPLRD--) * 0.01
      HALRD-- = (HLQRD-- * ALQRD--) * 0.98/(SEGRD-- - 2)
      SHLRD-- = (HLQRD-- * ALQRD--) * 0.01
      MCWRD-- = (MWLRD-- * CPWRD--) * 0.98/(SEGRD-- - 2)
      SCWRD-- = (MWLRD-- * CPWRD--) * 0.01
      BTZRD-- = BOLRD-- * 0.98/(SEGRD-- - 2)
      SBZRD-- = BOLRD-- * 0.01
      IF (SEGRD--.LT.3) THEN
        PRINT*, 'INSUFFICIENT # OF SEGMENTS'
        GO TO +++14
      ENDIF

```

C-----

```

C   When ICCALC = 1, EASY5 is calculating the initial conditions. This
C   is done in this program by setting all rates equal to zero. The
C   temperature at all nodes is set to TSKRD--, the inlet temp is set to
C   LIQTEM and program run until convergence which produces the steady
C   State temperature for that Inlet Temperature. Else the program uses
C   input from AF01 as the Liquid Inlet Temp.

```

C-----

```

      IF (ICCALC.EQ.1) THEN
        MCLRD-- = 0.
        SCLRD-- = 0.
        MCWRD-- = 0.
        SCWRD-- = 0.
        CONRD-- = SSCRD--
        LITRD-- = T1 RD--
        DO +++01 I RD--=1, SEGRD--
          TWLRD--(I RD--) = TSKRD--
          TLQRD--(I RD--) = TSKRD--
        +++01 CONTINUE
      ELSE
        LITRD-- = T1 RD--
        CONRD-- = DYCRD--
      ENDIF
      print*, 'time =', time
      print*, 'ICCALC =', iccalc

```

```

IF ((TIME.EQ.0.).AND.(ICCALC.NE.1)) GO TO +++02
SIZRD-- = 2*SEGRD--
DIMRD-- = 99
C-----
C Set bounds for the matrix TEMRD-- in which Temperatures are calculated
C-----
LQBRD-- = 1
LQERD-- = SEGRD--
WLBRD-- = LQBRD-- + SEGRD--
WLERD-- = 2*SEGRD--
DO +++15 I RD--=1,SEGRD--
    TWORD--(I RD--) = TWLRD--(I RD--)
    TLORD--(I RD--) = TLQRD--(I RD--)
+++15 CONTINUE
+++12 CONTINUE
C-----
C Small Segment of liquid
C-----
AMTRD--(LQBRD--,LQBRD--) = (SCLRD--/TINC) + SHLRD-- + FCLRD--
AMTRD--(LQBRD--,WLBRD--) = -SHLRD--
BMTRD--(LQBRD--) = (FCLRD--*LITRD--) + ((SCLRD--/TINC)*
$ TLQRD--(LQBRD--))
N RD--=0
C-----
C Regular segment of liquid
C-----
DO +++03 I RD--=LQBRD--+1,LQERD--1
    AMTRD--(I RD--,LQBRD--+N RD--) = -FCLRD--
    AMTRD--(I RD--,I RD--) = (MCLRD--/TINC) + HALRD-- + FCLRD--
    AMTRD--(I RD--,WLBRD--+N RD--+1) = -HALRD--
    BMTRD--(I RD--) = (MCLRD--/TINC) * TLQRD--(I RD--)
    N RD-- = N RD-- + 1
+++03 CONTINUE
C-----
C Small Segment of liquid
C-----
AMTRD--(LQERD--,LQBRD--+N RD--) = -FCLRD--
AMTRD--(LQERD--,LQERD--) = (SCLRD--/TINC) + SHLRD-- + FCLRD--
AMTRD--(LQERD--,WLBRD--+N RD--+1) = -SHLRD--
BMTRD--(LQERD--) = (SCLRD--/TINC) * TLQRD--(LQERD--)
C-----
C Small Segment of wall
C-----
N RD-- = 0
AMTRD--(WLBRD--,LQBRD--+N RD--) = -SHLRD--
AMTRD--(WLBRD--,WLBRD--) = (SCWRD--/TINC) + SHLRD-- +
$ SBZRD--*(TWORD--(N RD--+1)**3)
BMTRD--(WLBRD--) = (SCWRD--/TINC) * TWLRD--(N RD--+1) +
$ SBZRD--*(TSKRD--**4)
C-----
C Regular Segment of wall
C-----
N RD-- = 1
DO +++04 I RD--=WLBRD-- + 1,WLERD-- - 1
    AMTRD--(I RD--,LQBRD--+N RD--) = -HALRD--
    AMTRD--(I RD--,I RD--) = (MCWRD--/TINC) + HALRD-- +
$ BTZRD--*(TWORD--(N RD--+1)**3)
    BMTRD--(I RD--) = (MCWRD--/TINC) * TWLRD--(N RD--+1) +
$ BTZRD--*(TSKRD--**4)
    N RD--=N RD--+1
+++04 CONTINUE
C-----
C Small Segment of wall
C-----
AMTRD--(WLERD--,LQBRD--+N RD--) = -SHLRD--
AMTRD--(WLERD--,WLERD--) = (SCWRD--/TINC) + SHLRD-- +

```

```

$          SBZRD--*(TWORD--(N RD--+1)**3)
$          BMTRD--(WLRD--)= (SCWRD--/TINC) * TWLRD--(N RD--+1) +
$          SBZRD--*(TSKRD--**4)
C-----
C Beginning of the loop to calculate all temperatures at all
C points.
C-----
      CALL GAUSS(AMTRD--,BMTRD--,TEMRD--,SIZRD--,DIMRD--,CODRD--,DUNNA)
      IF (CODRD--.EQ.2) GO TO +++05
      L RD--=1
      DO +++06 I RD--=1,WLRD--,WLRD--
        TWNRD--(L RD--)= TEMRD--(I RD--)
        L RD--= L RD-- + 1
+++06 CONTINUE
      DO +++07 I RD--=1,SEGRD--
        IF ((ABS(TWORD--(I RD--)-TWNRD--(I RD--)).GT.
$          ((CONRD--/100)*TWORD--(I RD--)))
$ THEN
          GO TO +++09
        ELSE
          GO TO +++08
        ENDIF
+++07 CONTINUE

+++09 CONTINUE
      PRINT *, 'IN ITERATION LOOP. ITRD-- = ',ITRD--
      DO +++10 I RD--=1,SEGRD--
        TWORD--(I RD--)= (((TWORD--(I RD--))**4) +
$          ((TWNRD--(I RD--))**4))/2)**0.25
+++10 CONTINUE
      IF (ITRD--.GT.100) GO TO +++11
      ITRD--= ITRD-- + 1
      GO TO +++12

+++08 CONTINUE
      ITRD--= 0
      I RD--=1
      K RD--=1
      L RD--=1

C-----
C Assigning the temperatures to the correct slots in their
C individual matrices.
C-----
      DO +++13 I RD--=1,SIZRD--
        IF ((I RD--.GE.LQBRD--).AND.(I RD--.LE.LQERD--)) THEN
          TLQRD--(K RD--)= TEMRD--(I RD--)
          K RD--= K RD-- + 1
        END IF

        IF ((I RD--.GE.WLBRD--).AND.(I RD--.LE.WLERD--)) THEN
          TWLRD--(L RD--)= TEMRD--(I RD--)
          L RD--= L RD-- + 1
        END IF
+++13 CONTINUE
      DERIVATIVE OF, T2 RD--= LDTRD--
+++02 T2 RD--= TLQRD--(SEGRD--)
      P2 RD--= P1 RD--
      M2 RD--= M1 RD--
      GO TO +++14
+++05 PRINT *, 'SUBROUTINE GAUSS BOMBED'
      GO TO +++14
+++11 PRINT *, 'ITERATIONS FOR WALL TEMPERATURE EXCEED 100'

+++14 CONTINUE
RESUME SORT
END OF MACRO CODE

```

```

=====
*           H E A T   E X C H A N G E R   M A C R O
=====
DEFINE MACRO = HX , SYMBOL = 600
DESCRIPTION = COUNTERFLOW HEAT EXCHANGER
MACRO INPUTS = LP1, LT1, LM1, GP3, GT3, GM3, HSG, ILT, IGT,
CPL, CPG, CPW, HLQ, HGS, AGS, ALQ, MGS, MLQ, MWL, ILP, ILF, IGP,
IGF
MACRO OUTPUTS = LP2, LT2, LM2, GP4, GT4, GM4
MACRO CODE
STOP SORT
C23456789012345678901234567890123456789012345678901234567890123456789012
  DECLARATION, REAL*8 AMTHX--(99,99), BMTHX--(99), TEMHX--(99),
$      MCGHX--, SCGHX--, HAGHX--, SHGHX--, FCGHX--,
$      MCWHX--, SCWHX--, MCLHX--, SCLHX--, HALHX--,
$      SHLHX--, FCLHX--, GMINX--, LMINX--, GMOHX--,
$      LITHX--, GITHX--, TLOHX--(50), TWOHX--(50),
$      TGOHX--(50), GDRHX--, LMOHX--,
$      LDRHX--, TLOHX--(50), TWLHX--(50),
$      TGSHX--(50), LPIHX--, LPOHX--, GPIHX--,
$      GPOHX--
  DECLARATION, INTEGER I HX--, K HX--, L HX--, M HX--,
$      N HX--, O HX--, SIZHX--, DIMHX--, CODHX--,
$      IGBHX--, IGENX--, IWBHX--, IWEHX--, ILBHX--,
$      ILENX--, SEGHX--

C-----
C This EASY5 component calculates the dynamic parameters of a
C single pass counterflow Heat Exchanger divided into N
C segments. It takes as input the inlet temperature of the
C gas, as well as the inlet temperature of the fluid. Integration
C is done using a modified Euler method. The program produces the
C wall temperatures in each segment, as well as the inlet and outlet
C temperatures at these stations.
C
C List of constants and variables used in the program:
C LP1, LT1, LM1 = Liquid pressure, temperature, and massflow in.
C GP3, GT3, GM3 = Gas pressure, temperature and massflow in.
C HGS = Gas heat transfer coefficient.
C HLQ = Liquid heat transfer coefficient.
C HSG = Number of nodes in HX (real number).
C IGF = Initial massflow (gas).
C ILF = Initial massflow (liquid).
C ILT = Initial liquid temperature.
C IGT = Initial Gas temperature.
C CPG = Cp for the gas.
C CPL = Cp for the liquid.
C CPW = Cp for the wall.
C AGS = Area of contact for gas.
C ALQ = Area of contact for liquid.
C MGS = Mass of gas in control volume.
C MLQ = Mass of liquid in control volume.
C MWL = Mass of wall in control volume.
C MCG = (Mass)x(Cp) for the gas.
C SCG = Same as MCG but for small segment.
C HAG = (h)x(Area) for the gas.
C SHG = Same as HAG but for small segment.
C FCG = (Massflow)x(Cp) for the gas.
C MCW = (Mass)x(Cp) for the wall.
C SCW = Same as MCW but for small segment.
C MCL = (Mass)x(Cp) for the liquid.
C SCL = Same as MCL but for small segment.
C HAL = (h)x(Area) for the liquid.
C SHL = Same as HAL but for small segment.
C FCL = (Massflow)x(Cp) for the liquid.
C SEG = Number of segments Heat Exchanger is divided in.

```

```

C-----
      print*, 'in heat exchanger'
      SEGHX-- = NINT(HSGHX--)
      IF (SEGHX--.LT.3) THEN
        PRINT*, 'INSUFFICIENT # OF SEGMENTS'
        GO TO +++60
      END IF
      MCLHX-- = (MLQHX-- * CPLHX-- ) * 0.98/ (SEGHX-- - 2)
      SCLHX-- = (MLQHX-- * CPLHX-- ) * 0.01
      HALHX-- = (HLQHX-- * ALQHX-- ) * 0.98/ (SEGHX-- - 2)
      SHLHX-- = (HLQHX-- * ALQHX-- ) * 0.01
      MCWHX-- = (MWLHX-- * CPWHX-- ) * 0.98/ (SEGHX-- - 2)
      SCWHX-- = (MWLHX-- * CPWHX-- ) * 0.01
      MCGHX-- = (MGSHX-- * CPGHX-- ) * 0.98/ (SEGHX-- - 2)
      SCGHX-- = (MGSHX-- * CPGHX-- ) * 0.01
      HAGHX-- = (HGSHX-- * AGSHX-- ) * 0.98/ (SEGHX-- - 2)
      SHGHX-- = (HGSHX-- * AGSHX-- ) * 0.01
C-----
C This loop is executed if initial conditions need to be calculated.
C The variable ICCALC is then set to one, and all rates set to zero.
C-----
      IF (ICCALC.EQ.1) THEN
        MCLHX-- = 0.
        SCLHX-- = 0.
        MCWHX-- = 0.
        SCWHX-- = 0.
        MCGHX-- = 0.
        SCGHX-- = 0.
        LITX-- = ILTHX--
        GITX-- = IGTHX--
        LMIHX-- = ILPHX--
        GMIHX-- = IGFHX--
        LPIHX-- = ILPHX--
        GPIHX-- = IGFHX--
        DO +++51 I HX--=1,SEGHX--
          TWLHX--(I HX--)= LITX--
          TLOHX--(I HX--)= LITX--
          TGSHX--(I HX--)= LITX--
+++51 CONTINUE
        ELSE
          LITX-- = LT1HX--
          GITX-- = GT3HX--
          LMIHX-- = LM1HX--
          GMIHX-- = GM3HX--
          LPIHX-- = LP1HX--
          GPIHX-- = GP3HX--
        ENDIF
        FCLHX-- = LMIHX-- * CPLHX--
        FCGHX-- = GMIHX-- * CPGHX--
        print*, 'fcl = ',fclhx--, ' mcl = ',mclhx--, ' hal = ',halhx--
        print*, 'fcg = ',fcghx--, ' mcg = ',mcghx--, ' hag = ',haghx--
        print*, 'mcw = ',mcwhx--
        print*, 'time = ',time
        print*, 'ICCALC = ',iccalc

        IF ((TIME.EQ.0.).AND.(ICCALC.NE.1)) GO TO +++52

        print*, 'Did not jump out when time was zero'

        SIZHX-- = 3*SEGHX--
        DIMMX-- = 99
C-----
C Set bounds for temperatures in TEMHX--
C-----
        IGBHX-- = 1
        IGENX-- = SEGHX--

```

```

IWBHX-- = IGBHX-- + SEGHX--
IWEHX-- = 2*SEGHX--
ILBHX-- = IWBHX-- + SEGHX--
ILEHX-- = 3*SEGHX--
DO +++53 I HX--=1,SEGHX--
  TWOHX--(I HX--)= TWLHX--(I HX--)
  TLOHX--(I HX--)= TLQHX--(I HX--)
  TGOHX--(I HX--)= TGSHX--(I HX--)
+++53 CONTINUE
print*, 'two(5)= ',twohx--(5), ' twl(5)= ',twlhx--(5)
print*, 'tlo(5)= ',tlohx--(5), ' tlg(5)= ',tlghx--(5)
print*, 'tgo(5)= ',tgohx--(5), ' tgs(5)= ',tgs hx--(5)
CONTINUE
C-----
C      Small gas segment
C-----
  AMTHX--(IGBHX--,IGBHX--) = (SCGHX--/TINC) + SHGHX-- + FCGHX--
  AMTHX--(IGBHX--,IWBHX--) = -SHGHX--
  BMTHX--(IGBHX--) = (FCGHX--*GITHX--) + ((SCGHX--/TINC) *
$      TGSHX--(IGBHX--))
  N HX--=0
C-----
C      Regular gas segment
C-----
DO +++54 I HX--=IGBHX-- + 1,IGEHX-- - 1
  AMTHX--(I HX--,IGBHX--+N HX--) = -FCGHX--
  AMTHX--(I HX--,I HX--) = (MCGHX--/TINC) + HAGHX-- + FCGHX--
  AMTHX--(I HX--,IWBHX--+N HX-- + 1) = -HAGHX--
  BMTHX--(I HX--) = (MCGHX--/TINC) * TGSHX--(I HX--)
  N HX-- = N HX-- + 1
+++54 CONTINUE
C-----
C      Small gas segment
C-----
  AMTHX--(IGEHX--,IGBHX--+N HX--) = -FCGHX--
  AMTHX--(IGEHX--,IGEHX--) = (SCGHX--/TINC) + SHGHX-- + FCGHX--
  AMTHX--(IGEHX--,IWBHX--+N HX-- + 1) = -SHGHX--
  BMTHX--(IGEHX--) = (SCGHX--/TINC) * TGSHX--(IGEHX--)
C-----
C      Small wall segment
C-----
  N HX--=0
  AMTHX--(IWBHX--,IGBHX--+N HX--) = -SHGHX--
  AMTHX--(IWBHX--,IWBHX--) = (SCWHX--/TINC) + SHGHX-- + SHLHX--
  AMTHX--(IWBHX--,ILBHX--+N HX--) = -SHLHX--
  BMTHX--(IWBHX--) = (SCWHX--/TINC) * TWLHX--(N HX--+1)
C-----
C      Regular wall segment
C-----
  N HX--=1
DO +++55 I HX-- = IWBHX-- + 1,IWEHX-- - 1
  AMTHX--(I HX--,IGBHX--+N HX--) = -HAGHX--
  AMTHX--(I HX--,I HX--) = (MCWHX--/TINC) + HAGHX-- + HALHX--
  AMTHX--(I HX--,ILBHX--+N HX--) = -HALHX--
  BMTHX--(I HX--) = (MCWHX--/TINC) * TWLHX--(N HX--+1)
  N HX-- = N HX-- + 1
+++55 CONTINUE
C-----
C      Small wall segment
C-----
  AMTHX--(IWEHX--,IGBHX--+N HX--) = -SHGHX--
  AMTHX--(IWEHX--,IWEHX--) = (SCWHX--/TINC) + SHGHX-- + SHLHX--
  AMTHX--(IWEHX--,ILBHX--+N HX--) = -SHLHX--
  BMTHX--(IWEHX--) = (SCWHX--/TINC) * TWLHX--(N HX--+1)
C-----
C      Small liquid segment

```

```

C-----
N HX-- = 0
AMTHX--(ILBHX--,IWBHX--+N HX--) = -SHLHX--
AMTHX--(ILBHX--,ILBHX--) = (SCLHX--/TINC) + SHLHX-- + FCLHX--
AMTHX--(ILBHX--,ILBHX--+ N HX-- + 1) = -FCLHX--
BMTHX--(ILBHX--) = (SCLHX--/TINC) * TLQHX--(N HX-- + 1)
C-----
C Regular liquid segment
C-----
N HX-- = 1
DO +++56 I HX-- = ILBHX-- + 1,ILEHX-- - 1
AMTHX--(I HX--,IWBHX--+N HX--) = -HALHX--
AMTHX--(I HX--,I HX--) = (MCLHX--/TINC) + HALHX-- + FCLHX--
AMTHX--(I HX--,ILBHX--+ N HX-- + 1) = -FCLHX--
BMTHX--(I HX--) = (MCLHX--/TINC) * TLQHX--(N HX-- + 1)
N HX-- = N HX-- + 1
+++56 CONTINUE
C-----
C Small liquid segment
C-----
AMTHX--(ILEHX--,IWEHX--) = -SHLHX--
AMTHX--(ILEHX--,ILEHX--) = (SCLHX--/TINC) + SHLHX-- + FCLHX--
BMTHX--(ILEHX--) = (FCLHX--*LITHX--) + (SCLHX--/TINC) *
$ TLQHX--(SEGHX--)

print*, 'calculated matrices'

C-----
C Beginning of the loop to calculate all temperatures at all
C points.
C-----
CALL GAUSS(AMTHX--,BMTHX--,TEMHX--,SIZHX--,DIMHX--,CODHX--,DUNNA)

print*, 'back from gauss'

IF (CODHX--.EQ.2) GO TO +++58
I HX-- = 1
K HX-- = 1
L HX-- = 1
M HX-- = 1
N HX-- = 1
C-----
C Assigning the temperatures to the correct slots in their
C individual matrices.
C-----
DO +++59 I HX-- = 1,DIMHX--
IF ((I HX--.GE.IGBHX--).AND.(I HX--.LE.IGENHX--)) THEN
TGSHX--(K HX--) = TEMHX--(I HX--)
K HX-- = K HX-- + 1
END IF

IF ((I HX--.GE.IWBHX--).AND.(I HX--.LE.IWEHX--)) THEN
TWLHX--(L HX--) = TEMHX--(I HX--)
L HX-- = L HX-- + 1
END IF

IF ((I HX--.GE.ILBHX--).AND.(I HX--.LE.ILEHX--)) THEN
TLQHX--(N HX--) = TEMHX--(I HX--)
N HX-- = N HX-- + 1
END IF
+++59 CONTINUE

print*, 'assigned temperatures to matrices'

DERIVATIVE OF, LT2HX-- = LDRHX--
DERIVATIVE OF, GT4HX-- = GDRHX--

```



```

      LMOHX-- = LMIHX--
      GMOHX-- = GMIHX--
      GPOHX-- = GPIHX--
      LPOHX-- = LPIHX--

      print*, 'calculated fake derivatives'

+++52 LT2HX-- = TLQHX--(1)
      GT4HX-- = TGSHX--(SEGHX--)
      LP2HX-- = LPOHX--
      LM2HX-- = LMOHX--
      GP4HX-- = GPOHX--
      GM4HX-- = GMOHX--

      print*, 'set output to correct values'

      GO TO +++60
+++58 PRINT *, 'SUBROUTINE GAUSS BOMBED'
+++60 CONTINUE

      print*, 'finished HX'
      RESUME SORT
      END OF MACRO CODE
=====
*           R E C E I V E R / H X           M A C R O
=====
      DEFINE MACRO = RX , SYMBOL = 600
      DESCRIPTION = RECIEVER HEAT EXCHANGER
      MACRO INPUTS = BT1, GP3, GT3, GM3, HSG, IBT, IGT, IGF, IGP,
      CPG, CPW, HGS, AGS, HBD, ABD, MGS, MWL
      MACRO OUTPUTS = GP4, GT4, GM4
      MACRO CODE
      STOP SORT
      C23456789012345678901234567890123456789012345678901234567890123456789012
      DECLARATION, REAL*8 AMTRX--(99,99), BMTRX--(99), TEMRX--(99),
      $           MCGRX--, HAGRX--, FCGRX--, MCWRX--,
      $           HABRX--, GITRX--, TWORX--(50),
      $           TGORX--(50), GDRRX--, PINRX--, TWLRX--(50),
      $           TGSRX--(50), GPIRX--, GPORX--, GMIRX--,
      $           GMORX--
      DECLARATION, INTEGER I RX--, K RX--, L RX--, M RX--,
      $           N RX--, O RX--, SIZRX--, DIMRX--, CODRX--,
      $           IGBRX--, IGERX--, IWBRX--, IWERX--, SEGRX--

C-----
C This EASY5 component calculates the dynamic parameters of a
C single pass counterflow Heat Exchanger divided into N
C segments. It takes as input the inlet temperature of the
C gas, as well as the inlet temperature of the fluid. Integration
C is done using a modified Euler method. The program produces the
C wall temperatures in each segment, as well as the inlet and outlet
C temperatures at these stations.
C
C List of constants and variables used in the program:
C BT1 = Boundary temperature.
C GP3, GT3, GM3 = Gas pressure, temperature and massflow in.
C HGS = Gas heat transfer coefficient.
C HBD = Boundary heat transfer coefficient.
C HSG = Number of nodes in RX (real number).
C IGF = Initial gas flow (massflow).
C IGT = Initial Gas temperature.
C CPG = Cp for the gas.
C CPW = Cp for the wall.
C AGS = Area of contact for gas.
C MGS = Mass of gas in control volume.
C MWL = Mass of wall in control volume.

```

```

C MCG = (Mass)x(Cp) for the gas.
C HAG = (h)x(Area) for the gas.
C FCG = (Massflow)x(Cp) for the gas.
C MCW = (Mass)x(Cp) for the wall.
C SEG = Number of segments Heat Exchanger is divided in.
C-----
      print*, 'in heat exchanger'
      SEGRX-- = NINT(HSGRX--)
      MCWRX-- = MWLRX-- * CPWRX-- / SEGRX--
      MCGRX-- = MGSRX-- * CPGRX-- / SEGRX--
      HAGRX-- = HGSRX-- * AGSRX-- / SEGRX--
      HABRX-- = HBDRX-- * ABRX-- / SEGRX--
C-----
C This loop is executed if initial conditions need to be calculated.
C The variable ICCALC is then set to one, and all rates set to zero.
C-----
      IF (ICCALC.EQ.1) THEN
        MCWRX-- = 0.
        MCGRX-- = 0.
        TBDRX-- = IBTRX--
        GITRX-- = IGTRX--
        GMIRX-- = IGFRX--
        GPIRX-- = IGPRX--
        DO +++51 I RX--=1, SEGRX--
          TWLRX--(I RX--) = TBLRX--
          TGSRX--(I RX--) = TBSRX--
+++51 CONTINUE
      ELSE
        TBLRX-- = BT1RX--
        GT1RX-- = GT3RX--
        GP1RX-- = GP3RX--
        GM1RX-- = GM3RX--
      ENDIF
      FCGRX-- = GMIRX-- * CPGRX--

      print*, 'time =', time
      print*, 'ICCALC =', iccalc

      IF ((TIME.EQ.0.) .AND. (ICCALC.NE.1)) GO TO +++52

      print*, 'Did not jump out when time was zero'

      SIZRX-- = 2*SEGRX--
      DIMRX-- = 99
C-----
C Set bounds for temperatures in TEMRX--
C-----
      IGBRX-- = 1
      IGERX-- = SEGRX--
      IWBX-- = IGBRX-- + SEGRX--
      IWERX-- = 2*SEGRX--
      DO +++53 I RX--=1, SEGRX--
        TWORX--(I RX--) = TWLRX--(I RX--)
        TGORX--(I RX--) = TGSRX--(I RX--)
+++53 CONTINUE
      CONTINUE
      AMTRX--(IGBRX--, IGBRX--) = (MCGRX--/TINC) + HAGRX-- + FCGRX--
      AMTRX--(IGBRX--, IWBX--) = -HAGRX--
      BMTRX--(IGBRX--) = (FCGRX--*GITRX--) + ((MCGRX--/TINC) *
$          TGSRX--(IGBRX--))
      N RX--=0
C-----
      DO +++54 I RX--=IGBRX--+1, IGERX--
        AMTRX--(I RX--, IGBRX--+N RX--) = -FCGRX--
        AMTRX--(I RX--, I RX--) = (MCGRX--/TINC) + HAGRX-- + FCGRX--
        AMTRX--(I RX--, IWBX-- + N RX-- + 1) = -HAGRX--

```

```

      BMTRX--(I RX--) = (MCGRX--/TINC) * TGSRX--(I RX--)
      N RX-- = N RX-- + 1
+++54 CONTINUE
C-----
      N RX--=0
      DO +++55 I RX-- = IWBX-- , IWBX--
      AMTRX--(I RX-- , IGBX--N RX--) = -HAGRX--
      AMTRX--(I RX-- , I RX--) = (MCWRX--/TINC) + HAGRX-- + HABRX--
      BMTRX--(I RX--) = (MCWRX--/TINC) * TWLRX--(N RX--+1) +
      $ (HABRX--*TDBRX--)
      N RX-- = N RX-- + 1
+++55 CONTINUE
C-----
      print*,'calculated matrices'

C-----
C Beginning of the loop to calculate all temperatures at all
C points.
C-----
      CALL GAUSS(AMTRX-- , BMTRX-- , TEMRX-- , SIZRX-- , DIMRX-- , CODRX-- , DUNNA)

      print*,'back from gauss'

      IF (CODRX--.EQ.2) GO TO +++58
      I RX-- = 1
      K RX-- = 1
      L RX-- = 1
      M RX-- = 1
      N RX-- = 1

C-----
C Assigning the temperatures to the correct slots in their
C individual matrices.
C-----
      DO +++59 I RX-- = 1 , DIMRX--
      IF ((I RX-- .GE. IGBX--) .AND. (I RX-- .LE. IGERX--)) THEN
        TGSRX--(K RX--) = TEMRX--(I RX--)
        K RX-- = K RX-- + 1
      END IF

      IF ((I RX-- .GE. IWBX--) .AND. (I RX-- .LE. IWBX--)) THEN
        TWLRX--(L RX--) = TEMRX--(I RX--)
        L RX-- = L RX-- + 1
      END IF

+++59 CONTINUE

      print*,'assigned temperatures to matrices'

      DERIVATIVE OF, GT4RX-- = GDRX--
      GMORX-- = GMIRX--
      GPORX-- = GPIRX--

      print*,'calculated fake derivatives'

+++52 GT4RX-- = TGSRX--(SEGRX--)
      GP4RX-- = GPORX--
      GM4RX-- = GMORX--

      print*,'set output to correct values'

      GO TO +++60
+++58 PRINT *,'SUBROUTINE GAUSS BOMBED'
+++60 CONTINUE

      print*,'finished RX'
      RESUME SORT

```

END OF MACRO CODE

```

*-----*
*       P I P E   M A C R O
*-----*
DEFINE MACRO = PP, SYMBOL = 600
DESCRIPTION = COOLANT PIPE
MACRO INPUTS = P1      T1      M1      QLS, LGT, DIA
MACRO OUTPUTS = P2      T2      M2
MACRO CODE
STOP SORT
      DECLARATION, REAL*8 RENPP--, VELPP--, DPRPP--,
      $  FRIPP--, HEDPP--, HETPP--, VISPP--, RHOPP--,
      $  GRAPP--, PIEPP--
*-----*
*  VARIABLES USED AND THEIR UNITS:
*  M1, M2 = Mass Flow Rate (kg/s)
*  REN    = Reynolds Number
*  DIA    = Pipe Diameter (m)
*  VIS    = Viscosity (m**2/s)
*  RHO    = Liquid Density (kg/m**3)
*  FRI    = Friction Factor
*  HED    = Head Loss (m of liquid)
*  DPR    = Pressure Drop across pipe
*  GRA    = Gravity (m/s**2)
*  T1, T2, P1, P2 = Pressure and Temperature Inlet & Outlet
*  LGT    = Length of pipe
*  QLS    = Heat Loss from pipe.
*-----*
      VISPP-- = 2.03D-6
      RHOPP-- = 1058.5
      HETPP-- = 9.49E-1/62.5
      GRAPP-- = 9.81
      PIEPP-- = 3.14159
      RENPP-- = (4*M1 PP--) / (PIEPP-- * DIAPP-- * VISPP-- * RHOPP--)
      VELPP-- = (4*M1 PP--) / (PIEPP-- * (DIAPP--**2) * RHOPP--)

      IF ((ICCALC.EQ.1).OR.(TIME.EQ.0)) THEN
C        write (6,++22)t2 pp--,t1 pp--
C+++22  format(1x,'t2 pp-- =',f5.1,' t1 pp-- =',f5.1)
      T2 PP-- = T1 PP--
C        write (6,++23)t2 pp--,t1 pp--
C+++23  format(1x,'t2 pp-- =',f5.1,' t1 pp-- =',f5.1)
      P2 PP-- = P1 PP--
      M2 PP-- = M1 PP--
      GO TO ++10
      ELSE
      CONTINUE
      ENDIF
      IF (RENPP--.LT.2100) THEN
      FRIPP-- = 64 / RENPP--
      ELSE
      IF ((RENPP--.GE.2100).AND.(RENPP--.LE.2300)) THEN
      RENPP-- = 2300
      FRIPP-- = 0.316/(RENPP--**0.25)
      ELSE
      FRIPP-- = 0.316/(RENPP--**0.25)
      END IF
      END IF
      HEDPP-- = (FRIPP--*LGTPP--*(VELPP--**2)) / (2*DIAPP--*GRAPP--)
      DPRPP-- = HEDPP-- * RHOPP-- * GRAPP--
      P2 PP-- = P1 PP-- - DPRPP--
C        write (6,++11)time
C+++11  format (/1x,'time = ',f6.1)
C        write (6,++21)t1 pp--,t2 pp--
C+++21  format(1x,'t1 pp-- =',f5.1,' t2 pp-- =',f5.1)
      T2 PP-- = T1 PP-- - (QLSP--/(PIEPP--*LGTPP--*DIAPP--*HETPP--))

```

```

C      write (6,++20)t1 pp--,t2 pp--
C+++20  format(1x,'t1 pp-- =',f5.1,' t2 pp--=',f5.1)
C      write (6,++30)qlspp--,piepp--
C+++30  format(1x,'qlspp-- =',e6.1,' piepp--=',f5.3)
C      write (6,++40)lgtpp--,diapp--
C+++40  format(1x,'lgtpp-- =',f5.2,' diapp--=',f5.2)
C      write (6,++50)hetpp--
C+++50  format(1x,'hetpp-- =',e6.1)
      M2 PP-- = M1 PP--
++10 CONTINUE
RESUME SORT
END OF MACRO CODE
*-----
*           M A N I F O L D   M A C R O
*-----
DEFINE MACRO = MN, SYMBOL=400
DESCRIPTION = OUTLET MANIFOLD
MACRO INPUTS = P1, T1, M1, P3, T3, M3, P5, T5, M5, P7, T7, M7, NMI,
NMO, PR1, PR2, PR3, PR4
MACRO OUTPUTS = P2  T2  M2  P4  T4  M4  P6  T6  M6  P8  T8
M8
MACRO CODE
STOP SORT
*-----
*  VARIABLES USED
*  P1, T1, M1 = Pressure, temperature and massflow rate in a stream
*  NMI = Number of inlet streams.
*  NMO = Number of outlet streams.
*  PR1-PR4 = Percentage of massflow in pipe.
*-----
      DECLARATION, REAL*8 ZERMN--
      DECLARATION, INTEGER INOMN--, INIMN--
      INOMN-- = NINT(NMOMN--)
      INIMN-- = NINT(NMIMN--)
      IF (INOMN--.EQ.1) THEN
        P2 MN-- = ((PR1MN--*P1 MN--)+ (PR2MN--*P3 MN--)+
$          (PR3MN--*P5 MN--)+ (PR4MN--*P7 MN--))/100
        T2 MN-- = ((PR1MN--*T1 MN--)+ (PR2MN--*T3 MN--)+
$          (PR3MN--*T5 MN--)+ (PR4MN--*T7 MN--))/100
        M2 MN-- = M1 MN-- + M3 MN-- + M5 MN-- + M7 MN--
        ZERMN-- = 0.0
        P4 MN-- = ZERMN--
        T4 MN-- = ZERMN--
        M4 MN-- = ZERMN--
        P6 MN-- = ZERMN--
        T6 MN-- = ZERMN--
        M6 MN-- = ZERMN--
        P8 MN-- = ZERMN--
        T8 MN-- = ZERMN--
        M8 MN-- = ZERMN--
      ELSE
        P2 MN-- = P1 MN--
        P4 MN-- = P1 MN--
        P6 MN-- = P1 MN--
        P8 MN-- = P1 MN--
        T2 MN-- = T1 MN--
        T4 MN-- = T1 MN--
        T6 MN-- = T1 MN--
        T8 MN-- = T1 MN--
        M2 MN-- = PR1MN--*M1 MN-- / 100
        M4 MN-- = PR2MN--*M1 MN-- / 100
        M6 MN-- = PR3MN--*M1 MN-- / 100
        M8 MN-- = PR4MN--*M1 MN-- / 100
      ENDIF
RESUME SORT
END OF MACRO CODE

```

```

*-----
MODEL DESCRIPTION = SPACE STATION CBC POWER GENERATION SYSTEM
*-----
*      ANALYTIC FUNCTION GENERATOR FOR
*      GAS INLET TEMPERATURES.
*-----
*LOCATION = 201, TB02
*-----
*      P I P E   F R O M   H X   T O   R A D I A T O R
*-----
LOCATION = 51, PP01
INPUTS = MN04(T2-T1), MN04(P2-P1), MN04(M2-M1)
*-----
*      R A D I A T O R   I N L E T   M A N I F O L D
*-----
LOCATION = 42, MN01
INPUTS = PP01(P2-P1), PP01(T2-T1), PP01(M2-M1)
*-----
*      S I N K   T E M P E R A T U R E   T A B L E
*-----
LOCATION = 206, TB01
*-----
*      R A D I A T O R   P A N E L   #1
*-----
LOCATION = 34, RD01
INPUTS = MN01(T2-T1), MN01(P2-P1), MN01(M2-M1), TB01(S,2-TSK)
*-----
*      R A D I A T O R   P A N E L   #2
*-----
LOCATION = 26, RD02
INPUTS = MN01(T4-T1), MN01(P4-P1), MN01(M4-M1), TB01(S,2-TSK)
*-----
*      R A D I A T O R   P A N E L   #3
*-----
LOCATION = 14, RD03
INPUTS = MN01(T6-T1), MN01(P6-P1), MN01(M6-M1), TB01(S,2-TSK)
*-----
*      R A D I A T O R   P A N E L   #4
*-----
LOCATION = 6, RD04
INPUTS = MN01(T8-T1), MN01(P8-P1), MN01(M8-M1), TB01(S,2-TSK)
*-----
*      R A D I A T O R   O U T L E T   M A N I F O L D
*-----
LOCATION = 48, MN02
INPUTS = RD01(T2-T1), RD01(P2-P1), RD01(M2-M1),
        RD02(T2-T3), RD02(P2-P3), RD02(M2-M3),
        RD03(T2-T5), RD03(P2-P5), RD03(M2-M5),
        RD04(T2-T7), RD04(P2-P7), RD04(M2-M7)
*-----
*      P I P E   F R O M   R A D I A T O R   T O   P U M P
*-----
LOCATION = 60, PP02
INPUTS = MN02(M2-M1), MN02(P2-P1), MN02(T2-T1)
*-----
*      Tabular function to generate Mass Flow Rate.
*-----
LOCATION = 210, TB03
*-----
*      P U M P
*-----
LOCATION = 80, FOPU, INPUTS = P2 PP02, M2 PP02, T2 PP02, S2 TB03
ADD PARAMETERS = PDESIR, IMOPU
ADD TABLES = PERF
*ADD VARIABLES = TOPU
ADD STATES = POPU, MOPU, TOPU

```

FORTRAN STATEMENTS

```

      POPU = PDESIR
      PDEL = POPU - P2PP02
      MOPU = S2 TB03
      IF (ICCALC.EQ.1) THEN
        MOPU = IMOPU
        POPU = PDESIR
        TOPU = T2 PP02
      ELSE
        CONTINUE
      ENDIF
      TOPU = T2 PP02
      DERIVATIVE OF, POPU = INVENT*DUM2
      DERIVATIVE OF, MOPU = INVENT*DUM2
      DERIVATIVE OF, TOPU = INVENT*DUM2
*-----
*   H E A T   E X C H A N G E R   I N L E T   M A N I F O L D
*-----
LOCATION = 77, MN03
INPUTS = FOPU(MOPU=M1), FOPU(POPU=P1), FOPU(TOPU=T1)
*-----
*   G A S   C O O L E R   ( H X 0 1 )
*-----
LOCATION = 74, HX01
INPUTS = HX03(LP2=GP3), HX03(LM2=GM3), HX03(LT2=GT3),
MN03(P2=LP1), MN03(T2=LT1), MN03(M2=LM1)
*-----
*   B L E E D   C O O L E R   ( H X 0 2 )
*-----
*LOCATION = 57, HX02
*INPUTS = TB02(S,3=GP3), TB07(S,3=GM3), TB02(S,2=GT3),
*MN03(P4=LP1), MN03(T4=LT1), MN03(M4=LM1)
*-----
*   H E A T   E X C H A N G E R   O U T L E T   M A N I F O L D
*-----
LOCATION = 54, MN04
INPUTS = HX01(LT2=T1), HX01(LP2=P1), HX01(LM2=M1)
*, HX02(LT2=T3), HX02(LP2=P3), HX02(LM2=M3)
*-----
*   R E C U P E R A T O R   ( H X 0 3 )
*-----
LOCATION = 115, HX03
INPUTS = FOTR(TRPROUT=LP1), FOTR(TRTPOUT=LT1), FOTR(TRMFOUT=LM1),
FOCR(CRPROUT=GP3), FOCR(CRTPOUT=GT3), FOCR(CRMFOUT=GM3)
*-----
*   S O L A R   R E C E I V E R   ( R X 0 1 )
*-----
LOCATION = 118, RX01
INPUTS = HX03(GT4=GT3), HX03(GP4=GP3), HX03(GM4=GM3), TB05(S,3=BT1)
*-----
*   T A B L E   F O R   R E C E I V E R   T E M P   ( T B 0 5 )
*-----
LOCATION = 208, TB05
*-----
*   G A S   T U R B I N E
*-----
LOCATION = 139, FOTR, INPUTS = GT4RX01, GP4RX01, GM4RX01
ADD PARAMETERS = PRATTR, ETATR, CPTR, RTR, IMFTRIN, ITPTRIN, IPTRIN,
SWITCHT
ADD VARIABLES = WTURB, MINDEST, MINTDL
ADD STATES = TRPROUT, TRMFOUT, TRTPOUT
FORTRAN STATEMENTS
      DECLARATION, REAL*8 PINT, TINT, MINT, DUMMY, TOUTT, POUTT, MOUTT
      PINT = GP4RX01
      TINT = GT4RX01
      MINT = GM4RX01

```

```

      IF ((SWITCHT.EQ.1.).AND.(TIME.EQ.0.)) THEN
        MINDEST = (MINT * (TINT ** 0.5)/PINT)
      ELSE
        CONTINUE
      ENDIF
      IF (SWITCHT.NE.1.) GO TO 52
      MINTDL = (MINT * (TINT ** 0.5)/PINT) / MINDEST
52 CONTINUE
C-----
C   If simulation goes off the turbine map, i.e. the turbine
C   surges or stalls, the run is stopped and all data is saved.
C-----
      IF ((SWITCHT.EQ.1.).AND.((MINTDL.LT.0.45).OR.(MINTDL.GT.1.1)))
+ THEN
        ISTOP=1
        PRINT*, 'ABORT IN TURBINE'
      ELSE
        CONTINUE
      ENDIF
      IF (ICCALC.EQ.1) THEN
        MINT = IMFTRIN
        TINT = ITPTRIN
        PINT = IPTRIN
        TOUTT = TINT
        POUTT = PINT
        MOUTT = MINT
      ELSE
        IF (TIME.EQ.0.) GO TO 51
        TOUTT = TINT / (PRATTR*(ETATR*RTR/CPTR))
        MOUTT = MINT
      ENDIF
51 CONTINUE
      POUTT = PINT / PRATTR
      TRTPOUT = TOUTT
      TRPROUT = POUTT
      TRMFOUT = MOUTT
      WTURB = MINT * CPTR * (TINT - TRTPOUT)
      DERIVATIVE OF, TRPROUT = DUMMY
      DERIVATIVE OF, TRMFOUT = DUMMY
      DERIVATIVE OF, TRTPOUT = DUMMY
C-----
*           A L T E R N A T O R           P O W E R
C-----
      LOCATION = 134, FOAL, INPUTS = WTURB, WCOMP
      ADD PARAMETERS = ETAAL, SWITCHA
      ADD VARIABLES = POWER
      FORTRAN STATEMENTS
        POWER = ETAAL * (WTURB - WCOMP)
        IF ((POWER.LT.0.).AND.(SWITCHA.EQ.1.))
+ THEN
          ISTOP=1
          PRINT*, 'ZERO POWER - SYSTEM SHUT DOWN'
        ELSE
          CONTINUE
        ENDIF
C-----
*           C O M P R E S S O R
C-----
      LOCATION = 131, FOCR, INPUTS = GT4HX01, GP4HX01, GM4HX01
      ADD PARAMETERS = PRATCR, ETACR, CPCR, RCR, ITPCRIN, IMFCRIN, IPRCRIN,
      SWITCHR
      ADD VARIABLES = WCOMP, MINDES, MINRDL
      ADD STATES = CRPROUT, CRMFOUT, CRTPOUT
      FORTRAN STATEMENTS
        DECLARATION, REAL*8 PINR, TINR, MINR, DUMMY2, TOUTR, POUTR, MOUTR
        PINR = GP4HX01

```



```

TINR = GT4HX01
MINR = GM4HX01
IF ((SWITCHR.EQ.1.).AND.(TIME.EQ.0.)) THEN
    MINDESR = (MINR * (TINR ** 0.5)/PINR)
ELSE
    CONTINUE
ENDIF
IF (SWITCHR.NE.1.) GO TO 02
    MINRDL = (MINR * (TINR ** 0.5)/PINR) / MINDESR
02 CONTINUE
C-----
C   If simulation goes off the compressor map, i.e. the compressor
C   surges or stalls, the run is stopped and all data is saved.
C-----
    IF ((SWITCHR.EQ.1.).AND.((MINRDL.LT.0.75).OR.(MINRDL.GT.1.6)))
    + THEN
        ISTOP=1
        PRINT*, 'ABORT IN COMPRESSOR'
    ELSE
        CONTINUE
    ENDIF
    IF (ICCALC.EQ.1) THEN
        MINR = IMFCRIN
        TINR = ITPCRIN
        PINR = IPRCRIN
        TOUTR = TINR
        POUTR = PINR
        MOUTR = MINR
    ELSE
        IF (TIME.EQ.0.) GO TO 01
        TOUTR = TINR * (PRATCR** (RCR/(CPCR*ETACR)))
        MOUTR = MINR
    ENDIF
01 CONTINUE
    POUTR = PINR * PRATCR
    CRPROUT = POUTR
    CRTPOUT = TOUTR
    CRMFOUT = MOUTR
    WCOMP = MINR * CPCR * (CRTPOUT - TINR)
    DERIVATIVE OF, CRPROUT = DUMMY2
    DERIVATIVE OF, CRTPOUT = DUMMY2
    DERIVATIVE OF, CRMFOUT = DUMMY2
END OF MODEL
PLOT SCHEMATIC
PRINT SCHEMATIC

```

APPENDIX 8.2

Film Coefficient Calculations

The film coefficient  $h$ , was calculated by first computing the Reynolds number  $Re$ ,

$$Re = \frac{vD\rho}{\mu}$$

where

$v$  = velocity  
 $D$  = Diameter  
 $\mu$  = Viscosity

and the Prandtl number  $Pr$ ,

$$Pr = \frac{\mu c_p}{k}$$

where

$c_p$  = specific heat at constant pressure  
( $c$  for liquids)  
 $k$  = thermal conductivity

The Nusselt number  $Nu$ , is then calculated (reference 11),

$$Nu = 0.0155 (Pr)^{0.5} (Re)^{0.83}$$

Finally,

$$h = Nu \frac{k}{D}$$

The sensitivity of  $h$  to changes in fluid properties with temperature was examined to determine whether  $h$  could be specified as an input parameter for a model or would require dynamic computation during code execution. A change of 100 K about normal design conditions results in a 3% change in  $h$ ; well within the accuracy range for this formulation. Therefore  $h$  was included as a parameter in the EASY5 analysis file.

# APPENDIX 8.3

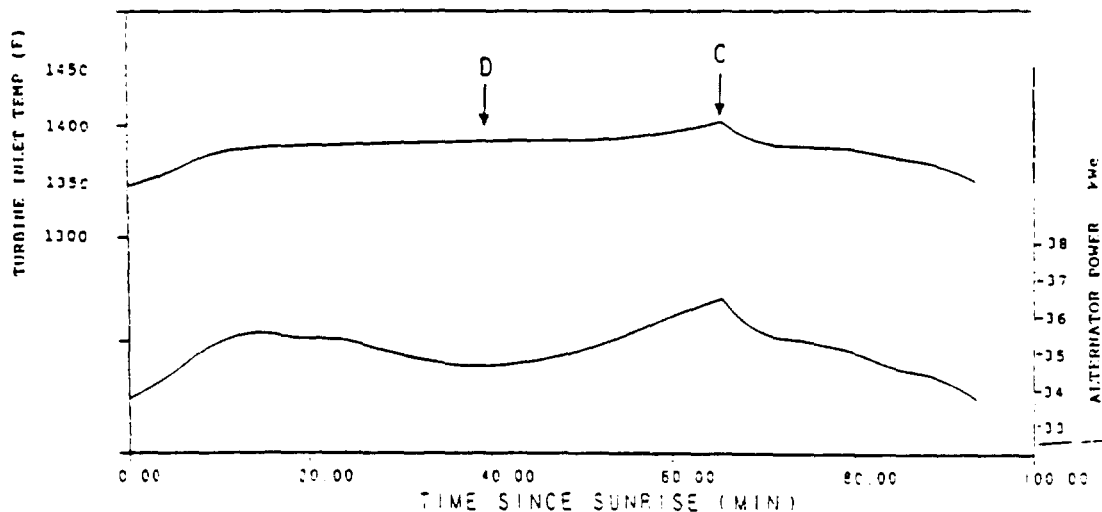
## CBC SUBSYSTEM PERFORMANCE OVER ONE ORBIT

FLUX IN = 207.8 KW  
INVENTORY = 2.630C LBM  
DATE RUN 20-NOV-86

TIME SINCE SUNRISE	MELT FRAC	T1 (R)	T2	T6P	THAX	SINK TEMP	VS (LBM/S)	GAG (KW)	P1 (PSI)	P2	QIN (KW)	E-STORED (KW-MIN)
07.00	.0341	605.67	1450.02	1801.00	1872.03	351.44	2.7438	33.32	45.63	79.60	126.1	0.
4.68	.0325	606.28	1463.24	1818.04	1880.48	346.77	2.7522	34.25	45.89	80.05	127.9	30.
9.37	.0640	606.92	1475.41	1833.61	1884.73	343.14	2.7595	35.08	46.13	80.46	129.4	593.
14.05	.1366	606.74	1479.78	1839.41	1885.06	339.17	2.7618	35.44	46.18	80.57	130.1	880.
18.74	.2075	608.45	1481.70	1840.91	1888.38	350.14	2.7612	35.29	46.30	80.67	129.9	1167.
23.42	.2650	609.16	1482.67	1841.75	1890.74	354.97	2.7595	35.25	46.32	80.66	129.7	1455.
28.11	.3180	611.69	1484.62	1842.60	1893.27	369.86	2.7573	34.93	46.48	80.78	129.2	1744.
32.79	.3683	613.64	1485.98	1843.17	1897.24	380.20	2.7554	34.67	46.60	80.85	128.9	2035.
37.47	.4221	615.03	1487.20	1843.86	1897.96	386.67	2.7553	34.50	46.72	80.96	128.7	2327.
42.16	.4647	615.02	1487.67	1844.45	1903.23	386.67	2.7548	34.55	46.70	80.94	128.7	2619.
46.84	.5120	613.72	1487.29	1844.80	1904.92	379.36	2.7577	34.75	46.67	80.95	129.1	2911.
51.52	.5572	611.61	1486.69	1845.29	1909.87	368.19	2.7586	35.06	46.53	80.85	129.5	3201.
56.20	.5996	609.92	1488.10	1848.35	1924.69	355.47	2.7643	35.52	46.50	80.93	130.4	3487.
60.88	.6327	608.65	1491.30	1853.38	1943.85	344.66	2.7679	36.00	46.49	81.01	131.2	3766.
65.54	.6640	608.98	1497.62	1861.44	1955.84	343.87	2.7698	36.42	46.58	81.16	132.0	4037.
70.22	.6107	607.78	1481.98	1841.70	1875.66	344.85	2.7627	35.43	46.29	80.69	130.1	336.
74.90	.4977	607.90	1479.37	1838.15	1875.59	348.68	2.7587	35.20	46.20	80.55	129.6	2687.
79.58	.3689	608.66	1478.01	1835.79	1875.43	354.26	2.7578	34.93	46.25	80.56	129.2	2013.
84.27	.2594	608.39	1472.31	1828.36	1875.09	357.38	2.7520	34.68	46.11	80.32	128.3	1342.
88.95	.1415	607.78	1466.56	1821.31	1873.67	355.54	2.7512	34.20	46.01	80.18	127.8	687.
93.63	.0577	605.90	1454.05	1806.02	1872.51	351.48	2.7440	33.56	45.67	79.69	126.5	38.
98.37	.0572	605.85	1453.63	1805.57	1872.49	351.44	2.7437	33.54	45.66	79.67	126.4	32.
0.00	.0572	605.83	1453.64	1805.54	1872.63	351.44	2.7437	33.54	45.66	79.67	126.4	32.
4.68	.0623	606.16	1463.50	1818.43	1879.99	346.77	2.7507	34.28	45.85	80.00	127.8	340.

### LEGEND:

- MELT FRAC = FRACTION OF SALT IN RECEIVER THAT IS LIQUID
- T1 = TEMPERATURE INTO COMPRESSOR (R)
- T2 = TEMPERATURE INTO RECEIVER
- T6P = TEMPERATURE OUT OF RECEIVER
- THAX = MAXIMUM RECEIVER TEMPERATURE
- SINK TEMP = SINK TEMPERATURE
- VS = MASS FLOW RATE AT RECEIVER (LBM/S)
- GAG = GROSS ALTERNATOR OUTPUT (KW)
- P1 = PRESSURE INTO COMPRESSOR
- P2 = PRESSURE OUT OF COMPRESSOR
- QIN = ENERGY INTO WORKING FLUID
- E-STORED = NET ENERGY STORED IN RECEIVER SINCE SUNRISE



9. BIBLIOGRAPHY

1. Niggeman, R. E., McKenna, R. F., Choudoir, D. W., Thallet, P. A., "A Solar Dynamic Power Conversion System for the Space Station", AIAA paper 85-1480, 21st Joint Propulsion Conference, July 8-10, 1985.
2. Boeing Computer Services, "EASY5 Engineering Analysis System Reference Manual", The Boeing Company, Second Edition, December, 1987.
3. Thal-Larsen, H., "Dynamics of Heat Exchangers and Their Models", Transactions of the ASME, Journal of Basic Engineering, June, 1960, pp. 489-504.
4. Myers, G. E., Mitchell, J. W., Norman, R. F., "The Transient Response of Crossflow Heat Exchangers, Evaporators, and Condensers", Transactions of the ASME, Journal of Heat Transfer, February, 1967, pp. 75-80.
5. Romie, F. E., "Transient Response of the Counterflow Heat Exchanger", Transactions of the ASME, Vol. 106, August, 1984, pp. 620-626.
6. Binz, E. and Hartung, J., "Solar Dynamic Power for the Space Station, IOC", American Chemical Society paper 869477, pp.2072-2076.
7. Rocketdyne, "Space Station Work Package WP-04 Power System Preliminary Analysis and Design Document", Rocketdyne RI/RD85-320-2, December, 1986. (AKA DR02 Documument)
8. Pearson, R., Dabrowski, D., "Optomization of Heat Rejection Subsystems for Solar Dynamic Brayton Cycle Power System", SAE paper 860999.
9. Hoffmann, K. A., "Computational Fluid Dynamics for Engineers", Engineering Education System, 1989.
10. Kern, D. Q., Kraus, A. D., "Extended Surface Heat Transfer", McGraw Hill Book Company, 1972.
11. Reynolds, W. C., Perkins, H. C. "Engineering Thermodynamics", McGraw Hill Book Company, 1970.
12. Faires V. M., Simmang, C. M., "Thermodynamics", McMillian Publishing Company, 6th edition, 1978.

13. Gerhart, P. M., Gross, R. J., "Fundamentals of Fluid Mechanics", Addison-Wesley Publishing Co., July, 1985.
14. Ali, M. S., "Lumped Parameter, Compressible, Transient Turbomachinery Models", Master's Thesis, Washington University, 1989.
15. Heywood, J. B., "Internal Combustion Engine Fundamentals", McGraw-Hill, Inc., 1988.
16. Horman, "Gas Turbine Engineering", 1981.

10. VITA

Biographical items on the author of the thesis, Mr. A. Iqbal

- 1) Born [REDACTED] in [REDACTED], [REDACTED]
- 2) Attended St. Mary's Academy, Rawalpindi, Pakistan. Received Cambridge University "O" Level Overseas Examination Certificate in December 1977.
- 3) Attended Aitchison College, Lahore, Pakistan. Received Cambridge University "A" Level Overseas Examination Certificate in December 1979.
- 4) Attended the Massachusetts Institute of Technology, Cambridge, Massachusetts. Received an S.B. in Aeronautics and Astronautics in June 1984.
- 5) Engineer, General Motors Corporation, Truck and Bus Group, Pontiac, MI, June 1984 to August 1986.
- 6) Attended Washington University, St. Louis, MO from January 1987 to January 1989 as a full-time student. Research Assistant June 1987 to January 1989. Continued till present as part-time graduate student.
- 7) Engineer, Structural Research, McDonnell Douglas Corporation, February 1989 to present.

May 1990

Short Title:      Solar Dynamic CBC Transient Model      Iqbal, M.Sc. 1990

## **Appendix B**

### **Modeling of Transient Thermodynamic Performance of Compressible Flow Turbomachines**



WASHINGTON UNIVERSITY  
SEVER INSTITUTE OF TECHNOLOGY

---

MODELING OF TRANSIENT THERMODYNAMIC PERFORMANCE  
OF COMPRESSIBLE FLOW TURBOMACHINES

by

MOHAMMAD SAMAD ALI

Prepared under the direction of

Dr. John I. Hochstein  
and  
Dr. Theodosios P. Korakianitis

---

A thesis presented to the Sever Institute of  
Washington University in partial fulfillment  
of the requirements for the degree of

MASTER OF SCIENCE

May, 1990

Saint Louis, Missouri

WASHINGTON UNIVERSITY  
SEVER INSTITUTE OF TECHNOLOGY

---

ABSTRACT

---

MODELING OF TRANSIENT THERMODYNAMIC PERFORMANCE  
OF COMPRESSIBLE FLOW TURBOMACHINERY

by Mohammad Samad Ali

---

ADVISORS:

Dr. John I. Hochstein  
Dr. Theodosios P. Korakianitis

---

May, 1990

Saint Louis, Missouri

---

The development of simple transient compressible turbomachinery models for the space station - closed Brayton cycle - power module is presented. The models employ simplified continuity, energy, moment-of-momentum, and polytropic equations. These simplified models do not neglect compressible flow physics. Total temperature, total pressure, and mass flow rate were selected as the state variables. In the absence of experimental data, the best model was identified on the basis of model response to simple input transients.

TABLE OF CONTENTS

No.	Page
1. Introduction.....	1
1.1 Closed Brayton Cycle.....	2
1.2 Control of the SDPCS.....	6
1.3 Classification of Thermodynamic Transients.....	9
2. Modeling Philosophy and Governing Equations.....	11
2.1 Modeling Philosophy.....	11
2.2 Governing Equations.....	12
3. Model Development and Simulation.....	18
3.1 Literature Review.....	19
3.2 Modeling Techniques.....	25
3.3 The State-Average Model.....	28
3.4 The Constant-Mach-Number-in-the-Middle Model.....	44
3.5 Choice of Integrator.....	56
3.6 The Upwind-Mass-Flow Model.....	63
3.6.1 Constant-Speed Variable-Rate-of-Work Model...	66
3.7 Outlet Response Dynamics.....	73
3.8 The Sliced Model.....	77
3.9 The State-Average Lagged-Mass-Flow-Rate Model.....	89
3.9.1 Constant-Speed Variable-Rate-of-Work Model...	90
3.9.2 Constant-Rate-of-Work Variable-Speed Model...	118
4. Discussion.....	130
5. Summary and Conclusions.....	133

6. Acknowledgements.....	135
7. Bibliography.....	136
8. Vita.....	138

LIST OF TABLES

No.	Page
1. Data for results presented in figures 10 - 16.....	33
2. Data for results presented in figures 18 - 24.....	47
3. Data for results presented in figures 25 - 28.....	57
4. Data for results presented in figures 31 - 34.....	67
5. Data for results presented in figures 39 - 42.....	83
6. Data for results presented in figures 45 - 48.....	93
7. Data for results presented in figures 49 - 51.....	100
8. Data for results presented in figures 52 - 63.....	105
9. Data for results presented in figures 64 - 67.....	119
10. Data for results presented in figures 68 - 71.....	125

LIST OF FIGURES

No.	Page
1.	The closed brayton cycle T-S diagram.....3
2.	The closed brayton cycle component configuration. The solid line shows the path of fluid flow. The dashed line shows the path of electrical signal.....4
3.	The inventory control schematic.....8
4.	General control volume.....13
5.	Control volume for moment of momentum equation, compressor shown.....15
6.	Greitzer's model schematic, reproduced from reference 11, page 192.....23
7.	Compressor, total-to-total polytropic efficiency map.....26
8.	Turbine, total-to-total polytropic efficiency map.....27
9.	The state-average model algorithm.....29
10.	Response of the outlet total temperature of the compressor to a step input of 0.1 K in inlet total temperature. Time step is 0.075 ms.....34
11.	Response of the outlet total temperature of the compressor to a step input of 5.0 K in inlet total temperature. Time step is 0.075 ms.....35
12.	Response of the outlet total temperature of the compressor to a step input of 20 K in inlet total temperature. Time step is 0.075 ms.....36
13.	Response of the outlet total temperature of the compressor to a step input of 50 K in inlet total temperature. Time step is 0.075 ms.....37
14.	Response of the outlet total temperature of the compressor to a step input of 100 K in inlet total temperature. Time step is 0.0375 ms.....38
15.	Response of the outlet total temperature of the compressor to a step input of 100 K in inlet total temperature while $dm/dt = 0$ in the compressor. Time step size is 0.01875 ms.....39

16.	The effect of $dm/dt$ on the response of the outlet total temperature of the compressor to a step input of 100 K in inlet total temperature. Time step is 0.075 ms.....	40
17.	Algorithm for the constant-mach-number-in-the-middle model.....	45
18.	Response of the outlet total temperature of the turbine to ramps described by table 2. Time step is 1 micro second.....	48
19.	Response of the middle total temperature of the turbine to ramps described by table 2. Time step is 1 micro second.....	49
20.	Response of the outlet total pressure of the turbine to ramps described by table 2. Time step is 1 micro second.....	50
21.	Response of the middle total pressure of the turbine to ramps described by table 2. Time step is 1 micro second.....	51
22.	Response of the outlet mass-flow rate of the turbine to ramps in described by table 2. Time step is 1 micro second.....	52
23.	Response of the middle mass-flow rate of the turbine to ramps described by table 2. Time step is 1 micro second.....	53
24.	Response of the middle and outlet mass-flow rate of the turbine to ramps described by table 2. Time step is 1 micro second.....	54
25.	Response of the outlet total temperature for the compressor to step input of 1 K in inlet total temperature. Time step is 1 micro second.....	58
26.	Expanded view of the response of outlet total temperature for the compressor to step input of 1 K in inlet total temperature. Time step of integration is 1 micro second.....	59
27.	Response of the outlet mass-flow rate for the compressor to step input of 1 K in inlet total temperature. Time step is 1 micro second.....	60

28.	Expanded view of the response of outlet mass-flow rate for the compressor to step input of 1 K in inlet total temperature. Time step of integration is 1 micro second.....	61
29.	Algorithm for variable-rate-of-work constant-speed-model.....	64
30.	Algorithm for constant-rate-of-work variable-speed-model.....	65
31.	Response of the outlet mass-flow rate for the turbine to ramps described by table 4. The three plots shown correspond to time steps of 5 micro seconds, 10 micro seconds, and 50 micro seconds.....	68
32.	Response of the rate of work output for the turbine to ramps described by table 4. The three plots shown correspond to time steps of 5 micro seconds, 10 micro seconds, and 50 micro seconds.....	69
33.	Response of the outlet total pressure, for the turbine, to ramps described by table 4. The three plots shown correspond to time steps of 5 micro seconds, 10 micro seconds, and 50 micro seconds.....	70
34.	Response of the outlet total temperature, for the turbine, to ramps described by table 4. The three plots shown correspond to time steps of 5 micro seconds, 10 micro seconds, and 50 micro seconds.....	71
35.	A duct representing a simplified turbomachine control volume.....	73
36.	Longitudinal section of turbomachine rotor.....	75
37.	The sliced model nodal temperature distribution.....	80
38.	Algorithm for variable-rate-of-work constant-speed-model.....	82
39.	Response of the outlet mass-flow rate for the turbine to ramps described by table 5. The three plots shown correspond to time steps of 0.5 micro seconds, 5 micro seconds, and 50 micro seconds.....	84



40.	Response of the middle mass-flow rate for the turbine to ramps described by table 5. The three plots shown correspond to time steps of 0.5 micro seconds, 5 micro seconds, and 50 micro seconds.....	85
41.	Response of the outlet total pressure, for the turbine, to ramps described by table 5. The three plots shown correspond to time steps of 0.5 micro seconds, 5 micro seconds, and 50 micro seconds.....	86
42.	Response of the outlet total temperature, for the turbine, to ramps described by table 5. The three plots shown correspond to time steps of 0.5 micro seconds, 5 micro seconds, and 50 micro seconds.....	87
43.	Algorithm for the state-average lagged-mass-flow-rate constant-speed variable-rate-of-work model.....	91
44.	Algorithm for the state-average lagged-mass-flow-rate constant-rate-of-work variable-speed model.....	92
45.	Response of the outlet mass-flow rate for the turbine to ramps described by table 6. The three plots shown correspond to time steps of 0.5 micro seconds, 5 micro seconds, and 50 micro seconds.....	95
46.	Response of the rate of work output for the turbine to ramps described by table 6. The three plots shown correspond to time steps of 0.5 micro seconds, 5 micro seconds, and 50 micro seconds.....	96
47.	Response of the outlet total pressure, for the turbine, to ramps described by table 6. The three plots shown correspond to time steps of 0.5 micro seconds, 5 micro seconds, and 50 micro seconds.....	97
48.	Response of the outlet total temperature, for the turbine, to ramps described by table 6. The three plots shown correspond to time steps of 0.5 micro seconds, 5 micro seconds, and 50 micro seconds.....	98
49.	Response of the total temperature, for the turbine, to ramps described by table 7. The time step is 5 micro seconds.....	101

50. Response of the total pressure, for the turbine, to ramps described by table 7. The time step is 5 micro seconds.....102
51. Response of the mass-flow rate, for the turbine, to ramps described by table 7. The time step is 5 micro seconds.....103
52. Response of the mass-flow rate, for the turbine, to sinusoidal input described by table 8. The time step is 1 micro seconds. Frequency is 2000 Hz....106
53. Response of the total temperature, for the turbine, to sinusoidal input described by table 8. The time step is 1 micro seconds. Frequency is 2000 Hz....107
54. Response of the total pressure, for the turbine, to sinusoidal input described by table 8. The time step is 1 micro seconds. Frequency is 2000 Hz....108
55. Response of the mass-flow rate, for the turbine, to sinusoidal input described by table 8. The time step is 1 micro seconds. Frequency is 1000 Hz....109
56. Response of the total temperature, for the turbine, to sinusoidal input described by table 8. The time step is 1 micro seconds. Frequency is 1000 Hz....110
57. Response of the total pressure, for the turbine, to sinusoidal input described by table 8. The time step is 1 micro seconds. Frequency is 1000 Hz....111
58. Response of the mass-flow rate, for the turbine, to sinusoidal input described by table 8. The time step is 1 micro seconds. Frequency is 500 Hz.....112
59. Response of the total temperature, for the turbine, to sinusoidal input described by table 8. The time step is 1 micro seconds. Frequency is 500 Hz.....113
60. Response of the total pressure, for the turbine, to sinusoidal input described by table 8. The time step is 1 micro seconds. Frequency is 500 Hz.....114
61. Response of the mass-flow rate, for the turbine, to sinusoidal input described by table 8. The time step is 1 micro seconds. Frequency is 50 Hz.....115
62. Response of the total temperature, for the turbine, to sinusoidal input described by table 8. The time step is 1 micro seconds. Frequency is 50 Hz.....116

- 63. Response of the total pressure, for the turbine, to sinusoidal input described by table 8. The time step is 1 micro seconds. Frequecny is 50 Hz.....117
- 64. Response of the mass-flow rate, for the turbine, to ramp described by table 9. The time step is 10 micro seconds.....120
- 65. Response of the total temperature, for the turbine, to ramp described by table 9. The time step is 10 micro seconds.....121
- 66. Response of the total pressure, for the turbine, to ramp described by table 9. The time step is 10 micro seconds.....122
- 67. Response of the rotor speed of the turbine to ramp described by table 9. The time step is 10 micro seconds.....123
- 68. Response of the mass-flow rate, for the turbine, to sinusoidal input described by table 10. The time step is 1 micro seconds. Frequency is 1000 Hz....126
- 69. Response of the total temperature, for the turbine, to sinusoidal input described by table 10. The time step is 1 micro seconds. Frequency is 1000 Hz....127
- 70. Response of the total pressure, for the turbine, to sinusoidal input described by table 10. The time step is 1 micro seconds. Frequecny is 1000 Hz....128
- 71. Response of the rotor speed of the turbine to sinusoidal input described by table 10. The time step is 1 micro seconds. Frequecny is 1000 Hz....129

NOMENCLATURE

A : area

Ak : friction factor

c : fluid velocity

Cp : specific heat

e : total enthalpy

Ff : frictional force

Fp : pressure force

h : enthalpy

L : characteristic length of control volume

m : mass of gas in control volume

$\dot{m}$  : mass flow rate

n : node number

nod: number of nodes chosen to span the control volume

M : Mach number

p : pressure

Q : rate of heat flow

R : gas constant

T : temperature

$\Delta\tau$  : time required for information to travel from inlet to the node  
being evaluated

V : volume of the control volume

$\rho$  : density

**Subscripts:**

i : inlet  
m : middle  
n : node number  
o : outlet  
s : static  
t : total

**Acronyms:**

CBC : closed Brayton cycle  
ECU : electronic control unit  
IOC : initial operating capability  
PLR : parasitic load radiator  
SALM : state-average lagged-mass-flow-rate model  
SDPCS : solar dynamic power control system  
UMFM : upwind mass flow model

**Symbols:**

$\Sigma$  : Summation

# MODELING OF TRANSIENT THERMODYNAMIC PERFORMANCE OF COMPRESSIBLE FLOW TURBOMACHINERY

## 1. INTRODUCTION

NASA is currently designing a space station to serve as a "permanent" manned facility to support a wide range of activities. The space station will orbit the Earth and provide experimental facilities as well as living quarters for the personnel manning it. 75 KW of electricity is required for the initial operating capability (IOC) of the space station [1]; 23.5 KW will be provided by a photovoltaic module, and the remaining 51.5 KW will be provided by a solar dynamic power conversion system (SDPCS). The 51.5 KW of electrical power is generated by two identical modules using a closed Brayton-cycle engine (CBC). The energy source for the CBC is solar radiation (insolation). Each module provides a nominal output of 25.75 KW and is designed for a peaking power of 28.75 KW. As the future power requirements of the space station grow, the modules will be replicated as required. The components required for the operation of a SDPCS are currently being designed by various contractors. Further details of the CBC system are presented in section 1.1.

The focus of the study reported by this thesis was to develop transient models for the turbine and the compressor, two of the major components of the SDPCS. These models will be used to support development of the control system for the SDPCS. The control scheme is discussed in section 1.2.

### 1.1 CLOSED BRAYTON CYCLE

The solar dynamic power conversion system (SDPCS) modules use the closed Brayton cycle (CBC) engine to convert solar insolation into mechanical power. An alternator converts this power to electricity. Figure 1 shows the thermodynamic closed Brayton cycle on a T-s diagram. Along path 1-2 the compressor raises the pressure and temperature of the working fluid. Between points 2 and 3, the temperature of the working fluid rises in the cold side of the recuperator. Energy is transferred from the receiver to the working fluid between points 3 and 4. From 4 to 5, the temperature and pressure of the working fluid are reduced in the turbine to produce work. Between points 5 and 6 the temperature of the working fluid decreases in the hot side of the recuperator. To complete the cycle, the working fluid is cooled in the gas cooler between points 6 and 1.

Figure 2 presents a schematic of the CBC hardware which shows the flow direction of the working fluid. Figure 2 also shows the electronic control unit (ECU) and the parasitic load radiator (PLR). The dashed line denotes an electronic signal. The compressor, turbine, and alternator are on the same shaft and hence have the same angular speed. Solar energy is collected by the concentrator which focuses incident radiation onto a receiver containing phase change

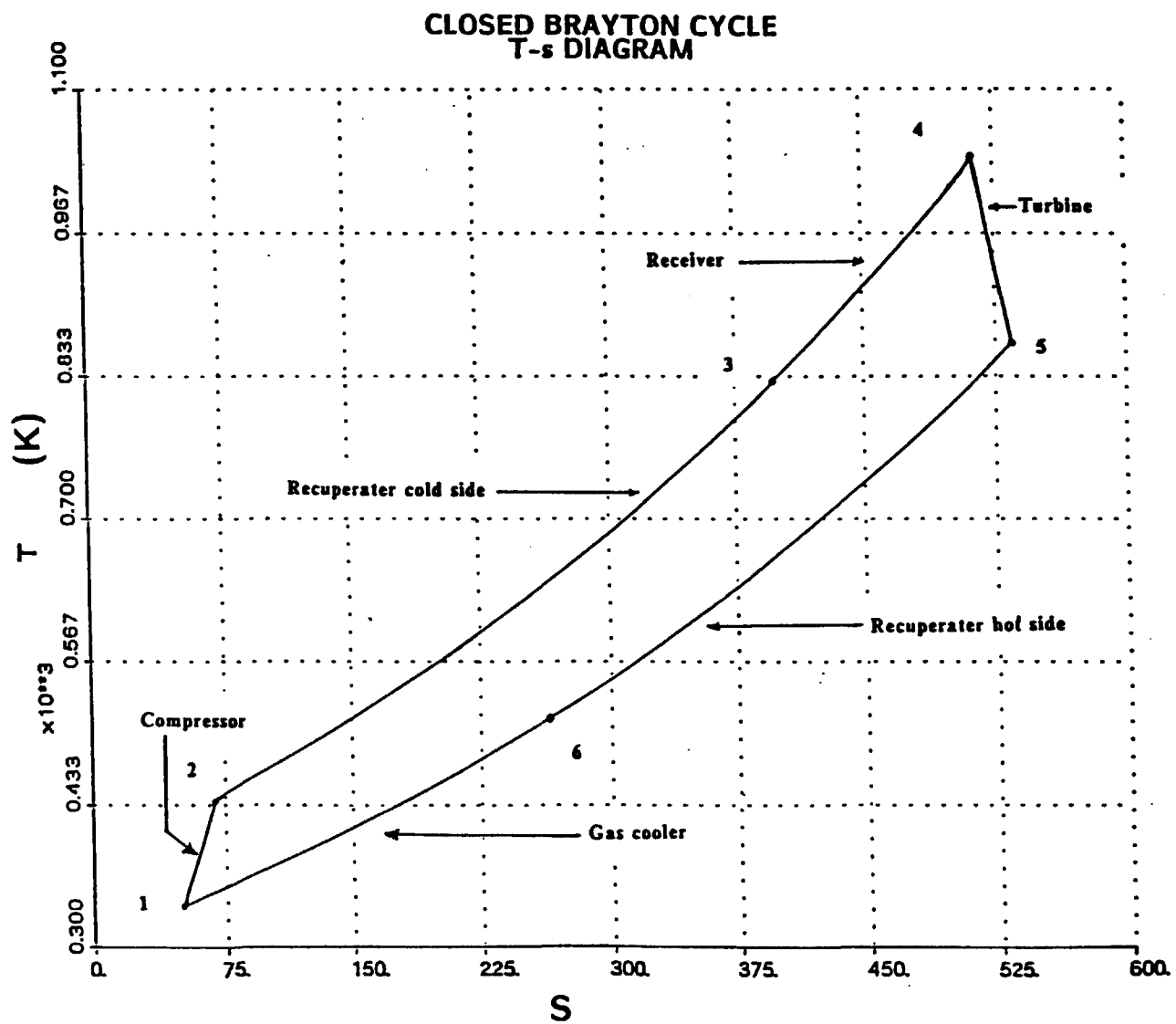


Figure 1. The closed brayton cycle T-S diagram.



# Brayton Cycle Component Configuration

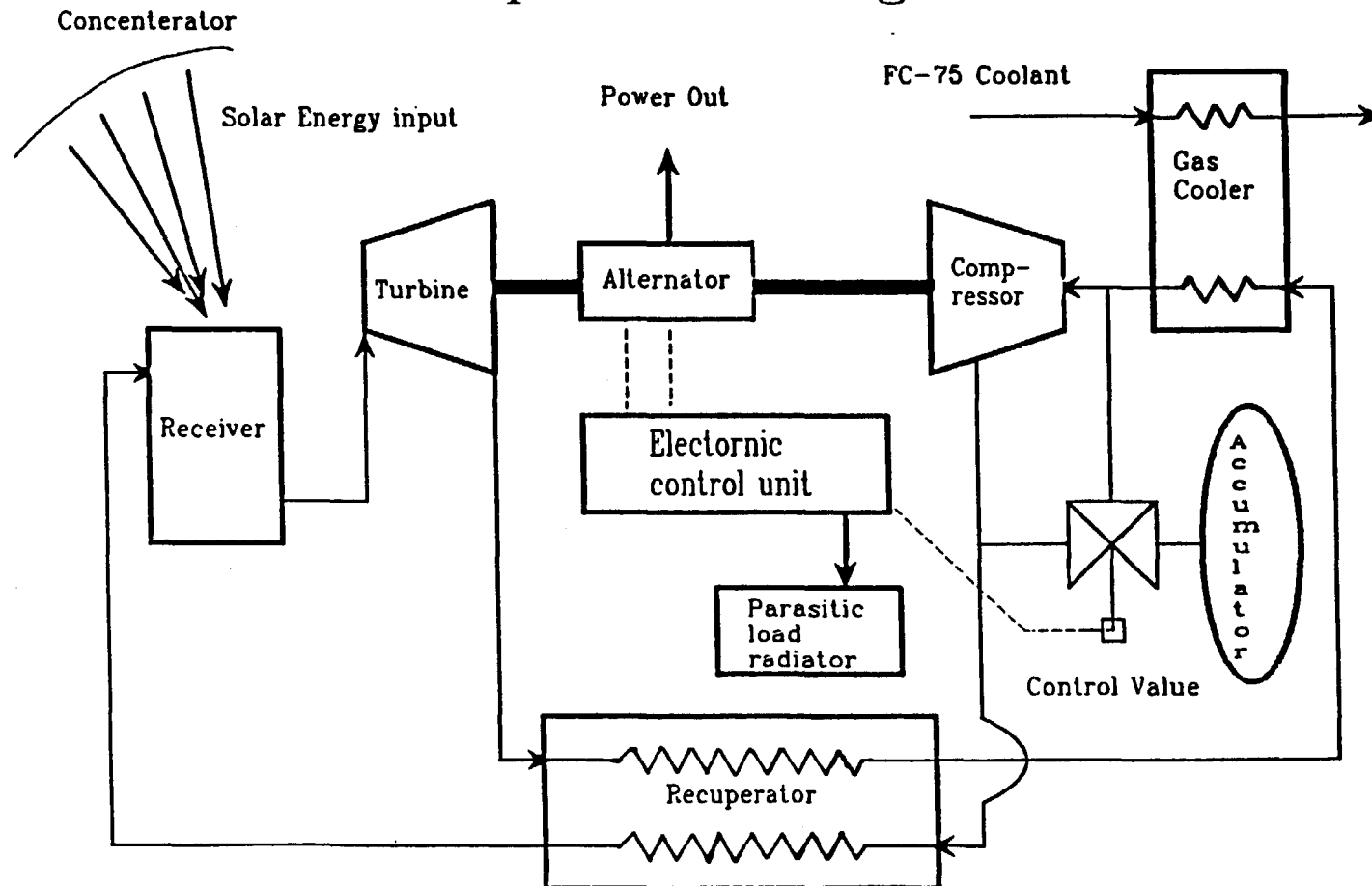


Figure 2. The closed brayton cycle component configuration. The solid line shows the path of fluid flow. The dashed line shows the path of electrical signal.

eutectic salts. The eutectic salts act as a thermal energy storage device. This stored energy is used to maintain constant power output even when the space station experiences variations in solar insolation. These variations periodically occur due to the changing distance between the sun and the space station. For a period of time during each orbit the space station is in the shadow (eclipse) of the Earth. During an eclipse, the solar insolation is virtually zero. Therefore, during the eclipse phase of the orbit, the energy stored in the eutectic salts provides the thermal energy required to power the CBC system.

The helium-xenon (He-Xe) working fluid extracts thermal energy from the receiver and then enters the turbine. As the fluid passes through the turbine it expands to produce shaft work and the temperature of the fluid decreases. The low pressure gas then passes through the hot side of the recuperator and gives up energy to the cold-side fluid. From the recuperator, the He-Xe mixture flows through the gas cooler where the working fluid is further cooled. The cold He-Xe mixture then enters the compressor where work is done on the fluid resulting in increased pressure and slightly increased temperature. The fluid then passes through the recuperator to gain energy from the hot exhaust coming from the turbine exhaust. The He-Xe mixture then enters the receiver to complete the cycle. The cycle

is shown in figure 1. The next section discusses the control system required to manage the CBC and the techniques used to achieve this control.

## 1.2 CONTROL OF THE SDPCS

The following list presents the objectives of the SDPCS control system.

- \* The speed of the rotor is to be maintained at 32,000 RPM to provide a constant 208 Volts ac.
- \* The temperature of the components is to be maintained below the maximum design temperature.
- \* The pressure in the components is to be maintained below the maximum design pressure.
- \* The temperature of eutectic salts is to be controlled to insure constant steady-state power output.
- \* Within the above stated limits, the system is to operate as efficiently as possible.

These objectives are achieved by the following control actions: variation in the load presented by the parasitic load radiator (PLR); change in inventory of the accumulator; and rotation of the concentrator.

The parasitic load radiator (PLR) controls the speed of the rotating unit and is connected in parallel with the user load. The purpose of the PLR is to maintain a constant total electrical load in order to maintain a constant power output from the alternator. The speed and the load are sensed by two separate sensors. If the rotor speed is sensed to be increasing, the PLR load is increased.

Conversely, if the speed of the alternator is sensed to be decreasing, the PLR load is decreased. Hence, a change in user load is compensated by the PLR to maintain constant speed of the rotating unit.

The accumulator controls both the temperature of the components and the power output of the module. During operation of the power plant, the concentrator experiences transients in solar insolation. This results in variation of the receiver salt temperature and hence the working fluid temperature. If the temperature rises above the design temperature for the receiver, the mass flow rate through the receiver is increased to reduce the temperature. Also, the concentrator can be redirected so that the solar radiation is no longer focused on the receiver salts. The extra mass required to increase the mass flow rate is provided by the accumulator. Variation in temperature of the working fluid will result in variation in the power generated by the turbine. To keep this power output constant, the mass flow rate is appropriately adjusted.

Figure 3 shows how the change in working fluid inventory is accomplished. If the turbine inlet temperature decreases, increased mass flow rate is required to maintain the power output from the turbine at a constant value. Opening valve B, upstream of the compressor, injects mass into the system producing an increase in mass flow rate. To reduce the mass flow rate, (decrease the working fluid inventory), valve A is opened downstream of the compressor, and mass flows back into the accumulator.

# Inventory control schematic

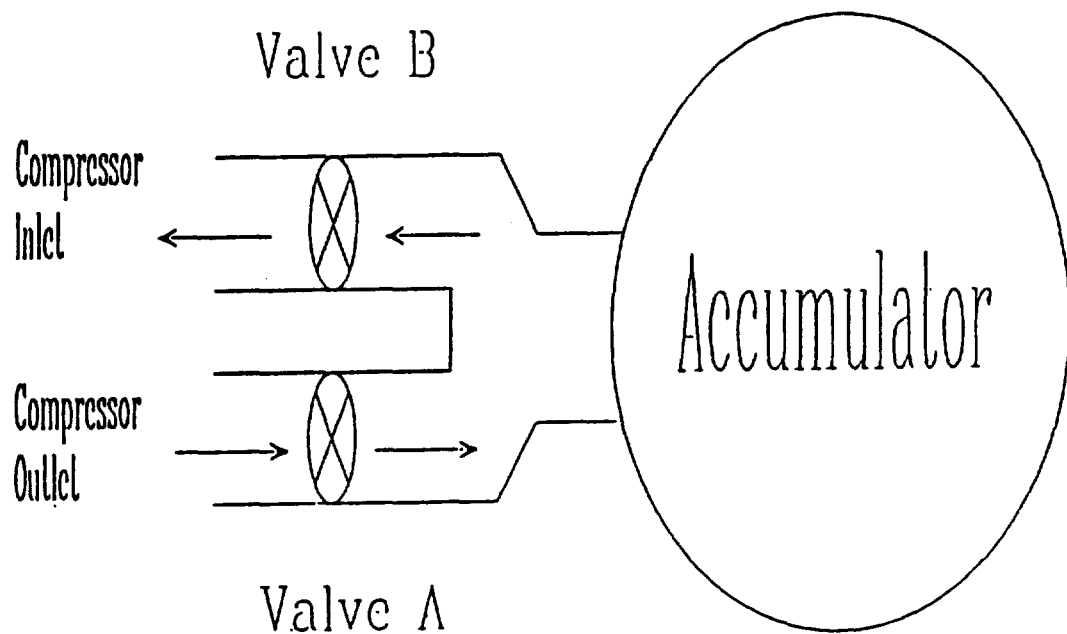


Figure 3. The inventory control schematic.

Rotation of the concentrator is used as the primary control over the flux of solar radiation into the receiver. As mentioned before, it is possible for this flux to be so large that the temperature of the receiver exceeds the allowable temperature of the structure. In such a case, the concentrator is rotated away from the receiver so that the solar radiation is no longer focused on the receiver. Note that all the controls mentioned above require electronic signals for various valves to open and close. Generally, valves are opened or closed slowly to avoid water-hammer.

### 1.3 CLASSIFICATION OF THERMODYNAMIC TRANSIENTS.

Bammert and Krey [2] classify thermodynamic transients into 3 groups on the basis of time constants. The first group has the most rapid transient response and is associated with pressure changes caused by gas pressure oscillations. These pressure changes occur due to the opening and closing of valves. The second group has relatively slower response, and physical processes which produce these transients include the storage of mass due to compressibility of working fluid and the storage of energy in rotating masses. The third group has the largest time constant, and these time constants are associated with heat storage in the thermal mass of the ducting and the heat exchangers.

The group 2 and group 3 transients are directly related to the inertia of the rotating units, the mass of fluid within the control volume, and the mass of the components. Since Bammert and Krey studied very large nuclear power plants with extremely large control volumes and rotating inertias, they are correct in distinguishing

between group 1 and group 2 transients. Since the inertia of the rotor and the volume inside the turbomachines for the SDPCS power module are very small, the group 2 time constants are expected to be of the same order of magnitude as the time constants of group 1. In fact, the investigation presented in this thesis proves this to be the case. Furthermore, since the transients associated with the control mechanisms (PLR, accumulator, control valves) are of the same order of magnitude as that of group 1 transients, the inclusion of group 1 and 2 transients in a model is important. Iqbal [3] studied group 3 transients associated with the SDPCS using instantaneous response turbomachine models. While such an approach is suitable for studying orbital fluctuations and other slow transients, it is not adequate for evaluating the load control system.

The following chapters discuss the development of the compressible-flow transient-thermodynamic-turbomachinery models. These models are capable of predicting the rapid response of group 1 and group 2 transients. These models can be incorporated in an overall model where group 1, group 2, and group 3 type transients can be studied. The results obtained from the simulation of these models are presented in chapter 4. The conclusions and recommended future work follow these results.

## 2. MODELING PHILOSOPHY AND GOVERNING EQUATIONS

### 2.1 MODELING PHILOSOPHY

Simulation of the transient thermodynamic performance of the solar dynamic power control system (SDPCS) closed Brayton cycle (CBC) required the development of several component models. Iqbal [3] developed incompressible flow, transient heat exchanger models (recuperator, gas cooler, radiator, receiver ), and instantaneous response turbomachinery models (compressor, turbine). As discussed in chapter 1, the instantaneous response turbomachinery models are not adequate for development of the load control system. The development of compressible transient-thermodynamic-turbomachinery models, suitable for studying rapid system transients, is the focus of this study.

Detailed compressible transient models for the various components of the SDPCS require solution of the three dimensional compressible Navier Stokes equations. Such an analysis is very complex and expensive and requires state-of-the-art computer resources. Repeated use of such a tool as part of a design and optimization process is prohibitively expensive and time consuming. Therefore, simplified models were sought which would produce the correct transient response and could be quickly executed with modest computational resources. The simplified models must retain the compressible flow physics and should provide considerable insight into the thermodynamic transient response of the SDPCS. The balance of this chapter presents the development of the governing equations for the simplified models.



## 2.2 GOVERNING EQUATIONS

The control volume shown in figure 4 is used to develop the continuity and energy equations. Figure 4 shows three points of interest: the inlet, middle and outlet. At each point of interest a thermodynamic state is uniquely defined by the three state variables (total temperature, total pressure, mass flow rate). The subscripts i, m and o refer to inlet middle and outlet respectively. For the control volume of figure 4 the continuity equation can be written as:

$$\left[ \begin{array}{c} \text{Rate of change} \\ \text{of mass in the} \\ \text{control volume} \end{array} \right] - \left[ \begin{array}{c} \text{Mass} \\ \text{flow rate} \\ \text{in} \end{array} \right] - \left[ \begin{array}{c} \text{Mass} \\ \text{flow rate} \\ \text{out} \end{array} \right]$$

$$\frac{dm}{dt} = \dot{m}_i - \dot{m}_o \quad (1)$$

For the same control volume, the energy equation can be written as

$$\left[ \begin{array}{c} \text{Rate of change} \\ \text{of energy in} \\ \text{control volume} \end{array} \right] - \left[ \begin{array}{c} \text{Rate} \\ \text{of Energy} \\ \text{Flow In} \end{array} \right] - \left[ \begin{array}{c} \text{Rate} \\ \text{of Energy} \\ \text{Flow Out} \end{array} \right]$$

$$+ \left[ \begin{array}{c} \text{Rate} \\ \text{of} \\ \text{Work In} \end{array} \right] - \left[ \begin{array}{c} \text{Rate} \\ \text{of} \\ \text{Heat Loss} \end{array} \right]$$

$$\frac{d(me)}{dt} = \dot{m}_i e_i - \dot{m}_o e_o + \dot{W} - \dot{Q} \quad (2)$$

or,

$$\frac{de}{dt} = \frac{1}{m} \left[ \dot{m}_i e_i - \dot{m}_o e_o + \dot{W} - \dot{Q} - e \frac{dm}{dt} \right] \quad (3)$$

For the development of centrifugal turbomachinery models the moment of momentum equation is more useful than the linear momentum equation. Figure 5 shows the compressor control volume used to develop the moment of momentum equation. Flow into the control

# General Control Volume

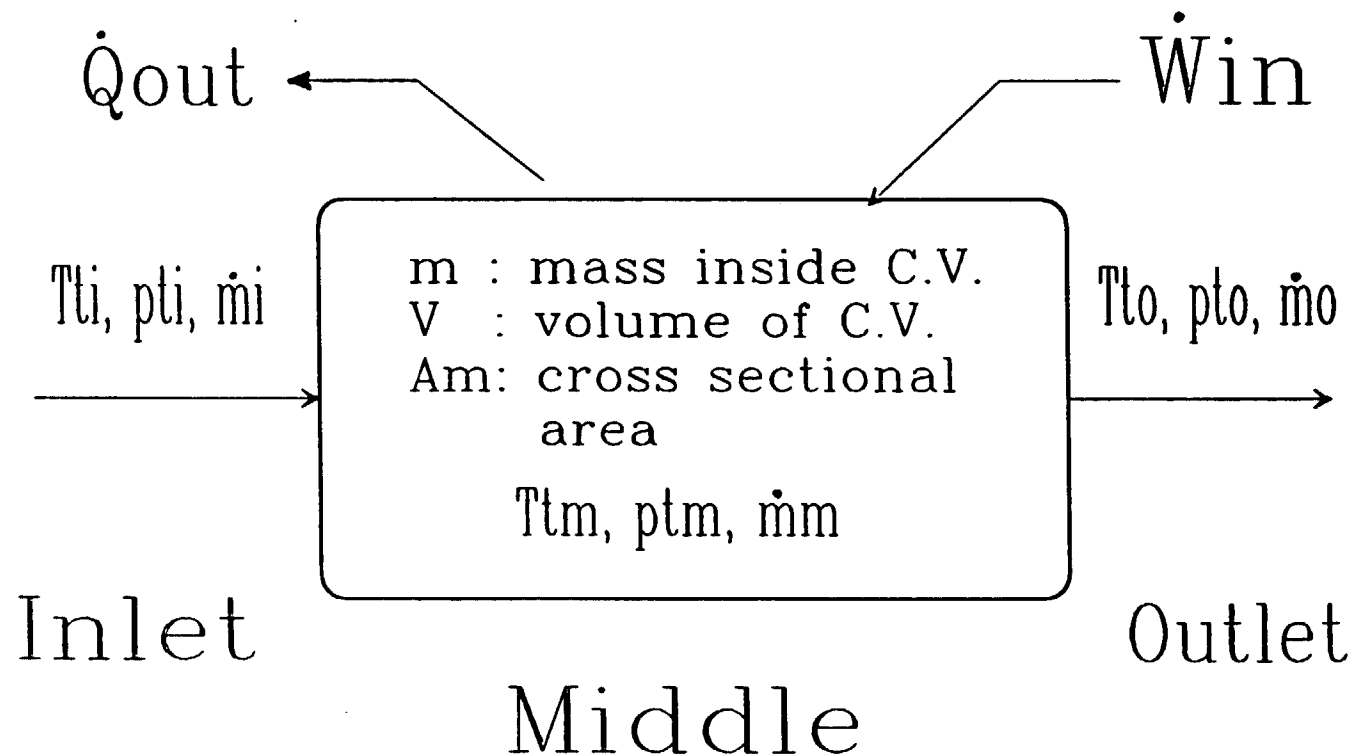


Figure 4. General control volume.

volume is assumed to be in the positive x direction. The flow out of the control volume contains both a radial component and a tangential component, but no axial component. The distance from the x axis to the outlet of the control volume is  $R_o$ , the distance from the x axis to the middle of the control volume is  $R_m$ .  $R_m$  was selected as half the distance from the rotor hub to the rotor tip. The velocity diagram for the flow is shown at the middle and the outlet. Summation of moments about the x axis gives the moment of momentum equation as:

$$\left[ \begin{array}{c} \text{Rate of change} \\ \text{of angular} \\ \text{momentum} \\ \text{in the} \\ \text{control volume} \end{array} \right] = \left[ \begin{array}{c} \text{Rate of flow} \\ \text{of angular} \\ \text{momentum} \\ \text{into the} \\ \text{control volume} \end{array} \right] - \left[ \begin{array}{c} \text{Rate of flow} \\ \text{of angular} \\ \text{momentum} \\ \text{out of the} \\ \text{control volume} \end{array} \right] + \left[ \begin{array}{c} \text{Sum of moments} \\ \text{acting on} \\ \text{the mass} \\ \text{in the} \\ \text{control volume} \end{array} \right]$$

The contribution of the angular momentum due to the flow into the control volume is zero because the direction of the flow is entirely in the positive x direction. For the compressor control volume the moment of momentum equation can be written:

$$\frac{d(m\Omega R_m^2)}{dt} = -\Omega R_o^2 \dot{m}_o + \Sigma T \quad (4)$$

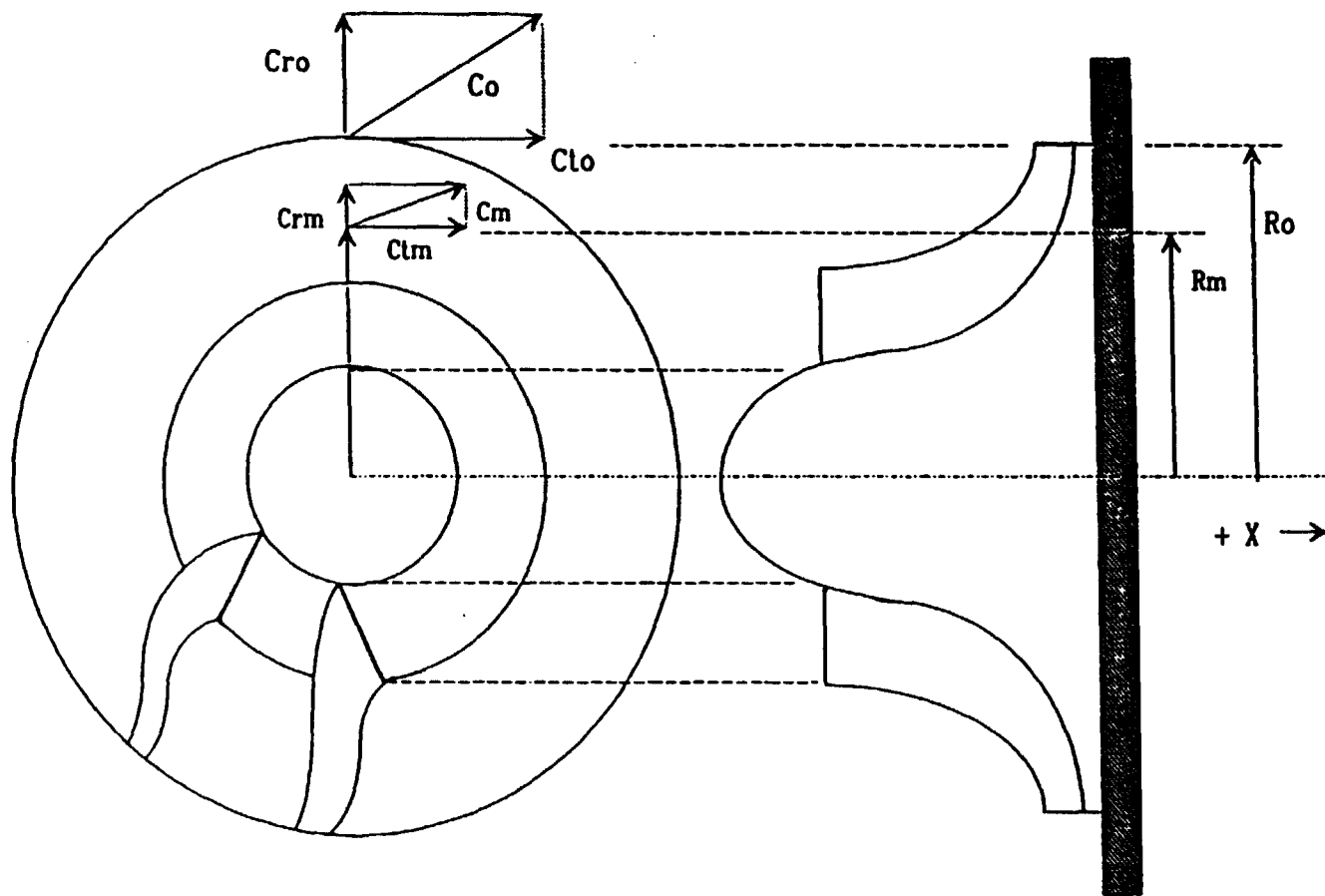


Figure 5. Control volume for moment of momentum equation.  
Compressor shown.

The torque on the control volume can be replaced with other more suitable variables by the following process:

$$\dot{W} = T\Omega$$

$$T = \dot{W} / \Omega$$

$$\dot{W} = \Omega^2 R_m^2 \frac{dm}{dt} + m\Omega R_m^2 \frac{d\Omega}{dt} + \Omega^2 R_o^2 \dot{m}_o \quad (5)$$

or,

$$\frac{d\Omega}{dt} = \frac{1}{m R_m^2} \left[ \frac{\dot{W}}{\Omega} - \Omega R_o^2 \dot{m}_o - \Omega R_m^2 \frac{dm}{dt} \right] \quad (6)$$

To compute any thermodynamic state variable from the three chosen state variables (total temperature, total pressure, mass flow rate), the following relations for a perfect gas are used:

$$p_s = \rho_s R T_s \quad (7)$$

$$p_t = \rho_t R T_t \quad (8)$$

$$\dot{m} = \rho_s C A \quad (9)$$

$$T_t = T_s + \frac{C^2}{2 C_p} \quad (10)$$

$$\frac{T_{to}}{T_{ti}} = \left[ \frac{p_{to}}{p_{ti}} \right]^{\frac{R}{C_p}} \quad (11)$$

Wilson [4] gives two very useful polytropic relations relating temperature ratio and pressure ratio across a compressor and a turbine. For the compressor the equation is,

$$\frac{T_{to}}{T_{ti}} = \left[ \frac{p_{to}}{p_{ti}} \right]^{\frac{R}{C_p \eta}} \quad (12)$$

For the turbine the equation is given as

$$\frac{T_{to}}{T_{ti}} = \left[ \frac{p_{to}}{p_{ti}} \right]^{\frac{R \eta}{C_p}} \quad (13)$$

$\eta$  represents total-to-total polytropic efficiency between the inlet and the exit. It should be noted that all of the losses (frictional, blading, etc.) are included in the polytropic efficiency of equations 12 and 13. Hence, instead of analyzing each loss separately, the efficiency charts for the machine can be used as an approximation to perform an analysis.

### 3. MODEL DEVELOPMENT AND SIMULATION

In this chapter, the general equations developed in chapter 2 are used to develop compressible transient thermodynamic models of turbomachinery. Total temperature, total pressure and mass flow rate are chosen as the state variables and the model geometry is specified by the DRO2 document [1]. The geometry and the 3 state variables are sufficient to uniquely identify a thermodynamic state. Figure 5, (in the preceeding chapter), shows a general control volume for a radial compressor; the turbine is similar. The inlet state of the turbomachine is known as it is the output of an upstream component. The states in the middle and at the outlet are unknown. Hence, there are six unknowns (3 state variables for the middle and 3 state variables for the exit) and only 3 equations (continuity, energy, and moment of momentum/polytropic). Therefore 3 additional equations are required to solve the system. This chapter is devoted to examining the various combinations of assumptions required to obtain a solution. Some candidate assumptions were:

- \* linear variation of state variables between inlet and outlet;
- \* non-linear variation of state variables between inlet and outlet; and
- \* use of steady state maps for the variation of the state variables.

### 3.1 LITERATURE REVIEW

A literature search provided little information about previously developed transient turbomachinery models. In fact, information uncovered by the search was limited to transient axial-flow compressor models trying to predict surge. The motivation behind the development of these transient compressor models was to predict surge. Furthermore, these compressor models neglected some of the compressible flow physics in their assumptions.

Kuhlberg & Sheppard [5] were among the first to report development of axial-flow-compressor transient models. They modeled a transient compressor using simplified continuity, energy and momentum equations. The simplification of the equations was based on the following assumptions:

- \* constant Mach number across chosen control volume;
- \* low Mach number approximation to compressible flow dynamics;
- \* isentropic flow (no losses); and
- \* no energy transfer between compressor walls and fluid.

They further assumed that steady-state characteristic maps could be used for transient analysis. They used maps relating temperature-rise function ( $\lambda$ ) to air-flow function ( $\phi$ ), and pressure-rise function ( $\psi$ ) to air-flow function. Specifically, these functions are normalized and are defined as follows:

$$\lambda \triangleq \left[ \frac{T_{t2} - T_{t1}}{T_{t1}} \right] * \left[ \frac{N/(\theta)^{1/2} \text{ DESIGN}}{N/(\theta)^{1/2}} \right] \quad (14)$$



$$\phi \triangleq \frac{W_1(\theta)^{1/2}}{\delta t_1} * \left[ \frac{N/(\theta)^{1/2} \text{ DESIGN}}{N/(\theta)^{1/2}} \right] \quad (15)$$

$$\psi \triangleq \left[ \frac{P_{t2} - P_{t1}}{P_{t1}} \right] * \left[ \frac{N/(\theta)^{1/2} \text{ DESIGN}}{N/(\theta)^{1/2}} \right] \quad (16)$$

$$\eta \triangleq \frac{\left[ T_{t2} - T_{t1} \right] \text{ IDEAL}}{\left[ T_{t2} - T_{t1} \right] \text{ ACTUAL}} \quad (17)$$

where they define,

W : air flow in lbs per second

P<sub>t</sub> : total pressure in psia

T<sub>t</sub> : total temperature in degrees Rankine

N : rotor speed

η : efficiency

θ<sub>t</sub> : total temperature ratio / 518.69

δ<sub>t</sub> : total pressure / 14.696

subscript 1 : inlet condition

subscript 2 : outlet condition

Using their model they were able to predict surge in a compressor. A modified version of their model was validated for predicting surge, by Elder, Gill, and Razak [6] in 1984.

MacCallum [7] identified the importance of heat transfer between the wall of the turbomachine and the fluid by analyzing transient heat transfer between the fluid and the blading. However, Sarantsev [8] makes the argument that heat transfer between the wall and the

fluid can be neglected as "Accumulation and discharging of heat energy in the metal parts, even at their intensive washing over, is carried out sufficiently slower." That is, the change in operating state due to compressibility of the fluid is much faster than that due to the storage of energy in the thermal mass of the blading. As a consequence, if a model is required to predict response due to the compressibility of fluid, the heat transfer between the walls and the fluid can be considered a second order effect.

Corbett and Elder [9] categorized their models under two main headings: lumped parameter ( L.P. ); and linearly-distributed parameter ( L.D.P. ). Both models use simplified continuity, energy and momentum equations. These simplifications are based on the following assumptions:

- \* constant viscous drag across the control volume;
- \* constant energy-transfer rate between the control volume and the surroundings; and
- \* low-Mach-number approximation to compressible-flow dynamics.

Additional simplifying assumptions specific to the L.P. model are:

- \* constant mass-flow rate between inlet and exit;
- \* constant volumetric-flow rate between inlet and exit; and
- \* constant value of energy in the control volume.

Additional simplifying assumptions unique to the L.D.P. model are:

- \* linear change in mass-flow rate between inlet and exit;
- \* linear change in volumetric-flow rate between inlet and exit;
- and
- \* linear change in energy in control volume between successive control volumes.

Corbet and Elder were able to predict surge a compressor with these models. However, they do not clearly identify the better of the two models. Modified versions of these models were validated again in 1984 by Elder, Gill, and Razak [6].

The modification made by Elder, Gill and Razak [6] in 1984 to the above models was the incorporation of a polytropic analysis done by Schultz [10] to represent real gases. Schultz [10] developed equations in terms of compressibility functions using the compressibility factor ( $Z$ ). He also introduced a polytropic-head factor to adjust test results for deviation from perfect gas behavior. The inclusion of the analysis done by Schultz in the compressor models provides greater thermodynamic flexibility as the models are not restricted to perfect gases.

The above models, when verified by Elder, Gill, and Razak [6], had two major restrictions:

- \* the length of the control volume had to be much less than the wave length of the expected flow perturbation at the inlet; and
- \* the volume of successive control volumes had to be approximately equal or the model became a "numerically stiff system."

Greitzer [11] developed a transient compressor model to predict surge and rotating stall. The components of his model are shown in figure 6.

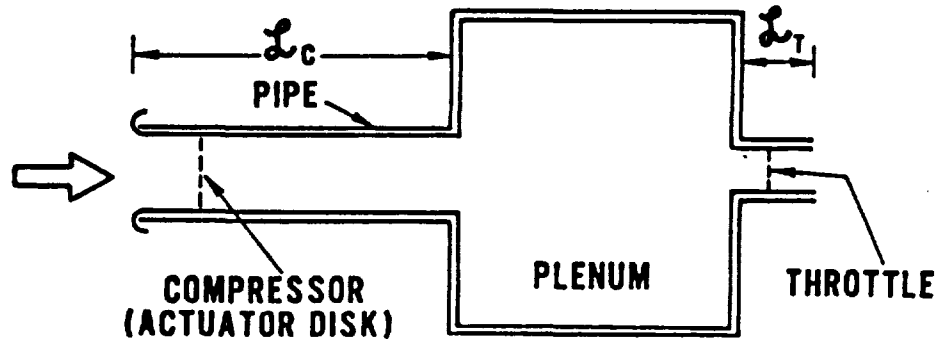


Figure 6: Greitzer's model schematic.  
(reproduced from reference 11, page 192)

Greitzer assumes that "all the kinetic energy of the oscillation is associated with the motion of fluid in the compressor and throttle ducts, and the potential energy is associated with the compression of gas in the plenum." The compressor model includes: an actuator disk; the compressor duct of length  $L_c$ ; and the throttle duct of length  $L_t$ . The duct  $L_c$  accounts for the dynamics of the fluid, while duct  $L_t$  represents the throttle valve. Greitzer assumes that the flow in the ducts is incompressible. Furthermore, he assumes that the velocity in the plenum is negligible and the thermodynamic process occurring in the plenum is isentropic. Greitzer was able to predict surge and rotating stall with this model.

Greitzer [12] also explains the inherent unsteady flow inside the turbomachinery. The sources of unsteadiness, according to Greitzer are: turbulence; wakes; potential field interactions; inlet distortion; rotating stall; and surge. However, since the purpose of this study is to develop models which use average (bulk) values at inlet and outlet, the unsteady characteristics of flow within the turbomachinery will be neglected.

It is clear from the literature review described above that a true transient compressible model having complete dynamic flexibility was not an existing technology. In fact, models of radial turbomachines are conspicuously absent in the literature. Models discussed and developed below do not neglect the compressible-flow physics which were neglected by models identified in the literature review.

### 3.2 MODELING TECHNIQUES

The simplest technique evaluated, in this study, for simulation of turbomachine performance was a Laplace-transform transfer-function model. This simple technique is well suited for modeling single-input single-output linear systems. Transfer functions can also be developed for multiple-input multiple-output systems, provided the set of equations defining the system can be decoupled. The equations describing turbomachinery performance are inherently non linear and coupled. Therefore, Laplace transform techniques were judged unsuitable for modeling turbomachinery.

The next class of techniques evaluated, in this study, use finite difference approximations to the governing set of equations. This solution technique can employ several different algorithms to obtain a solution. Some of the more successful models, and their algorithms, are discussed below. It should be noted that all models use typical total-to-total polytropic efficiency maps as shown in figures 7 and 8 [13]. In the upwind-mass-flow model, the sliced model, and the state-average lagged-mass-flow-rate model, the turbine efficiency data were represented by a third order curve fit as shown in figure 8. This third order curve was obtained by specifying: the slope at design-point as zero; the choice of design point; and the choice of another data point. This curve fit is a reasonable approximation of the actual efficiency data for a turbomachine. Note, that for all future discussions, the term middle will be used to define an average-thermodynamic state for the control volume.

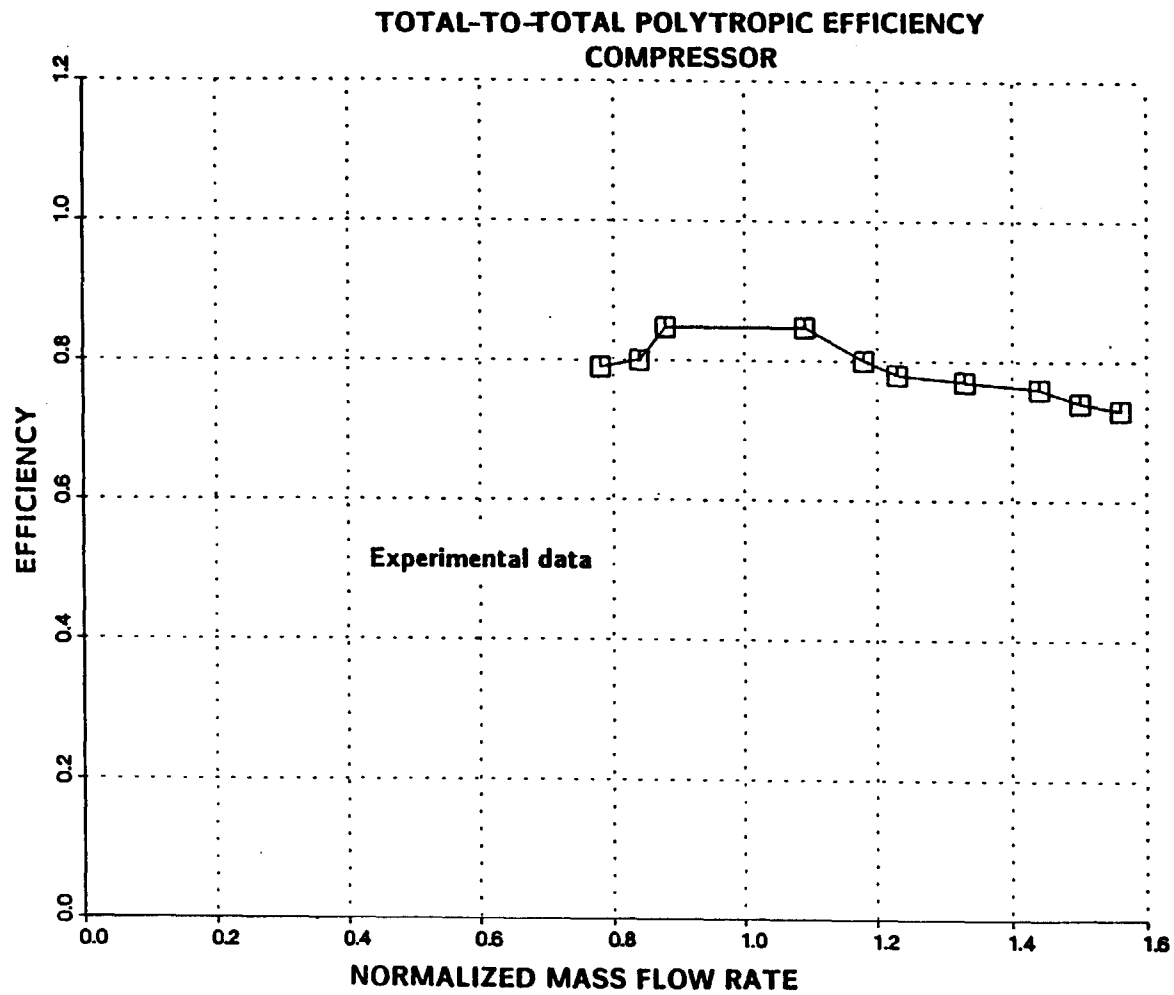


Figure 7. Compressor, total-to-total polytropic efficiency map.

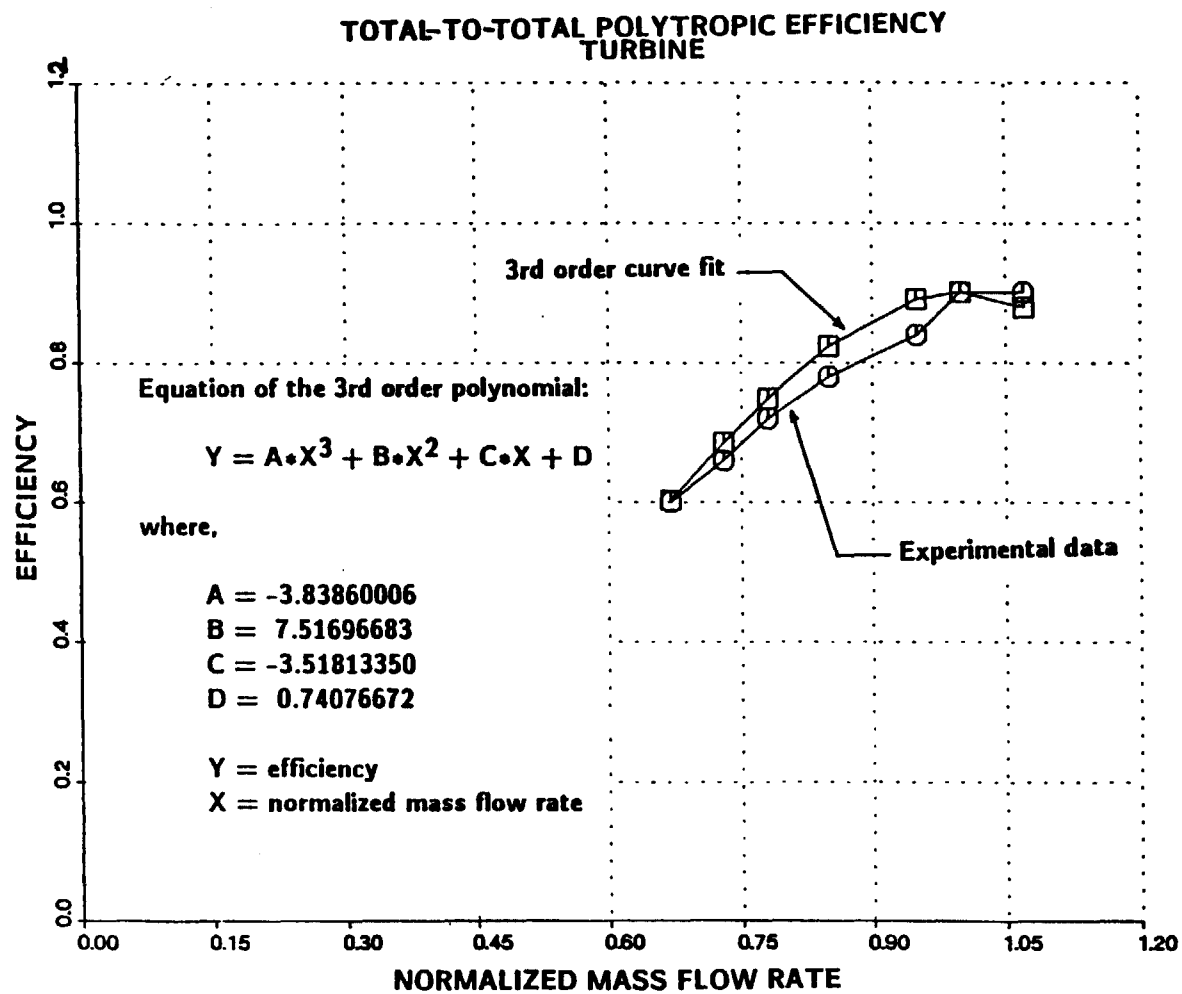


Figure 8. Turbine, total-to-total polytropic efficiency map.



### 3.3 THE STATE-AVERAGE MODEL

The earliest turbomachinery models were developed by applying the following assumptions, along with the continuity, energy and polytropic equations to a single control volume to model the turbomachine.

$$X_m = (X_i + X_o) / 2 \quad (18)$$

$$Y_m = (Y_i + Y_o) / 2 \quad (19)$$

$$Z_m = Z_i * (Y_m / Y_i)^{f(K, \eta)} \quad (20)$$

where,

X, Y, and Z, are any thermodynamic properties, such as total temperature, total pressure, etc.

i, m, and o, are inlet middle and outlet respectively,

K, is a combination of thermodynamic gas constants, &

$\eta$ , is an appropriately defined polytropic efficiency from inlet to middle of the machine.

The exponent  $\eta$  and K depend on the choice of the thermodynamic variables.

These appear to be a good set of assumptions as they are similar to the assumptions made for the solution of steady-state gas-dynamics problems including friction and thermal energy transfer. Figure 9 shows an implicit algorithm using an iteration scheme to obtain a solution at each time step.

To start the algorithm, all the state variables are defined for steady state. Once the variations at the inlet are defined, equations 18, 19, and 20 are used to estimate the value of the state variables in the middle. These estimates are based on the previous

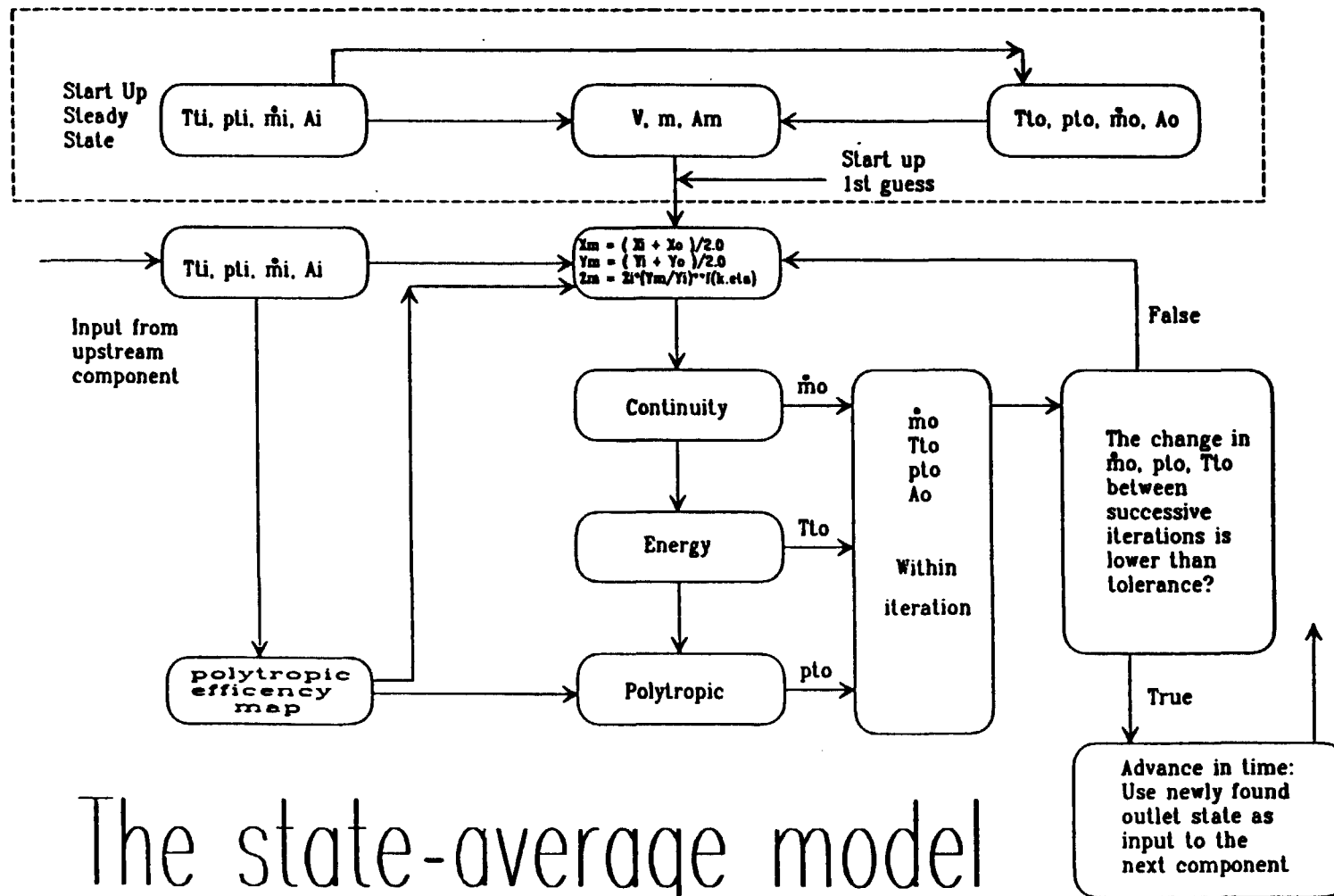


Figure 9. The state-average model algorithm.

time level outlet states. The same polytropic efficiency is used between inlet and outlet and between inlet and middle of the machine. This could be improved in the future if better efficiency data for the specific machine become available. Once the middle state variables have been estimated, the value of all the thermodynamic state variables are obtained by the use of equations 7-11. The mass in the control volume is then determined by:

$$m = \rho_{sm} * V \quad (21)$$

where  $\rho_{sm}$  is the static density in the middle and  $V$  is the volume of the control volume. Next, the rate of change of mass in the control volume is determined using equation 22.

$$\frac{dm}{dt} \Big|_{t+\Delta t} = \left[ m \Big|_{t+\Delta t} - m \Big|_t \right] / \Delta t \quad (22)$$

where,  $m$  is the mass in the machine,  $t$  is the previous time level and  $\Delta t$  represents the time increment. Once the rate of change of mass in the control volume is obtained, the outlet mass flow rate can be determined from the continuity equation.

$$\dot{m}_o \Big|_{t+\Delta t} = \dot{m}_i \Big|_{t+\Delta t} - \frac{dm}{dt} \Big|_{t+\Delta t} \quad (23)$$

Equation 24 is then used to determine the rate of change of energy in the control volume.

$$\frac{de}{dt} \Big|_{t+\Delta t} = \frac{1}{m} \left[ \dot{m}_i e_i - \dot{m}_o e_o + \dot{W} - e \frac{dm}{dt} \right] \Big|_{t+\Delta t} \quad (24)$$

The total temperature at the outlet is then determined from equation 26.

$$e_o \Big|_{t+\Delta t} = 2 * e \Big|_{t+\Delta t} - e_i \Big|_{t+\Delta t} \quad (25)$$

$$T_{to} \Big|_{t+\Delta t} = \frac{1}{C_p} \left[ 2 * C_v * T_{tm} - C_p * T_{ti} \right] \Big|_{t+\Delta t} \quad (26)$$

Based on the new estimate of outlet total temperature at  $t+\Delta t$ , equation 27 is used to determine the outlet total pressure for the compressor.

$$P_{to} \Big|_{t+\Delta t} = P_{ti} \Big|_{t+\Delta t}^* \left[ \frac{T_{to}}{T_{ti}} \right]^{\frac{C_p \eta}{R}} \Big|_{t+\Delta t} \quad (27)$$

The new outlet-state variables are substituted back in equations 18, 19 and 20 to obtain a better estimate for the middle state variables. This process continues until the percent change in successive outlet-thermodynamic states is within a specified tolerance. The tolerance is specified such that convergence is achieved to at least thirteen significant digits. This accuracy requirement was chosen to suppress round off errors affecting the solution. The affect of relaxing this requirement has not been determined and requires further investigation. Once the tolerance criteria are satisfied, the algorithm has converged for that particular time step, and the process starts again for the next time step.

Table 1 presents information used to perform a state-average turbomachinery analysis. Specifically, table 1 lists: the geometry of the compressor to be simulated; the design point data for the compressor; the perturbation to the design steady state value initiate a transient; and the thermodynamic steady-state values expected at the end of the simulation.

The initial steady-state operation of the compressor is perturbed by a step rise in the inlet total temperature. Several different simulations were performed with different size step increases in inlet total temperature. The results obtained from these simulations are presented in figures 10-16. The successive values of steps in inlet total temperature in table 1, and the expected outlet total temperature in table 1, correspond to this sequence of figures.

Figure 10 shows the response of outlet total temperature to a step rise in inlet total temperature of 0.1 K. The corresponding steady state outlet temperature is 440.1 K. Figure 10 shows that the transient model is able to correctly predict the expected final steady state. Figures 11-14 show plots for different size steps in inlet total temperature. For each of these figures the final steady state is predicted correctly as given by table 1. However, the smoothness of the response varies considerably. For smaller step rises in the inlet total temperature, the response fluctuates more than it does in response to a larger inlet total temperature step rise. This suggests that for the larger step rise in total inlet temperature the energy-storage term,  $(de/dt)$ , dominates the

**Table 1: Data for results presented in figures 10 - 16.**

**Compressor Geometry:**

Inlet normal area:	2.297E-3 m <sup>2</sup>
Middle normal area:	1.711E-3 m <sup>2</sup>
Outlet normal area:	1.125E-3 m <sup>2</sup>
Volume of compressor:	5.160E-5 m <sup>3</sup>
Tip radius:	4.480E-2 m
Hub radius:	1.250E-2 m

**Design point data:**

Inlet total temperature:	340.0 K
Outlet total temperature:	440.0 K
Inlet total pressure:	320.0 KPa
Outlet total pressure:	559.9 KPa
Mass flow rate:	1.2886 Kg/sec
Rotor speed:	3351.0 Hz
Total to total polytropic efficiency:	0.867

**Perturbation at inlet to obtain transient response:**

Step inlet total temperature to:	340.1 K 345.0 K 360.0 K 390.0 K 440.0 K
Keep inlet total pressure at:	320.0 KPa
Keep inlet mass flow at:	1.2886 Kg/sec

**Expected steady state outlet states:**

Outlet total temperature:	440.1 K 445.0 K 460.0 K 490.0 K 540.0 K
Outlet total pressure:	559.9 KPa
Outlet mass flow rate:	1.2886 Kg/sec

**Additional notes:**

Constant specific heat:	519.14 J/Kg/K
Gas constant:	207.44 J/Kg/K
Constant speed:	3351.00 Hz
Constant rate of work input:	66,865.2 J/sec

# Total Outlet Temp. Vs. Time

## Step 0.1 K

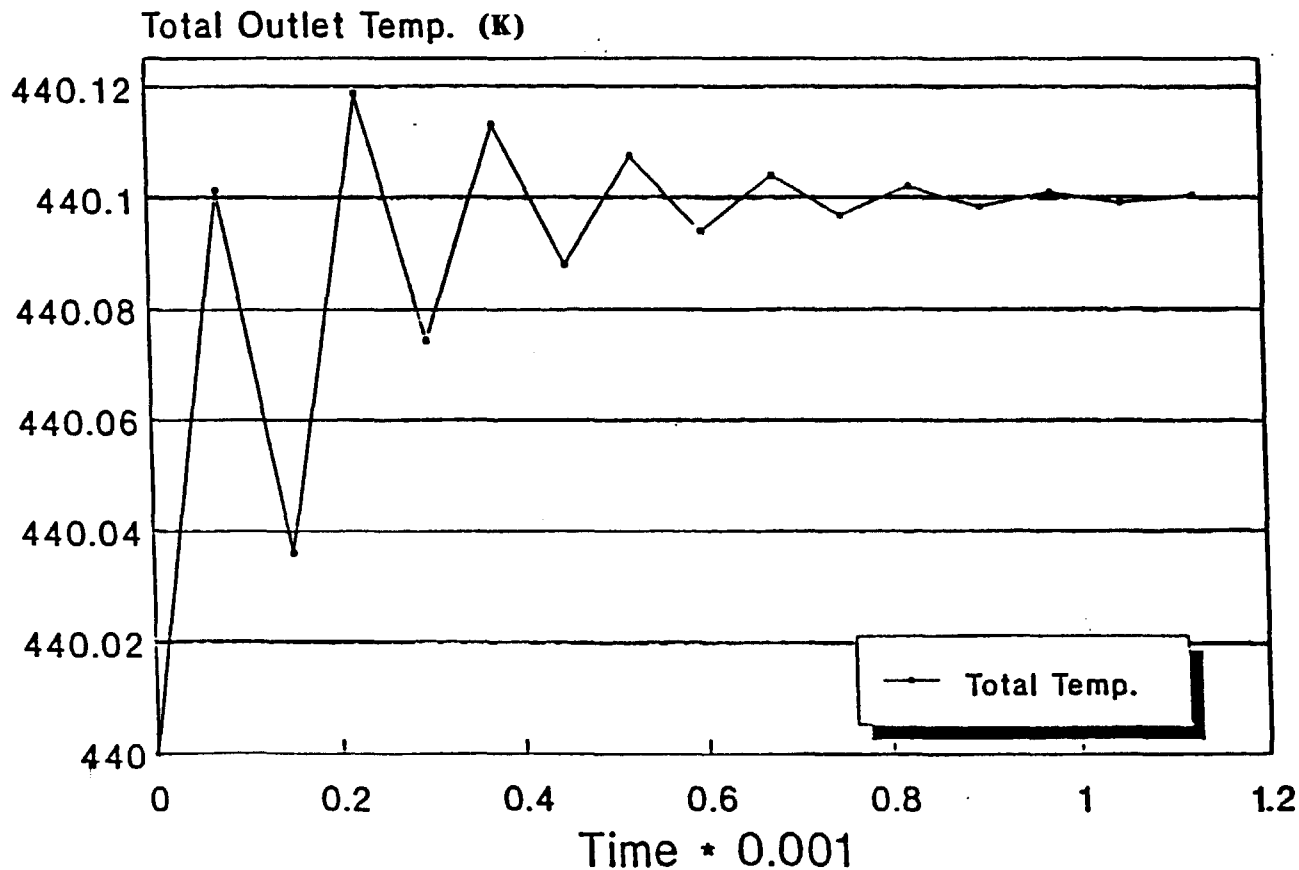


Figure 10. Response of the outlet total temperature of the compressor to a step input of 0.1 K in inlet total temperature. Time step is 0.075 ms.

# Total Outlet Temp. Vs. Time

## Step 5 K

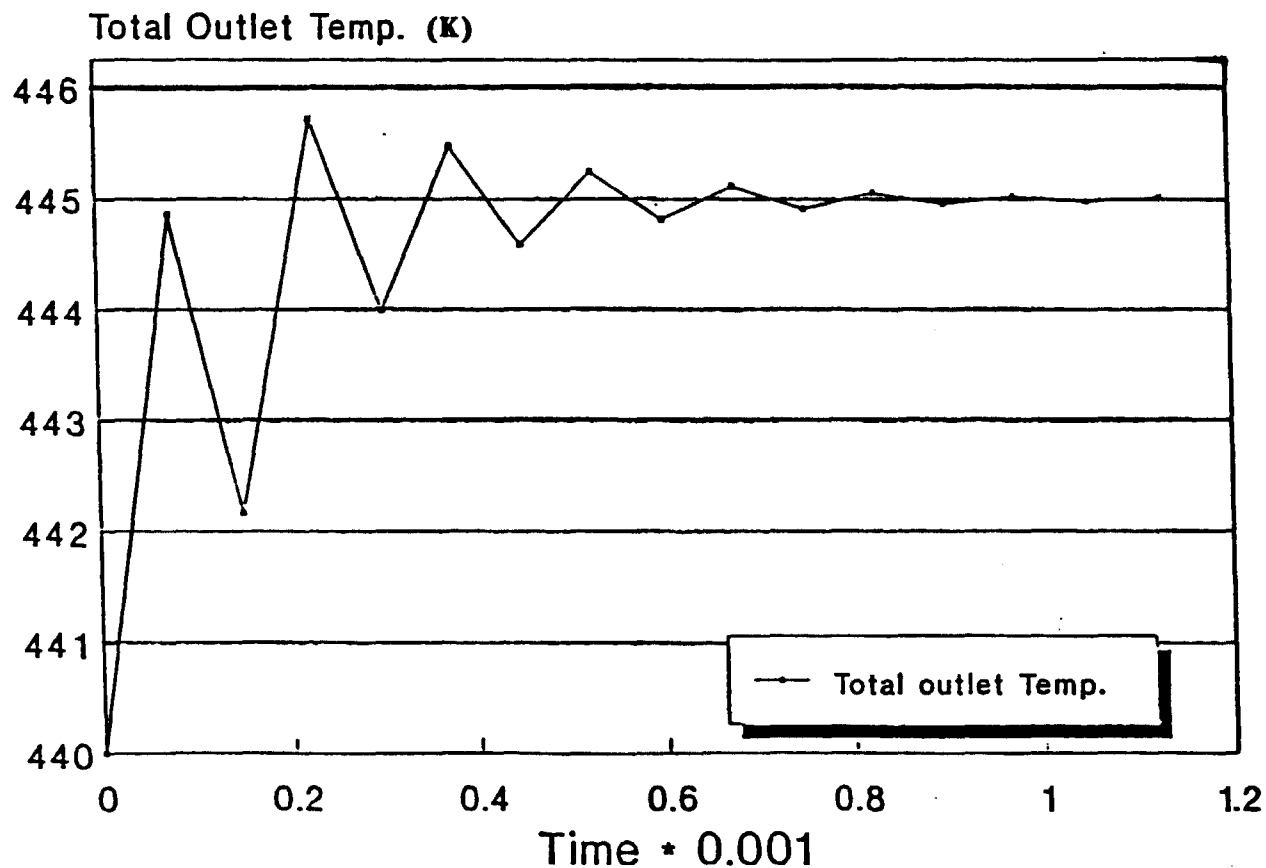


Figure 11. Response of the outlet total temperature of the compressor to a step input of 5.0 K in inlet total temperature. Time step is 0.075 ms.



# Total Temp. Vs. Time

## Step 20 K

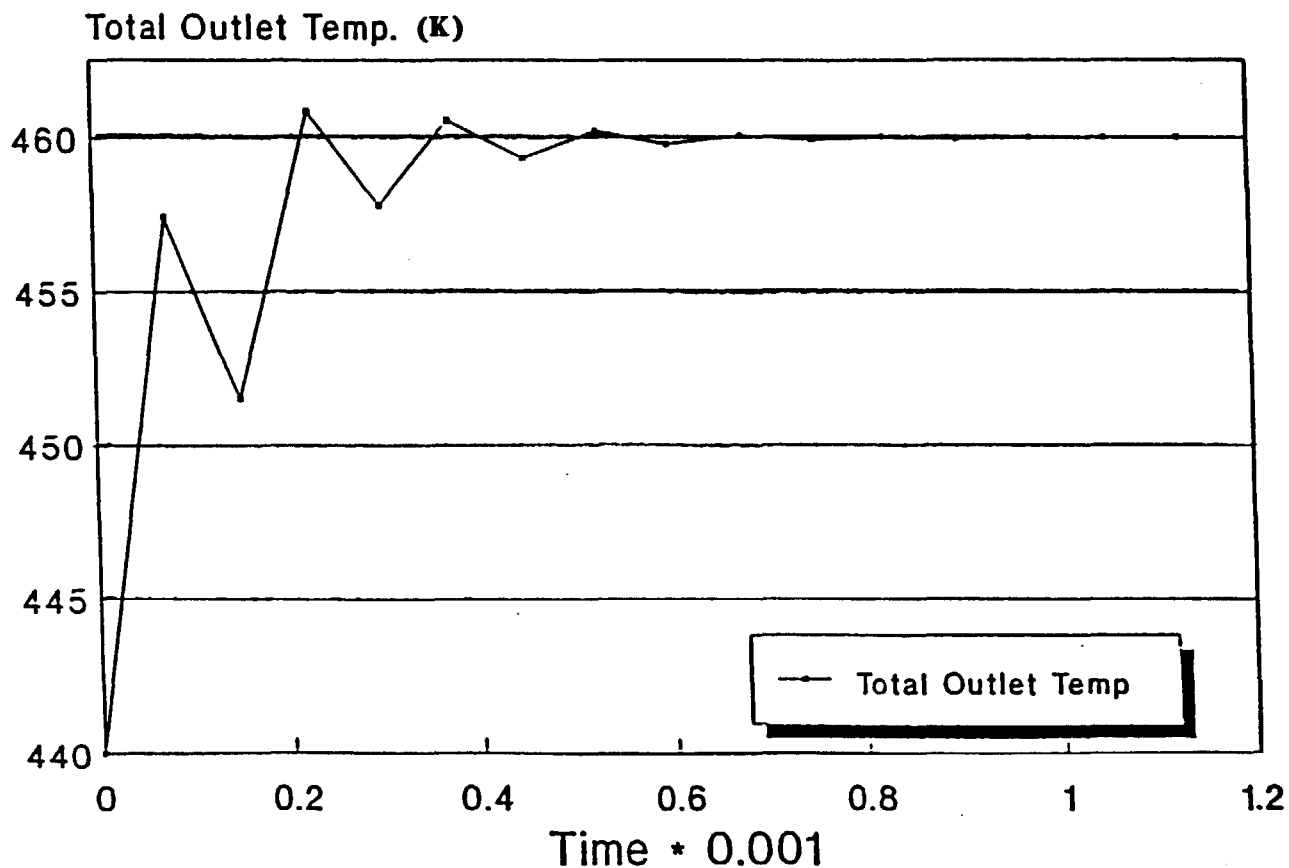


Figure 12. Response of the outlet total temperature of the compressor to a step input of 20 K in inlet total temperature. Time step is 0.075 ms.

# Total Temp. Vs. Time

## Step 50 K

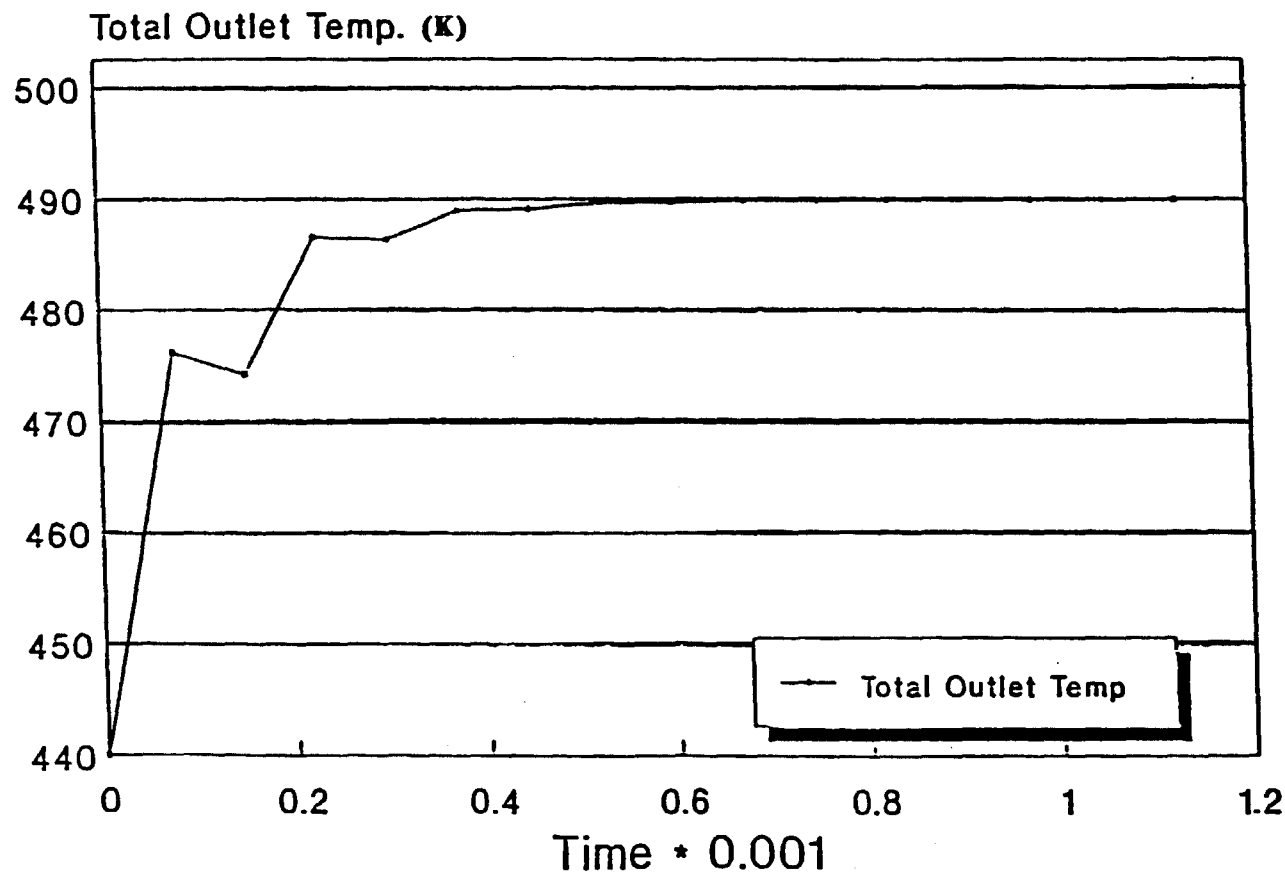


Figure 13. Response of the outlet total temperature of the compressor to a step input of 50 K in inlet total temperature. Time step is 0.075 ms.

# Total Temp. Vs. Time

## Step 100 K

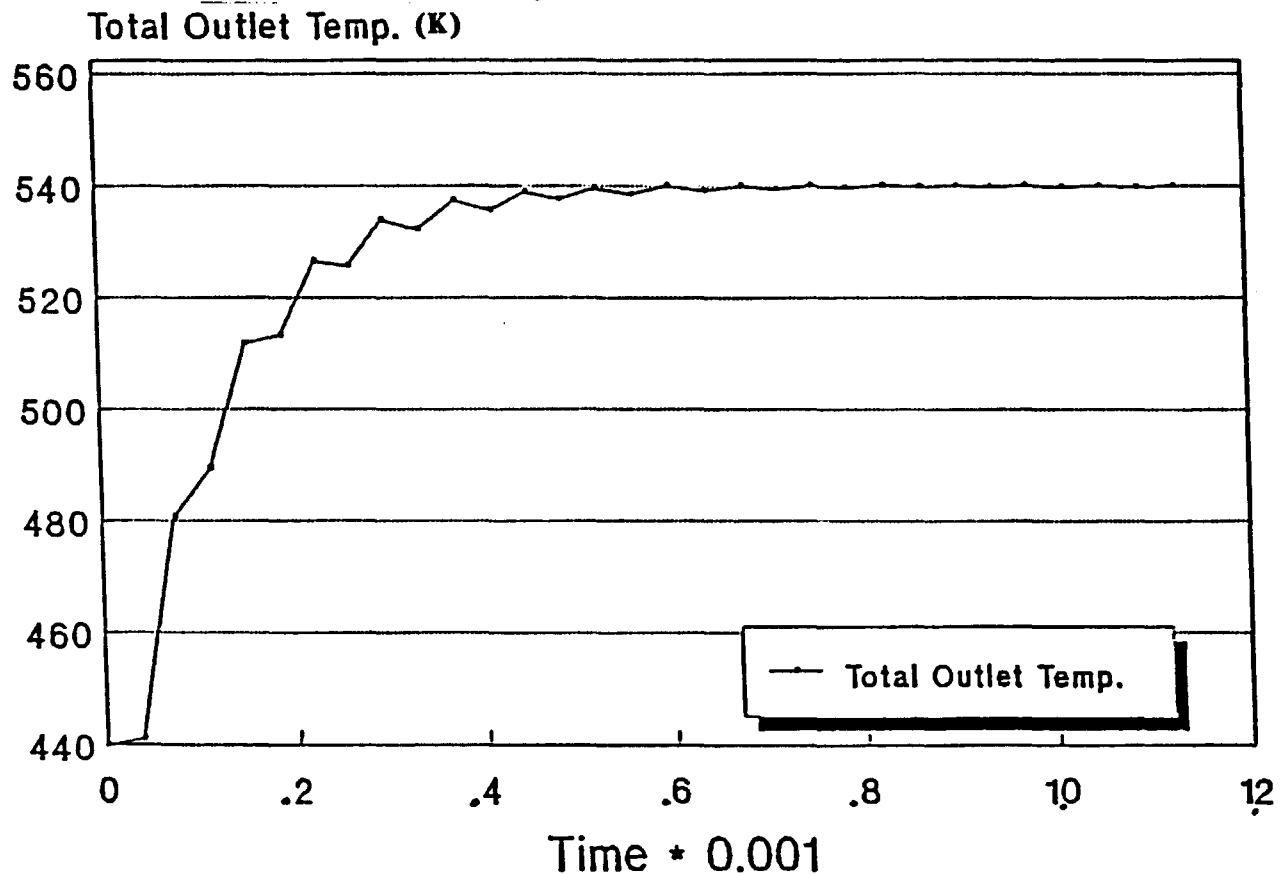


Figure 14. Response of the outlet total temperature of the compressor to a step input of 100 K in inlet total temperature. Time step is 0.0375 ms.

# Total Outlet Temp. Vs. Time

(K) Step 100 K,  $\frac{dm}{dt} = 0$

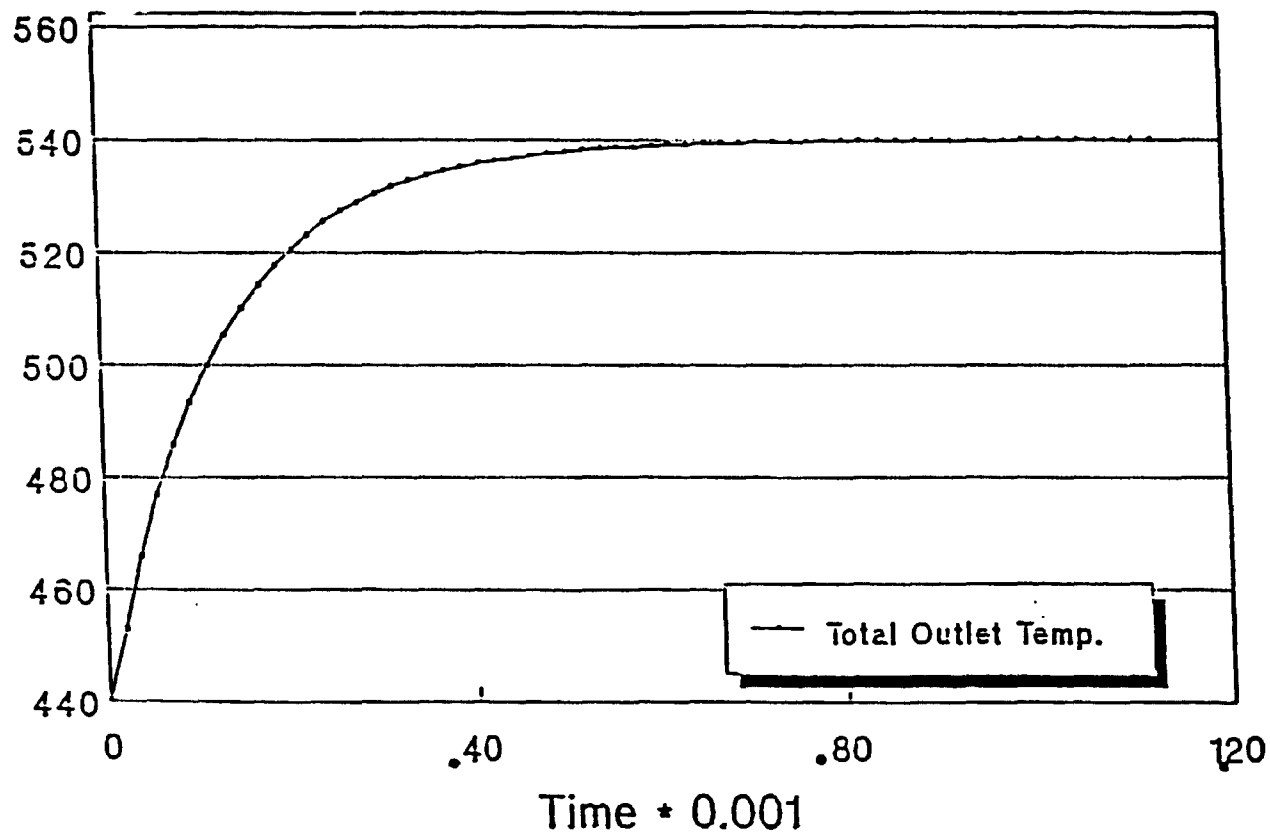


Figure 15. Response of the outlet total temperature of the compressor to a step input of 100 K in inlet total temperature while  $\frac{dm}{dt} = 0$  in the compressor. Time step size is 0.01875 ms.

# Total Temp. Vs. Time

## Step 100 K

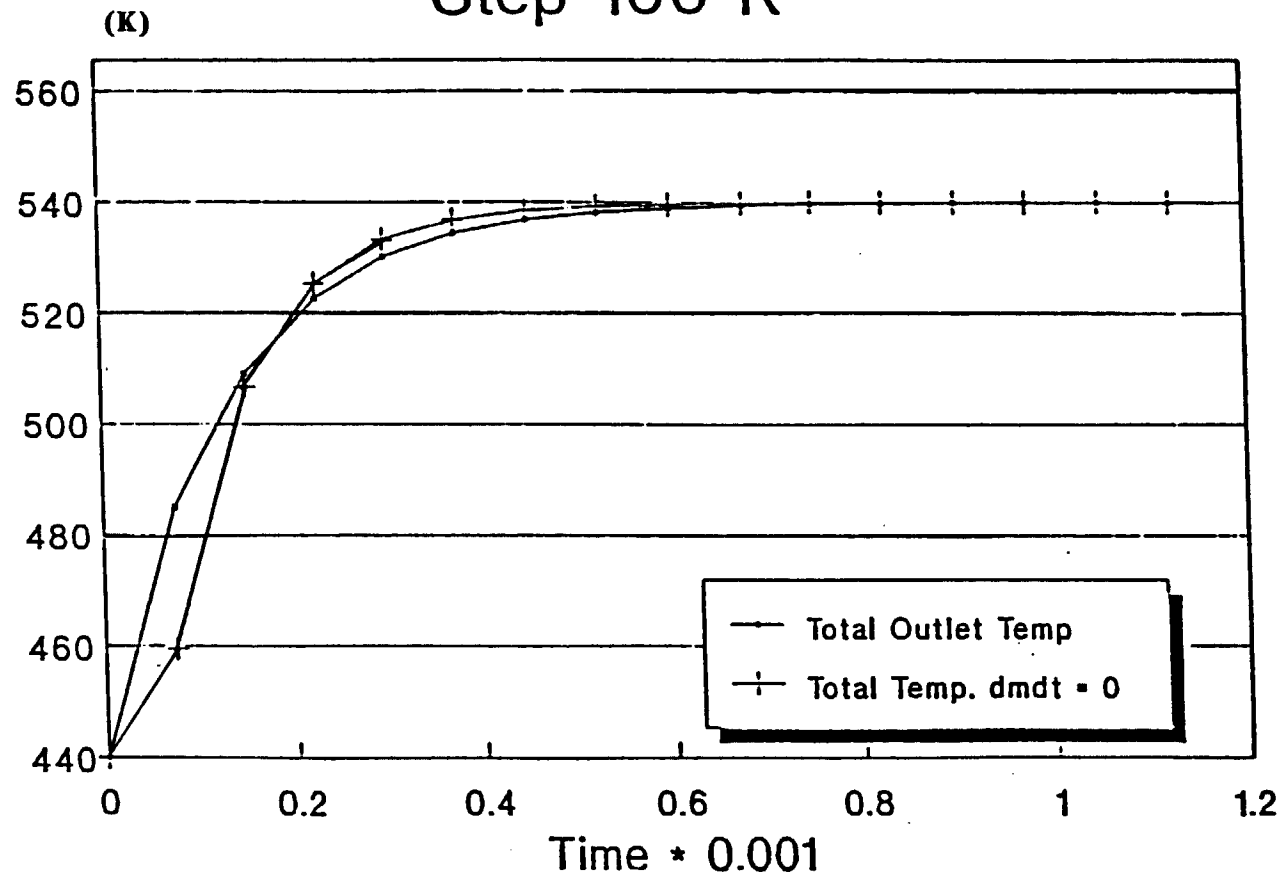


Figure 16. The effect of  $\frac{dm}{dt}$  on the response of the outlet total temperature of the compressor to a step input of 100 K in inlet total temperature. Time step is 0.075 ms.

mass-storage term,  $(dm/dt)$ . Therefore, a test model was developed neglecting the mass-storage term. The response predicted by the test model is presented in figure 15. This figure shows a monotonic response without the superimposed fluctuations predicted by the mass-storage model. Figure 16 shows a comparison of the predicted response when mass storage is included and when the mass storage is neglected. This comparison demonstrates that it is the mass storage term that is indeed producing fluctuations in the outlet total-temperature transient. Therefore, either the assumptions used to evaluate the mass in the middle were inconsistent, or the model is stiff (following paragraphs explain stiffness). Furthermore, there was a severe restriction on the size of the time step of integration in order to perform model analysis. The integrator time step had both an upper bound of 0.1 ms and a lower bound of 0.06 ms.

Based on the evaluation of the state average model, two major concerns were identified: fluctuations of questionable validity appear in the outlet total temperature; and a severe restriction of possible time step size is required for the analysis to run successfully.

These concerns led to a closer scrutiny of the underlying assumptions. Since the assumptions are algebraic equations, as soon as a change at the inlet occurs (such as a step), the middle state variables respond instantaneously. Since the outlet variables are related to the inlet variables through differential equations, the response of the outlet variables has a delay associated with it. Aiken [14] states that such a mixture of algebraic and differential

equations does indeed produce a stiff system. The small upper bound on time-step size is a classical symptom of a stiff system. The problem of stiffness occurs if the solutions of a system have severely different convergence rates. Aiken [14] gives a more formal definition of stiffness in his book. Interested readers are referred to pages 1 to 4. The lower bound on the time-step size of the integrator is explained by a closer examination of equations 22 and 23. The value of the mass in the machine is estimated at the new time level and is computed using specified changes at the inlet as the first guess. Hence, this new guess (numerator of equation 22) is independent of the time-step size. It is therefore possible to take such a small time step that the value of  $dm/dt$  becomes larger in magnitude than the value of inlet mass-flow rate. When this large value of  $dm/dt$  is inserted into equation 23, the value of mass flow rate out becomes negative. That is, the model predicts back flow at the outlet. This means that the choice of input variables and time step is such as to produce a condition that is unlikely to occur in practice (a step rise in inlet temperature over such a short time increment is very unlikely in practice). Under these conditions the solution algorithm fails to converge, and the state average model fails.

In summary: the state average model correctly predicted final steady state values; was severely limited in range of the time-step size required for execution; and exhibited a jagged response to a step change in input state. Therefore, it was decided to pursue the

development of an alternative algorithm, using the results produced by the state-average model for guidance.



### 3.4 THE CONSTANT-MACH-NUMBER-IN-THE-MIDDLE MODEL

Recognizing the stiffness problem of the state-average model, alternative assumptions were investigated in an effort to develop a better model. Assuming a constant Mach number through the middle of the machine appeared to accomplish this goal. This model incorporates the continuity, energy and momentum equations along with the following assumptions:

$$X_m = (X_i + X_o) / 2 \quad (28)$$

$$M_m = \text{constant} \quad (29)$$

$$Z_m = Z_i (X_m / X_i)^{f(K, \eta)} \quad (30)$$

where,

X, and Z are any thermodynamic properties such as total temperature, total pressure, etc.

M<sub>m</sub> is the Mach number in the middle of the machine

i, m, and o, are inlet middle and outlet respectively

K, is a combination of thermodynamic gas constants, and

η, is an appropriately defined polytropic efficiency from inlet to middle of the machine.

The exponent η and K depend on the choice of thermodynamic variables.

The algorithm used to solve this class of models is shown in figure 17. The assumption of constant Mach number in the middle of the machine seemed reasonable because the Mach number distribution through the blading is known after the design of a turbomachine is complete.

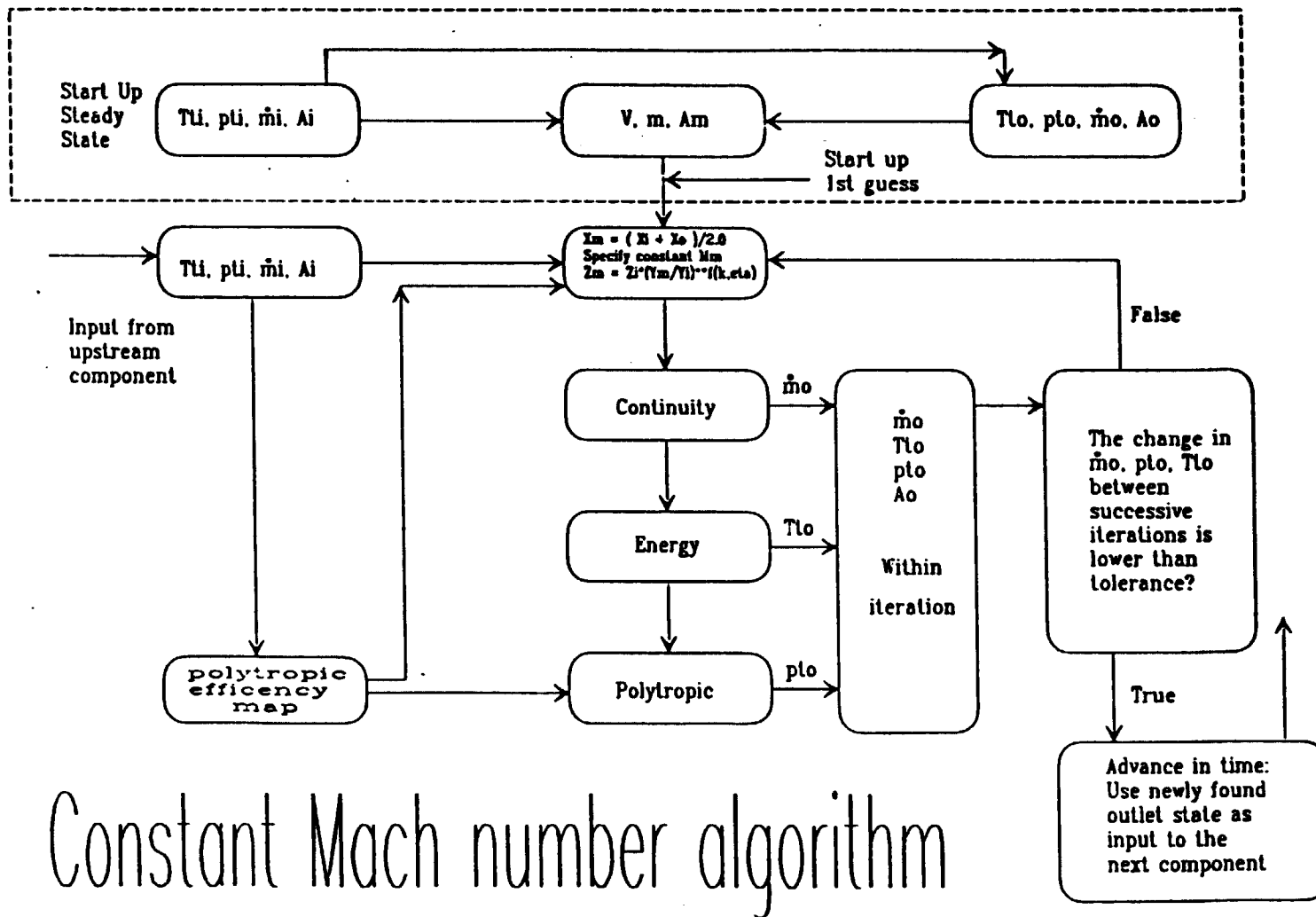


Figure 17. Algorithm for the constant-mach-number-in-the-middle model.

The algorithm for this model is the same as the one described in the previous section, except that the Mach number in the middle is kept constant through out the iteration procedure, and also throughout the time marching procedure.

Table 2 presents the information used to perform a turbomachinery analysis. Specifically table 2 lists; the geometry of the turbine to be simulated; the design point data for the turbine; the perturbation to the design steady-state value to initiate a transient; and the thermodynamic steady-state values expected at the end of the simulation. The perturbation of the initial steady-state is a ramp of input state variables over a period of 5 micro seconds. The ramp was chosen instead of a step so that the system experiences the same severity of transient independent of the selected time-step size. After 5 micro seconds the input remains constant at the new value. This new constant value of the inlet state results in a new steady-state value for the outlet-state variables. This outlet steady state is evaluated using the steady-state equations and then compared with the values predicted by the transient model. The purpose of the comparison is to provide a check of the transient model. The integration time-step size was chosen as 1 micro second. The simulation results obtained are presented in figures 18-24.

Figure 18 shows the transient in outlet total temperature obtained by the simulation. The initial rise in the outlet total temperature occurs during the time that the inlet is ramped up. At the end of the ramp, the outlet total temperature falls rapidly but rises again

**Table 2: Data for results presented in figures 18 - 24**

**Turbine Geometry:**

Inlet normal area:	4.668E-3 m <sup>2</sup>
Middle normal area:	5.158E-3 m <sup>2</sup>
Outlet normal area:	5.648E-3 m <sup>2</sup>
Volume of compressor:	1.000E-4 m <sup>3</sup>
Tip radius:	8.810E-2 m
Middle radius:	4.896E-2 m
Rotor Inertia:	0.082 Kg m <sup>2</sup>

**Design point data:**

Inlet total temperature:	1034.02 K
Outlet total temperature:	866.01 K
Inlet total pressure:	540.25 KPa
Outlet total pressure:	330.14 KPa
Mass flow rate:	1.2886 Kg/sec
Rotor speed:	3351.0 Hz
Total to total polytropic efficiency:	0.901

**Perturbation at inlet to obtain transient response:**

Ramp inlet total temperature to:	1035.02 K
Ramp inlet total pressure to:	540.35 KPa
Ramp inlet mass flow to:	1.3 Kg/sec

**Expected steady state outlet states:**

Outlet total temperature:	867.01 K
Outlet total pressure:	330.316 KPa
Outlet mass flow rate:	1.3 Kg/sec

**Additional notes:**

Constant specific heat:	519.14 J/Kg/K
Constant gas constant:	207.44 J/Kg/K
Constant speed:	3351.00 Hz
Variable rate of work out:	
Constant Mach number in middle:	0.45

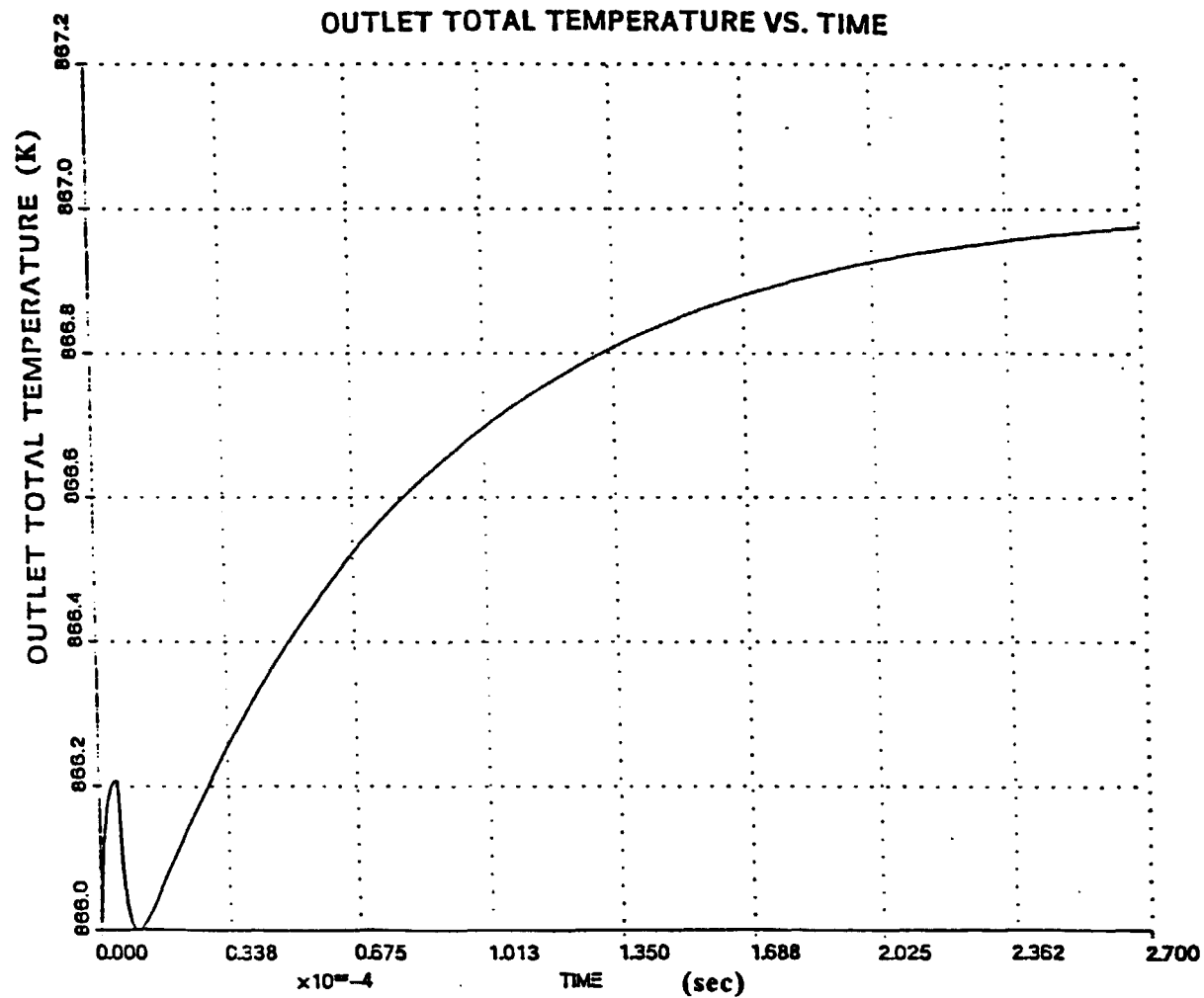


Figure 18. Response of the outlet total temperature of the turbine to ramps described by table 2. Time step is 1 micro second.

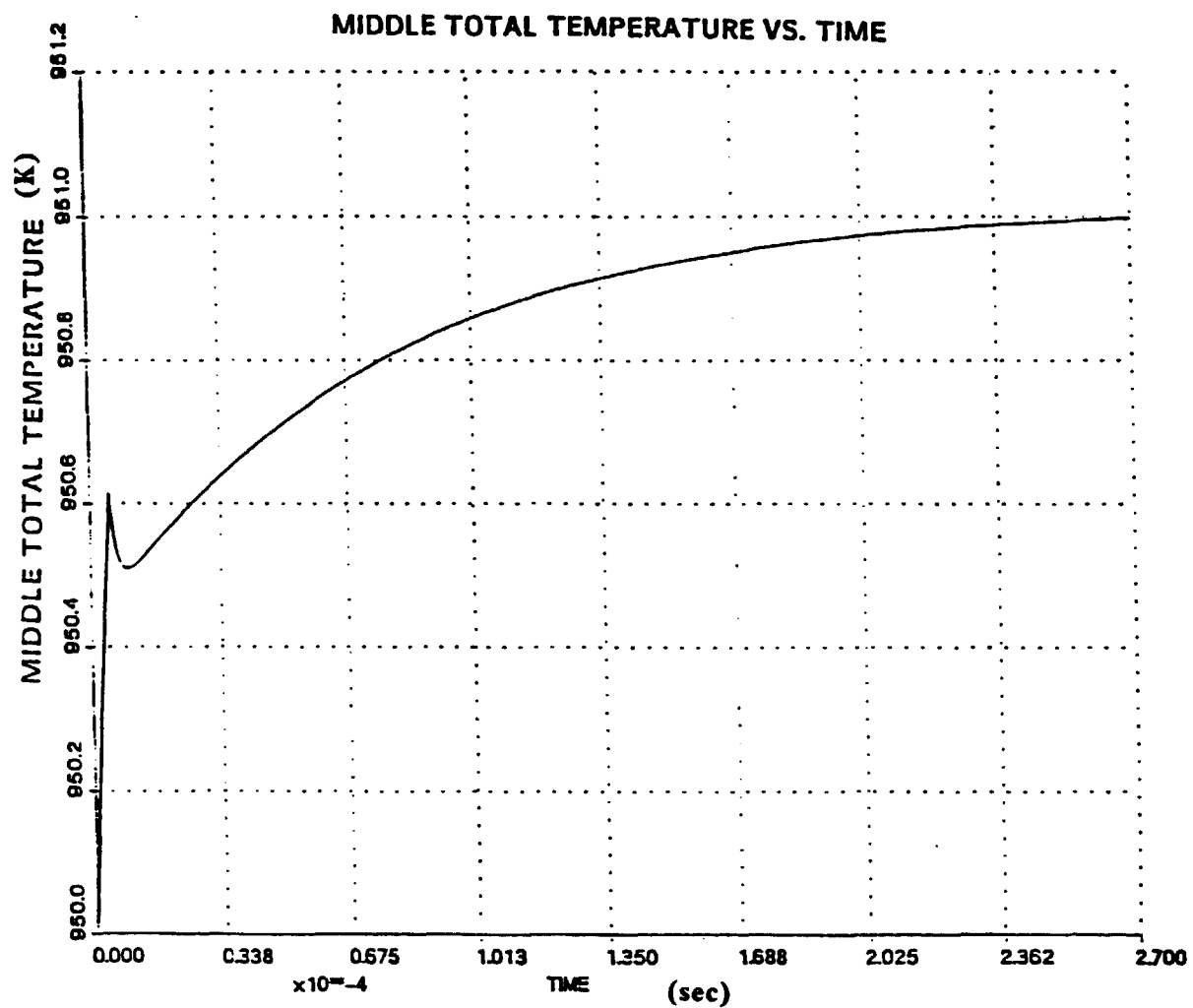


Figure 19. Response of the middle total temperature of the turbine to ramps described by table 2. Time step is 1 micro second.

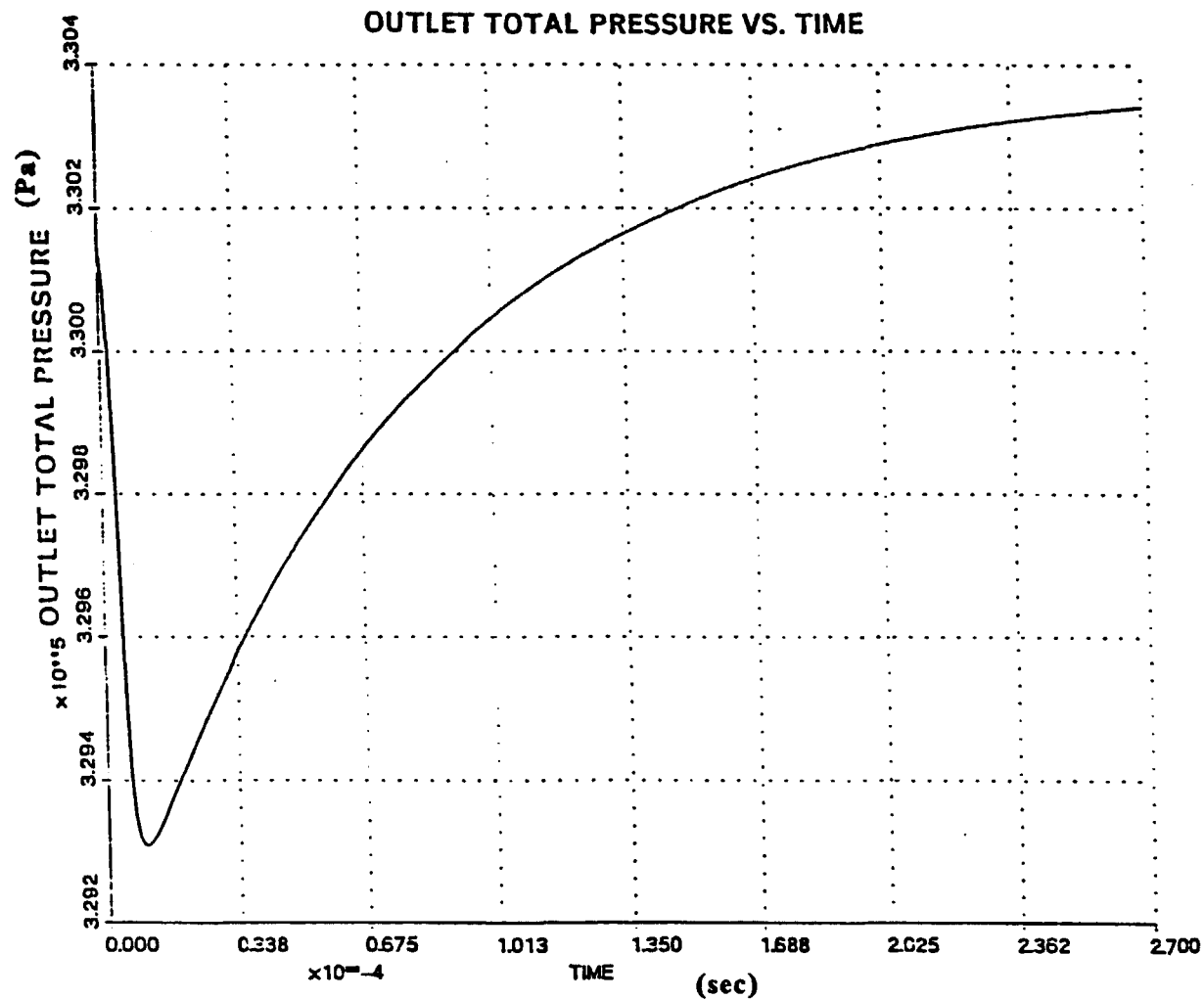


Figure 20. Response of the outlet total pressure of the turbine to ramps described by table 2. Time step is 1 micro second.

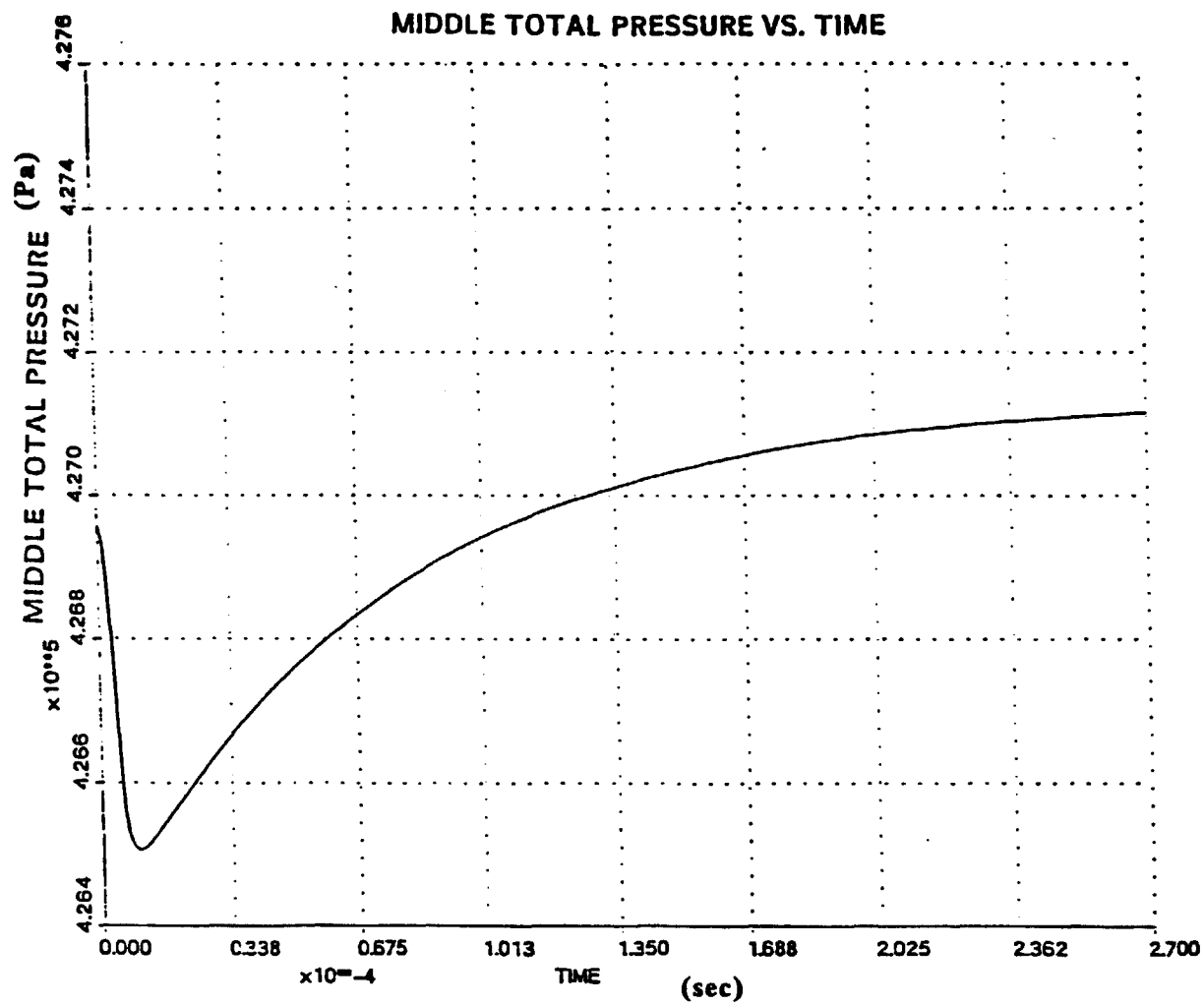


Figure 21. Response of the middle total pressure of the turbine to ramps described by table 2. Time step is 1 micro second.



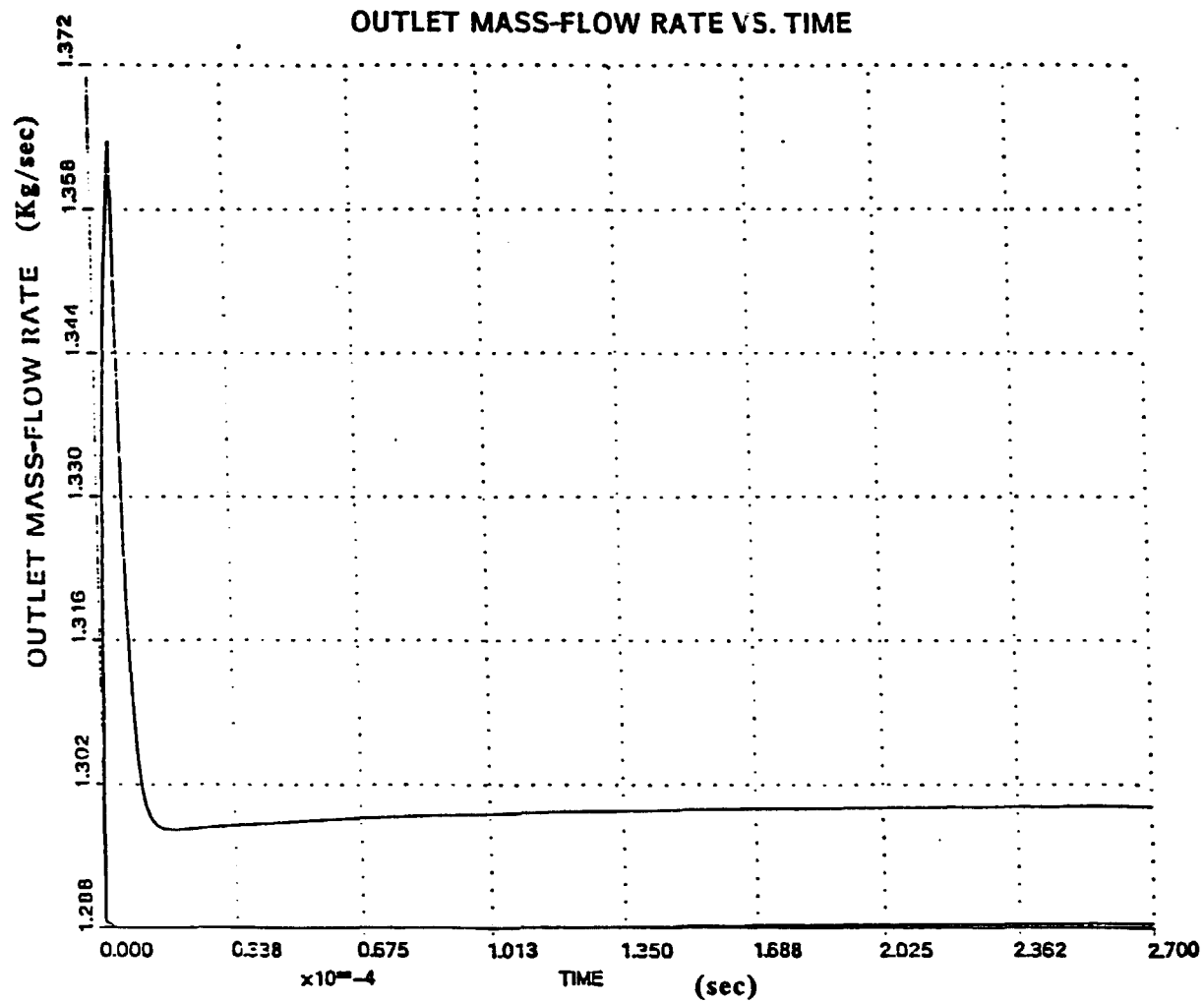


Figure 22. Response of the outlet mass-flow rate of the turbine to ramps in described by table 2. Time step is 1 micro second.

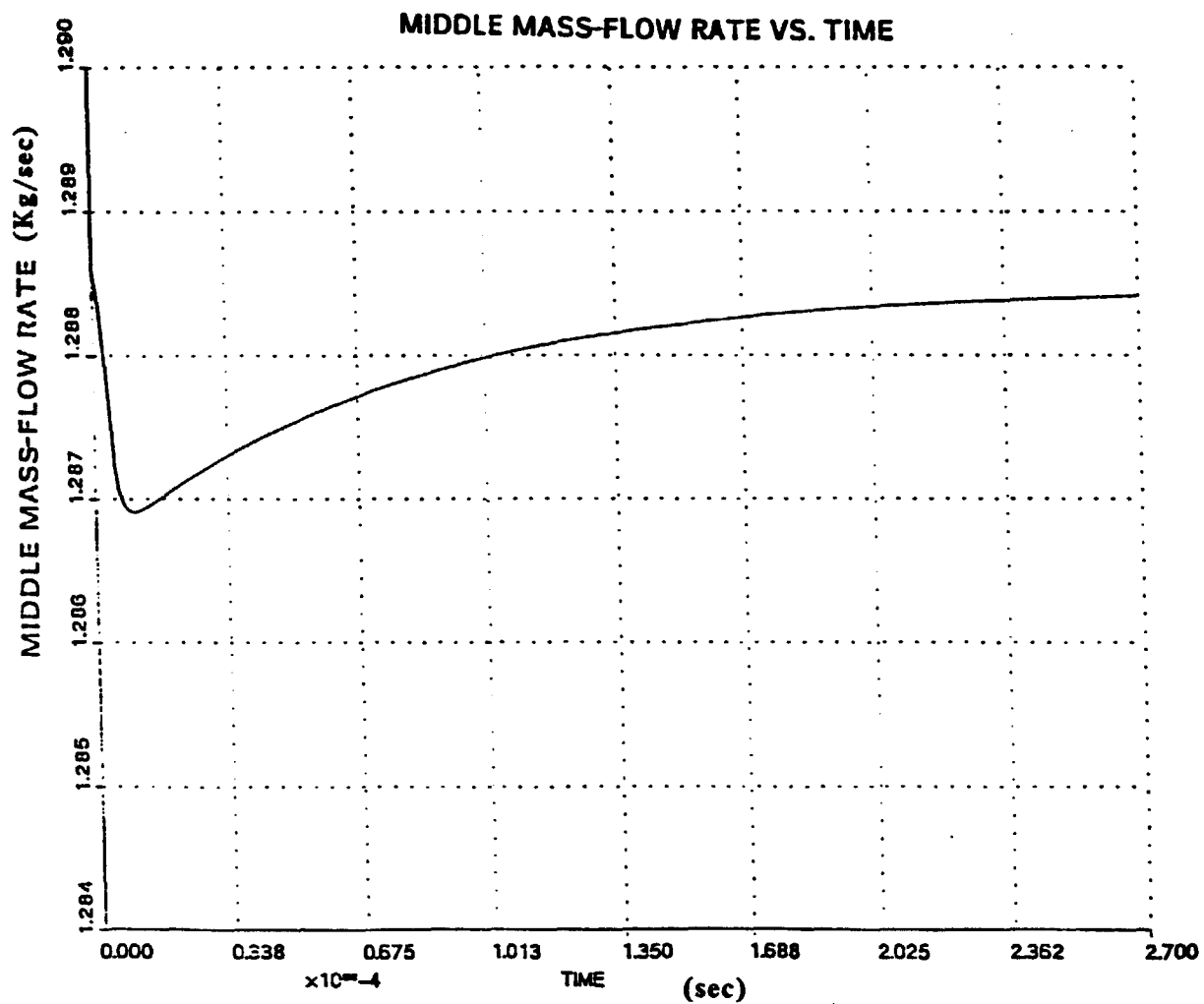


Figure 23. Response of the middle mass-flow rate of the turbine to ramps described by table 2. Time step is 1 micro second.

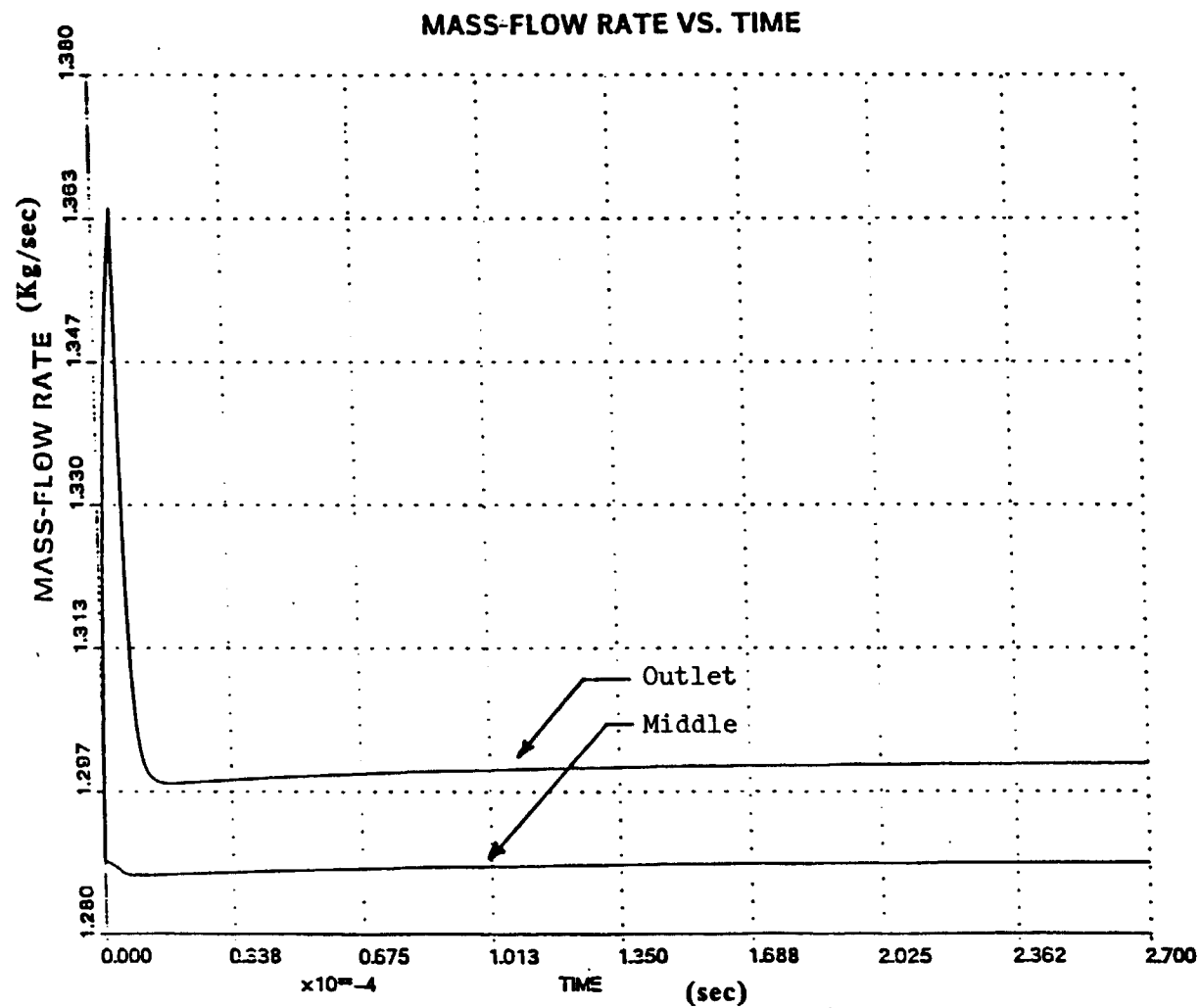


Figure 24. Response of the middle and outlet mass-flow rate of the turbine to ramps described by table 2. Time step is 1 micro second.

to predict the correct final steady-state temperature. Figure 19 shows the response of the total temperature in the middle of the turbine. The final steady-state value obtained by the transient model matches the steady-state values obtained from the steady-state equations. Figures 20 and 21 show the response of outlet total pressure and middle total pressure respectively. Once again the final steady-state values for total pressure match the expected values. Figures 22 and 23 show the response of both the outlet and the middle mass flow rates.

Figure 24 is a clear statement of the failure of this class of models. While the outlet mass flow rate is correctly predicted, the final steady-state mass flow rate in middle of the machine is incorrect. In fact, at final steady-state, mass flow rate through middle and outlet are predicted to be different. This difference in mass-flow rates violates conservation of mass! The root of the problem lies with the fact that the Mach number specified in the middle of the machine is only correct for a specific set of flow conditions. For all others it is incorrect.

Based on the failure of the constant-Mach-number-in-the-middle model to satisfy conservation of mass, it was judged unacceptable. Examination of the performance of this model, and preceding models, indicated that development of a successful transient model would require careful selection of the algorithm used for advancing the solution in time.

### 3.5 CHOICE OF INTEGRATOR

Initially, the solution algorithm was implemented using an implicit first order Euler integrator for the time terms. Aiken [14] states that this technique is the most stable available, but suffers from large truncation error. To obtain sufficient accuracy, the step size must be very small. Three integrators were chosen for evaluation: implicit Euler first order; implicit Euler second order; and implicit Runge Kutta fourth order (RK4). The constant-Mach-number-in-the-middle model was used to evaluate the performance of these algorithms.

Table 3 presents information used to evaluate performance of the integrators. Specifically table 3 lists: the geometry of the compressor to be simulated; the design point data for the compressor; the perturbation to the steady-state value to initiate a transient; and the thermodynamic steady-state values expected at the end of the simulation. The perturbation of the steady state is achieved by a step rise of 1 K in inlet total temperature. A time-step size of one micro second was selected to evaluate the performance of the solution technique.

As detailed elsewhere in the thesis the computational model has both an upper bound and a lower bound in time-step size. The basis for selecting an appropriate time-step size for a given application is discussed in section 3.7. The results of the simulations are presented in figures 25-28.

Figures 25 and 26 show the response of the outlet total temperature for the transients listed in table 3. Figure 26 shows an

**Table 3: Data for results presented in figures 25 - 28**

**Compressor Geometry:**

Inlet normal area:	2.297E-3 m <sup>2</sup>
Middle normal area:	1.711E-3 m <sup>2</sup>
Outlet normal area:	1.125E-3 m <sup>2</sup>
Volume of compressor:	5.160E-5 m <sup>3</sup>
Tip radius:	4.480E-2 m
Hub radius:	1.250E-2 m

**Design point data:**

Inlet total temperature:	340.0 K
Outlet total temperature:	440.0 K
Inlet total pressure:	320.0 KPa
Outlet total pressure:	559.9 KPa
Mass flow rate:	1.2886 Kg/sec
Rotor speed:	3351.0 Hz
Total to total polytropic efficiency:	0.867

**Perturbation at inlet to obtain transient response:**

Step inlet total temperature to:	341.0 K
Keep inlet total pressure at:	320.0 KPa
Keep inlet mass flow at:	1.2886 Kg/sec

**Expected steady state outlet states:**

Outlet total temperature:	441.0 K
Outlet total pressure:	559.9 KPa
Outlet mass flow rate:	1.2886 Kg/sec

**Additional notes:**

Constant specific heat:	519.14 J/Kg/K
Gas constant:	207.44 J/Kg/K
Constant speed:	3351.00 Hz
Constant rate of work input:	66,865.2 J/sec

# Total Outlet Temp. vs. Time

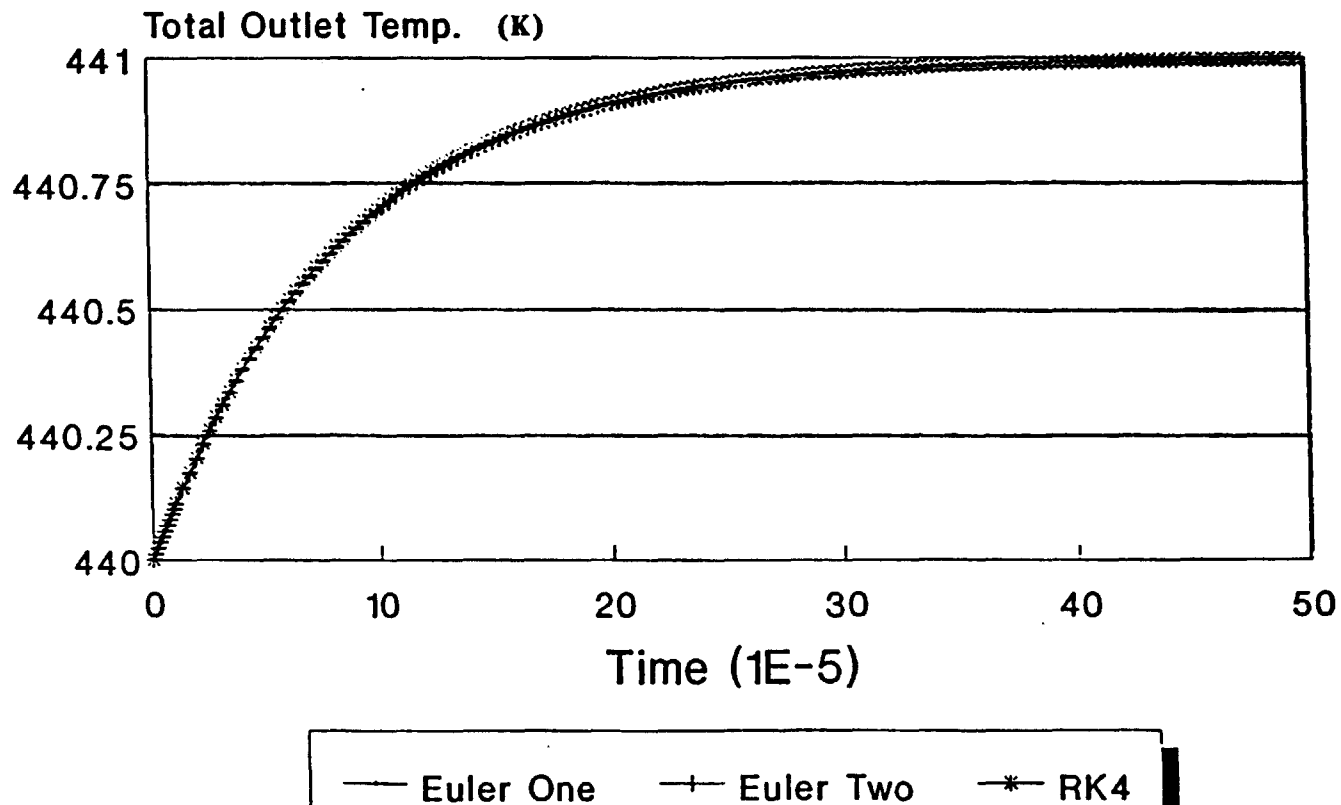


Figure 25. Response of the outlet total temperature for the compressor to step input of 1 K in inlet total temperature. Time step is 1 micro second.

# Total Outlet Temp. vs. Time

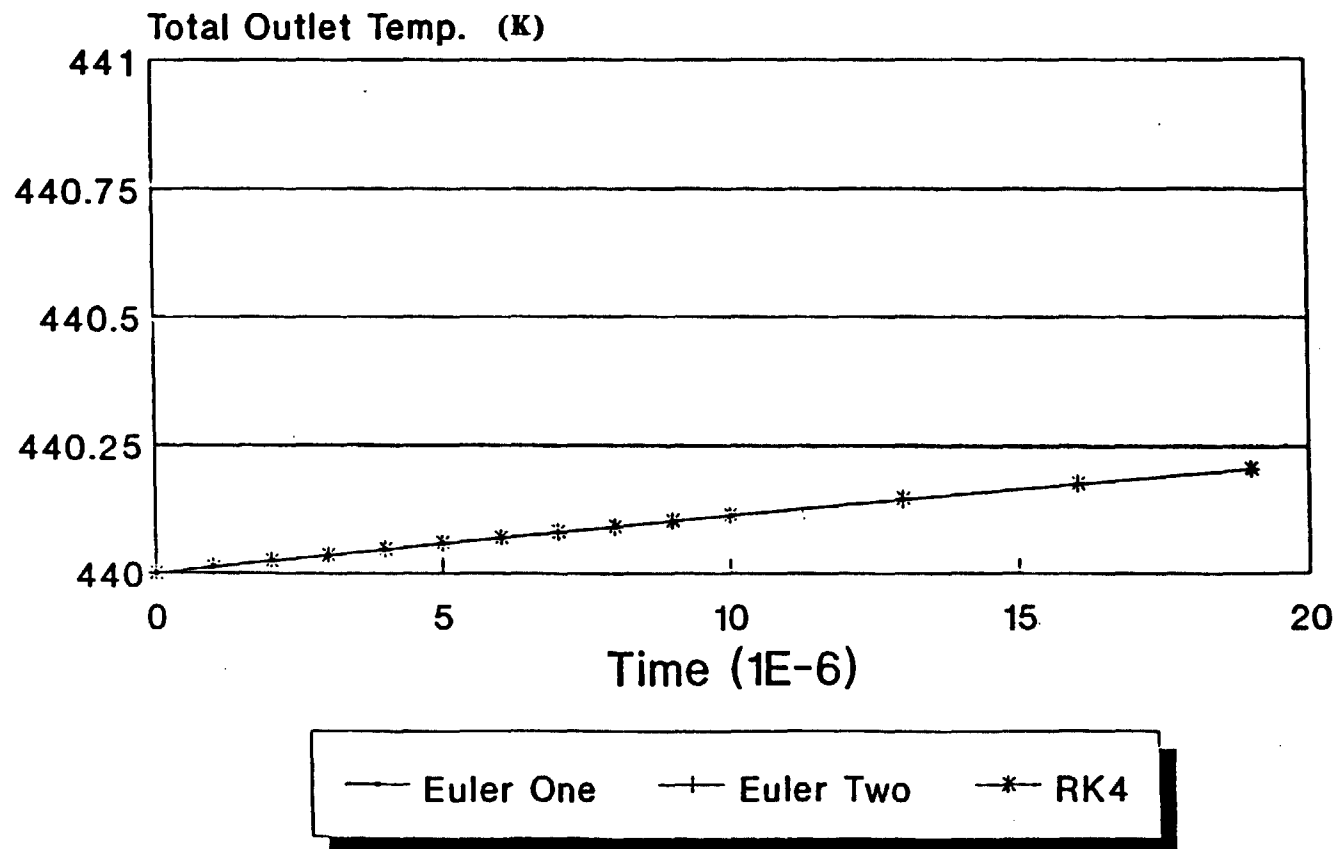
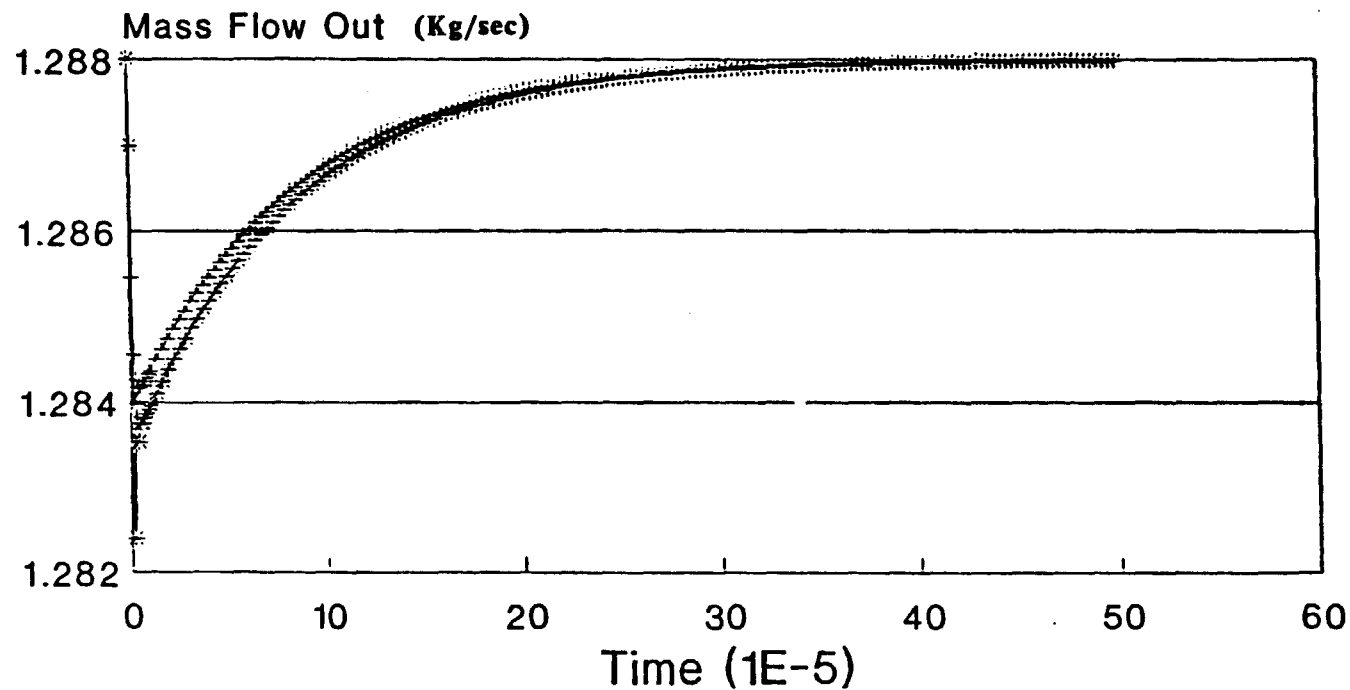


Figure 26. Expanded view of the response of outlet total temperature for the compressor to step input of 1 K in inlet total temperature. Time step of integration is 1 micro second.



# Mass Flow Out vs. Time



— Euler One    —+ Euler Two    \*— RK4

Figure 27. Response of the outlet mass flow rate for the compressor to step input of 1 K in inlet total temperature. Time step is 1 micro second.

# Mass Flow Out vs. Time

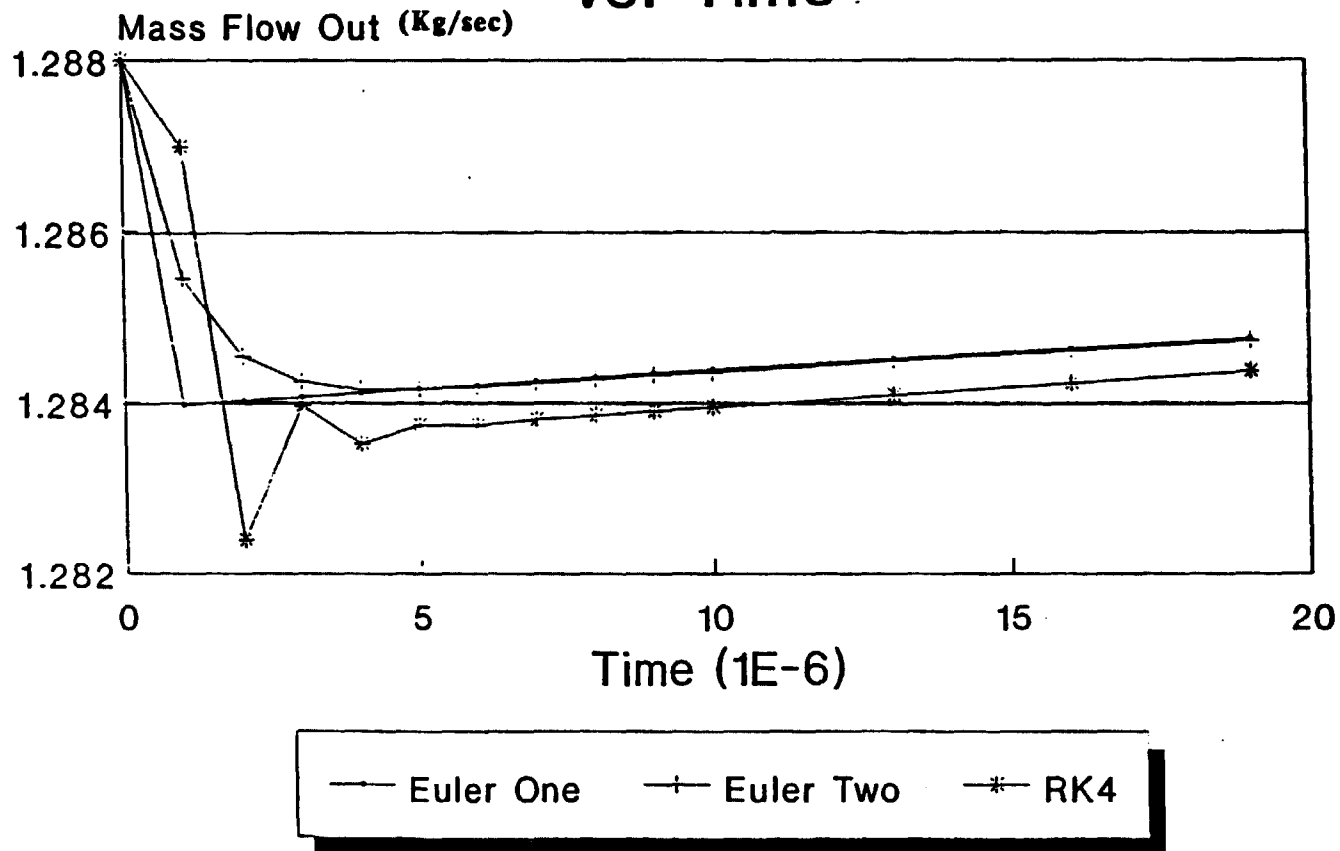


Figure 28. Expanded view of the response of outlet mass flow rate for the compressor to step input of 1 K in inlet total temperature. Time step of integration is 1 micro second.

expanded view of figure 25. The response obtained for the outlet total temperatures from the 3 integrators is indistinguishable. However, a comparison of outlet mass flow rate transients, shown in figure 27, does show differences. Figure 28 shows an expanded view of the initial transient. First order Euler is apparently the smoothest but from analysis it is known that the accuracy of implicit Euler 2nd order is better. RK4 shows questionable fluctuations and requires the greatest computational effort. This type of oscillatory response is typical of RK4 predictions of stiff systems [14].

Although the response predicted by both implicit algorithms appears reasonable, the response predicted by the second order algorithm is smoother and more closely resembles what one expects based on intuition. Further, it is known that the second order algorithm has a smaller truncation error for a given time-step size and therefore is more accurate.

Based on the above results, the implicit Euler second order algorithm was chosen as the integrator for future work. It provides both accuracy and stability and requires substantially less computing time than the RK4 integrator.

### 3.6 THE UPWIND-MASS-FLOW MODEL

Failure of the constant-Mach-number-in-the-middle model led to the development of the upwind mass flow model (UMFM). The UMFM was developed by applying the continuity, energy, polytropic, and moment of momentum equations to a single control volume which represents the turbomachine. The assumptions for this model are as follows:

$$T_{tm} = (T_{ti} + T_{to})/2 \quad (31)$$

$$\dot{m}_m = \dot{m}_i \quad (32)$$

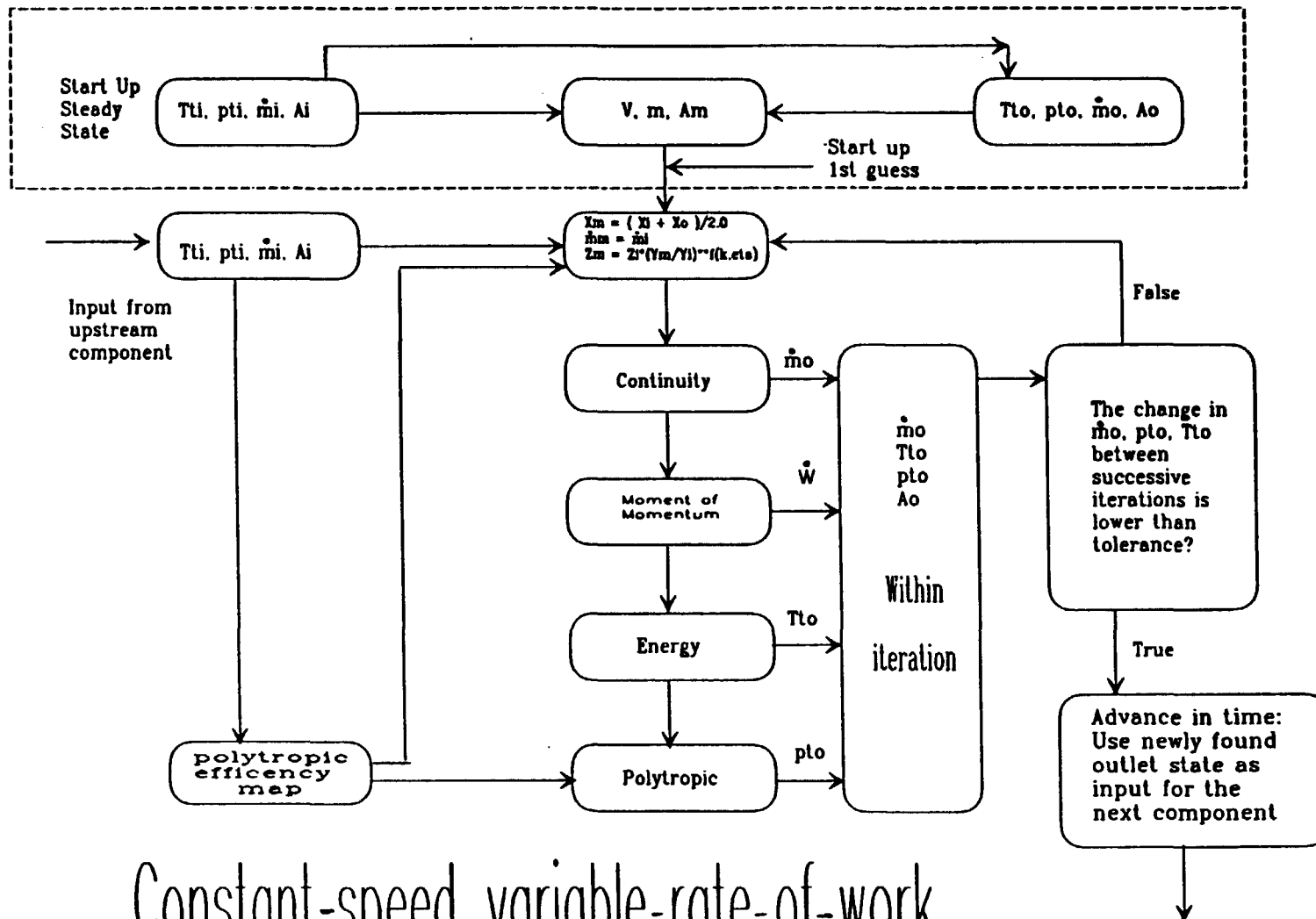
for the turbine:

$$P_{tm} = P_{ti} * (T_{tm} / T_{ti})^{Cp/R/\eta} \quad (33 a)$$

and for the compressor:

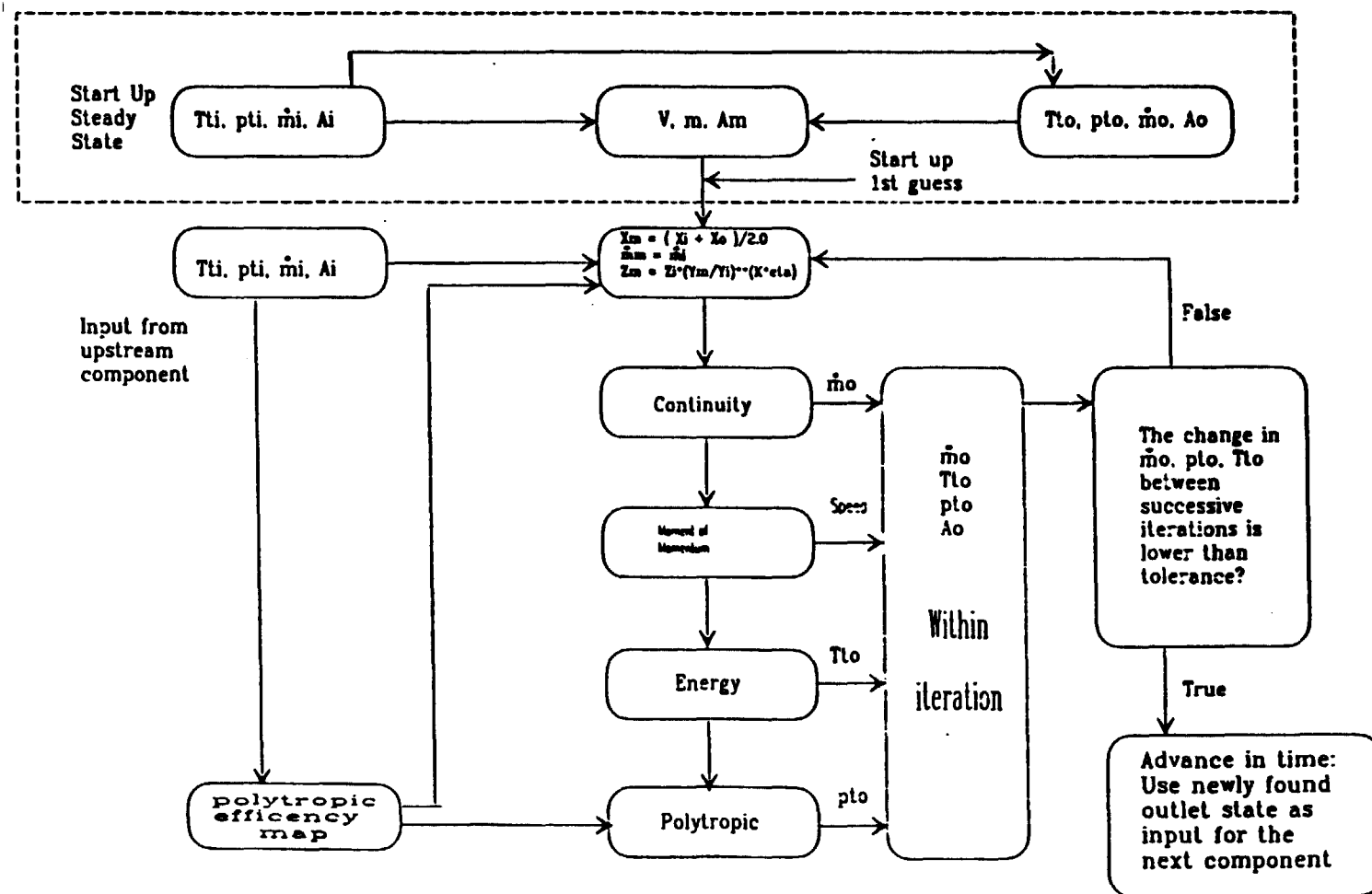
$$P_{tm} = P_{ti} * (T_{tm} / T_{ti})^{Cp*\eta/R} \quad (33 b)$$

Once again the general algorithm is the same as the one described previously, except that mass flow rate through the middle of the machine is assumed to be equal to the mass flow rate at the inlet. The moment of momentum equation is also added to this algorithm. The moment of momentum equation is utilized to obtain two different versions of the model. The first version of the model assumes constant speed operation and calculates the variable rate of work output. The second version assumes a constant rate of work while the rotor speed is allowed to change. Figure 29 shows the solution algorithm for the first version and figure 30 shows the solution algorithm for the second version. Only the results of the constant speed/variable rate of work model are presented below.



Constant-speed variable-rate-of-work

Figure 29. Algorithm for variable-rate-of-work constant-speed model.



## Constant-rate-of-work variable-speed

Figure 30. Algorithm for constant-rate-of-work variable-speed model.

### 3.6.1 Constant-Speed Variable-Rate-Of-Work Model

In this model, the rotor speed is assumed to be locked at 3351 Hz as specified by the DRO2 document [1]. A change in inlet total temperature results in a change in the rate of work output from the turbine.

Table 4 presents information used to perform the turbomachinery analysis. Specifically, table 4 lists: the geometry of the turbine to be simulated; the design point data for the turbine; the perturbation to the design steady state value to initiate a transient; and the thermodynamic steady-state values expected at the end of the simulation. The perturbation of the design steady state is achieved by ramping all the inlet state variables over a period of 250 micro seconds. After 250 micro seconds the inlet variables remain constant at their new values. Table 4 also shows that this transient is run for 3 different time steps, but that the ramp time of 250 micro seconds is the same for all the runs. This provides a good basis for the comparison of results obtained using different size time steps.

Figure 31 shows the response of mass-flow rate. There are 3 different curves shown in this figure. Each corresponds to a different time-step size. The difference in predicted response for the three time steps is small. Therefore, the larger integrator time step should be used to considerably reduce computational time. Figure 32 shows similar behavior in the rate of work output by the turbine. It also is clear that the difference in solutions reduces as smaller integration time step are chosen. In fact the difference

**Table 4: Data for results presented in figures 31 - 34**

**Turbine Geometry:**

Inlet normal area:	4.668E-3 m <sup>2</sup>
Middle normal area:	5.158E-3 m <sup>2</sup>
Outlet normal area:	5.648E-3 m <sup>2</sup>
Volume of compressor:	1.000E-4 m <sup>3</sup>
Tip radius:	8.810E-2 m
Middle radius:	4.896E-2 m
Rotor Inertia:	0.082 Kg m <sup>2</sup>

**Design point data:**

Inlet total temperature:	1034.02 K
Outlet total temperature:	866.01 K
Inlet total pressure:	540.25 KPa
Outlet total pressure:	330.14 KPa
Mass flow rate:	1.2886 Kg/sec
Rotor speed:	3351.0 Hz
Total to total polytropic efficiency:	0.9010

**Perturbation at inlet to obtain transient response:**

Ramp inlet total temperature to:	1035.02 K
Ramp inlet total pressure to:	540.35 KPa
Ramp inlet mass flow to:	1.3 Kg/sec

**Expected steady state outlet states:**

Outlet total temperature:	867.01 K
Outlet total pressure:	330.316 KPa
Outlet mass flow rate:	1.3 Kg/sec

**Additional notes:**

Constant specific heat:	519.14 J/Kg/K
Gas constant:	207.44 J/Kg/K
Constant speed:	3351.00 Hz
Variable rate of work out:	
3 different time steps:	50.0E-6 sec 10.0E-6 sec 5.0E-6 sec



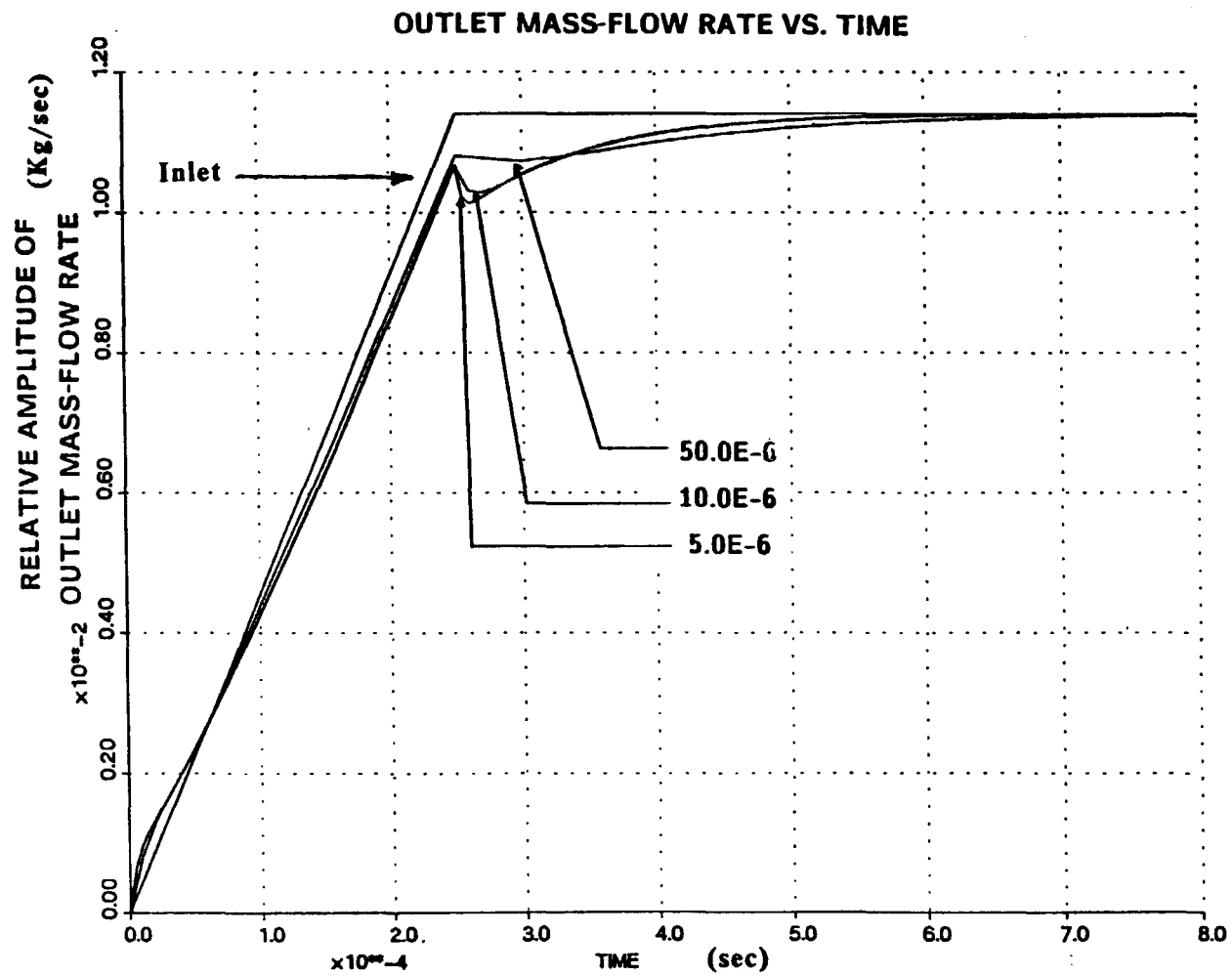


Figure 31. Response of the outlet mass-flow rate for the turbine to ramps described by table 4. The three plots shown correspond to time steps of 5 micro seconds, 10 micro seconds, and 50 micro seconds.

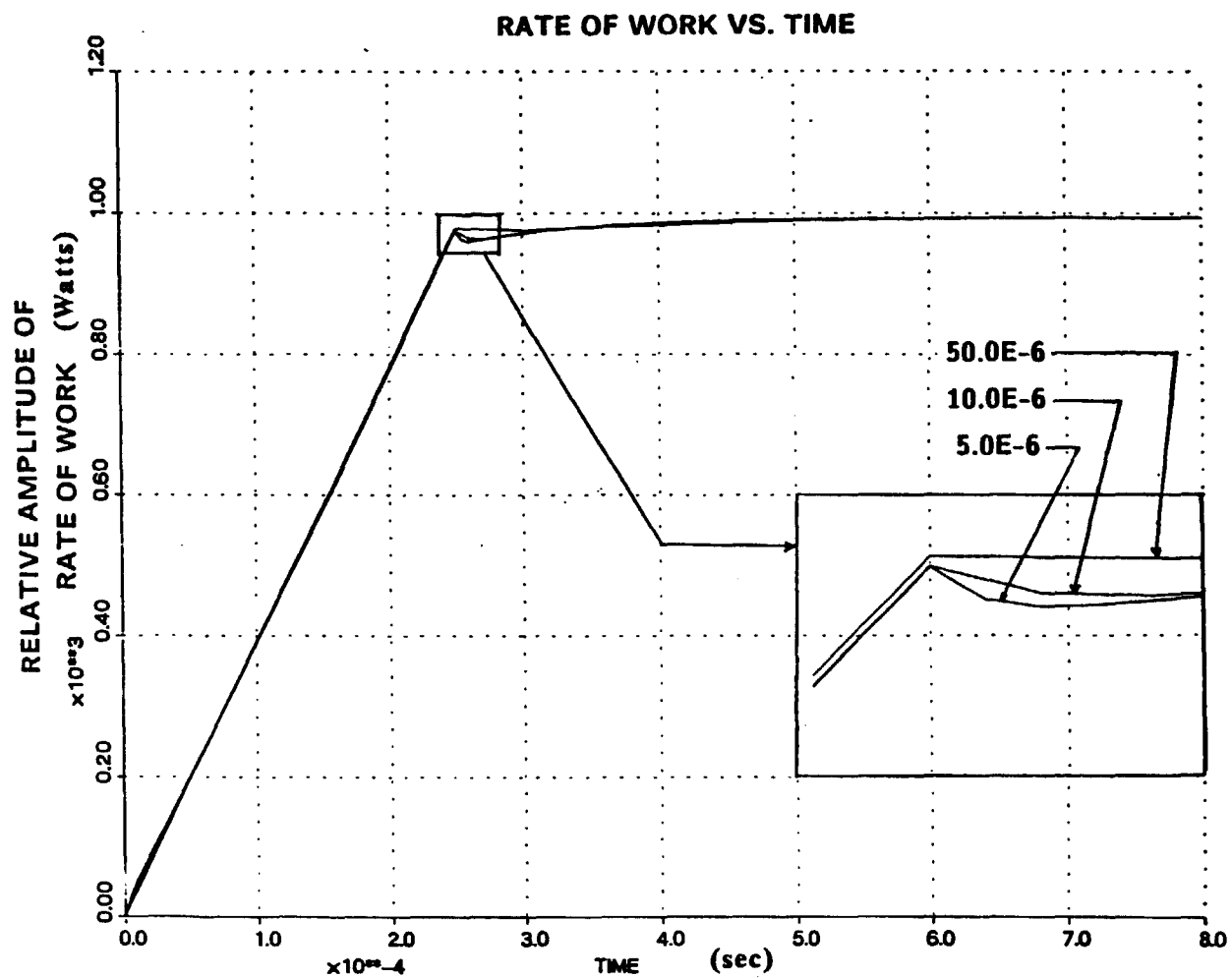


Figure 32. Response of the rate of work output for the turbine to ramps described by table 4. The three plots shown correspond to time steps of 5 micro seconds, 10 micro seconds, and 50 micro seconds.

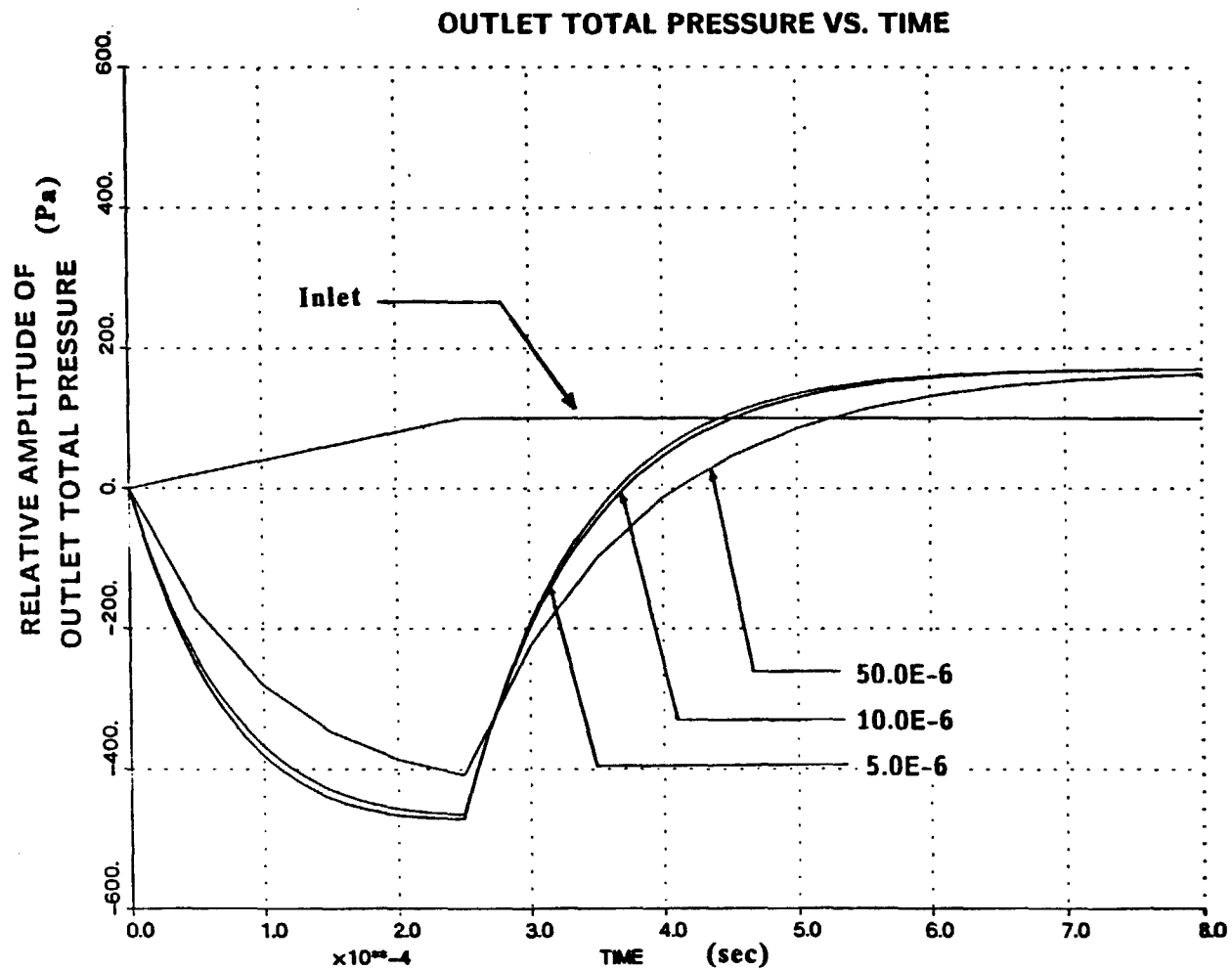


Figure 33. Response of the outlet total pressure, for the turbine, to ramps described by table 4. The three plots shown correspond to time steps of 5 micro seconds, 10 micro seconds, and 50 micro seconds.

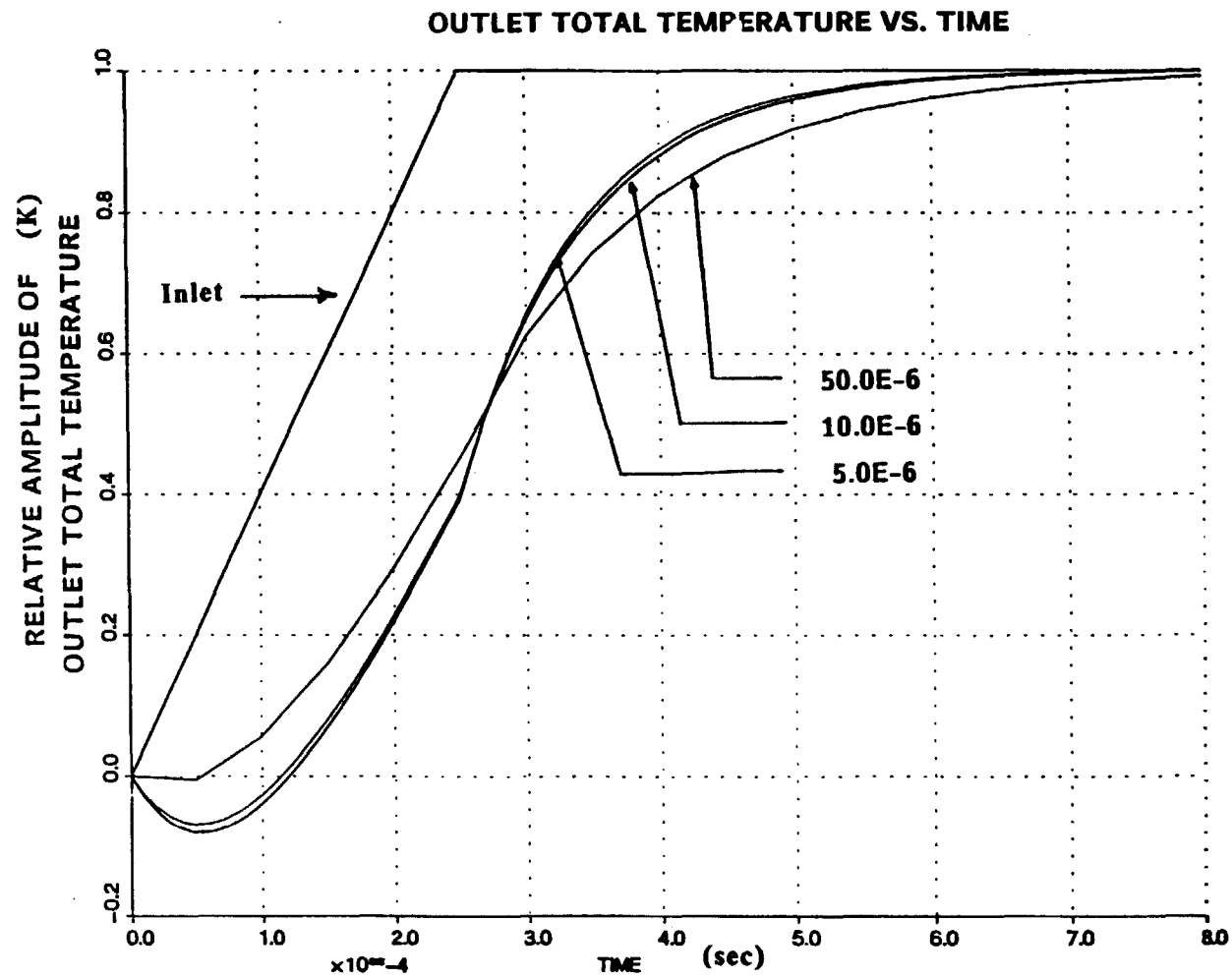


Figure 34. Response of the outlet total temperature, for the turbine, to ramps described by table 4. The three plots shown correspond to time steps of 5 micro seconds, 10 micro seconds, and 50 micro seconds.

between the 1 micro second solution and the 5 micro second solution is almost imperceptible. Even the 50 micro second solution appears to be satisfactory. Figure 33 shows the outlet total pressure response for the three time-step sizes. Once again, the solutions appear to converge as time-step size decreases. However, it should be noted that even the larger time step is representative of the solution obtained by the smaller time step. Figure 34 shows the total outlet temperature variation over time. Once again the solution obtained from the larger integrator time step is representative of the response.

In summary of the ramp test, two very useful conclusions can be drawn.

- 1) The steady state is predicted correctly for all state variables.
- 2) The differences in responses due to an order of magnitude larger time-step size is small and probably negligible for most applications.

It should be noted that the results show a small change in outlet thermodynamic state at the instant a change in inlet state occurs. The propriety of this instant response warrants further examination, and the issue of appropriate outlet response is examined in detail in the next section.

### 3.7 OUTLET RESPONSE DYNAMICS

Two methods of information travel through the turbomachine have been examined. In the first method, information travels along the characteristic lines of the flow through the turbomachine. In the second method, information is transmitted by the rigid rotating rotors inside the turbomachine.

Information travel in the first method is along the characteristic lines of the flow through the turbomachine passage just as one would consider flow through a duct. Consider the duct shown in figure 35.

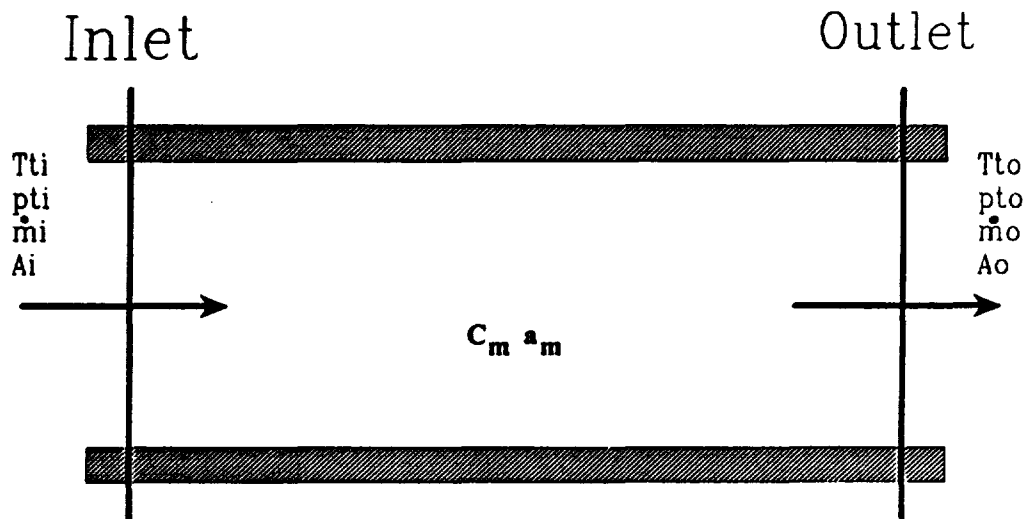


Figure 35: A duct representing a simplified turbomachine control volume.

It is assumed that the duct is operating under steady state conditions. At the inlet, the thermodynamic state of the fluid is described by the following state variables:

$T_{t1}$  - Total temperature of fluid at inlet;

$P_{t1}$  - total pressure of the fluid at inlet;

$\dot{m}_1$  - mass flow rate of fluid at inlet;

$A_1$  - Area normal to flow direction at the inlet.

From the state variables, the velocity of fluid and the speed of sound in the fluid are evaluated as  $C_1$  and  $a_1$ , respectively. Similarly, the outlet thermodynamic state is described by the following state variables:

$T_{t0}$  - Total temperature of fluid at outlet;

$P_{t0}$  - total pressure of the fluid at outlet;

$\dot{m}_0$  - mass flow rate of fluid at outlet;

$A_0$  - Area normal to flow direction at the outlet.

Again the velocity of the fluid ( $C_0$ ) and the speed of sound ( $a_0$ ) can be evaluated from the given outlet state variables. The approximate speed of fluid through the control volume, ( $C_m$ ), can then be evaluated by averaging the inlet and outlet fluid velocities. Similarly, the speed of sound through the control volume ( $a_m$ ) can be approximated.

If the operating steady state is perturbed by an infinitesimal disturbance at the inlet (change in state variables), then the disturbance will travel through the fluid at the speed  $C_m + a_m$ . If the length of control volume is  $L$ , then the order of magnitude of transit time for the disturbance is:

$$\tau = L / (C_m + a_m) \quad (34)$$

The order of magnitude of the transit time for the turbine model under investigation is 55 micro seconds.

Information travel in the second method is due to the rotation of the rigid rotors. To understand this method of information travel, consider figure 36.

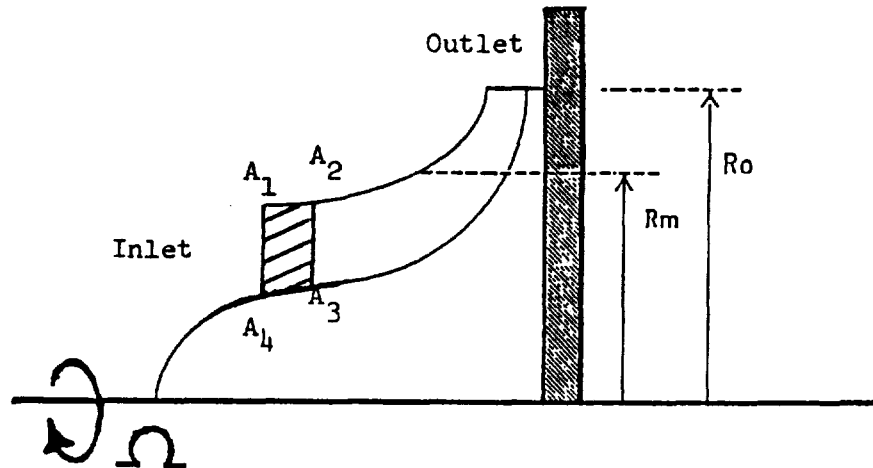


Figure 36: Longitudinal section of turbomachine rotor.



Figure 36 shows the side view of one of the rotors that rotate inside the control volume. It is assumed that the system is initially operating at a steady state. A disturbance, (change in thermodynamic inlet state variables). This disturbance will travel from inlet to line segment  $A_2A_3$  during one time step. Hence, a new thermodynamic state exists in the volume swept by the area  $A_1A_2A_3A_4$ . This new thermodynamic state changes the torque applied on the rotor. Since the rotor is rigid, this change affects fluid in contact with the entire length of the blade. Since the blade sweeps through the entire passage volume in less than 60 micro seconds, it is clear that the thermodynamic state of all fluid particles should change within this time period. Further, an infinitesimal disturbance will propagate across the passage in less than 10 micro seconds assuming that wave travels at sonic speed. Therefore, it is reasonable to use time-step sizes as small as 10 micro seconds in the models under evaluation by this study. It is concluded that prediction of an outlet response to an inlet disturbance within 10 micro seconds is not inconsistent with this method of information travel.

The rate of information travel predicted by the two methods is different. Since the two methods of information travel occur simultaneously in the turbomachine it is difficult to determine which method dominates the transient response. Both appear to have a measure of validity. This line of reasoning suggested the "sliced" model, introduced in the next section, as a compromise between the two points of view.

### 3.8 THE SLICED MODEL

In light of the discussion of section 3.7, the sliced model was developed to better approximate the wave model of information transmission. This model uses an averaging scheme to calculate the average total temperature, and average mass flow rate for the machine. These average states are not necessarily the states representing the middle of the machine, but rather they represent an average state for the control volume of the turbomachine. The representative temperature for the control volume is evaluated using the following equations:

$$\sum_{n=1}^{nod} T_{tn} = T_{ti}(t-\Delta\tau) + \frac{n-1}{nod-1} \left\{ T_{to}(t) - T_{ti}(t-\Delta\tau_n) \right\} \quad (35)$$

$$T_{tm}(t) = \frac{\sum_{n=1}^{nod} T_{tn}}{nod} \quad (36)$$

Similarly,

$$\sum_{n=1}^{nod} \dot{m}_n = \dot{m}_i(t-\Delta\tau) + \frac{n-1}{nod-1} \left\{ \dot{m}_o(t) - \dot{m}_i(t-\Delta\tau_n) \right\} \quad (37)$$

$$\dot{m}_m(t) = \frac{\sum_{n=1}^{nod} \dot{m}_n}{nod} \quad (38)$$

and the average total pressure in the machine (assumed turbine here) is evaluated using the following polytropic relationship:

$$P_{tm} = P_{ti} * ( T_{tm} / T_{ti} )^{C_p/\eta/R} \quad (39)$$

where in the above

$P_{tm}$  is the average total pressure for the control volume;

$T_{tm}$  is the average total temperature for the control volume;

$\dot{m}_m$  is the average mass-flow rate through the control volume;

$\Delta\tau_n$  is the time required for information to travel from the inlet to the node being evaluated;

$t$  is the current time level;

$dt$  is the integration time-step size;

$nod$  is the number of nodes chosen to span the control volume;

$n$  is the node number; and

$\eta$  is the total-to-total polytropic efficiency.

Note that the averaging equations reduce to a straight - inlet, outlet - average during steady-state operation. A geometric interpretation of the averaging procedure is presented in the following paragraphs.

The averaging procedure is based on the assumption that the inlet information travels only a finite distance through the control volume during an integration time step. Hence, if the inlet information travels only 1/4 the length of the control volume during an integration time step, only the first 25 percent of the flow passage should respond to the change in inlet conditions. The sequence of figures 37(a), 37(b), 37(c), 37(d), and 37(e), depict the values of the nodal temperature distribution as a function of time. These nodal temperatures are used for the evaluation of an average total

temperature in the control volume. Figure 37(a) shows the steady-state distribution of total temperatures along the length of the control volume. The control volume is divided into 4 equal segments. The segment boundaries are called nodes. Hence figure 37(a) has 4 segments and 5 nodes. For simplicity of discussion, it is assumed that information transverses one segment in one time step. The ovals in figure 37(a) show the value of total temperature at each node. Since figure 37(a) shows a steady-state operating condition, the averaging procedure will produce the same number as simply averaging the inlet and outlet total temperatures. The points chosen by the averaging procedure are represented by rectangles. Now, let the inlet total temperature be increased by a step, and then kept at the constant new value. Figure 37(b) shows the nodal values of total temperature (rectangles) that will be computed by the averaging procedure at that instant. After one time step, the information of the increased total temperature moves to node 1. Figure 37(c) shows the values of nodal temperatures (rectangles) that are computed by the averaging procedure. This process continues until the information has completely transversed the control volume. Figure 37(e) shows this condition. At this time the value of total temperature for the control volume is just the average of total temperatures at the inlet and the outlet. It should be noted that the steady-state condition is not reached until the outlet value ceases to change. The procedure to evaluate the average mass-flow rate through the control volume is very similar. However, rather than the value of the current outlet mass-flow rate, the value at the

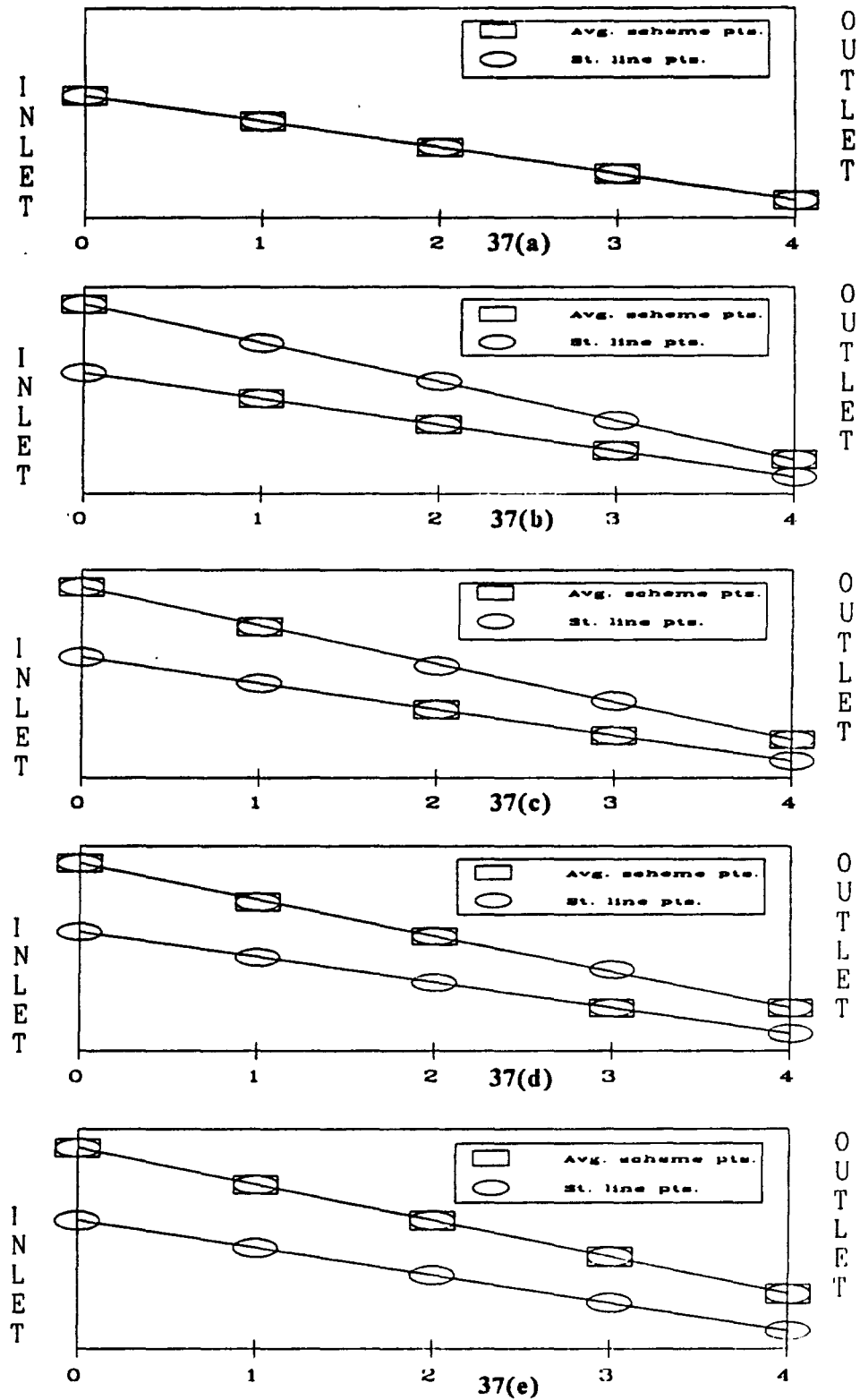


Figure 37. The sliced model nodal temperature distribution.

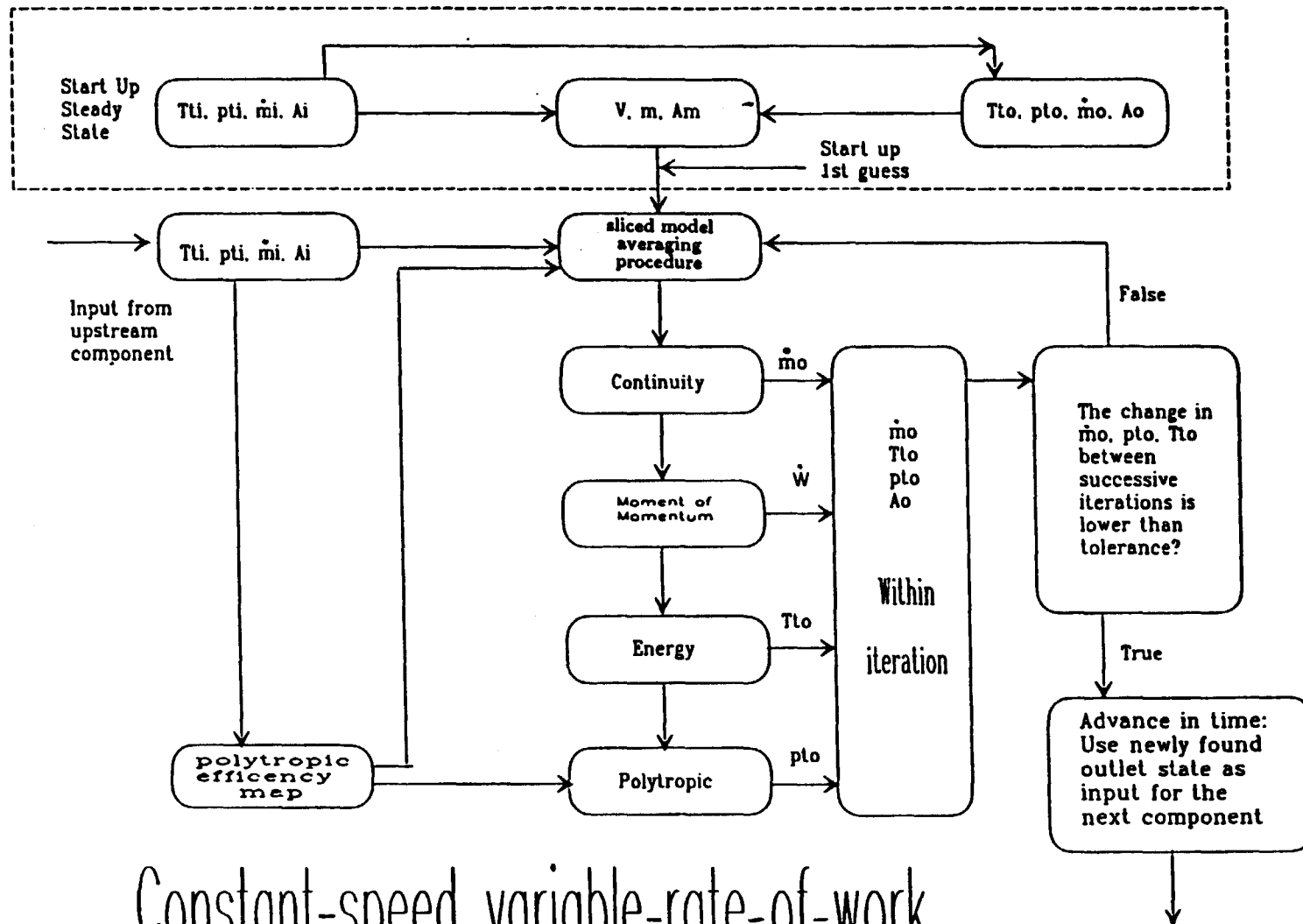
previous time step is used. The "lag" procedure for the mass flow rate in the control volume was selected to minimize numerical difficulties due to stiffness of the system of equations.

The moment-of-momentum equation can again be utilized to obtain two different versions of the model. The first version assumes a constant speed of operation and calculates the variable rate of work output. The second version assumes a constant rate of work while the rotor speed is allowed to change. Figure 38 shows the solution algorithm for the constant speed variable rate of work sliced model. Only results for the constant-speed variable-rate-of-work model are presented below.

#### 3.9.1 Constant-Speed Variable-Rate-Of-Work Model

In this model the rotor speed is assumed to be locked at 3351 Hz as specified by the DRO2 document [1]. A change in inlet total temperature results in a change in the rate of work output from the turbine.

Table 5 presents information used to perform the turbomachinery analysis. Specifically, table 5 lists: the geometry of the turbine to be simulated; the design point data for the turbine; the perturbation to the design steady-state value to initiate a transient; and the thermodynamic steady-state values expected at the end of the simulation. The perturbation of the design steady state is achieved by ramping all the inlet state variables over a period of 100 micro seconds. After 100 micro seconds the inlet remains constant at the new value. Table 5 also shows that this transient is run for 3 different time steps, but that the ramp time of 100 micro



Constant-speed variable-rate-of-work

Figure 38. Algorithm for variable-rate-of-work constant-speed-model.

**Table 5: Data for results presented in figures 39 - 42**

**Turbine Geometry:**

Inlet normal area:	4.668E-3 m <sup>2</sup>
Middle normal area:	5.158E-3 m <sup>2</sup>
Outlet normal area:	5.648E-3 m <sup>2</sup>
Volume of compressor:	1.000E-4 m <sup>3</sup>
Tip radius:	8.810E-2 m
Middle radius:	4.896E-2 m
Rotor Inertia:	0.082 Kg m <sup>2</sup>

**Design point data:**

Inlet total temperature:	1034.02 K
Outlet total temperature:	866.01 K
Inlet total pressure:	540.25 KPa
Outlet total pressure:	330.14 KPa
Mass flow rate:	1.2886 Kg/sec
Rotor speed:	3351.0 Hz
Total to total polytropic efficiency:	0.9010

**Pertubation at inlet to obtain transient response:**

Ramp inlet total temperature to:	1035.02 K
Ramp inlet total pressure to:	540.35 KPa
Ramp inlet mass flow to:	1.3 Kg/sec

**Expected steady state outlet states:**

Outlet total temperature:	867.01 K
Outlet total pressure:	330.316 KPa
Outlet mass flow rate:	1.3 Kg/sec

**Additional notes:**

Constant specific heat:	519.14 J/Kg/K
Gas constant:	207.44 J/Kg/K
Constant speed:	3351.00 Hz
Variable rate of work out:	
3 different time steps:	50.0E-6 sec 5.0E-6 sec 0.5E-6 sec



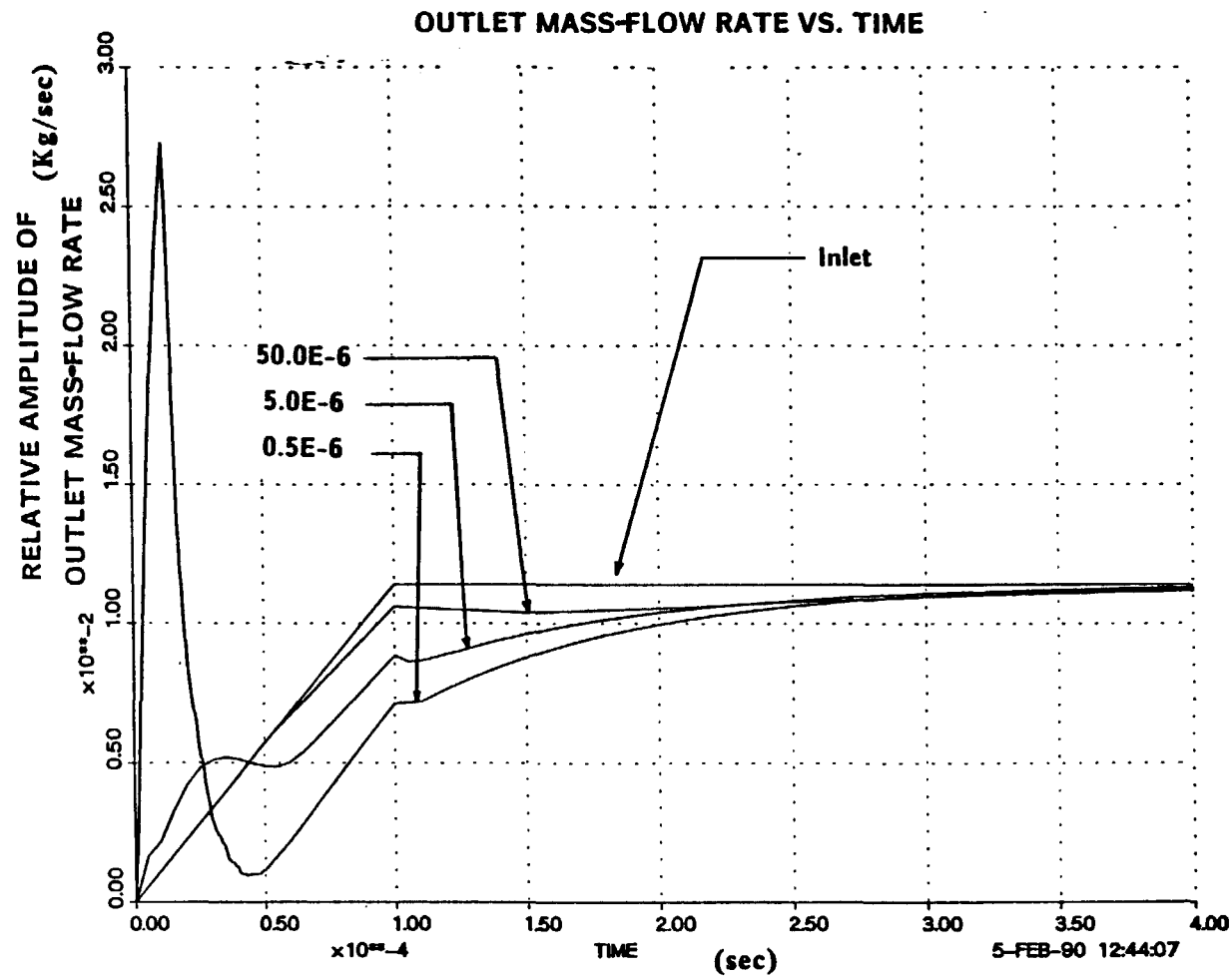


Figure 39. Response of the outlet mass-flow rate for the turbine to ramps described by table 5. The three plots shown correspond to time steps of 0.5 micro seconds, 5 micro seconds, and 50 micro seconds.

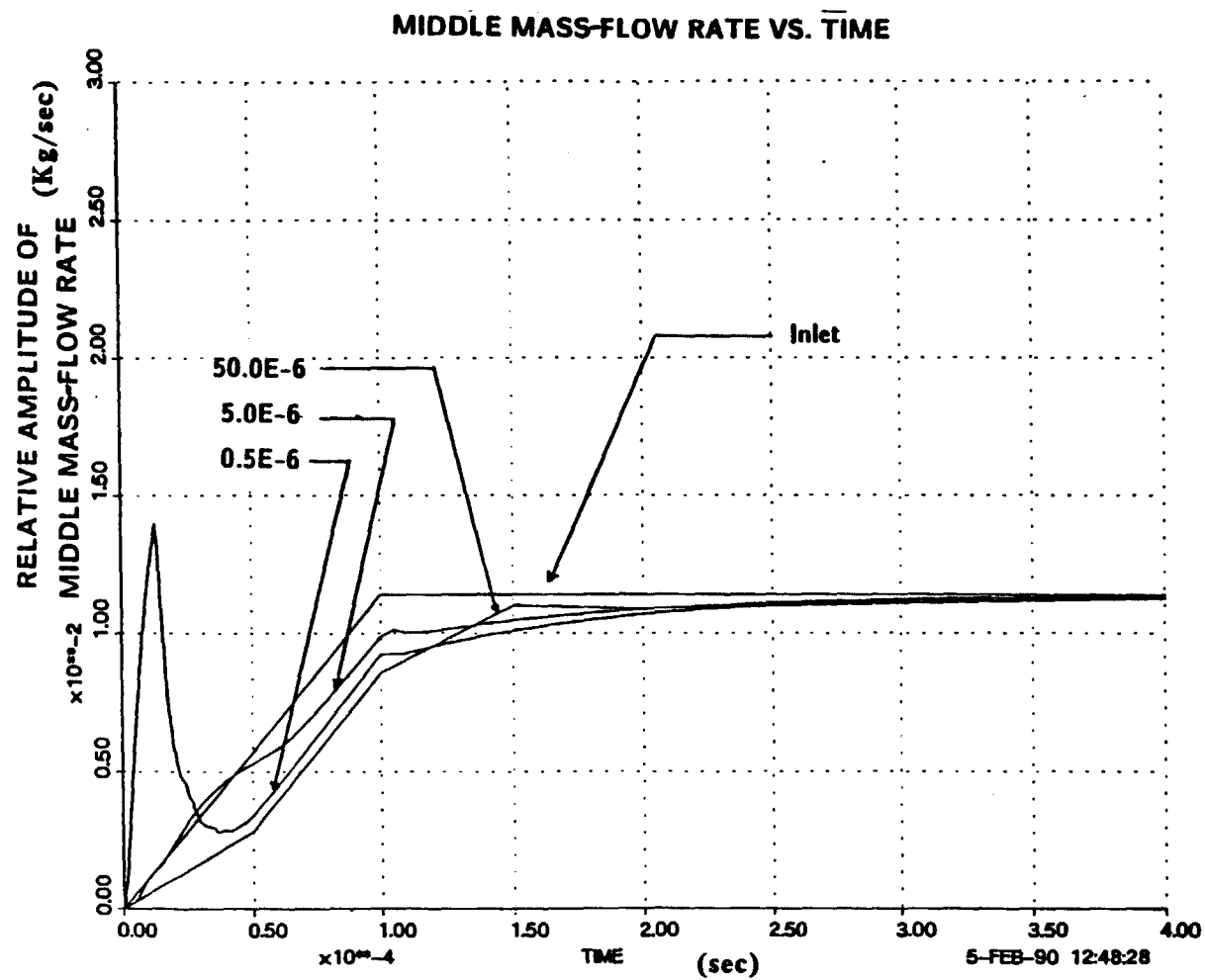


Figure 40. Response of the middle mass-flow rate for the turbine to ramps described by table 5. The three plots shown correspond to time steps of 0.5 micro seconds, 5 micro seconds, and 50 micro seconds.

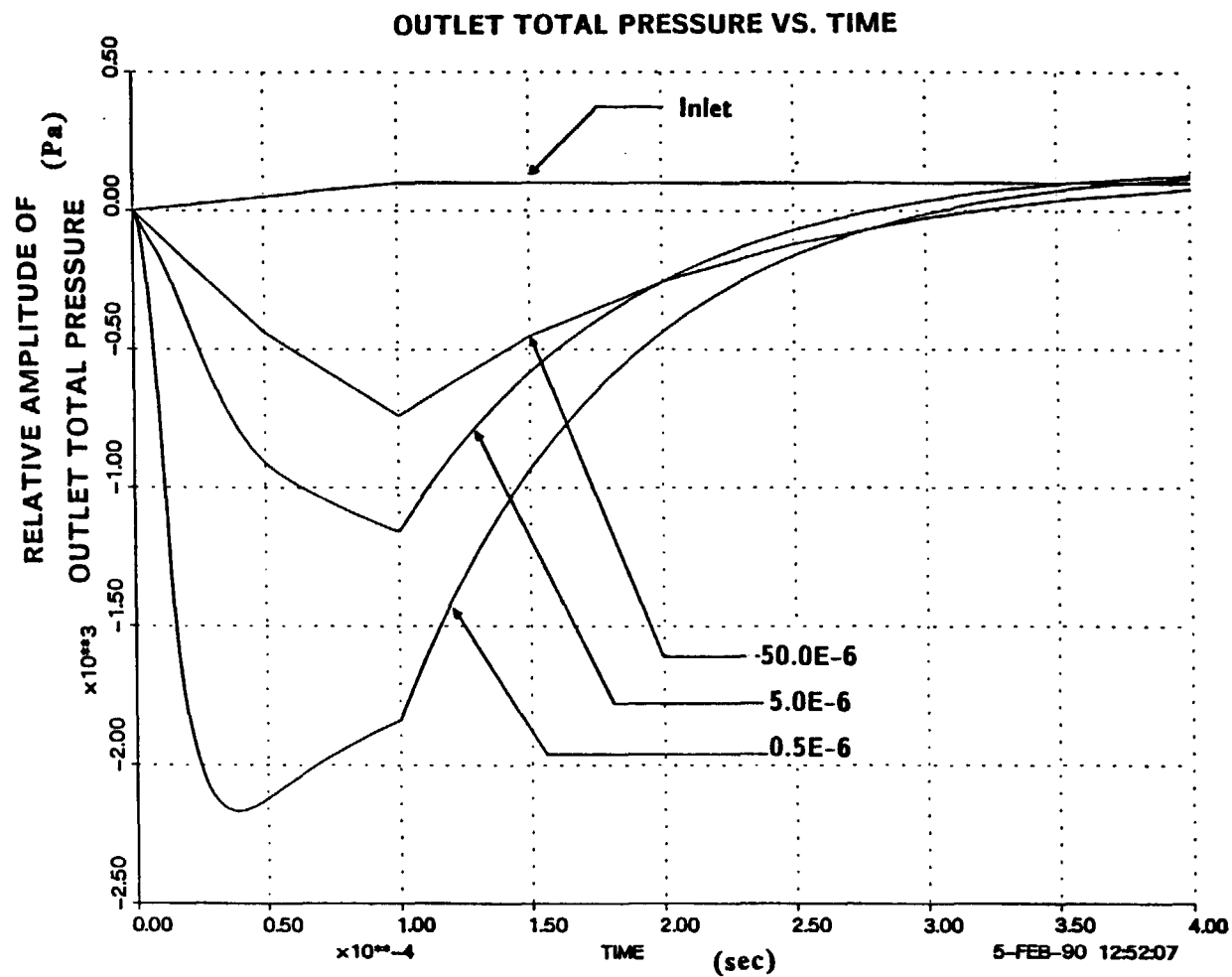


Figure 41. Response of the outlet total pressure, for the turbine, to ramps described by table 5. The three plots shown correspond to time steps of 0.5 micro seconds, 5 micro seconds, and 50 micro seconds.

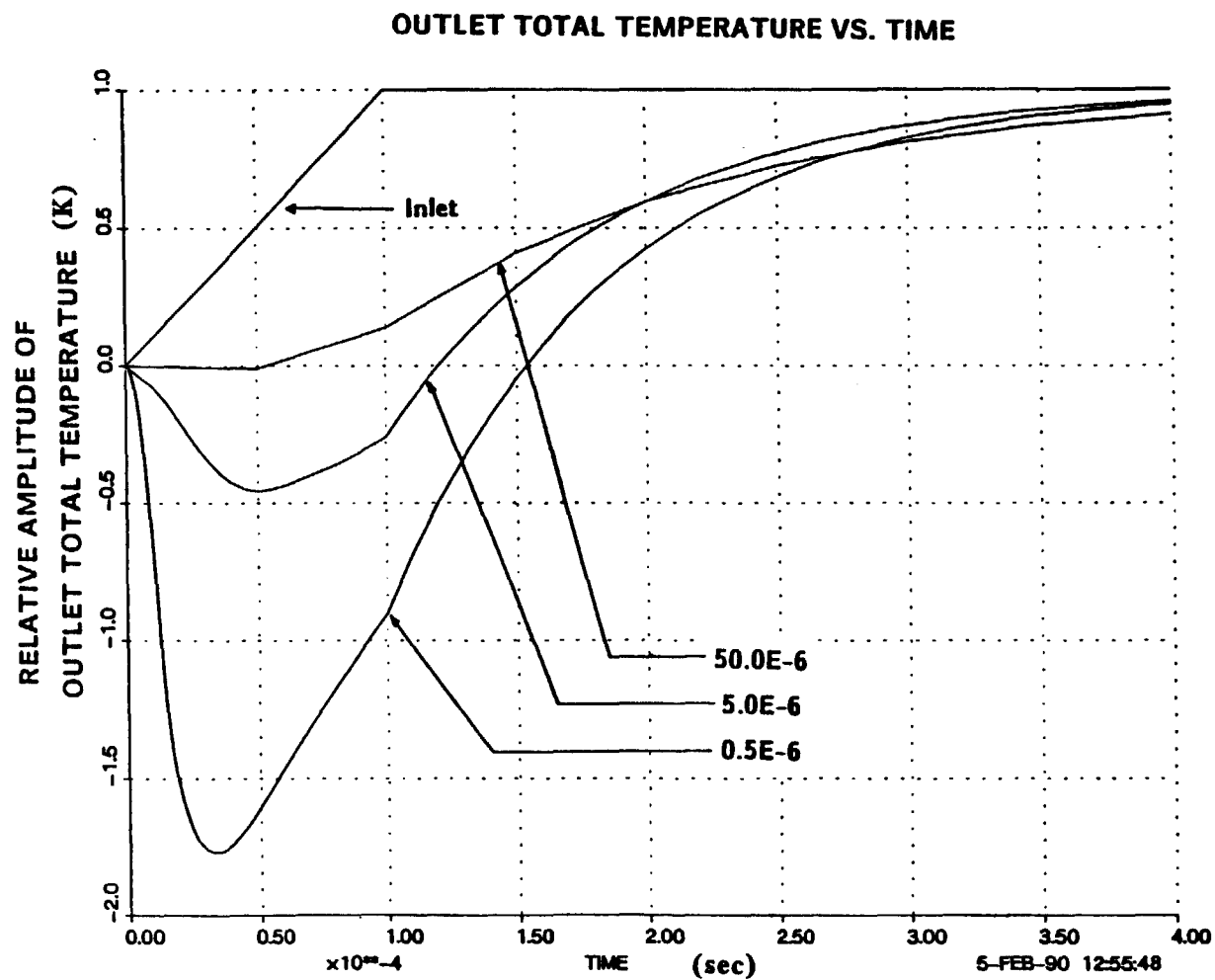


Figure 42. Response of the outlet total temperature, for the turbine, to ramps described by table 5. The three plots shown correspond to time steps of 0.5 micro seconds, 5 micro seconds, and 50 micro seconds.

seconds is the same for all the runs. This provides a good basis for comparison of the results obtained using different size time steps.

Figures 39 and 40 show the responses of outlet mass-flow rate and middle mass-flow rate respectively. There are 3 different curves shown in each figure. Each curve corresponds to a different time-step size. The difference in predicted response for the three time steps is very large. In fact the solution appears to be diverging with decreasing integration time-step size. Figure 41 shows the outlet total pressure response for the three time step sizes. Once again the solutions appear to be diverging with decreasing integrator time step. Figure 42 shows the total outlet temperature variation over time, and again the solution tends to diverge with the smaller time step.

The lack of convergence with decreased time-step size is clearly undesirable and this model is judged to be unsatisfactory. Study of this model demonstrated that lagging the outlet mass flow rate by 1 time step significantly reduced the numerical difficulties introduced by the stiffness of the governing equations. This suggested a return to the simpler state-average model but with a lagged-mass-flow calculation. A discussion of such a model, and its performance, is presented in the next section.

### 3.9 THE STATE-AVERAGE LAGGED-MASS-FLOW-RATE MODEL

Review of the sliced model performance suggested development of the state-average lagged mass flow rate model (SALM). The SALM was applies the continuity, energy, polytropic, and moment-of-momentum equations to a single control volume which represents the turbomachine. The assumptions for this model are as follows:

$$T_{tm}(t) = ( T_{ti}(t) + T_{to}(t) )/2 \quad (40)$$

$$\dot{m}_m(t) = ( \dot{m}_i(t) + \dot{m}_o(t-dt) )/2 \quad (41)$$

and for the turbine,

$$p_{tm}(t) = p_{ti}(t) * ( T_{tm}(t) / T_{ti}(t) )^{Cp/\eta/R} \quad (42)$$

where,

$T_{tm}$  is the total temperature in the middle of the machine

$p_{tm}$  is the total pressure in the middle of the machine

$\dot{m}_m$  is the mass flow rate through the machine

$dt$  is the magnitude of the integrator time step-size

$t$  is the current time level

$\eta$  is the total-to-total polytropic efficiency.

These assumptions are similar to those of the state-average model. However, there is a crucial difference. The outlet mass flow used in equation 41 to evaluate the mass flow rate through the machine is lagged by one integration time step, whereas the state-average model uses the current value of the mass flow rate. Another difference between the state-average model and SALM is that the state-average model did not include the moment-of-momentum equation.

The general algorithm for the SALM is very similar to the algorithm described for the upwind-mass-flow model but uses the new

procedure to evaluate the mass-flow rate for the average-state in the machine. The moment-of-momentum equation is once again utilized to obtain two different versions of the model. The first version of the model assumes constant speed operation, and calculates the variable rate of work output. The second version assumes a constant rate of work while the rotor speed is allowed to change. Figure 43 shows the solution algorithm for the first version while figure 44 shows the solution algorithm for the second version.

#### 3.9.1 Constant-Speed Variable-Rate-Of-Work Model

In this model the rotor speed is assumed to be locked at 3351 Hz as specified by the DRO2 [1]. A change in inlet total temperature results in a change in the rate of work output from the turbine.

Table 6 presents information used to perform turbomachinery analysis. Specifically table 6 lists: the geometry of the turbine to be simulated; the design point data for the turbine; the perturbation to the design steady-state value to initiate a transient; and the thermodynamic steady-state values expected at the end of the simulation. The perturbation of the steady-state is achieved by ramping all the inlet state variables over a period of 100 micro seconds. After 100 micro seconds the inlet remains constant at the new value. Table 6 also shows that this transient is run for 3 different time steps but that the ramp time of 100 micro seconds is the same for all the runs. This provides a good basis for comparison of the results obtained using different size time steps.

Figure 45 shows the response of the outlet mass-flow rate. There are 3 different curves shown in this figure. Each corresponds to a

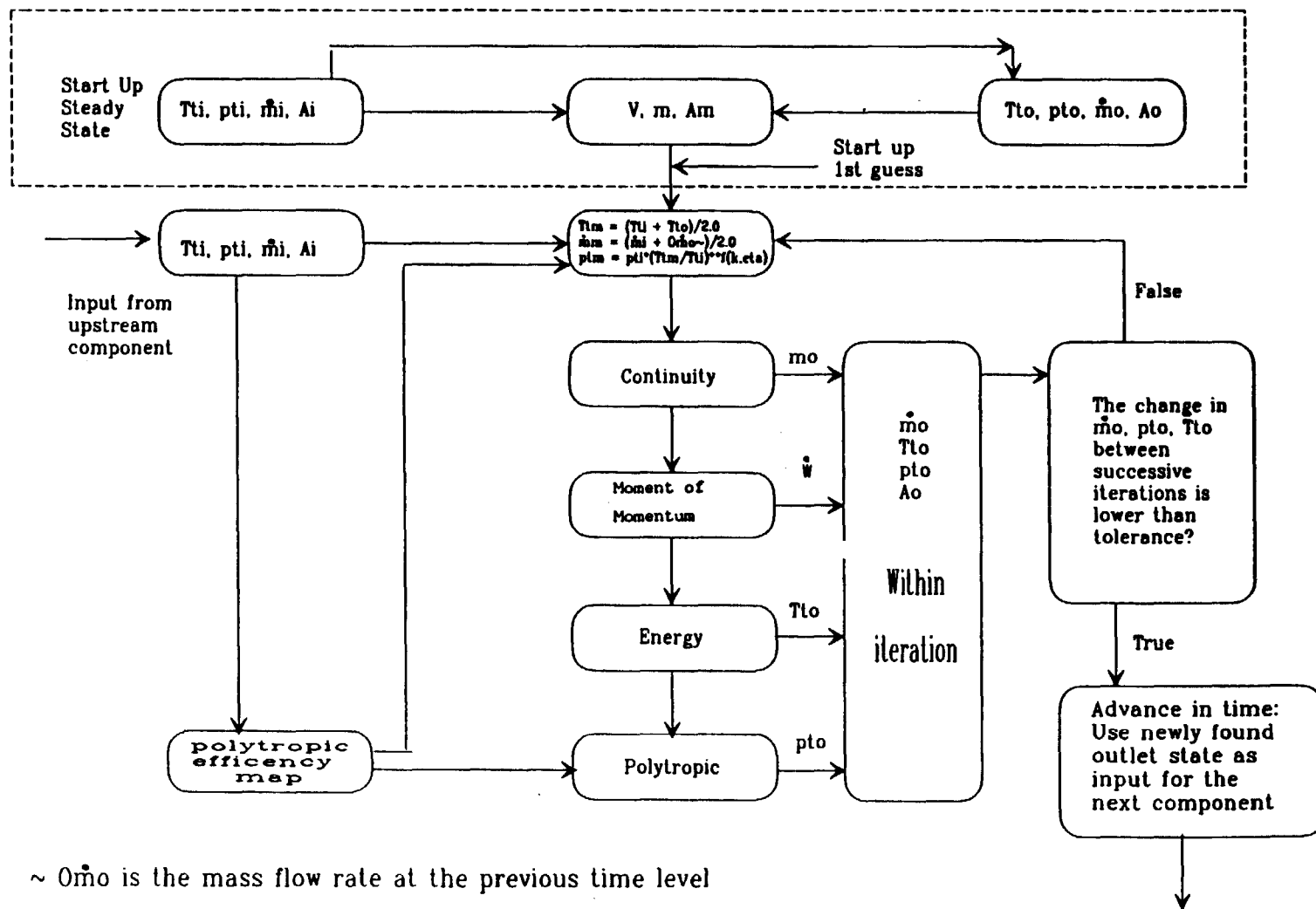


Figure 43. Algorithm for the state-average lagged-mass-flow-rate constant-speed variable-rate-of-work model.



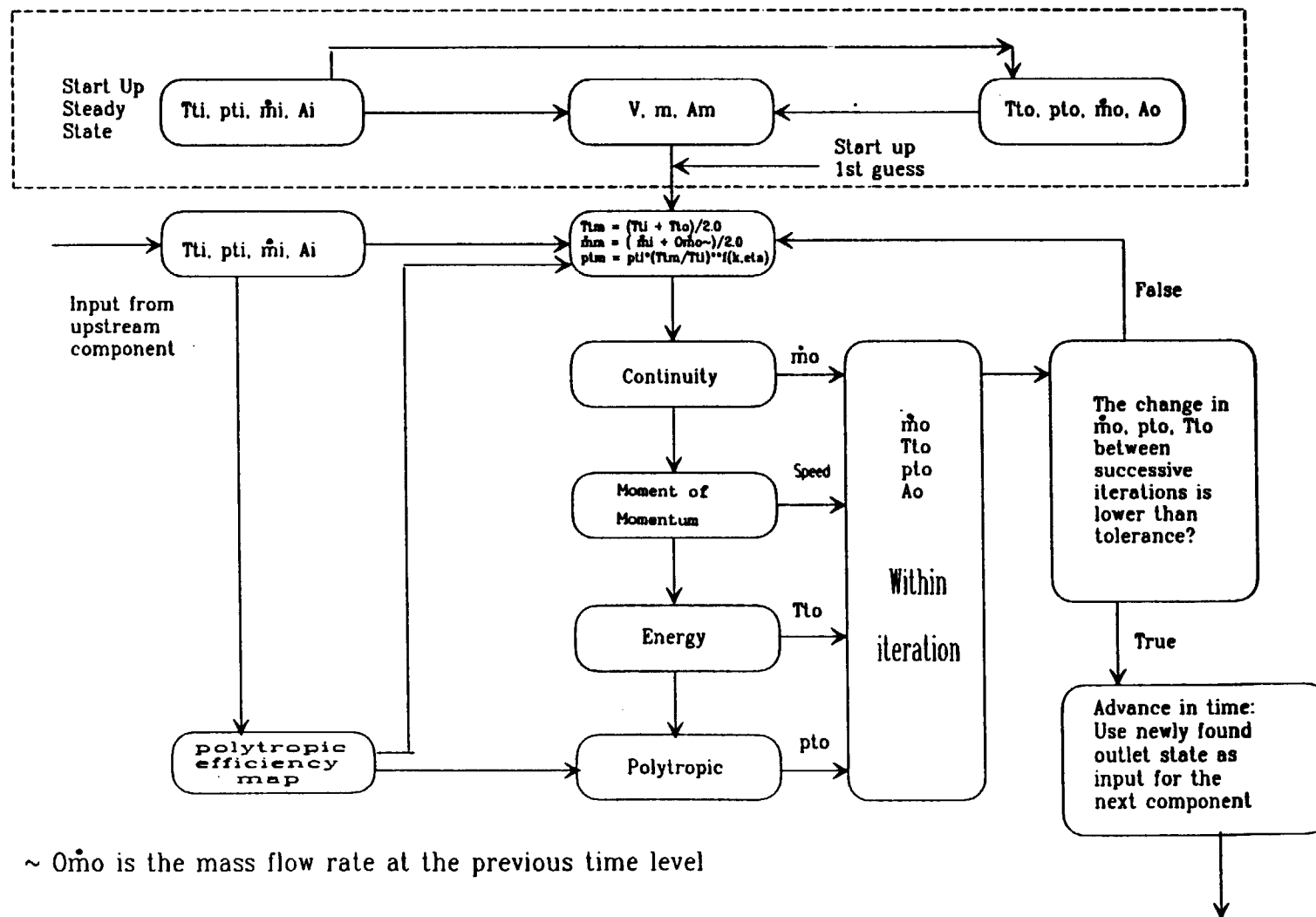


Figure 44. Algorithm for the state-average lagged-mass-flow-rate constant-rate-of-work variable-speed model.

**Table 6: Data for results presented in figures 45 - 48**

**Turbine Geometry:**

Inlet normal area:	4.668E-3 m <sup>2</sup>
Middle normal area:	5.158E-3 m <sup>2</sup>
Outlet normal area:	5.648E-3 m <sup>2</sup>
Volume of compressor:	1.000E-4 m <sup>3</sup>
Tip radius:	8.810E-2 m
Middle radius:	4.896E-2 m
Rotor Inertia:	0.082 Kg m <sup>2</sup>

**Design point data:**

Inlet total temperature:	1034.02 K
Outlet total temperature:	866.01 K
Inlet total pressure:	540.25 KPa
Outlet total pressure:	330.14 KPa
Mass flow rate:	1.2886 Kg/sec
Rotor speed:	3351.0 Hz
Total to total polytropic efficiency:	0.9010

**Pertubation at inlet to obtain transient response:**

Ramp inlet total temperature to:	1035.02 K
Ramp inlet total pressure to:	540.35 KPa
Ramp inlet mass flow to:	1.3 Kg/sec

**Expected steady state outlet states:**

Outlet total temperature:	867.01 K
Outlet total pressure:	330.316 KPa
Outlet mass flow rate:	1.3 Kg/sec

**Additional notes:**

Constant specific heat:	519.14 J/Kg/K
Gas constant:	207.44 J/Kg/K
Constant speed:	3351.00 Hz
Variable rate of work out:	
3 different time steps:	50.0E-6 sec
	5.0E-6 sec
	0.5E-6 sec

different time-step size. The difference in predicted response for the three time steps is small. Therefore, the larger integrator time step should be used to considerably reduce computational time.

Figure 46 shows similar behavior in the rate of work output by the turbine. It is also clear that the difference in solutions reduces considerably as smaller integration time step are chosen. In fact the difference between the 5 micro second solution and the 0.5 micro second solution is almost imperceptible. Even the 50 micro second solution appears to be satisfactory. Figure 47 shows the outlet total pressure response for the three time-step sizes. Once again, the solution appears to converge as time-step size decreases. However, it should be noted that even the larger time step is representative of the solution obtained by smaller time step. Figure 48 shows the total outlet temperature variation over time. Once again the solution obtained from the larger integrator time step is representative of the solution.

The SLAM was also tested for a ramp increase followed by a ramp decrease to the design point data for the inlet state. The object of this test is to determine if the model will return to the design steady-state outlet condition. Table 7 presents information used to perform turbomachinery analysis. Specifically table 7 lists: the geometry of the turbine to be simulated; the design point data for the turbine; the perturbation to the design steady-state value to initiate a transient; and the thermodynamic steady-state values expected at the end of the simulation. The perturbation of the steady state is achieved by ramping up input state variables over a

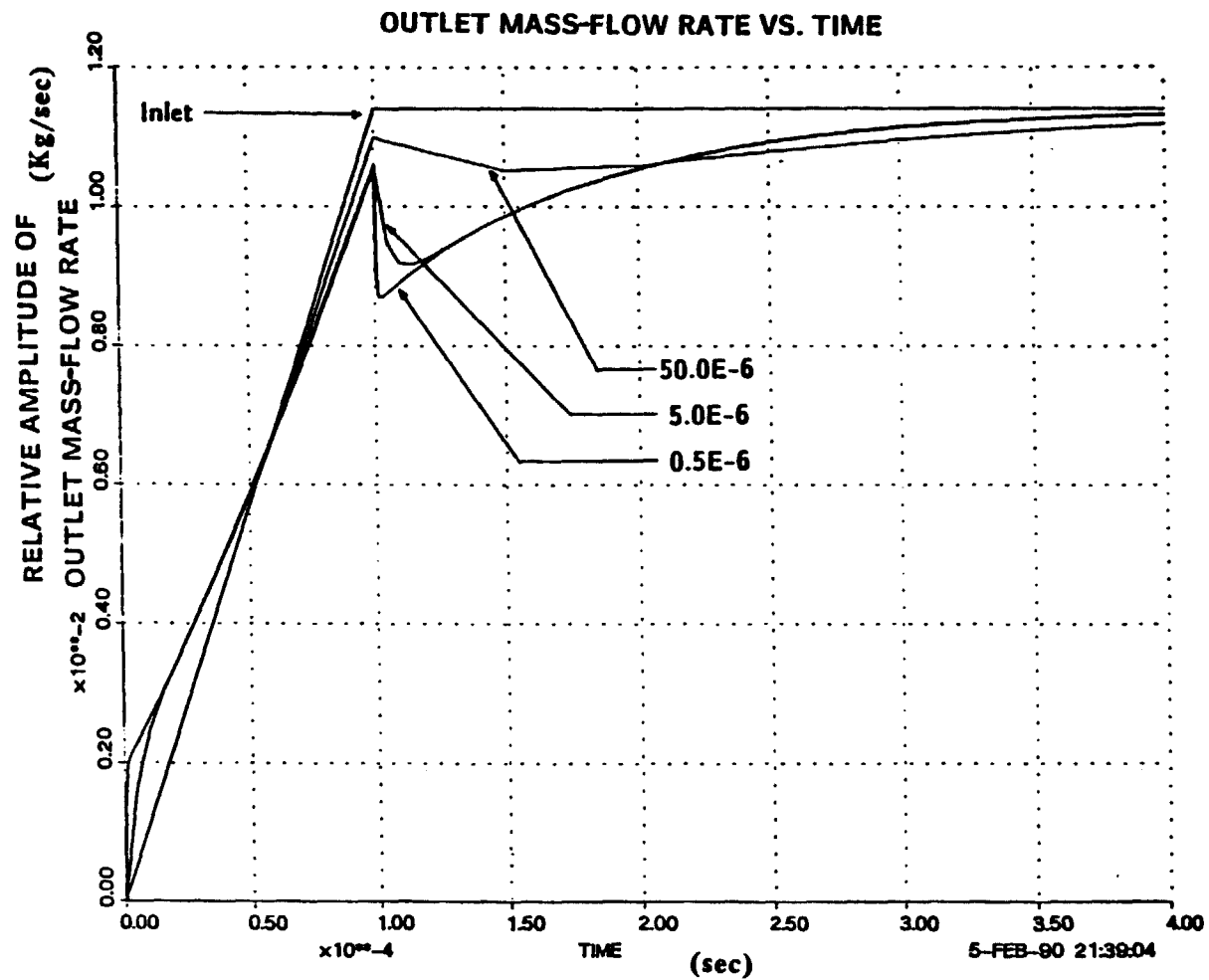


Figure 45. Response of the outlet mass-flow rate for the turbine to ramps described by table 6. The three plots shown correspond to time steps of 0.5 micro seconds, 5 micro seconds, and 50 micro seconds.

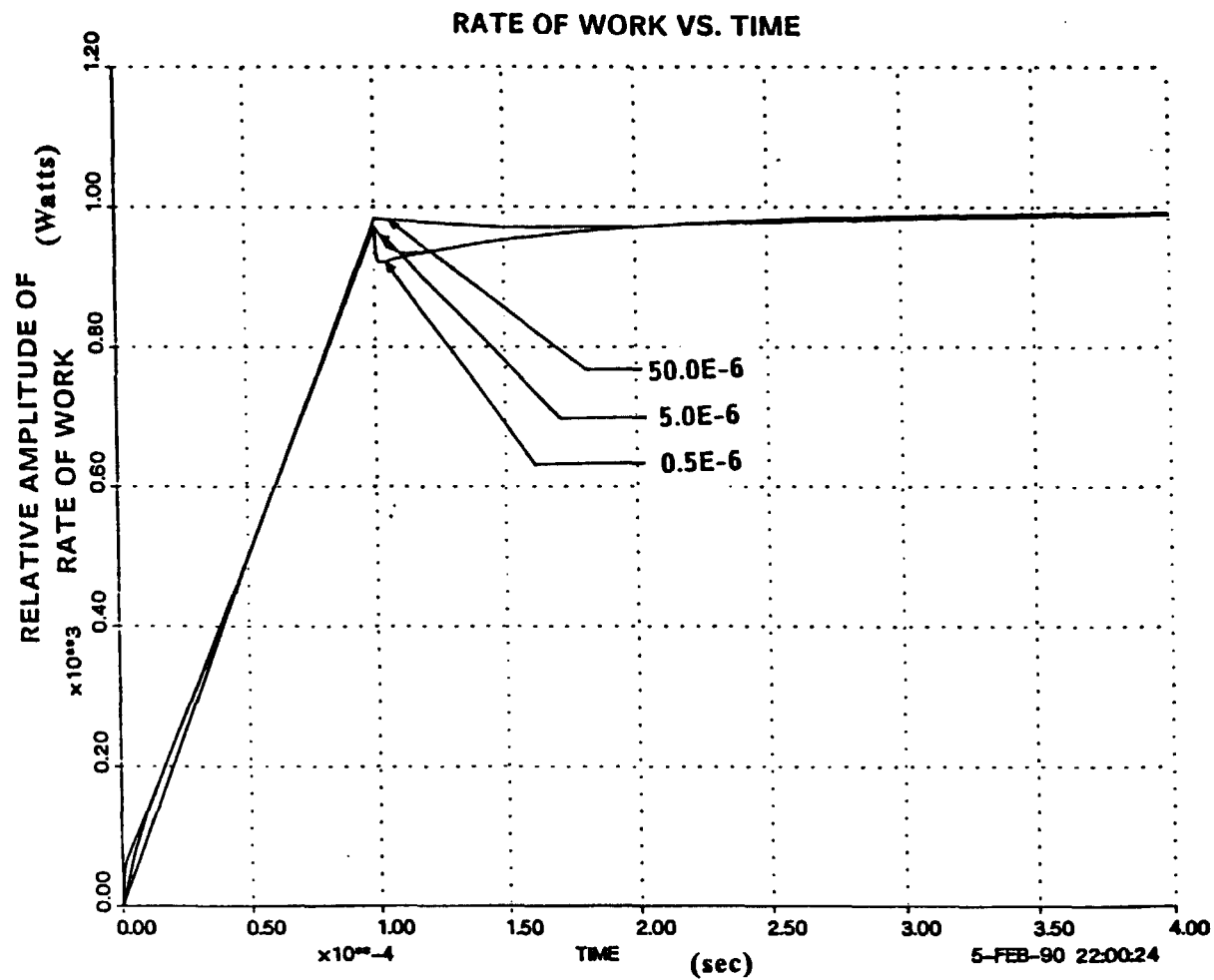


Figure 46. Response of the rate of work output for the turbine to ramps described by table 6. The three plots shown correspond to time steps of 0.5 micro seconds, 5 micro seconds, and 50 micro seconds.

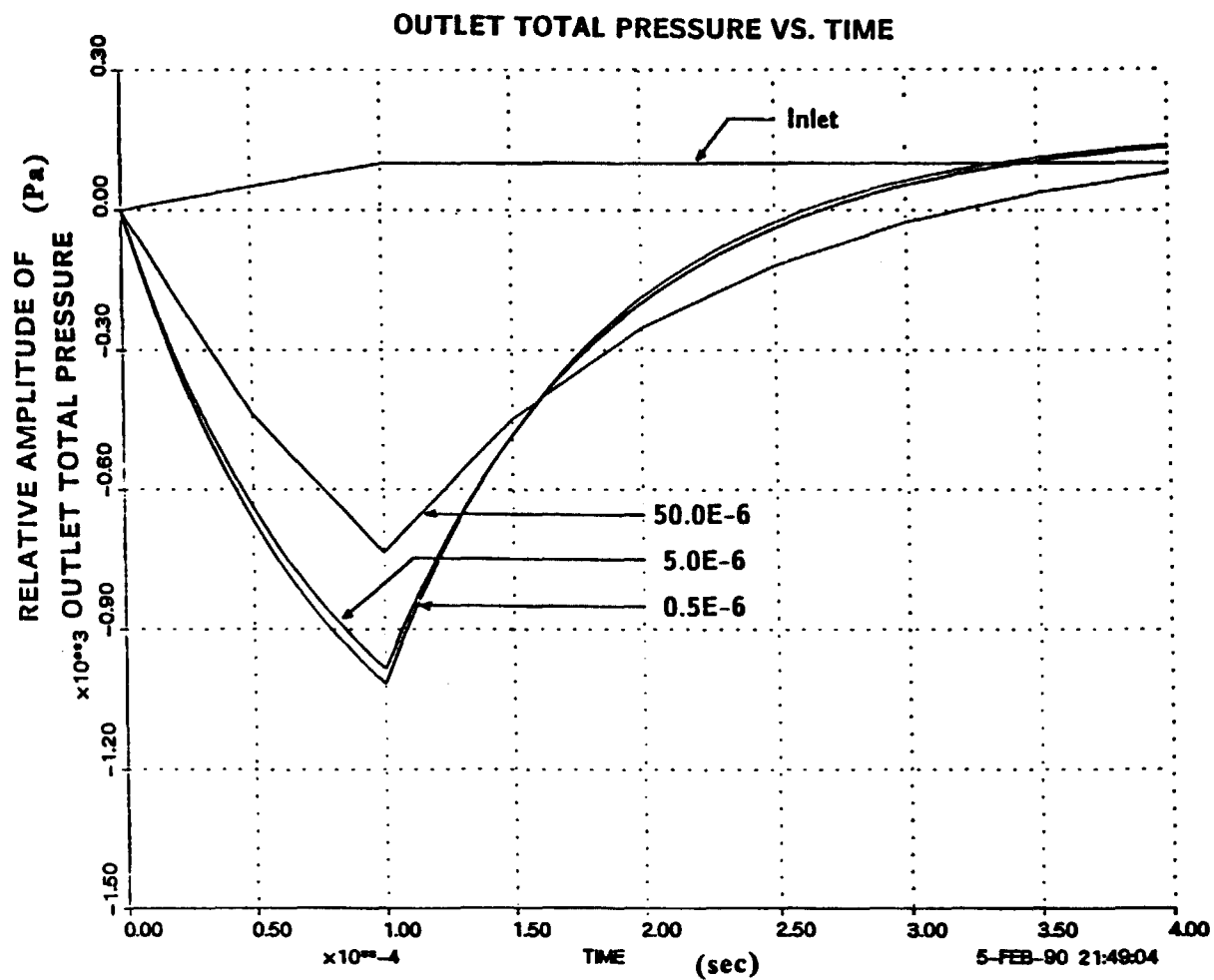


Figure 47. Response of the outlet total pressure, for the turbine, to ramps described by table 6. The three plots shown correspond to time steps of 0.5 micro seconds, 5 micro seconds, and 50 micro seconds.

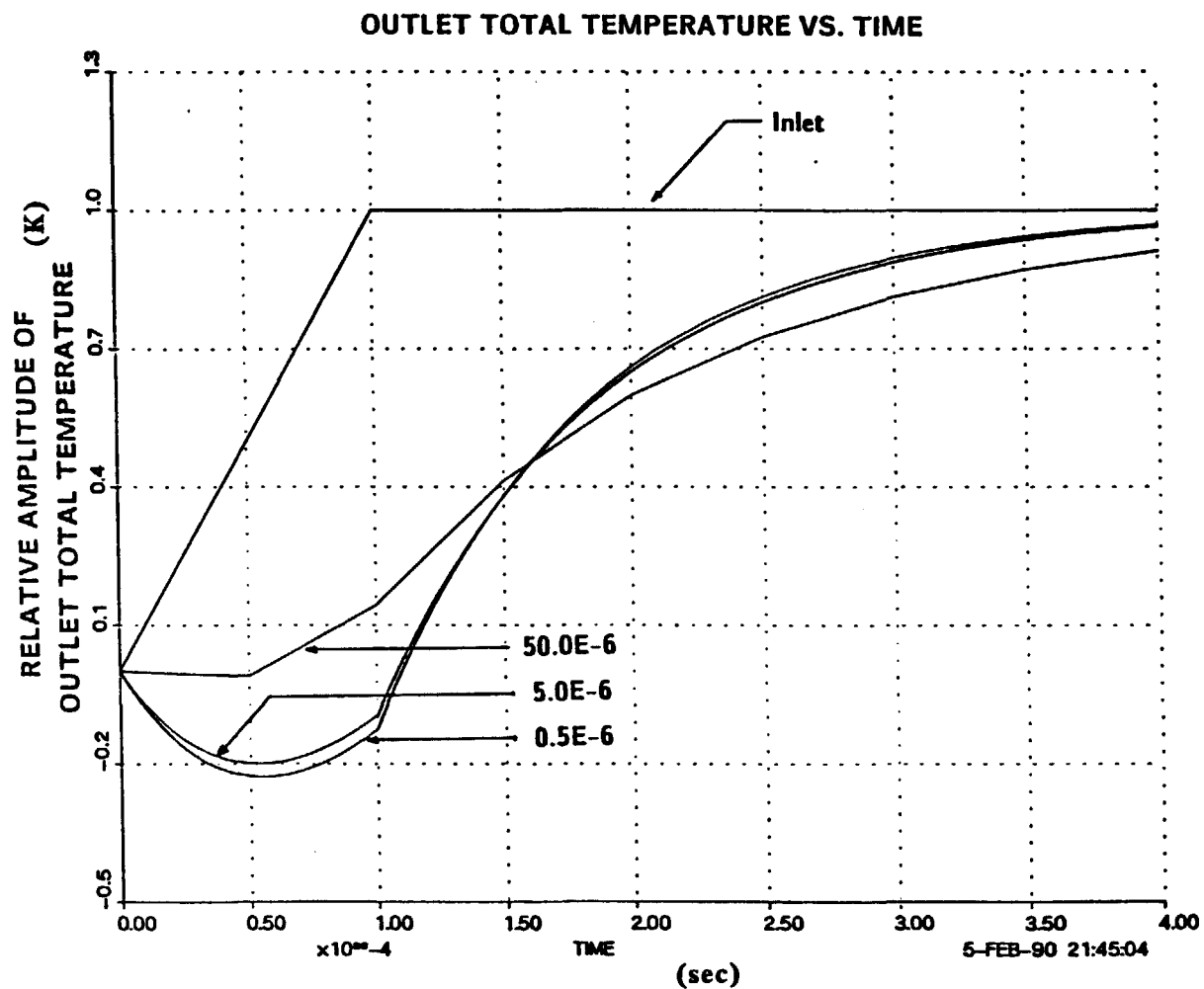


Figure 48. Response of the outlet total temperature, for the turbine, to ramps described by table 6. The three plots shown correspond to time steps of 0.5 micro seconds, 5 micro seconds, and 50 micro seconds.

period of 25 micro seconds. After 25 micro seconds the input remains constant at the new value. After 550 micro seconds the second ramp in inlet state variables begins and returns the inlet variables to the design point steady state values. The time elapsed for ramp up was 25 micro seconds but the time elapsed for ramp down was 50 micro seconds. Table 7 summarizes the details of the data used for this test.

Figures 49 to 51, show the transients in total temperature, total pressure, mass-flow rate, and rate-of-work output respectively. In each case the final steady state is predicted correctly by the transient model.

In summary, from the ramp up and the double ramp test, two important results were obtained: the steady state is predicted correctly for all state variables; and The differences in responses due to an order of magnitude larger time step size is negligible. Based on the above results it is postulated that since there is a discontinuity in the first derivative at the inlet when the ramp ends, the numerical method would require an infinitely small time-step size to precisely model this discontinuity. Therefore, if the model is excited by a sinusoidal input (or any other continuously differentiable function) the output should be smooth. To investigate this postulate, the model was excited by a 2,000 Hz sinusoidal input at the inlet. Table 8 summarizes the conditions used for this test. The transient results obtained from this test are presented in figures 52-54.



**Table 7: Data for results presented in figures 49 - 51**

**Turbine Geometry:**

Inlet normal area:	4.668E-3 m <sup>2</sup>
Middle normal area:	5.158E-3 m <sup>2</sup>
Outlet normal area:	5.648E-3 m <sup>2</sup>
Volume of compressor:	1.000E-4 m <sup>3</sup>
Tip radius:	8.810E-2 m
Middle radius:	4.896E-2 m
Rotor Inertia:	0.082 Kg m <sup>2</sup>

**Design point data:**

Inlet total temperature:	1034.02 K
Outlet total temperature:	866.01 K
Inlet total pressure:	540.25 KPa
Outlet total pressure:	330.14 KPa
Mass flow rate:	1.2886 Kg/sec
Rotor speed:	3351.0 Hz
Total to total polytropic efficiency:	0.9010

**Perturbation at inlet to obtain transient response:**

Ramp up inlet total temperature to:	1035.02 K
Ramp up inlet total pressure to:	540.35 KPa
Ramp up inlet mass flow to:	1.3 Kg/sec
then,	
Ramp down inlet total temperature to:	1034.02 K
Ramp down inlet total pressure to:	540.25 KPa
Ramp down inlet mass flow rate to:	1.2886 Kg/sec

**Expected steady state outlet states:**

Outlet total temperature:	867.01 K
Outlet total pressure:	330.316 KPa
Outlet mass flow rate:	1.3 Kg/sec

**Additional notes:**

Constant specific heat:	519.14 J/Kg/K
Gas constant:	207.44 J/Kg/K
Constant speed:	3351.00 Hz
Ramp up elapsed time	25.0E-6 sec
Ramp down elapsed time	550 E-6 sec
Variable rate of work out:	

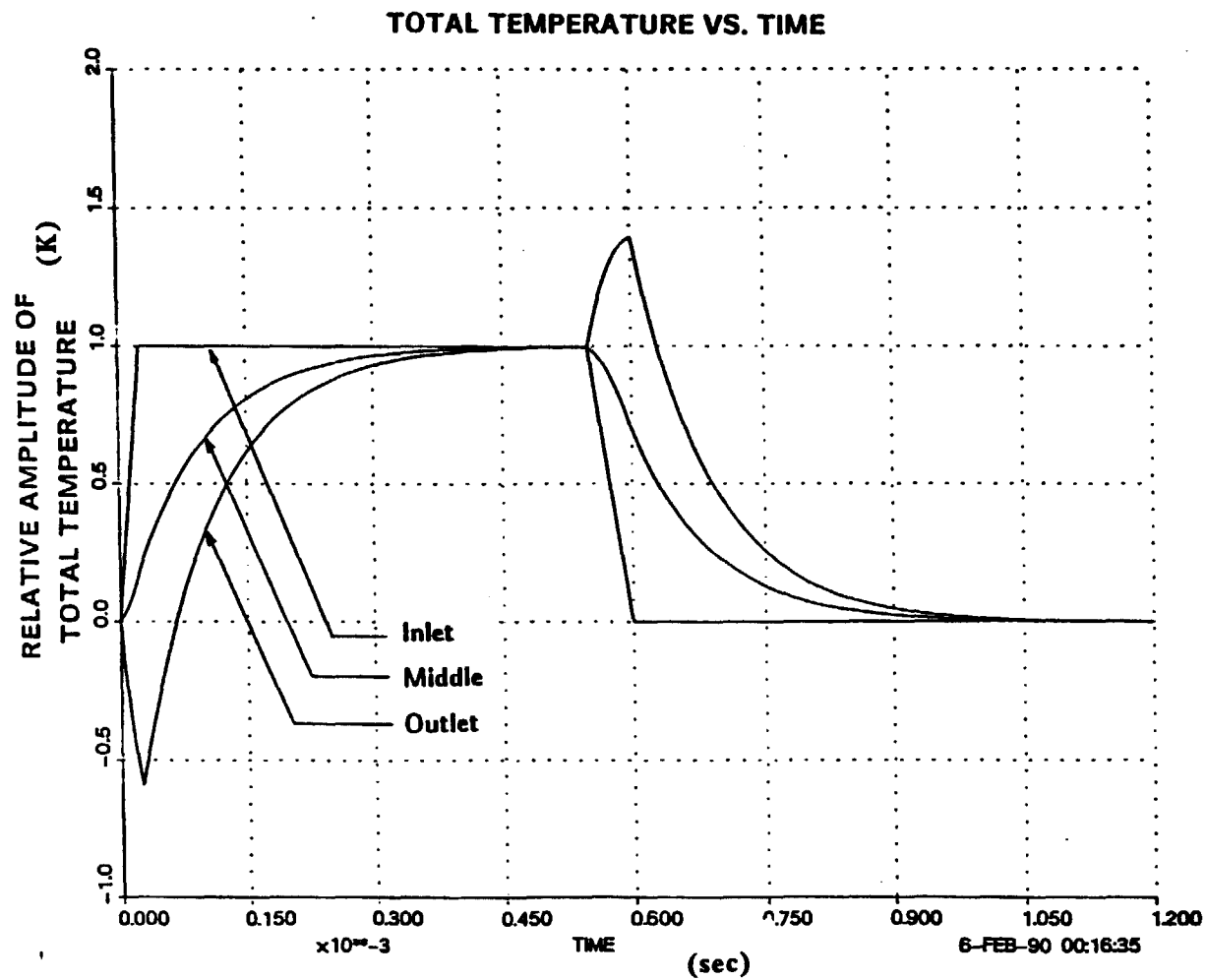


Figure 49. Response of the total temperature, for the turbine, to ramps described by table 7. The time step is 5 micro seconds.

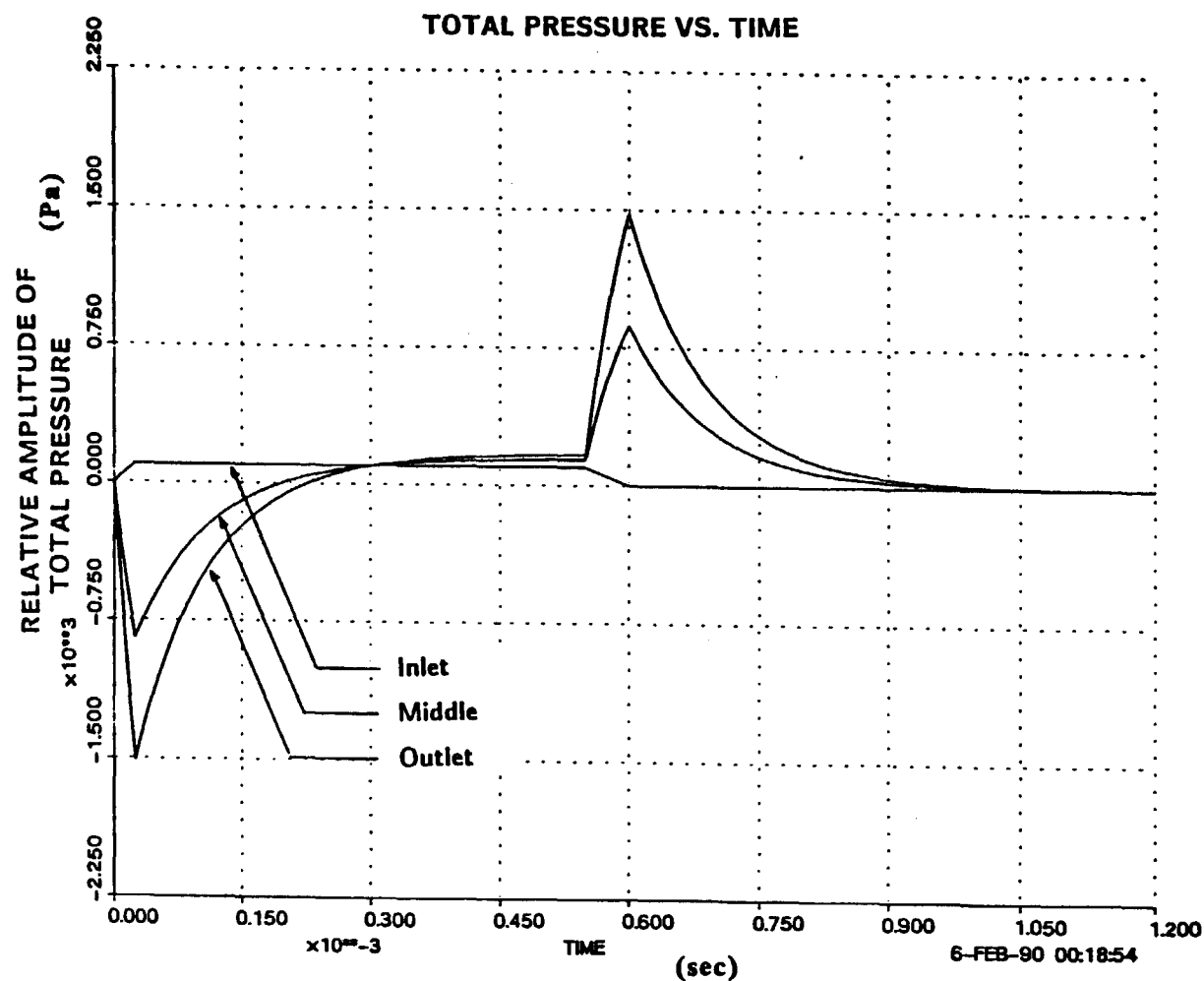


Figure 50. Response of the total pressure, for the turbine, to ramps described by table 7. The time step is 5 micro seconds.

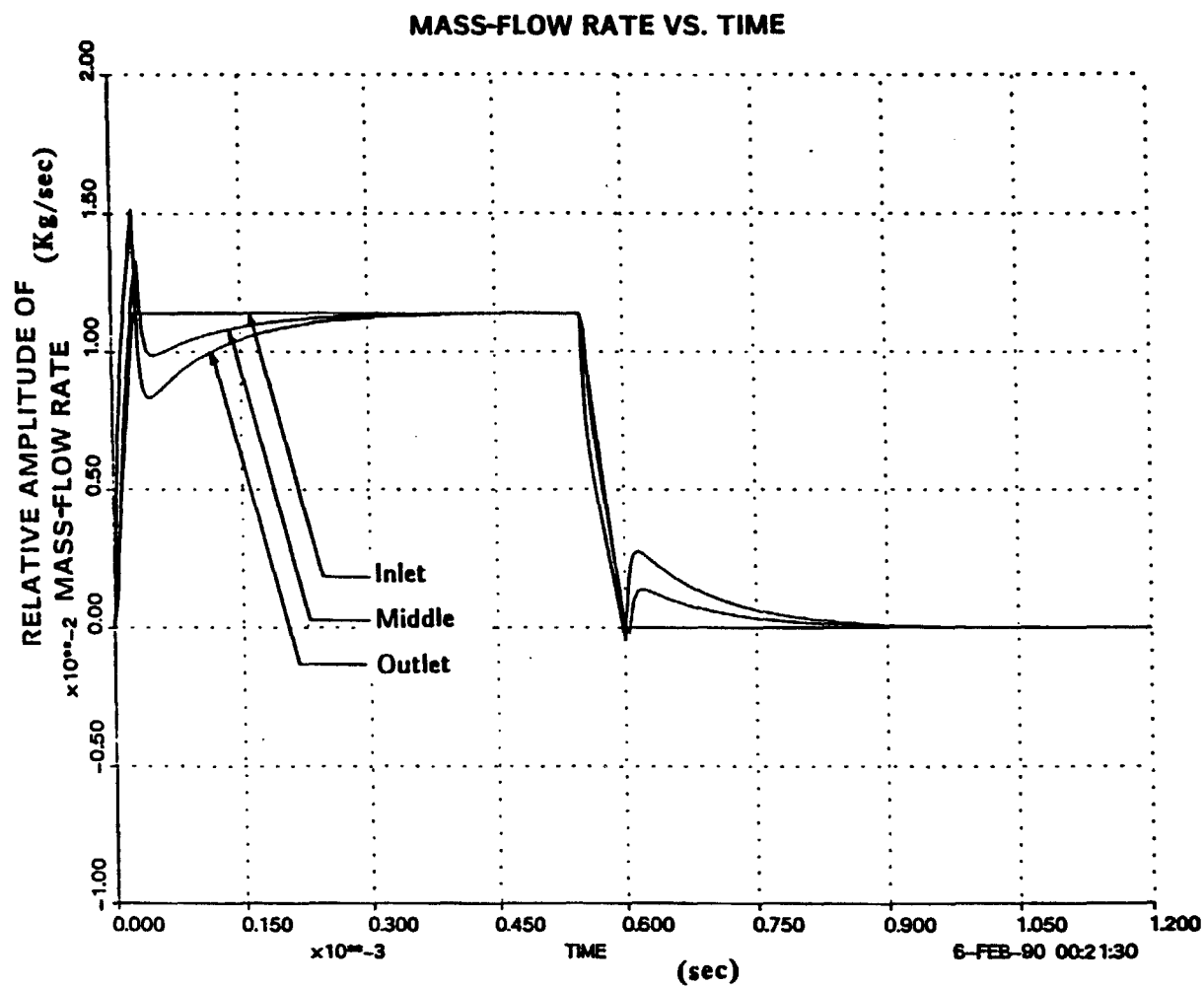


Figure 51. Response of the mass-flow rate, for the turbine, to ramps described by table 7. The time step is 5 micro seconds.

Figure 52 shows inlet, middle, and outlet mass-flow rates. Note that after initial perturbation from steady state, the outlet mass-flow rate lags the middle mass-flow rate which in turn lags the inlet-mass flow rate as expected. Also, no discontinuity is observed in the mass flow rate. Figure 53 shows the inlet, middle, and outlet total temperature. The zero on the vertical axis corresponds to the design point steady-state. Figure 54 shows the inlet, middle, and outlet total pressure. The pressure solutions also show no discontinuity. Hence, the postulate which predicts a smooth response of outlet variables for continuously differentiable variation in input variables was substantiated. The effect of slower inlet frequencies was also examined. Specifically the model was excited by inlet frequencies of 1,000 Hz, 500 Hz, and 50 Hz. The results of these transients are presented in figures 55 to 63. Examination of figures 55-63 reveals two very interesting results: the outlet state variable always lags the middle state variable and the middle state variable always lags the inlet state variable; and below excitation frequencies of 50 Hz, the mass storage term can be neglected.

**Table 8: Data for results presented in figures 52 - 63**

**Turbine Geometry:**

Inlet normal area:	4.668E-3 m <sup>2</sup>
Middle normal area:	5.158E-3 m <sup>2</sup>
Outlet normal area:	5.648E-3 m <sup>2</sup>
Volume of compressor:	1.000E-4 m <sup>3</sup>
Tip radius:	8.810E-2 m
Middle radius:	4.896E-2 m
Rotor Inertia:	0.082 Kg m <sup>2</sup>

**Design point data:**

Inlet total temperature:	1034.02 K
Outlet total temperature:	866.01 K
Inlet total pressure:	540.25 KPa
Outlet total pressure:	330.14 KPa
Mass flow rate:	1.2886 Kg/sec
Rotor speed:	3351.0 Hz
Total to total polytropic efficiency:	0.9010

**Perturbation at inlet to obtain transient response:**

Sine wave amplitude inlet total temperature:	1.0 K
Sine wave amplitude inlet total pressure:	100 KPa
Sine wave amplitude inlet mass flow:	0.0114 Kg/sec
Sine wave frequency inlet total temperature:	2,000 Hz - 50 Hz
Sine wave frequency inlet total pressure:	2,000 Hz - 50 Hz
Sine wave frequency inlet mass flow:	2,000 Hz - 50 Hz

**Additional notes:**

Constant specific heat:	519.14 J/Kg/K
Gas constant:	207.44 J/Kg/K
Variable Work out:	
Constant rotor speed:	

Sine wave is superimposed on already existing steady state:

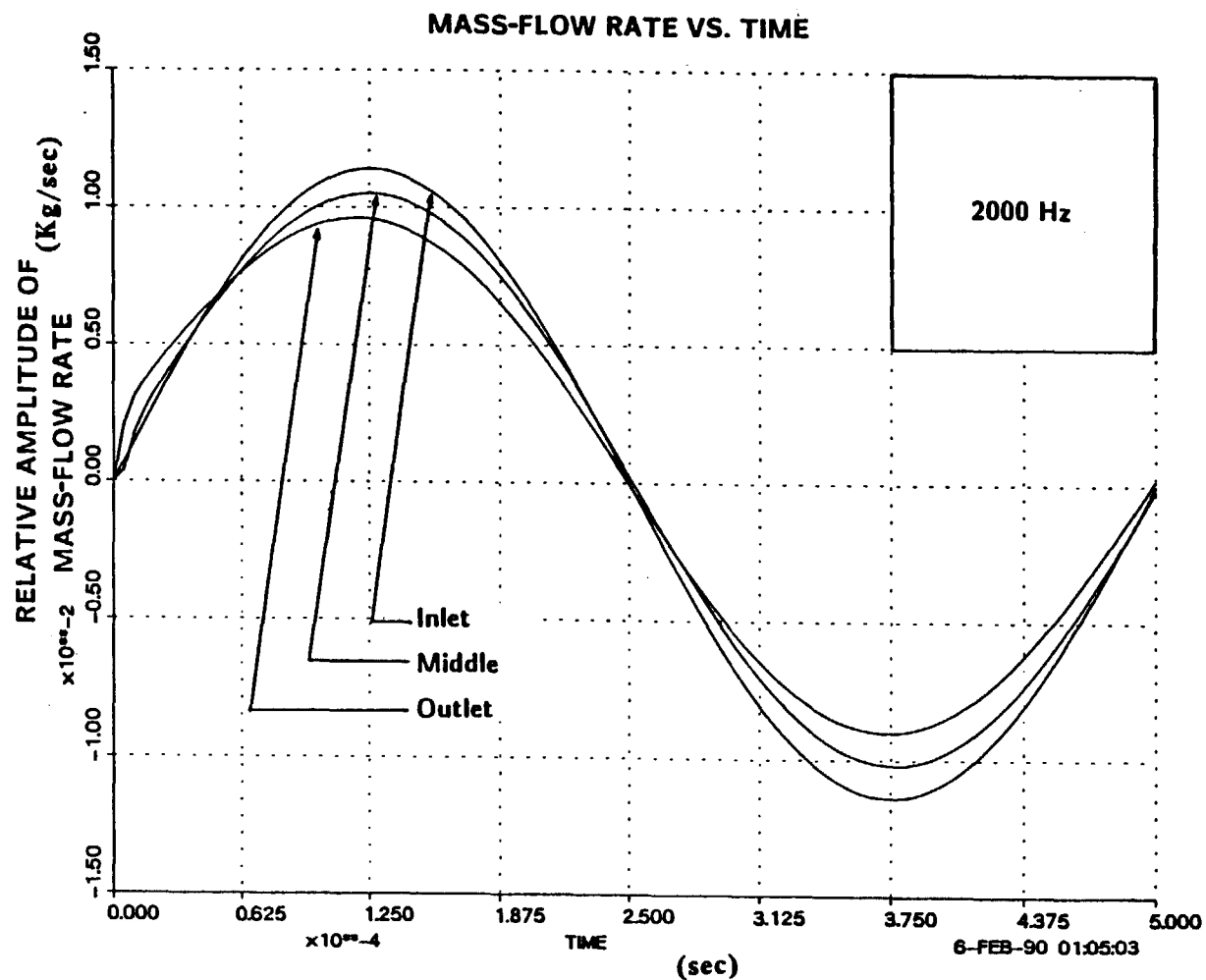


Figure 52. Response of the mass-flow rate, for the turbine, to sinusoidal input described by table 8. The time step is 1 micro seconds. Frequency is 2000 Hz.

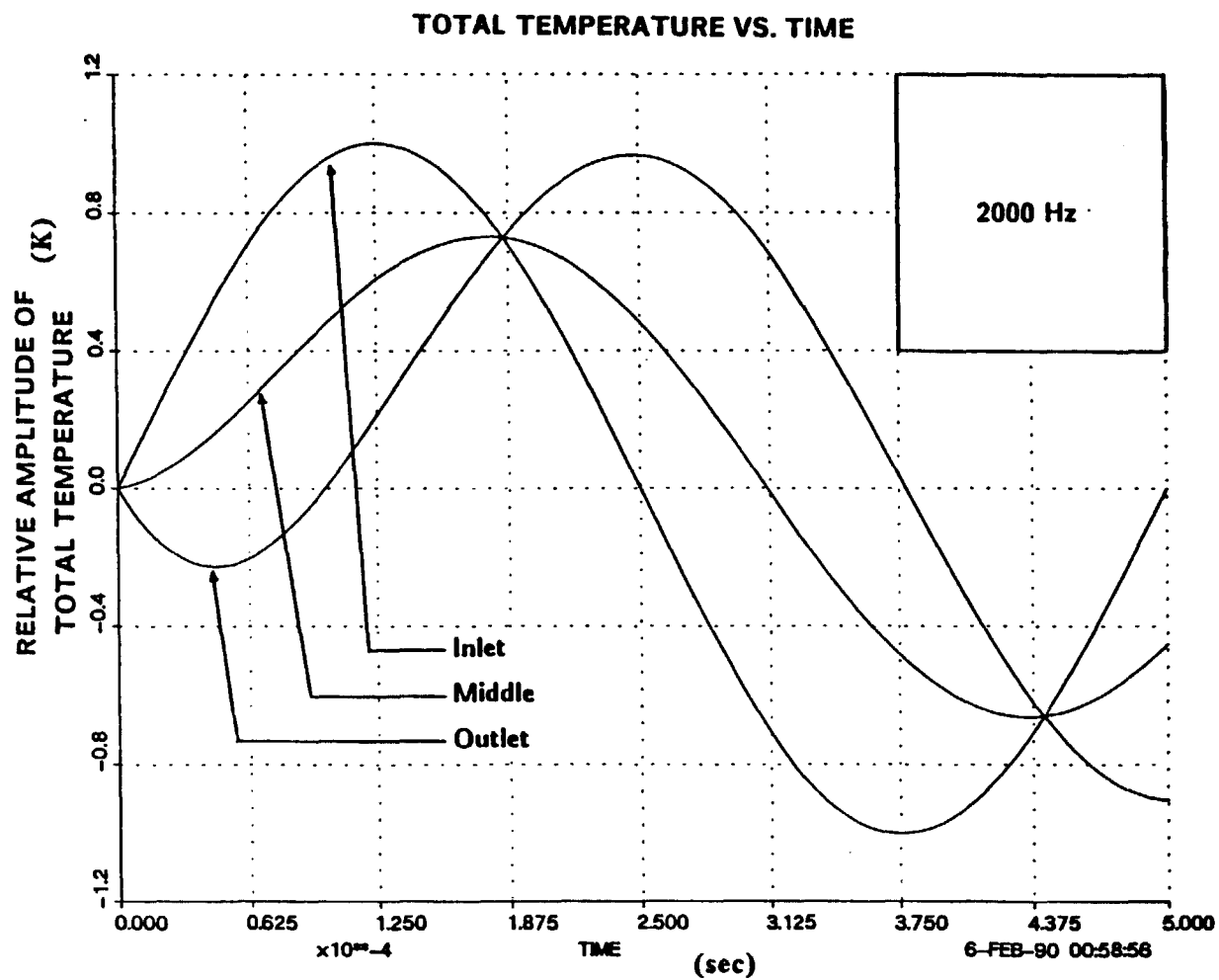


Figure 53. Response of the total temperature, for the turbine, to sinusoidal input described by table 8. The time step is 1 micro seconds. Frequency is 2000 Hz.



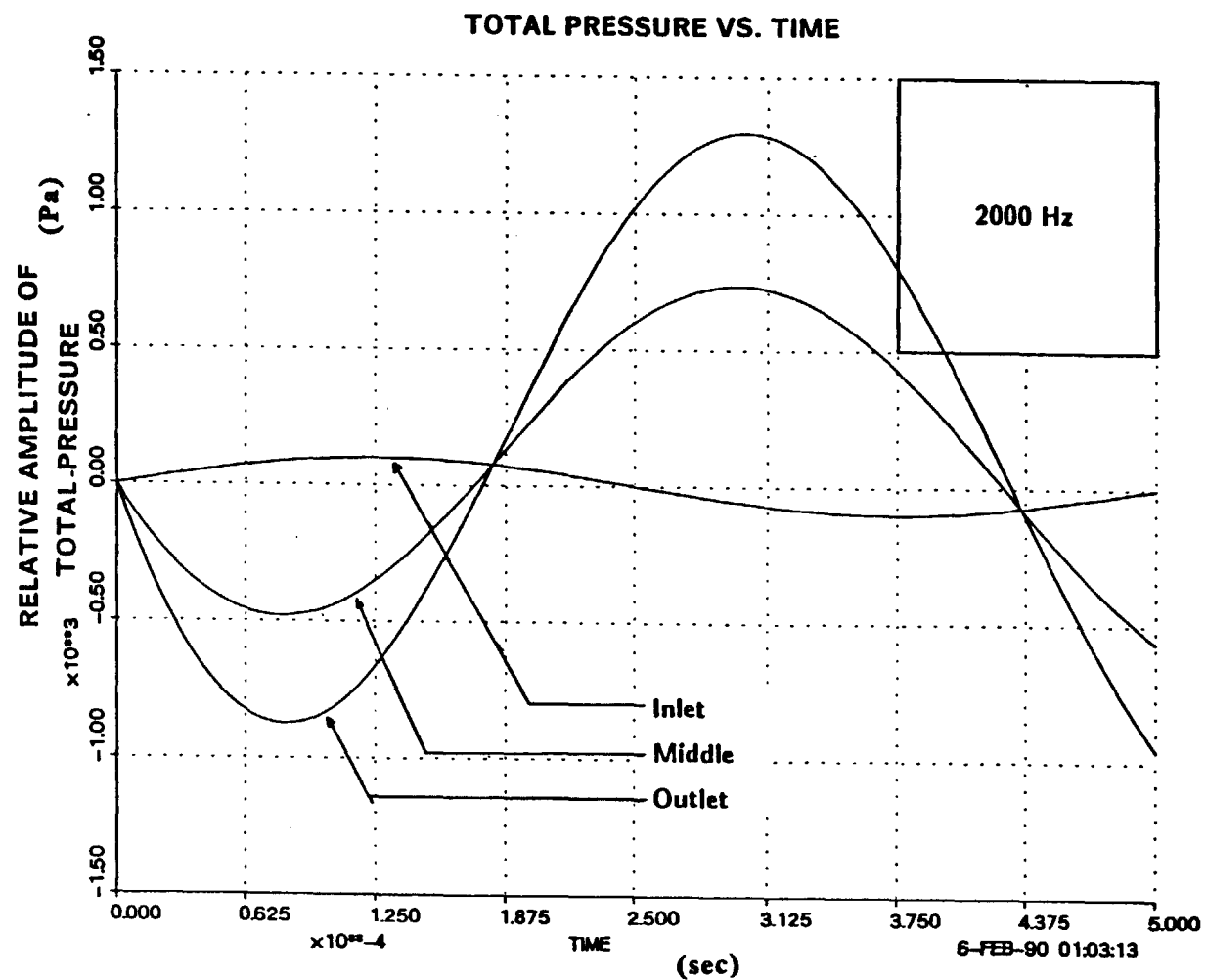


Figure 54. Response of the total pressure, for the turbine, to sinusoidal input described by table 8. The time step is 1 micro seconds. Frequency is 2000 Hz.

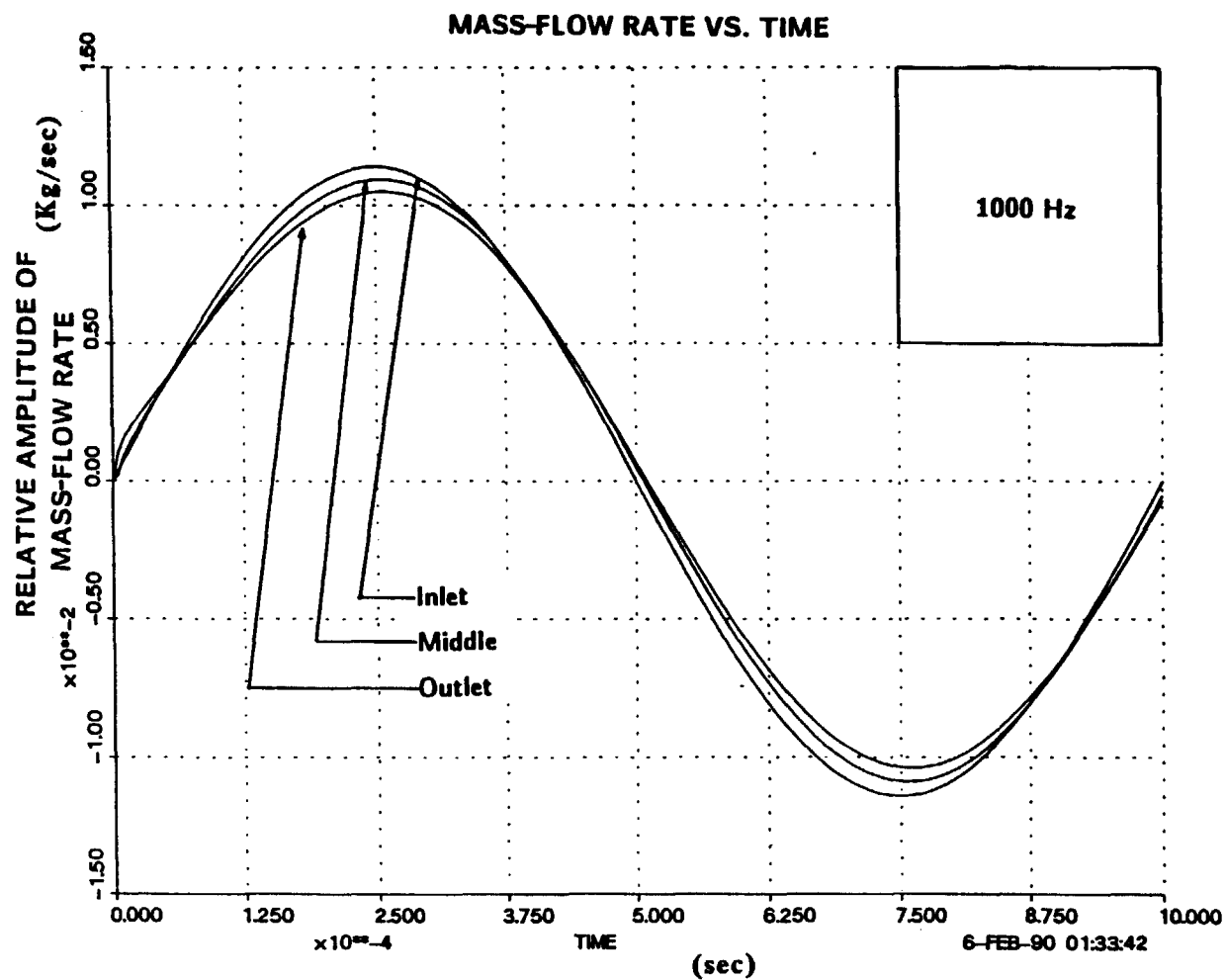


Figure 55. Response of the mass-flow rate, for the turbine, to sinusoidal input described by table 8. The time step is 1 micro seconds. Frequency is 1000 Hz.

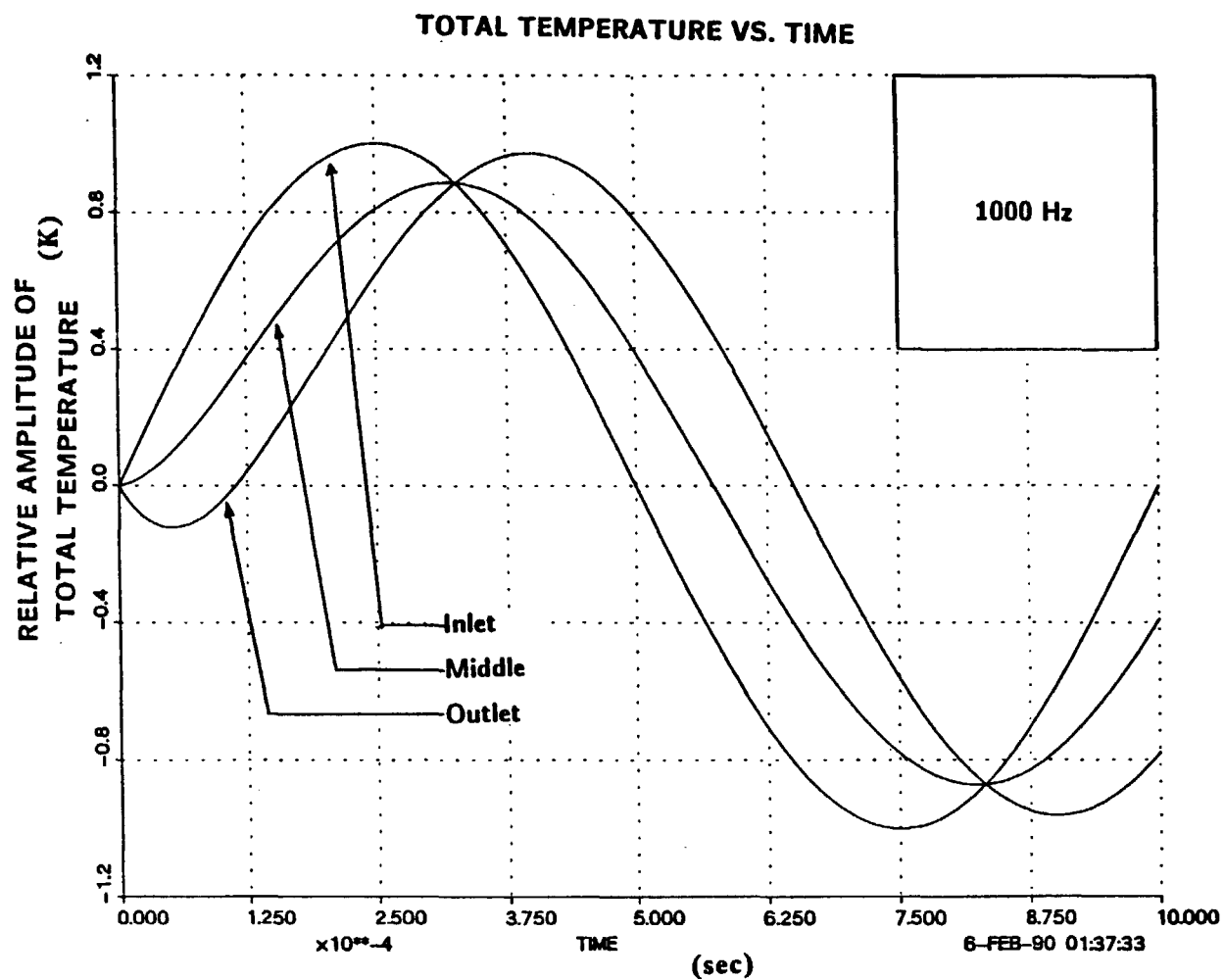


Figure 56. Response of the total temperature, for the turbine, to sinusoidal input described by table 8. The time step is 1 micro seconds. Frequency is 1000 Hz.

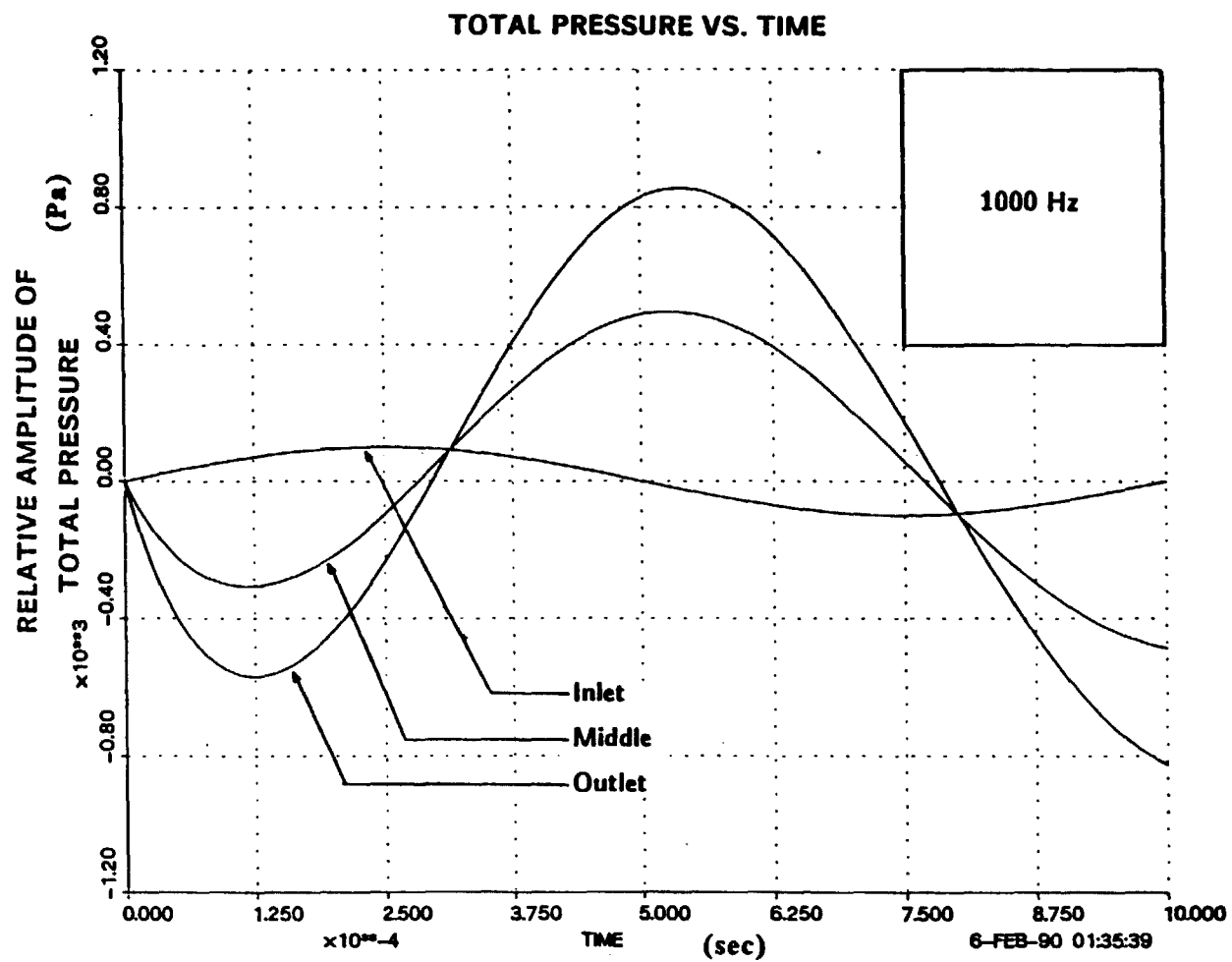


Figure 57. Response of the total pressure, for the turbine, to sinusoidal input described by table 8. The time step is 1 micro seconds. Frequency is 1000 Hz.

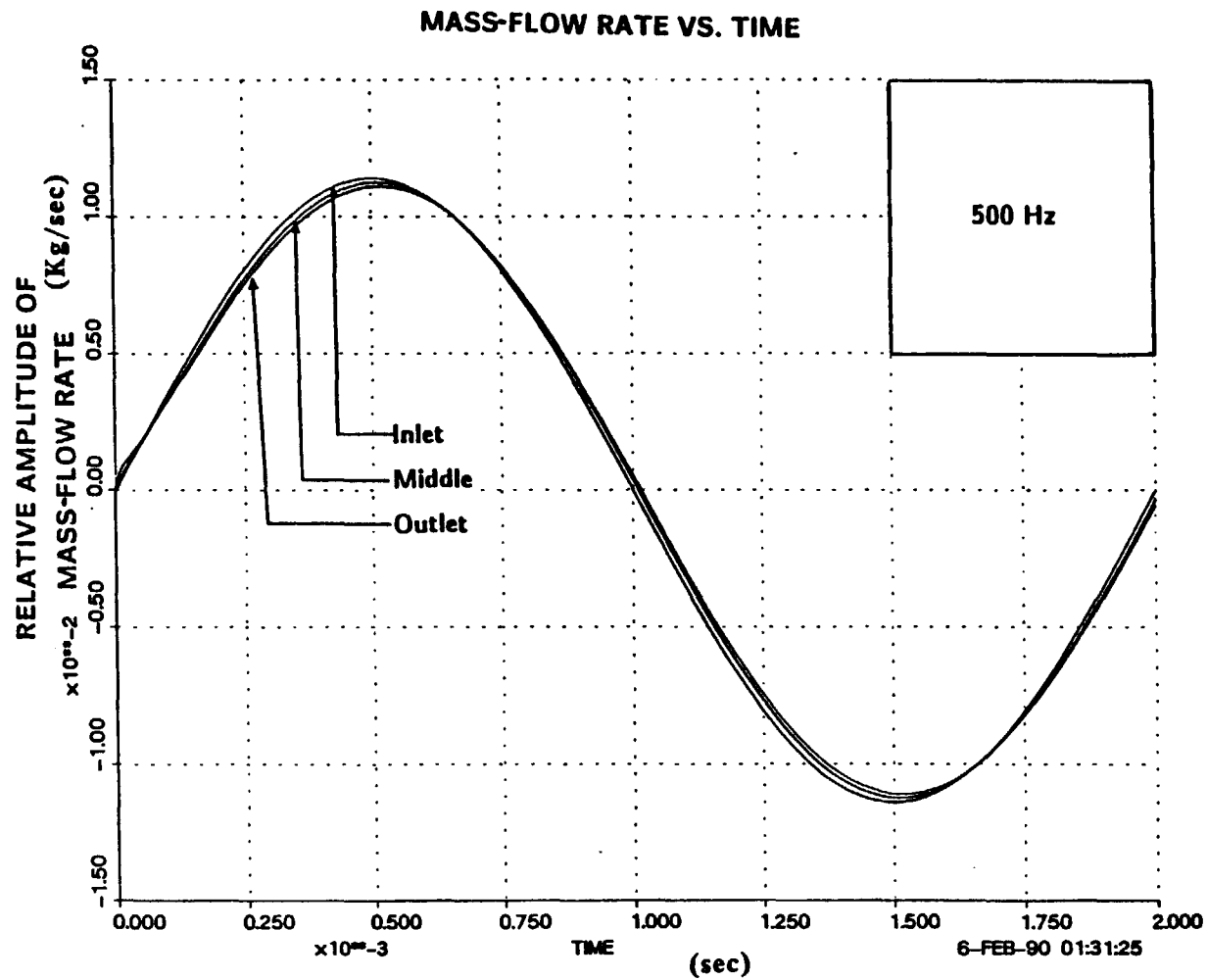


Figure 58. Response of the mass-flow rate, for the turbine, to sinusoidal input described by table 8. The time step is 1 micro seconds. Frequency is 500 Hz.

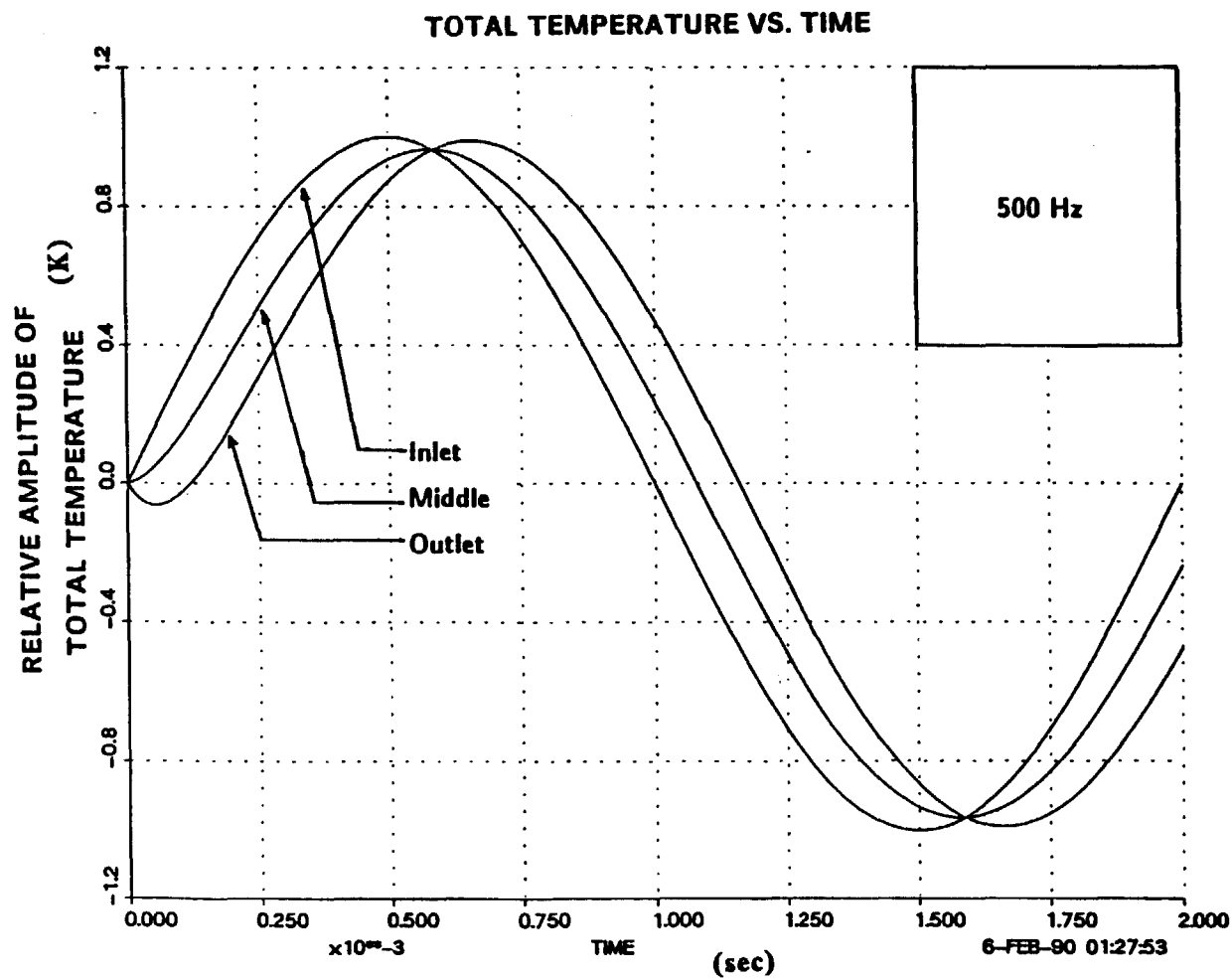


Figure 59. Response of the total temperature, for the turbine, to sinusoidal input described by table 8. The time step is 1 micro seconds. Frequency is 500 Hz.

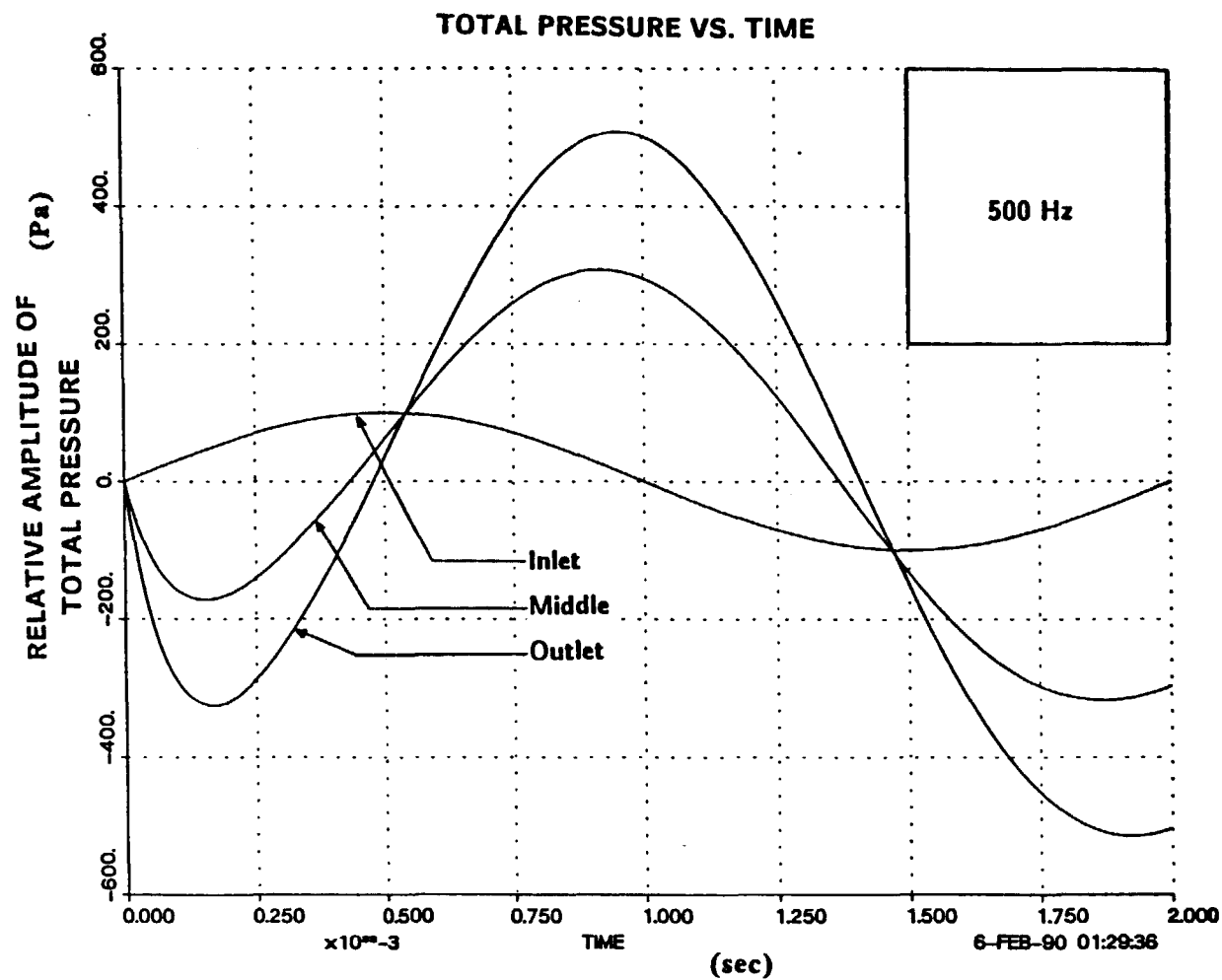


Figure 60. Response of the total pressure, for the turbine, to sinusoidal input described by table 8. The time step is 1 micro seconds. Frequency is 500 Hz.

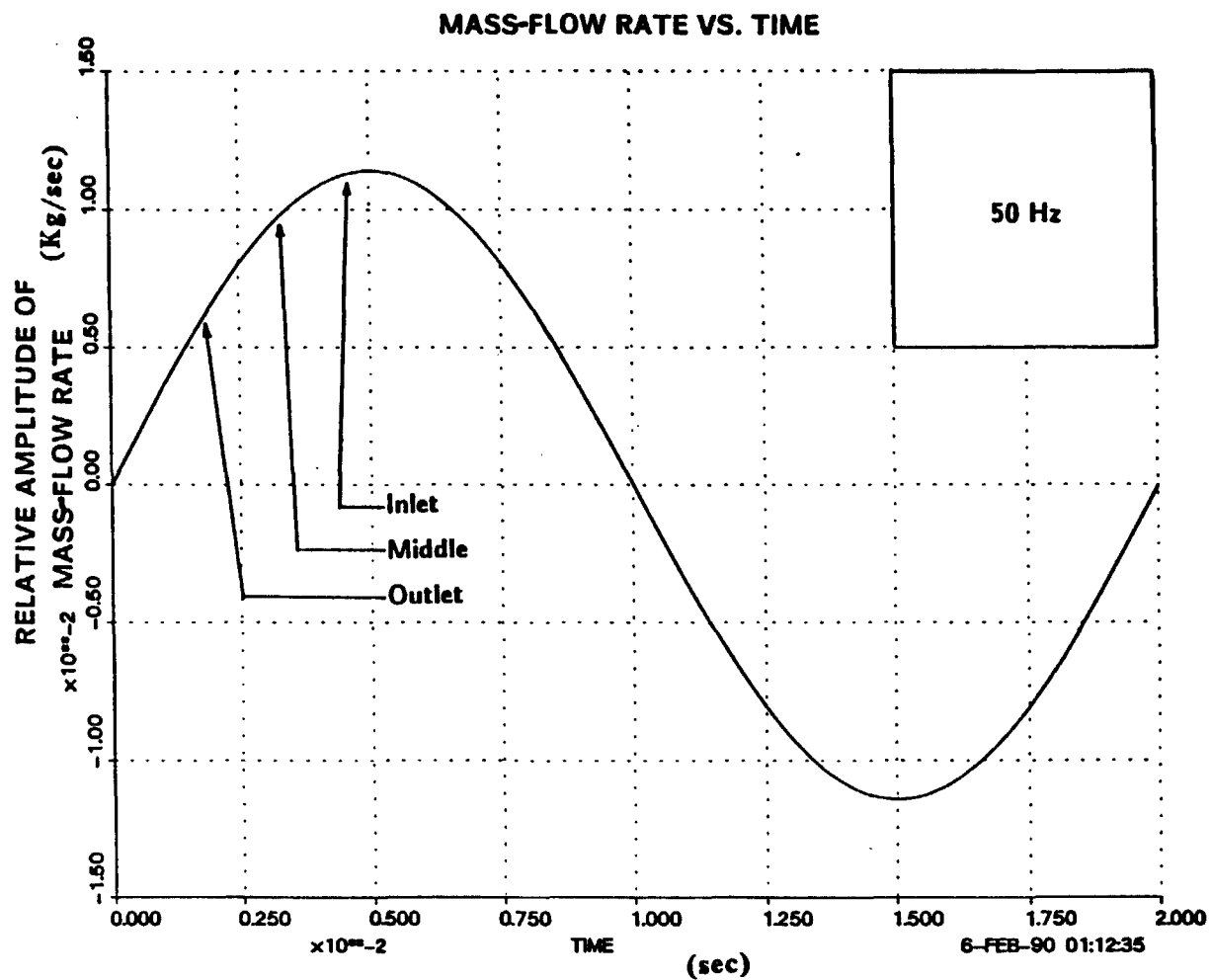


Figure 61. Response of the mass-flow rate, for the turbine, to sinusoidal input described by table 8. The time step is 1 micro seconds. Frequency is 50 Hz.



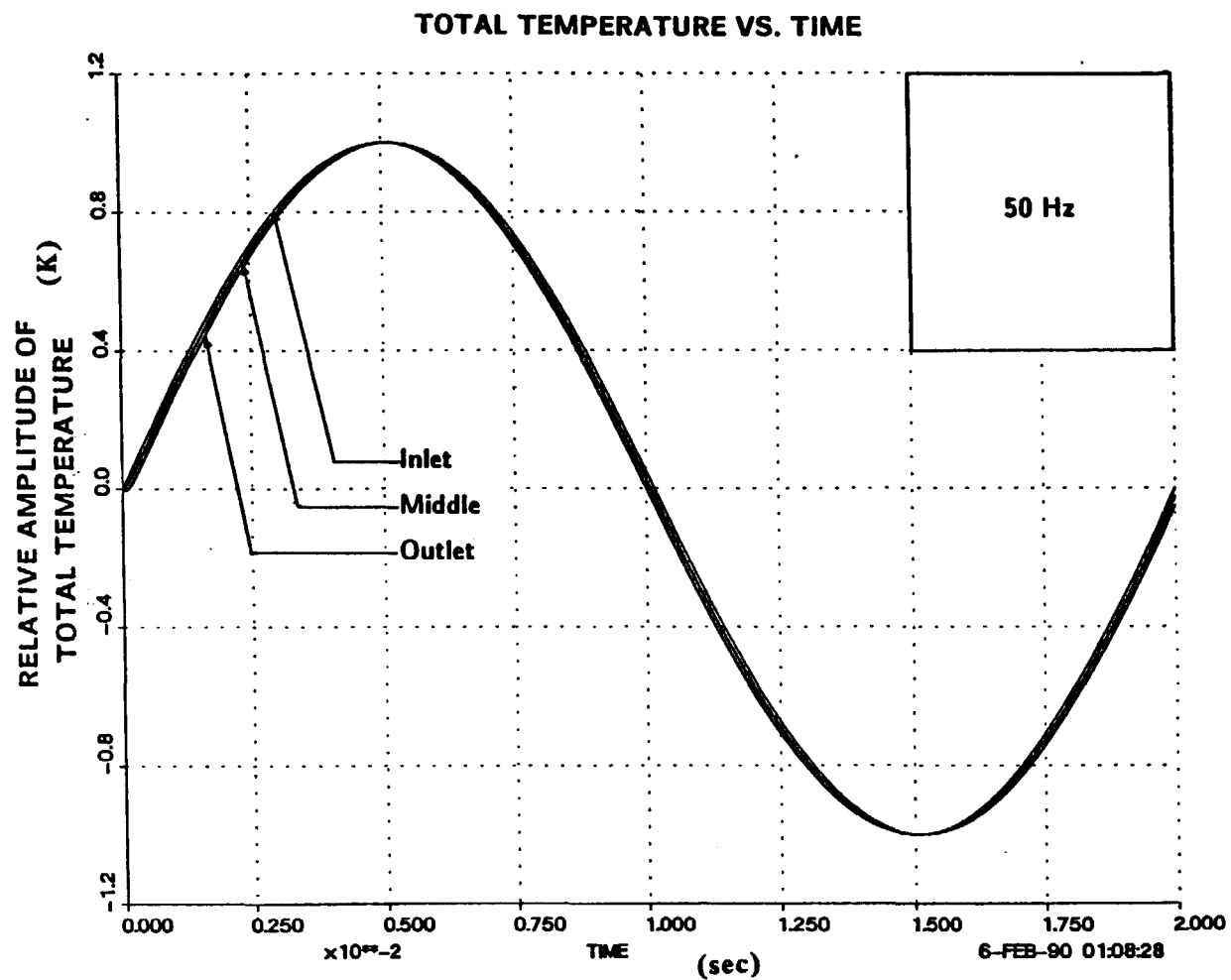


Figure 62. Response of the total temperature, for the turbine, to sinusoidal input described by table 8. The time step is 1 micro seconds. Frequency is 50 Hz.

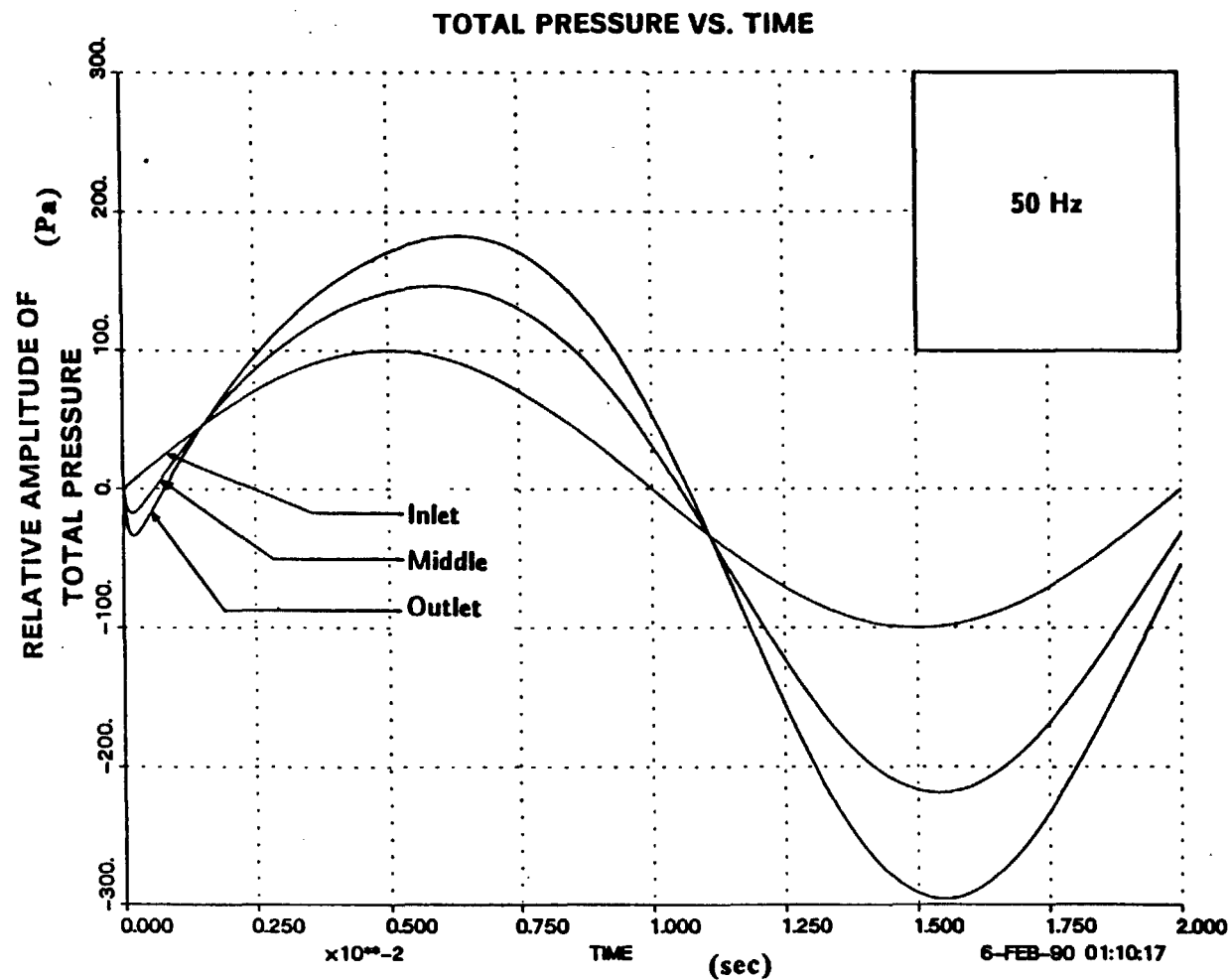


Figure 63. Response of the total pressure, for the turbine, to sinusoidal input described by table 8. The time step is 1 micro seconds. Frequency is 50 Hz.

### 3.9.2 Constant-Rate-Of-Work Variable-Speed Model

The second model developed by modification of the moment-of-momentum equation describes the performance of a constant-work-output turbine. The rotor speed is allowed to vary in response to thermodynamic changes at the inlet.

Table 9 presents information used to perform turbomachinery analysis. Specifically table 9 lists: the geometry of the turbine to be simulated; the design-point data for the turbine; the perturbation to the design steady-state value to initiate a transient; and the thermodynamic steady-state values expected at the end of the simulation. The perturbation of the steady-state is achieved by ramping the inlet state over a period of 100 micro seconds. After 100 micro seconds the inlet remains constant at the new value. The results of these analyses are presented in figures 64 to 67.

Figure 64 shows the mass-flow-rate response. Figures 65 and 66 show the response of total temperature and total pressure respectively. Figure 67 shows the reduction in rotor speed, due to increase in mass-flow rate. This decrease can be predicted by examining the steady-state equation relating rate of work and rotor speed.

$$\Omega = \left[ \frac{\dot{W}}{\dot{m}_* R^2} \right]^{1/2} \quad (43)$$

All the variables matched the expected final steady-state correctly.

This model was also excited by sinusoidal input according to data given in table 10. The predicted outlet response obtained for these

**Table 9: Data for results presented in figures 64 - 67**

**Turbine Geometry:**

Inlet normal area:	4.668E-3 m <sup>2</sup>
Middle normal area:	5.158E-3 m <sup>2</sup>
Outlet normal area:	5.648E-3 m <sup>2</sup>
Volume of compressor:	1.000E-4 m <sup>3</sup>
Tip radius:	8.810E-2 m
Middle radius:	4.896E-2 m
Rotor Inertia:	0.082 Kg m <sup>2</sup>

**Design point data:**

Inlet total temperature:	1034.02 K
Outlet total temperature:	866.01 K
Inlet total pressure:	540.25 KPa
Outlet total pressure:	330.14 KPa
Mass flow rate:	1.2886 Kg/sec
Rotor speed:	3351.0 Hz
Total to total polytropic efficiency:	0.9010

**Perturbation at inlet to obtain transient response:**

Ramp inlet total temperature to:	1035.02 K
Ramp inlet total pressure to:	540.35 KPa
Ramp inlet mass flow to:	1.3 Kg/sec

**Expected steady state outlet states:**

Outlet total temperature:	867.01 K
Outlet total pressure:	330.316 KPa
Outlet mass flow rate:	1.3 Kg/sec

**Additional notes:**

Constant specific heat:	519.14 J/Kg/K
Gas constant:	207.44 J/Kg/K
Variable speed:	
Constant rate of work out:	

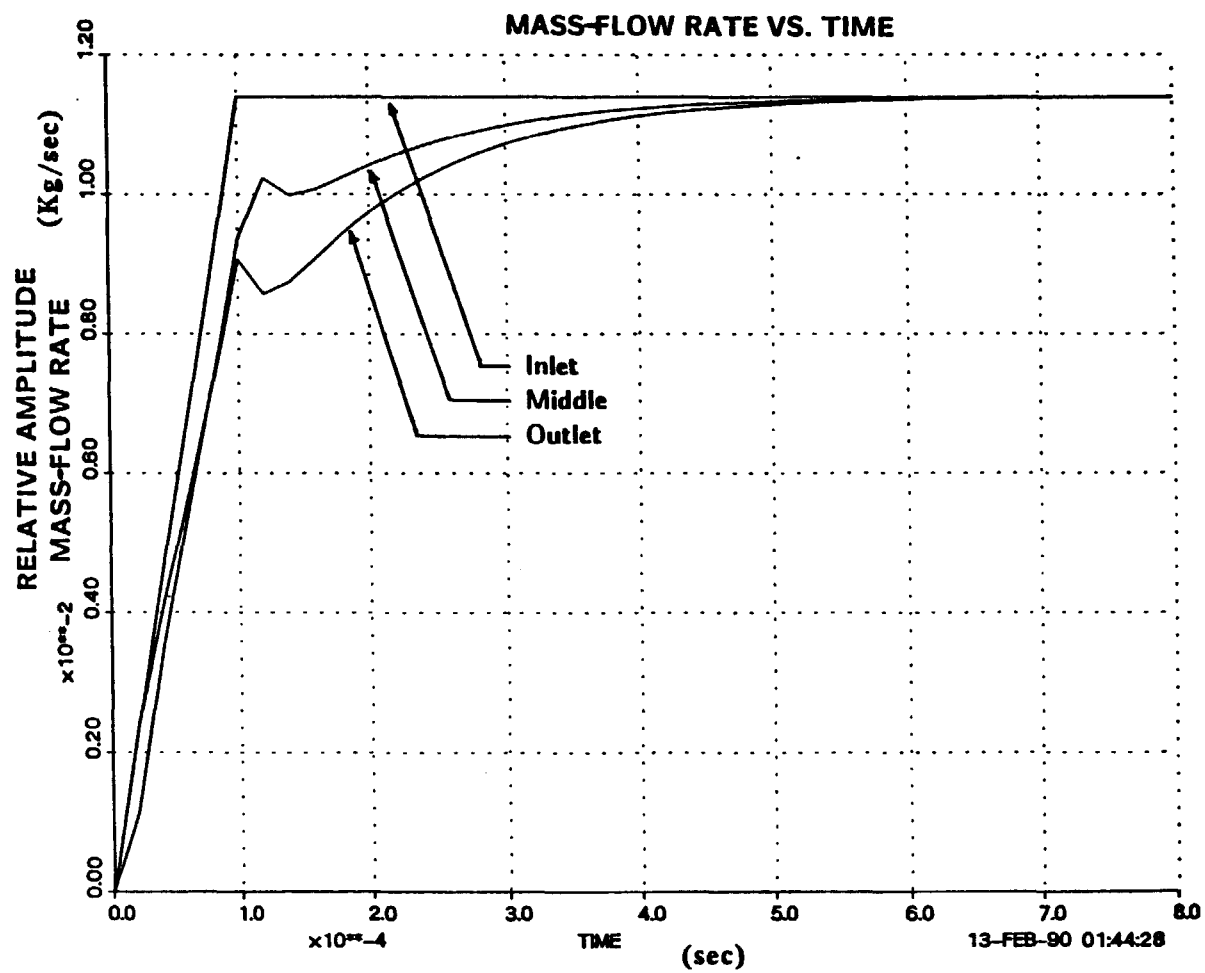


Figure 64. Response of the mass-flow rate, for the turbine, to ramp described by table 9. The time step is 10 micro seconds.

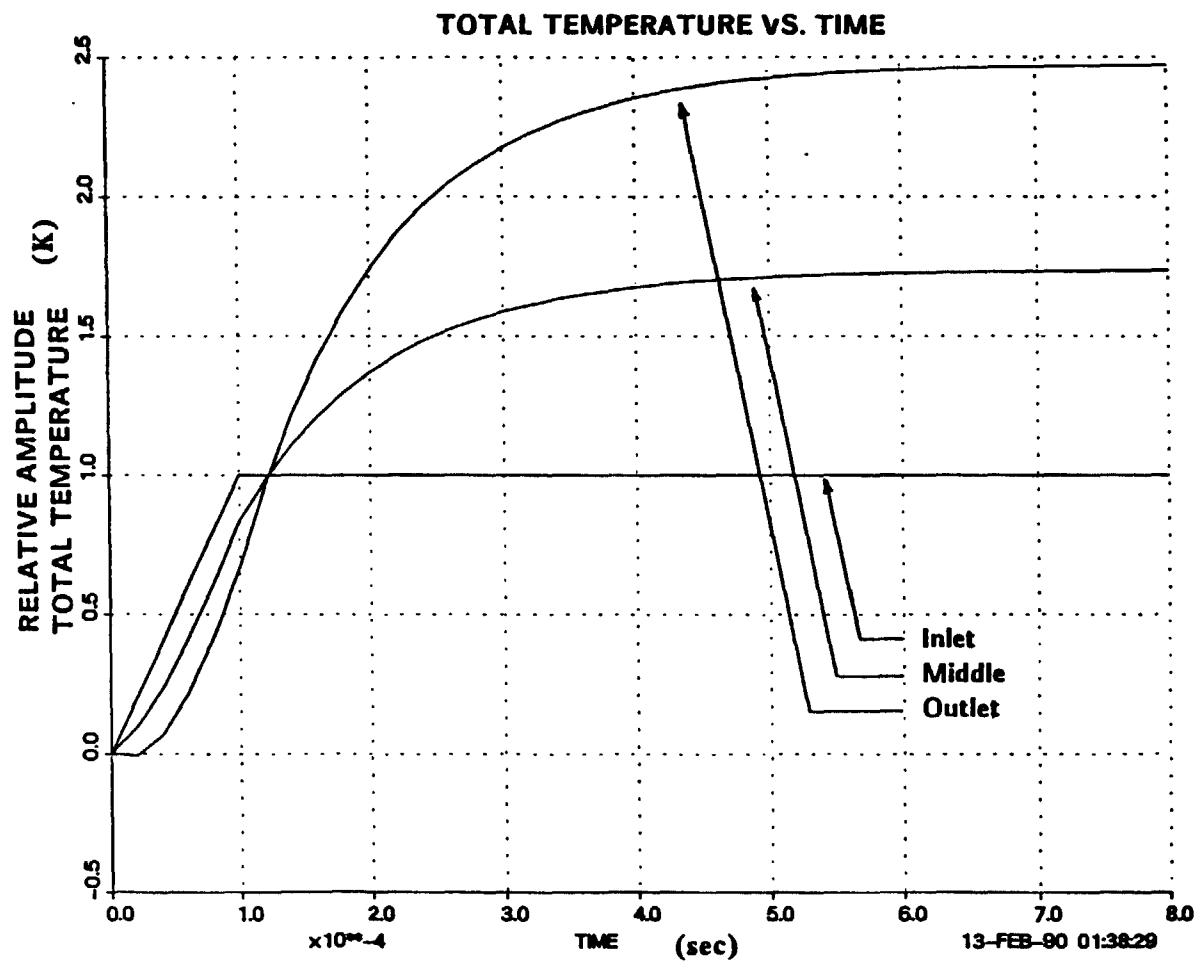


Figure 65. Response of the total temperature, for the turbine, to ramp described by table 9. The time step is 10 micro seconds.

Q-4

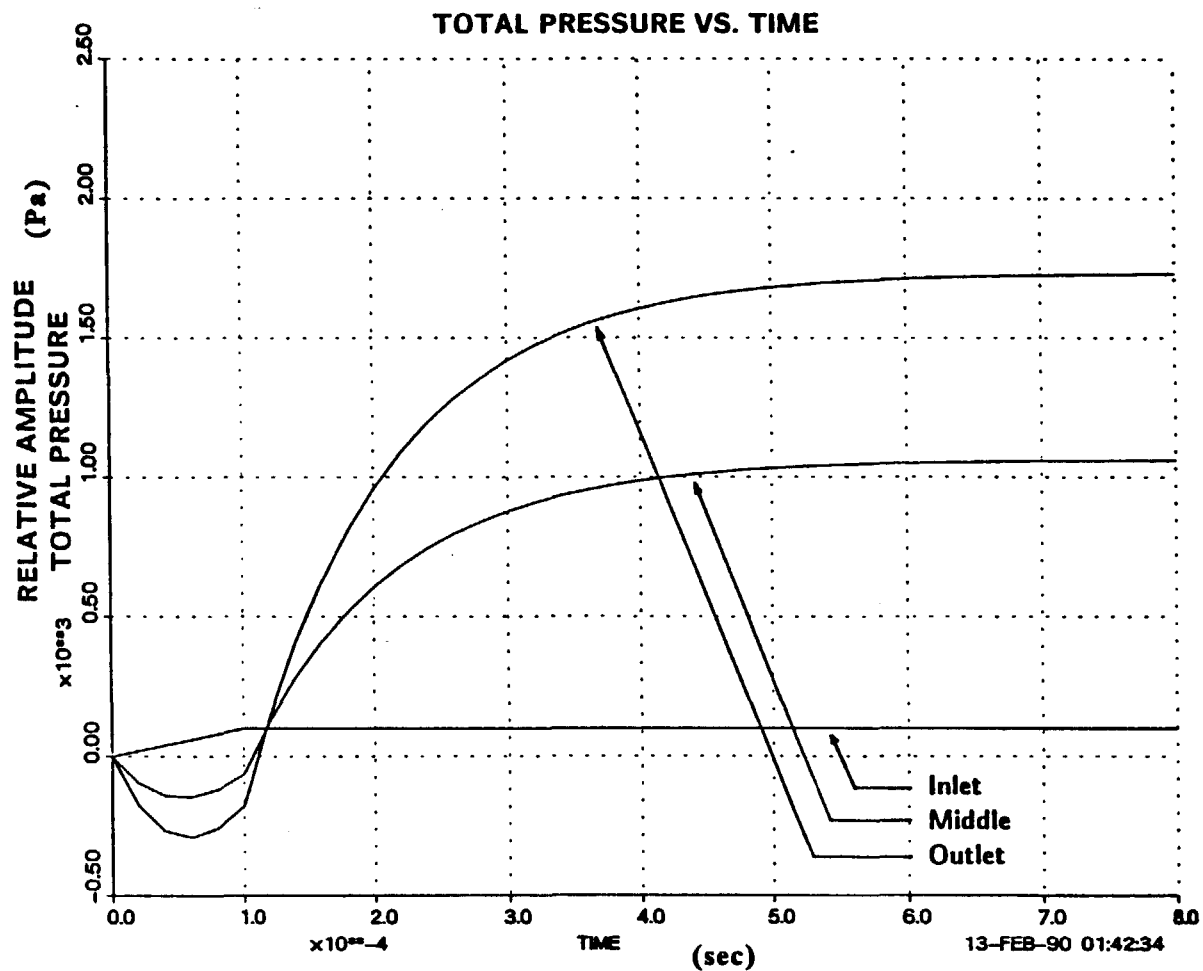


Figure 66. Response of the total pressure, for the turbine, to ramp described by table 9. The time step is 10 micro seconds.

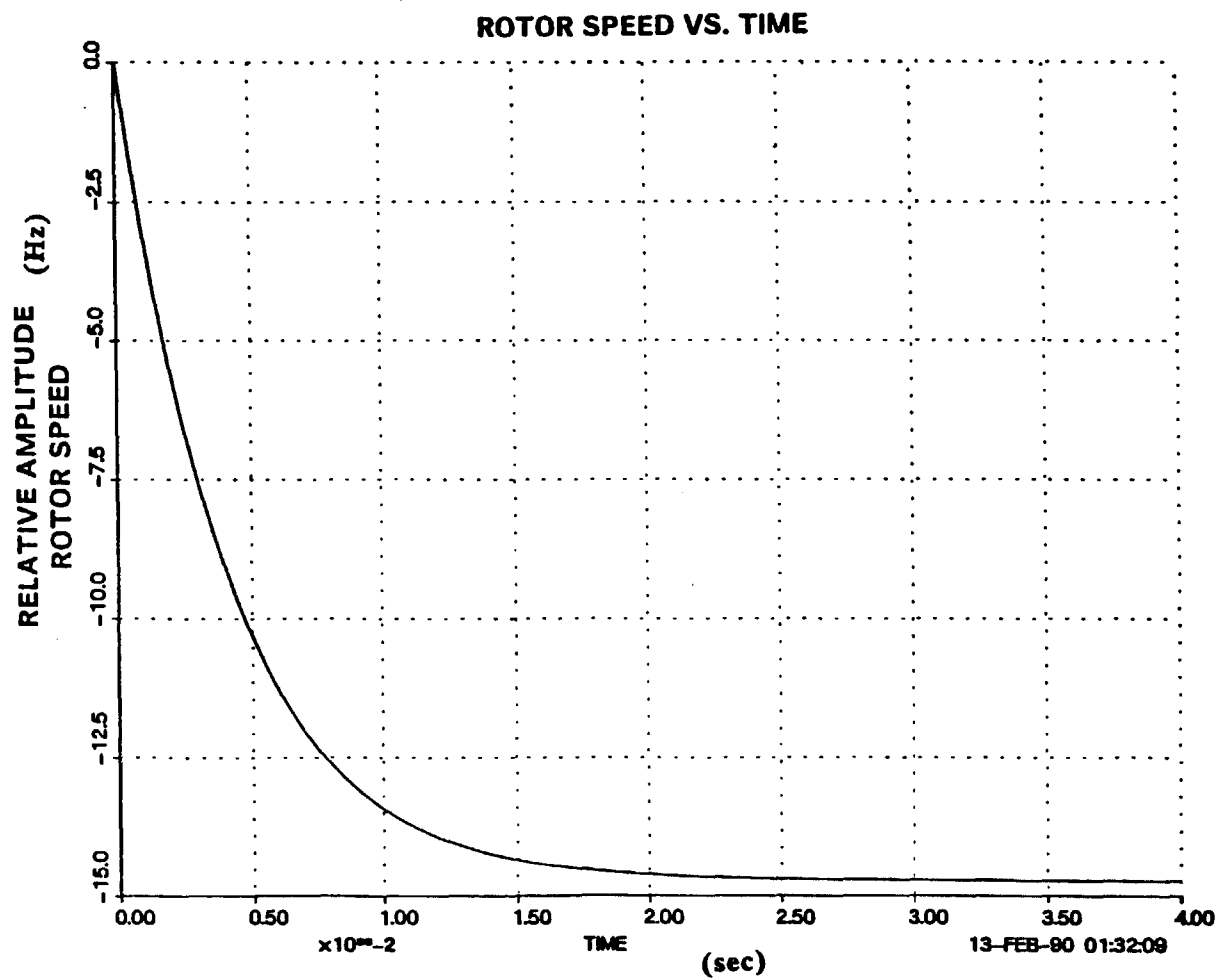


Figure 67. Response of the rotor speed of the turbine to ramp described by table 9. The time step is 10 micro seconds.



analyses are shown in figures 68-71. The zero on the abscissa represents the design-point steady-state value.

Figure 68 shows inlet, middle and outlet mass flow rate. Figure 69 shows inlet, middle and outlet total temperature. Figure 70 shows inlet, middle, and outlet total pressure. Figure 71 shows the rotor speed over time. Note the different time scale for this plot. A larger scale was selected to display rotor speed response because it is significantly slower than the response of the thermodynamic variables. The rotor response is related to both the thermodynamic state in the machine and inertia of the rotor.

In conclusion, the state-average lagged-mass-flow model was the most successful model. This model did not contradict any conservation laws, and the results predicted by it are not counter to intuition. However, the validity of this model is still dependent on the choice of a appropriate integration time-step size. In light of discussion of section 3.7, the results obtained for time-step size of 10 micro seconds are the most appropriate.

**Table 10: Data for results presented in figures 68 - 71**

**Turbine Geometry:**

Inlet normal area:	4.668E-3 m <sup>2</sup>
Middle normal area:	5.158E-3 m <sup>2</sup>
Outlet normal area:	5.648E-3 m <sup>2</sup>
Volume of compressor:	1.000E-4 m <sup>3</sup>
Tip radius:	8.810E-2 m
Middle radius:	4.896E-2 m
Rotor Inertia:	0.082 Kg m <sup>2</sup>

**Design point data:**

Inlet total temperature:	1034.02 K
Outlet total temperature:	866.01 K
Inlet total pressure:	540.25 KPa
Outlet total pressure:	330.14 KPa
Mass flow rate:	1.2886 Kg/sec
Rotor speed:	3351.0 Hz
Total to total polytropic efficiency:	0.9010

**Perturbation at inlet to obtain transient response:**

Sine wave amplitude inlet total temperature:	1.0 K
Sine wave amplitude inlet total pressure:	100 KPa
Sine wave amplitude inlet mass flow:	0.0114 Kg/sec
Sine wave frequency inlet total temperature:	1,000 Hz
Sine wave frequency inlet total pressure:	1,000 Hz
Sine wave frequency inlet mass flow:	1,000 Hz

**Additional notes:**

Constant specific heat:	519.14 J/Kg/K
Gas constant:	207.44 J/Kg/K
Constant Work out:	
Variable rotor speed:	

Sine wave is superimposed on already existing steady state:

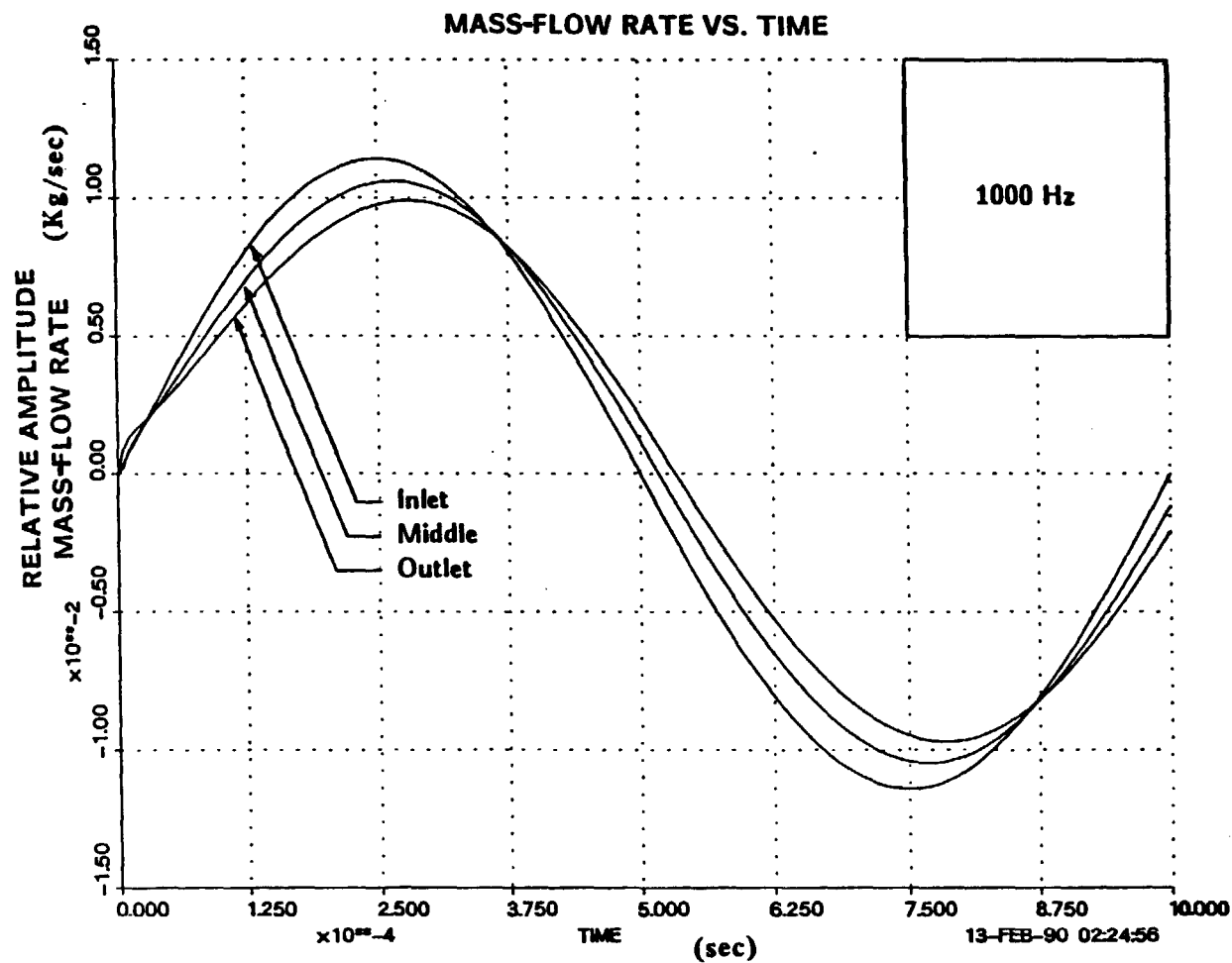


Figure 68. Response of the mass-flow rate, for the turbine, to sinusoidal input described by table 10. The time step is 1 micro seconds. Frequency is 1000 Hz.

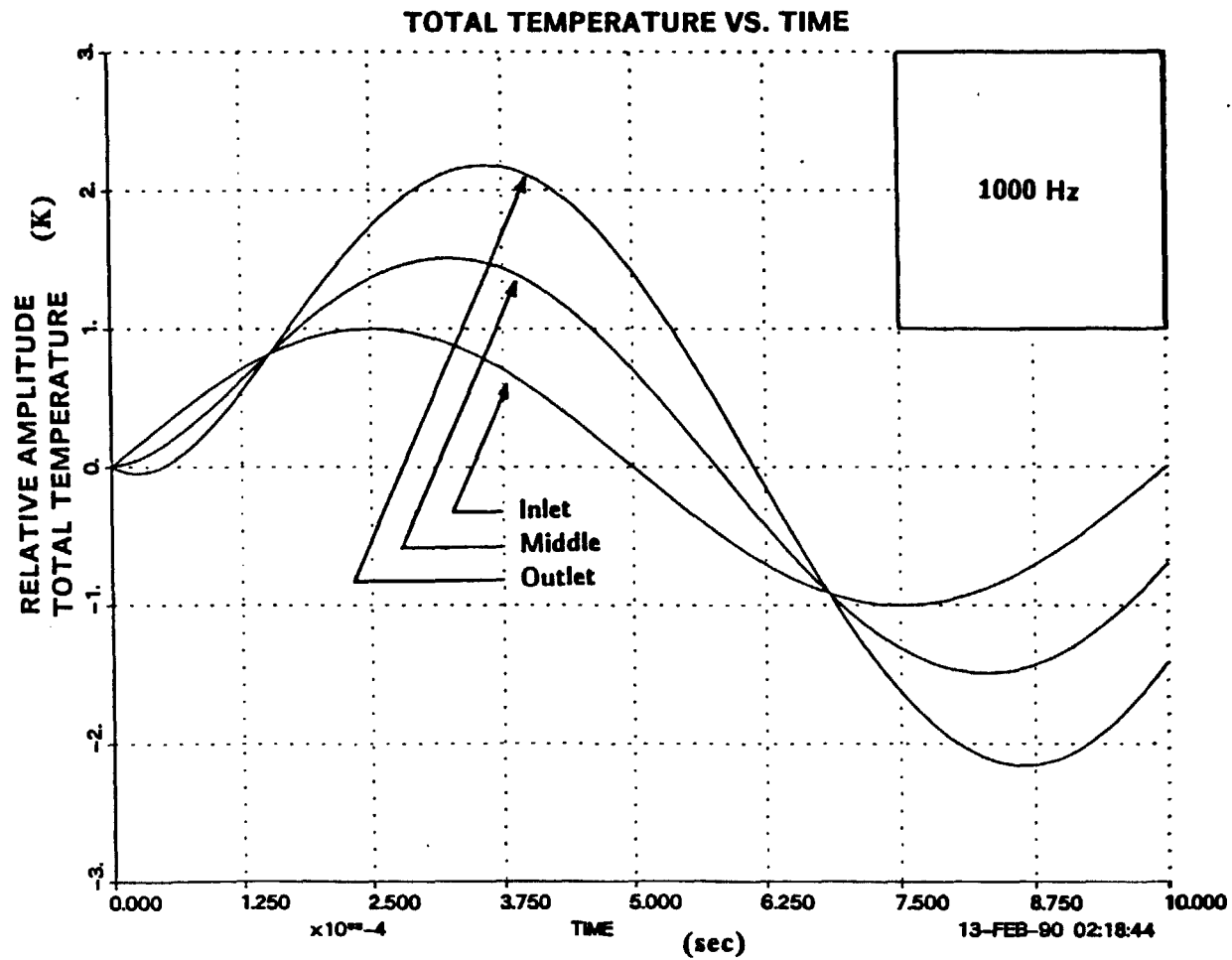


Figure 69. Response of the total temperature, for the turbine, to sinusoidal input described by table 10. The time step is 1 micro seconds. Frequency is 1000 Hz.

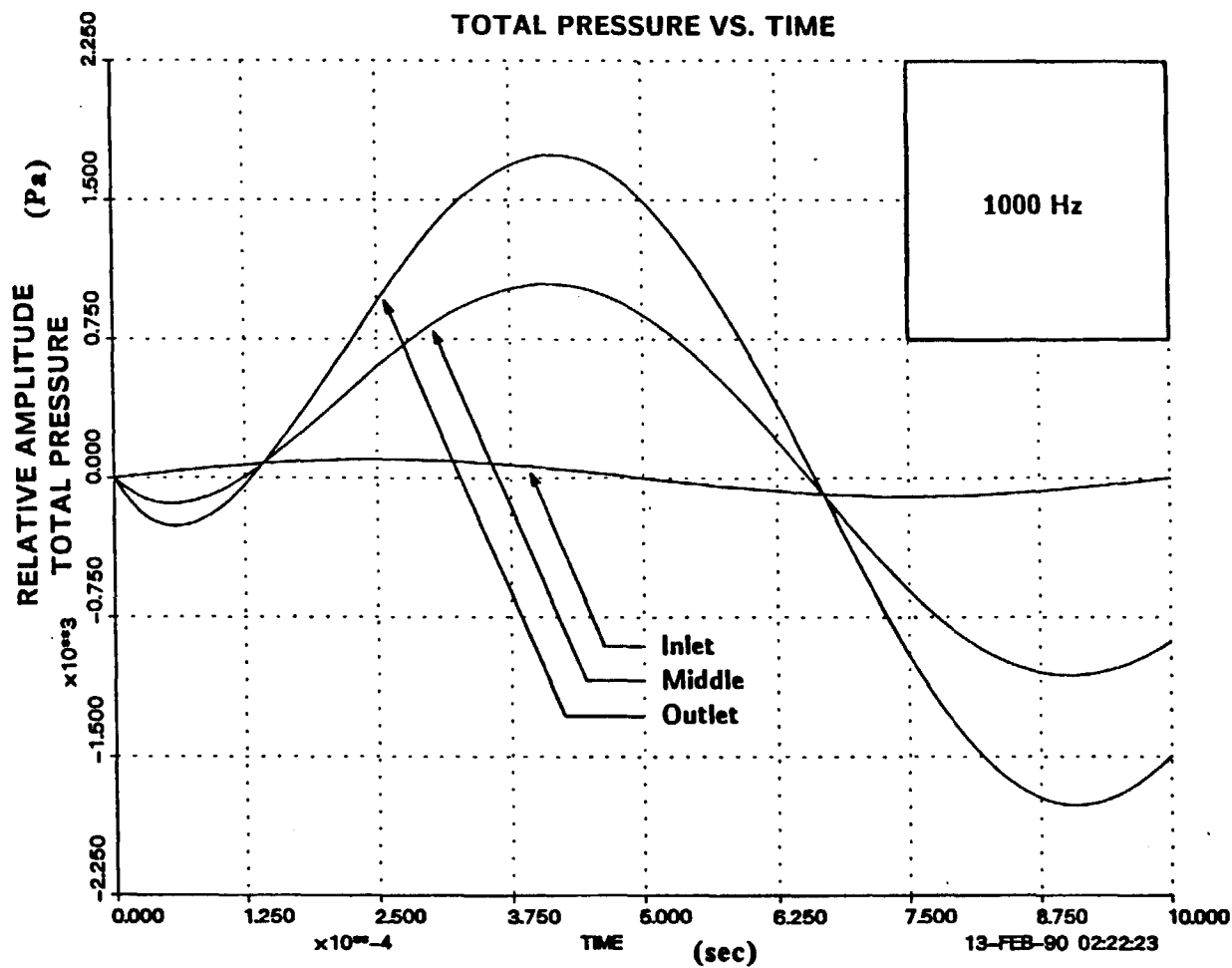


Figure 70. Response of the total pressure, for the turbine, to sinusoidal input described by table 10. The time step is 1 micro seconds. Frequency is 1000 Hz.

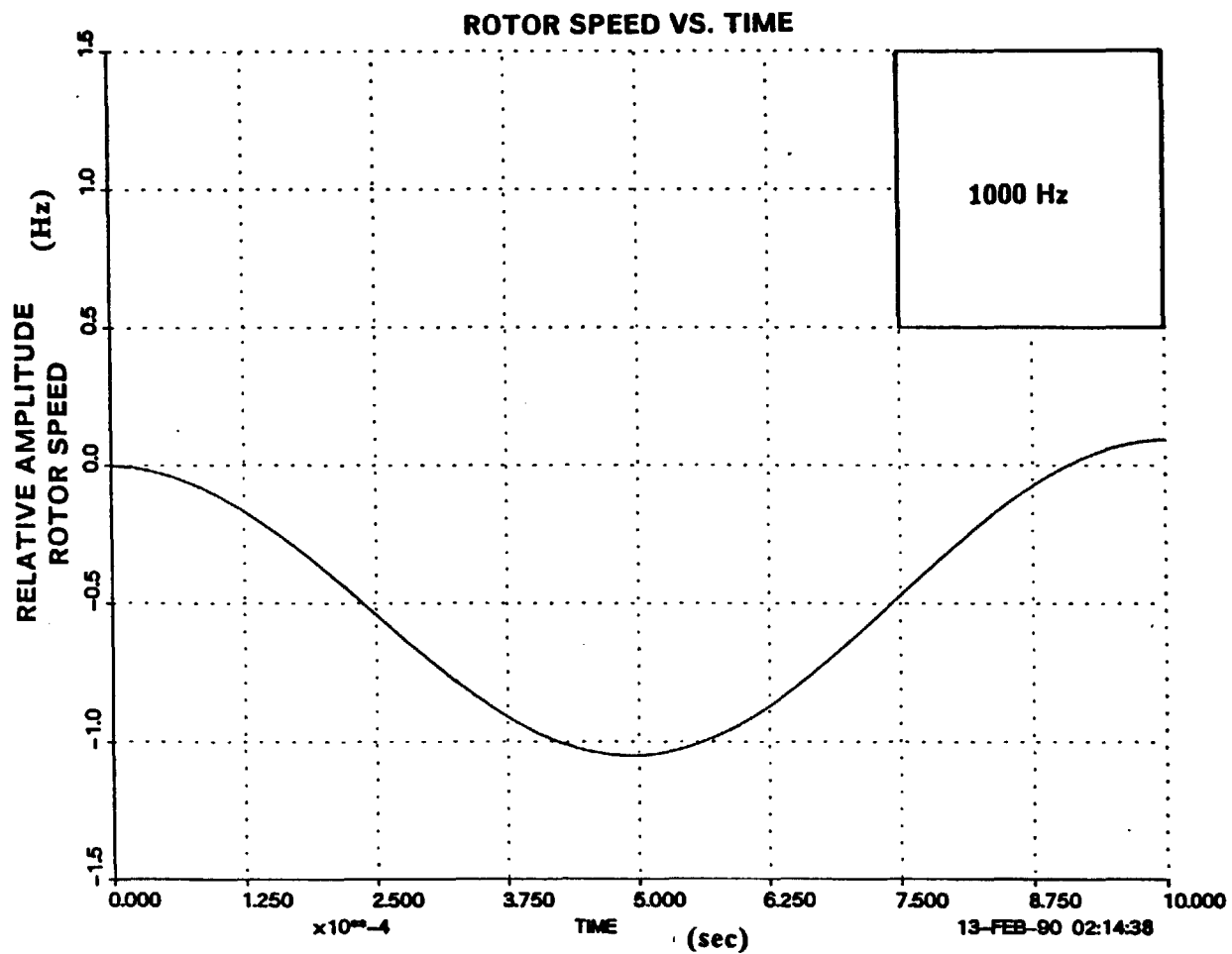


Figure 71. Response of the rotor speed of the turbine to sinusoidal input described by table 10. The time step is 1 micro seconds. Frequency is 1000 Hz.

#### 4. DISCUSSION

Chapter 3 presented the development of six different models for prediction of the transient performance of compressible flow turbomachines. Each model evolved from an understanding of the undesirable features of the model preceding it. The sixth and final model is considered to be the most successful. The following paragraphs summarize and compare the performance characteristics of each model.

The first model to be evaluated was based on Laplace transform transfer functions. This approach was found to be unsatisfactory due to the highly nonlinear and coupled nature of the governing equations.

The second model developed was the state-average model. A mixture of algebraic and differential equations are used to represent the physics governing the performance of the turbomachine. The thermodynamic state inside the machine is determined by a simple average of inlet and outlet values for two of the state variables. The outlet total temperature predicted by this model showed a questionable jagged response to a step change in inlet total temperature. Further, the integrator only functioned over a very restricted range of time-step sizes. Because of the jagged response and the severe restriction on the time-step size, this model was considered inadequate.

The third model developed was the constant-Mach-number-in-the-middle model. In an effort to address the time-step restriction of

the state-average model, one of the averaged internal state variables was replaced with the assumption of a constant Mach number in the middle of the machine. Although this did indeed eliminate the lower bound on time-step size, it violated conservation of mass for transient analyses.

The fourth model developed was the upwind-mass-flow model. The mass flow rate in the middle of the control volume is assumed to be equal to the inlet mass flow rate. This assumption directly addresses the shortcomings of both the constant-Mach-number-in-the-middle model and the state-average model. The general response predicted by this model appeared reasonable but raised concerns about the transit time of information through the control volume. Models of the transport of information through the control volume were examined to address these concerns. Further, it seemed desirable to develop a model which did not assume an instant response of the mass flow rate through the middle of the machine.

The fifth model developed was the sliced model. This model tried to incorporate the wave propagation of information through the control volume by a time-delay averaging procedure. Unfortunately the responses predicted by this model did not converge with decreasing time-step size. In fact, the responses diverge with decreasing time-step size. This characteristic was judged to be extremely undesirable and this model is therefore considered unsatisfactory.

The sixth and final model developed was the state-average lagged-mass-flow-rate model. The thermodynamic state inside the machine is



uniquely determined by a two step process. First, the total temperature in the middle of the machine is computed by a simple average of inlet and outlet values of total temperature at the new time-level. Second, the mass flow rate through the middle of the machine is computed as an average of the new time-level value of mass flow rate at the inlet and the old time-level value of mass flow rate at the outlet. This formulation directly addresses the shortcomings of the state-average and the upwind-mass-flow models. Several simulations using this model with various inputs were performed. The results obtained from these simulations do not contradict any of the conservation laws. In light of the discussion presented in section 3.7, a minimum time-step size consistent with the modeling assumptions is dictated by the size and speed of the turbomachine. A study conducted to investigate the response of the turbine to different perturbation frequencies below 50 Hz the mass storage term in the model can be neglected. The variable-speed constant-rate-of-work model (section 3.9.2) revealed that the rate of change of rotor speed depends on the inertia of the rotor. In fact the response time of rotor speed is orders of magnitude larger than the response time of the thermodynamics. Since no experimental data were found to validate the above results, the model performance could only be judged for simple transients.

## 5. SUMMARY AND CONCLUSIONS

The goal of this study was to develop transient models for two major components of the solar dynamic power conversion system (SDPCS) - the turbine and the compressor. These models are to be used to study the transient response of, and to develop controls for, the SDPCS. The models were required to simulate the physics associated with transients of the same order as the those associated with the control mechanisms.

Six models were developed. These were: the transfer function model; the state-average model; the constant-Mach-number-in-the-middle model; the upwind-mass-flow model; the sliced model; and the state-average lagged-mass-flow model. The first five models were considered to be unsatisfactory for reasons summarized in chapter 4.

The sixth and most successful model, the state-average lagged-mass-flow-rate model, was developed based on the experiences of the first five models. Several simulations using this model with various input transients were performed. The results obtained from these simulations do not contradict any of the conservation laws. In light of the discussion presented in section 3.7, a minimum time-step size consistent with the modeling assumptions is dictated by the size and speed of the turbomachine. The study conducted to investigate the response of the turbine to different perturbation frequencies revealed that for perturbation frequencies below 50 Hz the mass storage term can be neglected. The variable-speed constant-rate-of-work model (section 3.9.2) revealed that the rate of change of rotor

speed primarily depends on the inertia of the rotor. In fact the response time for the rotor speed is orders of magnitude larger than the response time of the thermodynamics. Since no experimental data were found to validate the above results, the model performance could only be judged for simple transients.

Therefore, the next step in validating the compressible flow turbomachinery models is to compare computational results with experimental data. The energy transfer between the blading and the fluid could also be included in the model. This inclusion would increase the flexibility of the model.

To further the study of SDPCS transients, a combined rotating unit model should be developed. This model would combine the turbine, the compressor, and the alternator models into one complete model. The response of this complete unit will determine the response times that will be required for the control of the SDPCS.

## 6. ACKNOWLEDGEMENT

The author would like to acknowledge the help and guidance of Dr. John I. Hochstein and Dr. Theodosios P. Korakianitis. During moments of intense frustration, Dr. Hochstein demonstrated infinite patience and provided encouragement, while Dr. Korakianitis induced in the author the energy and drive needed to proceed. The author will always remain indebted to Dr. Hochstein and Dr. Korakianitis not only for the academic knowledge, but also for their philosophical outlook on engineering and life in general. The author would like to thank Dr. Harold Brandon for his timely help in reading the thesis. Mr. Robert Watson also provided invaluable advice and guidance during this work. Finally, the author appreciates the assistance of Omar El-Ghazzawy, David William Dieckmeyer and the constant encouragement he received from his friends, family, and especially his parents.

## 7. BIBLIOGRAPHY

- 1) Rocketdyne, "Space Station Work Package WP-04 Power Systems Preliminary Analysis and Design Document," Rocketdyne RI/RD85--320-2, December 1986, (AKA DRO2 Document).
- 2) Bammert, K. and Krey, G., "Dynamic behavior and control of single shaft closed cycle Gas Turbines", ASME International Gas Turbine Institute, Technical Paper GT-16, 1971.
- 3) Iqbal Ahsan, "Transient Model of Space Station Solar Dynamic Power Generating System," Masters thesis, Sever Institute of Technology Washington University, May 1990.
- 4) Wilson, D.G., "The design of high-efficiency turbomachinery and gas turbine", The MIT press, Cambridge, Massachusetts, London, England 1984.
- 5) Khulberg, J. F., Sheppard, D.E., King, E.O. and Baker, J.R. "The dynamic simulation of turbine engine compressors", Fifth Propulsion Joint Specialist Conference, Colorado, 1969 (AIAA 69-486).
- 6) Elder, R.L., Gill, M.E. and Razak A.M.Y., "Validation of a compressor model", Transactions of the Institute of Measurement and Control, Volume 8, No 4, 1984.
- 7) Maccallum, N.R.L., "Thermal influences in gas turbine transients - effects of changes in compressor characteristics", ASME International Gas Turbine Institute, Technical Paper GT-143, 1979.
- 8) Sarantsev, L.B., "Analysis of the dynamics of gas turbines and their control systems", ASME International Gas Turbine Institute, Technical Paper GT-76, 1970.
- 9) Corbett, A.G., and Elder, R.L., "Stability of an axial flow compressor with steady inlet conditions", Journal of Mechanical Engineering Science, 16 (6), 377-385. December 1974.
- 10) Schultz, John M., "The polytropic analysis of centrifugal compressors", Journal of Engineering for Power, 84, 62-82. January 1962.
- 11) Greitzer, E.M., "Surge and rotating stall in axial flow compressors. Part 1: Theoretical Compression System Model," ASME International Gas Turbine Institute, Technical paper 75-GT-9, November 22, 1974.
- 12) Greitzer, E.M., "An introduction to unsteady flow in turbomachines," Massachusetts Institute of Technology, Cambridge, Massachusetts, U.S.A.

- 13) Heywood John D., "Internal Combustions Engine Fundamentals," McGraw Hill 1988.
- 14) Aiken, R.C., "Stiff Computation", Oxford University Press, Inc. 1985.

8. VITA

Biographical items on the author of the thesis,  
Mr. Mohammad Samad Ali

- 1) Born [REDACTED]
- 2) Attended Grinnell College from August, 1982 to May, 1985.  
Received the degree of Bachelor of Arts in May 1986. Major  
subject of study was Physics.
- 3) Attended Washington University from August, 1985 to May, 1987.  
Received the degree of Bachelor of Science in Mechanical  
Engineering in May 1987.
- 4) Maintenance Engineer, Exxon Chemicals Pakistan Ltd. August, 1987  
to November, 1987.
- 5) Attended Washington University from January, 1988 to present  
date.
- 6) Membership in Professional and Honor Societies: A.S.M.E.,  
A.I.A.A., and Pi Tau Sigma.

May, 1990

**Short Title:** Turbomachinery Transient Modeling    Ali, M.Sc. 1990



## Appendix C

### Dynamic Model of a Solar-Powered Closed Regenerative Turbine-Engine Cycle

WASHINGTON UNIVERSITY  
SEVER INSTITUTE OF TECHNOLOGY

---

DYNAMIC MODEL OF A SOLAR-POWERED CLOSED  
REGENERATIVE TURBINE-ENGINE CYCLE

by  
DEQUAN ZOU

Prepared under the direction of  
Professor Theodosios Korakianitis  
and  
Professor John I. Hochstein

---

A thesis presented to the Sever Institute of  
Washington University in partial fulfillment  
of the requirements for the degree of

MASTER OF SCIENCE

August, 1991

Saint Louis, Missouri

WASHINGTON UNIVERSITY  
SEVER INSTITUTE OF TECHNOLOGY

---

ABSTRACT

---

DYNAMIC MODEL OF A SOLAR-POWERED CLOSED  
REGENERATIVE TURBINE-ENGINE CYCLE

by Dequan Zou

---

ADVISORS :

Professor Theodosios Korakianitis

Professor John I. Hochstein

---

August, 1991

Saint Louis, Missouri

---

The development of quasi-steady, dynamic and mixed models of the Solar-Powered Closed Regenerative Turbine-Engine Cycle is presented. The development and refinement of component models are also presented. The system models were written in FORTRAN and based on the principles of conservation of mass, energy and momentum. An iteration scheme was used in the system model to find the mass-flow rate at every time step. Conservation of mass was used as a criterion of convergence of the iteration scheme. The system models were used to simulate the thermodynamic transient processes. The results with different system models were compared and discussed.

## TABLE OF CONTENTS

No.	Page
1. Introduction.....	1
1.1 The Solar-Powered Closed Regenerative Turbine-Engine Cycle.....	1
1.2 The Power Requirement of the Space Station.....	4
1.3 Previous Work.....	6
1.4 The Purpose of This Thesis.....	7
2. Component Modelling.....	9
2.1 Steady-State Models of the Components.....	9
2.1.1 Steady-State Heat Exchanger Model.....	10
2.1.2 Steady-State Radiator Model.....	14
2.1.3 Steady-State Turbine and Compressor Models.....	16
2.2 Dynamic Models of the Components.....	19
2.2.1 Dynamic Heat Exchanger Model.....	19
2.2.2 Dynamic Radiator Model.....	27
2.2.3 Dynamic Turbine and Compressor Models.....	31
2.2.4 Discussion of Minimum Time-Step for Turbomachinery Models.....	38
3. System Modeling.....	43
3.1 Control Equations and the Iteration Scheme for System Modeling.....	43
3.2 Quasi-Steady System Model.....	46
3.3 Dynamic Heat Exchangers/Quasi-Steady Turbomachines System Model.....	48
3.4 Dynamic Heat Exchangers/Dynamic Turbomachines System Model.....	52
4. The System Transient Performance Simulation.....	57
4.1 Transient Simulation with the Quasi-Steady System Model.....	57
4.2 Transient Simulation with Dynamic System Models.....	63

4.2.1 Performance Simulation by the Dynamic Heat Exchangers/Quasi-Steady Turbomachines System Model.....	63
4.2.1.1 Response to a Step of Receiver Salt Temperature.....	63
4.2.1.2 Response to a Double Step of Receiver Salt Temperature.....	70
4.2.1.3 Response to a Sinusoid of Receiver Salt Temperature.....	76
4.2.1.4 Response to a Ramp of Net Mechanical Power Output of the Turbomachinery.....	76
4.2.2 Performance Simulation by the Dynamic Heat Exchangers/Dynamic Turbomachines System Model.....	88
4.2.2.1 Response to a Step of Receiver Salt Temperature.....	88
4.2.2.2 Response to a Sinusoid of Receiver Salt Temperature.....	88
4.2.2.3 Response to a Ramp of Net Mechanical Power Output of the Turbomachinery.....	100
4.2.3 Discussion of Results Predicted by the Dynamic System Model with and without Turbomachine Dynamics.....	100
5. Summary and Conclusions.....	117
6. Recommendations for Further Study.....	119
7. Acknowledgements.....	121
8. References.....	122
9. Vita.....	123

## LIST OF TABLE

No.	Page
4.1 Design data for the components in the Solar-Powered Closed Regenerative Turbine-Engine Cycle.....	58-59

## **LIST OF FIGURES**

No.	Page
1.1 Schematic of the Solar-Powered Closed Regenerative Turbine-Engine Cycle.....	2
1.2 The temperature-entropy (T-S) diagram of the Solar-Powered Closed Regenerative Turbine-Engine Cycle.....	5
2.1 Section of radiator.....	15
2.2 Compressor characteristics.....	17
2.3 Turbine characteristics.....	18
2.4 Heat exchanger finite difference scheme.....	20
2.5 Radiator finite difference scheme.....	29
2.6 Control volume of turbomachinery.....	32
2.7 Control volume for moment of momentum equation.....	34
2.8 The flowchart of the iteration scheme used in the turbine and compressor models.....	39
2.9 The flow through one blade passage.....	41
3.1 Flowchart of the iteration scheme for system model.....	47
3.2 Flowchart of quasi-steady components system model.....	49-50
3.3 Flowchart of dynamic heat exchangers/quasi-steady turbomachines system model.....	53-54
3.4 Flowchart of dynamic heat exchangers/dynamic turbomachines system model.....	55-56
4.1 Response of receiver outlet parameters.....	60
4.2 Response of turbine outlet parameters.....	61
4.3 Response of compressor outlet parameters.....	62
4.4 Response of receiver outlet parameters.....	65
4.5 Response of turbine outlet parameters.....	66

4.6 Response of compressor outlet parameters.....	67
4.7 Response of gas cooler outlet parameters.....	68
4.8 Response of recuperator outlet parameters.....	69
4.9 Response of receiver outlet parameters.....	71
4.10 Response of turbine outlet parameters.....	72
4.11 Response of compressor outlet parameters.....	73
4.12 Response of recuperator outlet parameters.....	74
4.13 Response of gas cooler outlet parameters.....	75
4.14 Response of receiver outlet parameters (to sinusoidal driver).....	77
4.15 Response of turbine outlet parameters (to sinusoidal driver).....	78
4.16 Response of compressor outlet parameters (to sinusoidal driver).....	79
4.17 Response of recuperator outlet parameters (to sinusoidal driver).....	80
4.18 Response of gas cooler outlet parameters (to sinusoidal driver).....	81
4.19 Response of radiator outlet parameters (to sinusoidal driver).....	82
4.20 Response of compressor outlet parameters (to ramp of output power).....	83
4.21 Response of turbine outlet parameters (to ramp of output power).....	84
4.22 Response of recuperator outlet parameters (to ramp of output power).....	85
4.23 Response of receiver outlet parameters (to ramp of output power).....	86
4.24 Response of gas cooler outlet parameters (to ramp of output power).....	86
4.25 Response of radiator outlet parameters (to ramp of output power).....	87
4.26 Response of receiver outlet parameters (to ramp of salt temperature).....	89
4.27 Response of gas cooler outlet parameters (to ramp of salt temperature).....	89
4.28 Response of turbine outlet parameters (to ramp of salt temperature).....	90
4.29 Response of compressor outlet parameters (to ramp of salt temperature).....	91
4.30 Response of recuperator outlet parameters (to ramp of salt temperature).....	92
4.31 Response of radiator outlet parameters (to ramp of salt temperature).....	93



4.32 Response of receiver outlet parameters (to sinusoidal salt temp.).....	94
4.33 Response of turbine outlet parameters (to sinusoidal salt temp.).....	95
4.34 Response of compressor outlet parameters (to sinusoidal salt temp.).....	96
4.35 Response of recuperator outlet parameters (to sinusoidal salt temp.).....	97
4.36 Response of gas cooler outlet parameters (to sinusoidal salt temp.).....	98
4.37 Response of radiator outlet parameters (to sinusoidal salt temp.).....	99
4.38 Response of turbine outlet parameters (to ramp of output power).....	101
4.39 Response of compressor outlet parameters (to ramp of output power).....	102
4.40 Response of recuperator outlet parameters (to ramp of output power).....	103
4.41 Response of gas cooler outlet parameters (to ramp of output power).....	104
4.42 Response of receiver outlet parameters (to ramp of output power).....	105
4.43 Response of radiator outlet parameters (to ramp of output power).....	105
4.44 Response of receiver outlet parameters (to ramp of salt temperature) (time step = 0.000025 (sec)).....	106
4.45 Response of turbine outlet parameters (to ramp of salt temperature) (time step = 0.000025 (sec)).....	107
4.46 Response of compressor outlet parameters (to ramp of salt temperature) (time step = 0.000025 (sec)).....	108
4.47 Response of recuperator outlet parameters (to ramp of salt temperature) (time step = 0.000025 (sec)).....	109
4.48 Response of gas cooler outlet parameters (to ramp of salt temperature) (time step = 0.000025 (sec)).....	110
4.49 Response of radiator outlet parameters (to ramp of salt temperature) (time step = 0.000025 (sec)).....	110
4.50 Response of receiver outlet parameters (to ramp of salt temperature).....	112
4.51 Response of gas cooler outlet parameters (to ramp of salt temperature).....	112

4.52 Response of turbine outlet parameters (to ramp of salt temperature).....	113
4.53 Response of compressor outlet parameters (to ramp of salt temperature).....	114
4.54 Response of recuperator outlet parameters (to ramp of salt temperature).....	115
4.55 Response of radiator outlet parameters (to ramp of salt temperature).....	116

## NOMENCLATURE

### Latin Symbols:

$A$  - area

$A_r$  - radiation heat-transfer area

$A_x$  - heat-conduction area in x-direction

$A_y$  - heat-conduction area in y-direction

$C$  - fluid heat capacity rate

$C_p$  - constant-pressure specific heat

$C_v$  - constant-volume specific heat

$f$  - friction factor

$f_{cr}$  - correction factor

$f_e$  - relative error of calculated mass

$g$  - acceleration due to gravity

$h$  - heat-transfer coefficient

$k$  - heat conductivity

$K_{in}$  - entrance loss coefficient

$K_{out}$  - exit loss coefficient

$L$  - length

$L_d$  - length of radiator section

$L_w$  - width of radiator section

$M$  - Mach number

$m$  - mass

$\dot{m}$  - mass-flow rate

$N$  - rotation speed of rotor

$N_{tu}$  - number of heat exchanger heat-transfer units

$p$  - pressure

$\dot{Q}$  - heat-flow rate

$R$  - gas constant

$Re$  - Reynolds number

$R_{hub}$  - radius of rotor hub

$R_m$  - radius of the middle point of the control volume

$R_{tip}$  - radius of rotor tip

$S$  - entropy

$T$  - temperature

$T_{salt}$  - salt temperature

$T_{sink}$  - space temperature

$t$  - time

$V$  - velocity

$V_{cv}$  - control volume

$\dot{W}$  - power

Greek Symbols:

$\alpha$  - isothermal compressibility

$\beta$  - bulk expansion coefficient

$\varepsilon$  - heat exchanger heat transfer effectiveness

$\gamma$  - ratio ( $C_p/C_v$ )

$\eta$  - total-to-total isentropic efficiency

$\rho$  - density

$\sigma$  - ratio of the core free-flow area to the frontal-area

$\sigma_\varepsilon$  - product of the emissivity and the Stefan-Boltzmann constant

$\tau_q$  - torque

$\tau_0$  - unit surface shear stress

$\Omega$  - rotating frequency

$\Delta$  - denotes difference

$\Sigma$  - summation

Subscripts:

0 - reference parameter

a - fluid "a"

b - fluid "b"

c - cold fluid

comp - compressor

i - the  $i$ th element

in - inlet

j - the  $j$ th junction point between components

h - hot fluid

liq - liquid

m - middle

max - maximum

mean - mean value

min - minimum

out - outlet

p - polytropic

r - ratio

t - total

turb - turbine

w - wall

superscripts:

(k) - iteration step level

n - time step level

0 - reference parameters

\* - dimensionless parameter

' - corrected parameter

Acronyms:

SDPGS - Solar Dynamic Power Generation System

IOC - initial operation capacity

EASY5 - Engineering Analysis System 5

## 1. Introduction

The Solar-Powered Closed Regenerative Turbine-Engine Cycle is proposed for use in a Solar Dynamic Power Generating System (SDPGS) to provide electrical power for a space station under development by NASA<sup>[1]</sup>. The focus of the study presented in this thesis is the development of a dynamic model of the Solar-Powered Closed Regenerative Turbine-Engine Cycle.

### 1.1 The Solar-Powered Closed Regenerative Turbine-Engine Cycle

The Solar-Powered Closed Regenerative Turbine-Engine Cycle converts incident solar radiation into mechanical power. The mechanical power is then converted to electrical power by an alternator. Thermal energy is rejected from the cycle by radiation to space. The Solar-Powered Closed Regenerative Turbine-Engine Cycle consists of the following main components: receiver; turbine; compressor; heat exchanger (recuperator); gas cooler; and radiator. A schematic of the Solar-Powered Closed Regenerative Cycle is shown in Fig. 1.1.

The working fluid used in the Solar-Powered Closed Regenerative Turbine-Engine Cycle is a mixture of helium-xenon gas. Solar energy is collected by the concentrator which focuses incident solar energy onto the phase-change material (LiF-CaF<sub>2</sub> eutectic salt) in the receiver. When the concentrator is in direct sunlight, the salt in the receiver absorbs part of the incident solar energy flux and changes phase to liquid. The remainder of the collected solar energy is used to heat the cycle working fluid (helium-xenon). As the space station passes behind the Earth during its orbit, the solar energy flux is periodically interrupted by the Earth's shadow. When the space station is in the Earth's shadow, the eutectic salts return from the liquid state to a solid state and release

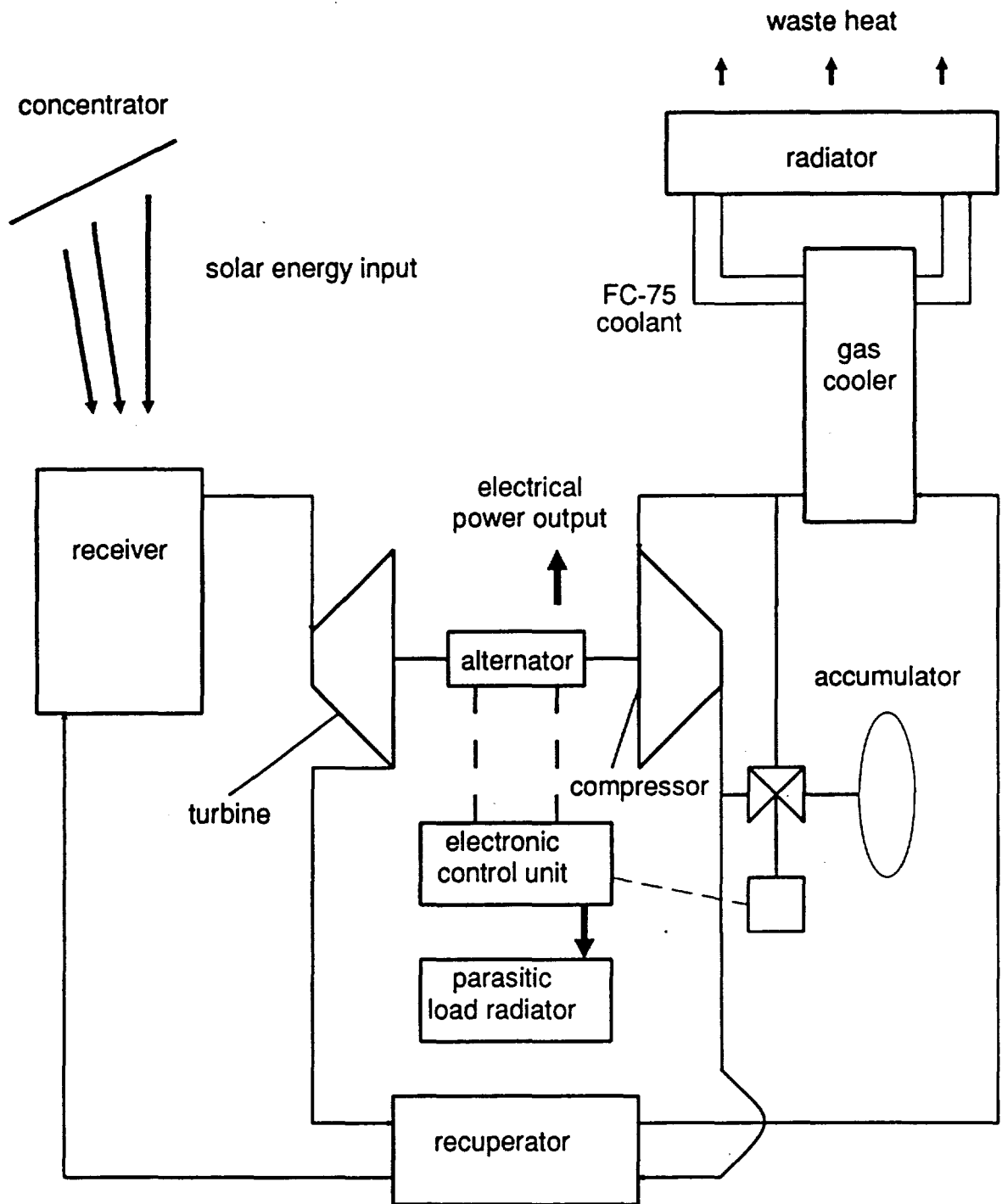


Fig. 1.1 Schematic of the Solar-Powered Closed Regenerative-Brayton Cycle



energy into the helium-xenon gas. The working process in the Solar-Powered Closed Regenerative Turbine-Engine Cycle can be described as follows:

(1). The low pressure, low temperature gas leaving the gas cooler passes through the compressor where it is compressed, and discharged at high pressure with a small rise in temperature.

(2). The compressed gas then passes through the high-pressure side of the recuperator where it is preheated by the turbine exhaust.

(3). The high pressure preheated gas is passed through the receiver where it is heated further to a high temperature while still at a high pressure.

(4). The high-pressure high-temperature gas leaving the receiver is passed through the turbine where it expands to produce work and its pressure and temperature are reduced.

(5). The low-pressure turbine-exhaust gas then passes through the low-pressure side of the recuperator and gives up energy to preheat the recuperator high-pressure side gas while the exhaust is itself precooled to a moderate temperature.

(6). The low-pressure precooled gas leaving the recuperator is further cooled in the gas cooler by FC-75 coolant. The low-pressure low-temperature gas is then returned to the compressor and the cycle is complete.

The net difference between shaft work required by the compressor and work delivered by the turbine is available for useful work in the alternator, once the frictional losses are deducted. Using the design data supplied in the DR02<sup>[1]</sup> document one concludes that the shaft power delivered by the gas expanding through the turbine is about 85% larger than the shaft power required by the compressor to compress the gas. The actual percentage depends on the efficiencies of the turbomachinery.

Fig. 1.2 shows the Solar-Powered Closed Regenerative Turbine-Engine Cycle on a temperature-entropy (T-S) diagram. Process (1) represented by path 1-2; Process (2) is represented by 2-3; Process (3) is represented by path 3-4; Process (4) is represented by path 4-5; Process (5) is represented by path 5-6; and Process (6) is represented by path 6-1.

## 1.2 The Power Requirement of the Space Station

The basic requirements of the SDPGS are to supply sufficient power for the space station. 75 kW of the electricity are required for the initial operation capacity (IOC) of the space station. 31.3% of the IOC will be provided by a photovoltaic module and the remaining 68.7% will be provided by a SDPGS. The SDPGS consists of two identical modules powered by Solar-Powered Closed Regenerative Turbine-Engine Cycles. The power output of each SDPGS module is 28.5 kW.

A number of control schemes have been designed to meet the dynamic-response requirements of the system. The objectives of the control schemes are:

- (1). The speed of the rotor is to be maintained at a constant value of 32,000 rpm to provide a constant voltage of 208 volts.

- (2). The flow of solar energy into the eutectic salt in the solar receiver is controlled to change the flow of energy into the working fluid, and hence to change the power output.

- (3). The power not required by the station is to be radiated into space.

These objectives are to be achieved by the control of the working fluid inventory by exchanging fluid between the accumulator and the system, the control of the rotation angle of the concentrator, and the control of the parasitic load. The accumulator and inventory control valves on the gas loop regulate the mass of gas in the loop. A change

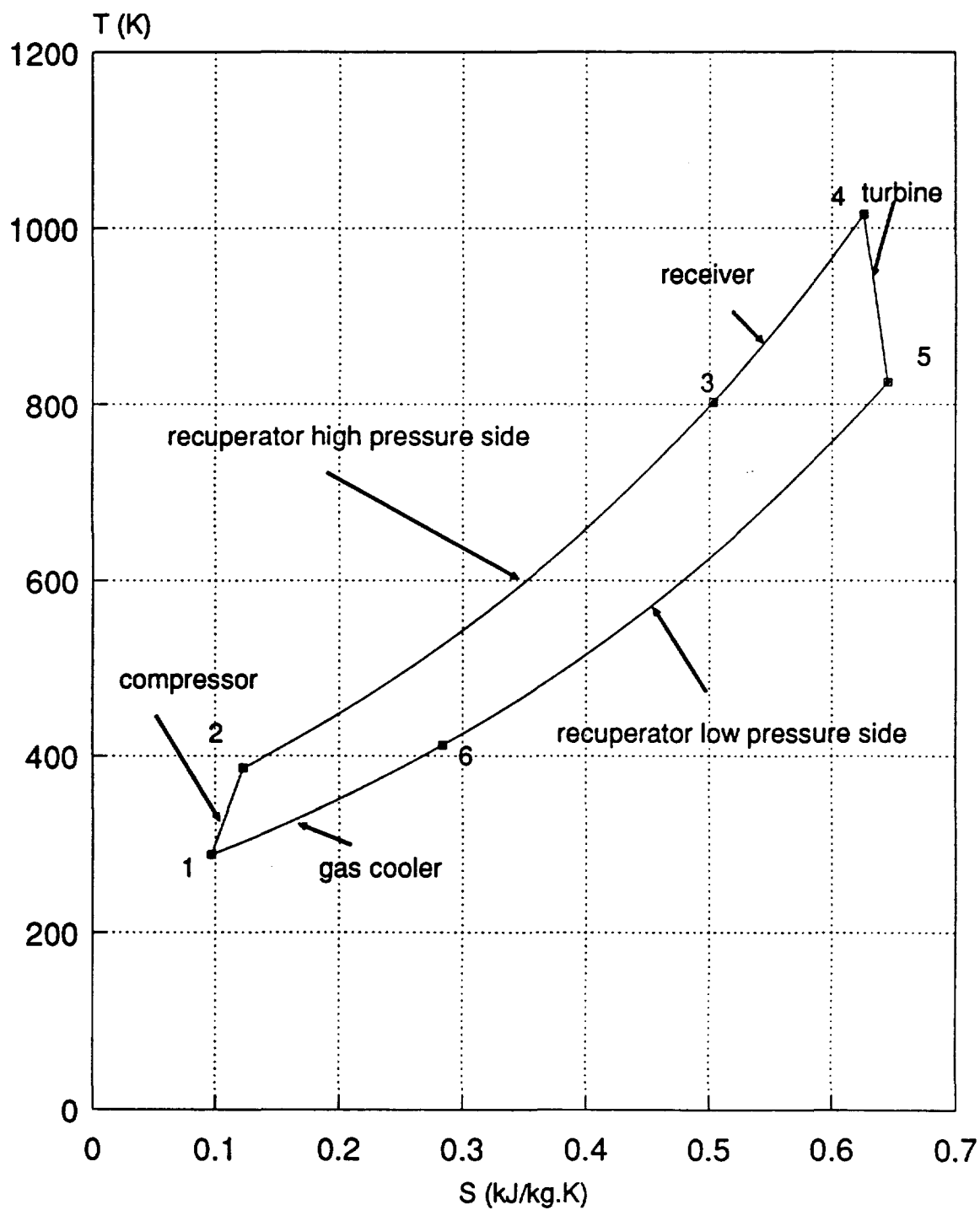


Fig. 1.2 The temperature-entropy (T-S) diagram of the Solar-Powered Closed Regenerative-Brayton Cycle

of mass in the gas loop will change the pressures and the temperatures in the gas loop. The pressure and temperature changes in the gas loop will cause performance changes in the turbine and the compressor, and hence the mass-flow rate in the gas loop will also change. The concentrator tracking and pointing control mechanism regulates the flow of energy into the working fluid. If the solar energy flux is so large that the temperature of the receiver approaches the allowable temperature of the structure, the concentrator is rotated away from the receiver so that the solar radiation is no longer focused on the receiver. The parasitic load radiator is connected in parallel with the user load. A change in user load can be compensated for by a change of the load presented by the parasitic load radiator in order to maintain a constant torque on the rotating unit, and hence a constant speed of the turbomachinery rotor. The power not required by the station is radiated to space.

### 1.3 Previous Work

A literature search provided little information about dynamic system modeling of power conversion systems. Some papers focused more on components than systems. The Electric Power Research Institute funded a research program on simulation of large power generation plants, but this work was tailored to very large machines and it is proprietary. Iqbal<sup>[2]</sup> developed a system model using the EASY5 program<sup>[3]</sup>. The EASY5 (Engineering Analysis System 5) is a proprietary simulation and control system analysis language developed by Boeing Computer Services Company. Since repeated calls to component models are not allowed at the same time level in EASY5, it is not possible to do a mass-flow-rate iteration inside the gas loop at a single time step. For this reason, the system model developed by Iqbal cannot be used to simulate the mass-flow response of the Solar-Powered Closed Regenerative Turbine-Engine Cycle. Further, Iqbal's heat exchanger models<sup>[2]</sup> do not include the effect of changes in pressure (and

therefore density) on the rate of heat transfer. These heat exchanger models need to be refined to include the pressure effect in the models. Ali<sup>[4]</sup> developed compressible transient turbomachinery models. Ali's work was concentrated on the transient thermodynamic performance modelling of the turbine. A FORTRAN subroutine of the compressor model needs to be developed for the system modeling. The component models developed by Ali and Iqbal provided useful information for the component modeling in this study.

#### 1.4 The Purpose of This Thesis

The current research is concerned with developing computational models of the transient thermodynamic performance of the Solar-Powered Closed Regenerative Turbine-Engine Cycle. The first step was to develop a quasi-steady system model based on steady-state component models. The quasi-steady system model was useful in the beginning stage of the development of the system modeling. It can be used to test the iteration scheme. The steady-state component models were developed for this purpose. The second step was to develop a dynamic (transient thermodynamic) system model based on the dynamic (transient thermodynamic) component models. The dynamic component models were developed for this purpose. The incompressible-flow heat exchanger model developed by Iqbal<sup>[2]</sup> was refined to include the effect of variable pressure into the model. A new transient thermodynamic radiator model was developed which includes a representation of the conduction heat-transfer through the radiator panels. Based on the compressible turbomachinery models developed by Ali<sup>[4]</sup>, a FORTRAN subroutine was developed for the compressor. By integrating the component models into the system model, the dynamic heat exchangers/quasi-steady turbomachines system model and the dynamic heat exchangers/dynamic turbomachines system model were developed. The system models were written in FORTRAN and based on the

principles of conservation of mass, energy and momentum. An iteration scheme was used in the system modeling to find the mass-flow rate at every time step. The details of the component models and the system models are presented in chapter 2 and chapter 3 respectively. The simulation results are presented and discussed in chapter 4.

## 2. Component Modelling

The simulation of the thermodynamic transient performance of the Solar-Powered Closed Regenerative Turbine-Engine Cycle required the development of component models. The steady-state component models were developed for the quasi-steady system model. Iqbal<sup>[2]</sup> developed transient incompressible-flow heat exchanger (recuperator, gas cooler, receiver) models. These heat exchanger models were refined to include the pressure effects. In the refined models, the density of the gas working fluid is evaluated according to the gas temperature and pressure. A new dynamic (transient thermodynamic) radiator model was developed. Conduction heat-transfer through the radiator panels was included in the new radiator models. The transient thermodynamic models of turbine and compressor were based on the "state-averaged lagged-mass-flow-rate" turbomachinery model developed by Ali<sup>[4]</sup>. In this chapter, the details of the development of the steady-state component models and the dynamic (transient thermodynamic) component models are presented.

### 2.1 Steady-State Models of the Components

The quasi-steady assumption produces models of the system based on the steady-state characteristics of the components. The steady-state component models were developed for the quasi-steady system model. The quasi-steady system model was used to perform initial evaluations of complete system-modeling strategies and was useful for determining steady-state system performance.

### 2.1.1 Steady-State Heat Exchanger Model

The steady-state heat exchanger model is based on the number of heat transfer unit method by which the  $\epsilon - N_{tu}$  relationship is used to analyze the heat-transfer in heat exchangers. Heat-exchanger heat-transfer effectiveness,  $\epsilon$ , is defined as<sup>[5]</sup>

$$\epsilon \triangleq \frac{C_h(T_{h,in} - T_{h,out})}{C_{min}(T_{h,in} - T_{c,in})}$$

$$\epsilon \triangleq \frac{C_c(T_{c,out} - T_{c,in})}{C_{min}(T_{h,in} - T_{c,in})}$$

where :  $C_h$  is the hot-fluid capacity rate ( $= (\dot{m}C_p)_h$ );

$C_c$  is the cold-fluid capacity rate ( $= (\dot{m}C_p)_c$ );

$T_{h,in}$  is the inlet temperature of hot-fluid;

$T_{h,out}$  is the outlet temperature of hot-fluid;

$T_{c,in}$  is the inlet temperature of cold-fluid;

$T_{c,out}$  is the outlet temperature of cold-fluid;

$C_{min}$  is the smaller of the two capacity rates  $C_h$  and  $C_c$ .

The number of heat exchanger heat transfer units is defined as<sup>[5]</sup>

$$N_{tu} \triangleq f(Ah, C_{min}) .$$

where :  $A$  is the heat-transfer area;

$h$  is the heat-transfer coefficient.

In general, it is possible to express  $\epsilon = f(N_{tu}, \frac{C_{min}}{C_{max}}, \text{flow arrangement})$ .  $C_{max}$  is the larger of the two capacity rates  $C_h$  and  $C_c$ . Consider a counter flow heat exchanger with  $C_h < C_c$ . The heat transfer rate can be computed by

$$\dot{Q} = Ah\Delta T_{mean} \quad (2.1)$$

where :  $\Delta T_{mean}$  is a suitably averaged mean temperature difference.



$$\Delta T_{\text{mean}} = \frac{(T_{h,\text{in}} - T_{c,\text{out}}) - (T_{h,\text{out}} - T_{c,\text{in}})}{\ln \frac{(T_{h,\text{in}} - T_{c,\text{out}})}{(T_{h,\text{out}} - T_{c,\text{in}})}} .$$

Two additional expressions may be written for  $\dot{Q}$  based on energy balance considerations:

$$\dot{Q} = C_h(T_{h,\text{in}} - T_{h,\text{out}}) \quad (2.2)$$

$$\dot{Q} = C_c(T_{c,\text{out}} - T_{c,\text{in}}) \quad (2.3)$$

The maximum possible heat-transfer rate is limited by mass-flow rates, heat capacities and inlet temperatures to

$$\dot{Q}_{\text{max}} = C_{\text{min}}(T_{h,\text{in}} - T_{c,\text{in}}) .$$

For  $C_h = C_{\text{min}}$  and  $C_c = C_{\text{max}}$  ,

$$\dot{Q}_{\text{max}} = C_h \Delta T_{\text{in}}$$

$$\text{where } \Delta T_{\text{in}} = T_{h,\text{in}} - T_{c,\text{in}} .$$

Normalizing (2.1), (2.2), and (2.3) with  $\dot{Q}_{\text{max}}$  yields

$$\epsilon = \frac{Ah \Delta T_{\text{mean}}}{C_h \Delta T_{\text{in}}} \quad (2.4)$$

$$\epsilon = \frac{(T_{h,\text{in}} - T_{h,\text{out}})}{\Delta T_{\text{in}}} \quad (2.5)$$

$$\epsilon = \frac{(T_{c,\text{out}} - T_{c,\text{in}})}{\Delta T_{\text{in}}} \frac{C_c}{C_h} . \quad (2.6)$$

Now from Equations (2.5) and (2.6), we have

$$T_{c,out} = T_{h,in} - (1 - \frac{\epsilon C_h}{C_c}) \Delta T_{in} \quad (2.7)$$

$$T_{h,out} = T_{c,in} + (1 - \epsilon) \Delta T_{in} . \quad (2.8)$$

Combining equations (2.1) and (2.3), and substituting equations (2.7) and (2.8) into the combined equation, produces the  $\epsilon - N_{tu}$  relation for counter-flow heat exchangers:

$$\epsilon = \frac{1 - e^{-N_{tu}(1 - C_r)}}{1 - C_r e^{-N_{tu}(1 - C_r)}} \quad (2.9)$$

$$\text{where } N_{tu} = \frac{Ah}{C_{min}} \text{ and } C_r = \frac{C_{min}}{C_{max}} .$$

Two limiting cases are  $\frac{C_{min}}{C_{max}} = 0$  and 1. The first case approximates the situation for the receiver. The salt temperature remains at a constant temperature throughout the exchanger when functioning under normal design conditions. Therefore, its specific heat (and thus its capacity rate) is equal to infinity. The second case is descriptive of a recuperator or a gas cooler, where  $C_c = C_h$ . For these conditions, Equation (2.9) reduces to

$$\epsilon = 1 - e^{-N_{tu}} \quad \text{for } \frac{C_{min}}{C_{max}} = 0$$

and

$$\epsilon = \frac{N_{tu}}{1 + N_{tu}} \quad \text{for } \frac{C_{min}}{C_{max}} = 1 .$$

A relation for the stream pressure-drop through a heat exchanger is given by Kays and London<sup>[5]</sup>. It is written in the form :

$$\Delta p = \frac{\rho_1 V_1^2}{2} \left[ \underbrace{(K_{in} + 1 - \sigma^2)}_{\text{entrance effect}} + 2 \underbrace{\left( \frac{\rho_1}{\rho_2} - 1 \right)}_{\text{flow acceleration}} + f \underbrace{\frac{A \rho_1}{A_{min} \rho_{mean}}}_{\text{core friction}} - \underbrace{(1 - \sigma^2 - K_{out}) \frac{\rho_1}{\rho_2}}_{\text{exit effect}} \right] \quad (2.10)$$

where :  $K_{in}$  and  $K_{out}$  are the entrance loss coefficient and the exit loss coefficient;

$V_1$  is the inlet velocity;

$A$  is the heat exchanger total heat transfer area on one side;

$A_{min}$  is the heat exchanger minimum free-flow area;

$\sigma$  is the ratio of the core free-flow area to the frontal-area;

$f$  is the mean friction factor

$$\rho_{mean} = \frac{2\rho_1\rho_2}{\rho_1 + \rho_2} .$$

The subscripts "1" and "2" represent the inlet and the outlet respectively. If the entrance and exit losses are included in the friction factor, equation (2.10) reduces to:

$$\Delta p = \frac{\rho_1 V_1^2}{2} \left[ (1 + \sigma^2) \left( \frac{\rho_1}{\rho_2} - 1 \right) + f \frac{A \rho_1}{A_{min} \rho_{mean}} \right] . \quad (2.11)$$

The mean friction factor is defined on the basis of the mean surface shear stress of the heat-exchanger core:

$$f \triangleq \frac{\tau_0}{\frac{1}{2g}(\rho V_1^2)}$$

The friction factor can also be expressed as a function of the Reynolds number,  $Re$ . For laminar flow ( $Re < 2100$ ), the friction factor can be expressed as

$$f = \frac{c_1}{Re} ,$$

whereas for turbulent flow,  $f$  can be expressed as

$$f = c_2 \text{Re}^{-\frac{1}{4}},$$

where  $c_1$  and  $c_2$  are constants [6]. Typical Reynolds numbers of fluids in the gas cooler are 940 at inlet and 1395 at outlet. For the given laminar flow,  $c_1$  is obtained from equation (2.11) using the pressure drop (a design input) through the gas cooler. Friction factors for the other heat exchangers are obtained in a similar manner.

### 2.1.2 Steady-State Radiator Model

Considering a section of radiator as shown in Fig. 2.1, the heat rejected from a differential slice of the radiator is equal to

$$d\dot{Q} = \sigma_{\epsilon} T^4 L_d dL \quad (2.12)$$

where :  $\sigma_{\epsilon}$  = the product of the emissivity and the Stefan-Boltzmann constant.

To simplify the analysis, the radiator metal temperature was taken to be equal to the fluid temperature. For this case, an energy balance on the differential slice yields

$$d\dot{Q} = -\dot{m} C_p dT. \quad (2.13)$$

Combining (2.12) and (2.13), and integrating along the length of the radiator

$$-\int_{T_{in}}^{T_{out}} \frac{\dot{m} C_p dT}{\sigma_{\epsilon} T^4} = \int_0^{L_w} L_d dL.$$

Assuming that  $L_d$  is constant, we have

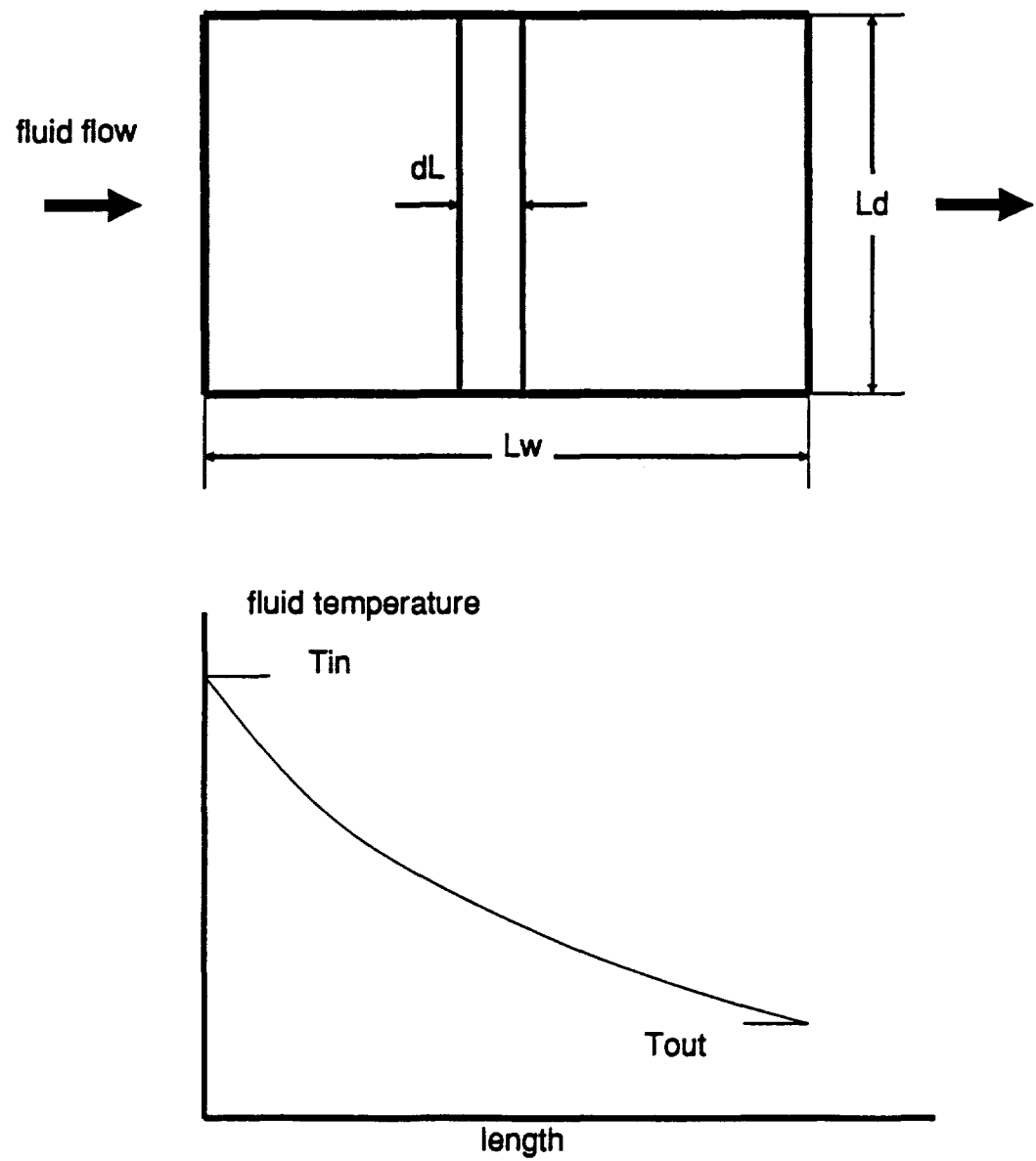


Fig. 2.1 Section of radiator

$$\frac{\dot{m}C_p}{3\sigma_e} \left( \frac{1}{T_{out}^3} - \frac{1}{T_{in}^3} \right) = L_d L_w$$

or

$$T_{out} = \left( \frac{3\sigma_e L_d L_w}{\dot{m}C_p} + \frac{1}{T_{in}^3} \right)^{-\frac{1}{3}}.$$

The last equation gives the temperature at the outlet of the radiator.

### 2.1.3 Steady-State Turbine and Compressor Models

The compressor and turbine are aerodynamic flow machines whose characteristics, plotted as corrected mass-flow rate against pressure ratio, with corrected rotational speed as parameter, depend on the geometry of both rotor and stator (impeller and diffuser for the radial flow turbomachines). Compressor characteristics are usually plotted in terms of the pressure ratio ( $\frac{P_{t2}}{P_{t1}}$ ) versus the corrected mass-flow rate ( $\dot{m}' = \frac{\dot{m}\sqrt{T_{t1}}}{P_{t1}}$ ) along lines of constant corrected speed ( $N' = \frac{N}{\sqrt{T_{t1}}}$ ). Contours of constant efficiency are superimposed, as shown in Fig. 2.2. Similar plots are used for the turbine: ( $\frac{P_{t4}}{P_{t5}}$ ) versus ( $\dot{m}' = \frac{\dot{m}\sqrt{T_{t4}}}{P_{t4}}$ ) along lines of constant ( $N' = \frac{N}{\sqrt{T_{t4}}}$ ), with contours of constant efficiency superimposed, as shown in Fig. 2.3. Subscripts "1" and "2" denote the compressor inlet and outlet flow stations and subscripts "4" and "5" denote the turbine inlet and outlet flow stations. Based on typical compressor and turbine characteristics given in reference [7], Fig. 2.2 and Fig. 2.3 have been generated using the design point data of the compressor and turbine specified for the Solar-Powered Closed Regenerative Turbine-Engine Cycle<sup>[1]</sup>. The working fluid is a mixture of helium and xenon.

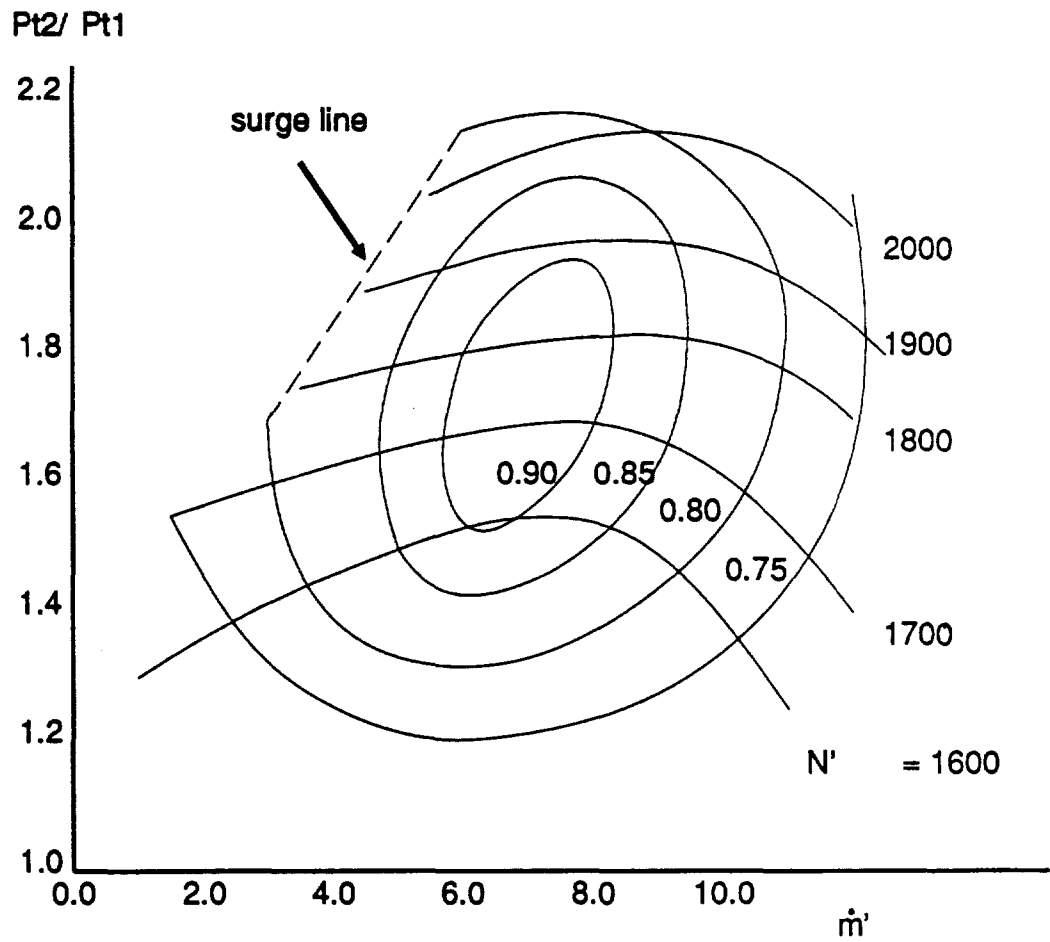


Fig. 2.2 Compressor characteristics with contours of constant isentropic total-to-total efficiency

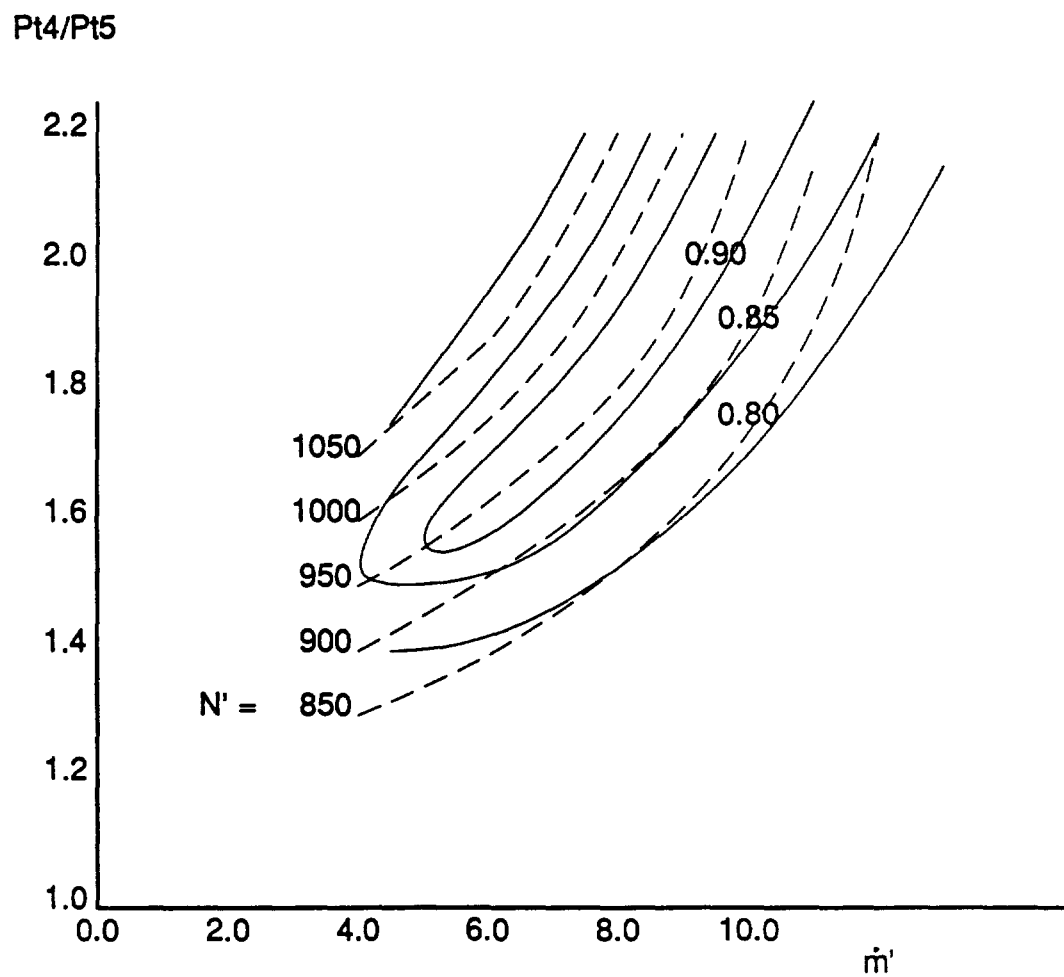


Fig. 2.3 Turbine characteristics with contours of constant isentropic total-to-total efficiency



Reference [1] does not specify the percentage of each constituent in the mixture, but it does give the specific heat capacities  $C_p = 0.5204 \text{ kJ/kg/K}$  and  $C_v = 0.3122 \text{ kJ/kg/K}$ .

The work-transfer rate, or power, required to drive the compressor can be expressed as

$$\dot{W}_{\text{comp}} = \dot{m}C_p(T_{t2} - T_{t1}) = \frac{\dot{m}C_pT_{t1}}{\eta_{\text{comp}}} \left[ \left( \frac{p_{t2}}{p_{t1}} \right)^{\frac{R}{C_p}} - 1 \right].$$

The power delivered by the turbine is given by

$$\dot{W}_{\text{turb}} = \dot{m}C_p(T_{t4} - T_{t5}) = \dot{m}C_p\eta_{\text{turb}}T_{t4} \left[ 1 - \left( \frac{p_{t5}}{p_{t4}} \right)^{\frac{R}{C_p}} \right].$$

where :  $\eta_{\text{comp}}$  is the total-to-total isentropic efficiency of the compressor;

$\eta_{\text{turb}}$  is the total-to-total isentropic efficiency of the turbine.

Fig. 2.2 and Fig. 2.3 show typical compressor and turbine performance maps.

## 2.2 Dynamic Models of the Components

### 2.2.1 Dynamic Heat Exchanger Model

The counter-flow/cross-counter-flow heat exchanger component model describes a number of heat exchangers in the Solar-Powered Closed Regenerative Turbine-Engine Cycle system that share approximately the same physical description. The heat exchanger is modeled by dividing the control volume into  $n$  sections along the flow direction. Each section consists of three elements, as shown in Fig. 2.4. Element (i) is fluid "a" flowing in the indicated direction. Element (ii) is a wall element in contact with fluid "a" on one side and fluid "b" on the other side. Element (iii) is the fluid "b" flowing in the counter-flow direction or the cross-counter-flow direction. No conduction energy

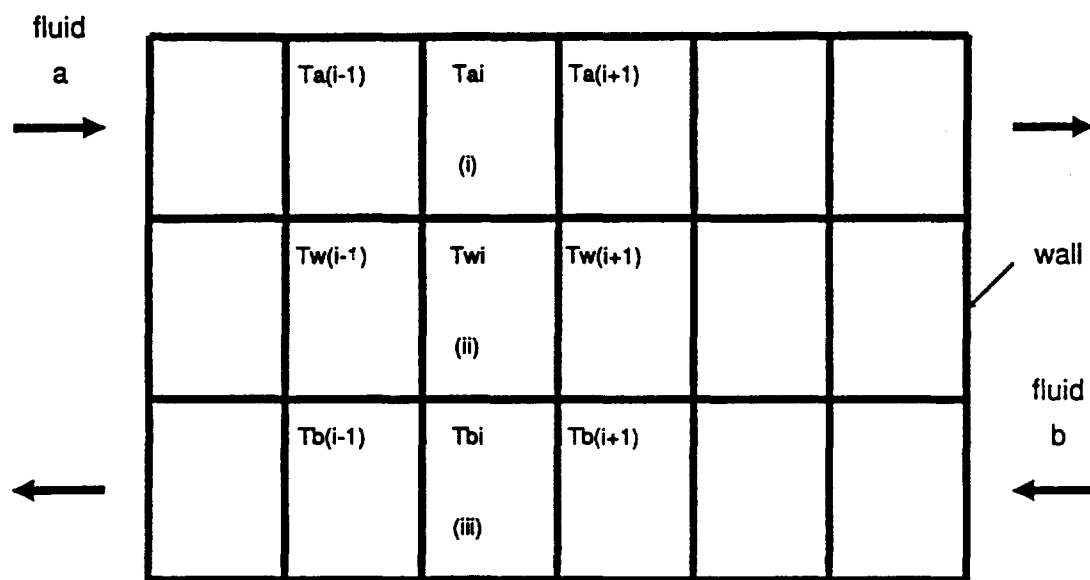


Fig. 2.4 Heat exchanger finite difference scheme

diffusion is assumed to occur between adjoining fluid elements, although adjoining fluid elements do have a net energy transfer by convective transport.

For the i-th section, the continuity equation is

$$\left[ \begin{array}{c} \text{RATE OF CHANGE} \\ \text{OF MASS IN THE} \\ \text{CONTROL VOLUME} \end{array} \right] = \left[ \begin{array}{c} \text{INLET} \\ \text{MASS} \\ \text{FLOW RATE} \end{array} \right] - \left[ \begin{array}{c} \text{OUTLET} \\ \text{MASS} \\ \text{FLOW RATE} \end{array} \right]$$

For fluid "a"

$$\frac{dm_a}{dt} = \dot{m}_{a(i-1)} - \dot{m}_{ai}$$

and for fluid "b"

$$\frac{dm_b}{dt} = \dot{m}_{b(i+1)} - \dot{m}_{bi}$$

where : m is the mass the fluid in the control volume;

$\dot{m}$  is the mass flow-rate defined at the downstream edge of the control volume.

The energy balance can be expressed as:

$$\left[ \begin{array}{c} \text{RATE OF CHANGE} \\ \text{OF ENERGY} \\ \text{IN C. V.} \end{array} \right] = \left[ \begin{array}{c} \text{NET RATE OF} \\ \text{CONVECTION} \\ \text{INTO C.V.} \end{array} \right]$$

If the temperatures in each element are given by an average temperature  $T_{\{ \}i}$ , where " $\{ \}$ " is the fluid "a", fluid "b", or wall "w", and "i" is the i-th section of the heat exchanger, then for a control volume of element (i) of fluid "a"

$$\frac{\partial(mC_v T)_a}{\partial t} = (Ah)_a(T_w - T_a) + \frac{\partial(\dot{m}C_p T)_a}{\partial x} dx \quad (2.14)$$

rate of change  
of energy in C. V.
convection heat-  
transfer into C. V.
net energy flow  
into C. V.

where :  $m$  is the mass of the fluid in the control volume;

$\dot{m}$  is the mass flow-rate;

$A$  is the heat-transfer area in the control volume;

$h$  is the heat-transfer coefficient;

$C_v$  is the constant volume specific heat;

$C_p$  is the constant pressure specific heat.

Assuming that there is no temperature gradient across the wall element (ii), the energy balance for element (ii) may be written as

$$\frac{\partial(mCT)_w}{\partial t} = (Ah)_a(T_a - T_w) + (Ah)_b(T_b - T_w). \quad (2.15)$$

Similar to (2.14), the energy balance for element (iii) yields

$$\frac{\partial(mC_vT)_b}{\partial t} = (Ah)_b(T_w - T_b) + \frac{\partial(\dot{m}C_pT)_b}{\partial x}dx. \quad (2.16)$$

The term on left side of the equation (2.14) can be expressed as:

$$\frac{\partial(mC_vT)_a}{\partial t} = m_a C_v \frac{\partial T_a}{\partial t} + C_v T_a \frac{\partial m_a}{\partial t} + m_a T_a \frac{\partial C_v}{\partial t}. \quad (2.17)$$

Assuming that  $C_v$  is constant, the value of the last term in the above equation is zero.

Substituting the continuity equation into equation (2.17) yields:

$$\frac{\partial(mC_vT)_a}{\partial t} = (mC_v)_a \frac{\partial T_a}{\partial t} + (C_vT)_a(\dot{m}_{a(i-1)} - \dot{m}_{ai}).$$

For element (ii),  $mC = \text{constant}$ , we have

$$\frac{\partial(mCT)_w}{\partial t} = (mC)_w \frac{\partial T_w}{\partial t}.$$

Similarly we have, for fluid "b":

$$\frac{\partial(mC_v T)_b}{\partial t} = (mC_v)_b \frac{\partial T_b}{\partial t} + (C_v T)_b (\dot{m}_{b(i+1)} - \dot{m}_{bi}).$$

Using the subscript "i" for the node location, the equations (2.14), (2.15), (2.16) can be written as

$$\begin{aligned} (mC_v)_{ai} \left[ \frac{\partial T_a}{\partial t} \right]_i &= (hA)_{ai} (T_{wi} - T_{ai}) + (\dot{m} C_p T)_{a(i-1)} - (\dot{m} C_p T)_{ai} \\ &\quad - (C_v T)_a (\dot{m}_{a(i-1)} - \dot{m}_{ai}) \end{aligned} \quad (2.18)$$

$$(mC_v)_{wi} \left[ \frac{\partial T_w}{\partial t} \right]_i = (hA)_{ai} (T_{ai} - T_{wi}) + (hA)_{bi} (T_{bi} - T_{wi}) \quad (2.19)$$

$$\begin{aligned} (mC_v)_{bi} \left[ \frac{\partial T_b}{\partial t} \right]_i &= (hA)_{bi} (T_{wi} - T_{bi}) + (\dot{m} C_p T)_{b(i+1)} - (\dot{m} C_p T)_{bi} \\ &\quad - (C_v T)_b (\dot{m}_{b(i+1)} - \dot{m}_{bi}). \end{aligned} \quad (2.20)$$

The following two pages show that the terms  $(C_v T)_a (\dot{m}_{a(i-1)} - \dot{m}_{ai})$  and  $(C_v T)_b (\dot{m}_{b(i+1)} - \dot{m}_{bi})$  are negligible. To do so we can express the density as a function of the temperature and the pressure<sup>[8]</sup>

$$\rho = \rho(T, p).$$

The rate of change of density can be expressed as:

$$\frac{d\rho}{dt} = \left[ \frac{\partial \rho}{\partial T} \right]_p \frac{dT}{dt} + \left[ \frac{\partial \rho}{\partial p} \right]_T \frac{dp}{dt}.$$

Dividing both sides by  $\rho$  we can express the above equation in a nondimensional form :

$$\frac{1}{\rho^*} \frac{d\rho^*}{dt^*} = \gamma_0 M^2 \alpha^* \frac{dp^*}{dt^*} - \beta^* B \left[ \frac{T_w - T_0}{T_0} \right] \frac{dT^*}{dt^*} \quad (2.21)$$

where  $T^* = \frac{T - T_0}{T_w - T_0}$ ;  $\rho^* = \frac{\rho}{\rho_0}$ ;  $\beta^* = \frac{\beta}{\beta_0}$ ;  $\gamma_0 = \frac{C_{p0}}{C_{v0}}$ ;  $\alpha^* = \frac{\alpha}{\alpha_0}$ ;  $M = \frac{V_0}{a_0}$ ;  
 $p^* = \frac{p - p_0}{\rho_0 V_0^2}$ ;  $t^* = \frac{t V_0}{L}$ ;  $B = \beta_0 T_0$ . The subscript "0" indicates the reference state.

$\beta$  is the bulk expansion coefficient which is defined as

$$\beta \triangleq -\frac{1}{\rho} \left( \frac{\partial \rho}{\partial T} \right)_p$$

and  $\alpha$  is the isothermal compressibility which is defined as

$$\alpha \triangleq \frac{1}{\rho} \left( \frac{\partial \rho}{\partial p} \right)_T.$$

$V_0$  and  $a_0$  are the reference speed of fluid and the speed of sound respectively. The speed of sound  $a_0$  can be expressed as

$$a_0 = \frac{\gamma_0}{\rho_0 \alpha_0}.$$

The Mach number,  $M$ , and the temperature difference,  $T_w - T_0$ , are small for the heat exchangers used in the Solar-Powered Closed Regenerative Turbine-Engine Cycle system. Take the recuperator as a example. The average wall temperature is  $T_w = 605$  K. The average temperature of the "hot" fluid is  $T_0 = 618$  K. The average temperature of the "cold" fluid is  $T_0 = 593$  K. Then  $(T_w - T_0) / T_0 = -0.02$  for the "hot" fluid side and  $(T_w - T_0) / T_0 = 0.02$  for the "cold" fluid side. In these cases, equation (2.21) reduces to

$$\frac{dp^*}{dt} \approx 0.$$

So we have

$$\frac{dm}{dt} = V_{cv} \frac{d\rho}{dt} = V_{cv} \rho_0 \frac{d\rho^*}{dt} \approx 0$$

where :  $V_{cv}$  is the control volume of the element.

Since the  $\frac{dm}{dt}$  term is small, we may assume  $\dot{m}_{a(i-1)} = \dot{m}_{ai}$  and  $\dot{m}_{b(i+1)} = \dot{m}_{bi}$  by the continuity equation. Applying the simple Euler method of integration to the control volume for the time derivative, and using an implicit formulation for the convective terms in equations (2.18)-(2.20), produces the following difference equations. These are written with superscript "n" representing the time step.

$$(mC_v)_{ai} \left[ \frac{T_{ai}^n - T_{ai}^{n-1}}{\Delta t} \right] = (hA)_{ai} \left[ T_{wi}^n - T_{ai}^n \right] + (\dot{m}C_p)_{ai} \left[ T_{a(i-1)}^n - T_{ai}^n \right] \quad (2.22)$$

$$(mC)_{wi} \left[ \frac{T_{wi}^n - T_{wi}^{n-1}}{\Delta t} \right] = (hA)_{ai} \left[ T_{ai}^n - T_{wi}^n \right] + (hA)_{bi} \left[ T_{bi}^n - T_{wi}^n \right] \quad (2.23)$$

$$(mC_v)_{bi} \left[ \frac{T_{bi}^n - T_{bi}^{n-1}}{\Delta t} \right] = (hA)_{bi} \left[ T_{wi}^n - T_{bi}^n \right] + (\dot{m}C_p)_{bi} \left[ T_{b(i+1)}^n - T_{bi}^n \right] \quad (2.24)$$

It was shown by Ali<sup>[4]</sup> that the response of outlet pressure to oscillations induced by changes in inlet pressure is the most rapid transient response compared with the other thermodynamic transient responses. Assuming an equilibrium state at every time step, the pressure drop through the heat exchanger can be calculated by equation (2.11) developed for the steady-state heat exchanger models. The pressure distribution is assumed to be linear along the heat exchanger flow passage. The mass in the elements can be calculated by the following equation

$$m_i = V_{cvi} \rho_i$$

For a gas working fluid, the density  $\rho$  can be calculated from the state equation for an ideal gas:

$$\rho_i = \frac{P_i}{RT_i}$$

The recuperator, gas cooler and receiver transient models can be built from the above equations with small variations in constants to account for design details. The fluids "a" and "b" are the same (a mixture of helium and xenon) in the recuperator. Reference [1] does not specify the percentage of each constituent in the mixture, but it does give the specific heat capacities  $C_p = 0.5204$  kJ/kg/K and  $C_v = 0.3122$  kJ/kg/K. Equations (2.22), (2.23) and (2.24) can be used directly for the recuperator. For the gas cooler, fluid "a" is the working fluid (helium-xenon), and the fluid "b" is the coolant which is liquid FC75. On the liquid side, we have  $C_{vb} = C_{pb} = C_b$  and  $\rho_b = \text{constant}$ . Equations (2.22), (2.23) and (2.24) can be used for the liquid side of gas cooler with substitution of  $C_{pb}$  for  $C_{vb}$  and constant  $\rho_b$ . For the receiver, the fluid "a" is the working fluid, helium-xenon and the fluid "b" is the salt (eutectic LiF-CaF<sub>2</sub> mixture). For the remainder of this thesis it is assumed that the salt temperature is an input variable which drives the thermodynamic transients of the Solar-Powered Closed Regenerative Turbine-Engine Cycle. It is also assumed that the salt properties do not change with time as it is cycled between the liquid and solid phases. The salt mixture melts during insolation, absorbing some of the incident flux, and solidifies during eclipse. It is therefore assumed that the salt temperature  $T_{\text{salt}}$  is specified and is uniform along the length of the tube in the receiver. Element "(iii)" (in Fig. 2.4, representing fluid "b", the eutectic salt) uses the same temperature for all sections throughout the length of the receiver, which is an input to the system and varies with time. The temperature of element "(i)" (in Fig. 2.4, representing fluid "a", the helium-xenon mixture) is derived



from equation (2.22). The temperature of element "(ii)" (in Fig. 2.4, representing the wall "w") is included in equation (2.23), which is modified to include the salt temperature  $T_{\text{salt}}$  :

$$(mC_v)_{wi} \left[ \frac{T_{wi}^n - T_{wi}^{n-1}}{\Delta t} \right] = (hA)_{ai} \left[ T_{ai}^n - T_{wi}^n \right] + (hA)_{bi} \left[ T_{\text{salt}}^n - T_{wi}^n \right] \quad (2.25)$$

Equations (2.22), (2.23), and (2.24) can be rearranged to produce a system of equations of the form

$$[A]\{T\} = \{B\} \quad (2.26)$$

where A is an (nxn) matrix of known coefficients, T is a (1xn) vector of unknown temperatures, and B is a (1xn) vector of known quantities. The set of simultaneous equations (2.26) is solved using a Gaussian elimination method with scaling and partial pivoting. Similarly equations (2.22), (2.25) can be solved for the receiver in the same manner.

### 2.2.2 Dynamic Radiator Model

The radiator in the Solar-Powered Closed Regenerative Turbine-Engine Cycle system is of the pumped fluid loop type. The coolant is circulated in a coolant loop consisting of the gas cooler and the radiator. A mechanical pump, which draws its power from the electrical bus, is used to circulate the liquid in the coolant loop. The radiator rejects the cycle waste energy to the space environment by thermal radiation. The liquid coolant conveys the heat to the radiator as it circulates through channels embedded in the radiator panels. There are two coolant loops, a primary loop and a secondary loop, arranged in a redundant alternating design.

The following assumptions are made for the radiator model: the heat leaves the radiator surface by radiation from the two large surfaces only (no heat is radiated from the edges); the emissivity of the surface is constant; heat radiates from the surface in accordance with the Stefan-Boltzmann law; and the sink temperature is assumed to be a function of time but spatially constant across the panel.

As shown in Fig. 2.5, the radiator is modeled by dividing it into "N" sections for each loop. Each section consists of two elements. Element (i) is the fluid "a" flowing in the direction indicated. Element (ii) is the wall element in contact with fluid "a" on one side and radiating to space on the other side. For each element, an energy balance is enforced:

$$\left[ \begin{array}{c} \text{RATE OF CHANGE} \\ \text{OF ENERGY} \\ \text{IN C. V.} \end{array} \right] = \left[ \begin{array}{c} \text{NET RATE OF} \\ \text{CONVECTION} \\ \text{INTO C. V.} \end{array} \right] + \left[ \begin{array}{c} \text{NET RATE OF} \\ \text{CONDUCTION} \\ \text{INTO C. V.} \end{array} \right] + \left[ \begin{array}{c} \text{NET RATE OF} \\ \text{RADIATION} \\ \text{INTO C. V.} \end{array} \right] .$$

Let the subscripts "a" and "w" represent fluid "a" and the wall respectively. For a control volume in element (i) the energy balance can be written as

$$\frac{\partial(mC_v T)_a}{\partial t} = (Ah)_a(T_w - T_a) + \frac{\partial(\dot{m}C_p T)_a}{\partial x} dx . \quad (2.27)$$

In the above equation, it is assumed there is no radiation heat transfer and no conduction between adjoining fluid elements. For element (ii), assuming a uniform temperature in the element, the energy equation for the wall control volume may be written as

$$\frac{\partial(mCT)_w}{\partial t} = (Ah)_a(T_a - T_w) + \sigma_\epsilon A_r \left( T_{\text{sink}}^4 - T_w^4 \right) - kA_x \frac{\partial T_w}{\partial x} - kA_y \frac{\partial T_w}{\partial y} \quad (2.28)$$

where :  $\sigma_\epsilon$  is the product of the emissivity and the Stefan-Boltzmann constant;

A is the convection heat-transfer area of the wall control volume;

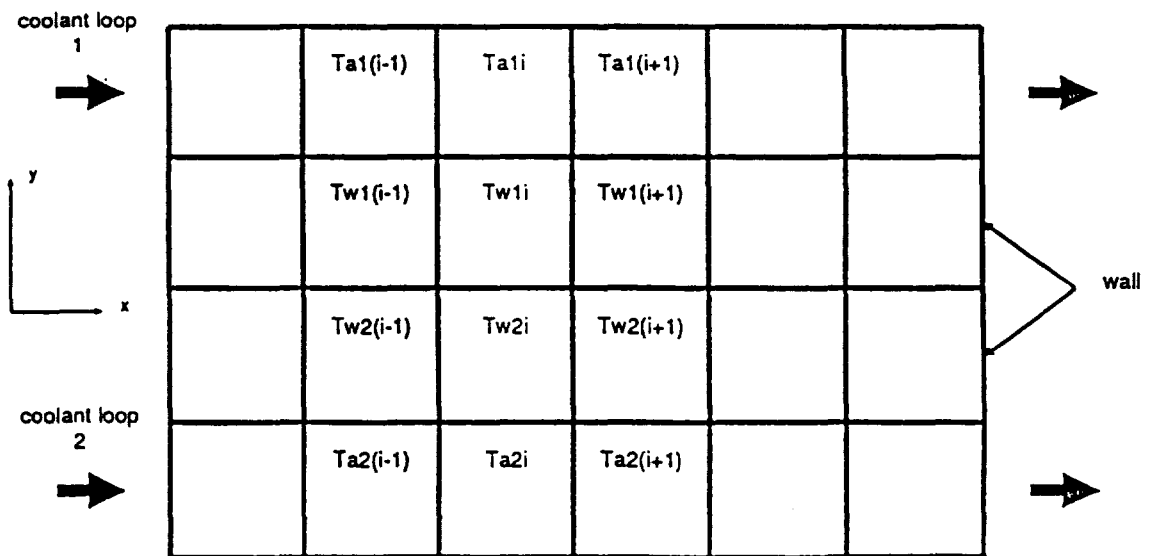
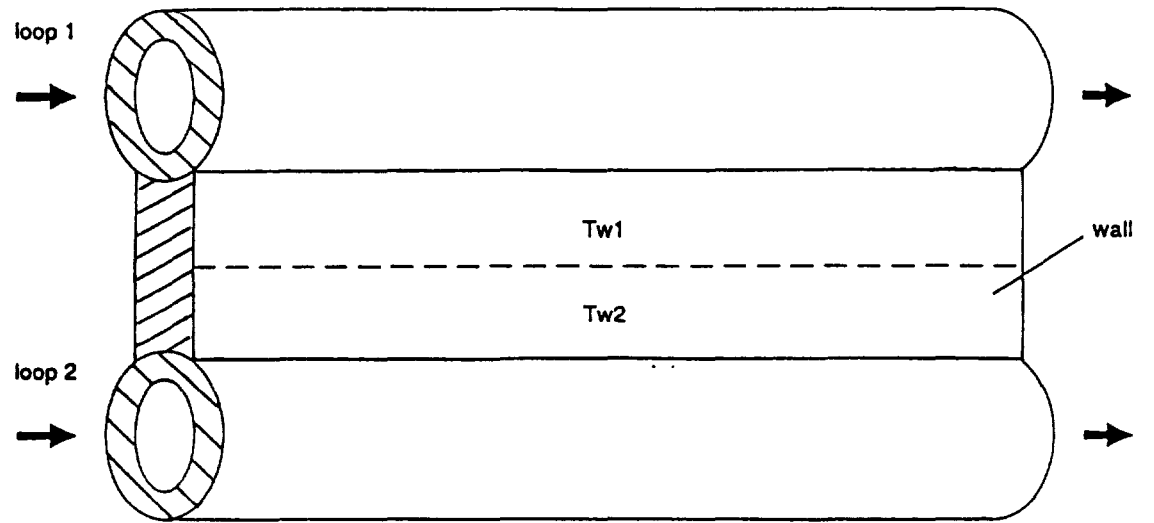


Fig. 2.5 Radiator finite difference scheme

$A_r$  is the radiation heat-transfer area of the wall control volume;

$A_x$  is the heat-conduction area of the wall control volume in

x-direction;

$A_y$  is the heat-conduction area of the wall control volume in

y-direction;

$k$  is the heat conductivity of the wall.

Equations (2.27) and (2.28) can be applied to both the primary loop and the redundant loop. Using the subscript "i" for the node location, "1" for the primary loop, and "2" for the redundant loop, we can rewrite equations (2.27) and (2.28). For the primary loop, using an explicit formulation, we can write

$$\left[ \frac{\partial T_{a1}}{\partial t} \right]_i = \frac{1}{(mC_v)_{a1i}} \left[ (hA)_{a1i} (T_{w1i} - T_{a1i}) + (\dot{m}C_p)_{a1i} (T_{a1(i-1)} - T_{a1i}) \right] \quad (2.29)$$

$$\begin{aligned} \left[ \frac{\partial T_{w1}}{\partial t} \right]_i &= \frac{1}{(mC)_{w1i}} \left[ (hA)_{a1i} (T_{a1i} - T_{w1i}) + (\sigma_{\epsilon} A_r)_{w1i} \left[ T_{\text{sink}}^4 - T_{w1i}^4 \right] \right] \\ &- \frac{1}{(mC)_{w1i}} \left[ \left( \frac{kA_x}{\Delta x} \right)_{w1i} (2T_{w1i} - T_{w1(i-1)} - T_{w1(i+1)}) - \left( \frac{kA_y}{\Delta y} \right)_{w1i} (T_{w1i} - T_{w2i}) \right]. \end{aligned} \quad (2.30)$$

For the redundant loop, using an explicit formulation, we can write

$$\left[ \frac{\partial T_{a2}}{\partial t} \right]_i = \frac{1}{(mC_p)_{a2i}} (hA)_{a2i} (T_{w2i} - T_{a2i}) \quad (2.31)$$

$$\left[ \frac{\partial T_{w2}}{\partial t} \right]_i = \frac{1}{(mC)_{w2i}} \left[ (hA)_{a2i} (T_{a2i} - T_{w2i}) + (\sigma_{\epsilon} A_r)_{w2i} \left[ T_{\text{sink}}^4 - T_{w2i}^4 \right] \right]$$

$$- \frac{1}{(mC)_{w2i}} \left[ \left( \frac{kA_x}{\Delta x} \right)_{2i} (2T_{w2i} - T_{w2(i-1)} - T_{w2(i+1)}) - \left( \frac{kA_y}{\Delta y} \right)_{2i} (T_{w2i} - T_{w1i}) \right]. \quad (2.32)$$

The temperatures on the right hand side of equation (2.29), (2.30), (2.31) and (2.32) are known at time level "n - 1". Therefore, these equations are in an explicit form. The set of differential equations (2.29), (2.30), (2.31) and (2.32) are solved by the Runge-Kutta numerical-integration method. The order of the Runge-Kutta method is selectable from the first order to the fourth order.

### 2.2.3 Dynamic Turbine and Compressor Models

The turbine and compressor dynamic (transient thermodynamic) models were based on the state-averaged lagged-mass-flow-rate turbomachinery model developed by Ali<sup>[4]</sup>. A discussion on the time step for which these models can be applied is included in the next section. A control volume for a turbine or compressor is shown in Fig. 2.6. It is assumed that the thermodynamic state parameters at the middle point of the control volume are the average values in the control volume. The subscript "in" represents the inlet state parameters, the subscript "m" represents the state parameters in the middle point, and the subscript "out" represents the outlet state parameters. The continuity equation for the control volume can be written as :

$$\left[ \begin{array}{c} \text{RATE OF CHANGE} \\ \text{OF MASS IN THE} \\ \text{CONTROL VOLUME} \end{array} \right] = \left[ \begin{array}{c} \text{INLET} \\ \text{MASS} \\ \text{FLOW RATE} \end{array} \right] - \left[ \begin{array}{c} \text{OUTLET} \\ \text{MASS} \\ \text{FLOW RATE} \end{array} \right]$$

or

$$\frac{dm}{dt} = \dot{m}_{in} - \dot{m}_{out}. \quad (2.33)$$

The energy equation can be written as

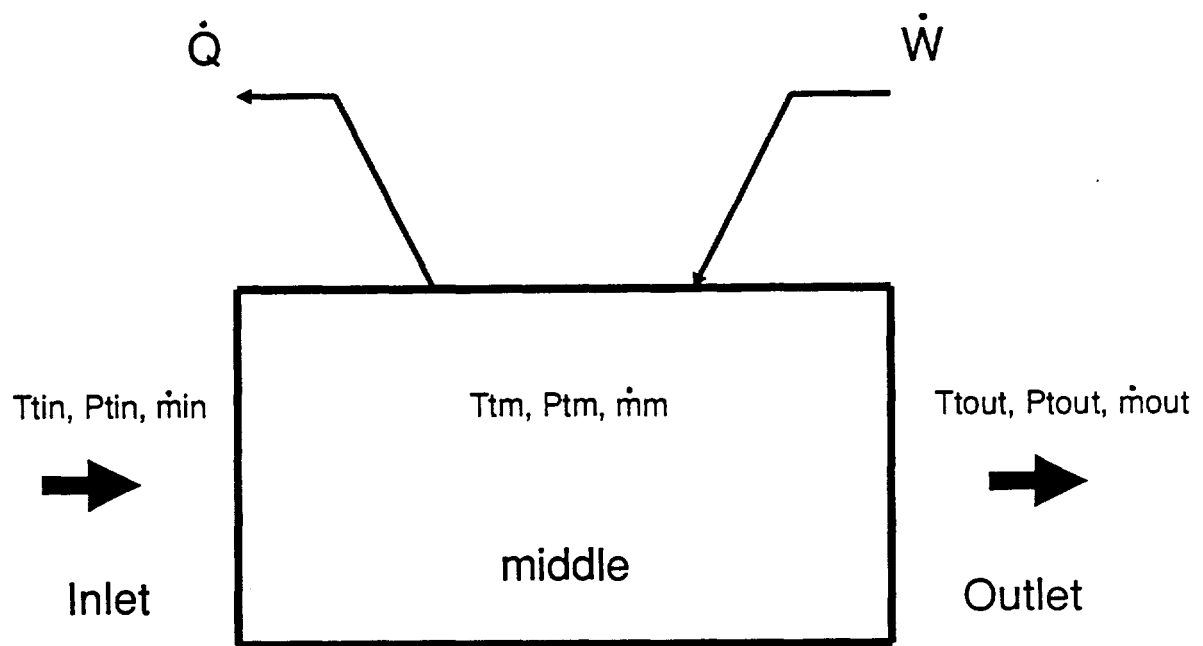


Fig. 2.6 Control volume of turbomachinery

$$\left[ \begin{array}{c} \text{RATE OF CHANGE} \\ \text{OF ENERGY IN} \\ \text{CONTROL VOLUME} \end{array} \right] = \left[ \begin{array}{c} \text{NET RATE OF} \\ \text{ENTHALPY FLOW} \\ \text{INTO C.V.} \end{array} \right] + \left[ \begin{array}{c} \text{RATE OF WORK} \\ \text{DONE ON MASS} \\ \text{IN C.V.} \end{array} \right] + \left[ \begin{array}{c} \text{RATE OF} \\ \text{HEAT FLOW} \\ \text{INTO C.V.} \end{array} \right]$$

or

$$\frac{d(mC_vT)_m}{dt} = (\dot{m}C_pT)_{in} - (\dot{m}C_pT)_{out} + \dot{W} - \dot{Q} . \quad (2.34)$$

For constant specific heat, we can rewrite equation (2.34) as

$$\frac{dT_m}{dt} = \frac{1}{mC_v} \left[ (\dot{m}C_pT)_{in} - (\dot{m}C_pT)_{out} + \dot{W} - \dot{Q} - C_vT_m \frac{dm}{dt} \right] . \quad (2.35)$$

An expression for the work term  $\dot{W}$  in equation (2.35) can be derived from the moment-of-momentum equation. Take the axis of the rotor as the x direction. The distance from the x axis to the rotor tip is  $R_{tip}$ , the distance from the x axis to the rotor hub is  $R_{hub}$ , and the distance from the x axis to the middle of the control volume is  $R_m$ . As shown in Fig. 2.7,  $R_m$  was selected as the average of  $R_{tip}$  and  $R_{hub}$ . Summation of moments about the x axis gives the moment-of-momentum equation as :

$$\left[ \begin{array}{c} \text{RATE OF CHANGE} \\ \text{OF ANGULAR} \\ \text{MOMENTUM} \\ \text{IN THE} \\ \text{CONTROL VOLUME} \end{array} \right] = \left[ \begin{array}{c} \text{RATE OF FLOW} \\ \text{OF ANGULAR} \\ \text{MOMENTUM} \\ \text{INTO THE} \\ \text{C. V.} \end{array} \right] - \left[ \begin{array}{c} \text{RATE OF FLOW} \\ \text{OF ANGULAR} \\ \text{MOMENTUM} \\ \text{OUT OF THE} \\ \text{C. V.} \end{array} \right] + \left[ \begin{array}{c} \text{SUM OF MOMENTS} \\ \text{ACTING ON} \\ \text{THE MASS} \\ \text{IN THE} \\ \text{CONTROL VOLUME} \end{array} \right] .$$

Since the flow into the compressor and out of the turbine has zero angular momentum (by design), the above equation can be written as

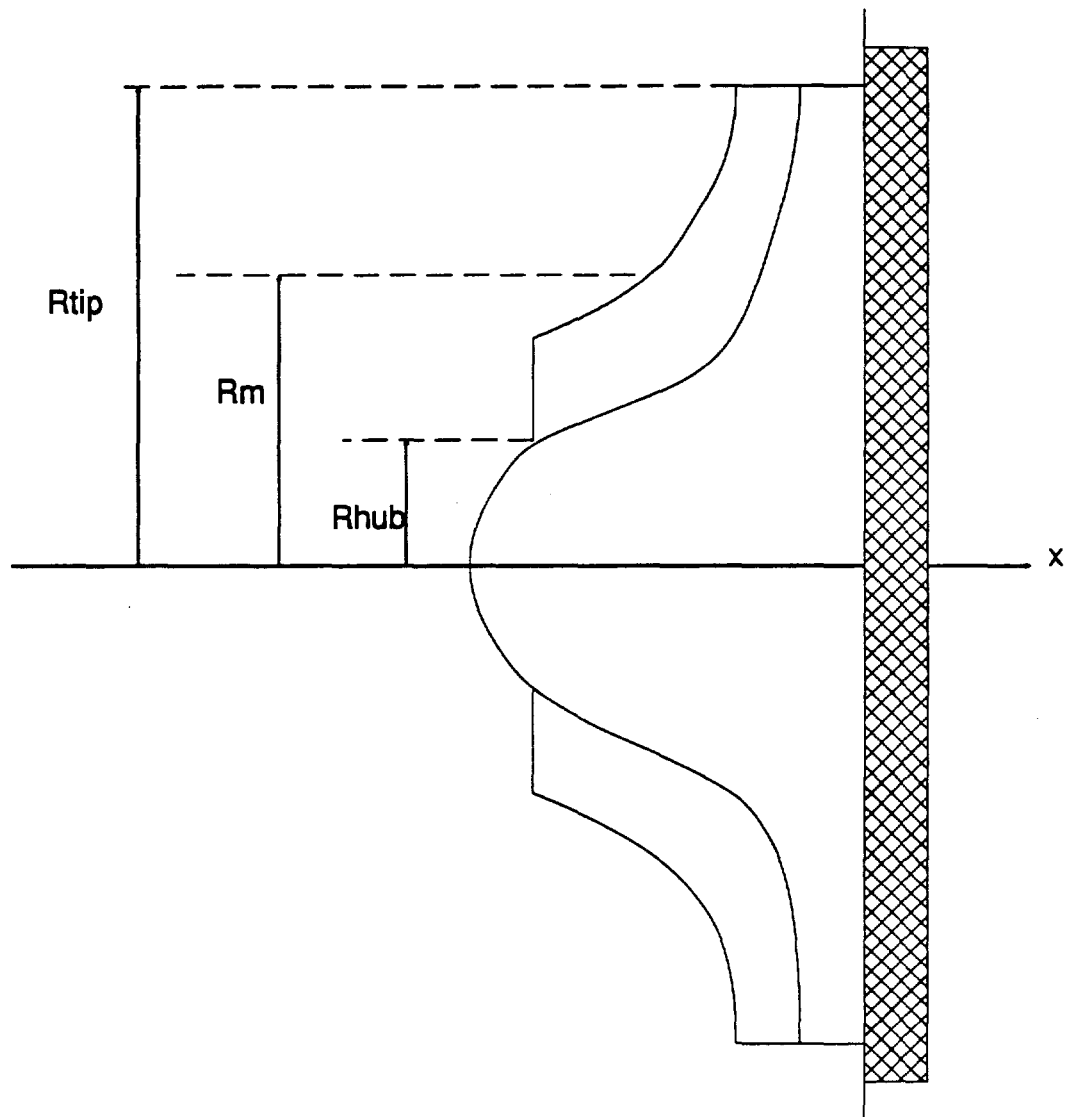


Fig. 2.7 Control volume for moment of momentum equation



$$\frac{d(m\Omega R_m^2)}{dt} = \pm \Omega R_{tip}^2 \dot{m} + \tau_q \quad (2.36)$$

where the sign of the first term on the right hand side is "+" for the turbine and "-" for the compressor;  $\Omega$  is the rotating frequency of rotor; and  $\tau_q$  is the torque acting on the mass in the control volume. For the turbine, the mass-flow rate at the rotor tip is into the control volume. Therefore, the sign of the first term on the right side of equation (2.36) is positive. For the compressor, the mass-flow rate at the rotor tip is out of the control volume, so the sign of the first term on the right side of equation (2.36) is negative. The torque acting on the control volume can be expressed as

$$\tau_q = \frac{\dot{W}}{\Omega}$$

Substituting this expression for  $\tau_q$  into equation (2.36), and rearranging the equation, we have:

$$\dot{W} = \Omega^2 R_m^2 \frac{dm}{dt} + \Omega m R_m^2 \frac{d\Omega}{dt} \pm \Omega^2 R_{tip}^2 \dot{m} \quad (2.37)$$

The sign of the last term on the right side of equation (2.37) is negative for the turbine and positive for the compressor. The heat transfer rate  $\dot{Q}$  is assumed to be negligible. Equation (2.37) can be used to model : a constant speed ( $\frac{d\Omega}{dt} = 0$ ), variable work ( $\frac{d\dot{W}}{dt} \neq 0$ ) component ; a constant work ( $\frac{d\dot{W}}{dt} = 0$ ), variable speed ( $\frac{d\Omega}{dt} \neq 0$ ) component; and to specify the time dependence of one of ( $\dot{W}$ ,  $\Omega$ ) to find the other.

In addition to the above equations, the following relations for a perfect gas are used in modeling the turbomachinery:

$$p = \rho R T$$

$$p_t = \rho_t R T_t$$

$$T_t = T + \frac{V^2}{2C_p}$$

$$\frac{T_t}{T} = \left( \frac{p_t}{p} \right)^{\frac{R}{C_p}}.$$

The total temperature in the middle point of the control volume is assumed to be a linear average of inlet and outlet temperatures:

$$T_{tm}(t) = \frac{1}{2} [T_{tin}(t) + T_{tout}(t)] . \quad (2.38)$$

A "state-averaged lagged-mass-flow-rate" model<sup>[4]</sup> was used for the mass-flow rate at the middle point of the control volume, i.e., the mass-flow rate in the middle point is computed as a average of the inlet mass-flow rate at the new time level and the outlet mass-flow rate at the old time level.

$$\dot{m}_m(t) = \frac{1}{2} [\dot{m}_{in}(t) + \dot{m}_{out}(t-\Delta t)] \quad (2.39)$$

The mass in the control volume can be computed by

$$m = \rho_m V_{cv}$$

where :  $\rho_m$  is the static density in the middle point of the control volume;

$V_{cv}$  is the volume of the control volume.

The pressure at the middle point of the control volume is evaluated by the following polytropic relations. For the turbine:

$$P_{tm}(t) = P_{tin}(t) \left[ \frac{T_{tm}(t)}{T_{tin}(t)} \right]^{\frac{C_p}{(\eta_p)_{turb} R}} \quad (2.40)$$

For the compressor:

$$P_{tm}(t) = P_{ti}(t) \left[ \frac{T_{tm}(t)}{T_{ti}(t)} \right]^{\frac{(\eta_p)_{comp} C_p}{R}} \quad (2.41)$$

where :  $(\eta_p)_{turb}$  is total-to-total polytropic efficiency between the inlet and middle of the turbine;

$(\eta_p)_{comp}$  is total-to-total polytropic efficiency between the inlet and middle of the compressor.

The total-to-total polytropic efficiencies can be evaluated from the total-to-total isentropic efficiencies shown in Fig. (2.2) and Fig. (2.3) using the following expressions.

$$(\eta_p)_{turb} = \frac{\ln \left[ 1 - \eta_{turb} \left( 1 - \left( \frac{P_{tout}}{P_{tin}} \right)^{\frac{R}{C_p}} \right) \right]}{\frac{R}{C_p} \ln \frac{P_{tout}}{P_{tin}}} \quad .$$

$$(\eta_p)_{comp} = \frac{\frac{R}{C_p} \ln \frac{P_{tout}}{P_{tin}}}{\ln \left[ 1 + \frac{1}{\eta_{comp}} \left( \left( \frac{P_{tout}}{P_{tin}} \right)^{\frac{R}{C_p}} - 1 \right) \right]} \quad .$$

Assuming all of the losses (frictional, blading, etc.) are included in the polytropic efficiency, the efficiency charts for the machine can be used as an approximation to perform an unsteady analysis.

Based on the above governing equations, relations for the thermodynamic state parameters, and assumptions, an implicit algorithm using an iteration scheme was developed for the turbine and compressor models. Fig. 2.8 shows the flow chart of the implicit algorithm<sup>[4]</sup>. Given the inlet parameters, equations (2.38)-(2.41) are used to estimate the values of the state variables at the middle point. Once the middle state variables have been estimated, the values of all state variables are obtained by the use of the energy equation, the continuity equation and the moment of momentum equation. The new outlet state variables are substituted back in equations (2.38)-(2.41) to obtain a better estimate for the middle state variables. This process continues until the percent change in successive outlet state variables is less than a specified tolerance. Once the tolerance criteria are satisfied, the algorithm has converged for that particular time step, and the process starts again for next time step.

#### 2.2.4 Discussion of Minimum Time-Step for Turbomachinery Models

A discussion of turbomachinery outlet response dynamics was given by Ali<sup>[4]</sup>. It was shown that the inlet information (or perturbation) may be modeled as traveling through the turbomachine in two ways. In the first way, information travels along the characteristic lines of the flow. In the second way, information is transmitted by the rigid rotating rotor inside the turbomachine.

Information travel in the first way is along the characteristic lines of the flow through the turbomachine passage. It is assumed that the turbomachine is operating under steady-state conditions. Consider the control volume of the turbomachine as shown in Fig. 2.6. The inlet velocity of fluid and the inlet speed of sound in the fluid are evaluated as  $v_{in}$  and  $a_{in}$  from the inlet state variables. The outlet velocity of the fluid ( $v_{out}$ ) and the outlet speed of sound ( $a_{out}$ ) can be evaluated from the given outlet state

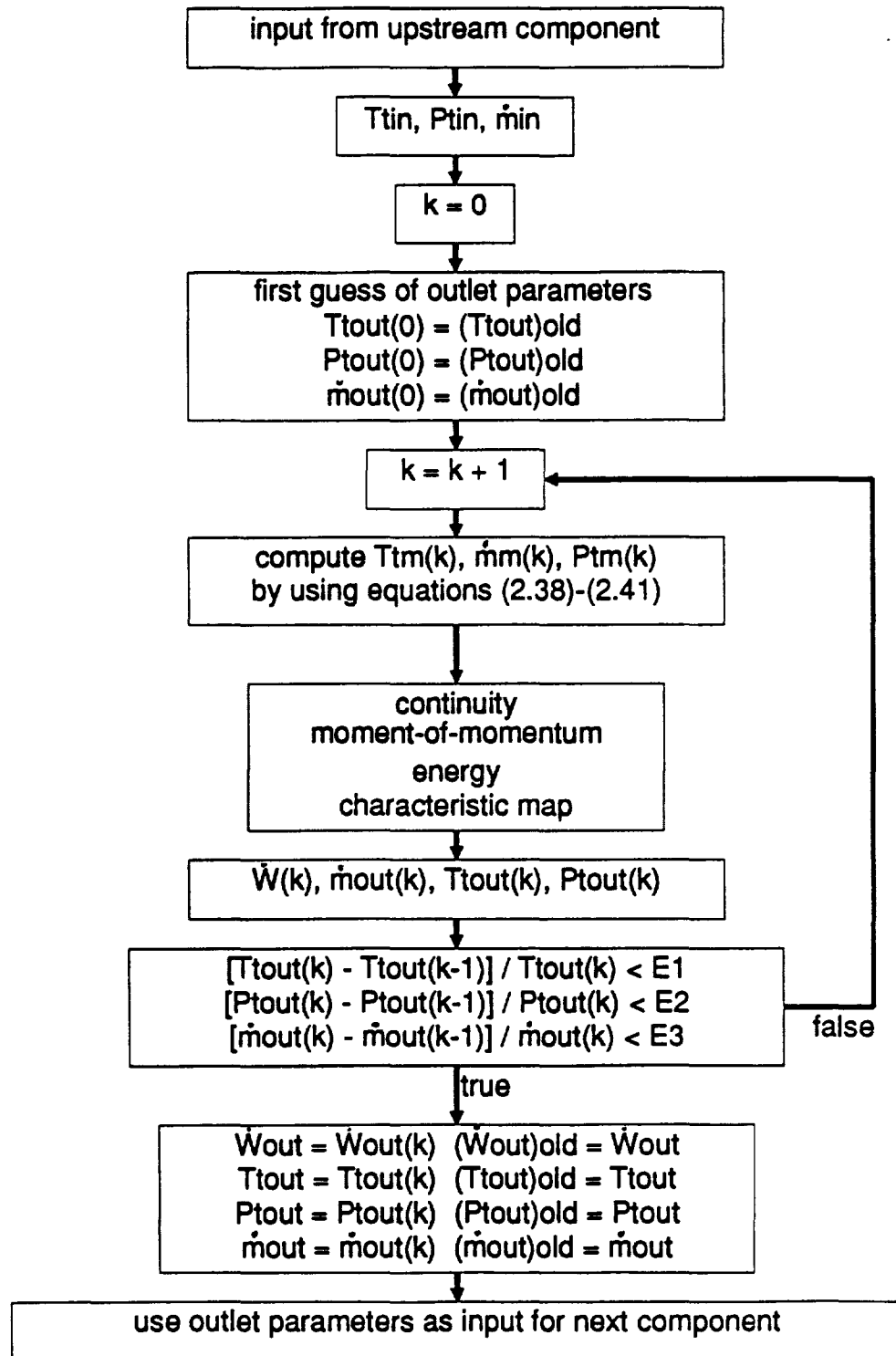


Fig. 2.8 The flowchart of the iteration scheme used in the turbine and compressor models

variables. The approximate speed of fluid through the control volume ( $v_m$ ) can then be evaluated by averaging the inlet and outlet fluid velocities. Similarly, the speed of sound through the control volume ( $a_m$ ) can be approximated. If the operating steady-state is perturbed by an infinitesimal disturbance (change in state variables) at the inlet, then the disturbance will travel through the fluid at the speed  $v_m + a_m$ . If the length of the flow path in the control volume is  $L$ , then the order of magnitude of transit time for the disturbance is

$$t = \frac{L}{v_m + a_m} \quad (2.42)$$

For the turbine,  $L = 0.1$  m,  $v_m = 137.6$  m/s,  $a_m = 563.8$  m/s. From (2.42), the transmit time is  $t = 0.00015$  seconds. Similarly, for the compressor,  $L = 0.06$  m,  $v_m = 79.0$  m/s,  $a_m = 341.4$  m/s. From (2.42), the transit time is  $t = 0.00014$  seconds.

Information travel in the second way is due to the rotation of the rigid rotors. Fig. 2.9 shows the flow through one blade passage. It is assumed that the rotor is initially operating at a constant speed. Consider the infinitesimal control volume  $A_1A_2A_3A_4$ , which is in contact with the blade at the inlet. A disturbance (change in thermodynamic state variables) at the inlet will cause a change of the thermodynamic state variables in the infinitesimal control volume  $A_1A_2A_3A_4$ . The change of thermodynamic state variables in  $A_1A_2A_3A_4$  will cause a change of force acting on the blade. This change of force will change the torque applied on the rotor. Since the rotor is rigid, this change of torque instantaneously affects fluid in contact with entire length of the blade. So, the thermodynamic state variables in an infinitesimal control volume  $B_1B_2B_3B_4$ , which is in contact with the blade at outlet, will be affected instantaneously. Further, an infinitesimal disturbance in  $B_1B_2B_3B_4$  will propagate across the passage at sonic speed. The speed of sound at the outlet is  $a_{out} = 535.1$  m/s for the turbine and  $a_{out}$

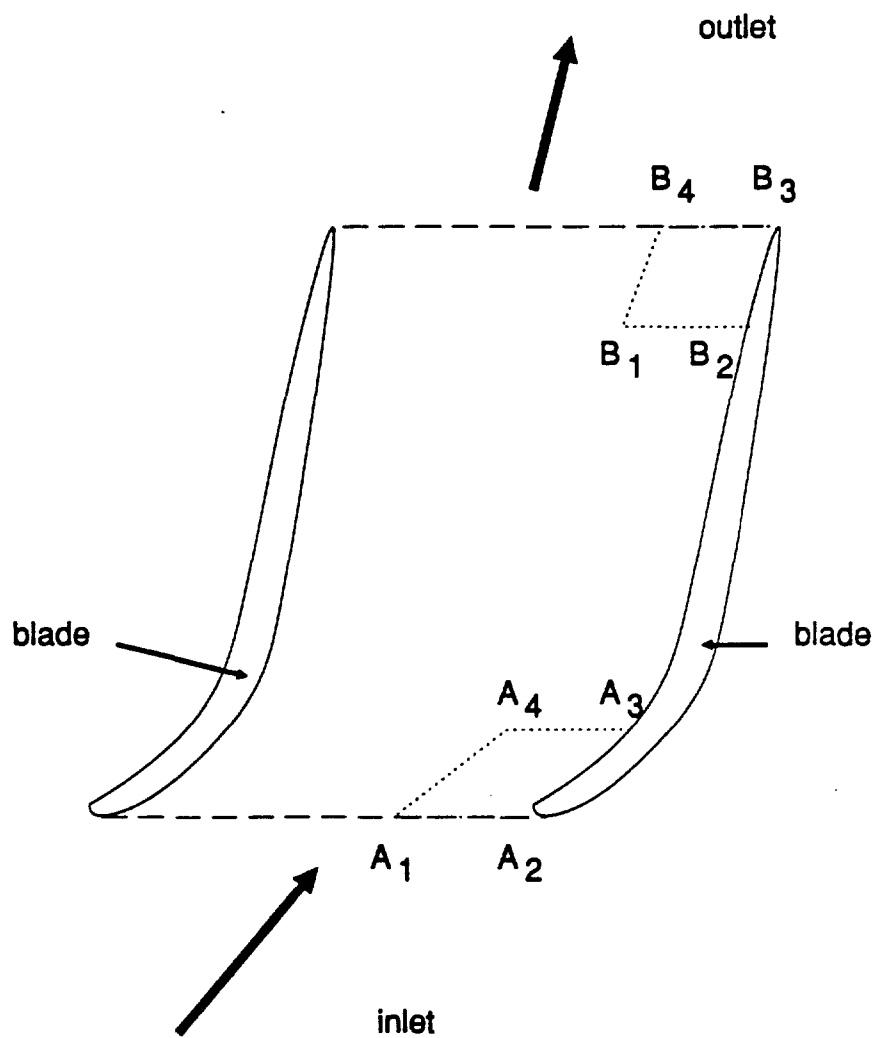


Fig. 2.9 The flow through one blade passage

= 366.9 m/s for the compressor. The width of the blade passage at the outlet is 0.013 m for the turbine and 0.006 m for the compressor. Thus, information travelling in the second way, will reach completely across the outlet in 0.000025 seconds for the turbine and in 0.000015 seconds for the compressor respectively.

The modes of information travel in the two ways are different. Since the two ways of information travel occur simultaneously in the turbomachine, it is difficult to determine which way dominates the transient response. Both appear to have a measure of validity. Therefore, it is reasonable to use a minimum time-step size as small as 0.000025 seconds in the system model under evaluation by this study provided that the variation at the inlet is not affecting the outlet of the dynamic turbomachine models in less than 0.00014 seconds.

In summary, this chapter has presented the component models for the components used in the Closed Regenerative Turbine-Engine Cycle. Details of implementation and use of the component models will be presented in later chapters.



### 3. System Modeling

#### 3.1 The Control Equations and the Iteration Scheme for System Modeling

The system model for the Solar-Powered Closed Regenerative Turbine-Engine Cycle was developed by integrating the component models into a system model. The control equations for the Solar-Powered Closed Regenerative Turbine-Engine Cycle system are based on the equation for conservation of mass and on the equation for conservation of energy. The equation for conservation of energy is:

$$\left[ \begin{array}{c} \text{RATE OF CHANGE} \\ \text{OF ENERGY IN} \\ \text{THE SYSTEM} \end{array} \right] = \left[ \begin{array}{c} \text{RATE OF} \\ \text{COLLECTED} \\ \text{SOLAR} \\ \text{ENERGY} \end{array} \right] - \left[ \begin{array}{c} \text{RATE OF} \\ \text{OUTPUT} \\ \text{ELECTRICAL} \\ \text{POWER} \end{array} \right] - \left[ \begin{array}{c} \text{RATE OF} \\ \text{WASTE HEAT} \\ \text{RADIATED} \\ \text{TO SPACE} \end{array} \right] \quad (3.1)$$

The equation for conservation of mass is:

$$\left[ \begin{array}{c} \text{TOTAL MASS} \\ \text{OF FLUID} \\ \text{IN SYSTEM} \end{array} \right] = \text{CONSTANT}$$

and

$$\left[ \begin{array}{c} \text{TOTAL MASS} \\ \text{OF COOLANT} \\ \text{IN SYSTEM} \end{array} \right] = \text{CONSTANT}$$

Equation (3.1) can be satisfied by applying an energy balance to the control volume for each component. The equation for conservation of mass is used as a criterion of convergence for the integrated system model. The mass-flow-rate iteration scheme is used in the transient simulation to insure that conservation of mass is satisfied at each time step. This is done by adjusting the inlet mass-flow-rate of the receiver during the iteration.

The state of the Solar-Powered Closed Regenerative Turbine-Engine Cycle is represented by the parameters ( $T_j$ ,  $p_j$  and  $\dot{m}_j$ ) at the junction points between the components. When a boundary condition of the Solar-Powered Closed Regenerative Turbine-Engine Cycle is given at time level  $n+1$ , the parameters at time level  $n+1$  are evaluated by the iteration scheme with known  $T_j^n$ ,  $p_j^n$ , and  $\dot{m}_j^n$  at time step  $n$ . The initial values of the parameters are given by

$$T_j^{(0)} = T_j^n$$

$$p_j^{(0)} = p_j^n$$

$$\dot{m}_j^{(0)} = \dot{m}_j^n$$

The parameters at iteration step  $(k)$  ( i.e.,  $T_j^{(k)}$ ,  $p_j^{(k)}$ ,  $\dot{m}_j^{(k)}$ , etc. ) can be evaluated by the component models. The total mass of the fluid in the system at iteration  $(k)$  is evaluated by

$$m^{(k)} = \sum_{j=1}^N m_j^{(k)},$$

where  $N$  is the number of components;  $m_j^{(k)}$  is the mass of working fluid in component "j" at iteration  $(k)$ . The value of  $m_j^{(k)}$  is the sum of all masses in the elements of the component

$$m_j^{(k)} = \sum_i m_i^{(k)}$$

where  $m_i^{(k)}$  is the mass in the element "i" at iteration  $(k)$ .

The mass in the element "i" can be evaluated by

$$m_i^{(k)} = \rho_i^{(k)} V_{cvi}$$

where  $\rho_i^{(k)}$  is the density of fluid in the element "i" at iteration (k);

$V_{cvi}$  is the control volume of the element "i".

The convergence criterion of the conservation of mass iteration is

$$\frac{m^{(k)} - m_0}{m_0} < \varepsilon, \quad (3.2)$$

where  $m_0$  (a given constant) is the total mass of the working fluid in the system. If the above inequality is not satisfied, the inlet mass-flow rate of the receiver is adjusted for the next iteration.

$$\dot{m}_3^{(k+1)} = \dot{m}_3^{(k)} + \Delta \dot{m}_3^{(k)}$$

or

$$\dot{m}_3^{(k+1)} = \dot{m}_3^{(k)} + f_{cr}^{(k)} f_e^{(k)} \dot{m}_3^{(k)}$$

where:  $\Delta \dot{m}_3^{(k)} = f_{cr}^{(k)} f_e^{(k)} \dot{m}_3^{(k)}$ ; superscript (k) is the iteration number; subscript "3"

represents the flow station at the inlet of the receiver;  $f_e^{(k)}$  is the relative error of the calculated mass at iteration (k)

$$f_e^{(k)} = \frac{m_0 - m^{(k)}}{m_0};$$

and  $f_{cr}^{(k)}$  is the correction factor (  $f_{cr}^{(0)} = 0.5$  ). To prevent "over-shooting" during the iteration, the value of  $f_{cr}^{(k)}$  is halved when  $f_e^{(k)}$  changes the sign between iteration (k) and (k+1), i.e.,

$$f_{cr}^{(k+1)} = 0.5f_{cr}^{(k)} .$$

The sign of  $\Delta \dot{m}_3^{(k)}$  is controlled by the sign of the relative calculated mass error  $f_e^{(k)}$ .

If inequality (3.2) is satisfied, then the parameters at next time step n+1 are given by

$$T_j^{n+1} = T_j^{(k)}$$

$$p_j^{n+1} = p_j^{(k)}$$

$$\dot{m}_j^{n+1} = \dot{m}_j^{(k)}$$

A flowchart of the iteration scheme is shown in Fig. 3.1.

### 3.2 Quasi-Steady System Model

The quasi-steady system model was developed to support steady-state calculations and to test the iteration scheme in the system model. The quasi-steady technique models the system in terms of "steady-state" characteristics of the components. FORTRAN subroutines have been developed to model each of the components. These subroutines are integrated into a system model using the iteration scheme described in chapter 3.1. The main computer program is designed such that each component model can be changed or replaced.

A transient process in the Closed Regenerative Turbine-Engine Cycle can be caused by an "outside disturbance" or an "inside disturbance". An "outside disturbance" can be caused by the change of environment such as occurs during orbit about the earth.

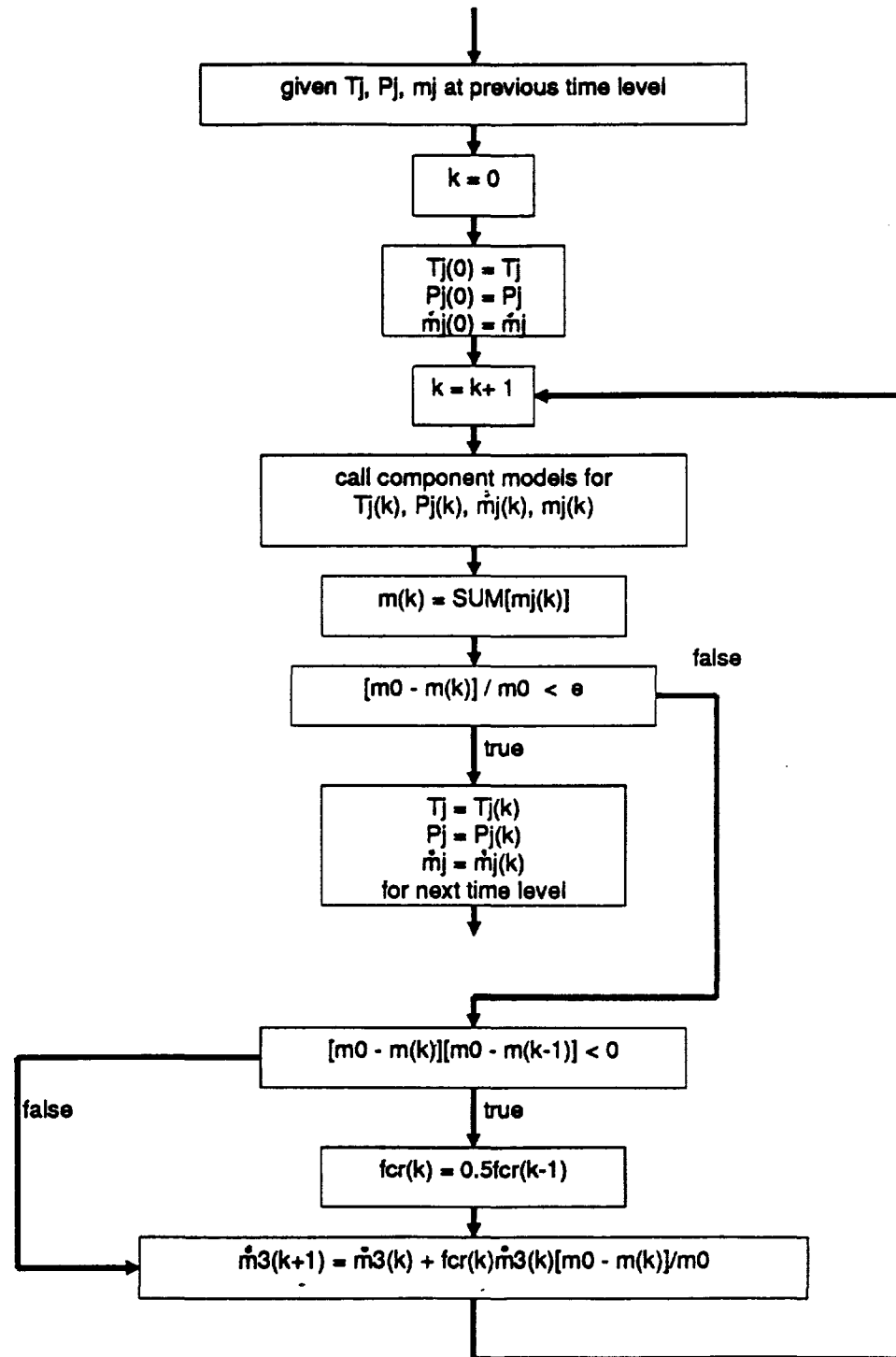


Fig. 3.1 Flowchart of the iteration scheme for system model

An "inside disturbance" may be a change of inventory, electrical load or rotation of the concentrator. The space temperature "seen" by the radiator can be used to represent the influence of the environment. The salt temperature in the receiver can be changed to represent the influence of rotation of the concentrator. The change of the total mass of working fluid can be used to represent the change of inventory. The space temperature and salt temperature can be specified as functions of time according to the orbital condition or the operating condition. The rotor speed of the turbomachinery is assumed to be fixed at 32,000 rpm as specified by the DR02 document<sup>[1]</sup>. This is the ideal operating condition for the Solar-Powered Closed Regenerative Turbine-Engine Cycle when the appropriate control scheme is used.

The mass of working fluid in a component is evaluated by

$$m = \frac{V_{cv}}{R} \left( \frac{p_{in} + p_{out}}{T_{in} + T_{out}} \right)$$

where  $V_{cv}$  is the volume of the working fluid in the component;  $R$  is the gas constant;  $T_{in}$  and  $p_{in}$  are inlet temperature and pressure;  $T_{out}$  and  $p_{out}$  are outlet temperature and pressure. The total mass of working fluid inventory in the system is the sum of the masses of the working fluid in all components. For a given total working fluid mass in the system, the inequality (3.2) is used to check the conservation of mass. The heat loss and pressure loss in the connecting pipes between the components are neglected. A flowchart of the quasi-steady system model is shown in Fig. 3.2.

### 3.3 Dynamic Heat Exchangers/Quasi-Steady Turbomachines System Model

It was shown by Iqbal<sup>[2]</sup> and Ali<sup>[4]</sup> that the response time for the turbine and for the compressor are many orders of magnitude smaller than for the heat exchangers. The assumption of instantaneous response of the turbine and the compressor has been shown

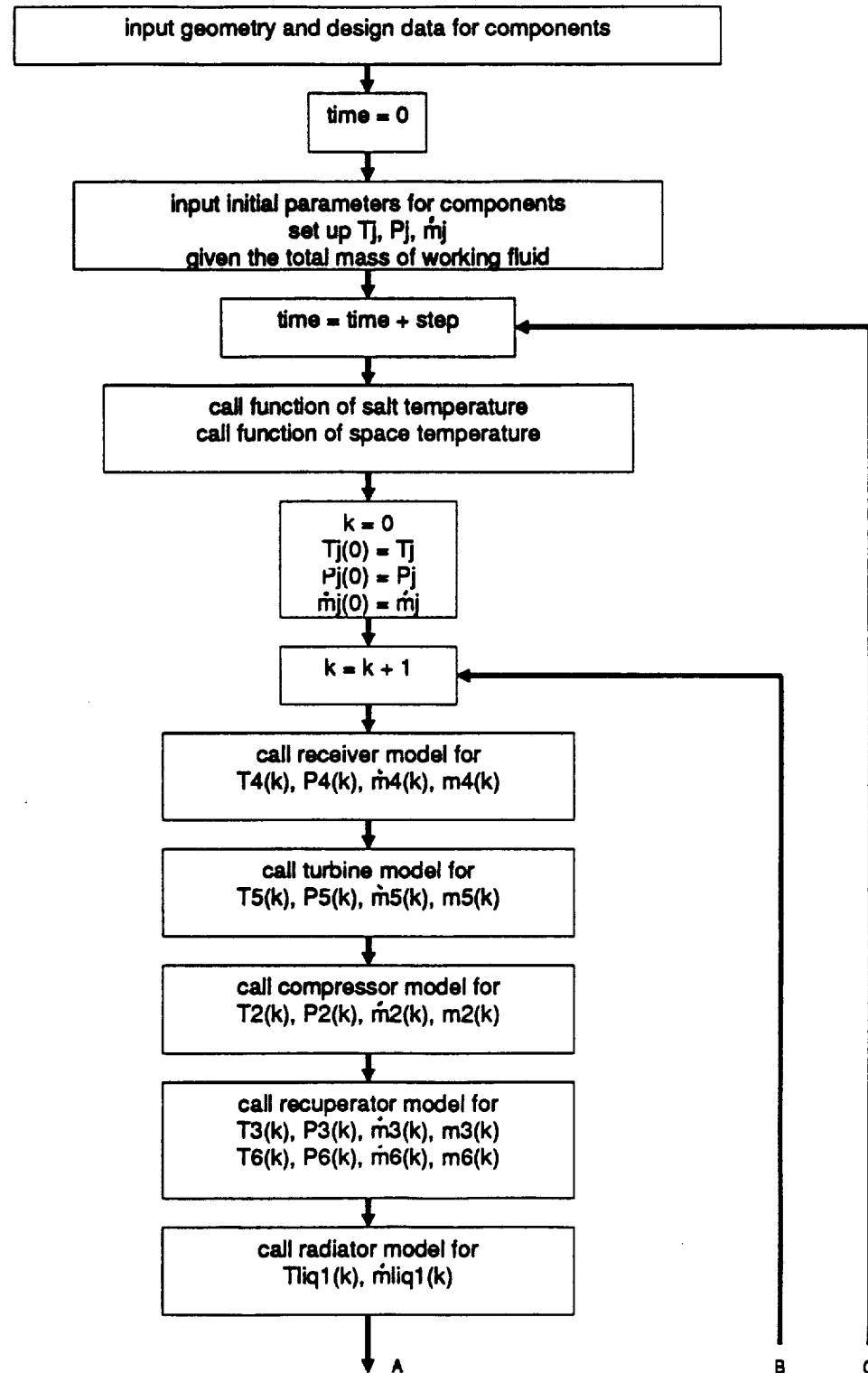


Fig. 3.2 Flowchart of quasi-steady components system model  
(continued on next page)

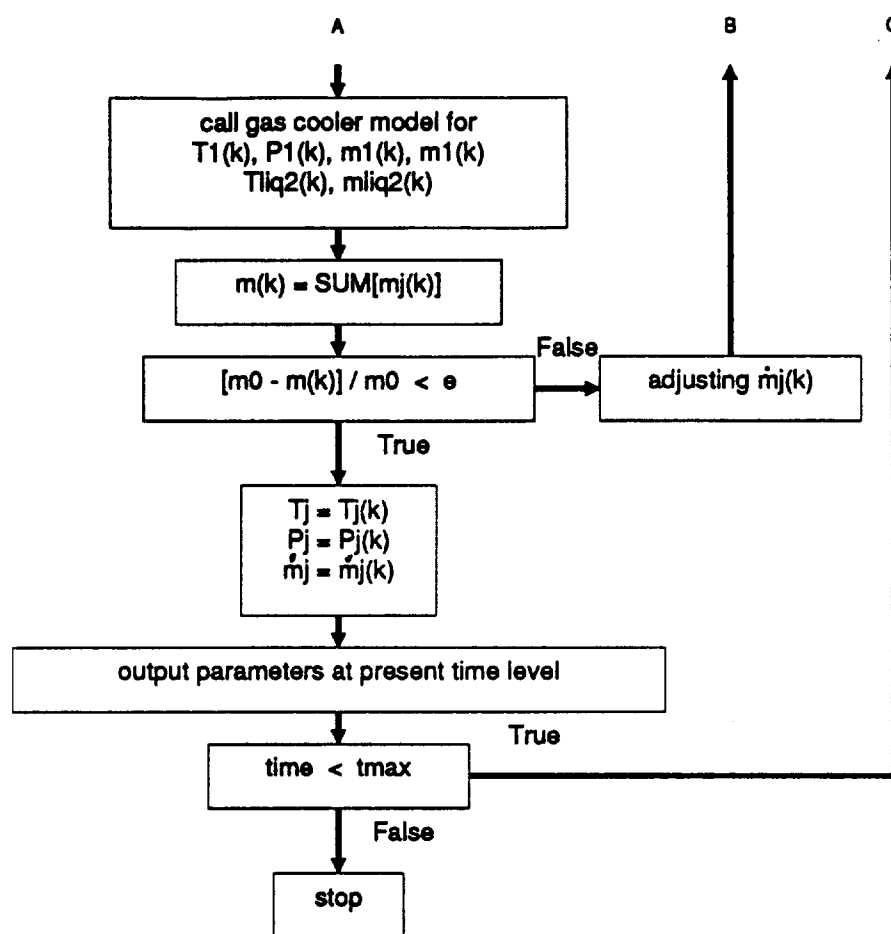


Fig. 3.2 Flowchart of quasi-steady components system model  
(continued from previous page)



to be a good assumption for studying system performance. Based on the quasi-steady system model, the dynamic heat exchangers/quasi-steady turbomachines system model was developed. The FORTRAN subroutines developed for the dynamic heat exchanger models and the steady-state turbine and compressor models are integrated to build a system model. The control equations and the iteration scheme used in the system modeling are the same as used for the quasi-steady system model. The change of storage of mass in components due to the change of pressure and temperature was considered in the system model. The mass-flow rate was found using the iteration scheme based on the conservation of mass. Two kinds of integrators are used by the system model: the Runge-Kutta integration method is used for the dynamic radiator model; and the simple Euler method is used for the receiver, gas cooler and recuperator dynamic models.

In the iteration loop, the quantities at time level "n" are stored and used during the iteration until the solution for the next time level is found. The mass of working fluid in the heat exchangers is the sum of the mass of the working fluid in the control volume of the elements. The total mass of the working fluid in the system is the sum of the masses of the working fluid mass in all components. Conservation of mass is used as a criterion of convergence for the iteration scheme, i.e., inequality (3.2) is used to check the conservation of mass in the system. The iteration scheme was described in section 3.1.

The space temperature and the salt temperature are specified as functions of time. The rotor speed of the turbomachinery is assumed to be fixed at 32,000 (rpm) as specified by the DR02 document<sup>[1]</sup>. The heat and pressure losses in the connecting pipes between the components are neglected.

The computer model (written in FORTRAN) can simulate a transient process caused by a change in space temperature or/and the rotation of the concentrator (i.e., the

change of salt temperature). The program can also be used to simulate a radiator panel loss and coolant pump loss by changing the number of panels and setting coolant mass-flow rate to zero. A flowchart of the program is shown in Fig. 3.3.

### 3.4 Dynamic Heat Exchangers/Dynamic Turbomachines System Model

The FORTRAN subroutines of the dynamic turbine and compressor models described in chapter 2.2.3 have been used to develop a complete dynamic system model. The dynamic heat exchangers/dynamic turbomachines system model is developed by substituting the dynamic turbomachinery models for the quasi-steady turbomachinery models into the dynamic heat exchanger/quasi-steady turbomachines system model. The implicit Euler second order algorithm is used as the time integrator for the dynamic turbine and compressor models. The integrator used for the receiver, gas cooler and recuperator dynamic models is the simple Euler method. The integrator used for the radiator dynamic model is the Runge-Kutta method. The iteration scheme in the main program of the dynamic heat exchangers/dynamic turbomachines system model is similar to that used in the main program of dynamic heat exchangers/quasi-steady turbomachines system model. The space temperature and salt temperature are given as functions of time. The rotor speed of the turbomachinery is assumed to be 32,000 rpm as specified by the DR02 document<sup>[1]</sup>. The heat and pressure losses in the connecting ducts between the components are assumed negligible. A flowchart of the program is shown in Fig. 3.4.

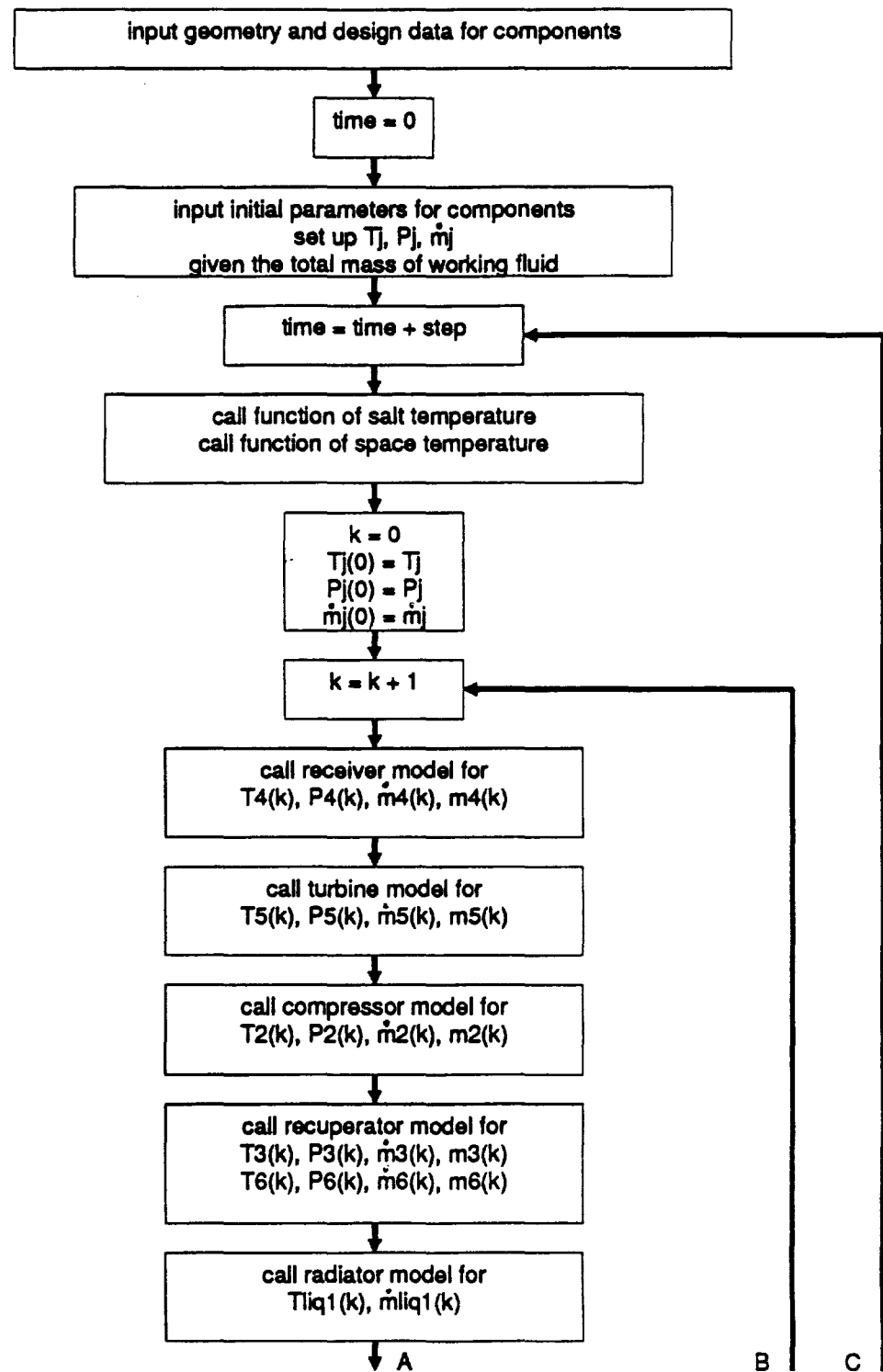


Fig. 3.3 Flowchart of dynamic heat exchangers/quasi-steady turbomachines system model  
(continued on next page)

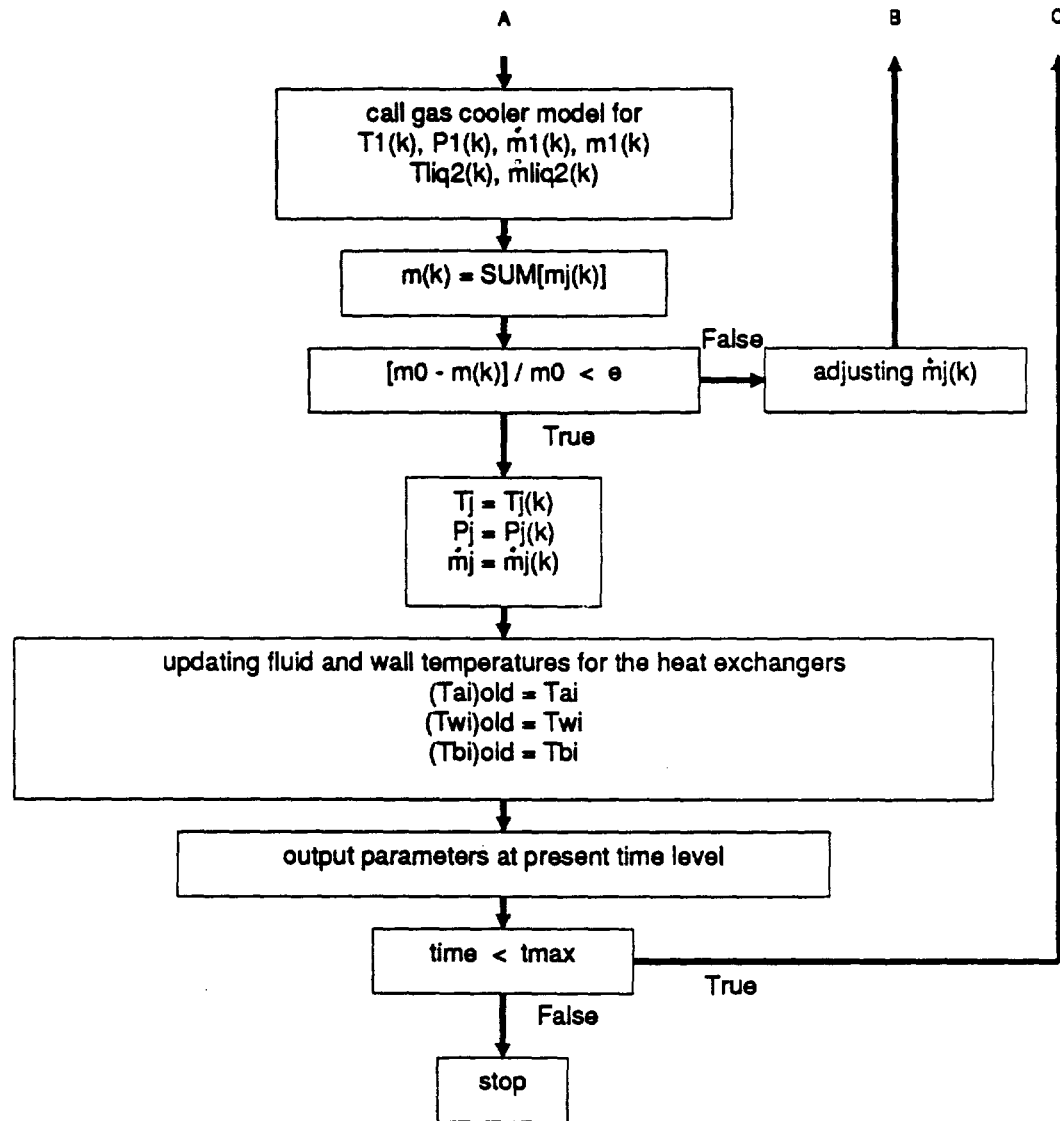


Fig. 3.3 Flowchart of dynamic heat exchangers/quasi-steady turbomachines system model  
(continued from previous page)

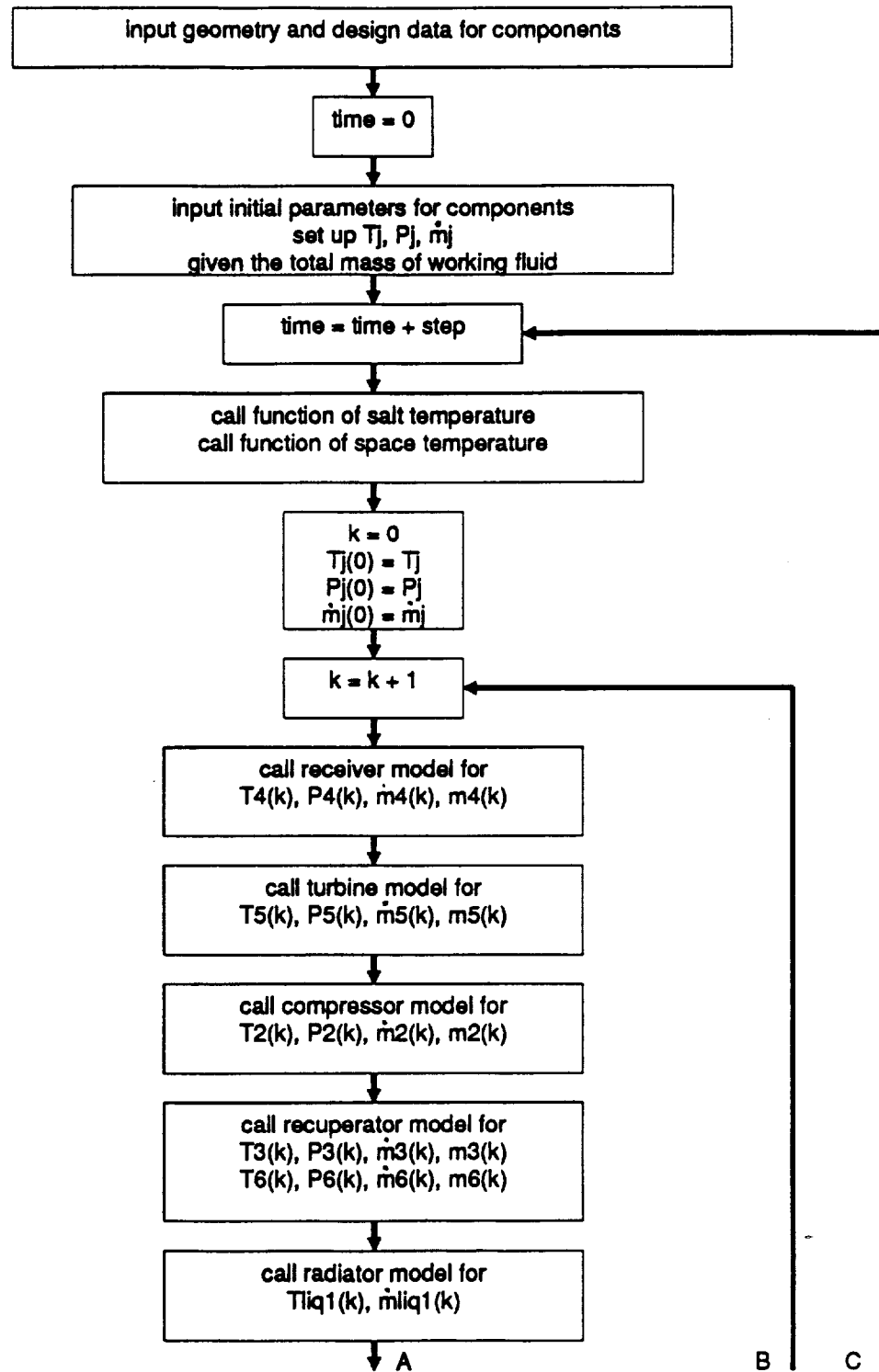


Fig. 3.4 Flowchart of dynamic heat exchangers/dynamic turbomachines system model  
(continued on next page)

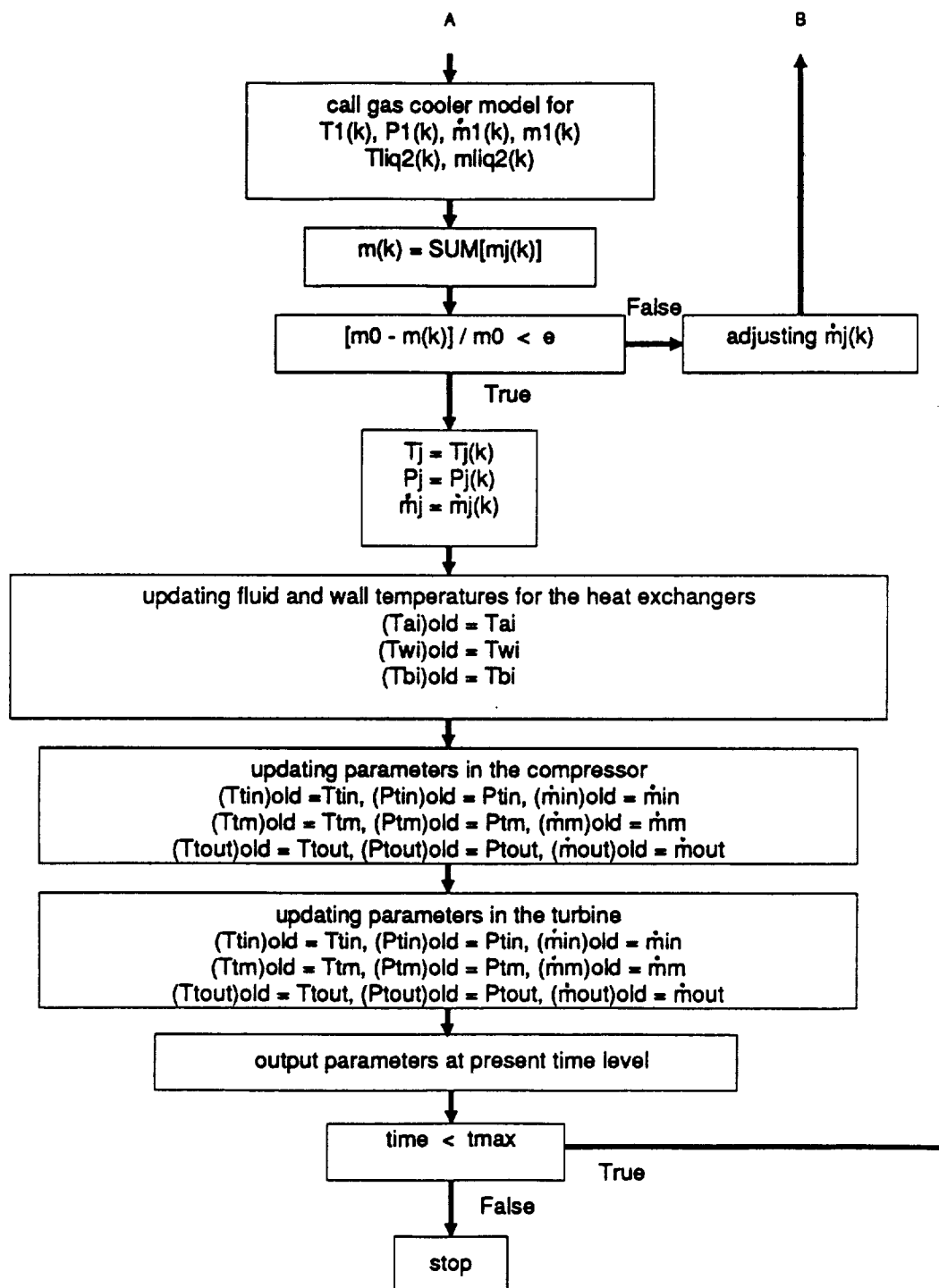


Fig. 3.4 Flowchart of dynamic heat exchangers/dynamic turbomachines system model  
(continued from previous page)

#### 4. The System Transient Performance Simulation

The Solar-Powered Closed Regenerative Turbine-Engine Cycle system performs its function by collecting energy in the form of incident solar flux and converting a portion of the collected energy to electrical power to meet the space station needs. During operation, the Solar-Powered Closed Regenerative Turbine-Engine cycle controller must maintain constant alternator speed and output line voltage despite variations in load including peaking demands and varying receiver energy input rates. The dynamic system models described in the previous chapter are used to predict the transient performance of the Solar-Powered Closed Regenerative Turbine-Engine Cycle. The design data for the components in the Solar-Powered Closed Regenerative Turbine-Engine Cycle are shown in Table 4.1.

##### 4.1 Transient Simulation with the Quasi-Steady System Model

The motivation for developing the quasi-steady system model was to test the iteration scheme in the system model. The simulation results of the quasi-steady system model can also be compared to the results of the dynamic system model to evaluate the importance of including dynamic turbomachinery models in the system simulation.

The quasi-steady system model was subjected to a number of tests to verify the performance of the iteration scheme. The response of the system to a double step of 10 K in the salt temperature of the receiver was simulated with this model. The integrator time step used for the simulation was 1.0 second. Fig. 4.1, 4.2 and 4.3 show the responses of receiver, turbine and compressor outlet parameters to the double step in salt temperature. We can see that all parameters of the system, pressure, temperature and mass-flow rates at the inlet and outlet of the components, change back to the exact points

Table 4.1 Design Data for the Components in the Solar-Powered Closed  
Regenerative Turbine-Engine Cycle

<b>Receiver</b>	
Phase-Change Material.....	LiF-CaF <sub>2</sub> Eutectic
Active Tube Length, (m).....	2.5
Number of Tubes.....	82
Inner Tube OD, (m).....	$2.22 \times 10^{-2}$
Tube Wall Thickness, (m).....	$8.9 \times 10^{-2}$
Tube material.....	Haynes 188
Total Active Tube Weight (estimated), (kg).....	150.0
<b>Heat Exchanger (Recuperator)</b>	
Flow Length, (m).....	$3.66 \times 10^{-1}$
Flow Width, (m).....	$3.18 \times 10^{-1}$
<b>High Pressure Side Fin</b>	
Height, (m).....	$3.2 \times 10^{-3}$
Fins per m.....	630
Thickness, (m).....	$1.5 \times 10^{-4}$
Number of Sandwiches.....	62
Type : Rectangular Offset	
<b>Low Pressure Side Fin</b>	
Height, (m).....	$3.9 \times 10^{-3}$
Fins per m.....	630
Thickness, (m).....	$1.5 \times 10^{-4}$
Number of Sandwiches.....	63
Type : Rectangular Offset	
Material.....	CRES 304L
Total Recuperator Weight (dry), (kg).....	162
<b>Gas Cooler</b>	
Gas Flow Length, (m).....	$2.68 \times 10^{-1}$
Liquid Flow Length (per pass), (m).....	$2.54 \times 10^{-1}$
Number of Liquid Pass.....	8
<b>Gas Side Fins</b>	
Height, (m).....	$2.3 \times 10^{-3}$

(Table 4.1 continued on next page)



Table 4.1 Design Data of the Components in the Solar-Powered Closed  
Regenerative Turbine-Engine Cycle (continued from previous page)

Fins per m.....	470
Thickness, (m).....	$1.5 \times 10^{-4}$
Type : Rectangular Offset	
Liquid Side Fins	
Height, (m).....	$1.9 \times 10^{-3}$
Fins per m.....	790
Thickness, (m).....	$1.5 \times 10^{-4}$
Type : Rectangular Offset	
Number of Gas Sandwiches.....	103
Material.....	CRES 304L
Total Gas Cooler Weight (dry), (kg).....	85.3
<hr/>	
Radiator	
Panel Size, (m <sup>2</sup> ).....	2.3x8.0
Number of Panels.....	8
Material.....	Aluminum
Total Panel Weight (dry), (kg).....	825
<hr/>	
Turbine	
Inlet Normal Area, (m <sup>2</sup> ).....	$4.0 \times 10^{-3}$
Middle Normal Area, (m <sup>2</sup> ).....	$5.058 \times 10^{-3}$
Outlet Normal Area, (m <sup>2</sup> ).....	$5.648 \times 10^{-3}$
Volume of Turbine, (m <sup>3</sup> ).....	$1.0 \times 10^{-4}$
Tip Radius, (m).....	$9.49 \times 10^{-2}$
Middle Radius, (m).....	$5.26 \times 10^{-2}$
<hr/>	
Compressor	
Inlet Normal Area, (m <sup>2</sup> ).....	$3.6 \times 10^{-3}$
Middle Normal Area, (m <sup>2</sup> ).....	$3.05 \times 10^{-3}$
Outlet Normal Area, (m <sup>2</sup> ).....	$2.5 \times 10^{-3}$
Volume of Compressor, (m <sup>3</sup> ).....	$6.0 \times 10^{-5}$
Tip Radius, (m).....	$6.654 \times 10^{-2}$
Middle Radius, (m).....	$3.739 \times 10^{-2}$

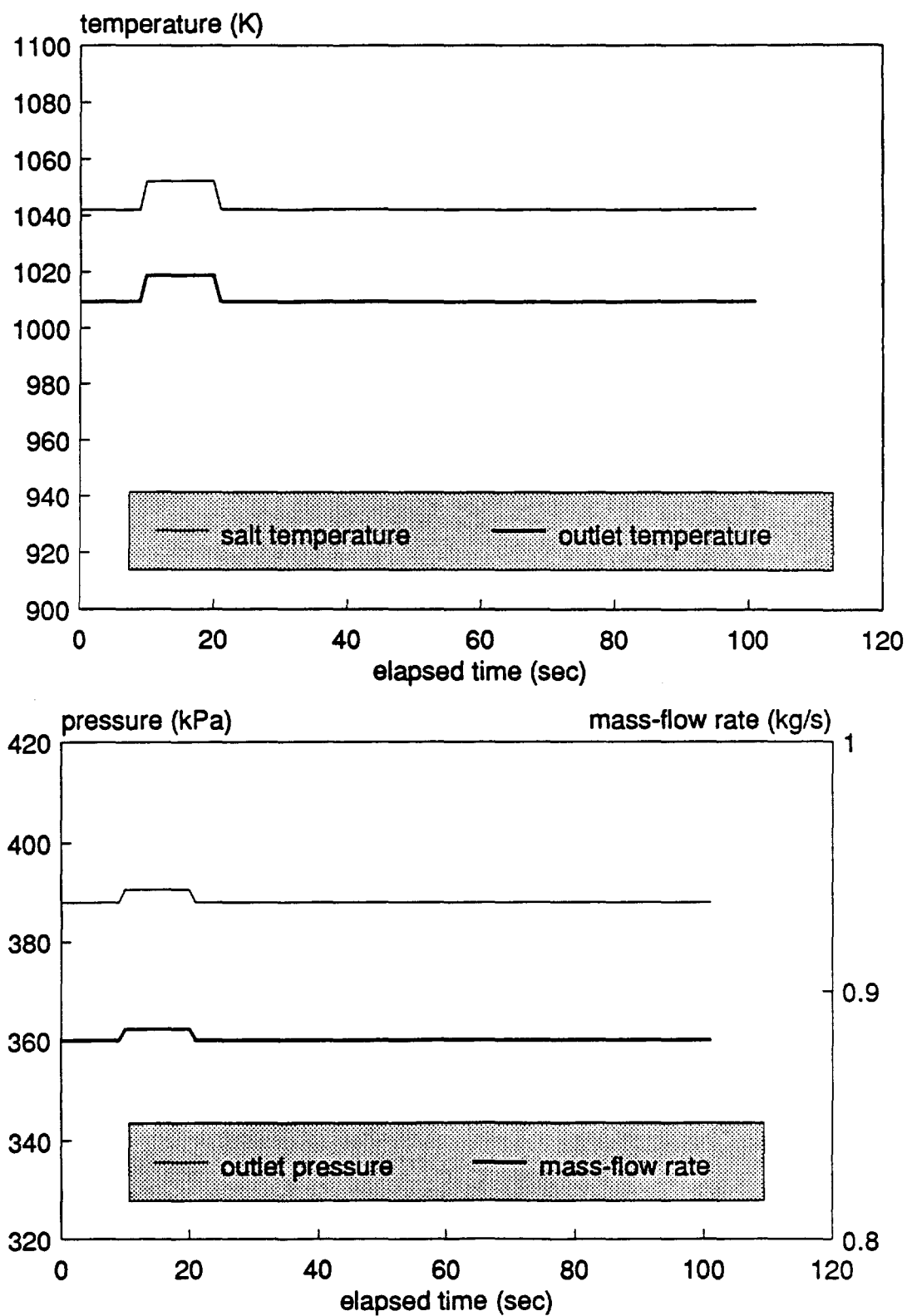


Fig. 4.1 Response of receiver outlet parameters

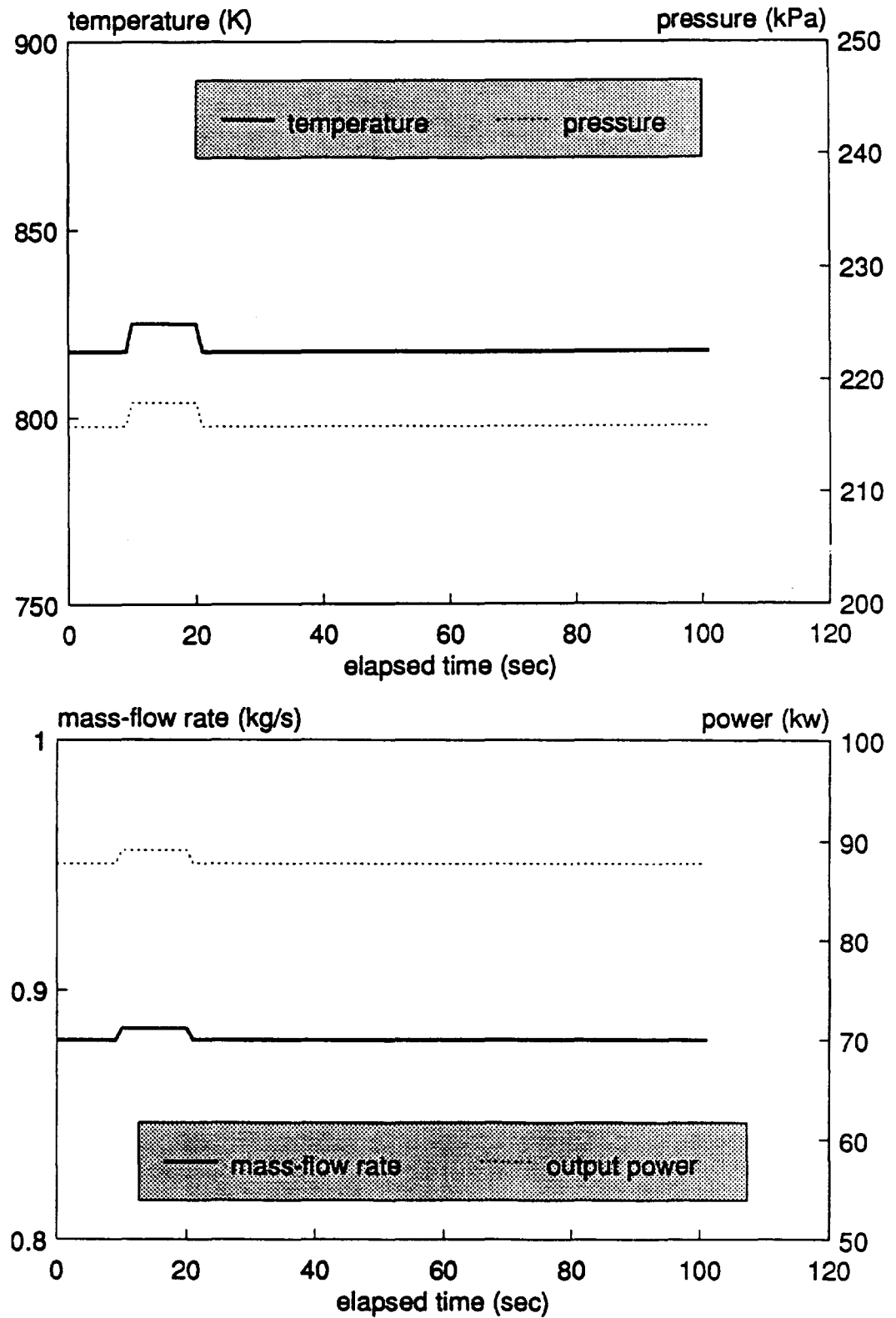


Fig. 4.2 Response of turbine outlet parameters

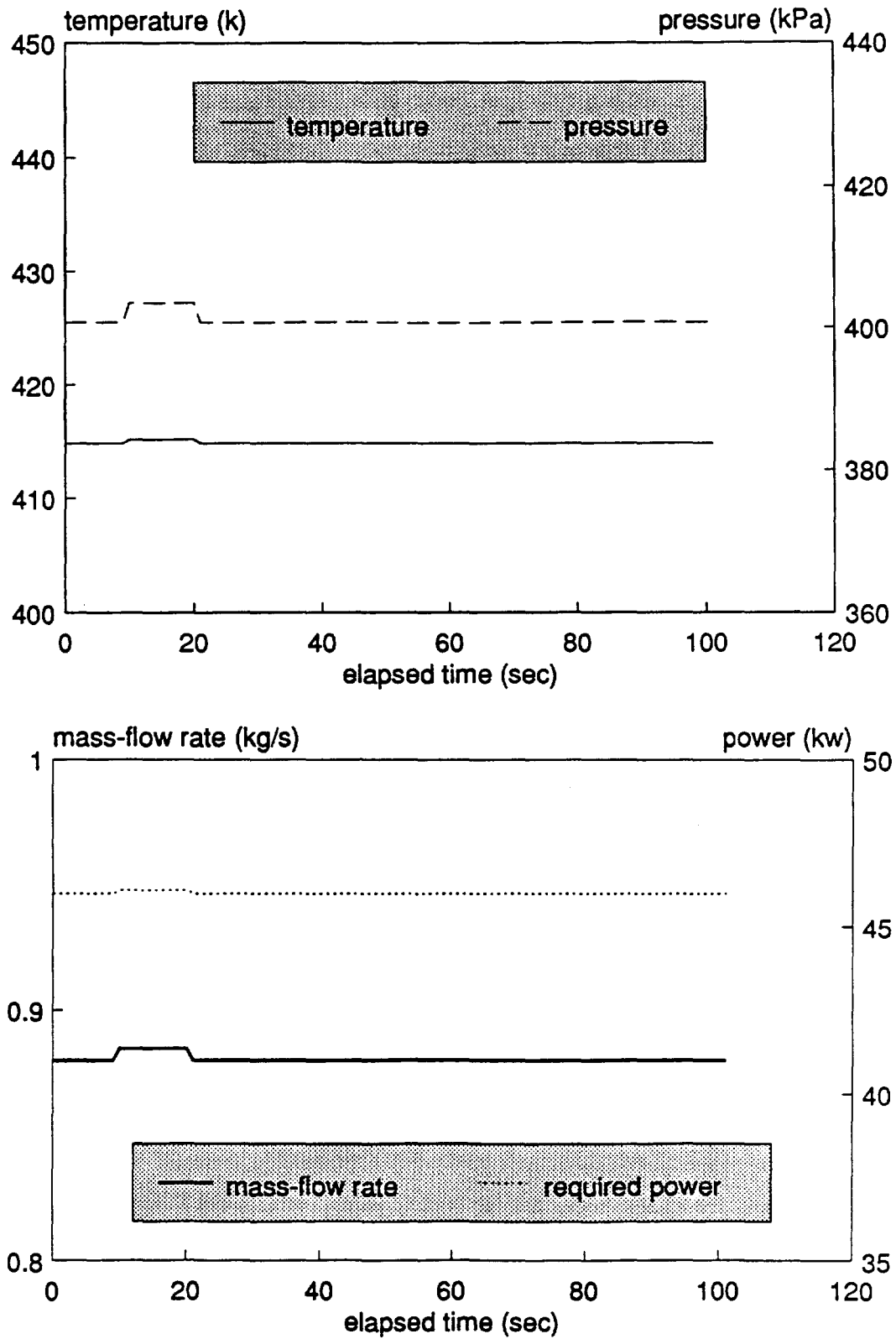


Fig. 4.3 Response of compressor outlet parameters

after the double step change in salt temperature. This verifies that the iteration scheme is correctly locating a new operating point of the system. This test was important for proving the validity of the iteration scheme and logic of the program.

## 4.2 Transient Simulation with Dynamic System Models

The dynamic system models developed in chapter 3.3 and 3.4 were used to simulate the transient processes in the Solar-Powered Closed Regenerative Turbine-Engine Cycle. The simulation results with the dynamic heat exchangers/quasi-steady turbomachines system model and the dynamic heat exchangers/dynamic turbomachines system model were compared for the same transient processes.

### 4.2.1 Performance Simulation by the Dynamic Heat Exchangers/Quasi-Steady

#### Turbomachines System Model

Since response times for the turbine and compressor are many orders of magnitude smaller than the heat exchangers, the assumption of instantaneous response turbomachinery has been used in the dynamic heat exchangers/quasi-steady turbomachines system model. To verify the performance of this model, the transient response of the Solar-Powered Closed Regenerative Turbine-Engine Cycle to a single step, double step and sinusoidally varying receiver salt temperature was simulated with the dynamic heat exchangers/quasi-steady turbomachines system model. The integrator time step used for the simulation was 1.0 second.

#### 4.2.1.1 Response to a Step Change of Receiver Salt Temperature

The system is initially working at a steady-state operating point. At the 10th time step, the perturbation is provided by a step of receiver salt temperature from 1042 K to 1062 K. The response of the outlet parameters of receiver, turbine, compressor and gas

cooler are shown in Fig. 4.4 to 4.8. The outlet temperatures of the components lag from up-stream components to down-stream components as shown in the figures. The outlet temperature of recuperator at low-pressure side lags the receiver outlet temperature. The outlet temperature of the gas cooler in turn lags the outlet temperature of recuperator. We can see that the response of recuperator outlet temperature at low-pressure side is much slower than the response of the recuperator outlet temperature of the high-pressure side as shown in Fig. 4.8. This is because that the high pressure side fluid at the outlet exchanges heat energy with the turbine outlet flow at up stream position. At the starting period of the transient, because of the lag in temperature, the inlet temperature of the compressor does not change much even though the salt temperature was given a big step. But the mass-flow rate in the compressor is changing (increasing in this case) with the same response as the up-stream components. The change in mass-flow rate causes the change in compressor efficiency which is determined by the characteristic map. The change in compressor efficiency causes the changes of outlet temperature and pressure even with unchanged inlet temperature. For the given process, the increase of mass-flow rate causes the increase of compressor efficiency. Because the change in compressor inlet temperature is small, the increased efficiency causes the slight decrease of outlet temperature at the beginning period as shown in Fig. 4.6. Since the compressor is at the most down-stream position along the flow path from the receiver, the responses of compressor outlet temperature and pressure are the most slow ones compared to the other components. But the system pressure level is much affected by the pressure ratio of the compressor, this explains the slow pressure response in the system. It can be seen that the response time of the system to the perturbation is greater than 2500 seconds. This supports the assumption that the instantaneous response turbomachinery can be a good assumption for studying system performance.

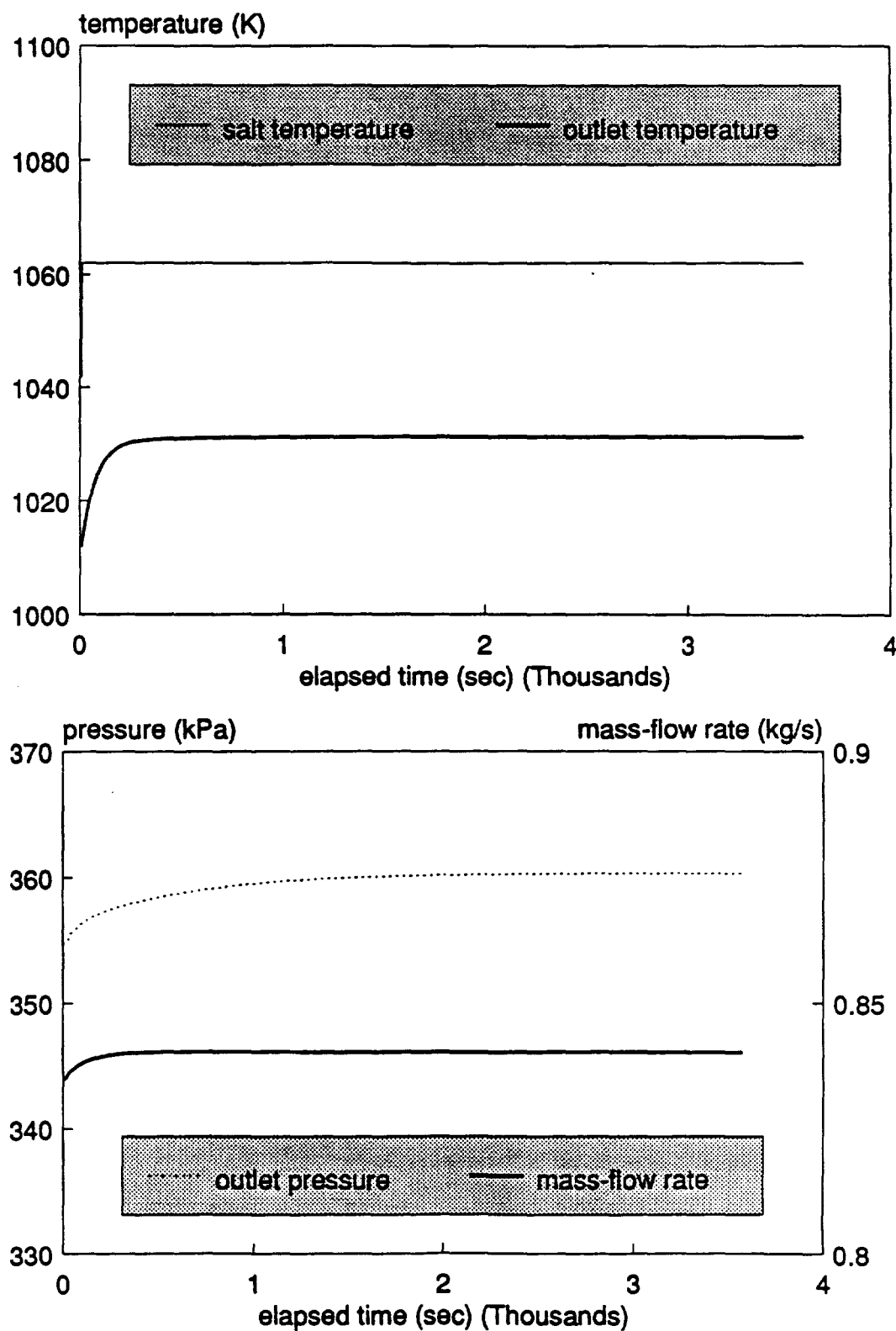


Fig. 4.4 Response of receiver outlet parameters

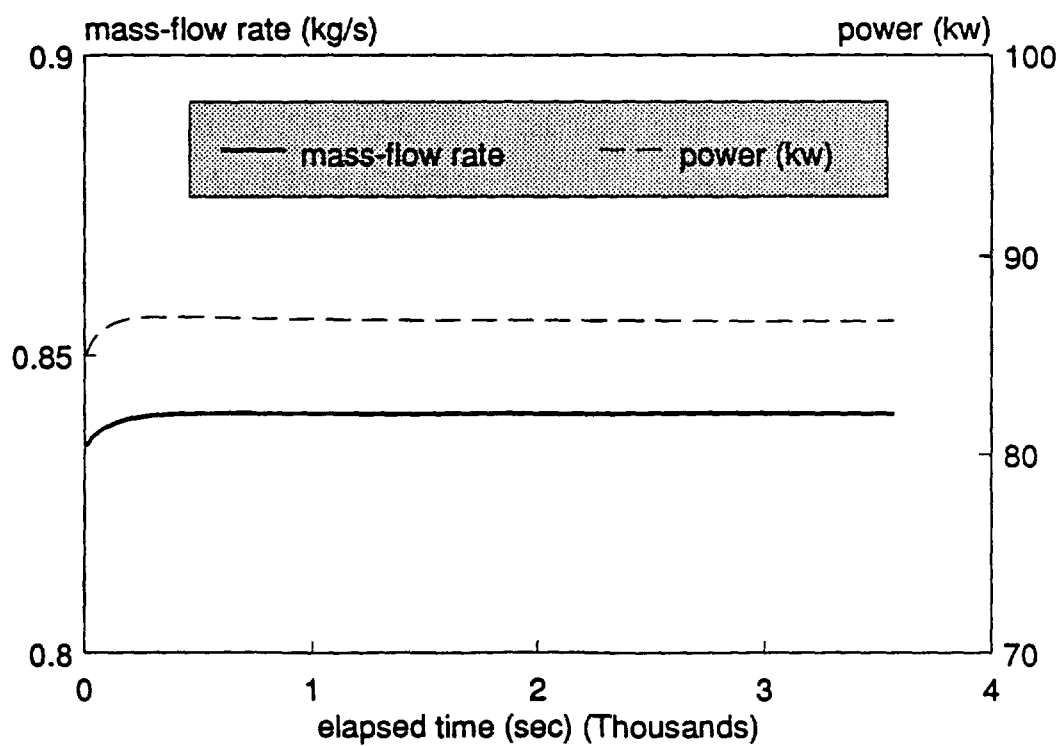
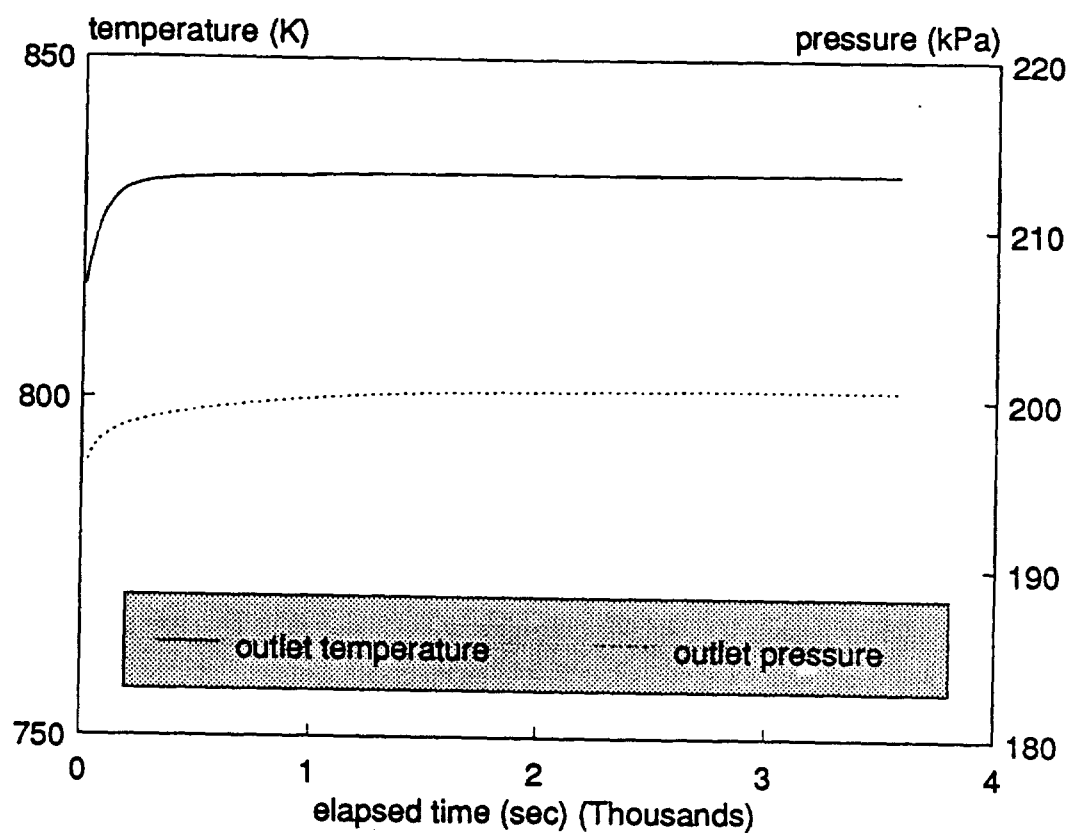


Fig. 4.5 Response of turbine outlet parameters

C-5



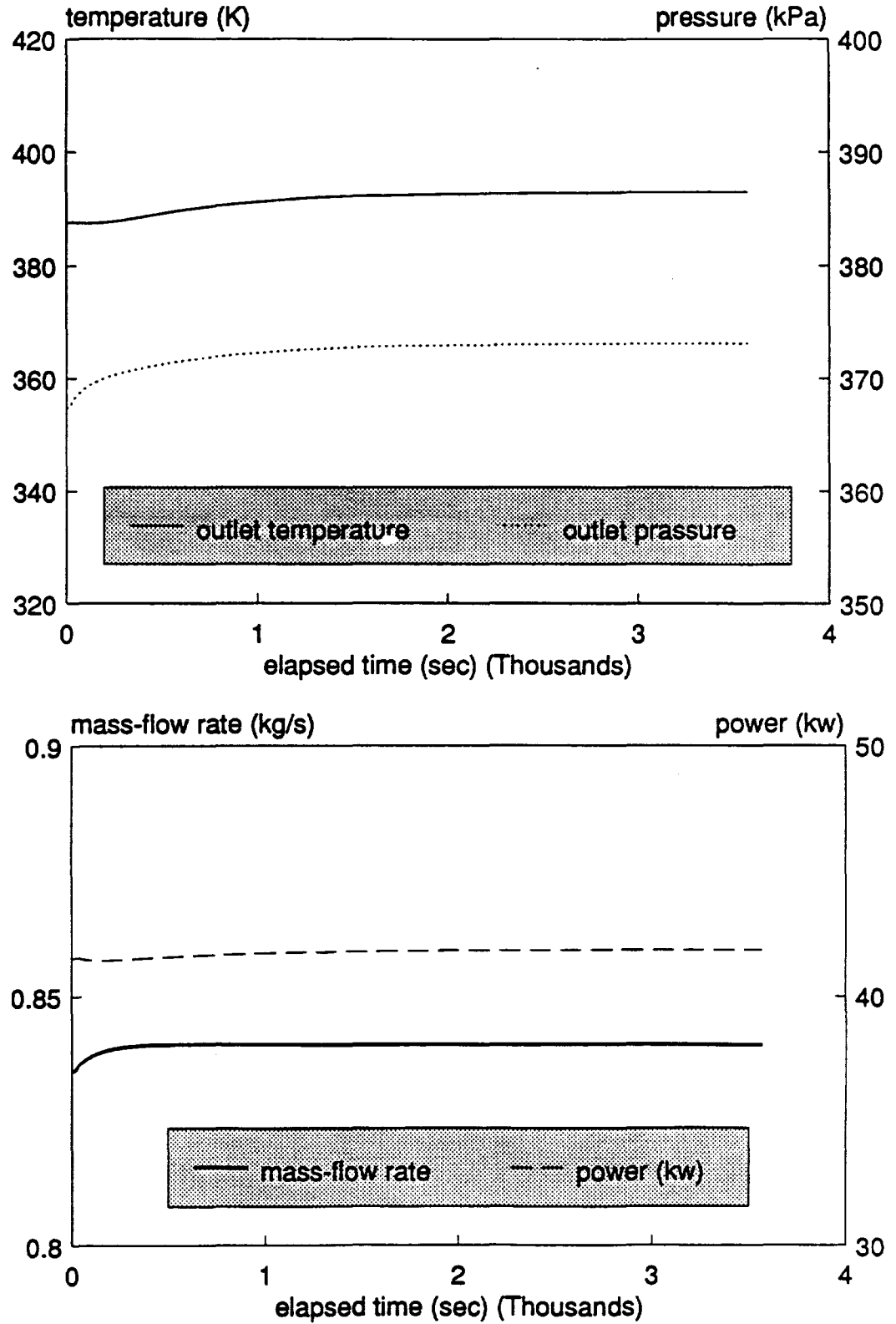


Fig. 4.6 Response of compressor outlet parameters

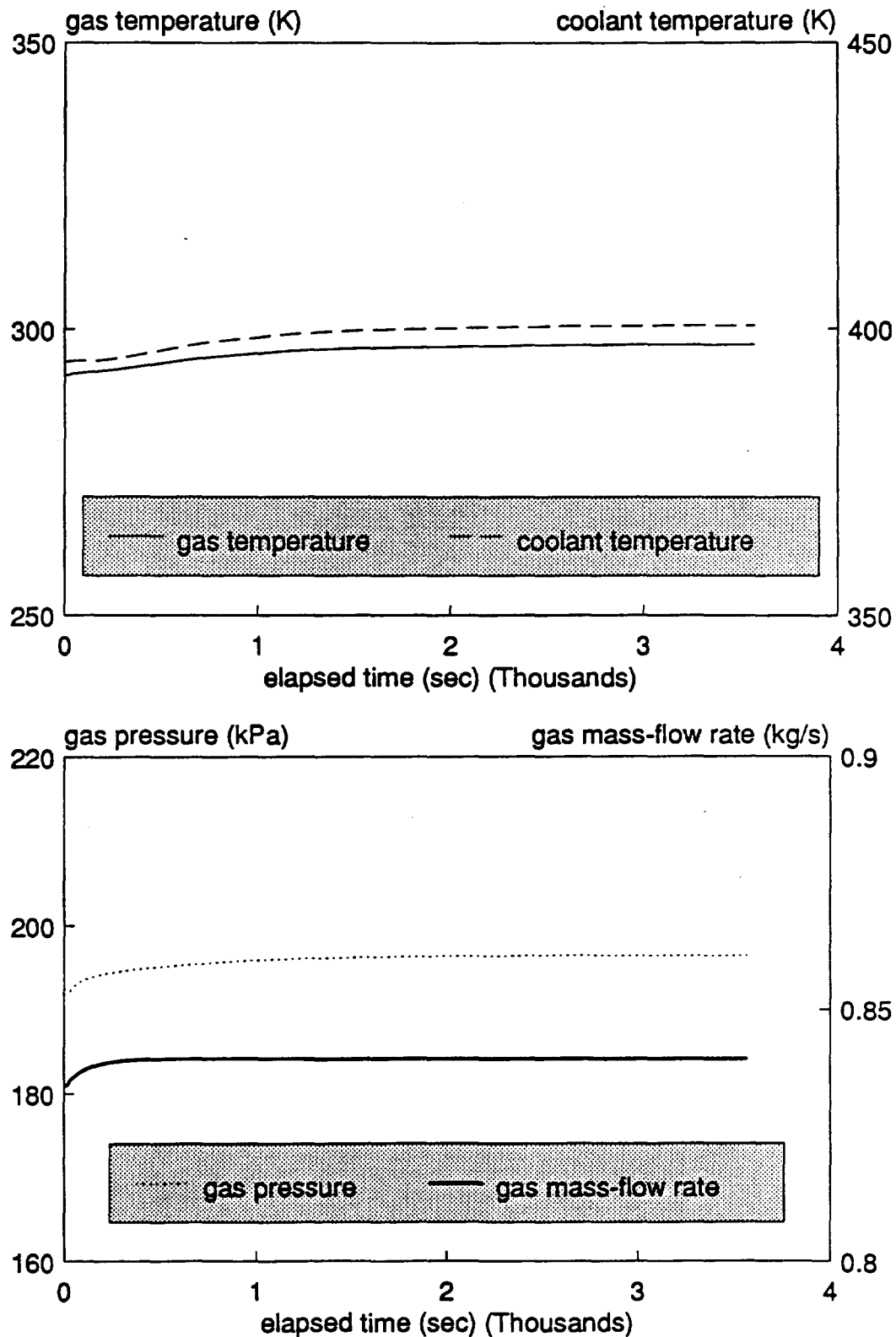


Fig. 4.7 Response of gas cooler outlet parameters

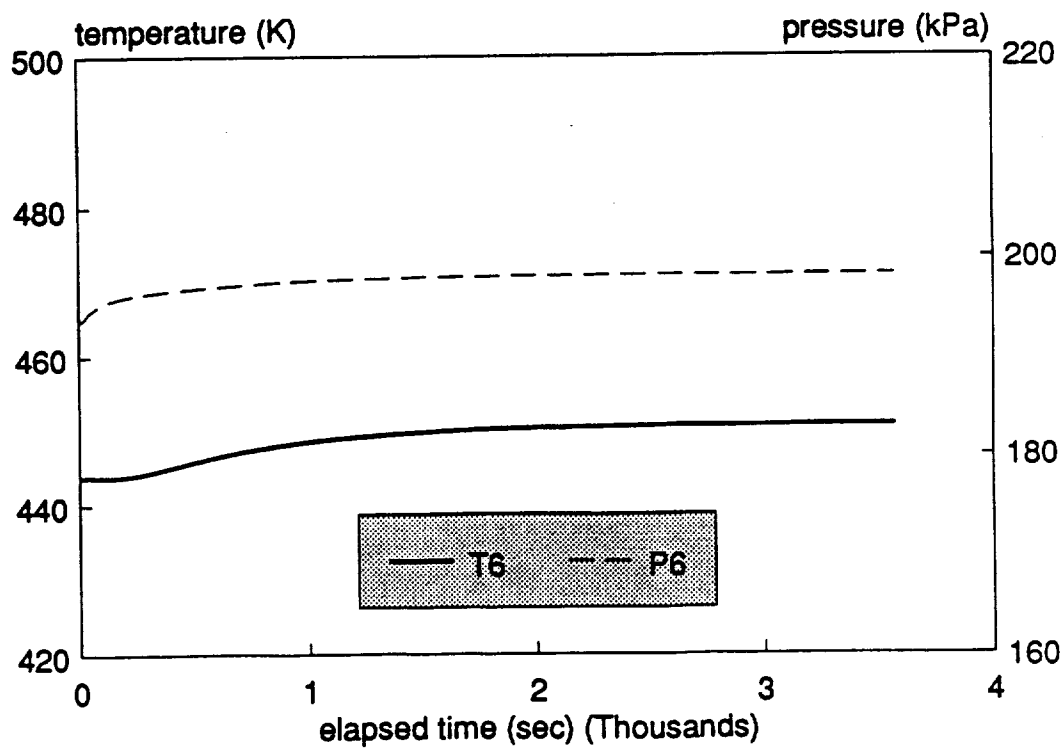
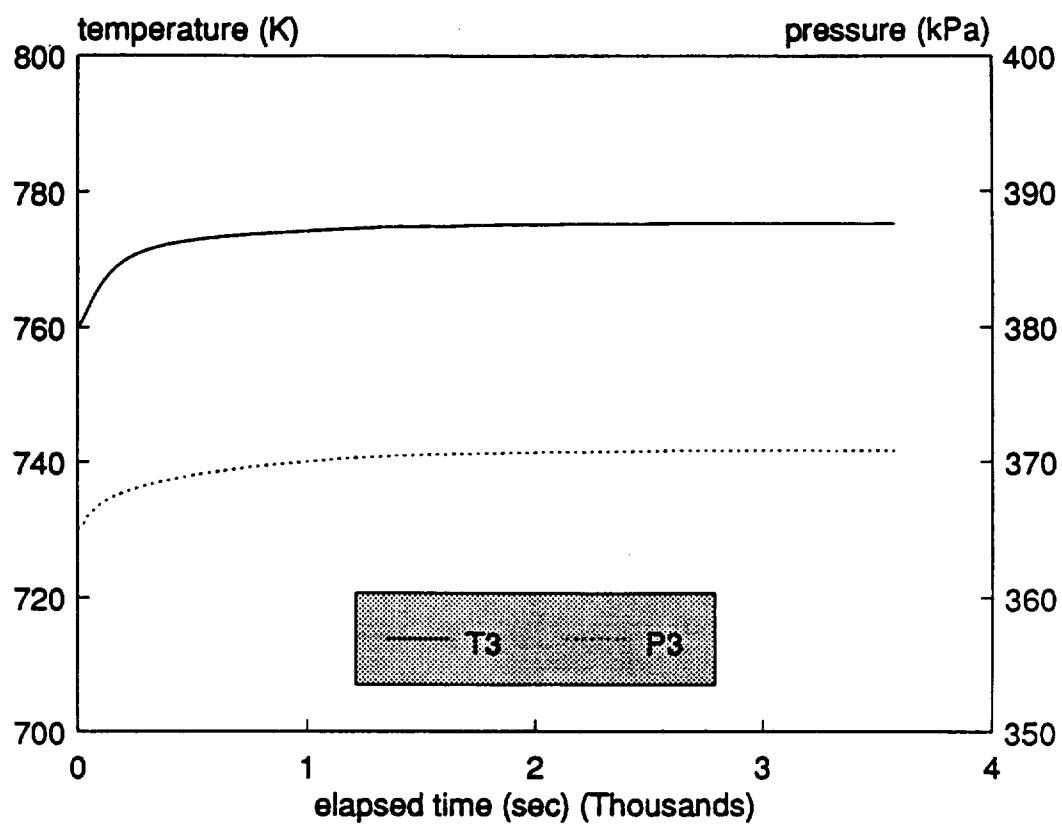


Fig. 4.8 Response of recuperator outlet parameters

#### 4.2.1.2 Response to a Double Step of Receiver Salt Temperature

This test resembled the previous one, except that the salt temperature was stepped down to the original 1042 K after 1000 seconds. The system response to the double step is shown in Fig. 4.9 to 4.13. The simulation results of the quasi-steady system model for the same perturbation in receiver salt temperature are also plotted in Fig. 4.9 to 4.13. Since the mass in a component is calculated with the averaged temperature and pressure at the inlet and outlet positions of the component for the quasi-steady system model, this causes the error of calculated mass in the system compared with the dynamic heat exchanger/quasi-steady turbomachines system model. The differences in calculated mass cause the differences in the calculated mass-flow rate and other parameters which can be seen from the responses to the step in the salt temperature as shown in Fig. 4.9 to 4.13. We can see that the quasi-steady system model cannot predict the lag in parameters. It is shown in Fig. 4.11 that the outlet temperature of compressor keeps increasing after the salt temperature stepped down from 1062 K to 1042 K. This is caused by the dropping of efficiency of the compressor and the lag of gas cooler outlet temperature. The drop in the efficiency is caused by the drop of mass-flow rate. The increased compressor-outlet temperature in turn causes the increase of the recuperator outlet temperature at the low-pressure side as shown in Fig. 4.12. The simulation results show that the operating points predicted by the dynamic heat exchangers/quasi-steady turbomachines system model and the quasi-steady system model are very close at the end of transient process. This agreement provides confidence in the dynamic heat exchangers/quasi-steady turbomachines system model.

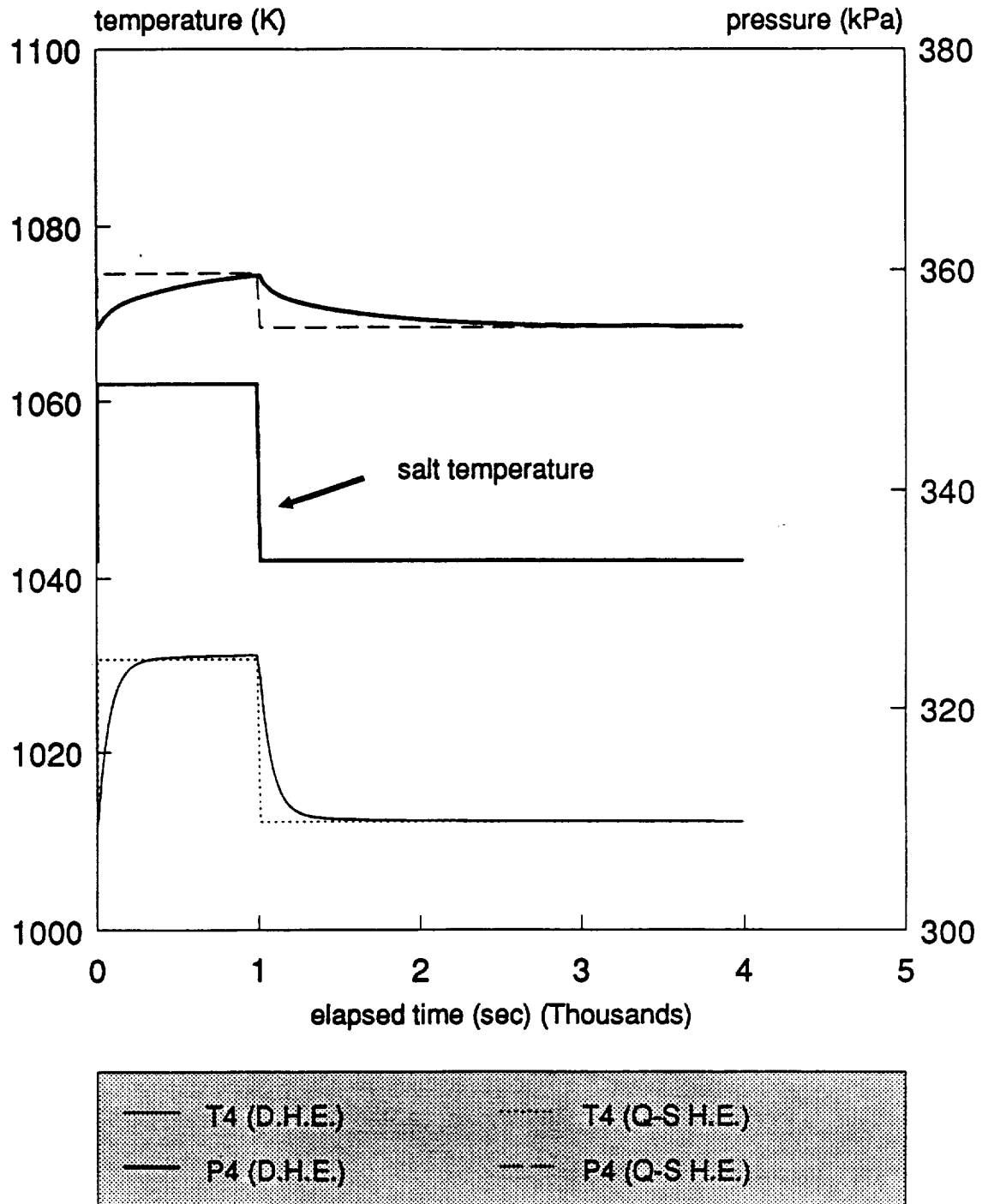


Fig. 4.9 Response of receiver outlet parameters

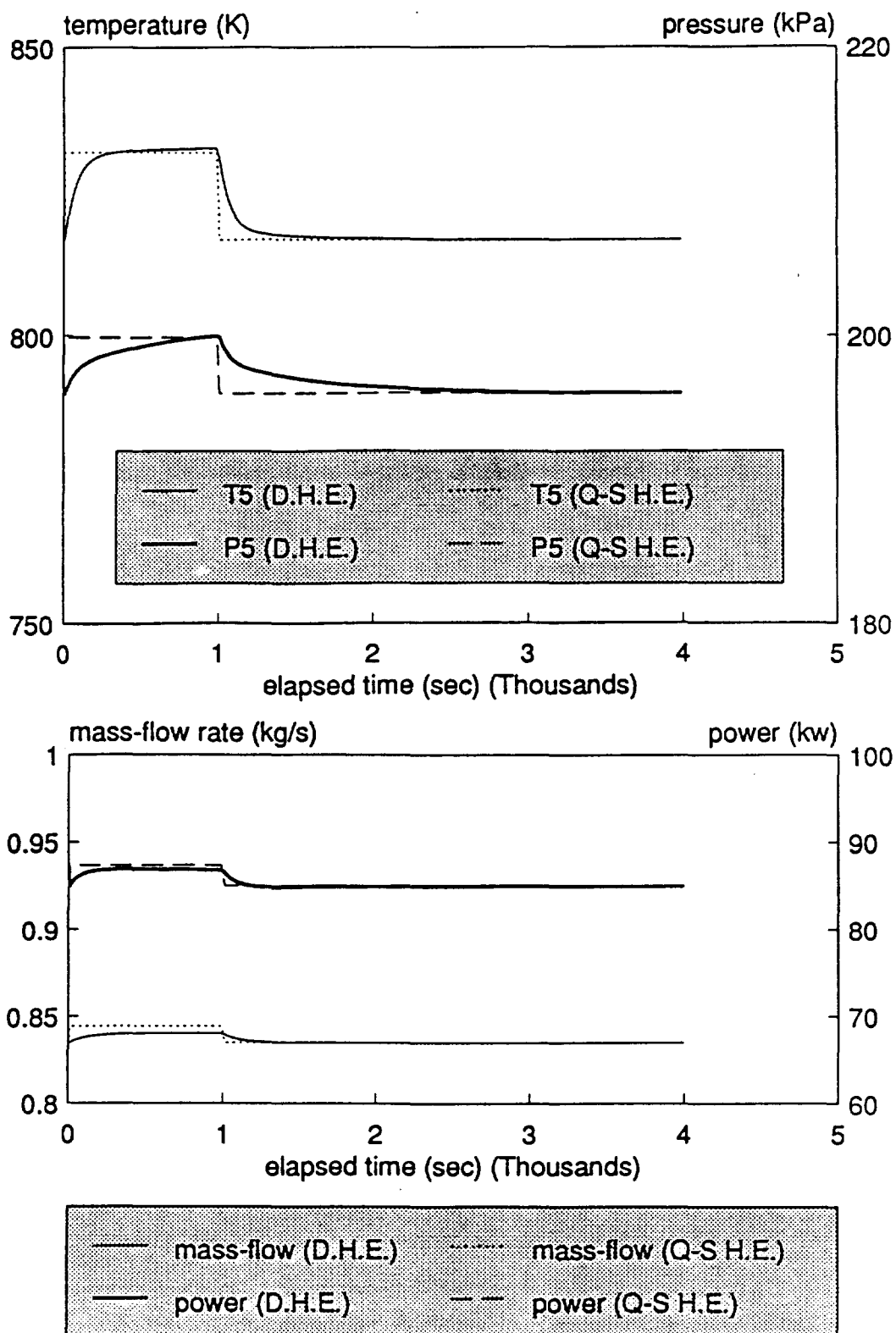


Fig. 4.10 Response of turbine outlet parameters

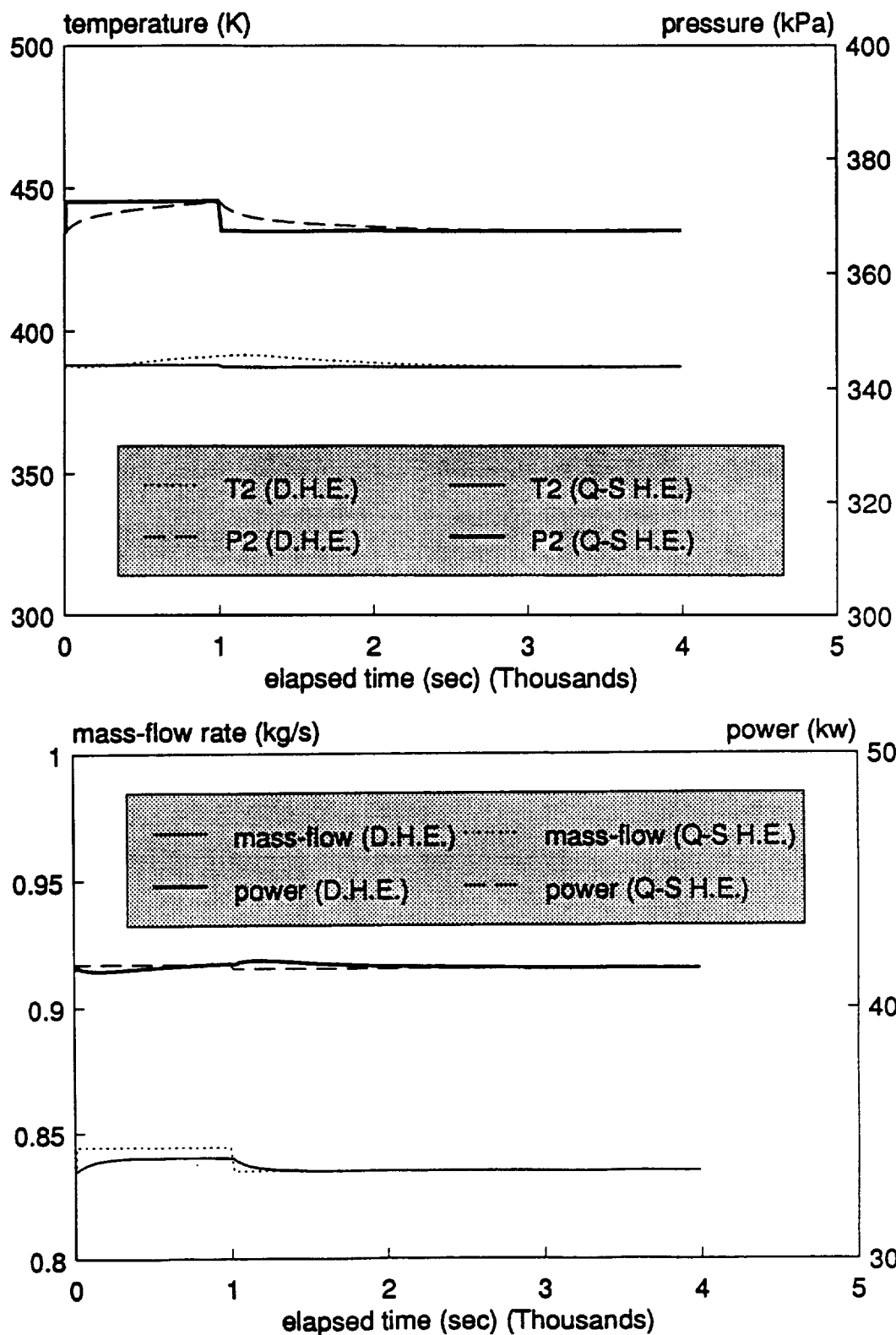


Fig. 4.11 Response of compressor outlet parameters

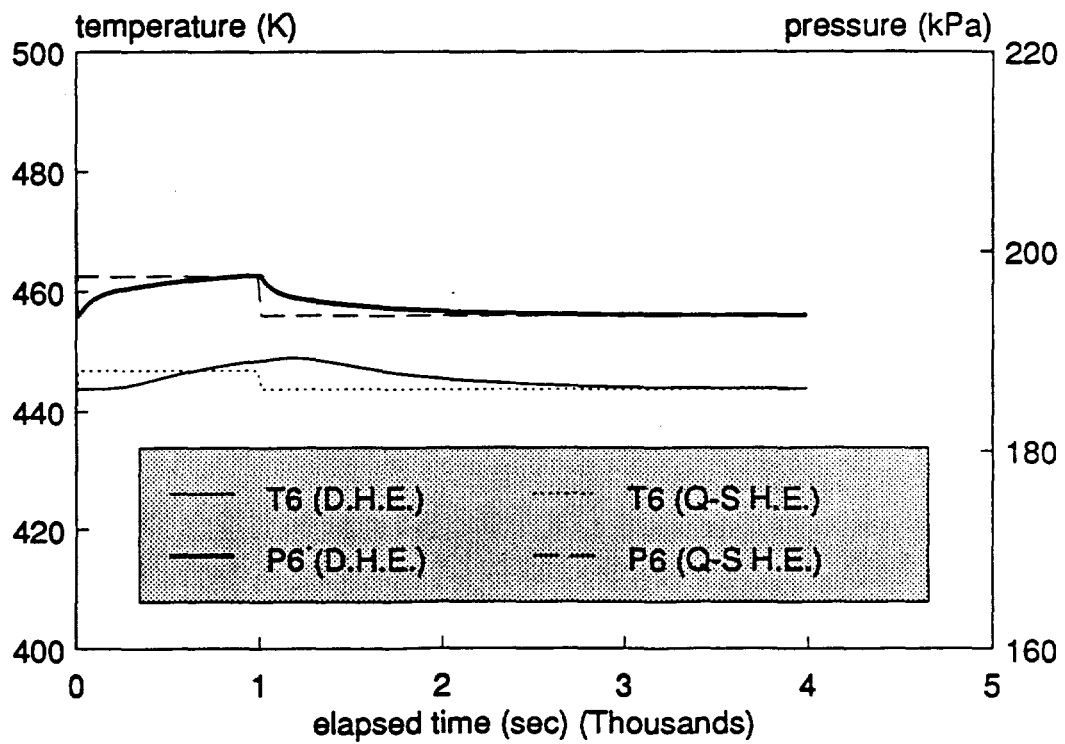
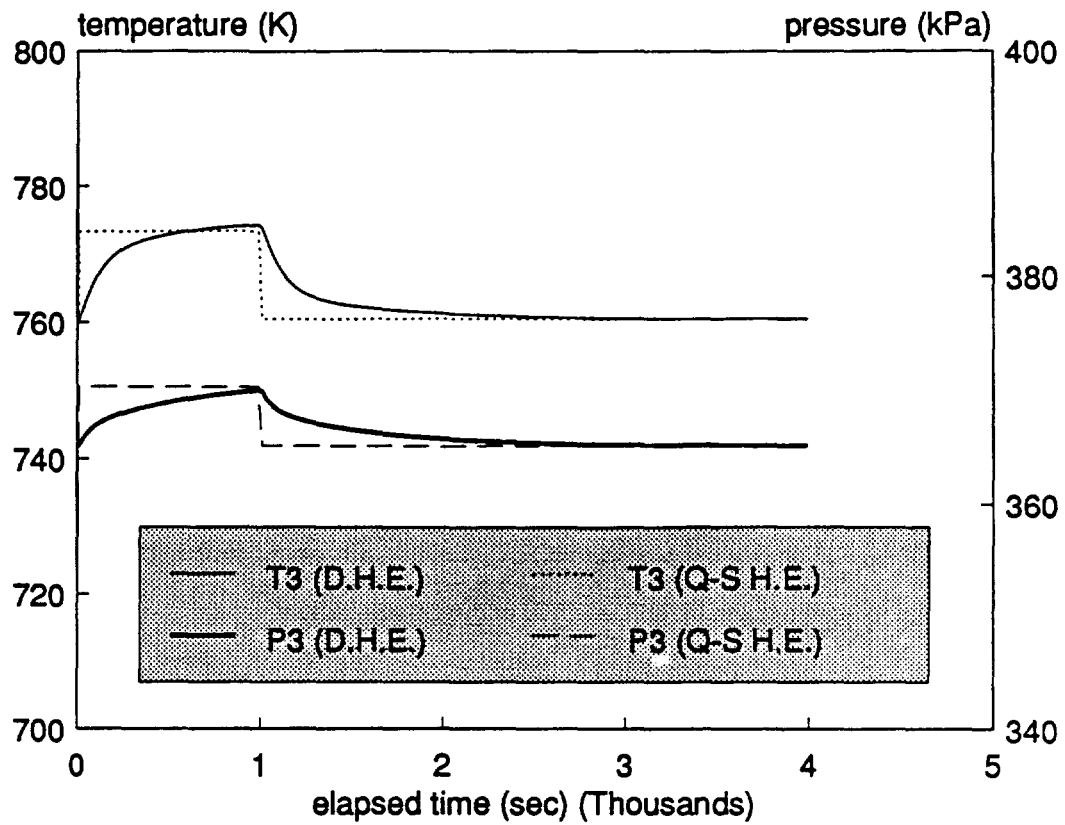


Fig. 4.12 Response of recuperator outlet parameters



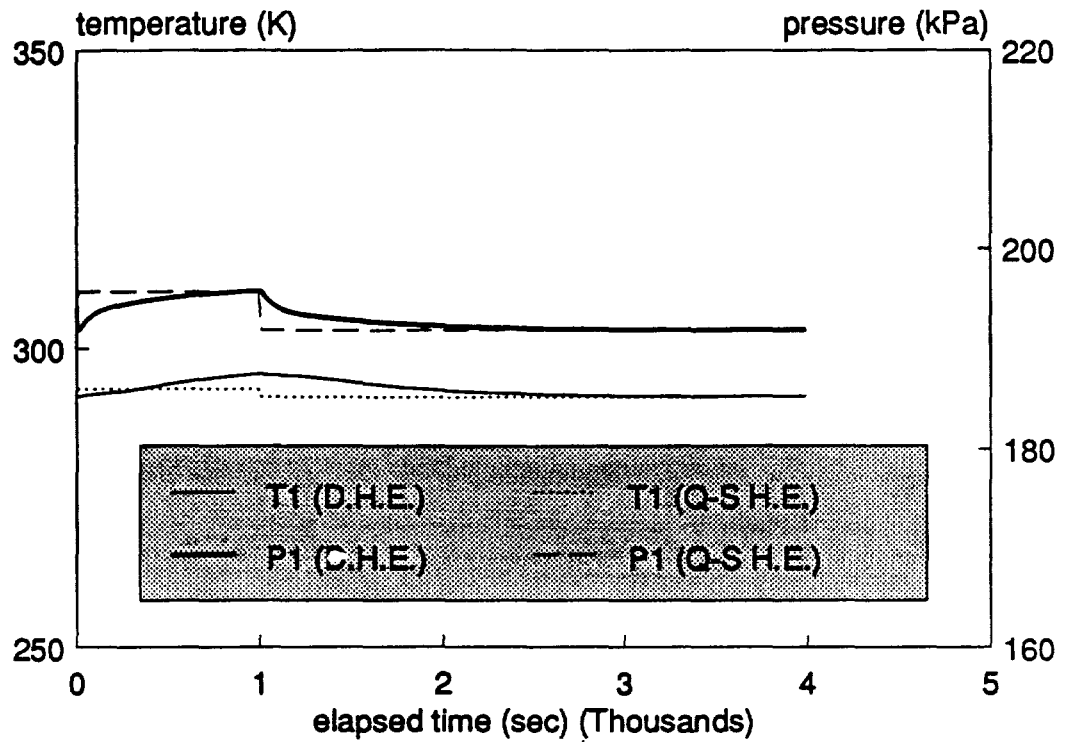


Fig. 4.13 Response of gas cooler outlet parameters

#### 4.2.1.3 Response to a Sinusoid of Receiver Salt Temperature

A sinusoid variation of receiver temperature produces the transients shown in Fig. 4.14 to 4.19. The frequency of the sinusoid is 0.016 Hz. The receiver outlet temperature lags the salt temperature. The gas cooler outlet temperature lags the recuperator outlet temperature which in turn lags the receiver outlet temperature. The outlet temperature of the down stream components are not a sinusoid response for the first few cycles of the receiver salt temperature because of the lag. The mass-flow rate and pressure variations in the system also lag the salt temperature. As shown in Fig. 4.19, the response of radiator outlet temperature lags the gas cooler outlet temperature. The amplitude of the radiator outlet-temperature oscillation is small because of the bigger heat capacity of the coolant and the large radiator panels. At the beginning of the transient process, there is a "starting transient". After several cycles in the salt temperature, the sinusoidal variation of other parameters established with various phase lags from component to component.

#### 4.2.1.4 Response to a Ramp of Net Mechanical Power Output of the Turbomachinery

The responses of parameters in the system to a ramp change of net mechanical power output are shown in Fig. 4.20 to 4.25. The net mechanical power demand was increased 1.0 kW over a 0.25 second period, which means that the compressor input power was decreased 1.0 kW. The integrator time step is  $5.0 \times 10^{-5}$  second. It can be seen that the ramp variation of the net output mechanical power causes a ramp variation of compressor outlet temperature. It can be seen in Fig. 4.21 that the turbine outlet pressure and temperature increased at the beginning of the transient process. This is the result of the decrease in pressure ratio of the turbine which is caused by the decrease of mass-flow rate and the lagging of the receiver outlet temperature.

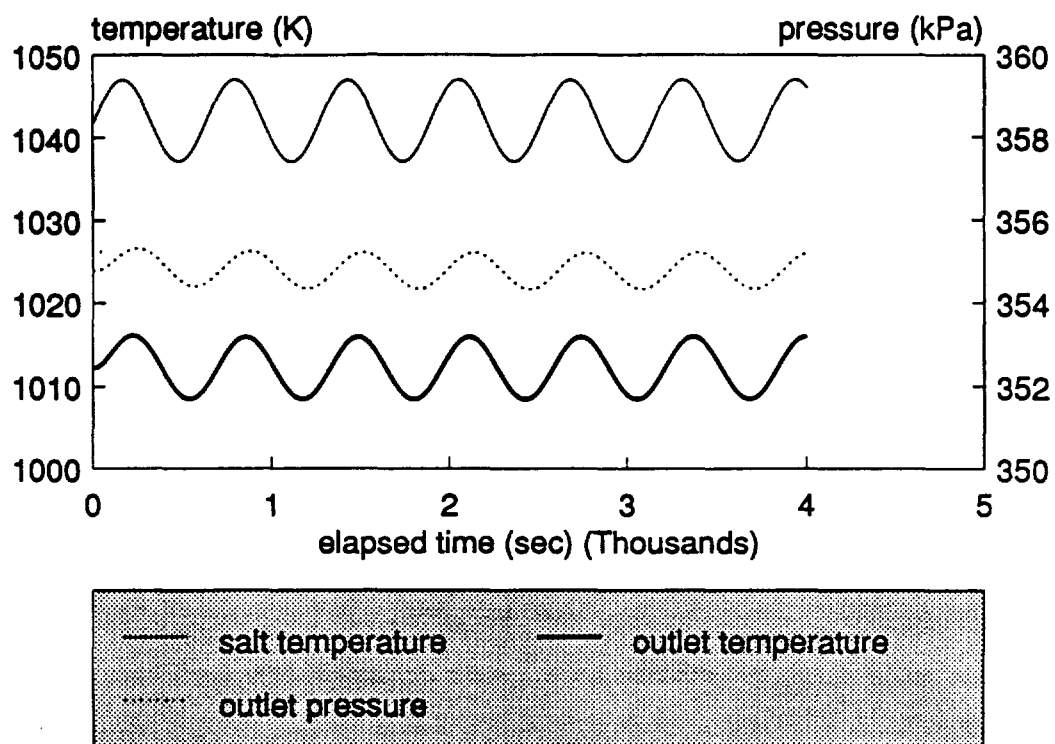


Fig. 4.14 Response of receiver outlet parameters (to sinusoidal driver)

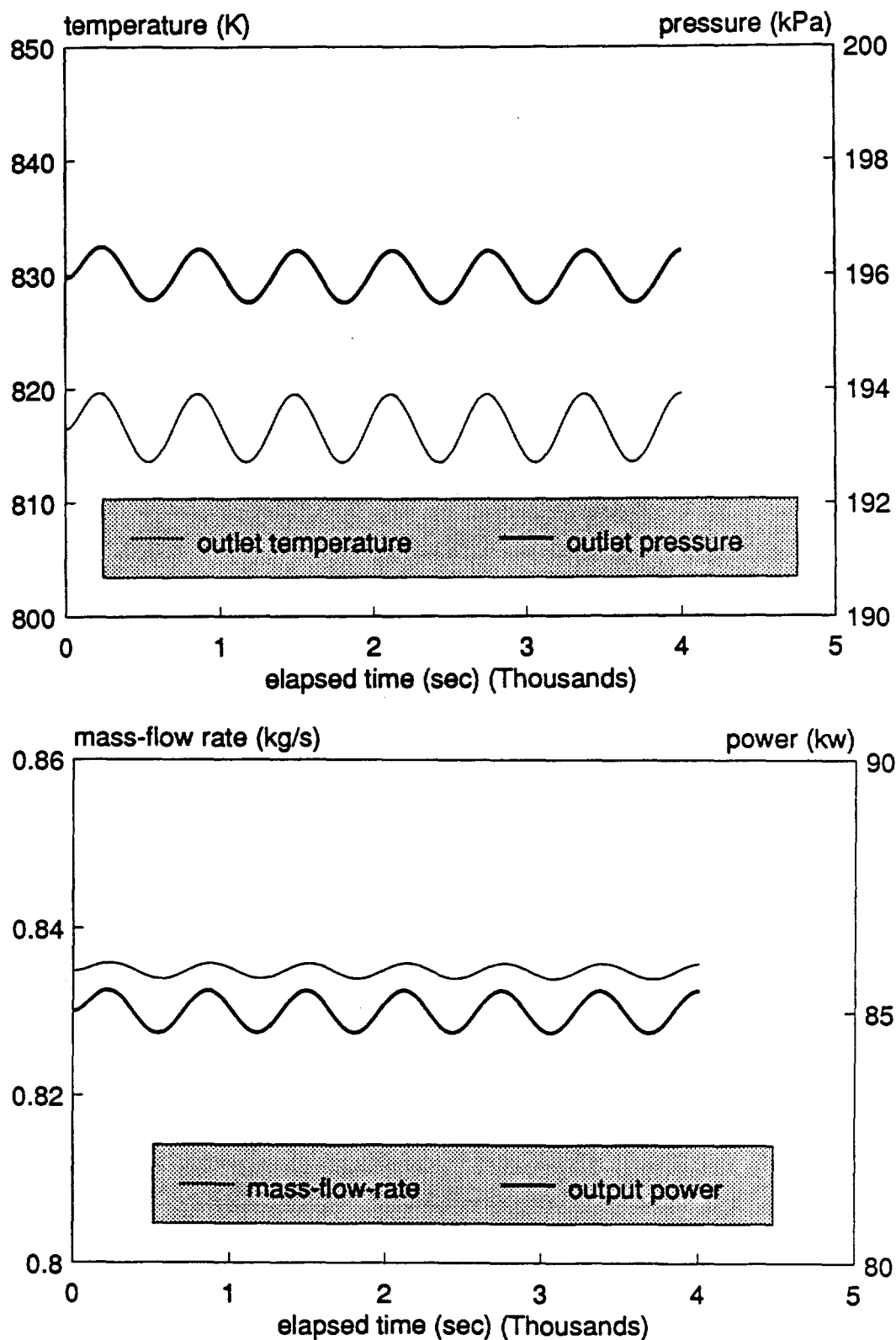


Fig. 4.15 Response of turbine outlet parameters (to sinusoidal driver)

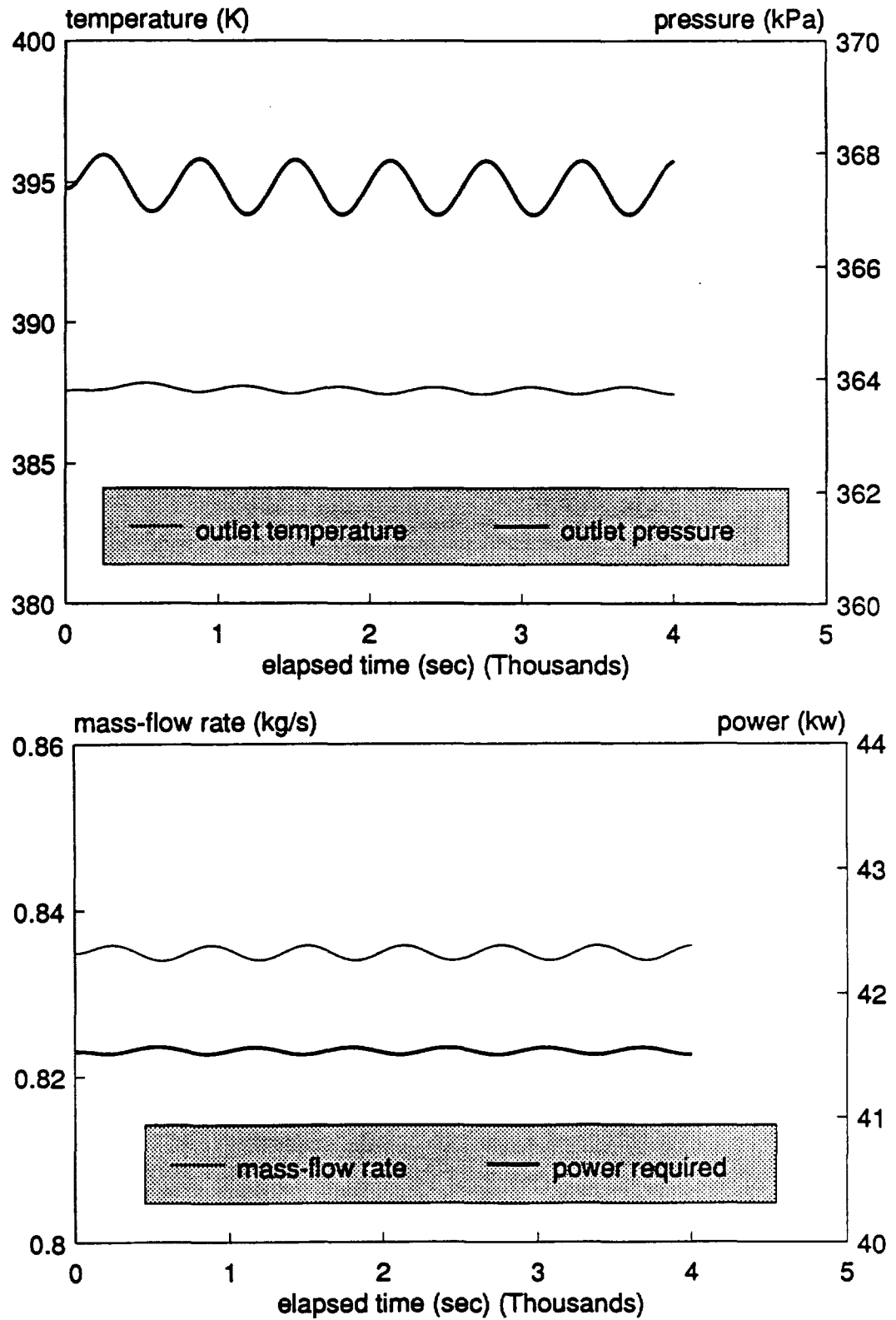


Fig. 4.16 Response of compressor outlet parameters (to sinusoidal driver)

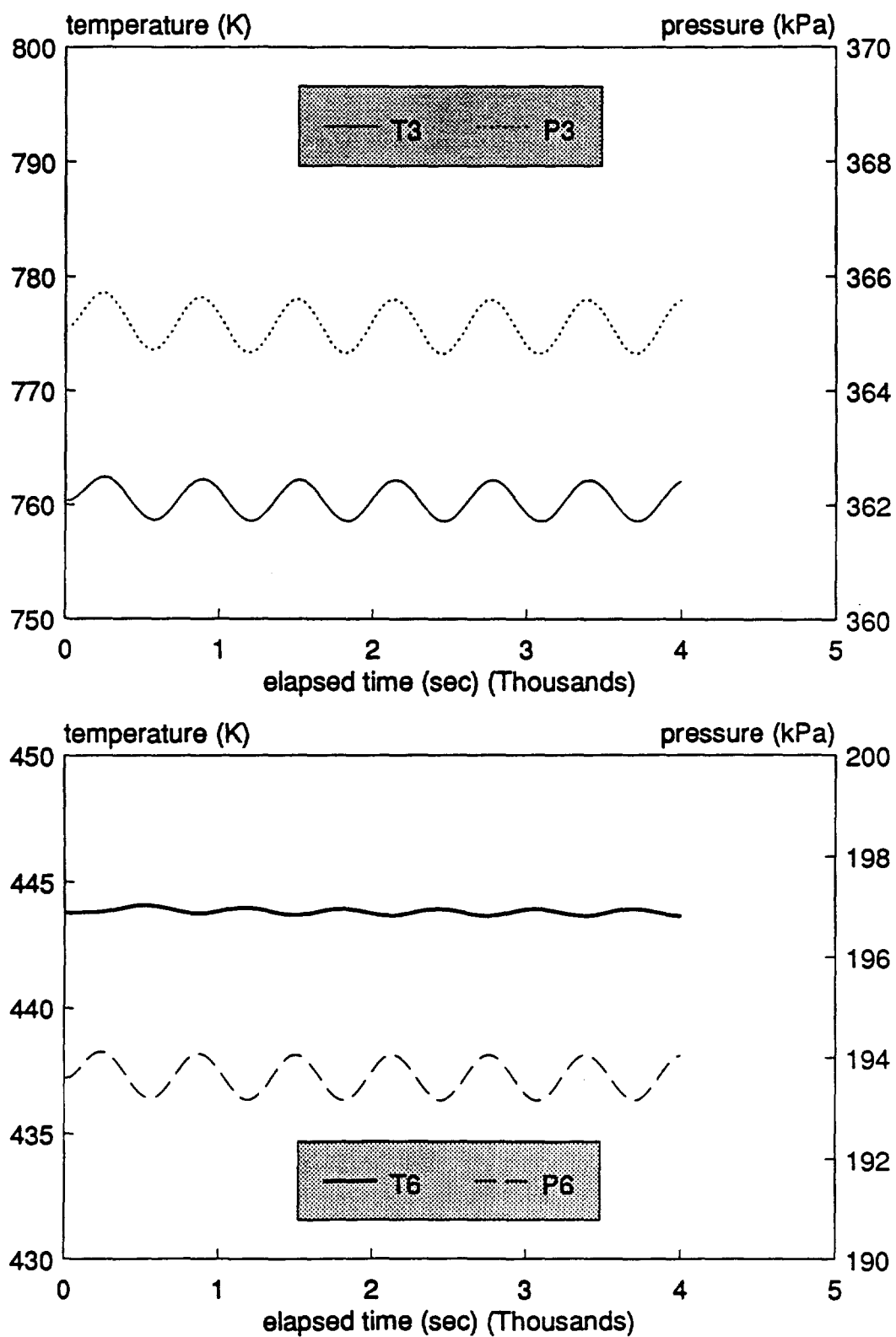


Fig. 4.17 Response of recuperator outlet parameters (to sinusoidal driver)

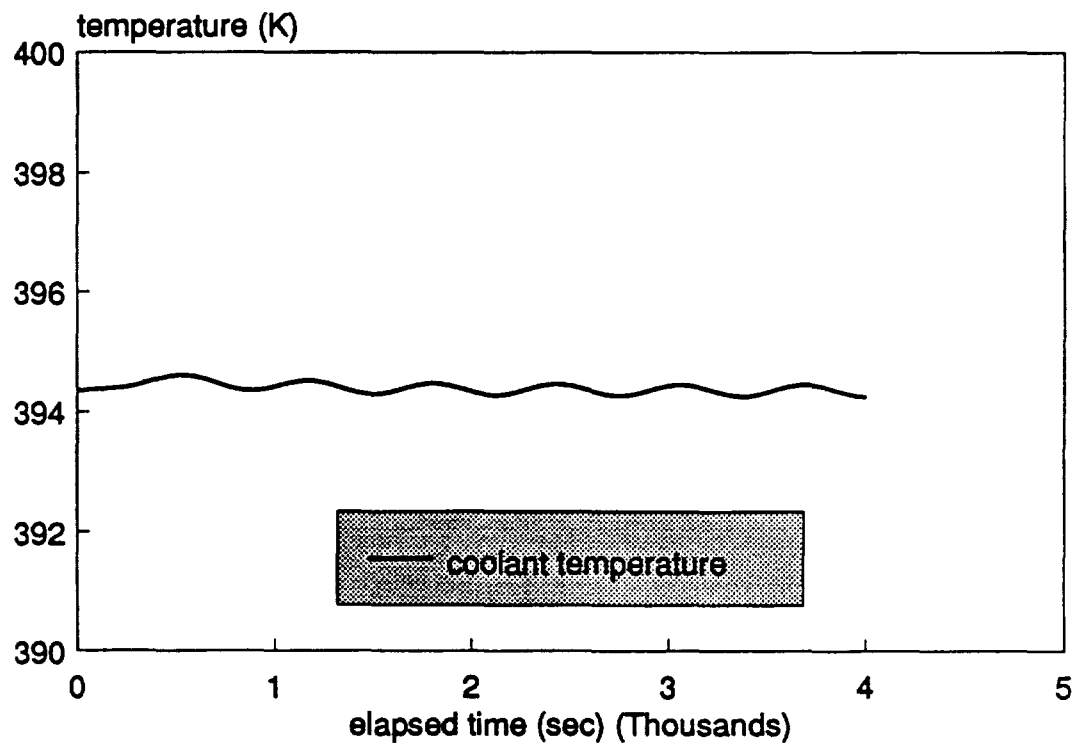
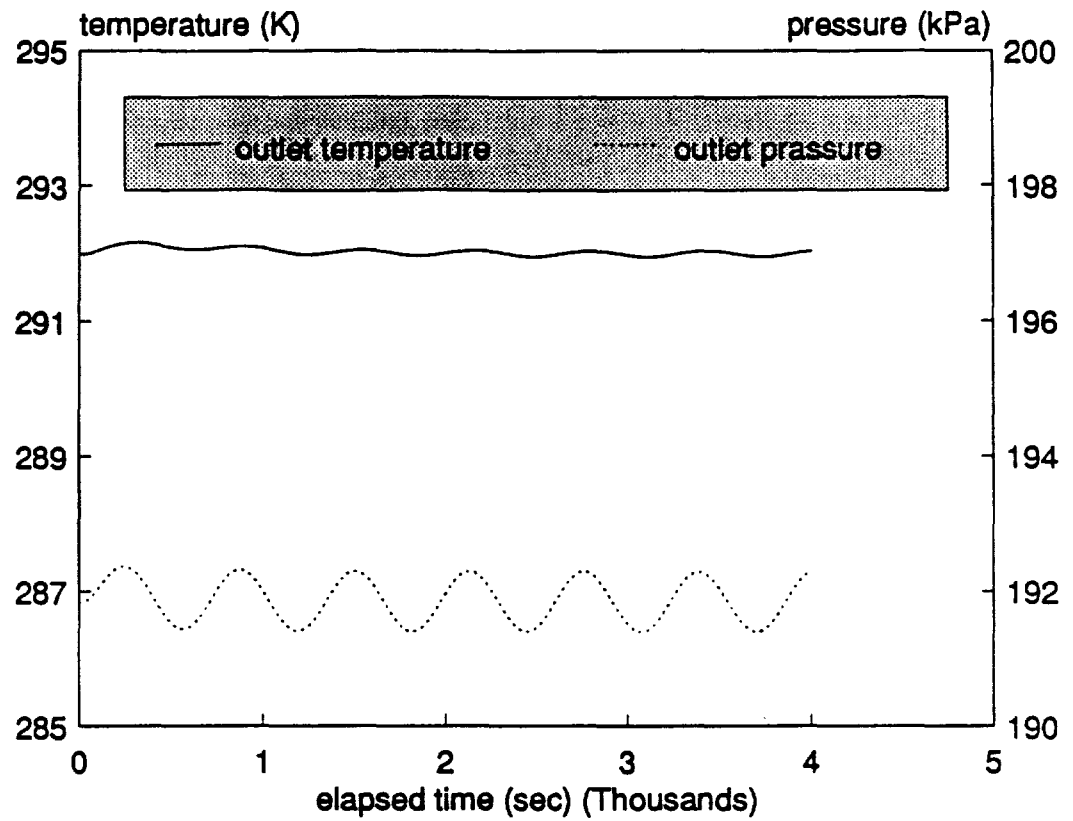


Fig. 4.18 Response of gas cooler outlet parameters (to sinusoidal driver)

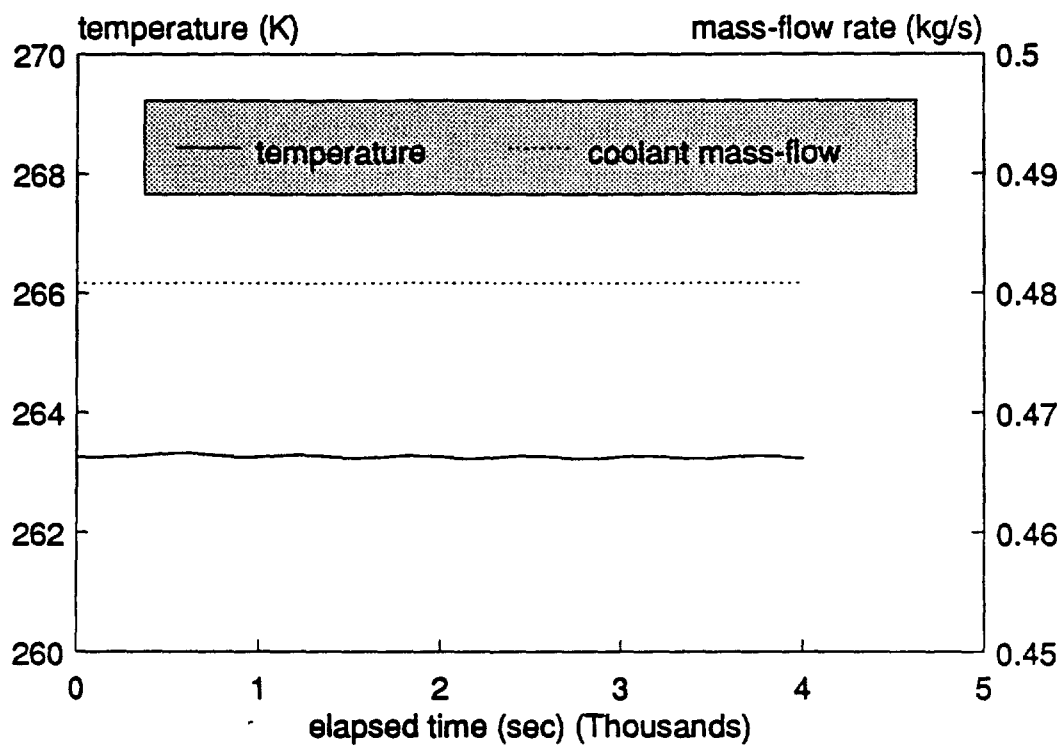


Fig. 4.19 Response of radiator outlet parameters (to sinusoidal driver)



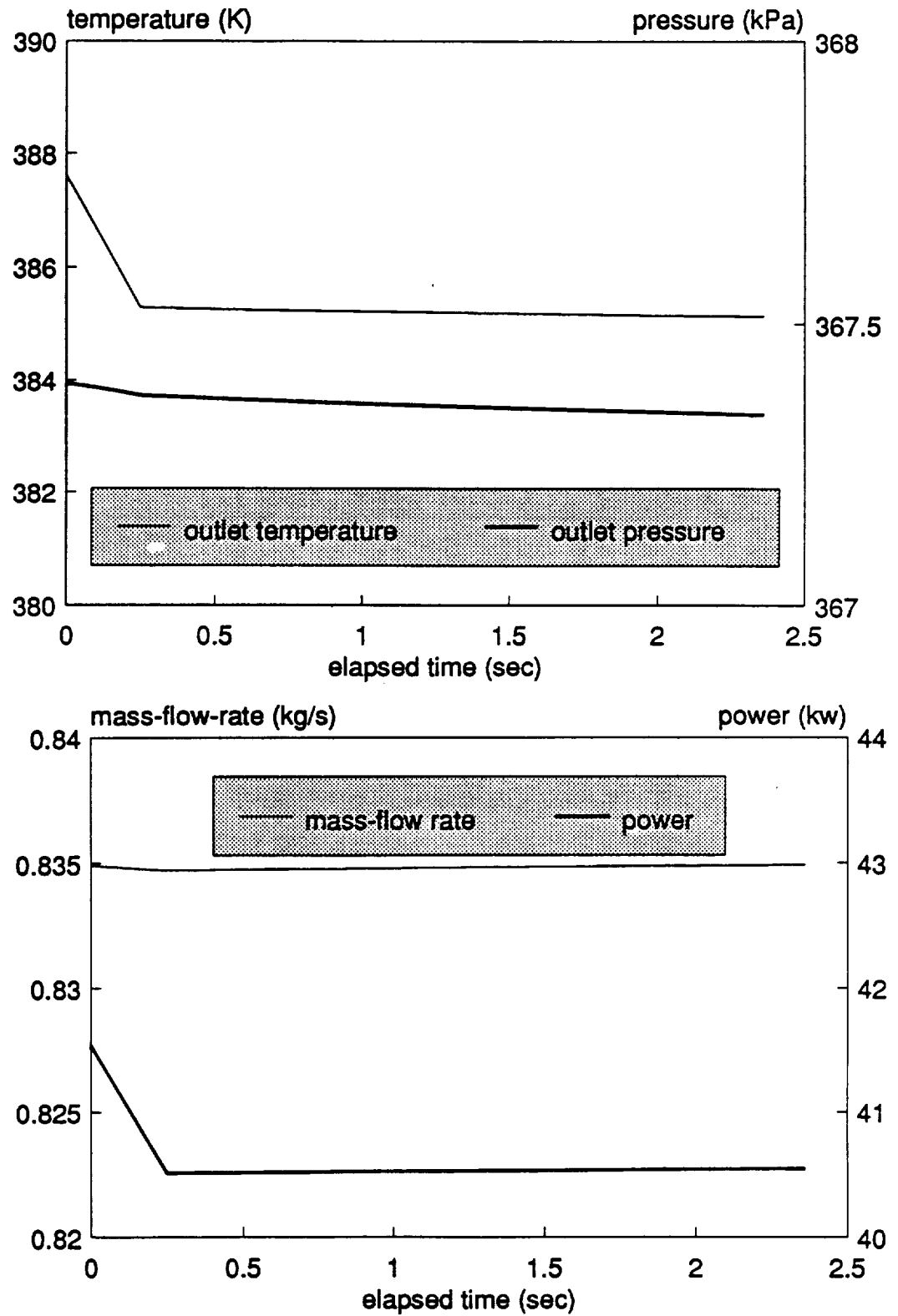


Fig. 4.20 Response of compressor outlet parameters (to ramp of output power)

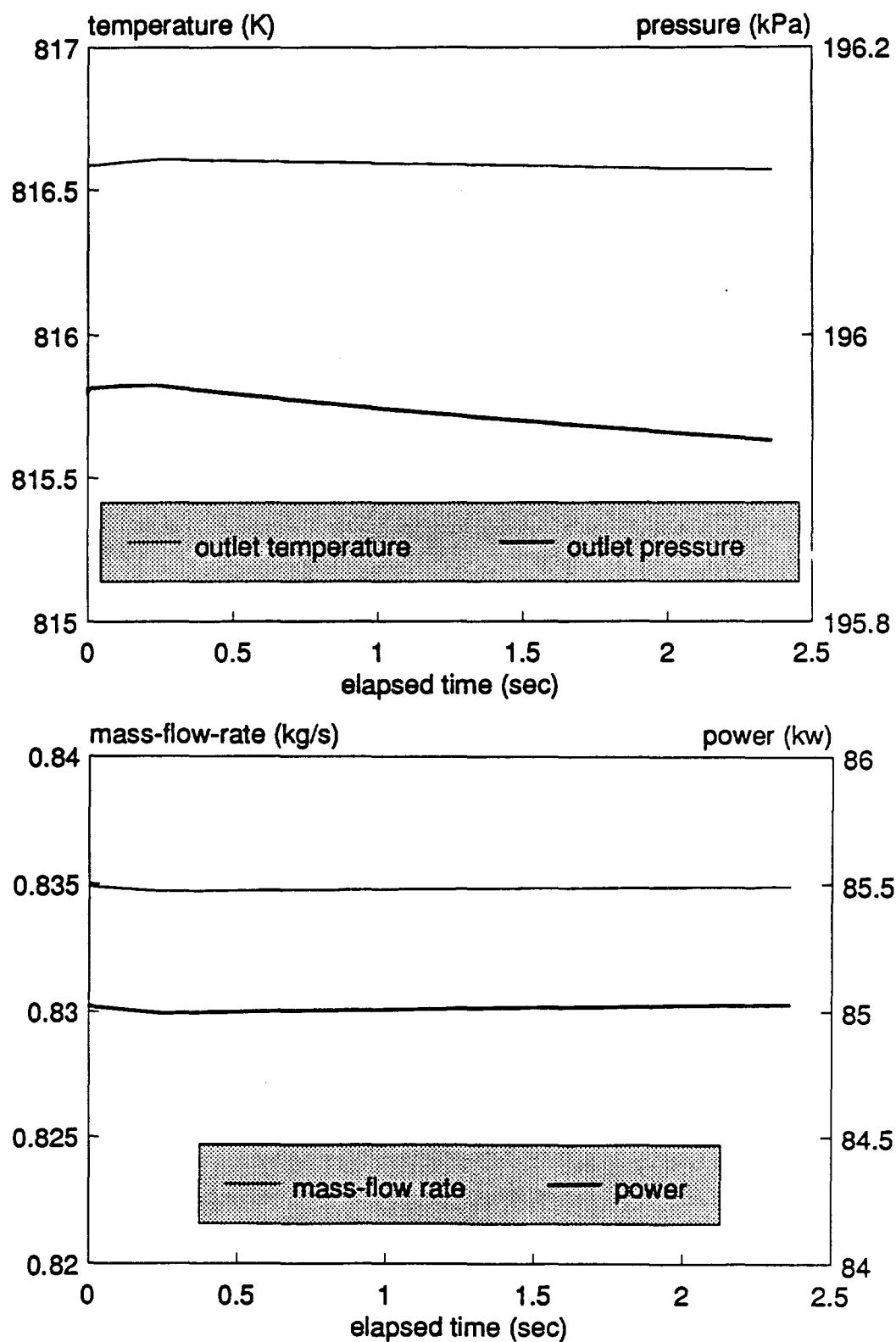


Fig. 4.21 Response of turbine outlet parameters (to ramp of output power)

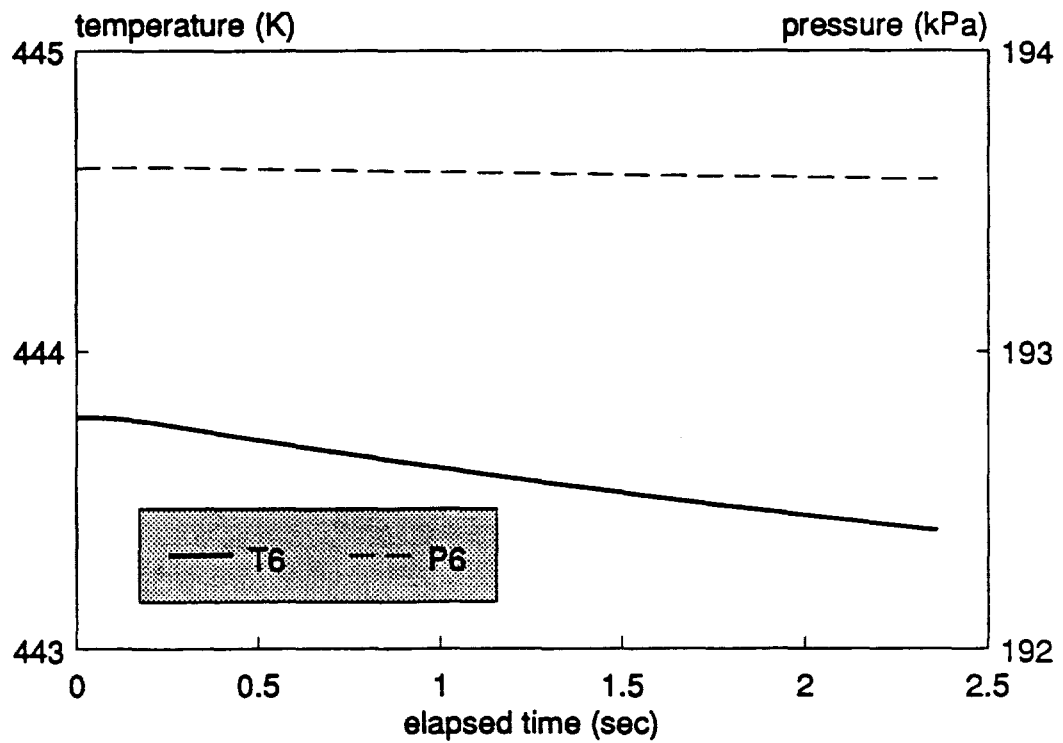
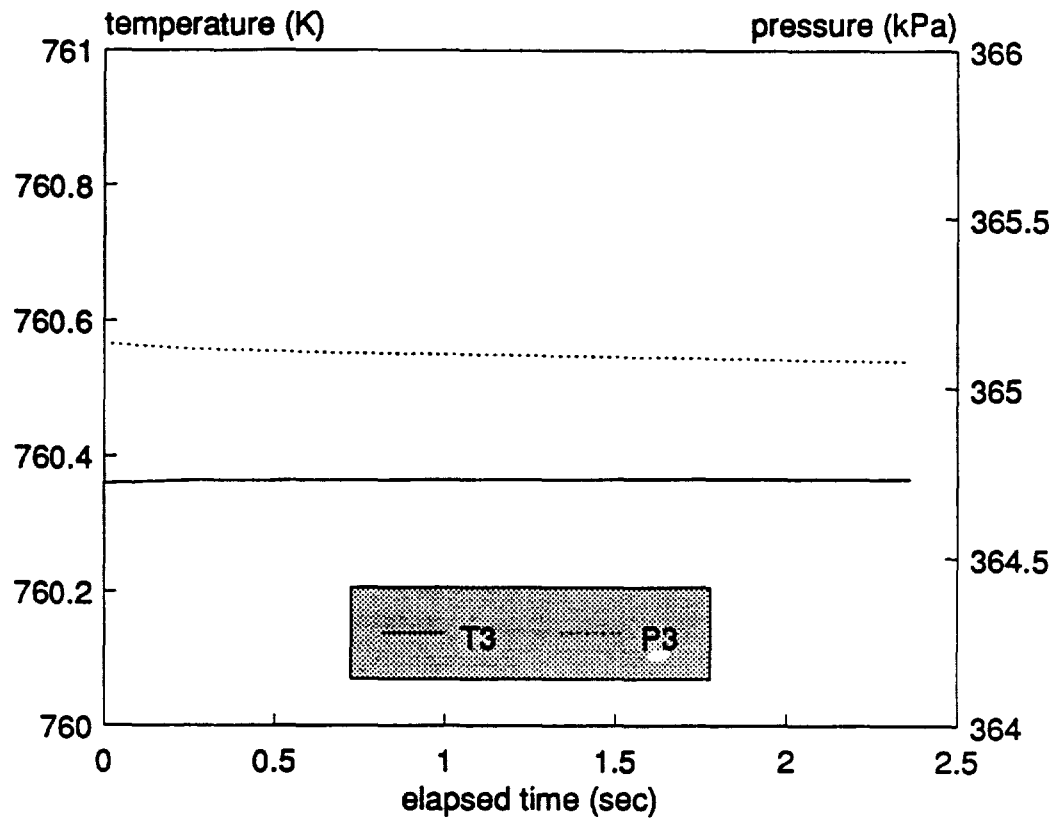


Fig. 4.22 Response of recuperator outlet parameters (to ramp of output power)

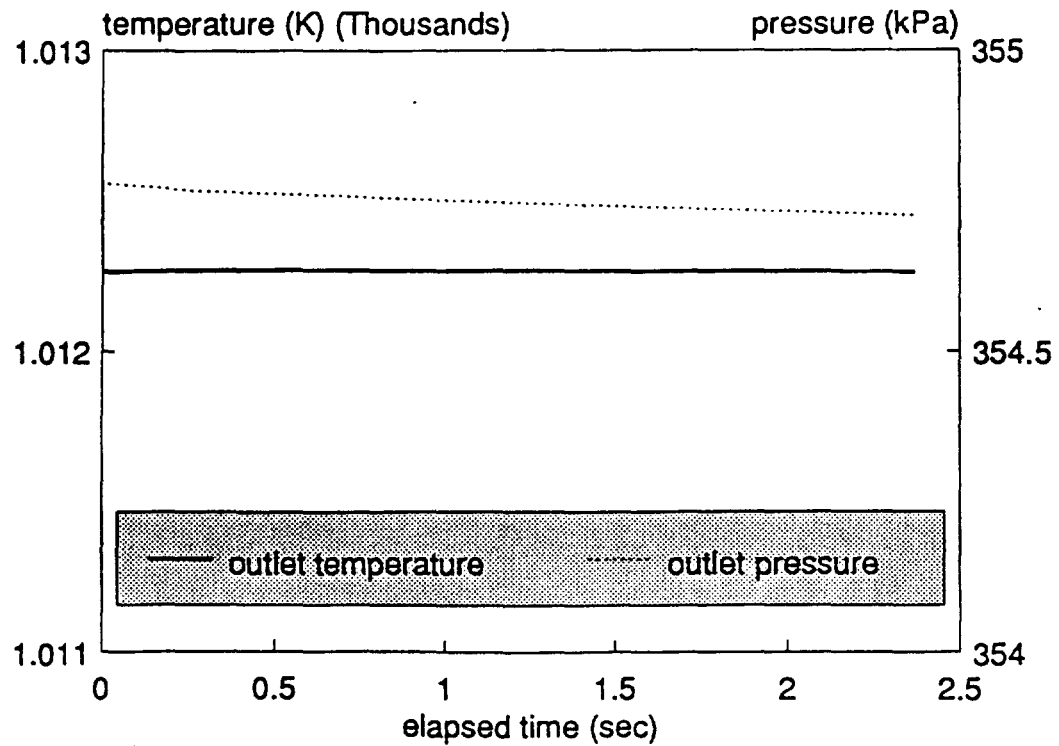


Fig. 4.23 Response of receiver outlet parameters (to ramp of output power)

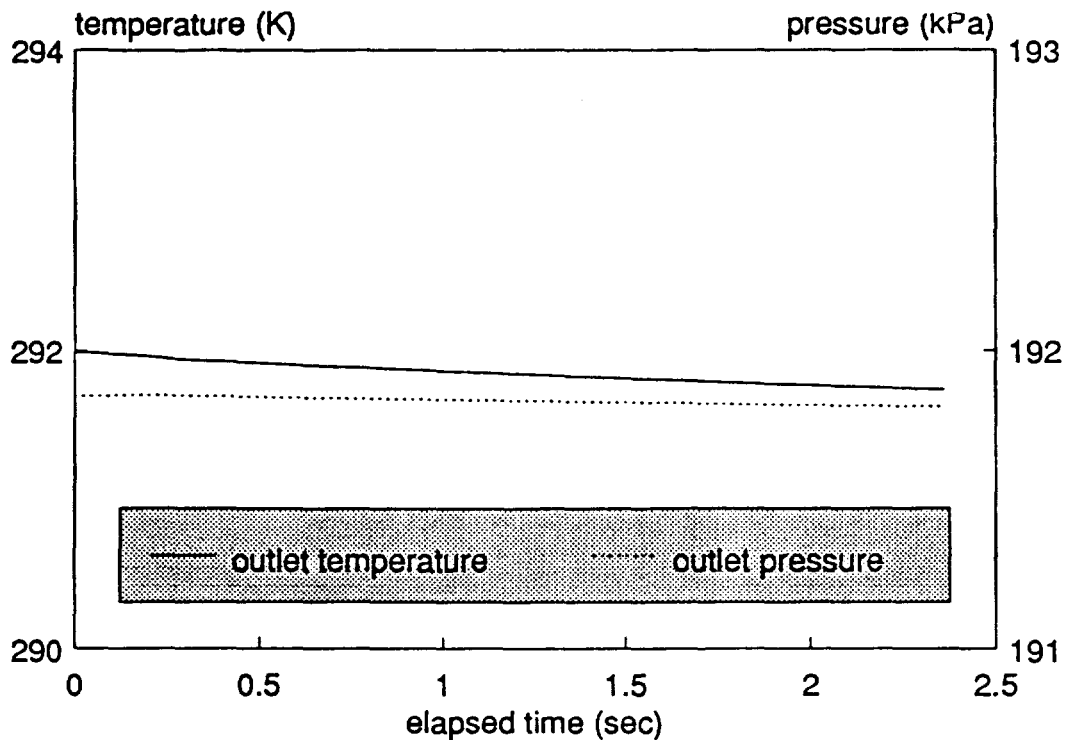


Fig. 4.24 Response of gas cooler outlet parameters (to ramp of output power)

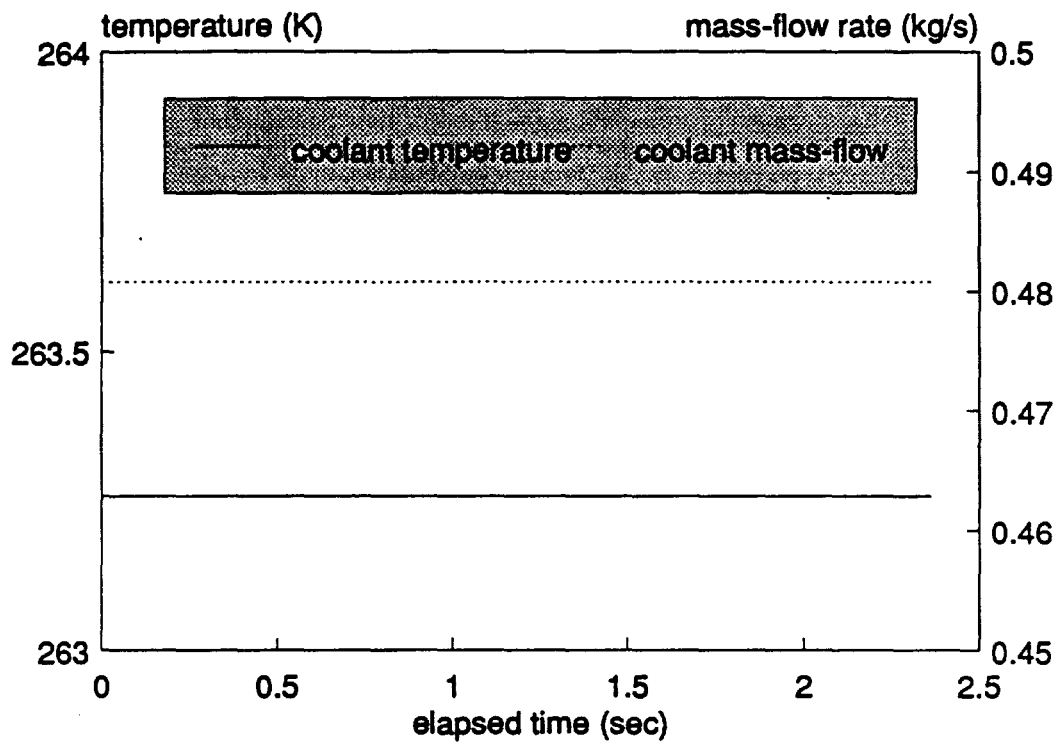


Fig. 4.25 Response of radiator outlet parameters (to ramp of output power)

#### 4.2.2 Performance Simulation by the Dynamic Heat Exchangers/Dynamic Turbomachines System Model

The dynamic heat exchangers/dynamic turbomachines system model described in section 3.4 is used to simulate transient processes in the Solar-Powered Closed Regenerative Turbine-Engine Cycle. The integrator time-step had both an upper bound of  $8 \times 10^{-5}$  second and a lower bound of  $1 \times 10^{-5}$  second. The upper bound is imposed by traditional numerical stability considerations. The lower bound is required to prevent the procedure for computing mass storage in the machine from producing a negative (inflow) velocity at the component exit. Following the discussion in section 2.2.4, the minimum integrator time-step was chosen as  $2.5 \times 10^{-5}$  second. The iteration required for the dynamic turbine and compressor models and the small integrator time step greatly increased the CPU time needed for simulation. This limits the usage of the dynamic heat exchangers/dynamic turbomachines system model for long elapsed time simulation.

##### 4.2.2.1 Response to a Step of Receiver Salt Temperature

The response of the system parameters to a 10 K step of receiver salt temperature are shown in Fig. 4.26 to 4.31. The elapsed time for the simulated transient process is 5 seconds. It can be seen that the process is dominated by the slow transient process in the heat exchangers. The responses of parameters in the system to the perturbation in salt temperature in the receiver are very slow as shown in Fig. 4.27 to 4.31.

##### 4.2.2.2 Response to a Sinusoidal Variation of Receiver Salt Temperature

The transients produced by a sinusoidal variation of receiver temperature are shown in Fig. 4.32 to 4.37. The amplitude of the sinusoid is 50 K and the frequency of the sinusoid is 1.6 Hz. As shown in Fig. 4.32, the outlet temperature of the receiver

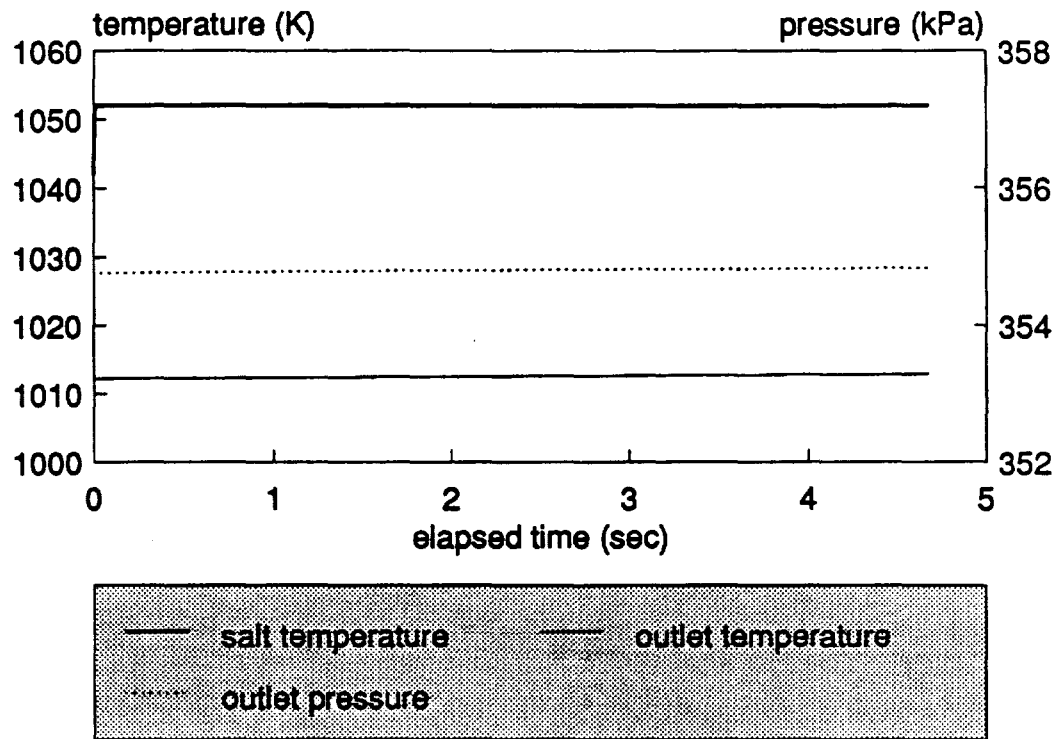


Fig. 4.26 Response of receiver outlet parameters (to ramp of salt temperature)

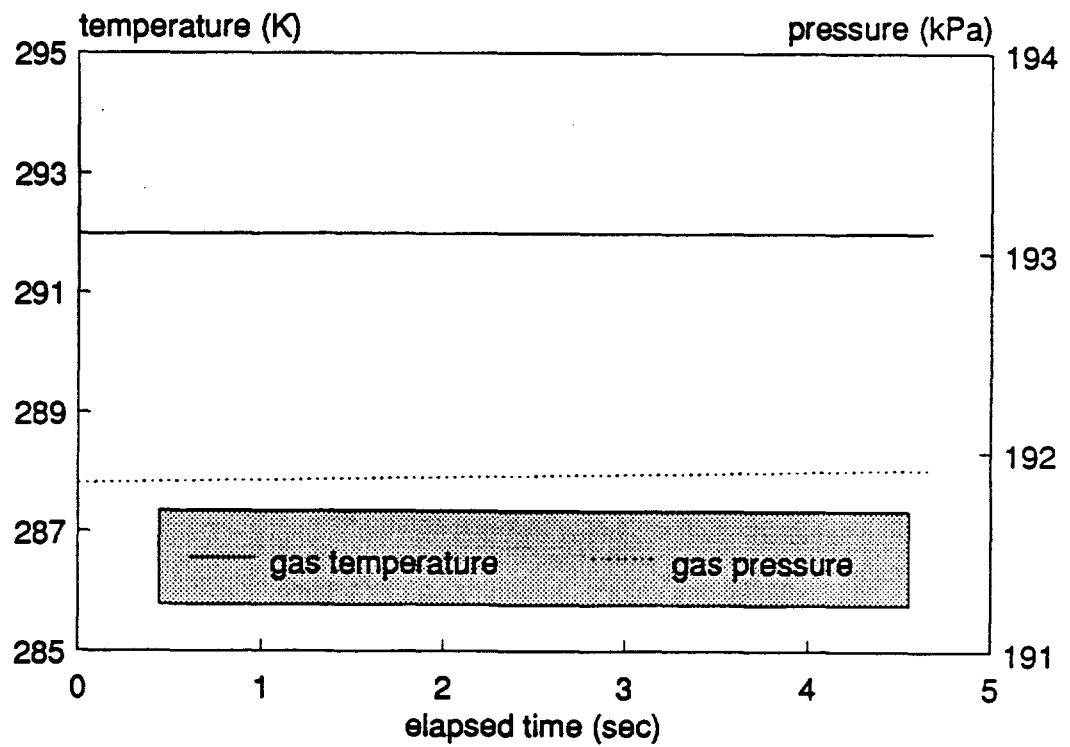


Fig. 4.27 Response of gas cooler outlet parameters (to ramp of salt temperature)

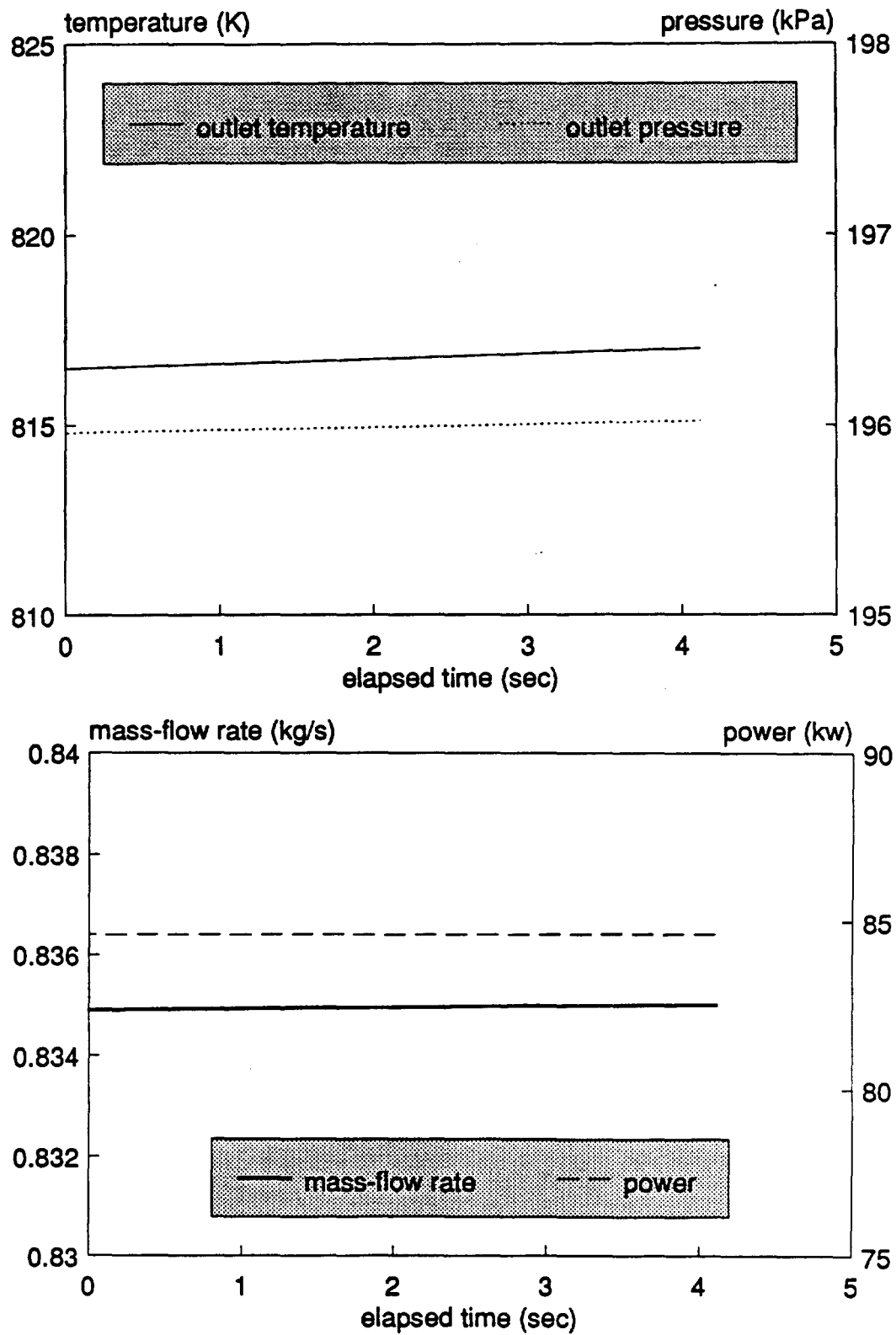


Fig. 4.28 Response of turbine outlet parameters (to ramp of salt temperature)



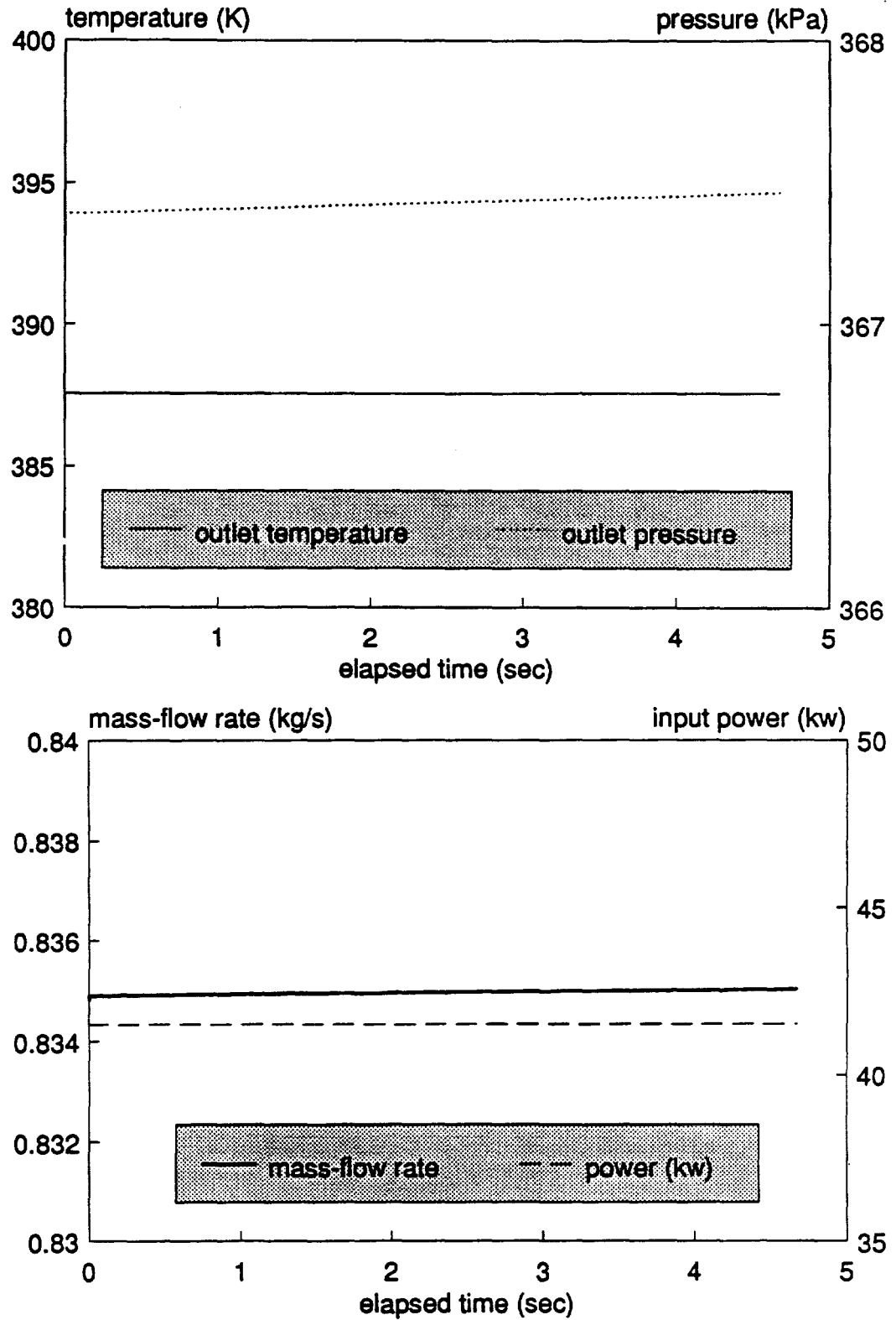


Fig. 4.29 Response of compressor outlet parameters (to ramp of salt temperature)

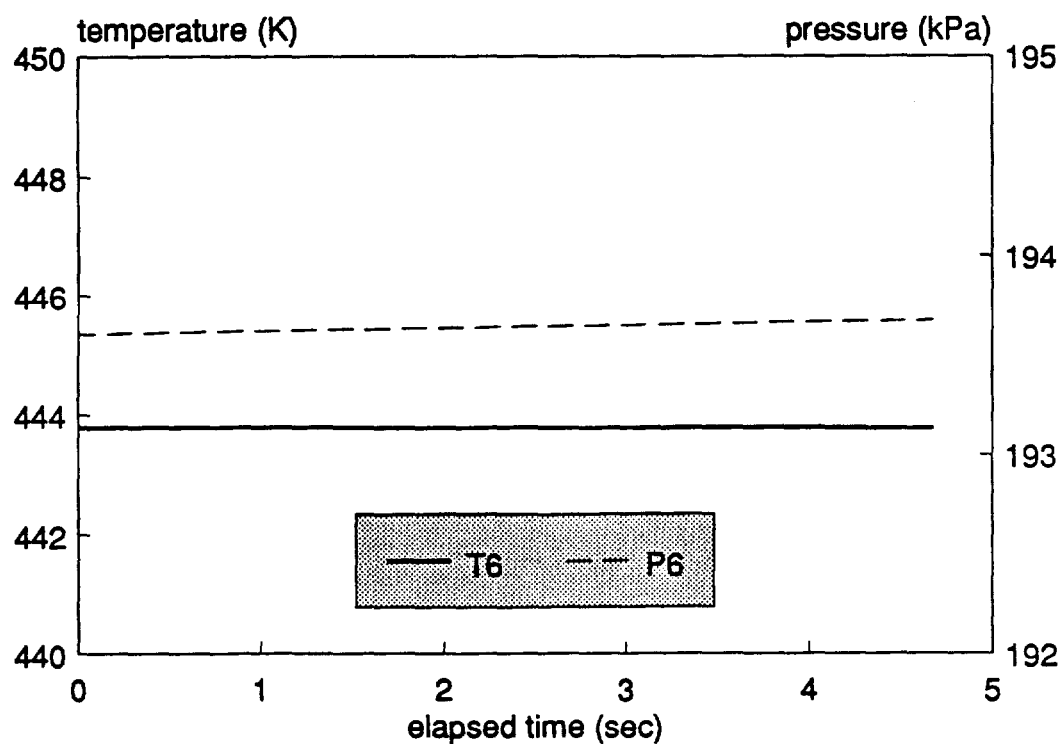
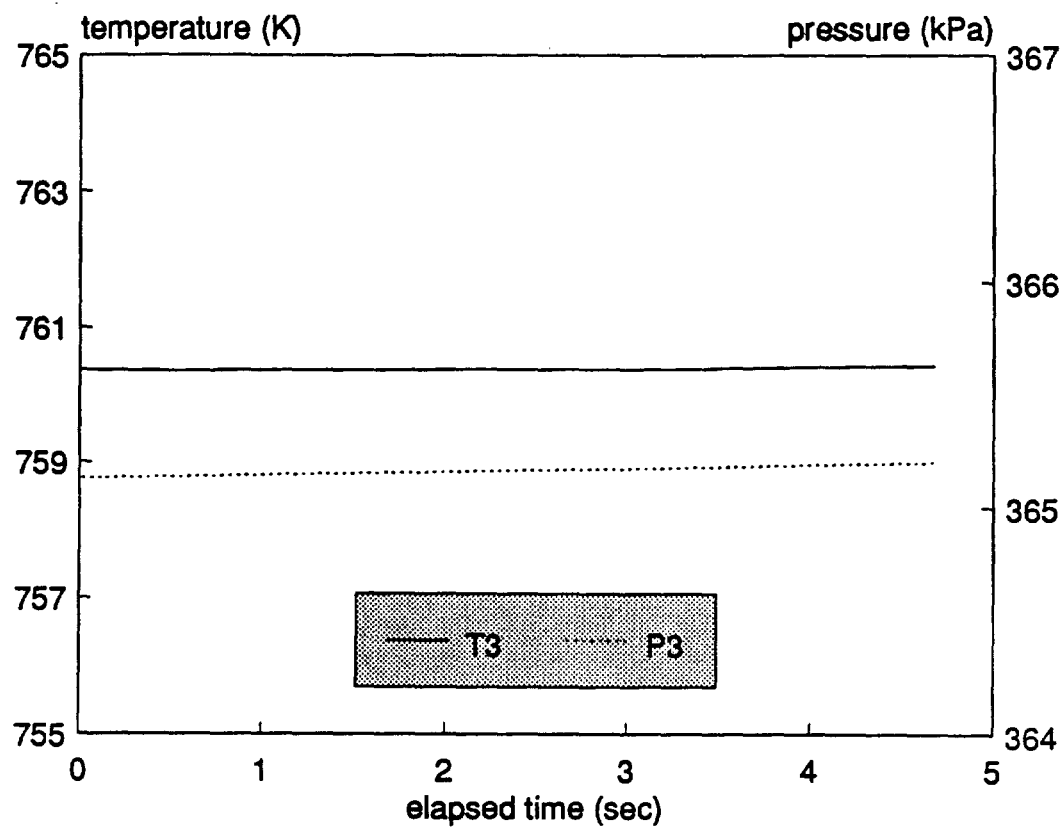


Fig. 4.30 Response of recuperator outlet parameters (to ramp of salt temperature)

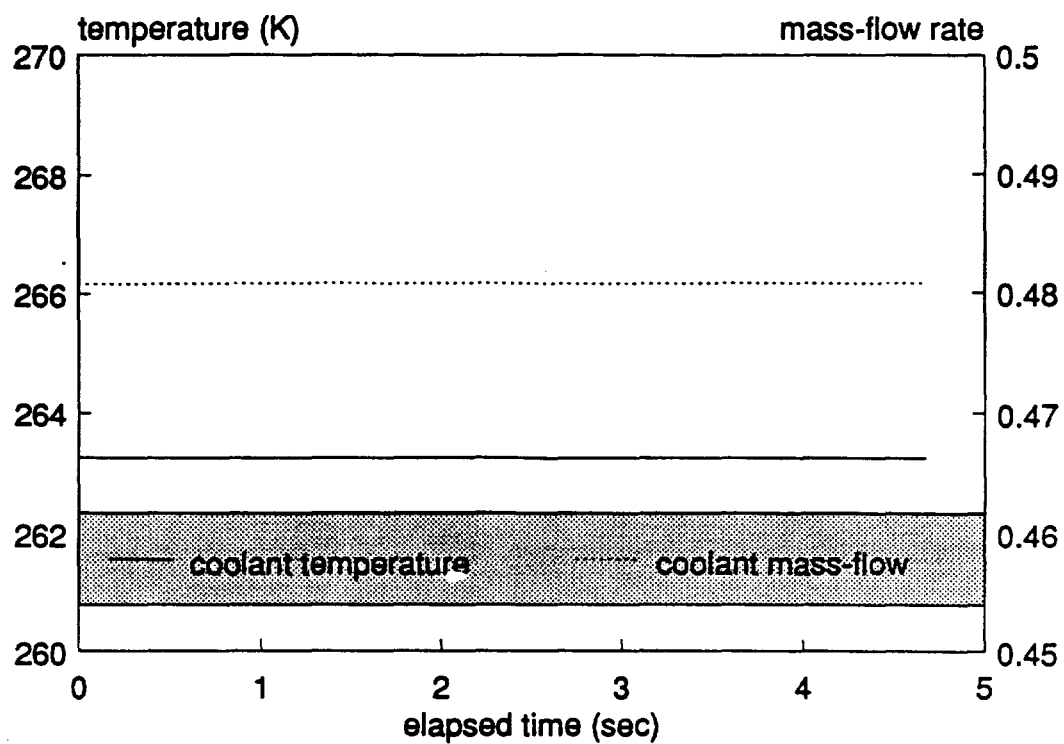


Fig. 4.31 Response of radiator outlet parameters (to ramp of salt temperature)

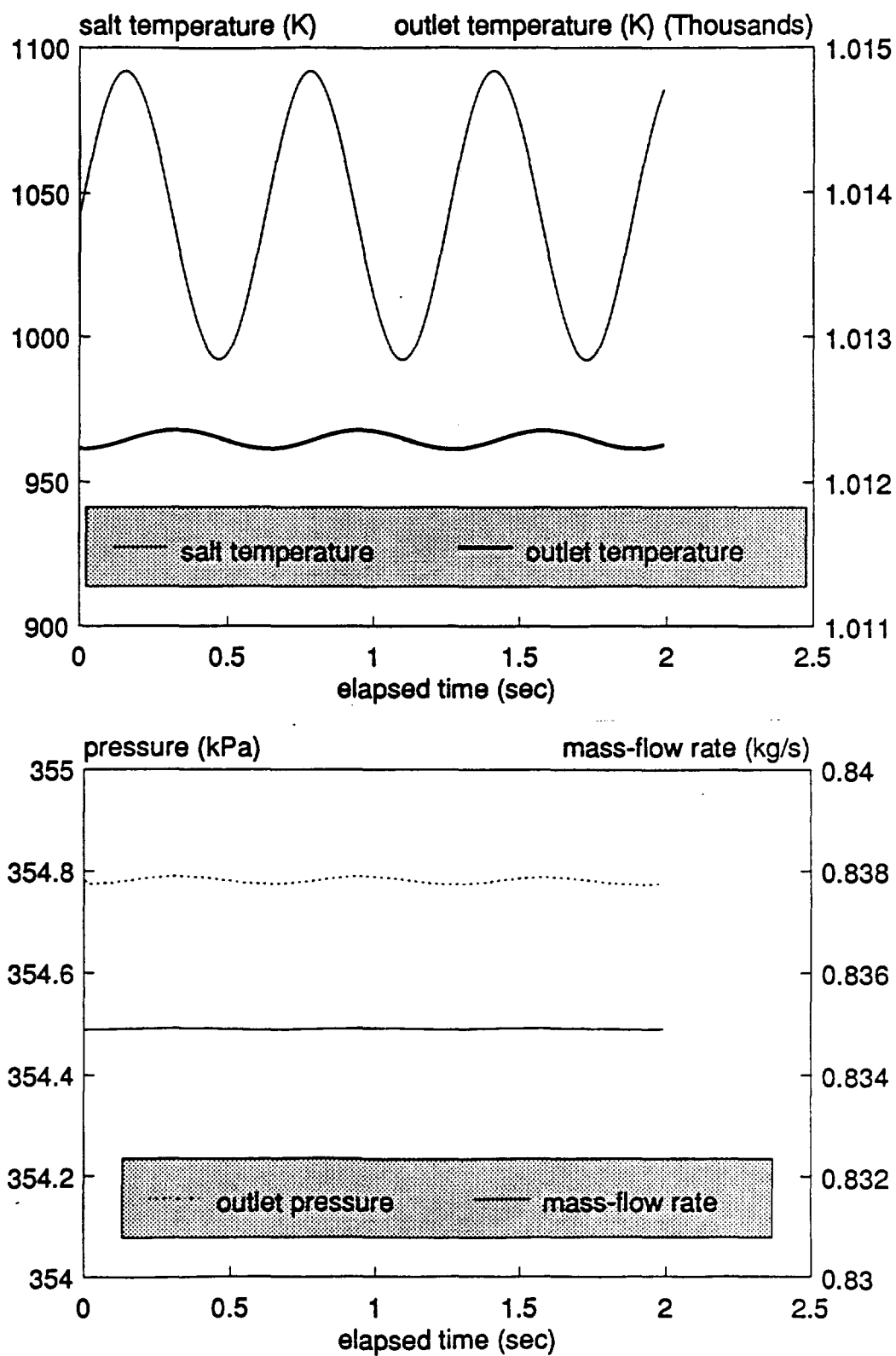


Fig. 4.32 Response of receiver outlet parameters (to sinusoidal salt temp.)

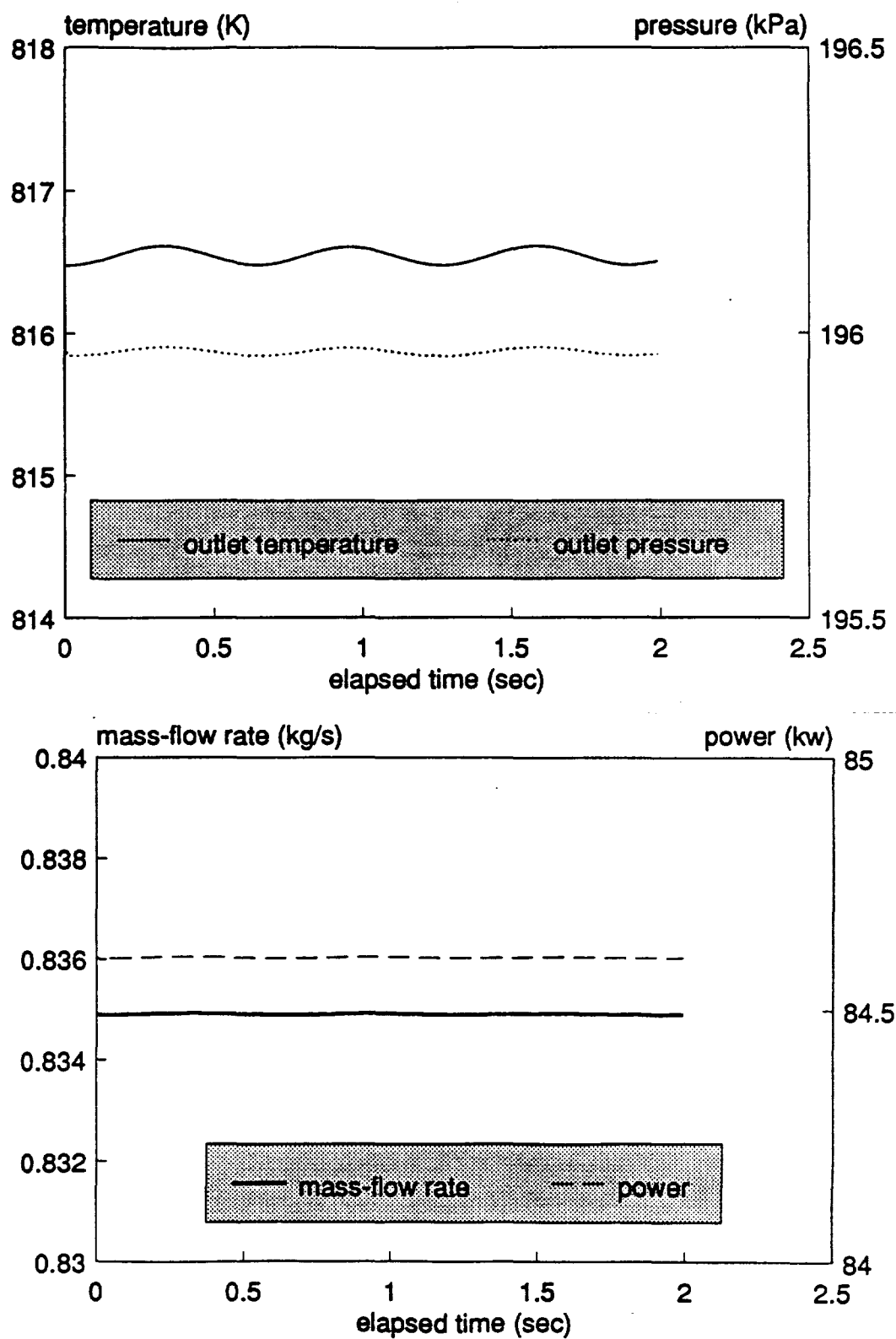


Fig. 4.33 Response of turbine outlet parameters (to sinusoidal salt temp.)

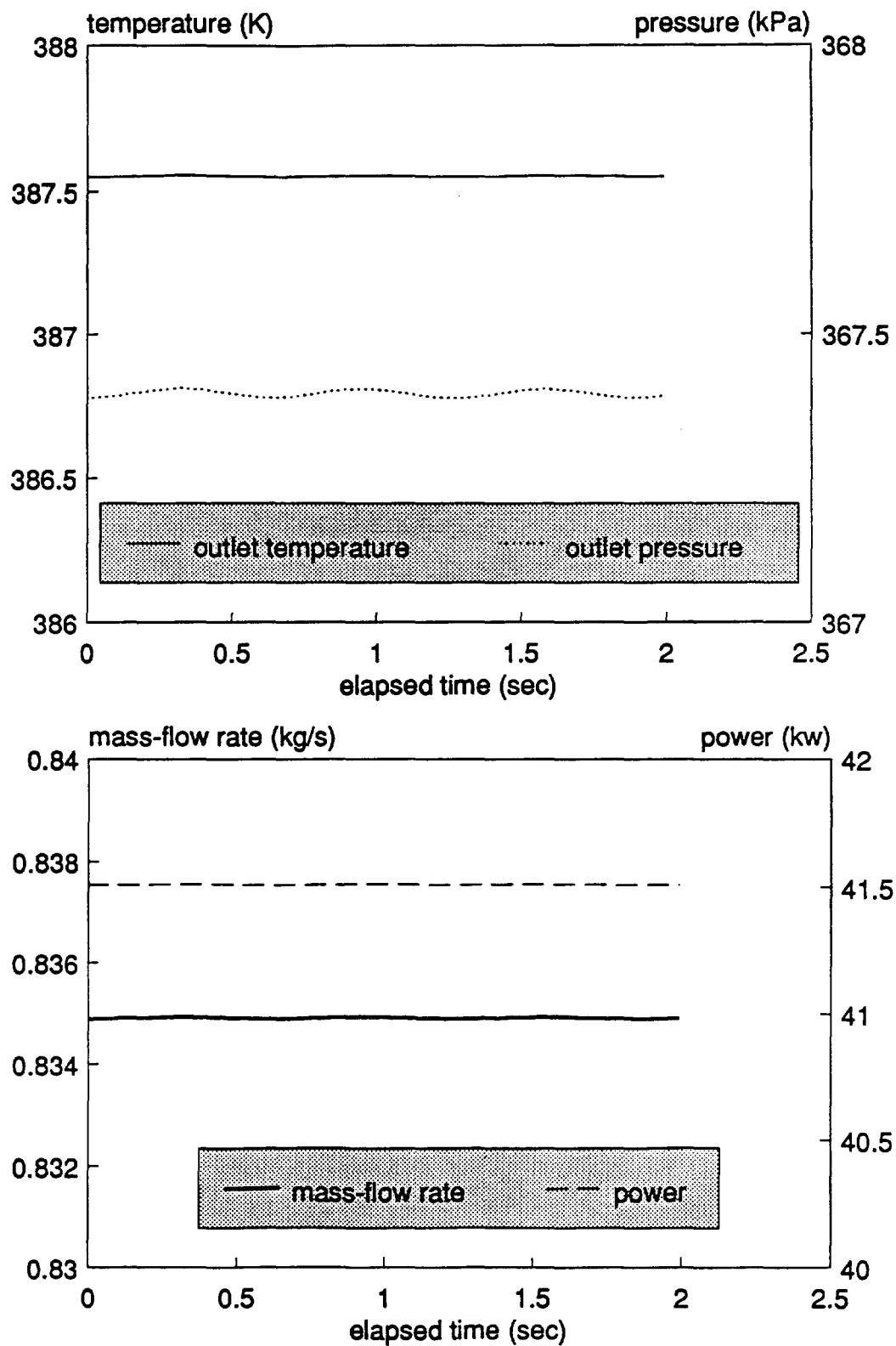


Fig. 4.34 Response of compressor outlet parameters (to sinusoidal salt temp.)

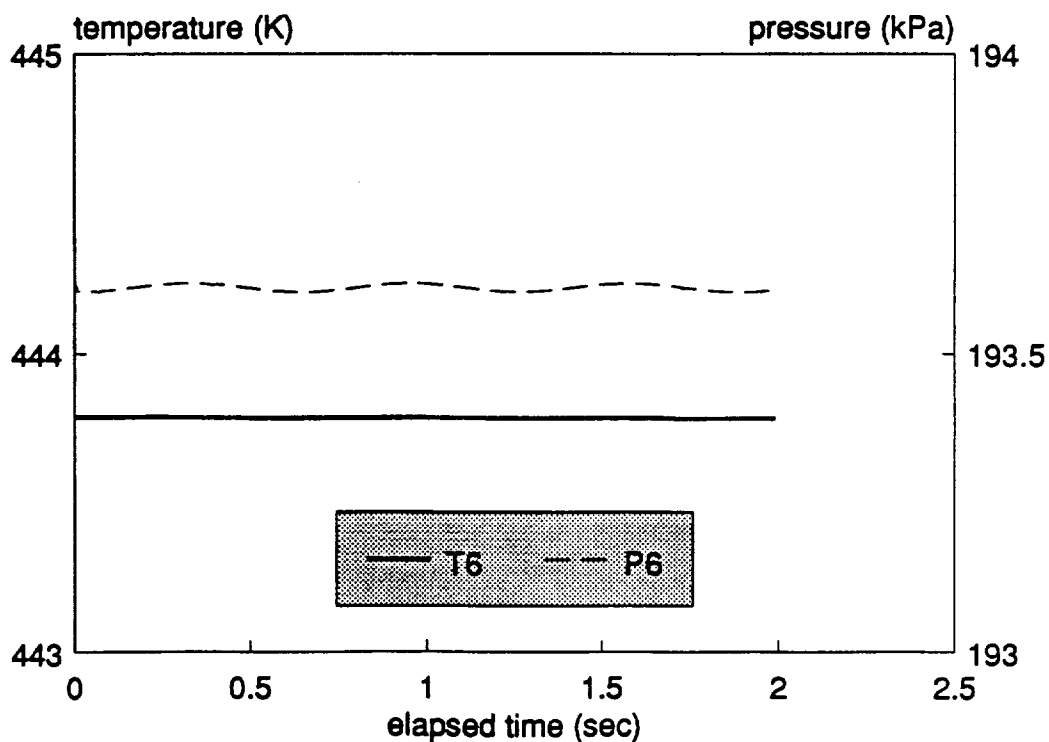
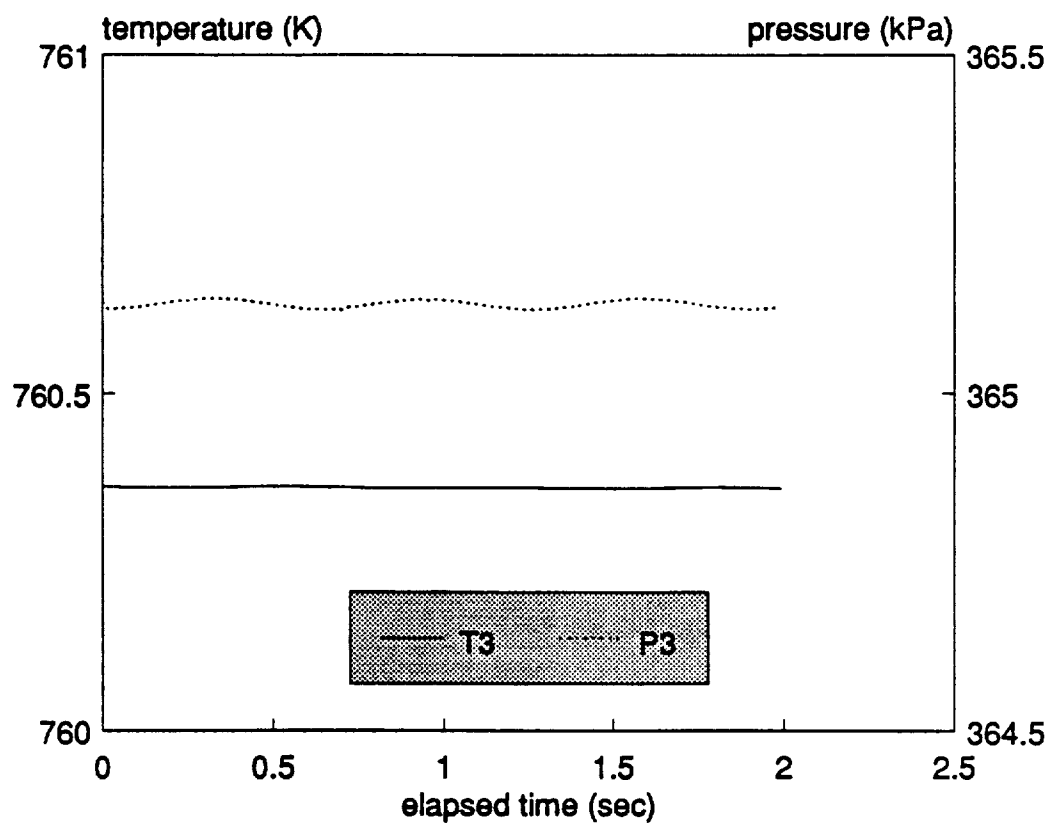


Fig. 4.35 Response of recuperator outlet parameters (to sinusoidal salt temp.)

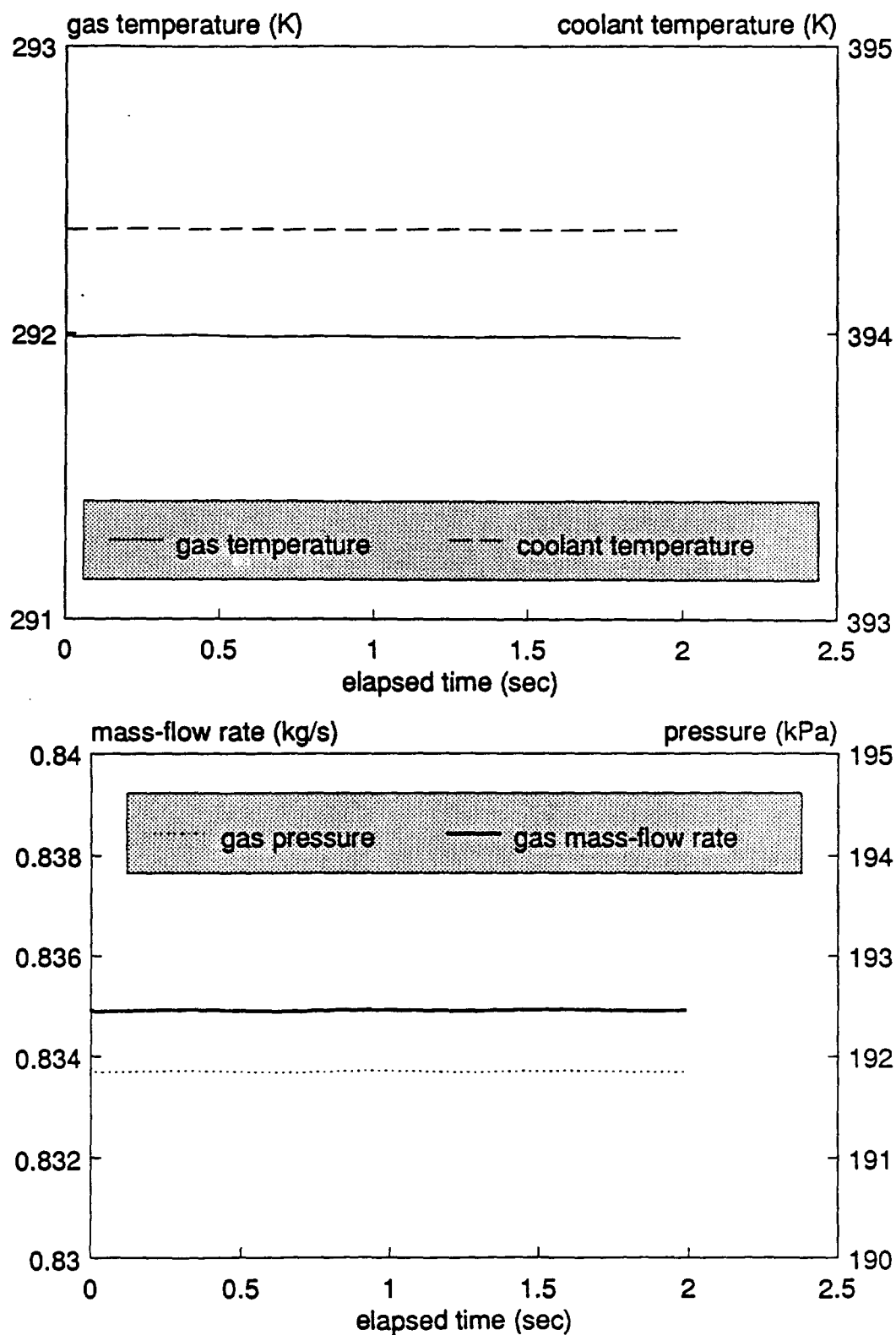


Fig. 4.36 Response of gas cooler outlet parameters (to sinusoidal salt temp.)



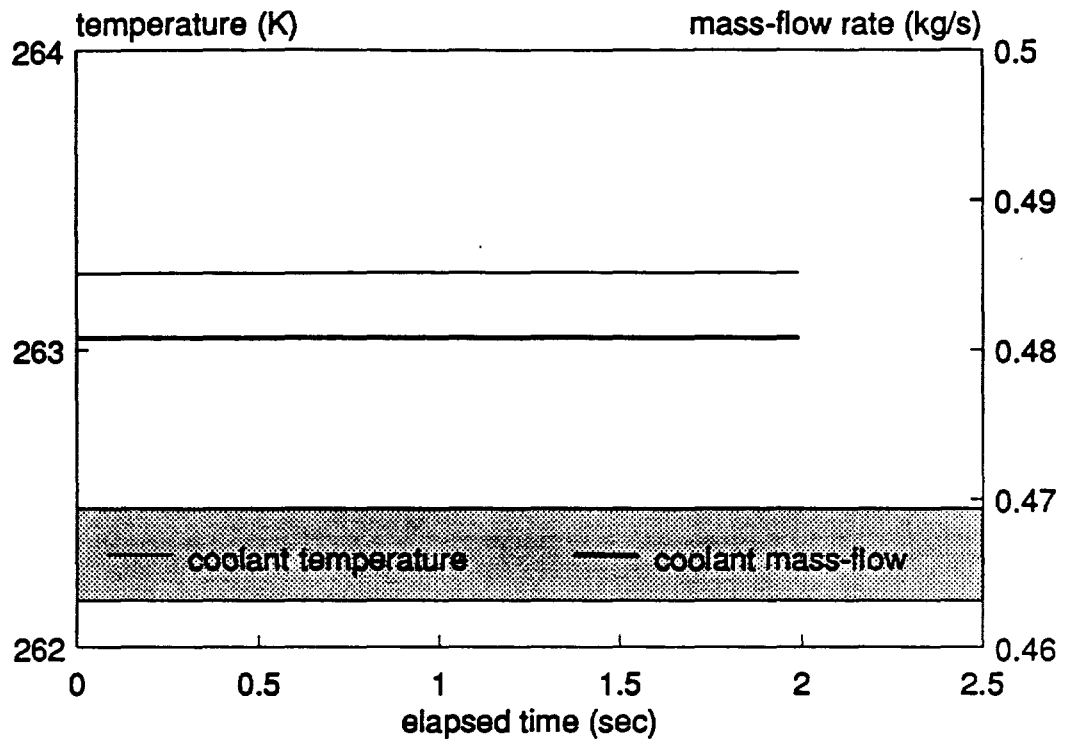


Fig. 4.37 Response of radiator outlet parameters (to sinusoidal salt temp.)

follows the sinusoid with a much smaller amplitude compared to the amplitude of the sinusoidal variation in the salt temperature. The lagging of outlet temperature to the salt temperature is obvious even in the same component. It can be seen that the pressure and mass-flow rate are oscillating with very small amplitude during the transient. This oscillation is caused by the compressibility incorporated in the turbine and compressor model.

#### 4.2.2.3 Response to a Ramp Change of Net Mechanical Power

##### Output of the Turbomachinery

The transient responses produced by a ramp of net mechanical power output are shown in Fig. 4.38 to 4.43. The net mechanical power output increased by 1.0 kW within 0.25 second. The integrator time step is  $5.0 \times 10^{-5}$  second. It is shown that the responses of the parameters in the system to the ramp change of net mechanical power output of turbomachinery are faster than the responses of parameters in the system to the step change of salt temperature. It can be seen that the predicted transients have the same trends as predicted by dynamic heat exchangers/quasi-steady turbomachines system model. The difference between the results predicted by the two system models is small.

#### 4.2.3 Discussion of Results Predicted by the Dynamic System Models

##### with and without Turbomachinery Dynamics

The transient responses predicted by the two system models (with and without turbomachinery dynamics) are shown in Fig. 4.44 to 4.49. The transient process is produced by a ramp (from 1042 K step to 1092 K) change of receiver salt temperature. The same integration time step is used for both two system models. It can be seen that the differences in the simulation results are small. This shows that the instantaneous turbomachinery is a good assumption for such a transient. Further the dynamic heat

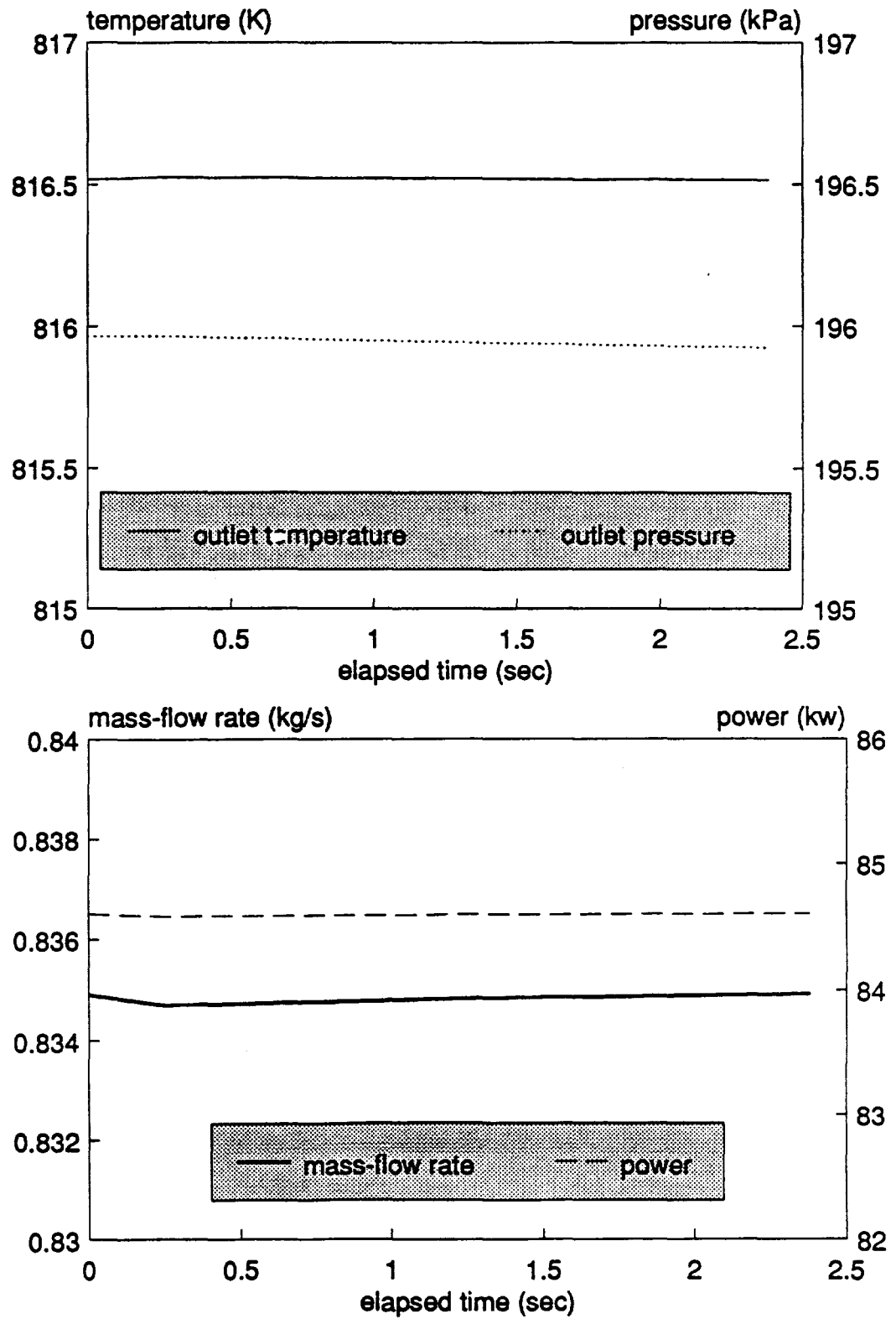


Fig. 4.38 Response of turbine outlet parameters (to ramp of output power)

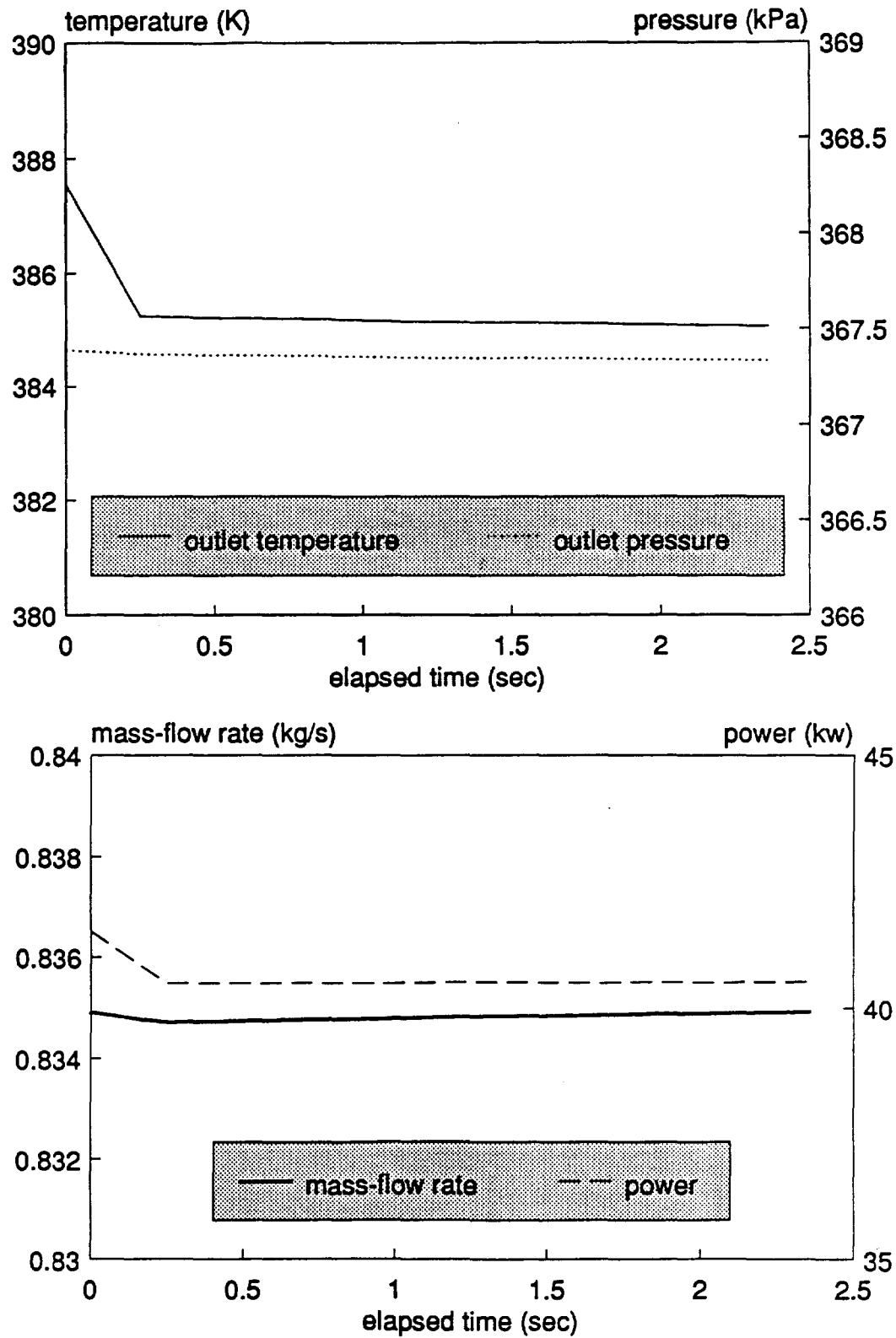


Fig. 4.39 Response of compressor outlet parameters (to ramp of output power)

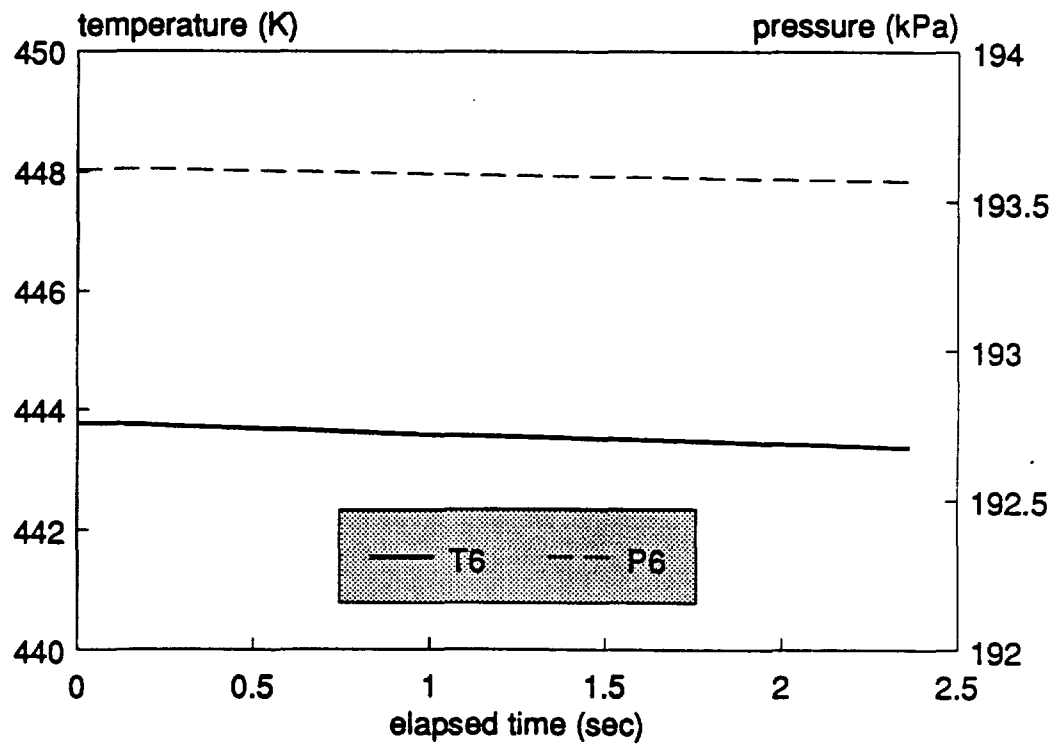
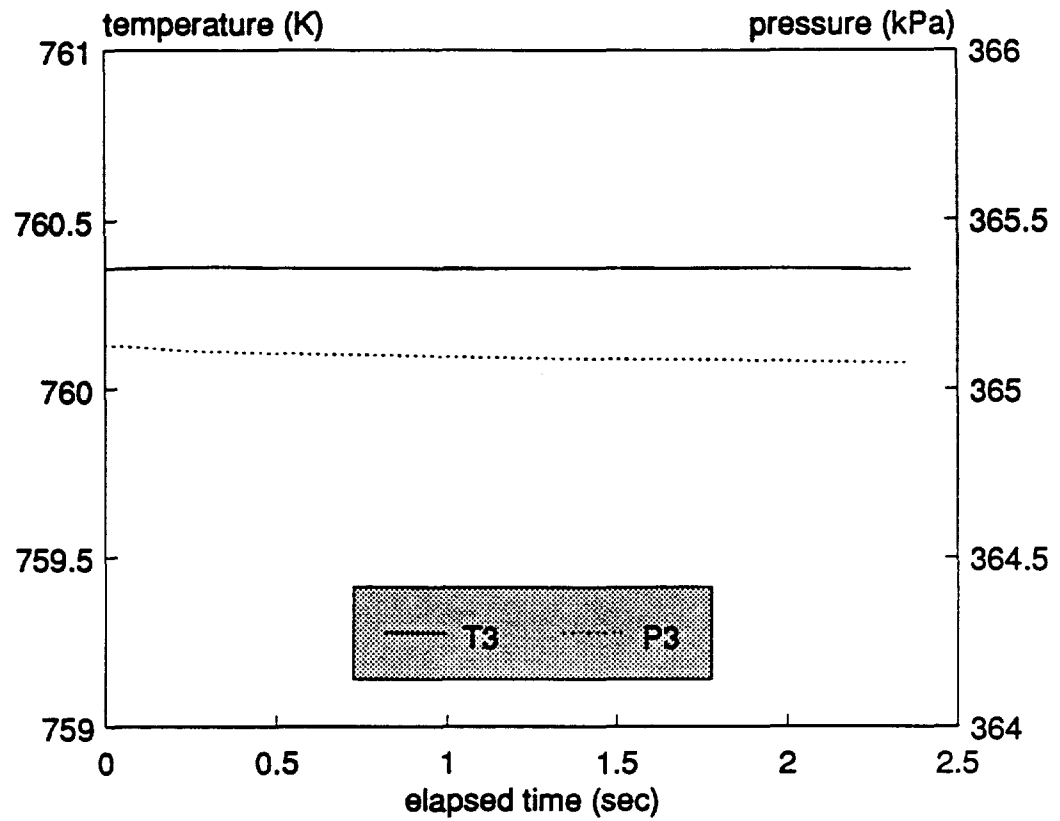


Fig. 4.40 Response of recuperator outlet parameters (to ramp of output power)

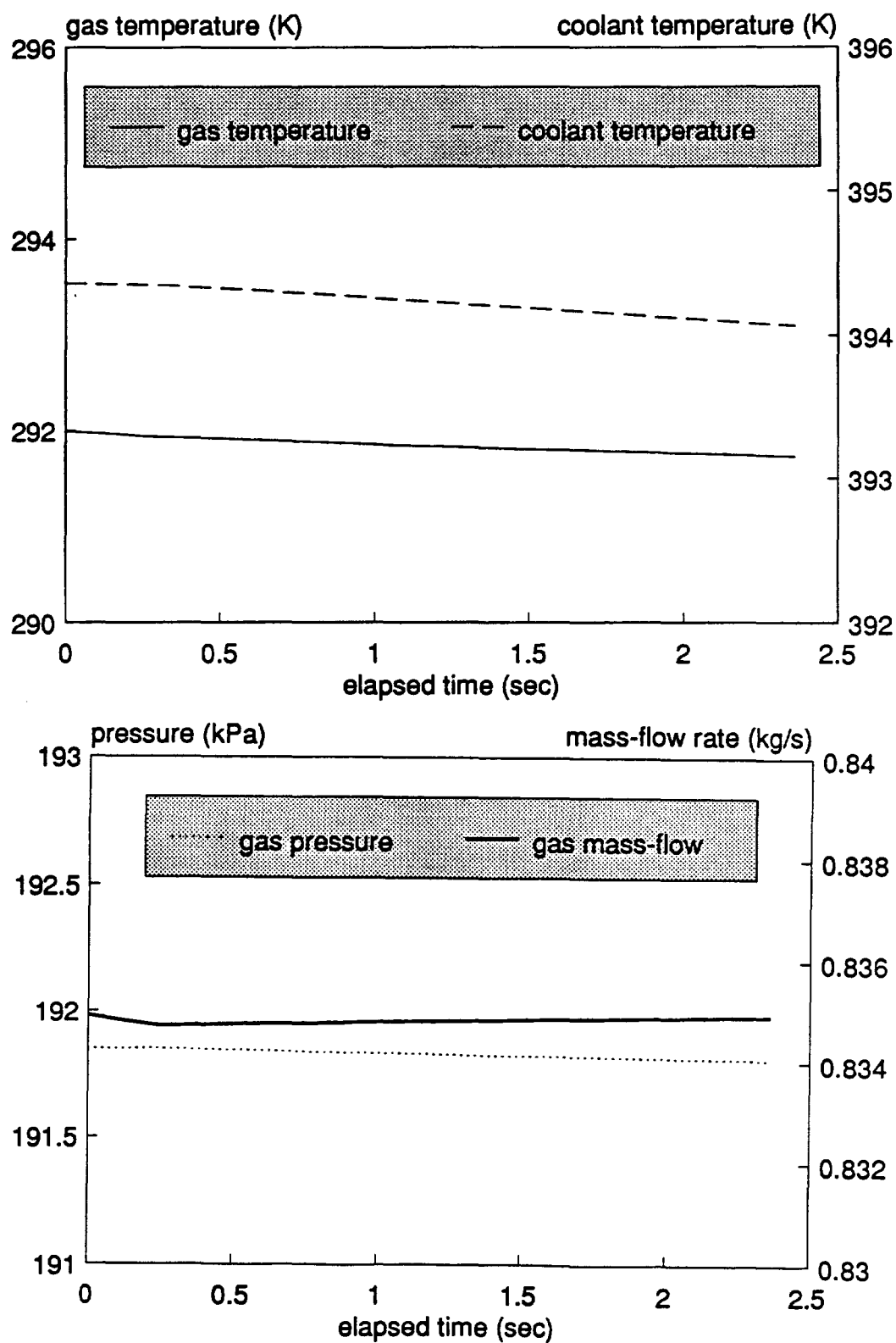


Fig. 4.41 Response of gas cooler outlet parameters (to ramp of output power)

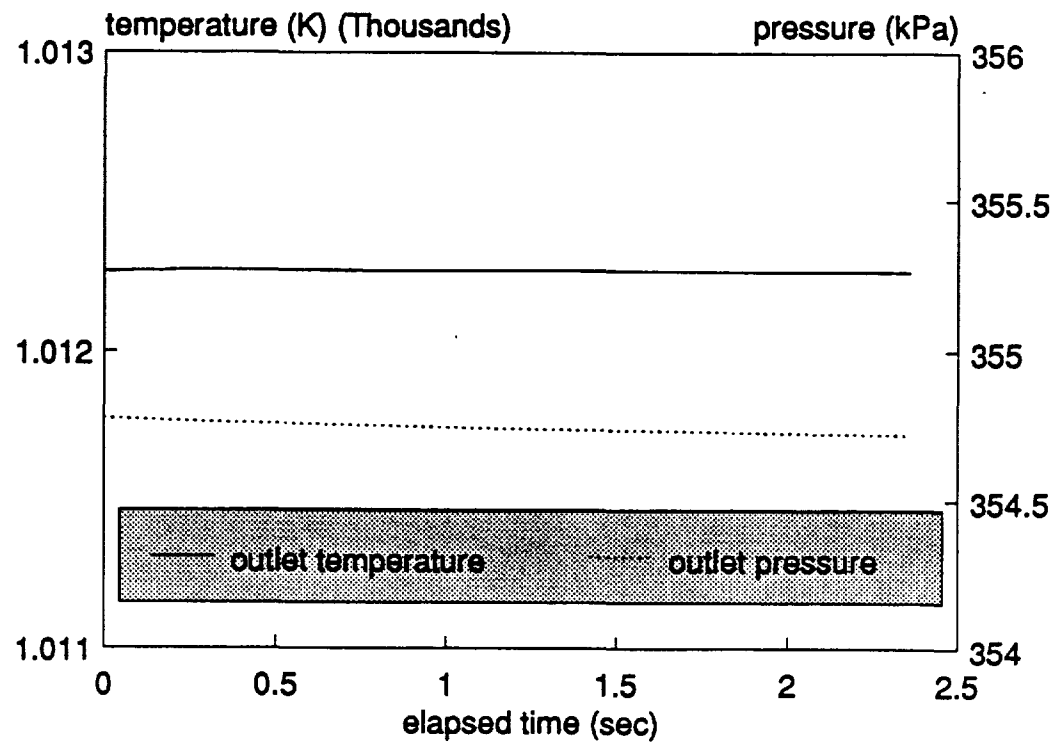


Fig. 4.42 Response of receiver outlet parameters (to ramp of output power)

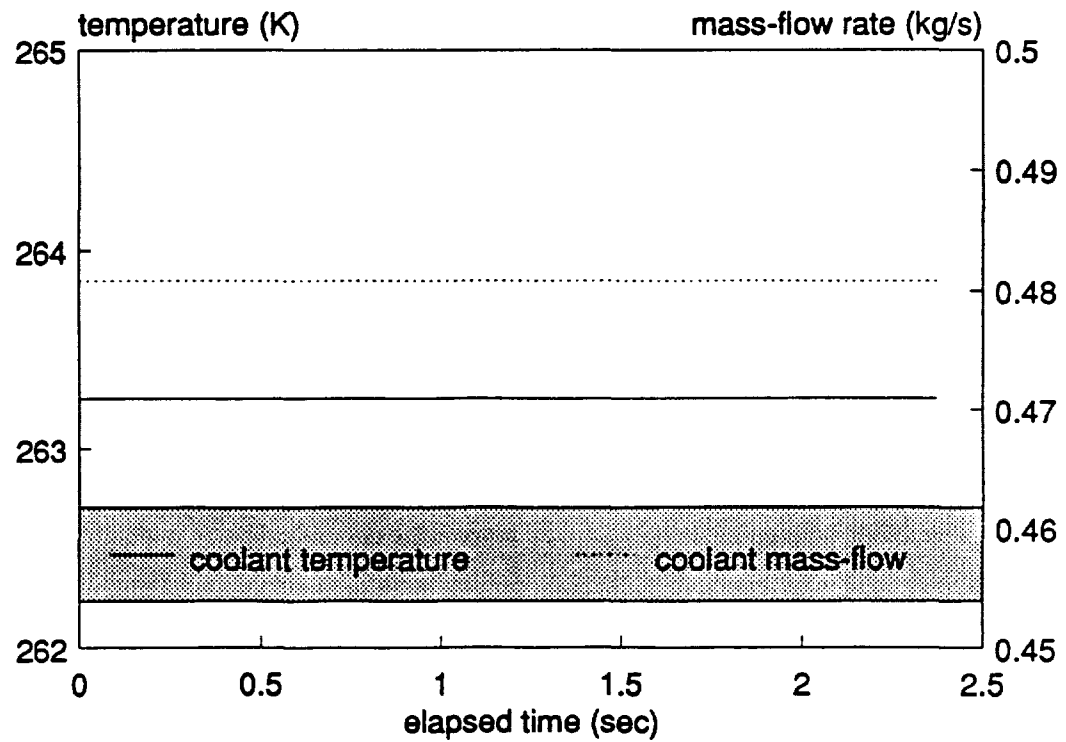


Fig. 4.43 Response of radiator outlet parameters (to ramp of output power)

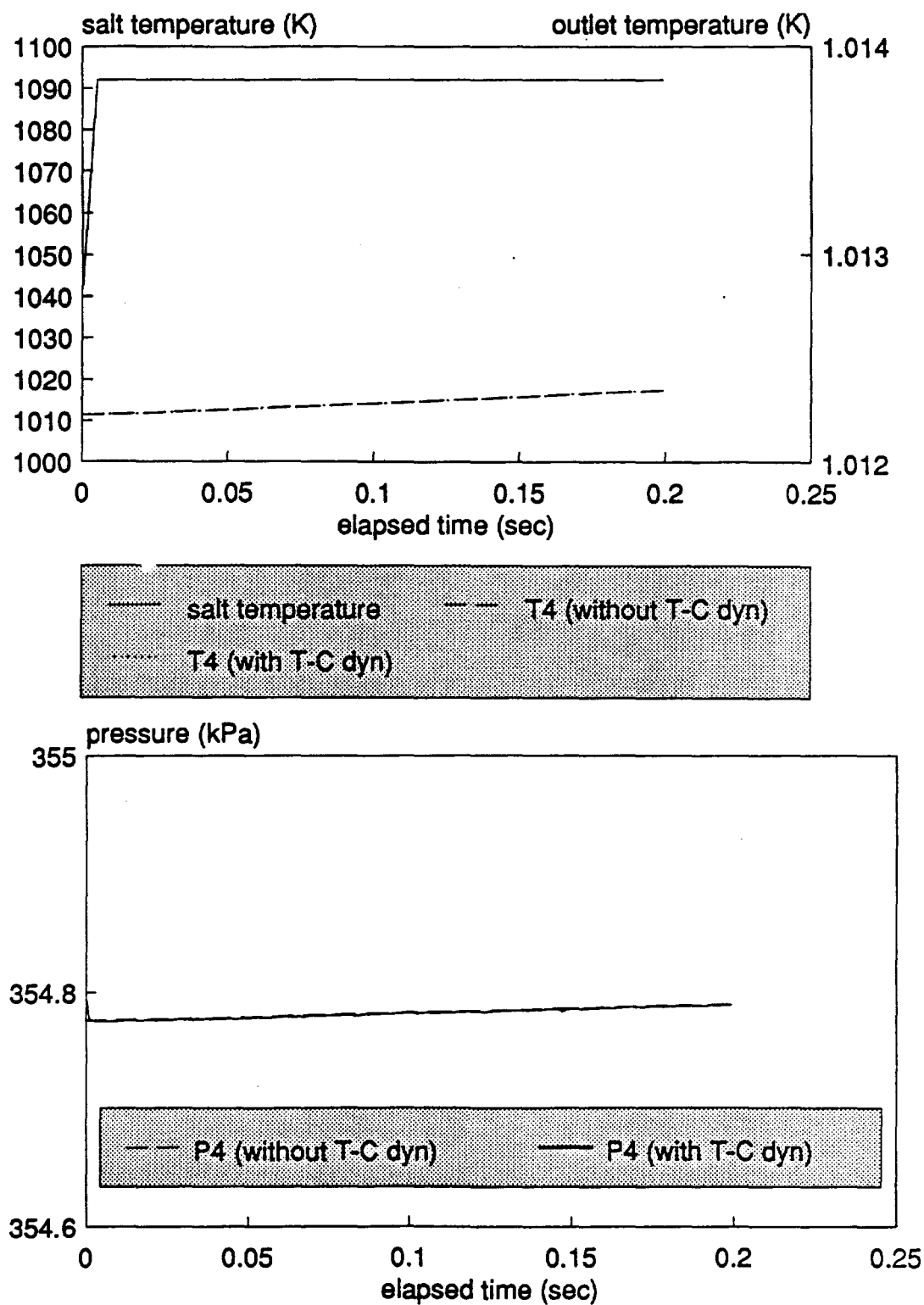


Fig. 4.44 Response of receiver outlet parameters (to ramp of salt temperature) (time step = 0.000025 (sec))



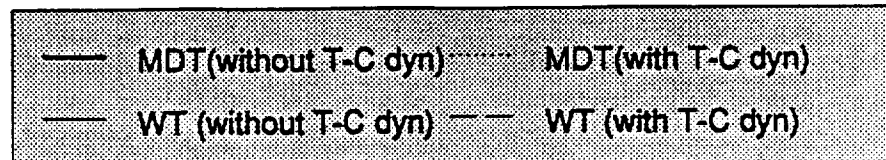
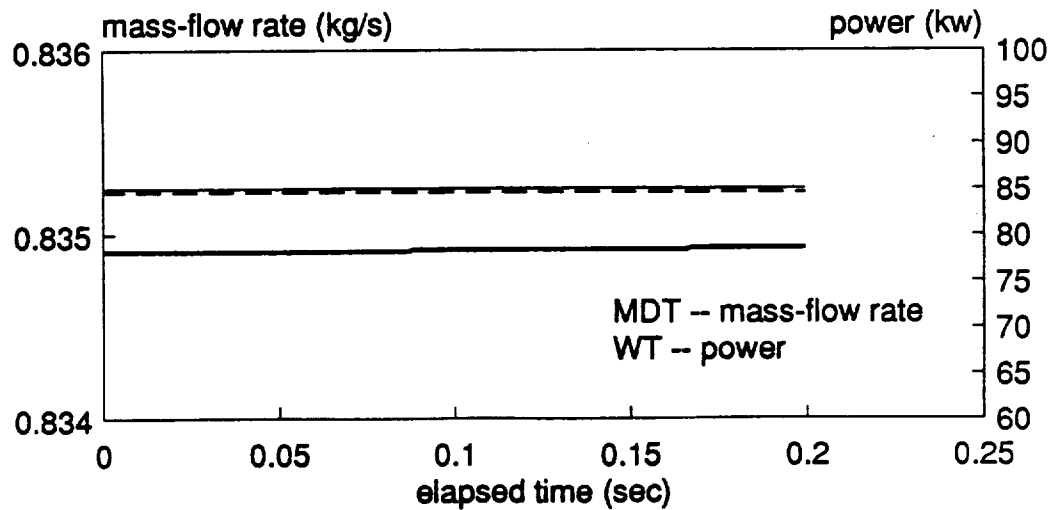
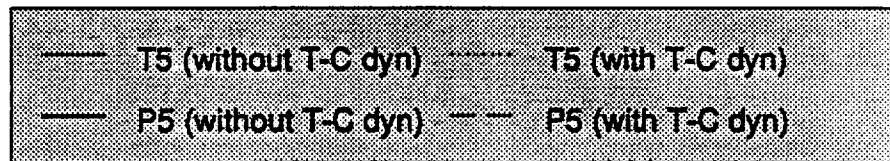
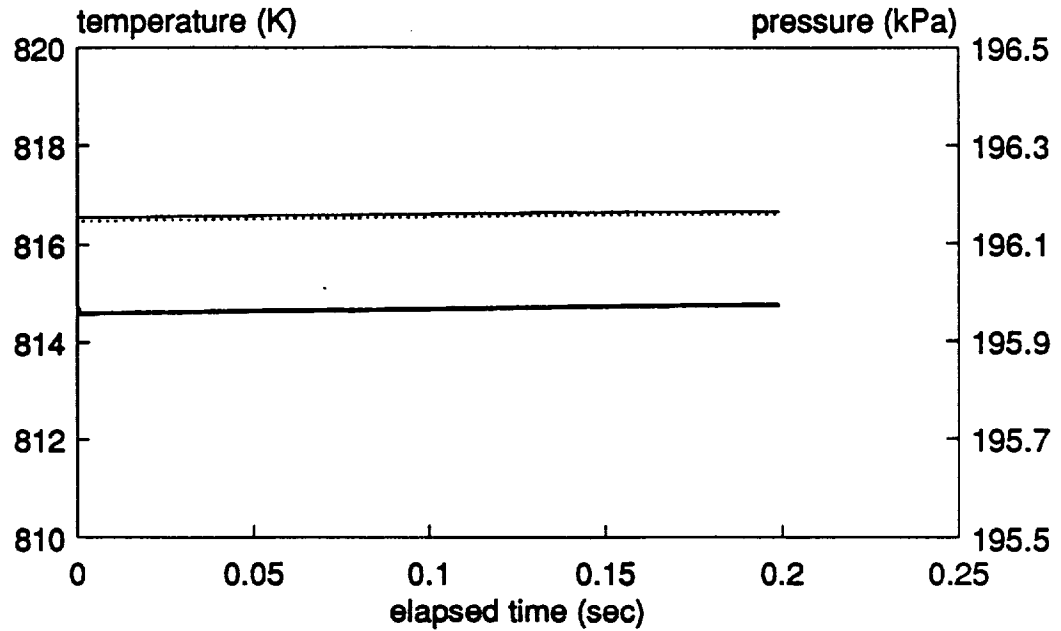


Fig. 4.45 Response of the turbine outlet parameters (to ramp of salt temperature) (time step = 0.000025 (sec))

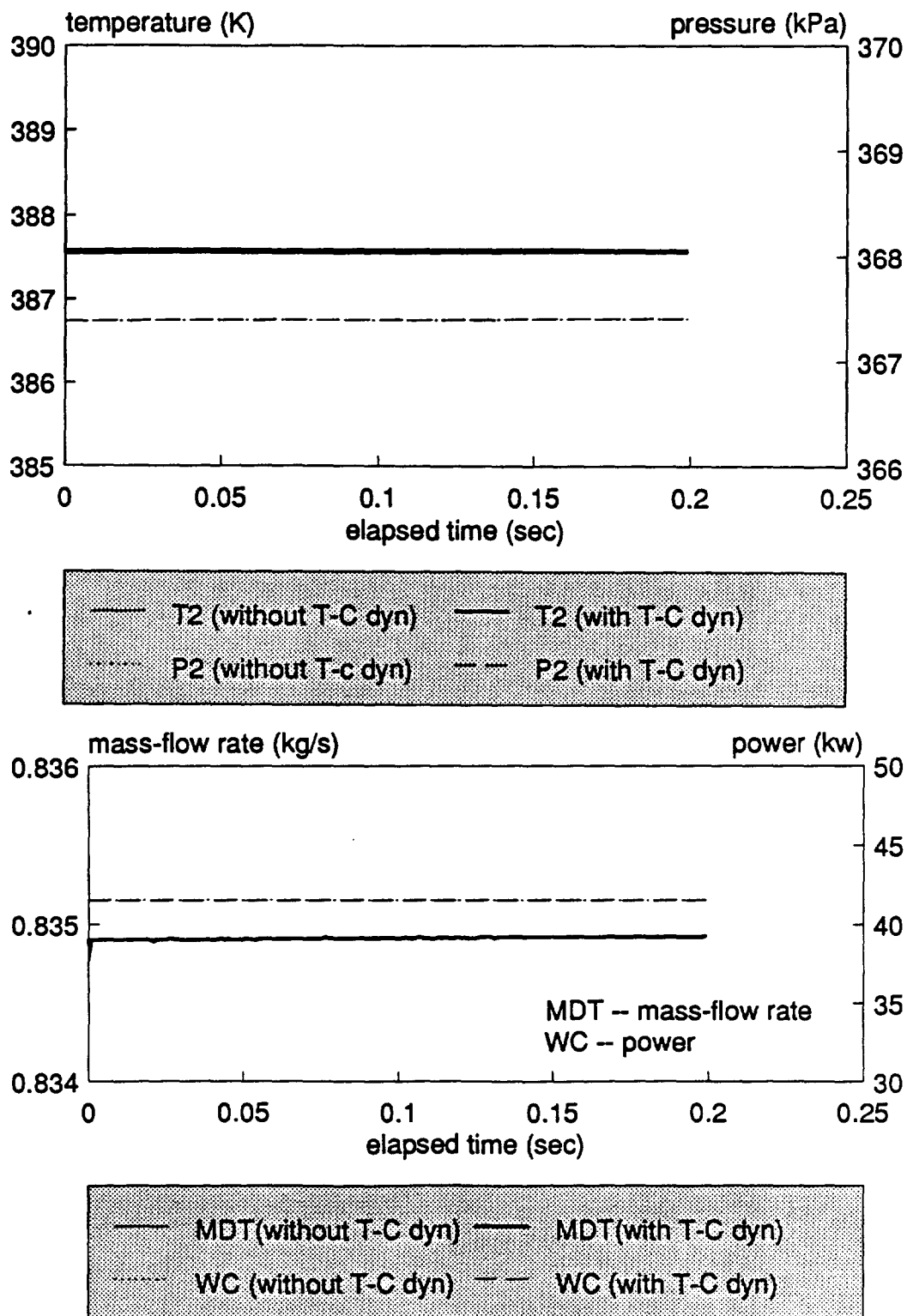


Fig. 4.46 Response of compressor outlet parameters (to ramp of salt temperature)  
(time step = 0.000025 (sec))

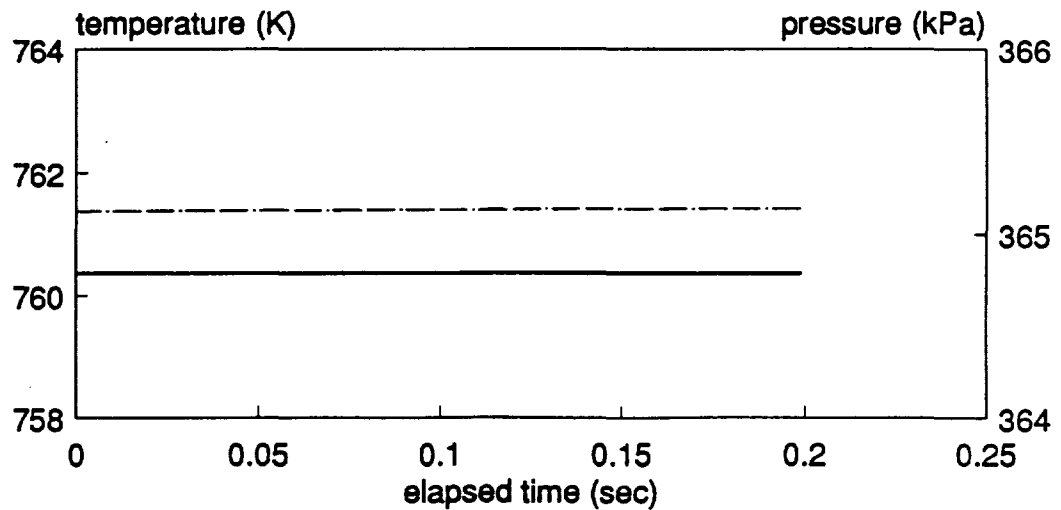
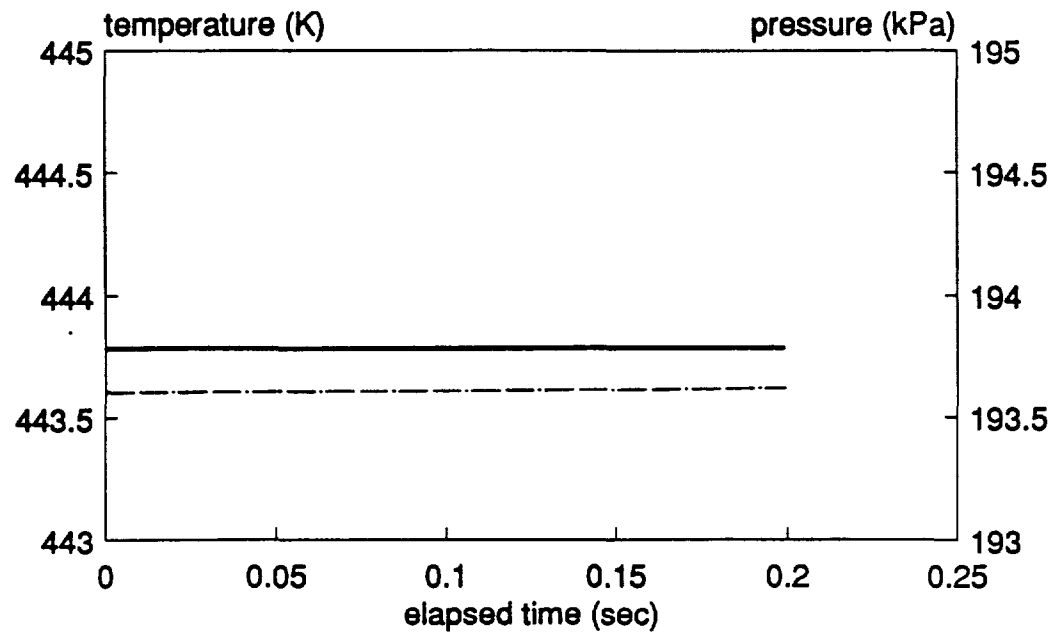


Fig. 4.47 Response of recuperator outlet parameters (to ramp of salt temperature) (time step = 0.000025 (sec))

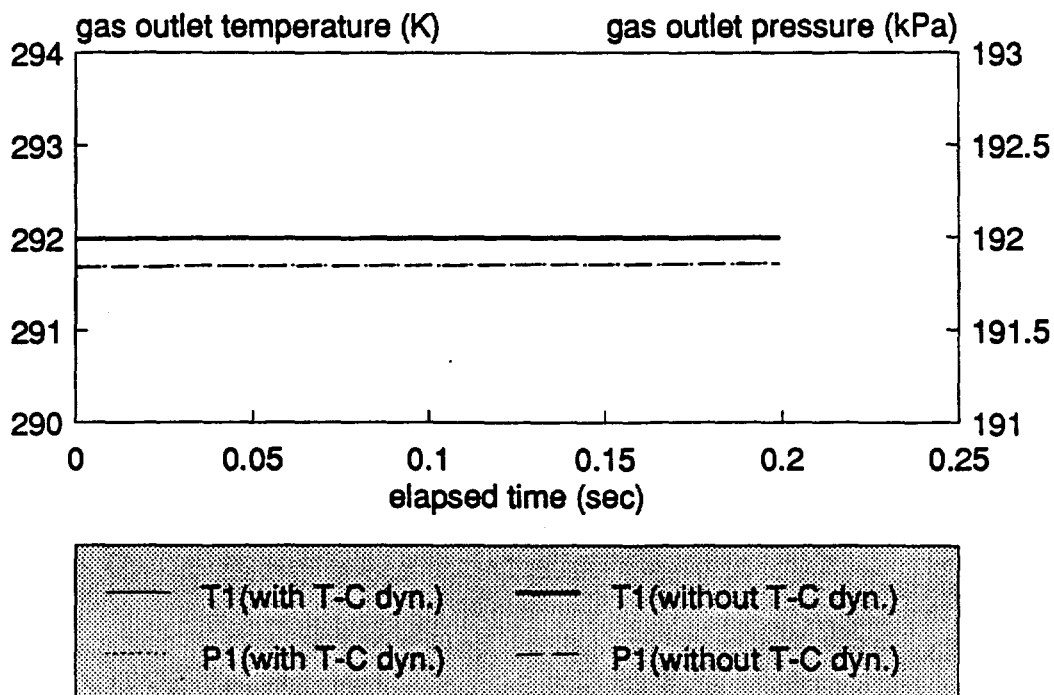


Fig. 4.48 Response of gas cooler outlet parameters (to ramp of salt temperature) (time step = 0.000025 (sec))

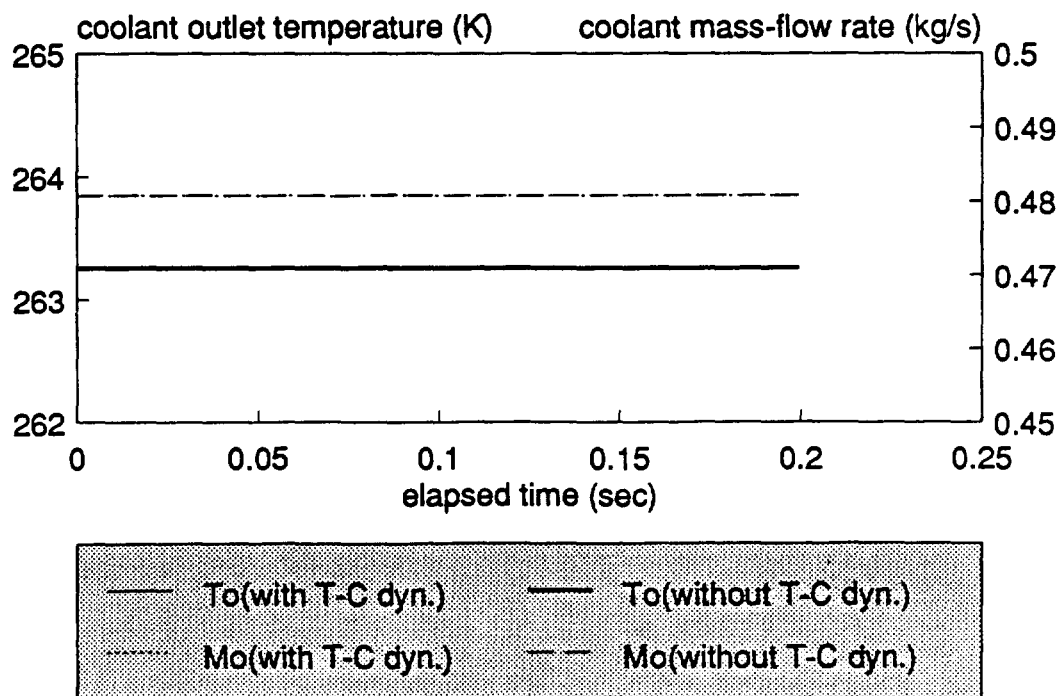


Fig. 4.49 Response of radiator outlet parameters (to ramp of salt temperature) (time step = 0.000025 (sec))

exchangers/quasi-steady turbomachines system model can be run with a much larger integration time step than the dynamic heat exchanger/dynamic turbomachines system model. Fig. 4.50 to 4.55 show the simulation results predicted by the dynamic heat exchangers/quasi-steady turbomachines system model with 1.0 second and  $2.5 \times 10^{-5}$  second time steps respectively. The difference in transient responses predicted using the two time step size is small. This verifies the conclusion of the discussion of the integration time step in section 2.2.4 is right. Therefore, for sufficiently slow transients, the CPU time required for the transient simulation of the Solar-Powered Closed Regenerative Turbine-Engine Cycle can be greatly reduced by using the dynamic heat exchanger/quasi-steady turbomachines system model.

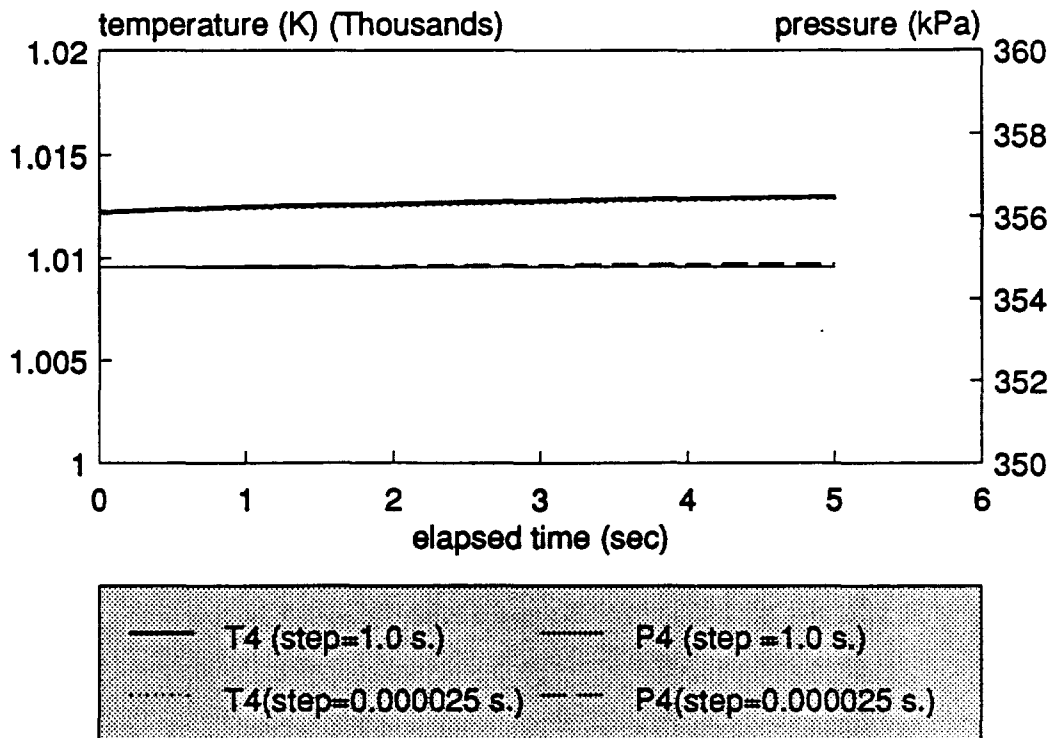


Fig. 4.50 Response of receiver outlet parameters (to ramp of salt temperature)

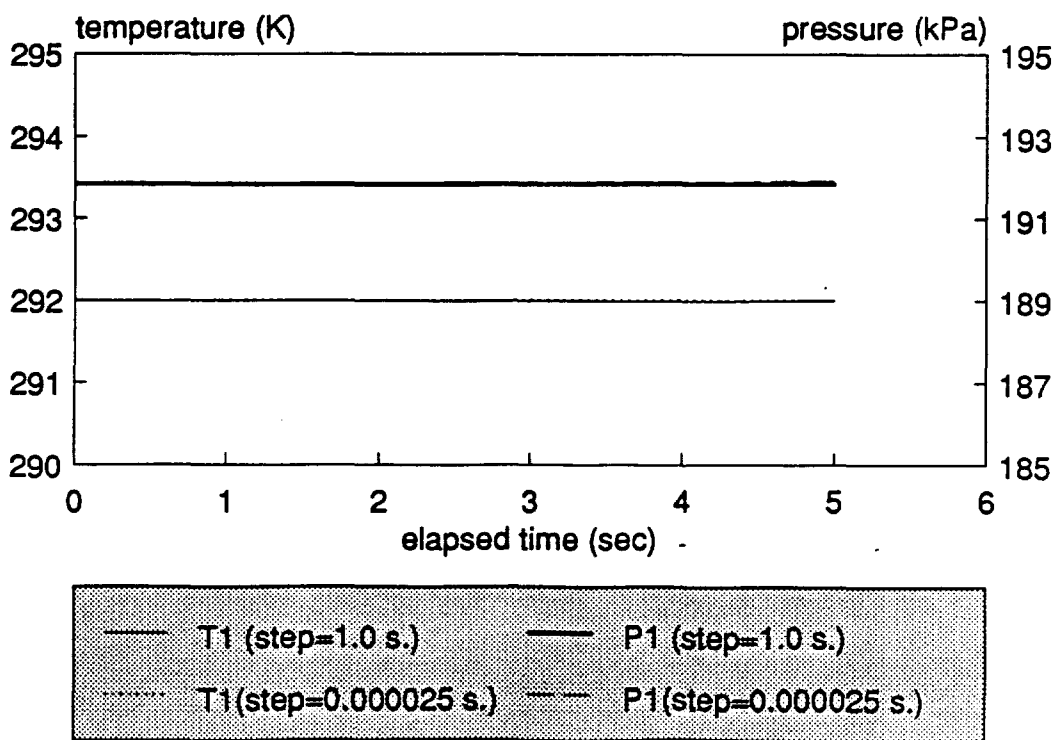


Fig. 4.51 Response of gas cooler outlet parameters (to ramp of salt temperature)

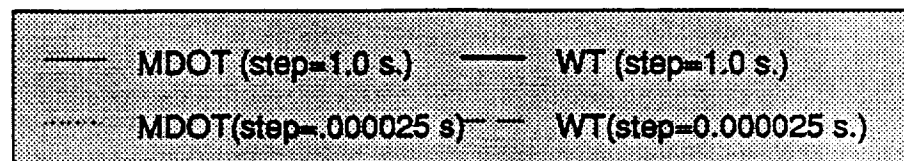
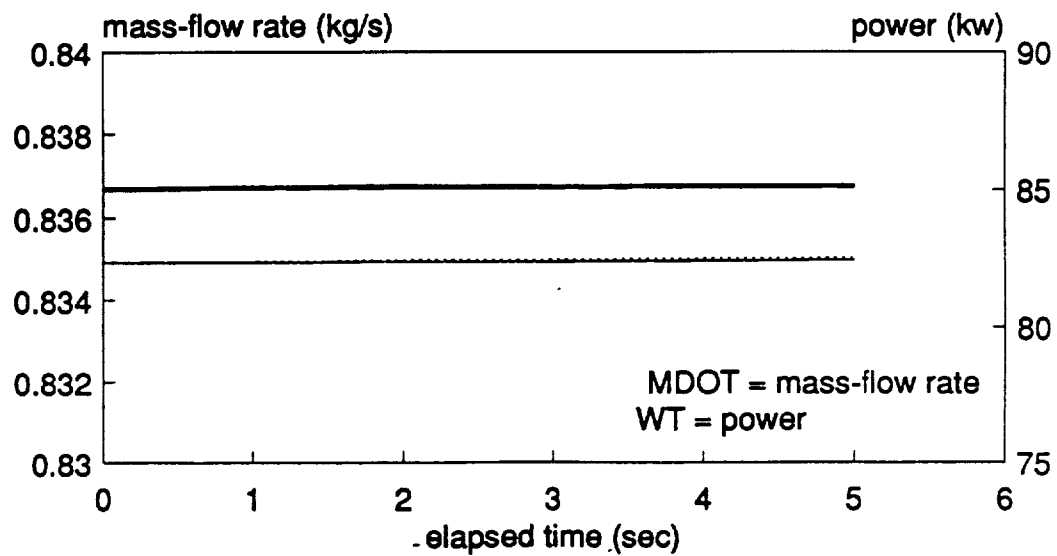
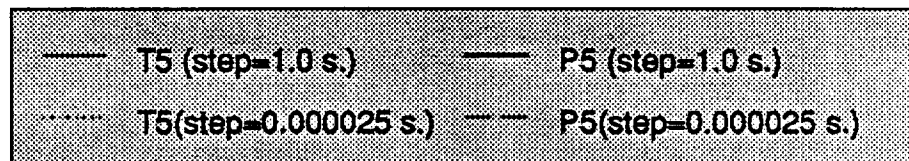
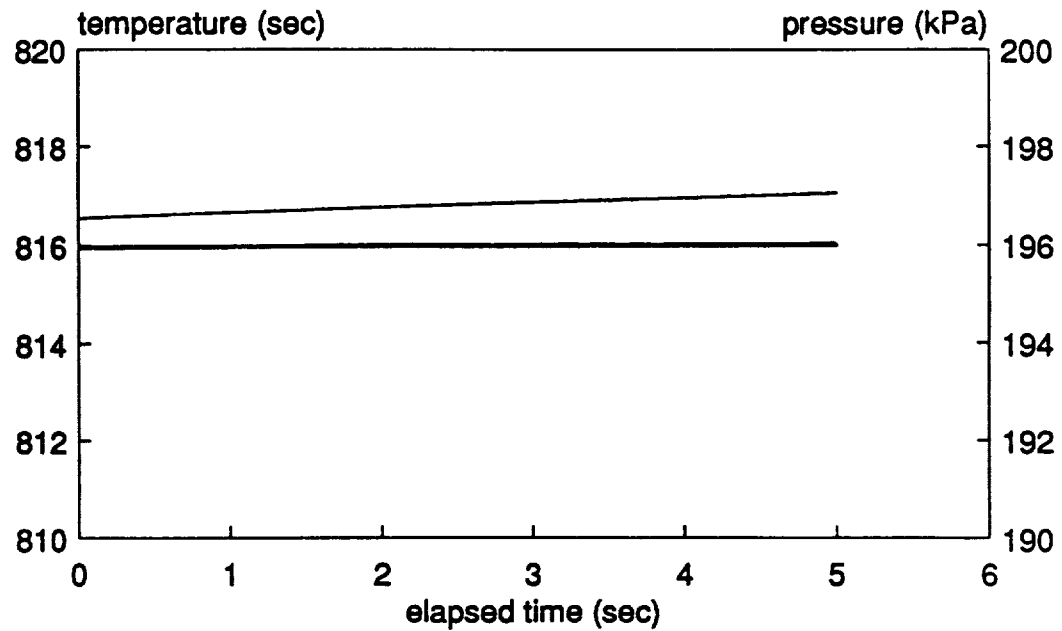


Fig. 4.52 Response of the turbine outlet parameters (to ramp of salt temperature)

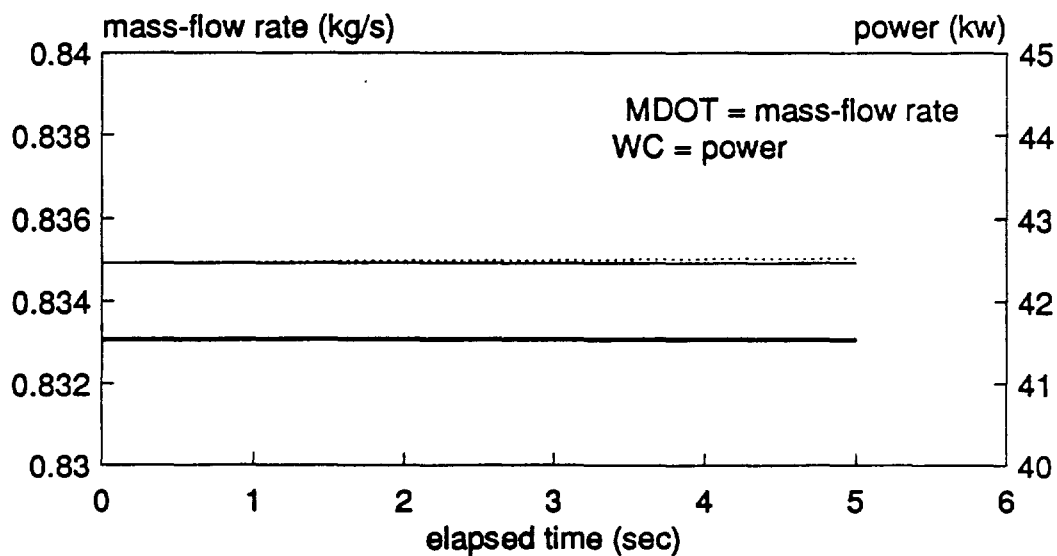
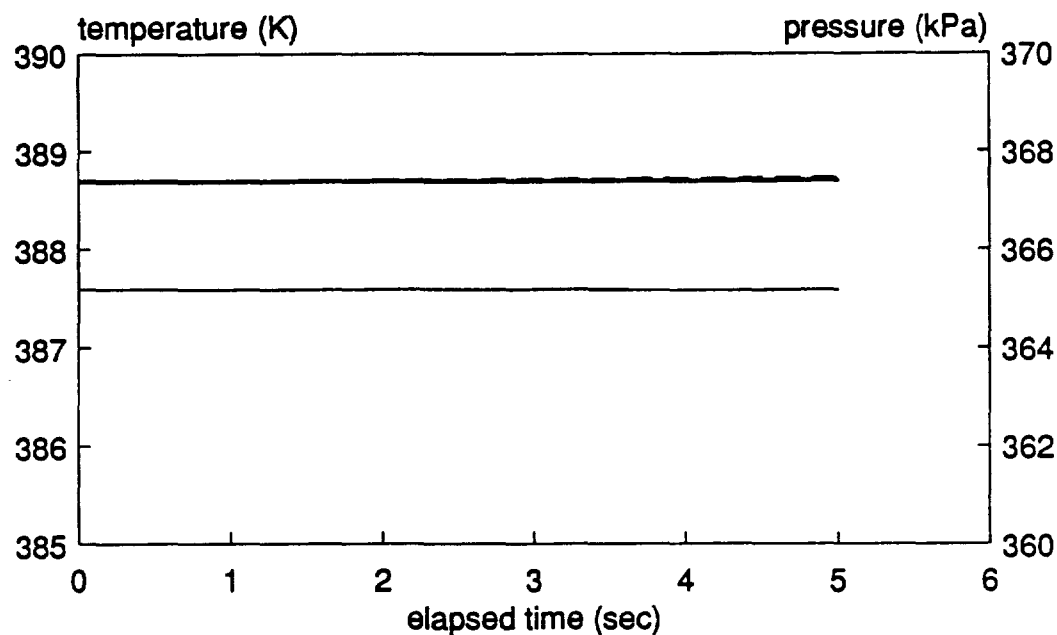


Fig. 4.53 Response of compressor outlet parameters (to ramp of salt temperature)



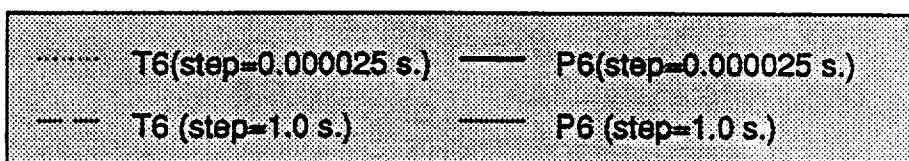
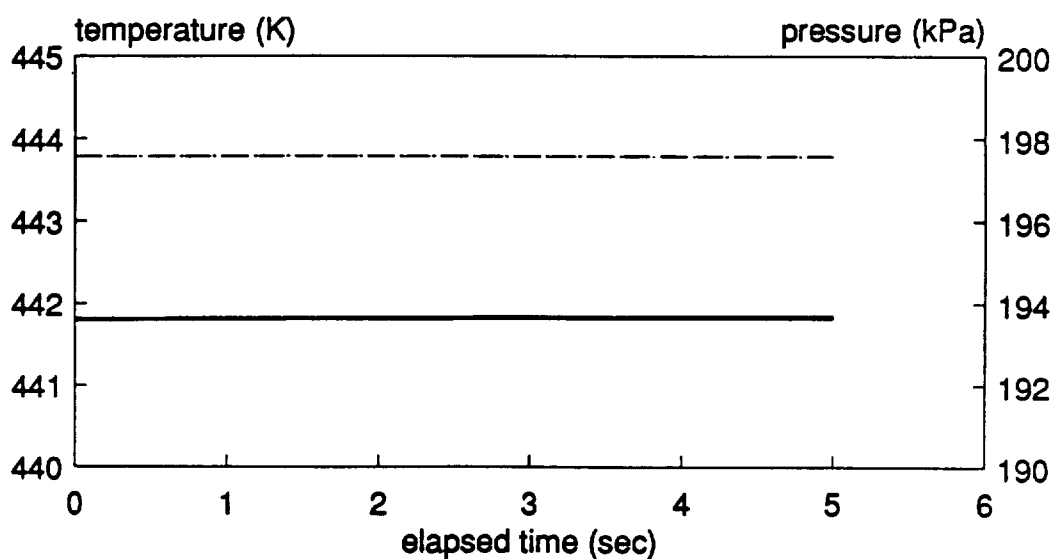
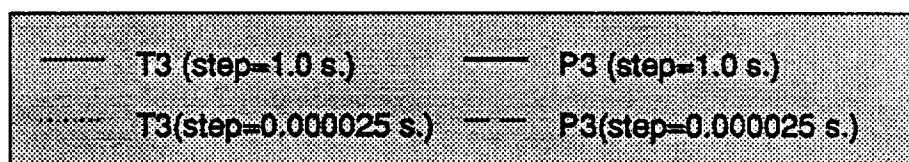
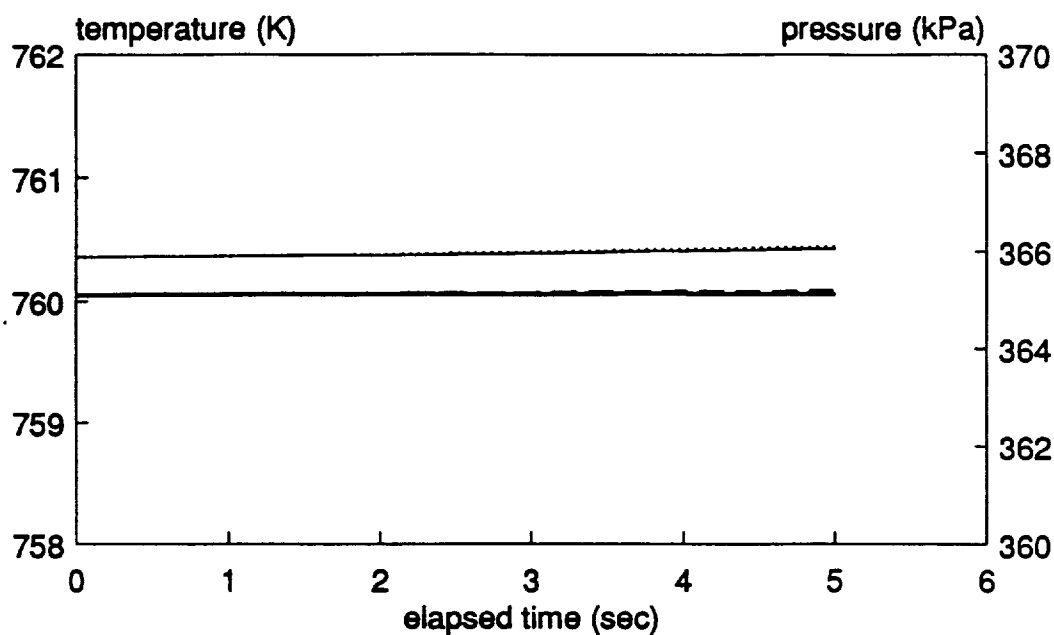


Fig. 4.54 Response of recuperator outlet parameters (to ramp of salt temperature)

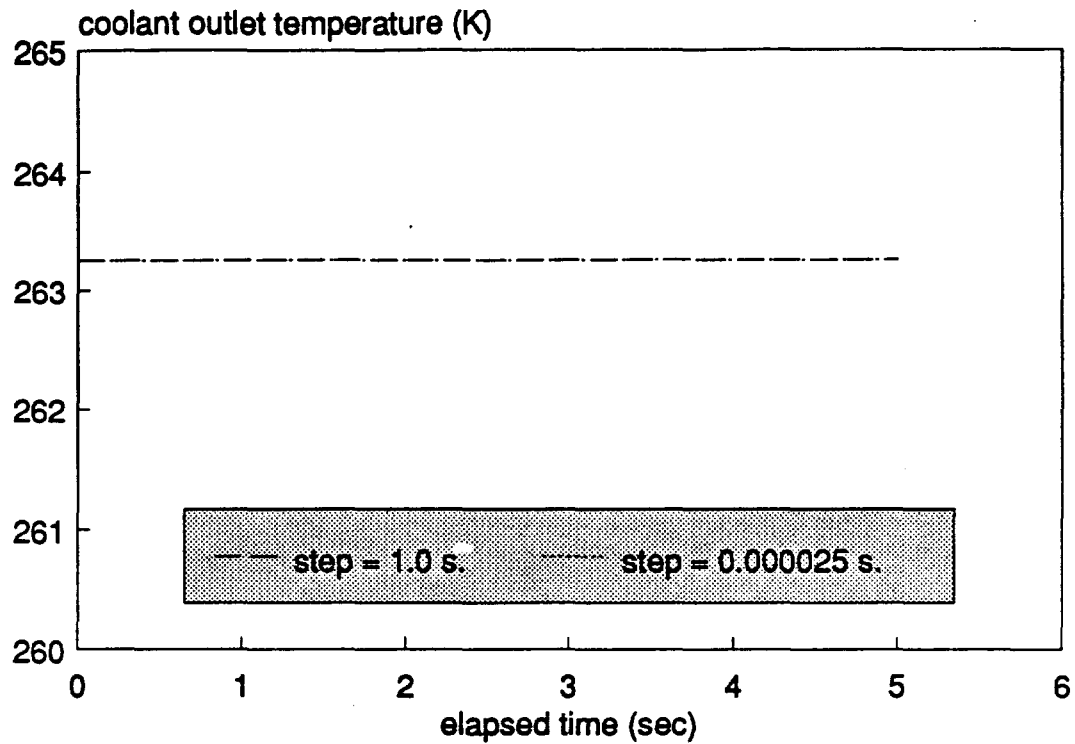


Fig. 4.55 response of radiator outlet temperature(to ramp of salt temperature)

### 5. Summary and Conclusions

Quasi-steady and dynamic models were developed and written in FORTRAN for the components (receiver, gas cooler, recuperator, radiator, compressor and turbine) used in the Solar-Powered Closed Regenerative Turbine-Engine Cycle. The component models were integrated into the quasi-steady system model, the dynamic heat exchangers/quasi-steady turbomachines system model, and the dynamic heat exchangers/dynamic turbomachines system model. The system models were written in FORTRAN and based on the equations for conservation of energy and the equation of conservation of mass.

The quasi-steady system model was used to calculate the steady-state performance and to debug the iteration scheme during the development of the system model. The "mixed" (dynamic heat exchangers and quasi-steady turbomachines) system model and the dynamic components system model was developed on the basis of the quasi-steady components system model.

The transient processes simulated by the dynamic heat exchangers/quasi-steady turbomachines system model include:

- (1). Transient process caused by a step increase in the receiver salt temperature
- (2). Transient process caused by a double step in the receiver salt temperature
- (3). Transient process caused by a sinusoid function in the receiver salt temperature
- (4). Transient process caused by a ramp of the net mechanical power output of the turbomachinery.

The time lag of the temperature response can be seen from component to component downstream of the perturbation location. It can also be seen that for the above transient

processes, the response of mass-flow rate and pressure lags the receiver salt temperature. System simulation showed the response time of the system to a step of the receiver salt temperature to be greater than 2500 seconds. The system transient response was also slow in the transient process (4) which was caused by a ramp of the net output mechanical power (i. e., a ramp of the compressor input power). These analyses provided evidence that the response time of the system is dominated by the heat exchangers. To verify this, the dynamic heat exchangers/dynamic turbomachines system model was used to simulate the system response. Comparison between the simulation results of the dynamic heat exchangers/quasi-steady turbomachines system model and the dynamic heat exchangers/dynamic turbomachines system model showed only very small differences. It is therefore concluded that the dynamic heat exchangers/quasi-steady turbomachines system model can be used to simulate the transient performance of the Closed Regenerative Turbine-Engine Cycle with sufficient accuracy for these types of events.

The simulation results of the dynamic heat exchangers/quasi-steady turbomachines system model with different integration time steps ( $2.5 \times 10^{-5}$  second and 1.0 second) showed very small differences. This demonstrates that the larger integration time step can be used by the dynamic heat exchangers/quasi-steady turbomachines system model with satisfactory accuracy. The CPU time needed for the transient simulation is therefore greatly reduced when using the dynamic heat exchangers/quasi-steady turbomachines system model. The dynamic heat-exchangers/quasi-steady turbomachines system model has shown the capability for simulation over a wide range of transient processes.

## 6. Recommendations for Further Study

The system transient response to the change in space temperature and the change in inventory (total mass in the system) have not yet been simulated. Since the existing dynamic heat exchangers/quasi-steady turbomachines system model and dynamic heat exchangers/dynamic turbomachines system model were designed to be able to simulate these transient processes, execution of such analyses is a logical step in studying the performance of the power generation system. Improvements in model performance can be obtained by increasing the accuracy and the range of transient performance simulation by component-model refinement and system-model expansion.

A simplified transient turbomachine model should be the subject of further investigation. The dynamic turbine and compressor models may be refined to increase the integration time step by carefully selecting the iteration scheme and the assumptions in the models.

The component models can be refined further by using more design details of the actual construction. The receiver model can be refined by including the behavior of the phase-change material as more details of the property of the phase change material become known. Actual performance maps can be incorporated into the compressor and turbine models to predict the performance more accurately.

The modular construction of the existing FORTRAN program of the system model makes it easy to add component models into the system model. An accumulator model can be added into the system model to simulate the response to inventory change. The system model can be improved to become variable-speed system model by including the rotating-unit dynamics. This would greatly increase the range of possible analyses.

Dynamic models of the ducting can also be added into the system model. Finally, the control-system model can be integrated into the thermodynamic system model, to produce a complete Solar-Powered Closed Regenerative Turbine-Engine Cycle system model.

## 7. Acknowledgements

I would like to express my sincere appreciation to Dr. John I. Hochstein and Dr. Theodosios Korakianitis for their help and guidance. They demonstrated infinite patience and timely foresight which induced in the author the energy and drive to proceed with the work. They have been the most significant influence in my graduate study. I would like to thank Mr. Mohammad Samad Ali and Mr. Ahsan Iqbal for their help and advice during this work.

I am grateful to my wife, Shufang Zheng, for her understanding and patience. I appreciate the help and encouragement received from my family and friends

### 8. References

1. Rocketdyne, "Space Station Work Package WP-04 Power System Preliminary Analysis and Design Document", Rocketdyne RI/RD85-320-2, December, 1986. (AKA DR02 Document)
2. Iqbal, A., "Transient Model of Space Station Solar Dynamic Power Generating System", Master's Thesis, Washington University, 1990.
3. Boeing Computer Services, "EASY5 Engineering Analysis System Reference Manual", The Boeing Company, Second Edition, December, 1987.
4. Ali, M. S., "Modelling of Transient Thermodynamic Performance of Compressible Flow Turbomachines", Master's Thesis, Washington University, 1990.
5. Kays, W. M. and London, A. L., "Compact Heat Exchangers", McGraw-Hill Book Company, 1984.
6. Gerhart, P. M., Gross, R. J., "Fundamentals of Fluid Mechanics", Addison-Wesley Publishing Co., 1985.
7. Heywood, J. B., "Internal Combustion Engine Fundamentals", McGraw-Hill Inc., 1988.
8. Panton, R. L., "Incompressible Flow", John Wiley & Sons Inc., 1984.



Dequan Zou

## VITA

**Date of Birth:** [REDACTED]

**Place of Birth:** [REDACTED].

**Undergraduate Study:** Harbin Shipbuilding Engineering Institute, Harbin, China  
B.Sc. 1981

**Graduate Study:** Harbin Shipbuilding Engineering Institute, Harbin, China  
M.Sc. 1984  
Washington University, St. Louis, Missouri,  
1989-present  
M.Sc. expected August, 1991;  
D.Sc. expected August, 1993

**Professional Societies:** SAE

**Honors/Awards:** Tuition Scholarship, Washington University,  
1989-present

**Scholastic and Professional Experience:** Lecturer, Harbin Shipbuilding Engineering Institute,  
1985-1988  
Visiting Research Assistant, University of Bath, U.K.  
1988-1989  
Research Assistant, Washington University,  
1989-present

**Publications:**

1. "Optimization of Rankine Cycle Waste Heat Recovery System", Journal of Harbin Shipbuilding Engineering Institute, 1985, No. 4.
2. "Calculation of Thermodynamic Properties of Organic Working Fluids Used in

Rankine Cycle Waste Heat Recovery Systems", Journal of Harbin Shipbuilding Engineering Institute, 1986, No. 1.

3. "Research and Application of Methanal-Gasolene Emulsified Fuel", Journal of Harbin Shipbuilding Engineering Institute Science and Technology, 1988, No. 1.
4. "Transient Response and Route Simulation for Heavy Vehicles with Alternative Engine-Transmission Systems", SAE Congress, Detroit, Feb. 1989, Paper 890393.

August, 1991

**Short Title: Turbine-Engine Cycle Modeling**

**Zou, M.Sc. 1991**

## Appendix D

### View-Foils for Final Oral Presentation

# Dynamic Modeling of Solar Dynamic Power Components and Systems

Final Report  
NASA Grant NAG3-817  
January 28, 1991

John I. Hochstein, Principal Investigator  
T. Korakianitis, Co-Principal Investigator

## Personnel & Activities

J. Hochstein - all phases

T. Korakianitis - all phases

J. McTavish - Initial phase: EASY5, Rankine Cycle

A. Iqbal - Steady & Quasi-Steady Models

S. Ali - Centrifugal Models

D. Zou - Model Refinement, Control Algorithm

1. Introduction
2. First Component & System Models
  - System fabric and component models
  - System transients
3. Improved Turbomachinery Models
  - Sequence of models
  - Component transients
4. Final System and Component Models
  - Improved component models
  - System modeling
  - Transients
5. Conclusions

- 
- Solar Dynamic Power Generation System (SDPGS) proposed for higher electrical power demands of Space Station freedom.
  - Early candidates for thermodynamic system
    - Rankine Cycle
    - Closed Brayton Cycle
  - Directed by NASA to use EASY5 program as modeling tool
    - Motivation was to provide consistent basis for mechanical and electrical models
  - Initial effort focused on Rankine Cycle
    - Built system fabric in EASY5
    - Developed thermodynamic properties block
    - Stopped work when Brayton cycle selected by NASA
  - Balance of effort devoted to Closed Regenerative Brayton Cycle



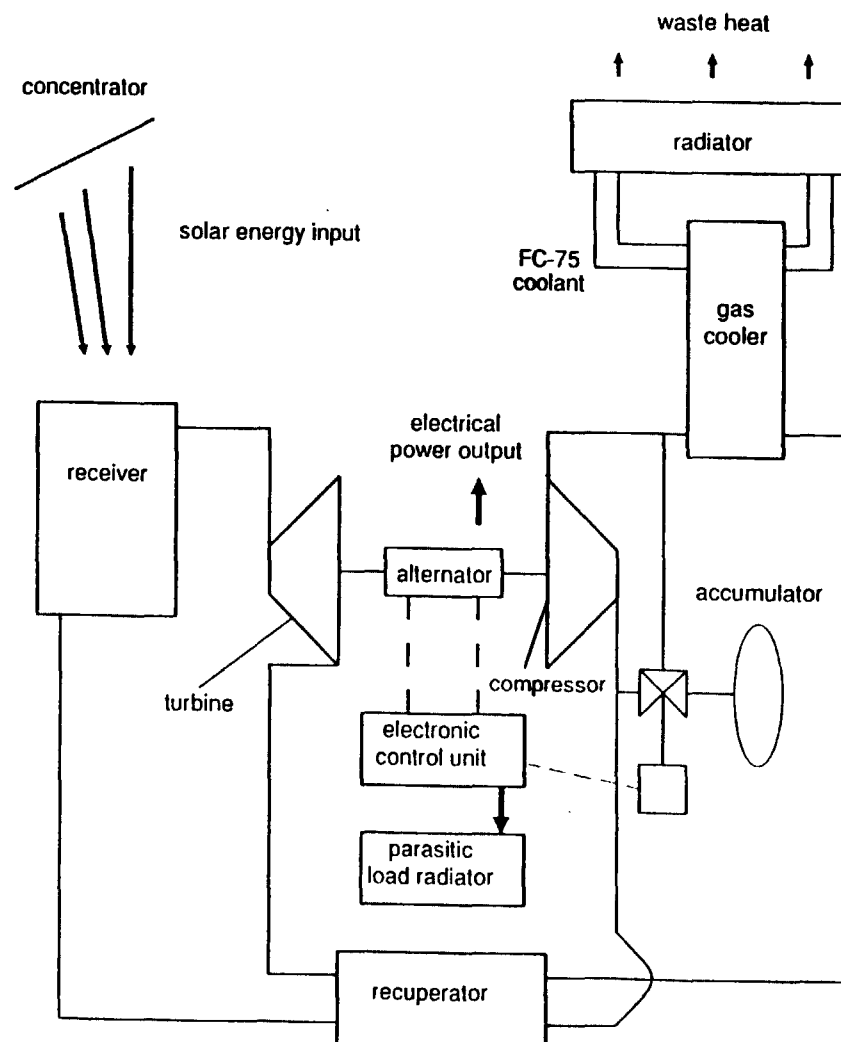
- Commercial software for system modeling available from Boeing
- At various times, installed on:
  - Cray XMP (LeRC) difficult to use interface & missing features
  - VAX 11/780 (WU) errors in manual
  - VAXstation 2000 (WU) buggy implementation
  - MicroVAX II (WU) final installation, bulk of analyses
- Strengths: - establishes standard interface
  - "standard" component models provided
  - facilities for graphical display of results
- Negatives: - large computational overhead (slow)
  - "standard" components not suitable for this study
  - "loop" procedures not suitable for iterative solutions



## Closed Regenerative-Brayton Cycle

- Heat source: incident solar radiation captured by collector
- Heat sink: gas cooler transfers heat to liquid cooling loop, which rejects heat to space through radiator
- Combined Rotating Unit: centrifugal compressor, centrifugal turbine, alternator
- System designed to function at fixed operating speed; excess electrical power consumed by parasitic load to present a constant power demand to the power generation system

# Brayton Cycle



First models based on steady or quasi-steady assumptions for all components.

Coding development cycle for component models:

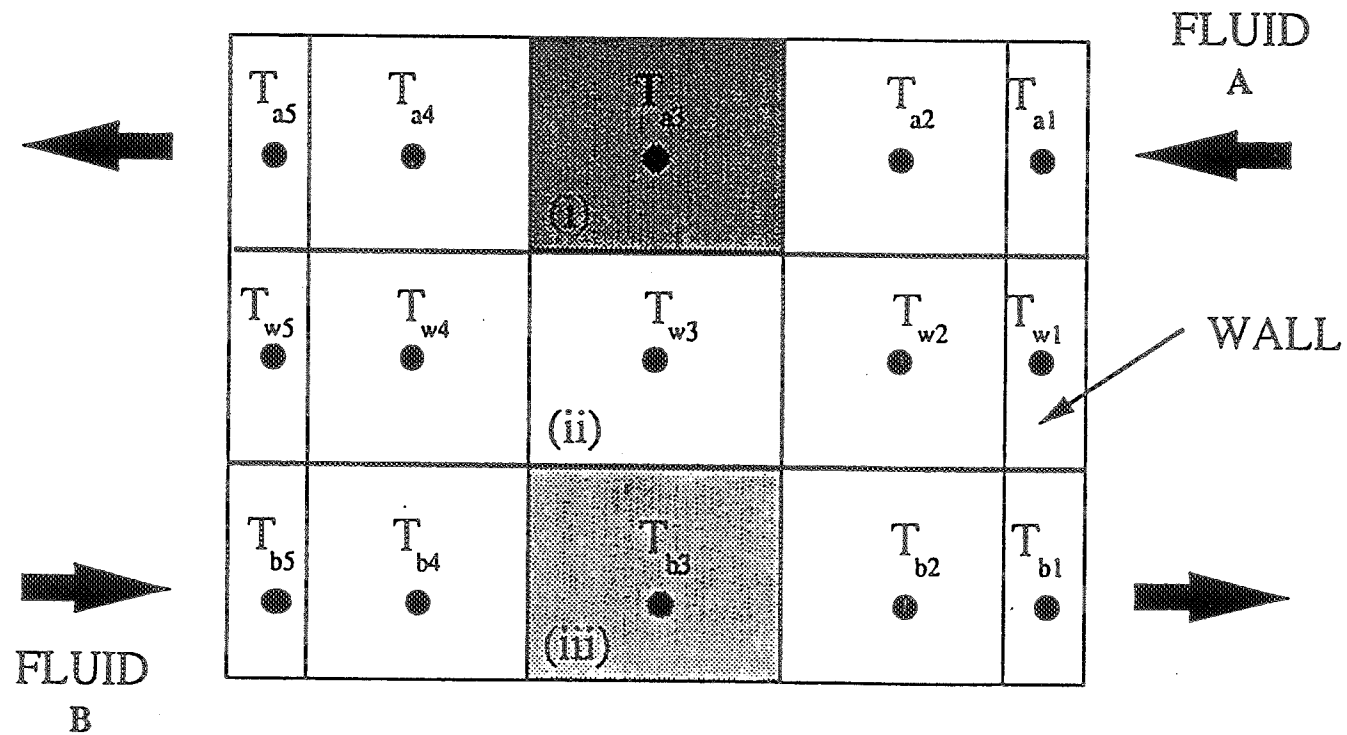
- Write standard FORTRAN model as a subroutine and test
- Convert subroutine into EASY5 FORTRAN block and test
- Convert FORTRAN block into Macro if appropriate
- Install component model in system fabric

Coolant Loop:

- Built system fabric: identify & name each component  
name each input & output variable  
establish connectivity between components
- First radiator model:
  - single element
  - explicit Euler solution of energy equation

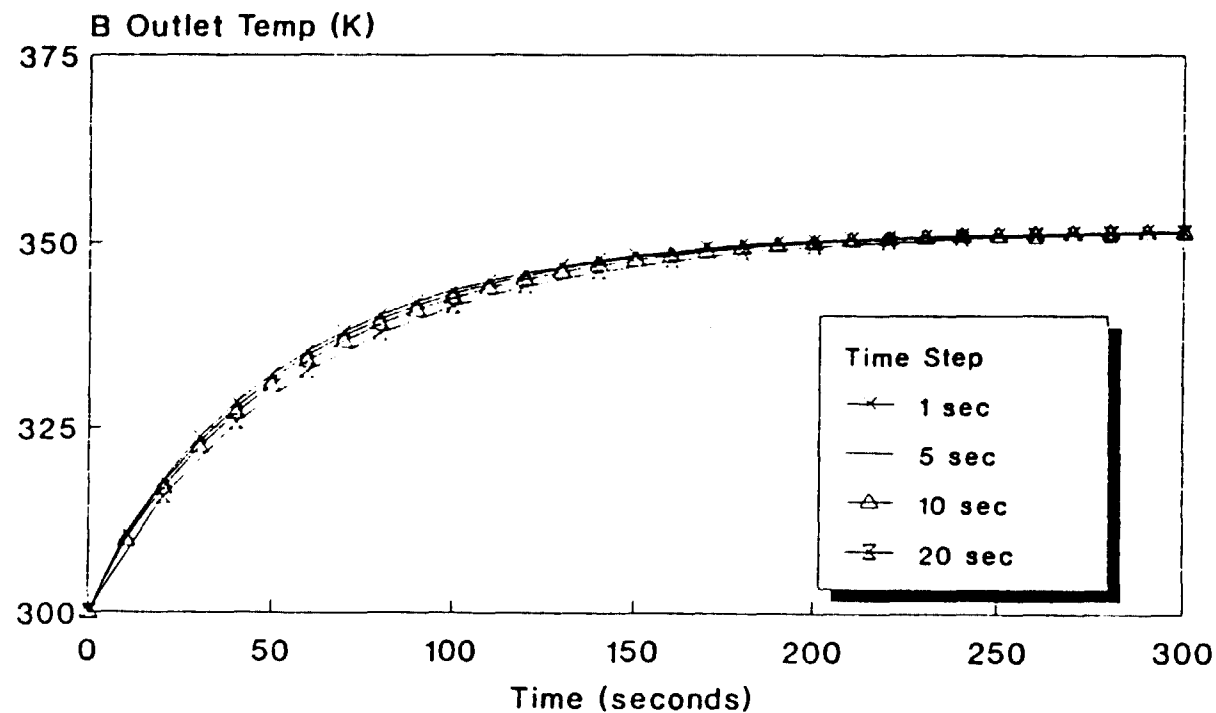
- Gas-Liquid Heat Exchanger
  - 2D Multi-element
  - Fully implicit (Gauss with partial pivoting)
  - Tested sensitivity to time-step size and number of elements
- Second Radiator Model
  - Multi-element
  - Fully implicit (split  $T^4$  term and iterate)
  - Test model sensitivity to  $\Delta t$  and number of elements
- Develop simple component models for:
  - connecting ducts (specified heat flow, simple friction loss)
  - pump (specified flow rate)
  - manifold (specified flow ratios)
- Assemble and test coolant loop

# COOLANT LOOP



Gas Cooler Model

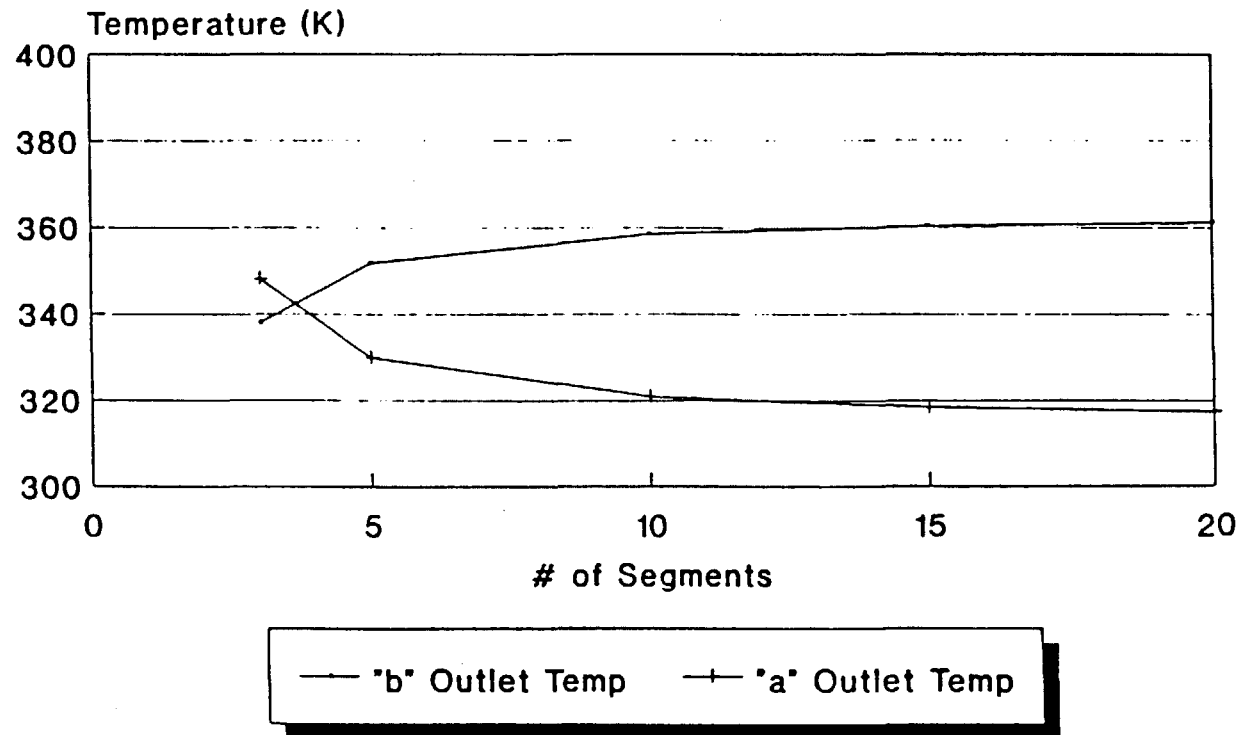
## Gas Cooler Fluid B Transient Performance



A Intemp=400 K, B Intemp=300 K  
# of segments=5,  
A. Iqbal 11/8/89 SMALL.FOR

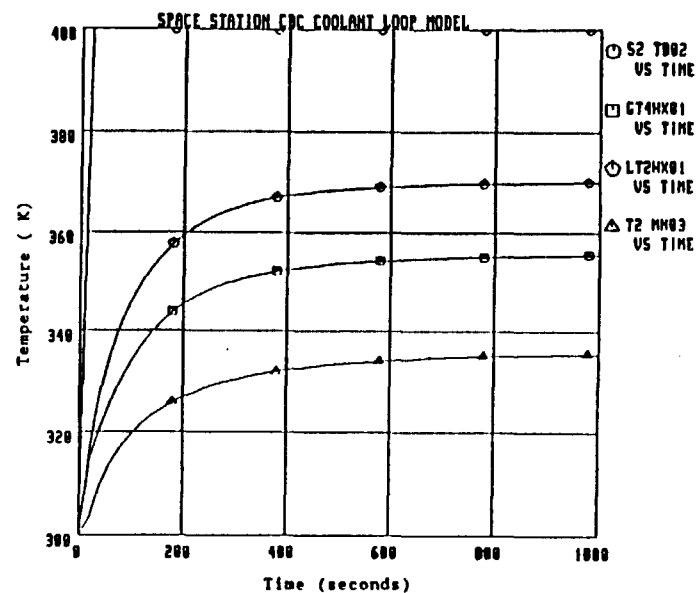


## Gas Cooler Number of Segments Convergence Study



'a' Intemp=400 K, 'b' Intemp=300K  
Delta T=10 s,  
A. Iqbal 11/9/89 SMALL.FOR

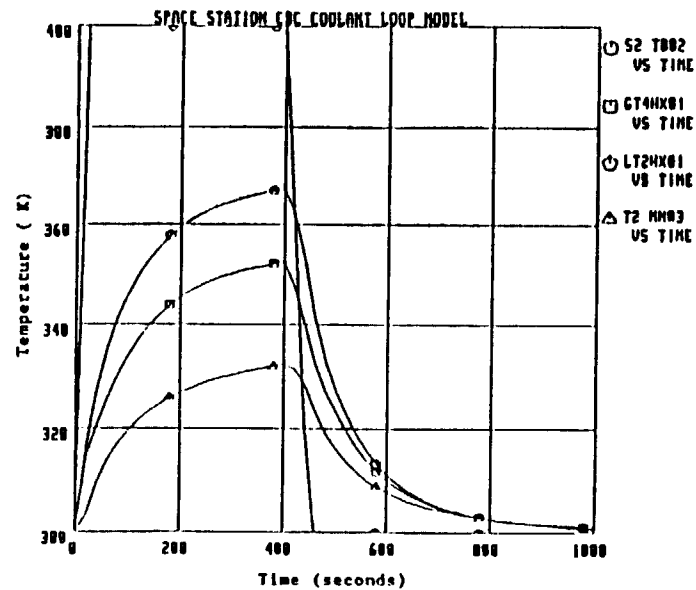
[illegible]



S2 T802 - GAS INLET TEMP., GAS COOLER  
GT4HX01 - GAS OUTLET TEMP., GAS COOLER  
LT2HX01 - COOLANT OUTLET TEMP., GAS COOLER  
T2 MN03 - COOLANT OUTLET TEMP., MANIFOLD 3

Response to a Step in Salt Temperature

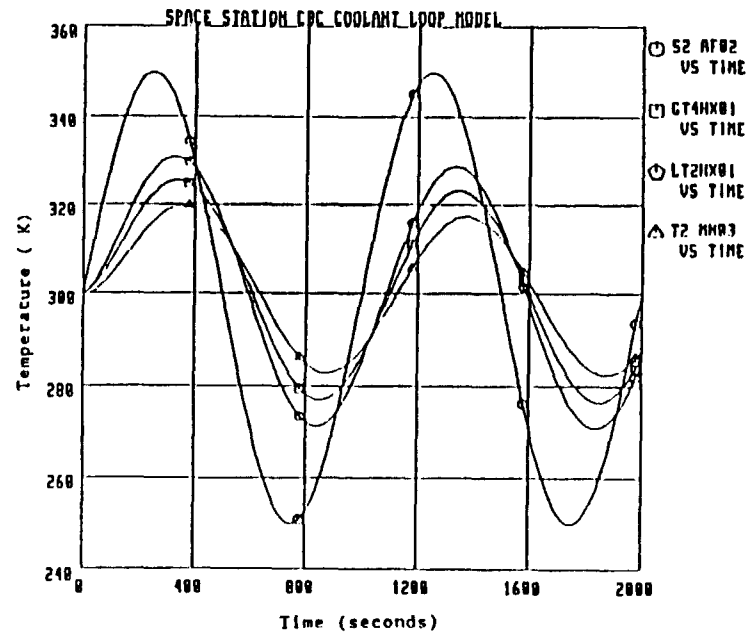
# COOLANT LOOP



S2 T802 - GAS INLET TEMP., GAS COOLER  
GT4HX01 - GAS OUTLET TEMP., GAS COOLER  
LT2HX01 - COOLANT OUTLET TEMP., GAS COOLER  
T2 MN03 - COOLANT OUTLET TEMP., MANIFOLD 3

Response to a Double Step in Salt Temperature

# COOLANT LOOP



S2 AF02 - GAS INLET TEMP., GAS COOLER  
GT4HX01 - GAS OUTLET TEMP., GAS COOLER  
LT2HX01 - COOLANT OUTLET TEMP., GAS COOLER  
T2 MN03 - COOLANT OUTLET TEMP., MANIFOLD 3

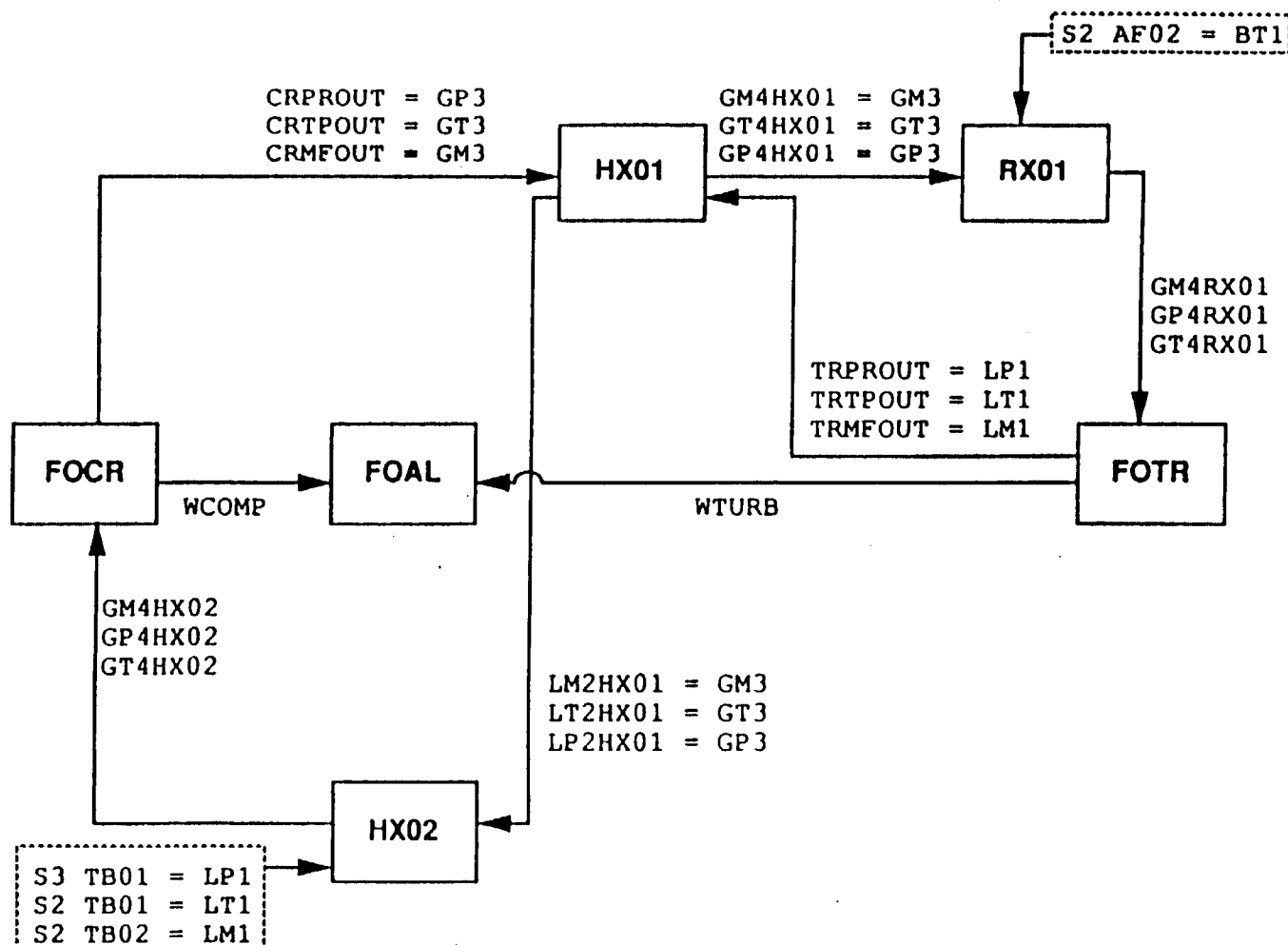
Response to a Sinusoidal Variation in Salt Temperature

## Gas Loop Components:

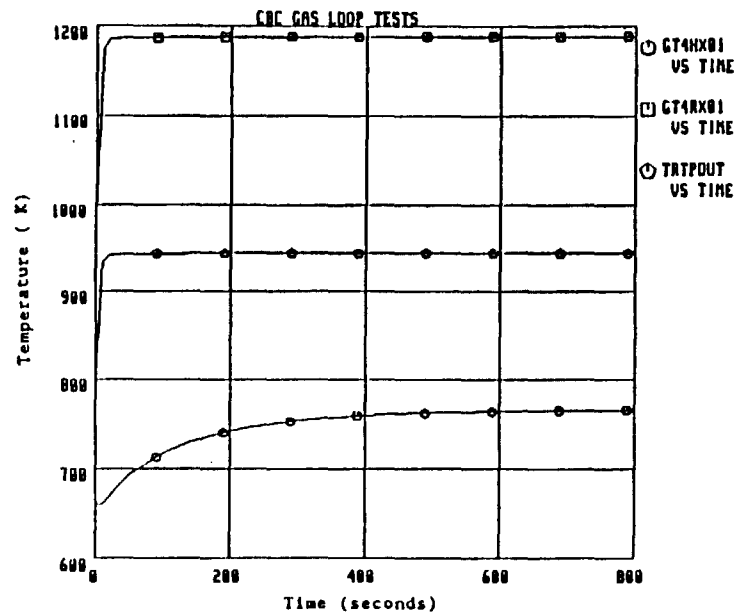
- Receiver
  - Multi-element
  - Fully implicit solution of energy equation
  - Specified uniform salt temperature
- Combined Rotating Unit: Turbine, Alternator, Compressor
  - Constant-speed operation
  - Quasi-steady model
    - enforce steady state balances for mass and energy
    - use steady state performance parameters (ie  $\eta$ )
    - neglect mass storage in components
    - more details in turbomachinery modeling section
  - Also developed variable speed model to evaluate performance during an intentional change of speed

- Assemble and test gas loop against simple transient drivers (fixed coolant temperature in gas cooler).
- Assemble Full Power Generation System
- Run analyses of interest

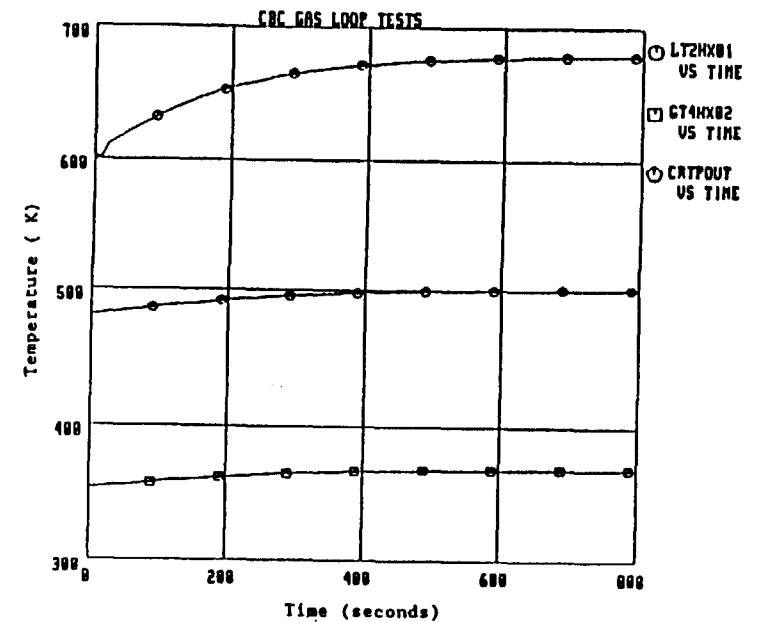
# GAS LOOP





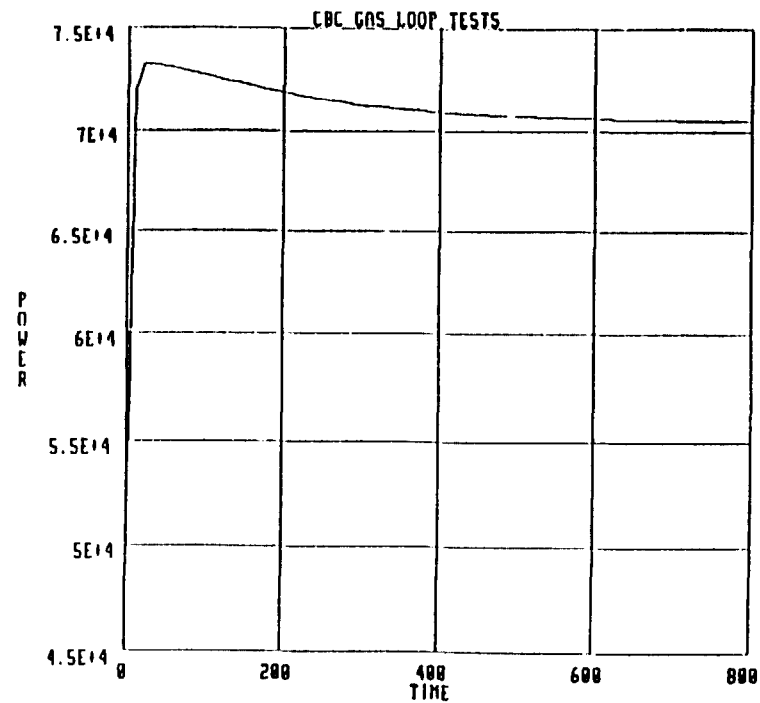


GT4HX01 - GAS OUTLET TEMP., RECUPERATOR  
GT4RX01 - GAS OUTLET TEMP., RECEIVER  
TRTPOUT - GAS OUTLET TEMP., TURBINE

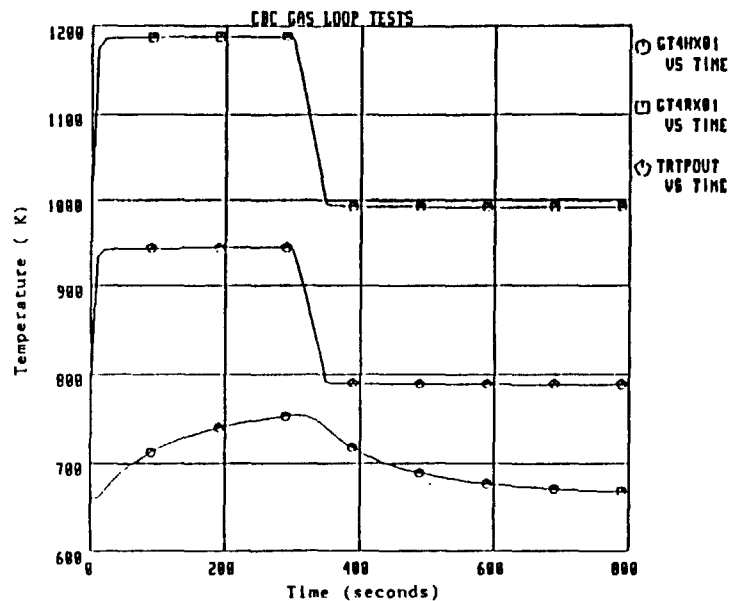


LT2HX01 - GAS OUTLET TEMP., RECUPERATOR  
GT4HX02 - GAS OUTLET TEMP., GAS COOLER  
CRTPOUT - GAS OUTLET TEMP., COMPRESSOR

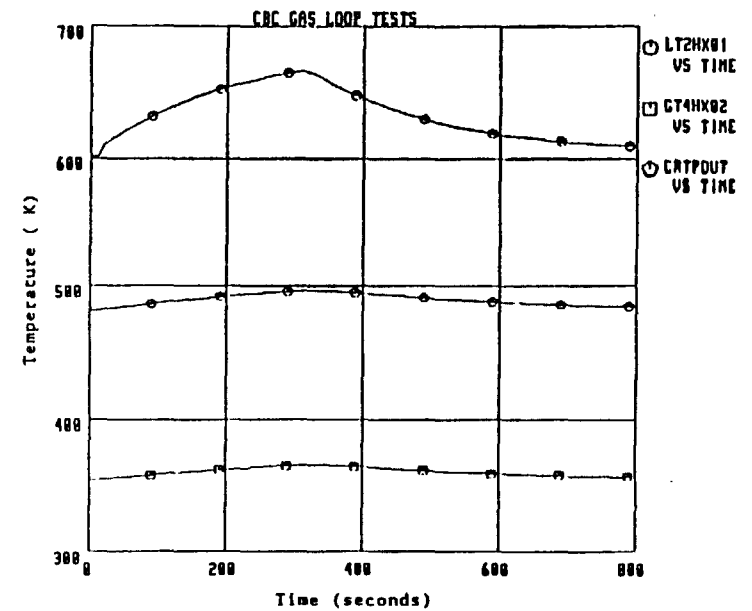
Response to a Step in Salt Temperature



Response to a Step in Salt Temperature

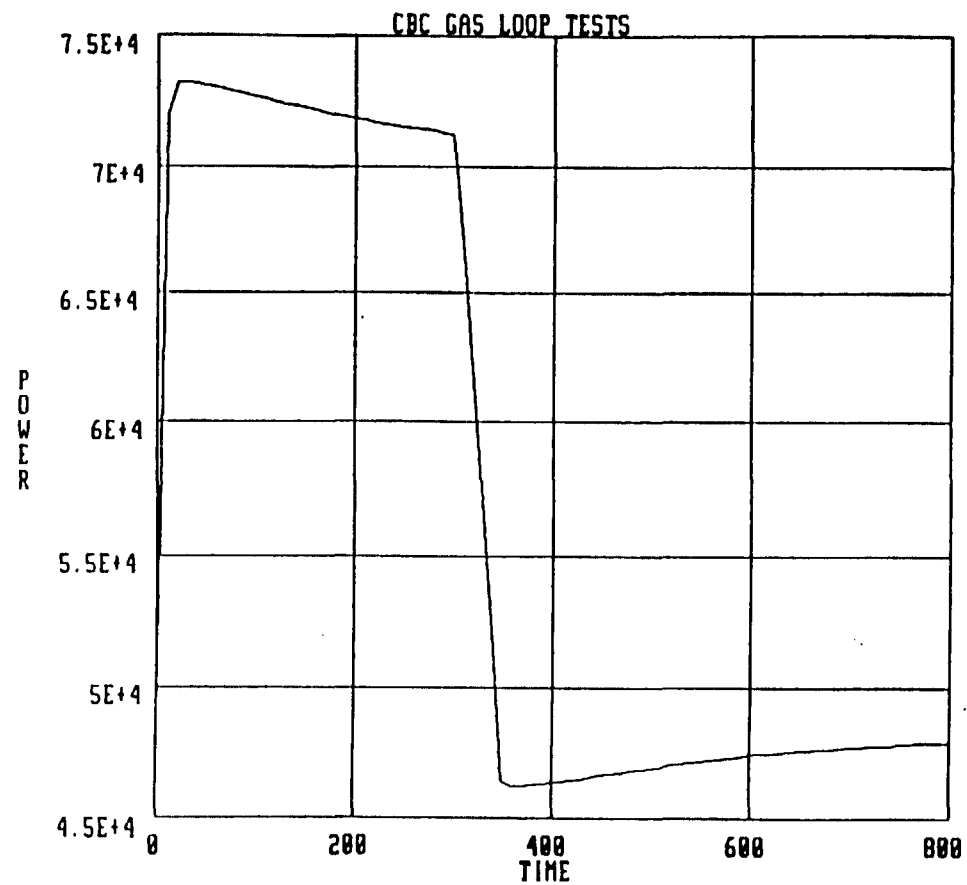


GT4HX01 - GAS OUTLET TEMP., RECUPERATOR  
GT4RX01 - GAS OUTLET TEMP., RECEIVER  
TRTPOUT - GAS OUTLET TEMP., TURBINE



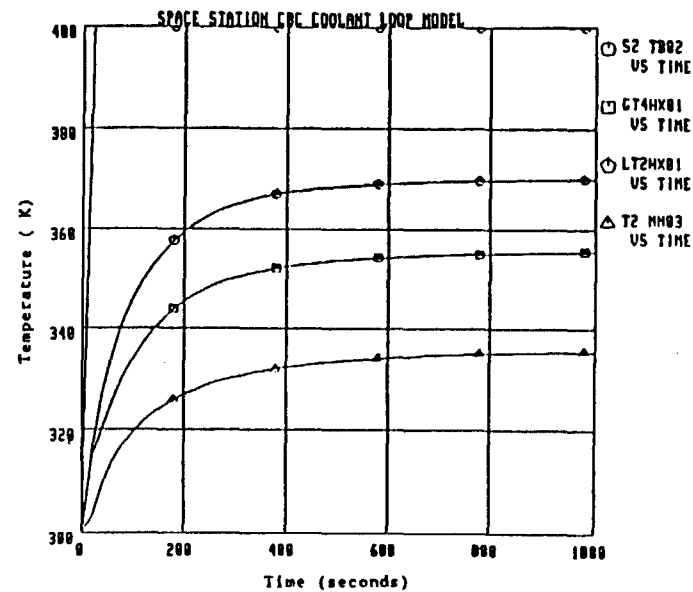
LT2HX01 - GAS OUTLET TEMP., RECUPERATOR  
GT4HX02 - GAS OUTLET TEMP., GAS COOLER  
CRTPOUT - GAS OUTLET TEMP., COMPRESSOR

Response to a Double Step in Salt Temperature



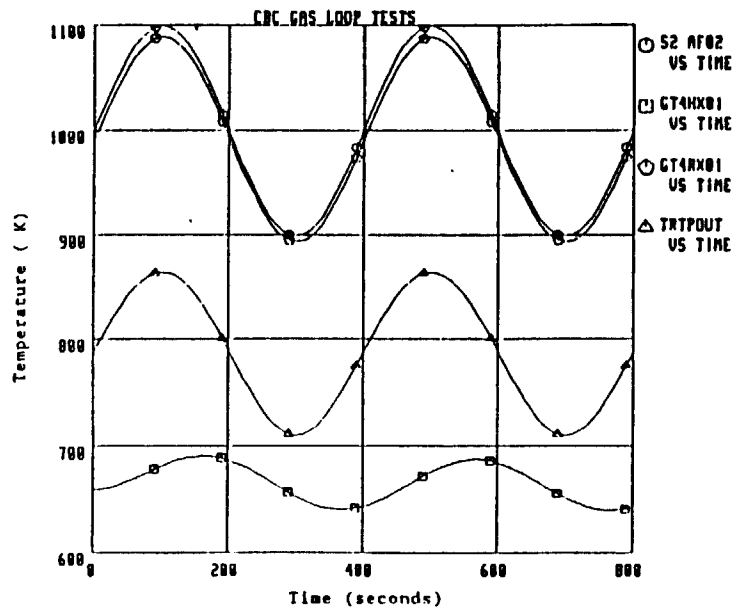
Response to a Double Step in Salt Temperature

# COOLANT LOOP

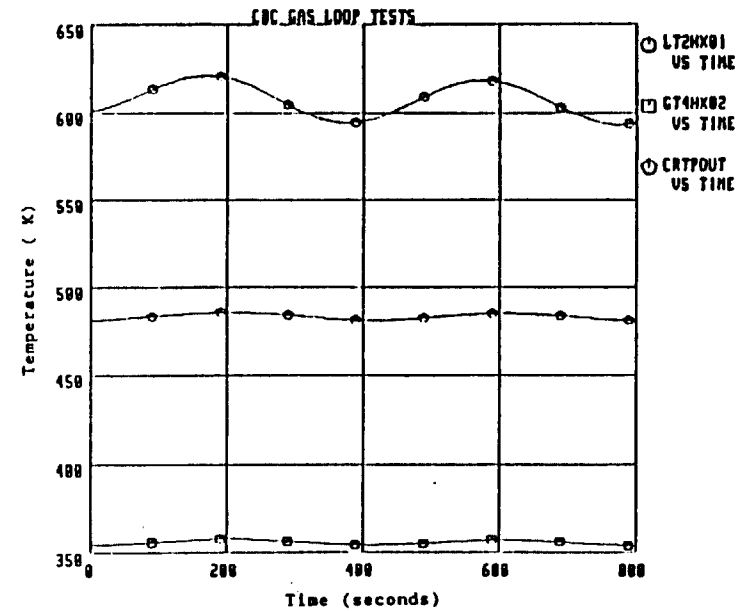


S2 TB02 - GAS INLET TEMP., GAS COOLER  
GT4HX01 - GAS OUTLET TEMP., GAS COOLER  
LT2HX01 - COOLANT OUTLET TEMP., GAS COOLER  
T2 MN03 - COOLANT OUTLET TEMP., MANIFOLD 3

Response to a Step in Salt Temperature

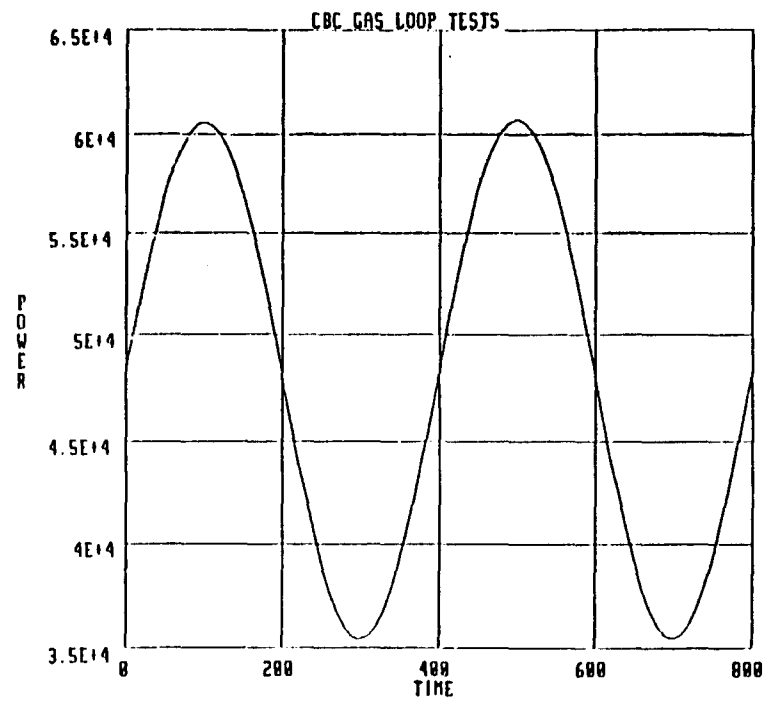


S2 AF02 - SALT TEMP., RECEIVER  
GT4HX01 - GAS OUTLET TEMP., RECUPERATOR  
GT4RX01 - GAS OUTLET TEMP., RECEIVER  
TRTPOUT - GAS OUTLET TEMP., TURBINE

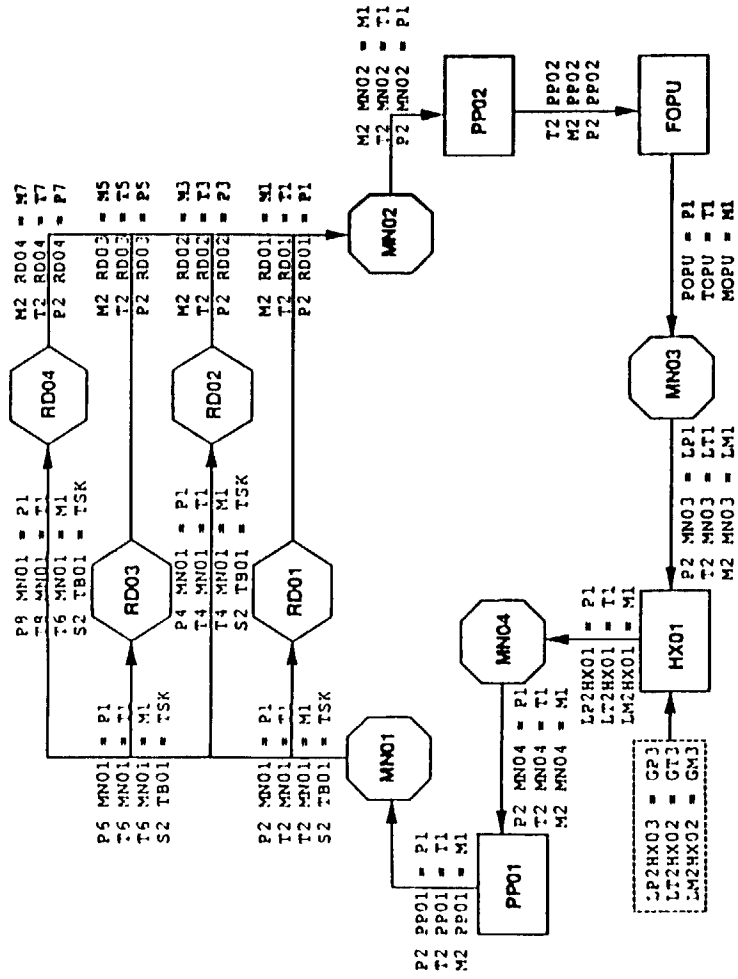


LT2HX01 - GAS OUTLET TEMP., RECUPERATOR  
GT4HX02 - GAS OUTLET TEMP., GAS COOLER  
CRTPOUT - GAS OUTLET TEMP., COMPRESSOR

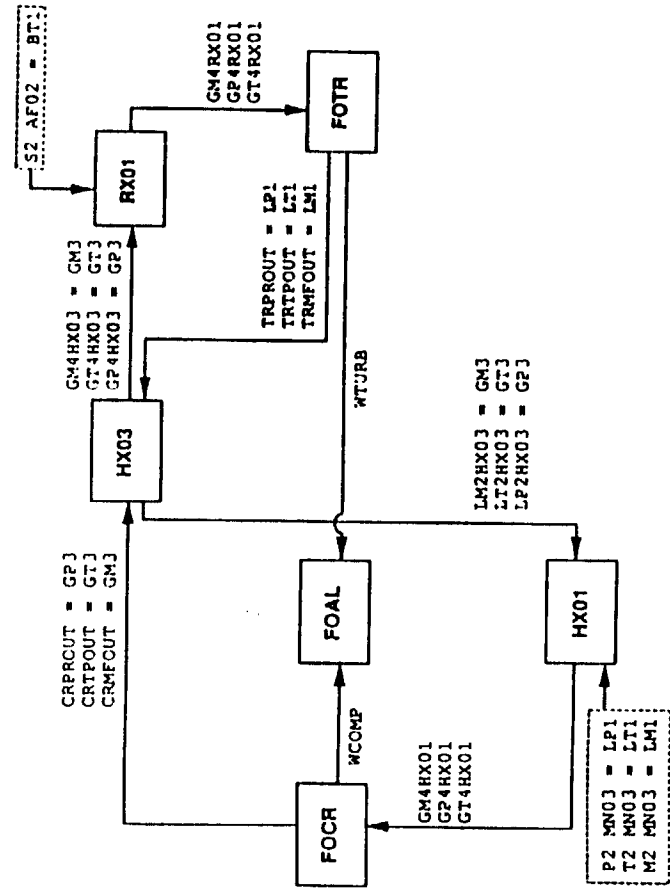
Response to a Sinusoidal Variation in Salt Temperature



Response to a Sinusoidal Variation in Salt Temperature

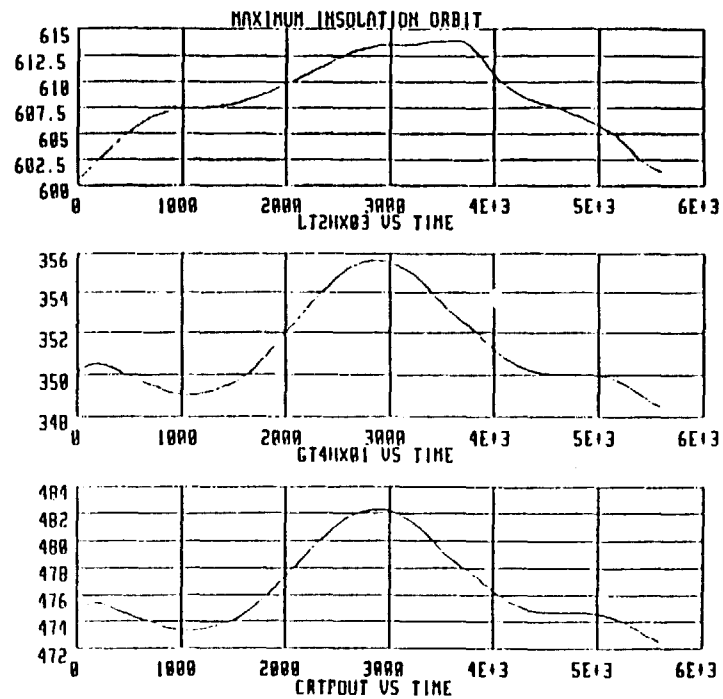


CBC Full System Schematic (Coolant Loop)

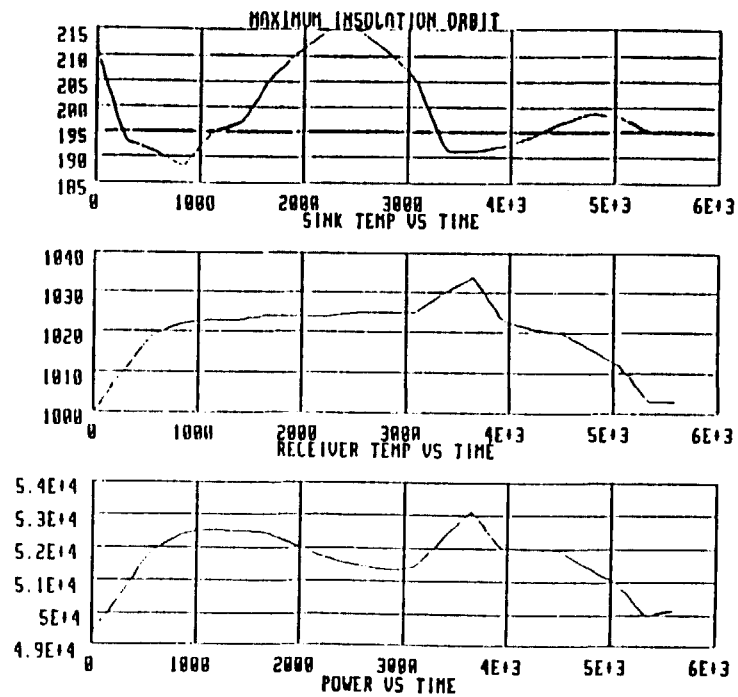


CBC Full System Schematic (Gas Loop)

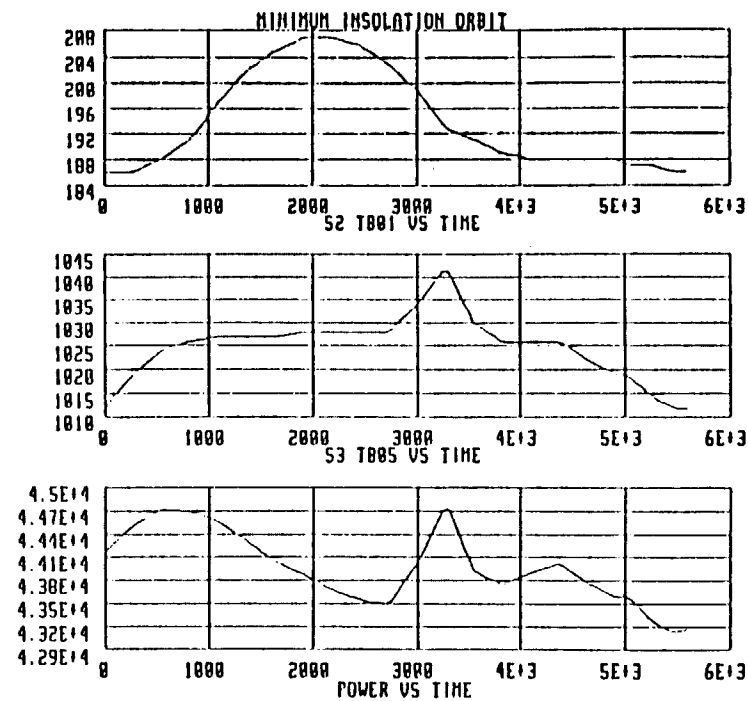




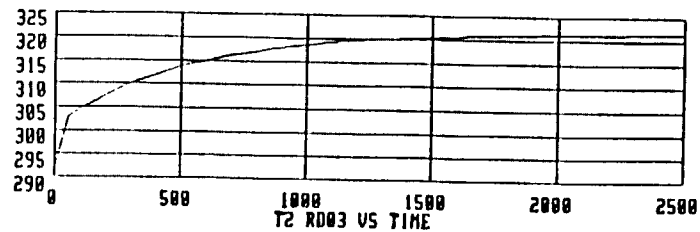
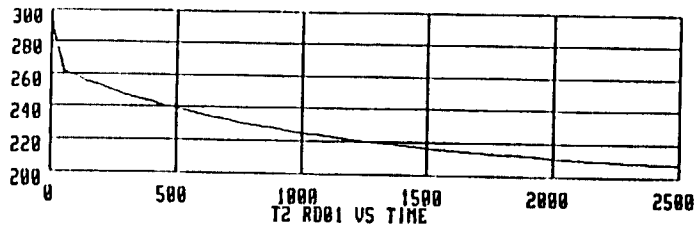
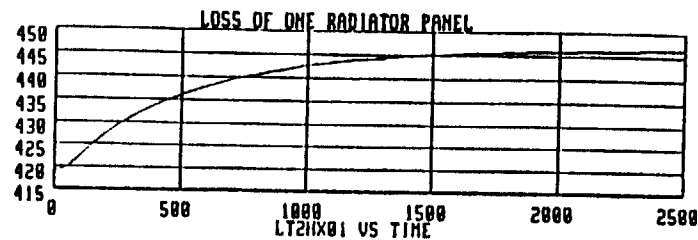
LT2HX03 - GAS OUTLET TEMP., RECUPERATOR  
GT4HX01 - GAS OUTLET TEMP., GAS COOLER  
CRTPOUT - GAS OUTLET TEMP., COMPRESSOR



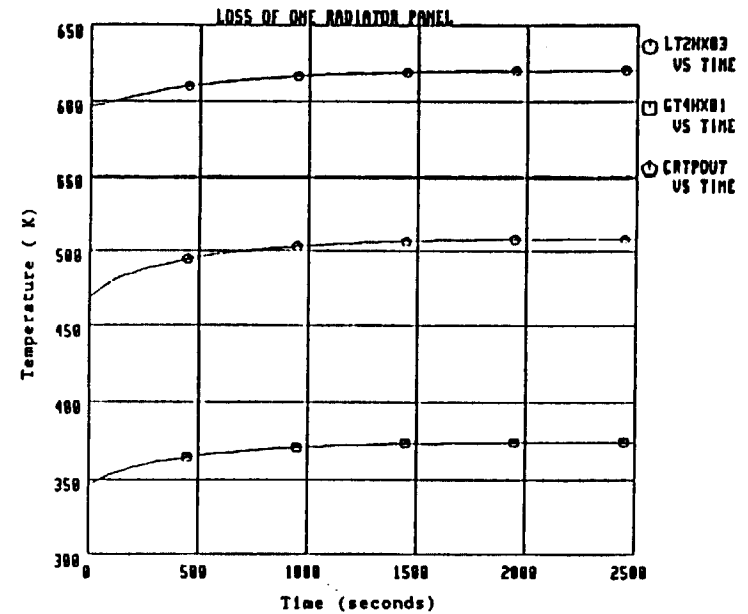
# FULL SYSTEM



S2 TR01 - SINK TEMPERATURE  
S3 TR05 - SALT TEMP., RECEIVER  
POWER - ALTERNATOR POWER

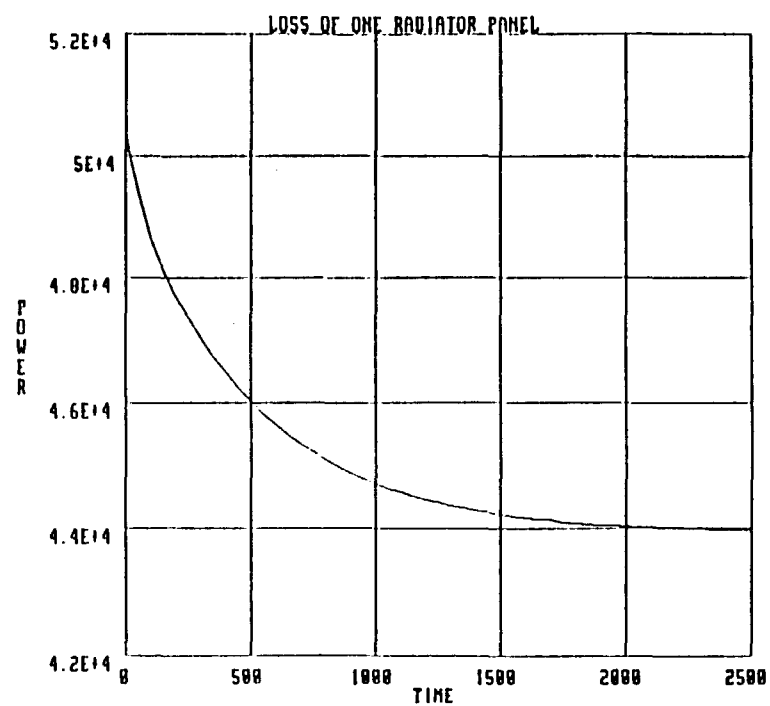


LT2HX01 - COOLANT OUTLET TEMP., GAS COOLER  
T2 RD01 - COOLANT OUTLET TEMP., RADIATOR 1  
T2 RD03 - COOLANT OUTLET TEMP., RADIATOR 3



LT2HX03 - GAS OUTLET TEMP., RECUPERATOR  
GT4HX01 - GAS OUTLET TEMP., GAS COOLER  
CRTPOUT - GAS OUTLET TEMP., COMPRESSOR

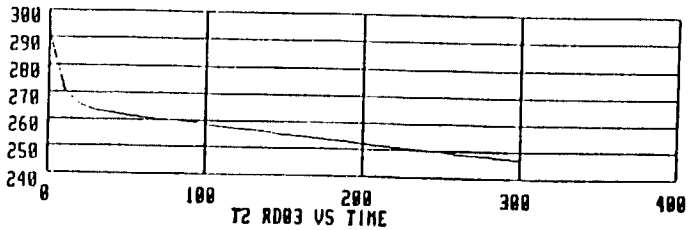
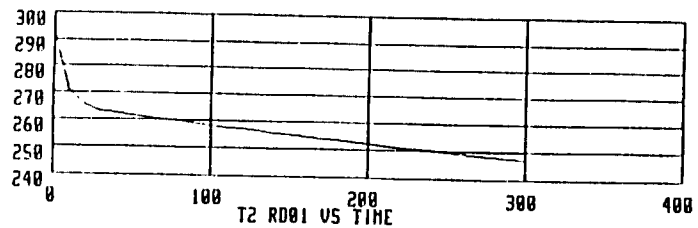
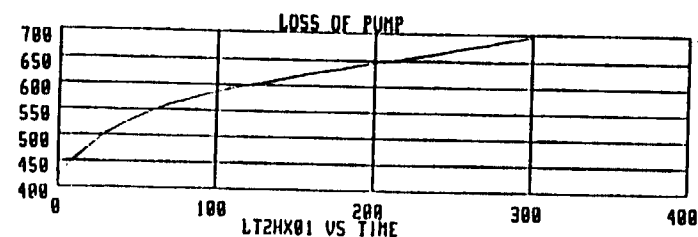
# FULL SYSTEM



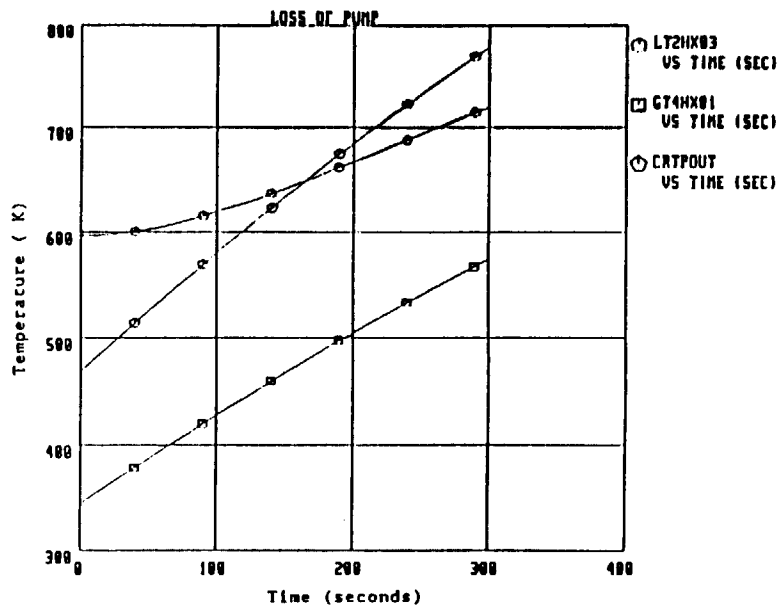
Washington  
University

# FULL SYSTEM

SDPG  
MODELING

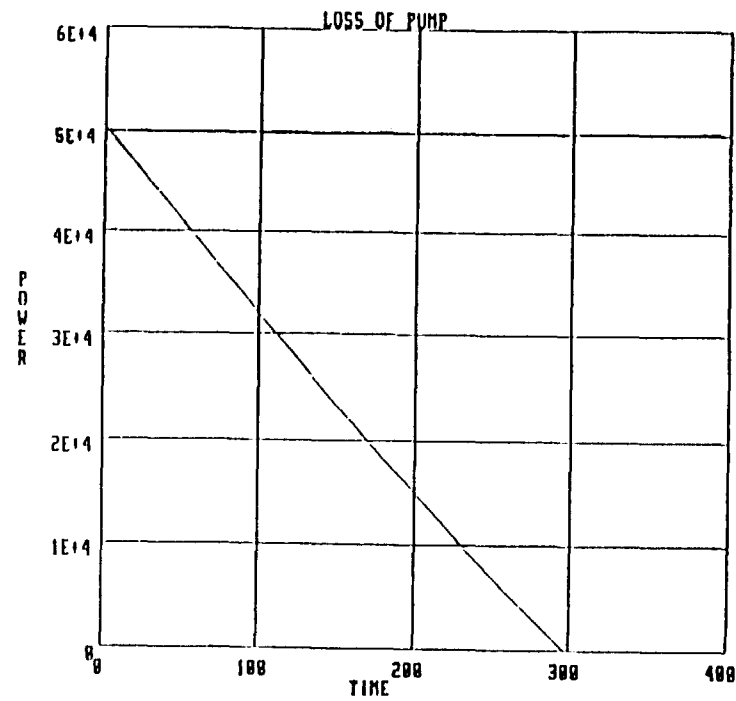


LT2HX01 - COOLANT OUTLET TEMP., GAS COOLER  
T2 RD01 - COOLANT OUTLET TEMP., RADIATOR 1  
T2 RD03 - COOLANT OUTLET TEMP., RADIATOR 3



GT4HX03 - GAS OUTLET TEMP., RECUPFRATOR  
GT4RX01 - GAS OUTLET TEMP., RECEIVER  
TRTPOUT - GAS OUTLET TEMP., TURBINE

# Full System



- Model refinement with more accurate component data
- Integrate thermodynamic model with control system model
- Improve turbomachinery models by attacking "stiffness" to allow larger time-steps.



- Additional information became available on details of components and experience was gained with model performance.
- Developed true steady-state model for system testing.
- Developed new dynamic models
- Developed new system integration logic
- Run Dynamic Heat Exchangers/Quasi-Steady Turbo. model
- Run Dynamic Heat Exchangers/Dynamic Turbo. model

Q-6

Steady-State Models

- Heat Exchangers
  - $\epsilon$ -NTU model
  - improved  $\Delta p$  calculation
- Radiator
  - direct solution of energy balance
- Turbine and Compressor
  - better information on performance

## Dynamic Component Models

- Heat Exchangers
  - Obtained new data on cross-counterflow heat exchangers
  - Multi-element 2D finite-difference model
  - Developed compressible flow analysis to substantiate assumption of no mass storage within a component during a transient flow
- Radiator
  - Improved model details
  - Reformulated as explicit model to avoid iterative solution
- Turbine and Compressor
  - Based on developments of previous section.
  - Improved estimate of actual geometry

Steady-state and quasi steady state models assembled by logically connecting component models.

This could be accomplished using either EASY5 or a FORTRAN main program.

A system model which includes mass storage in the components requires an iterative procedure to solve for the system state at each time-step and ***CANNOT BE IMPLEMENTED IN EASY5.***

#### System Integration Constraint

- Conservation of mass for the entire gas loop must be satisfied.
- begin time-step by using dynamic models to compute a first estimate of new time-level state for each component
  - adjust inlet mass flow rate to the receiver using under-relaxation formula
  - iterate until system mass conserved to within specified tolerance

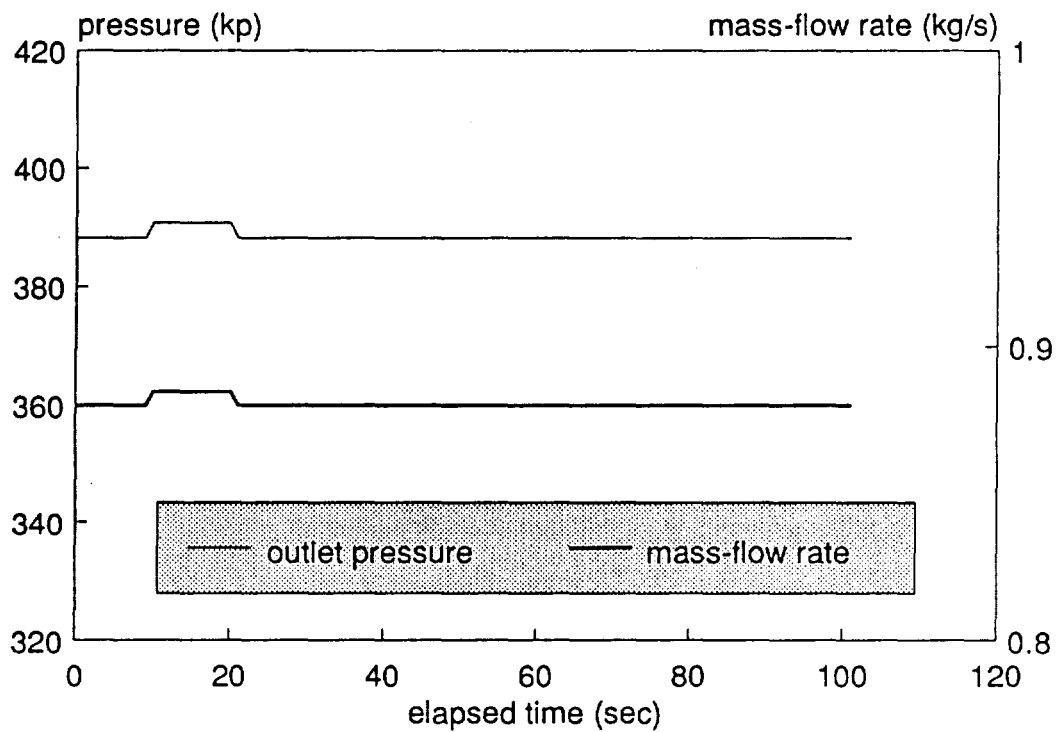
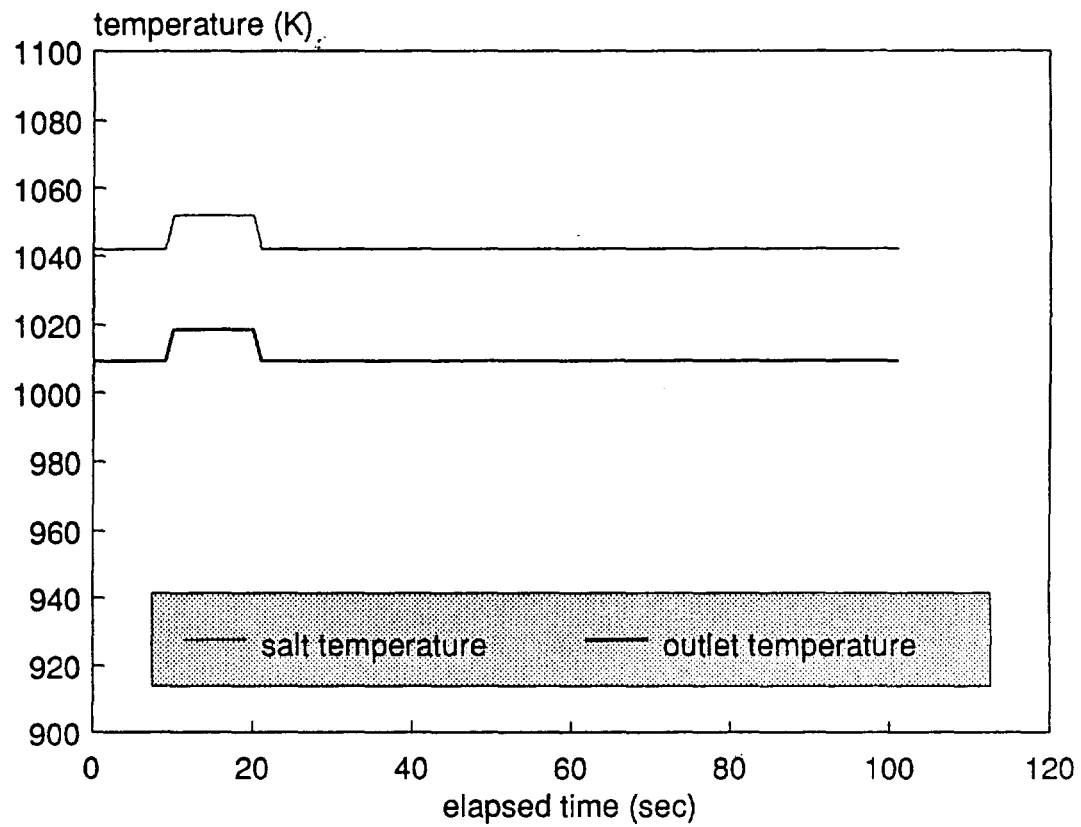


Fig. 4.1 Response of receiver outlet parameters

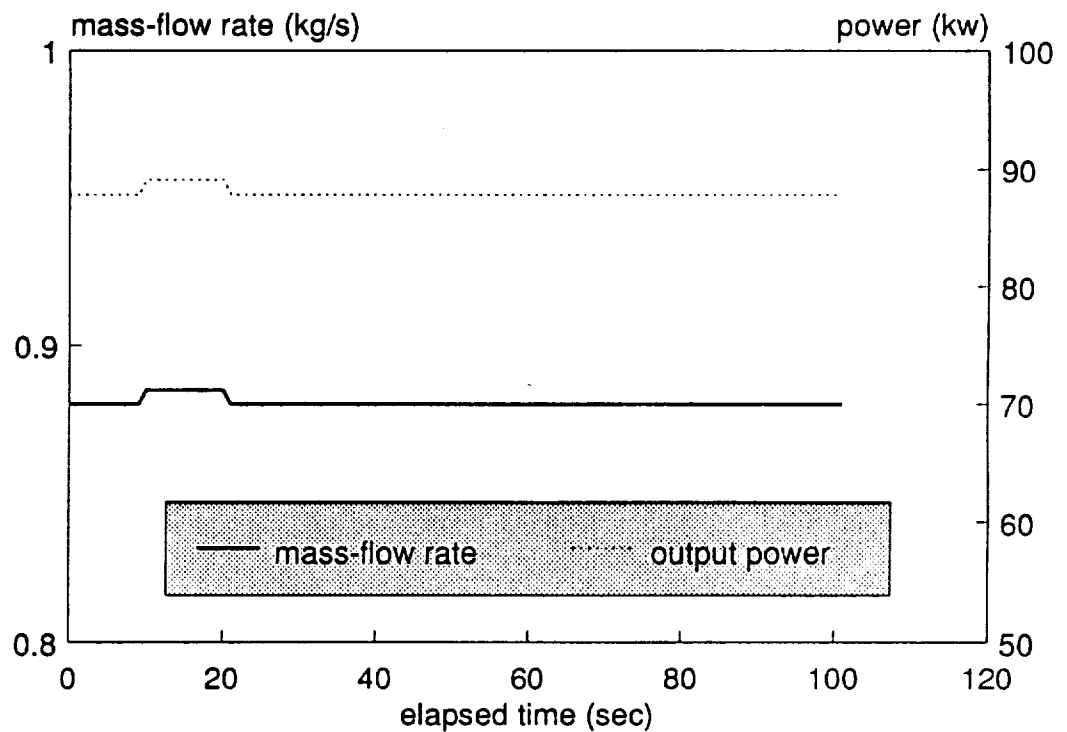
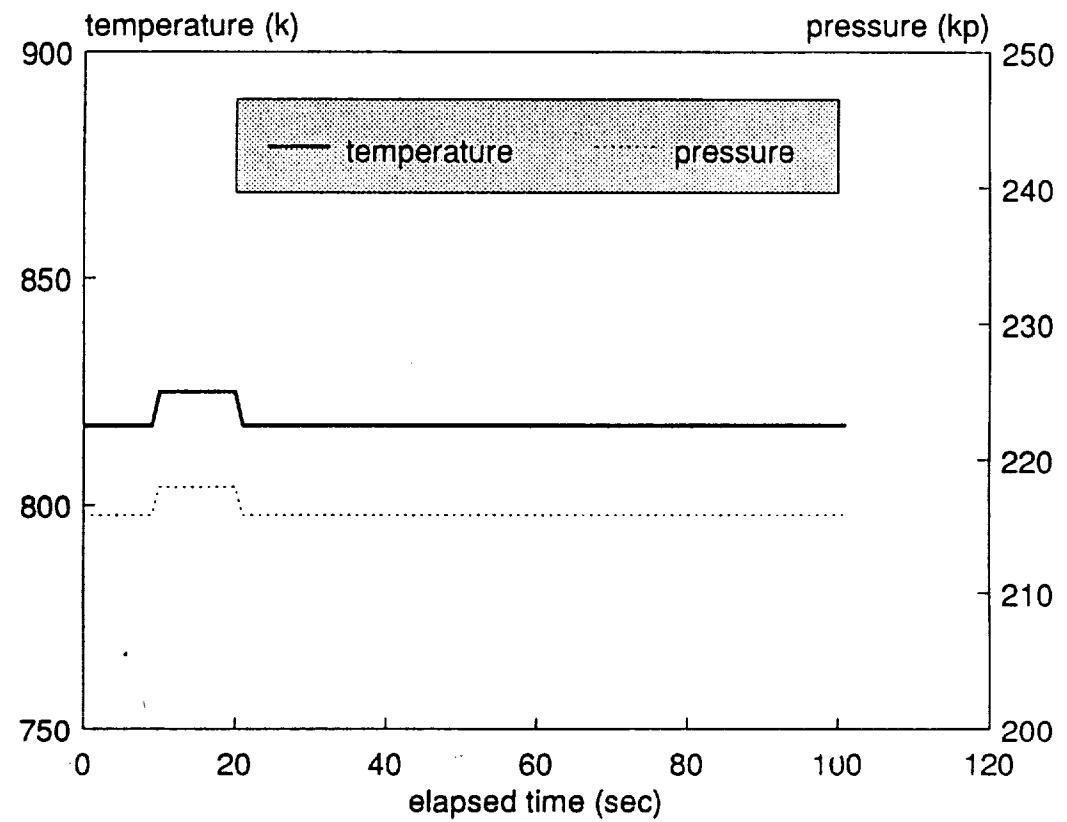


Fig. 4.2 Response of turbine outlet parameters

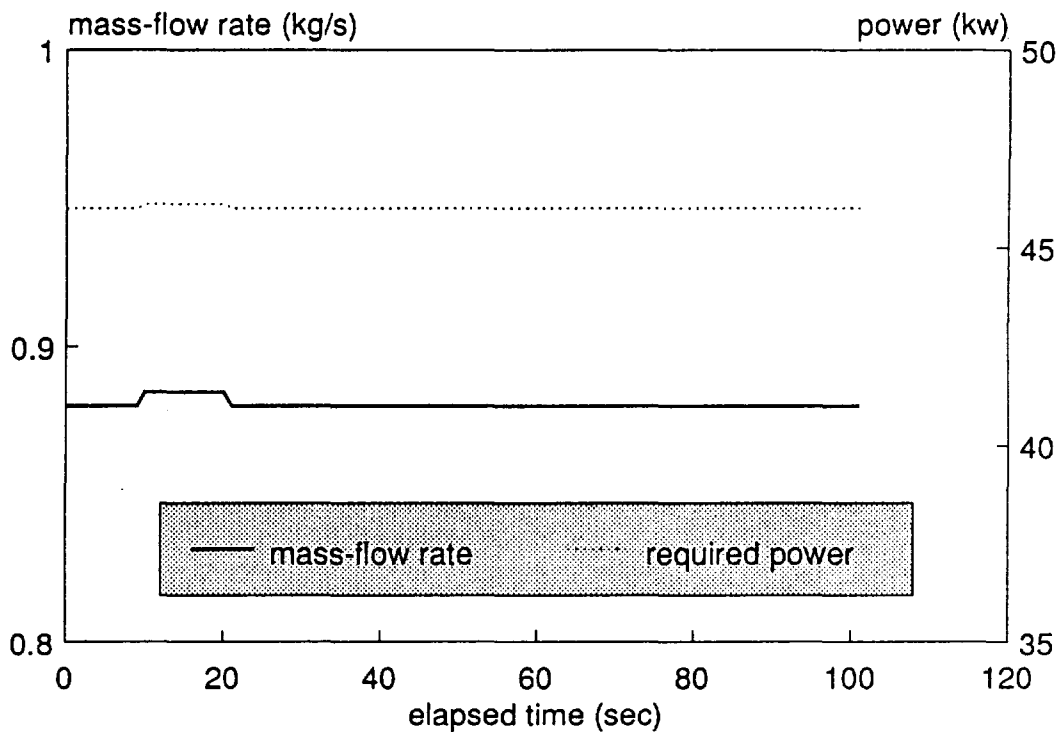
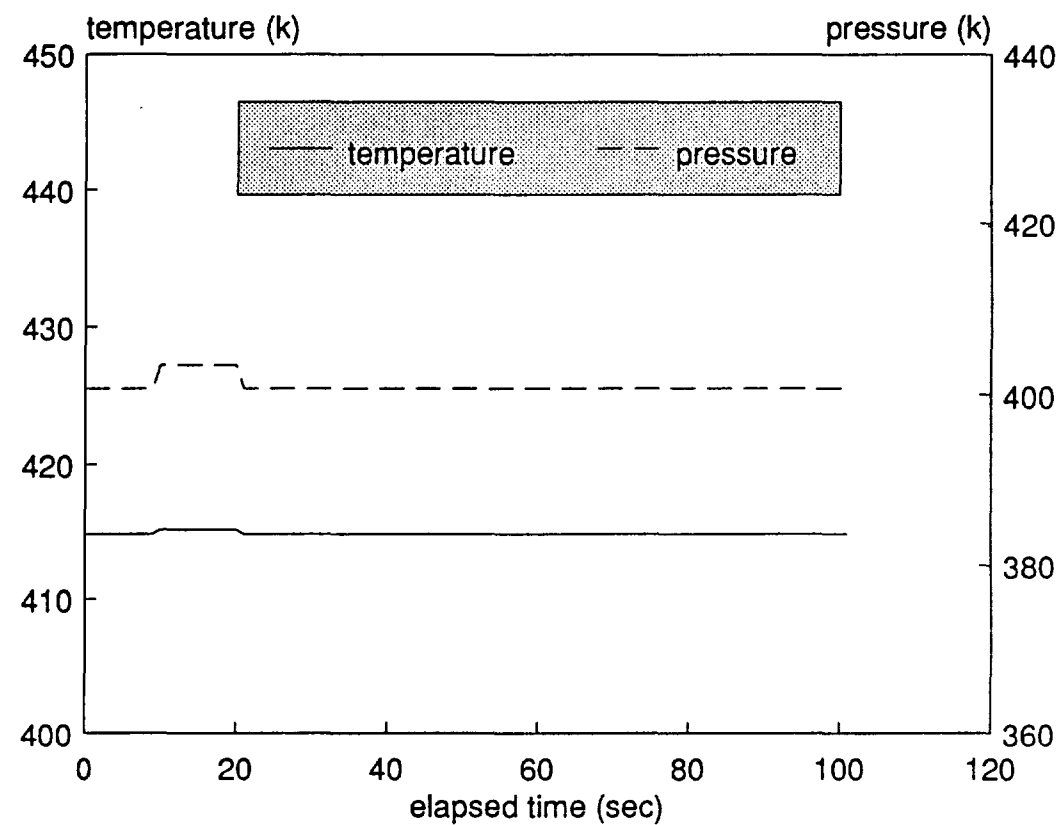


Fig. 4.3 Response of compressor outlet parameters

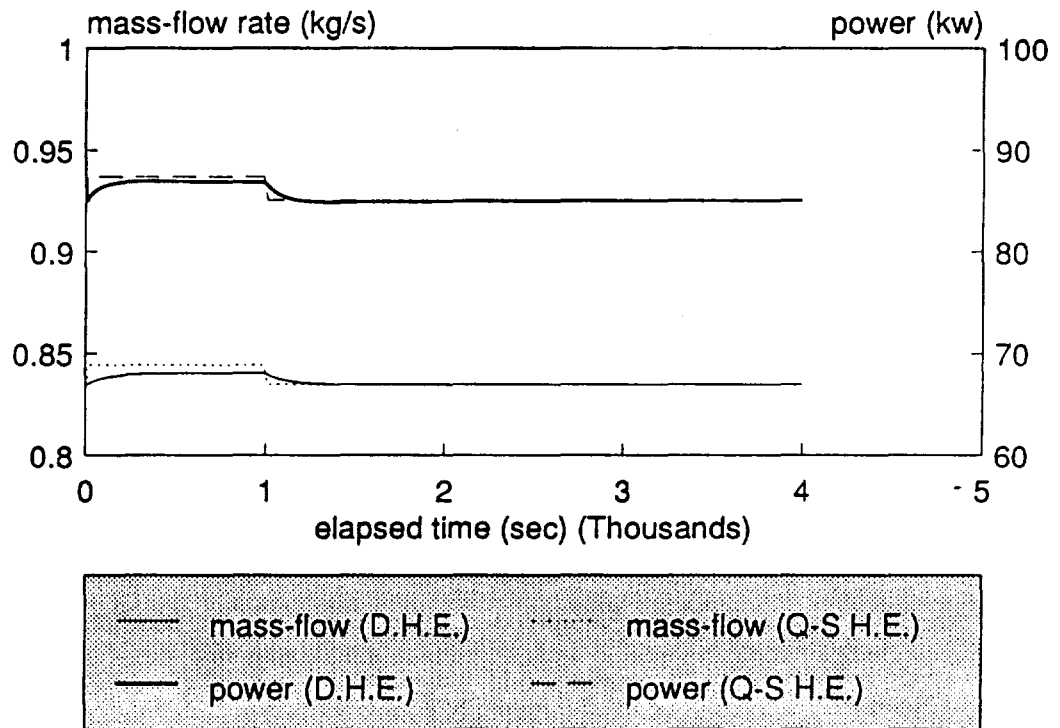
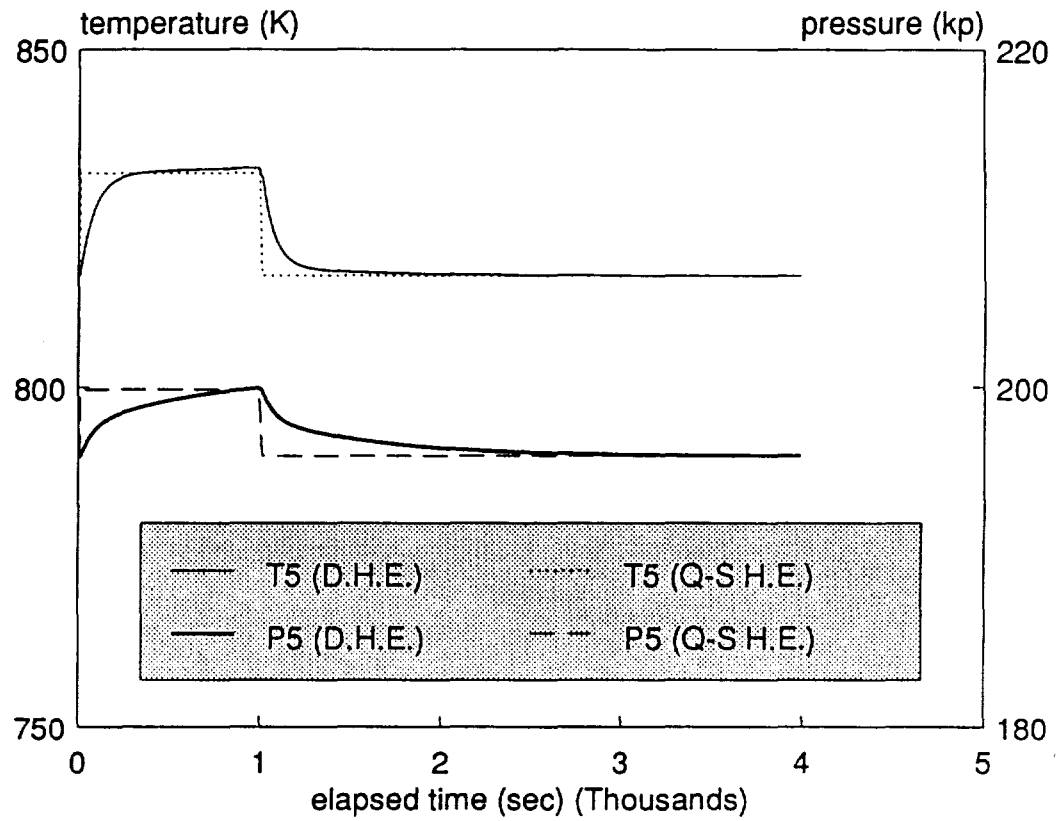


Fig. 4.10 Response of turbine outlet parameters



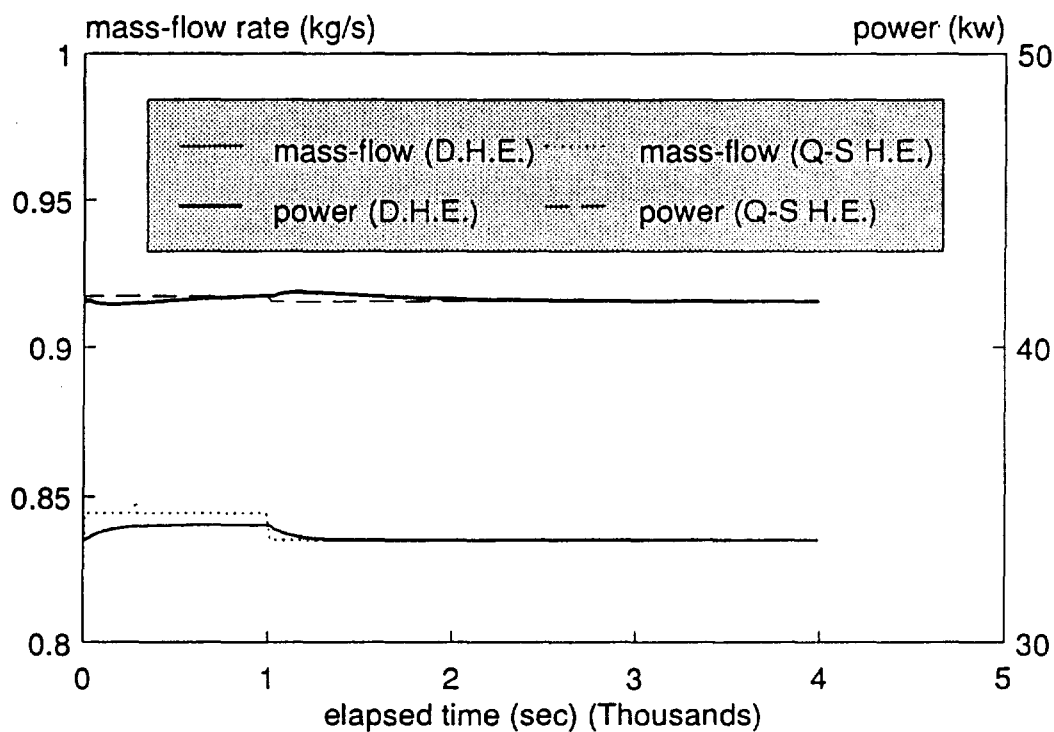
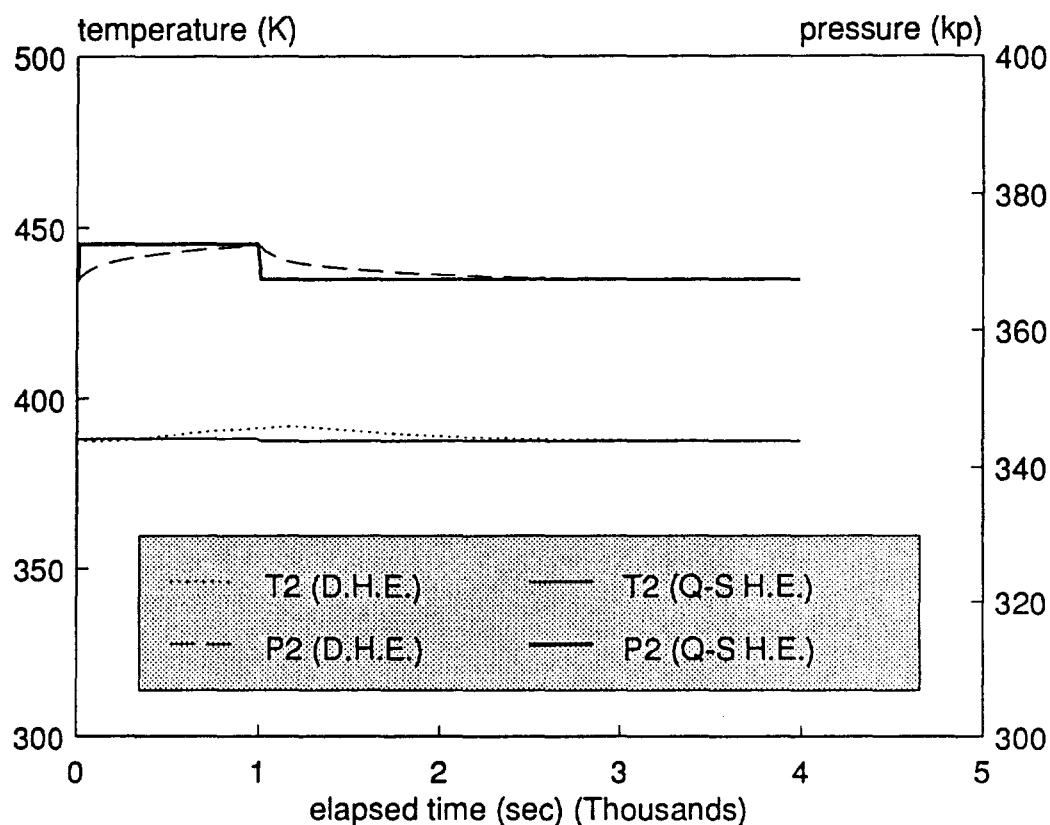


Fig. 4.11 Response of compressor outlet parameters

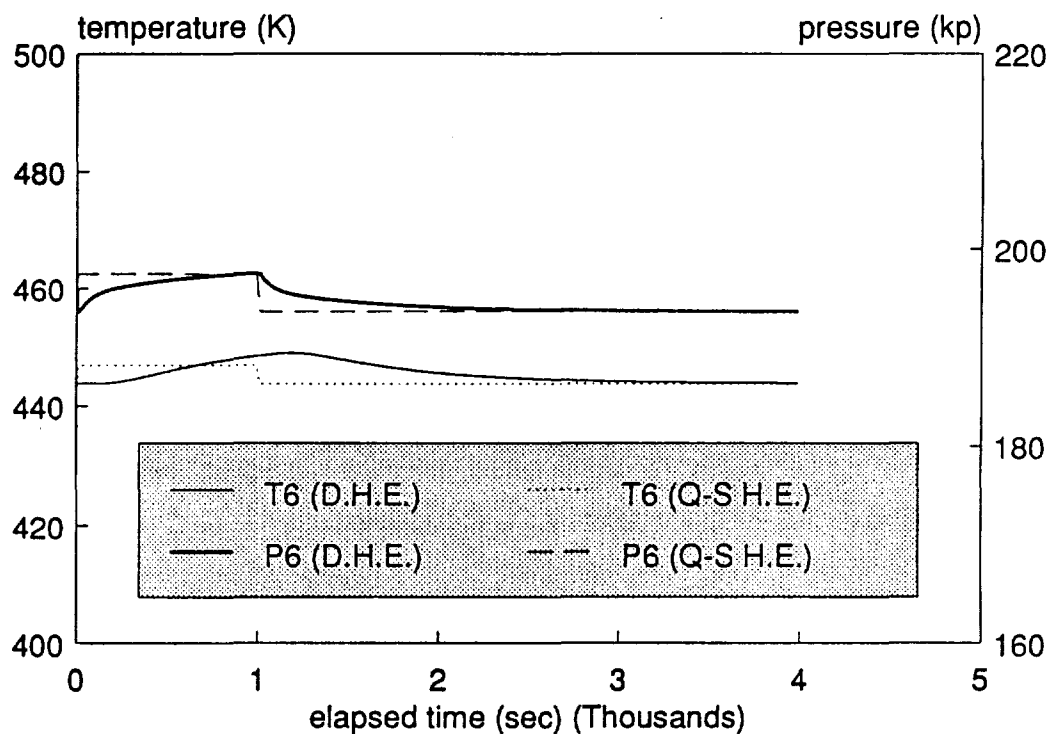
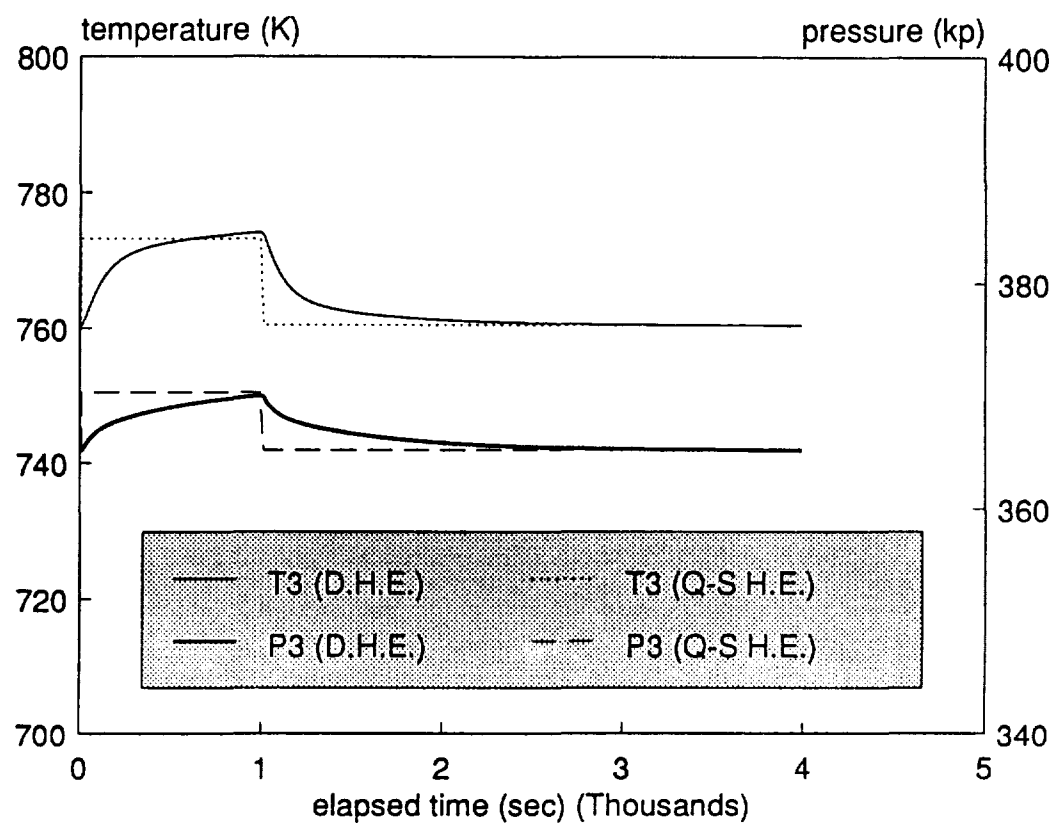


Fig. 4.12 Response of recuperator outlet parameters

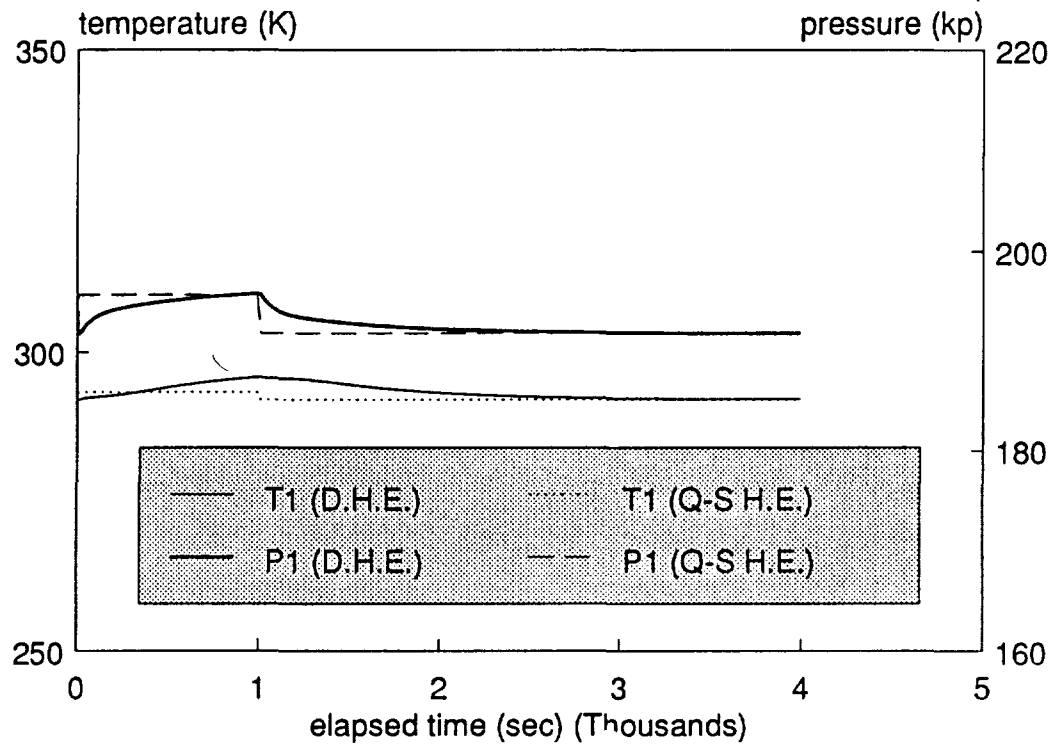


Fig. 4.13 Response of gas cooler outlet parameters

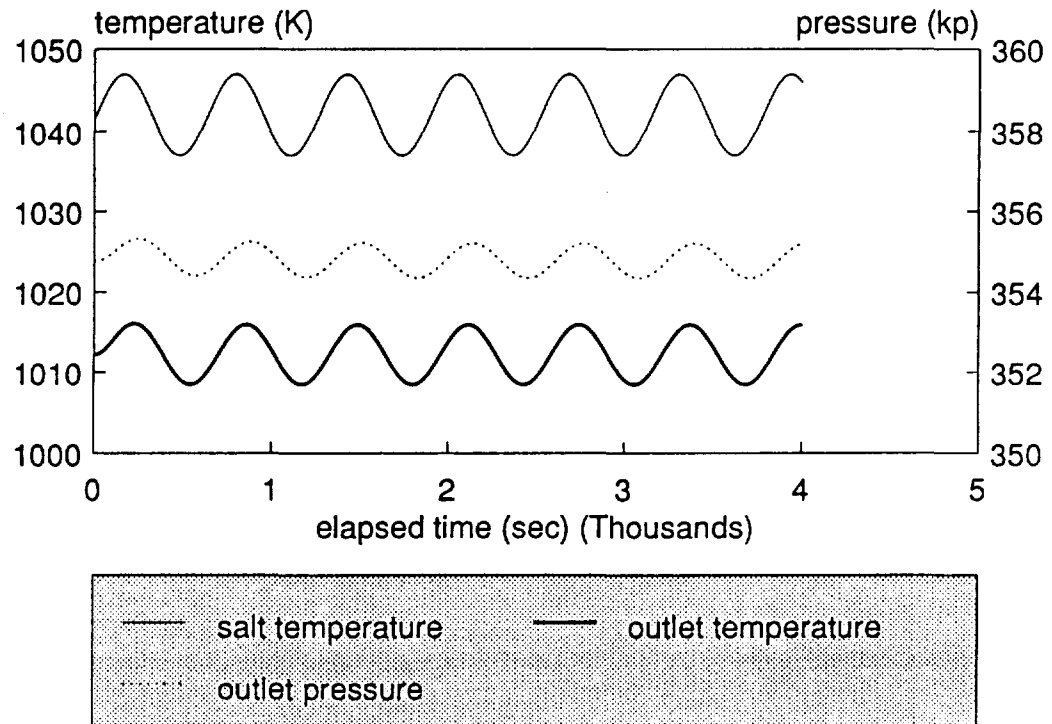


Fig. 4.14 Response of receiver outlet parameters (to sinusoidal driver)

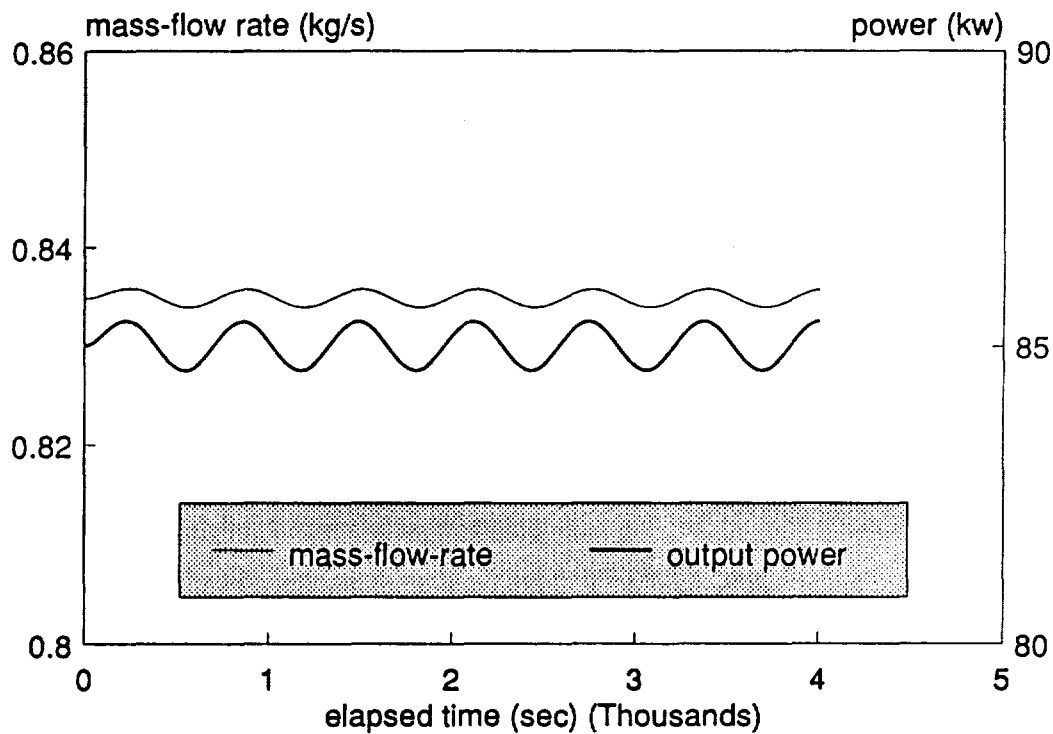
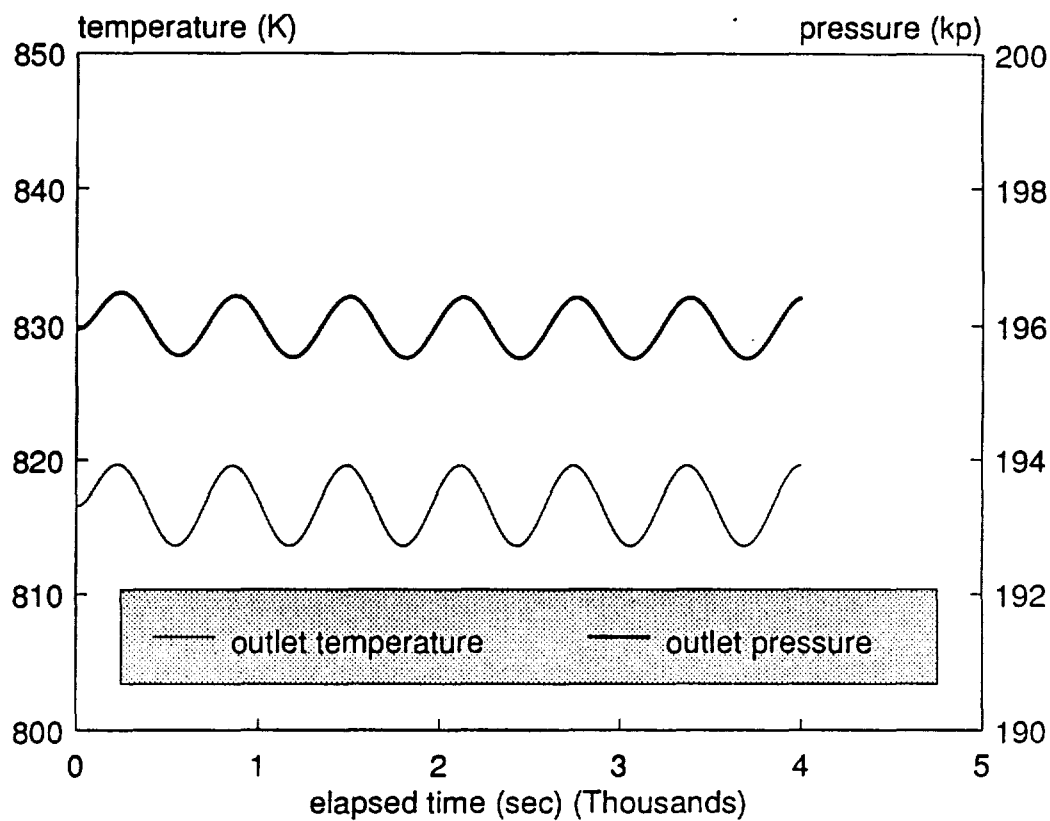


Fig. 4.15 Response of turbine outlet parameters (to sinusoidal driver)

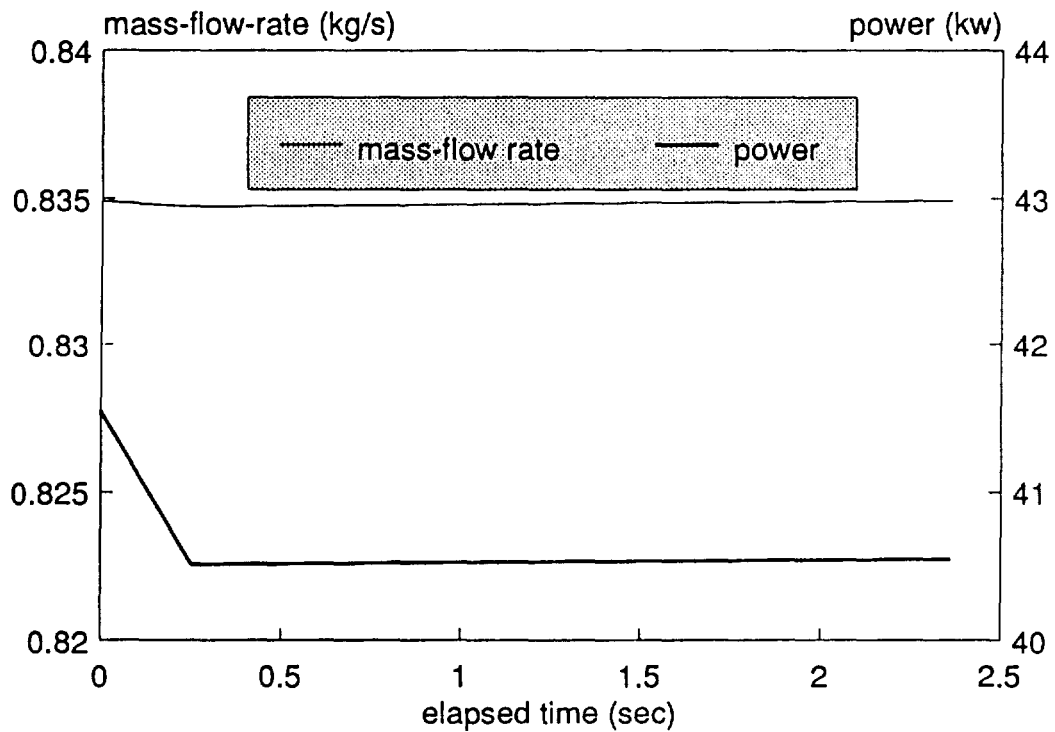
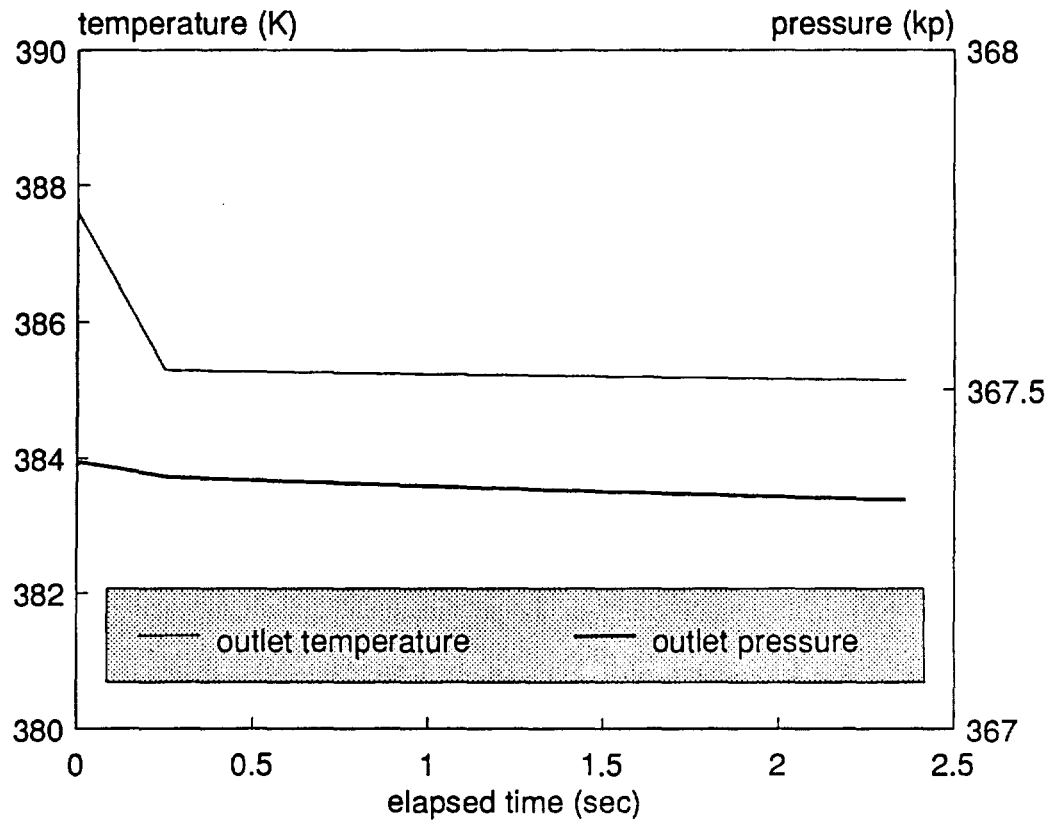


Fig. 4.20 Response of compressor outlet parameters (to ramp of output power)

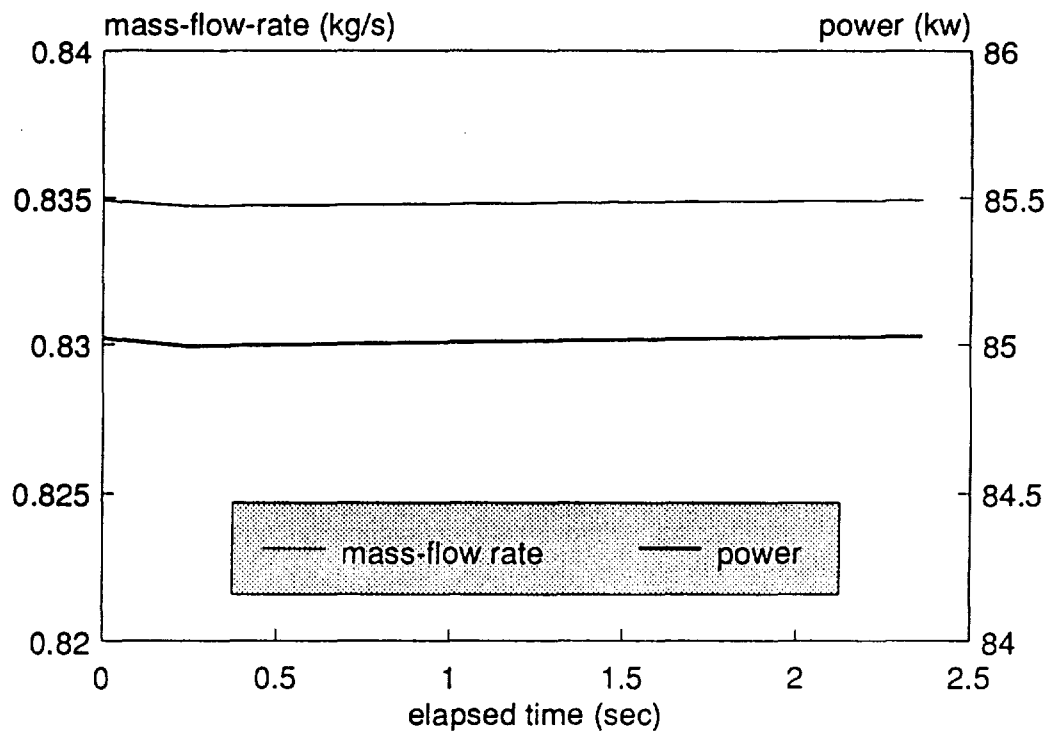
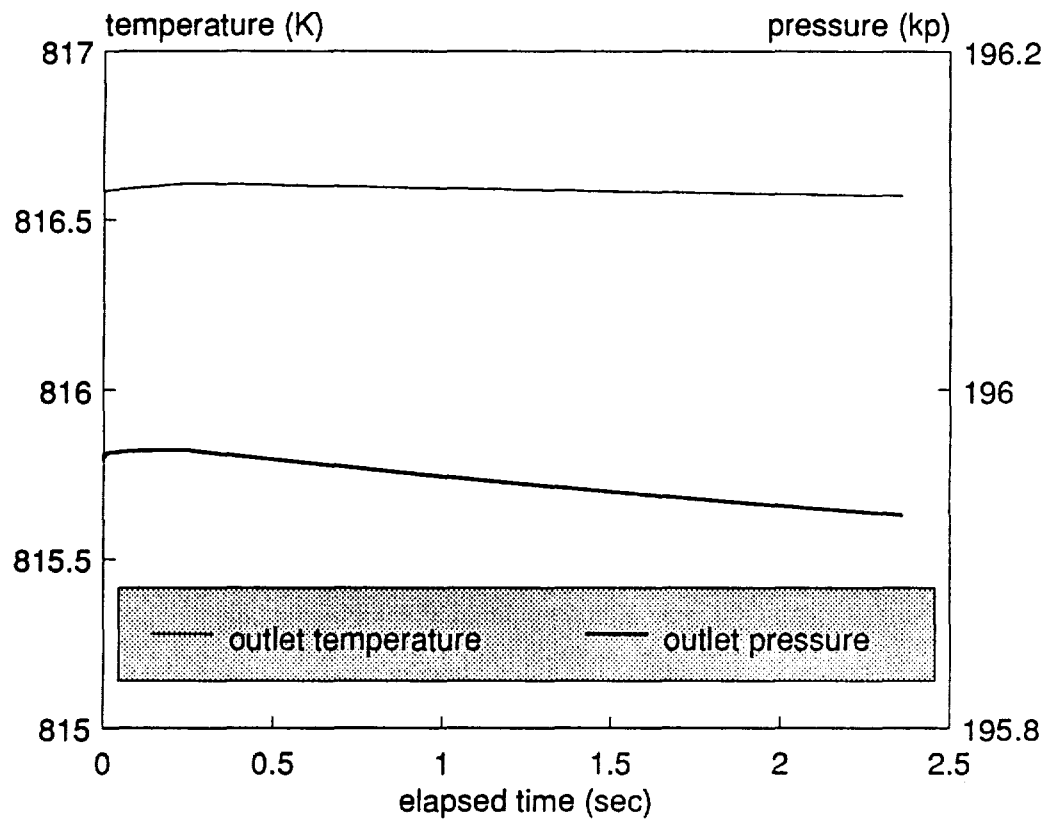


Fig. 4.21 Response of turbine outlet parameters (to ramp of output power)

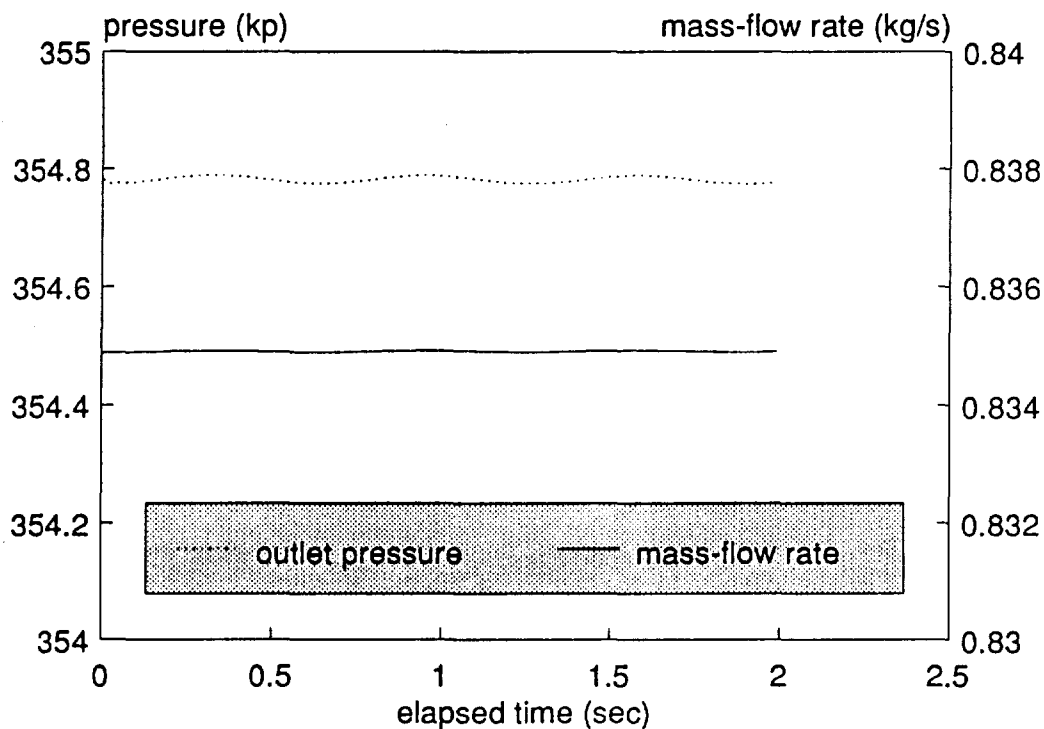
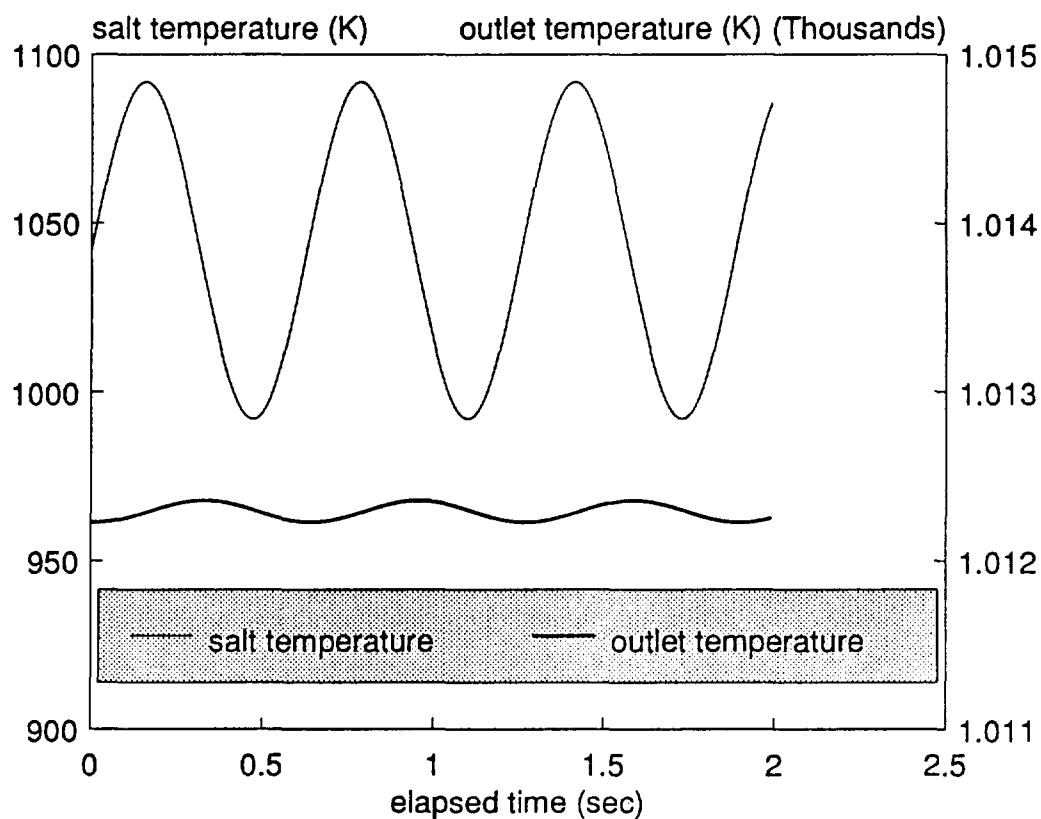


Fig. 4.32 Response of receiver outlet parameters (to sinusoidal salt temp.)

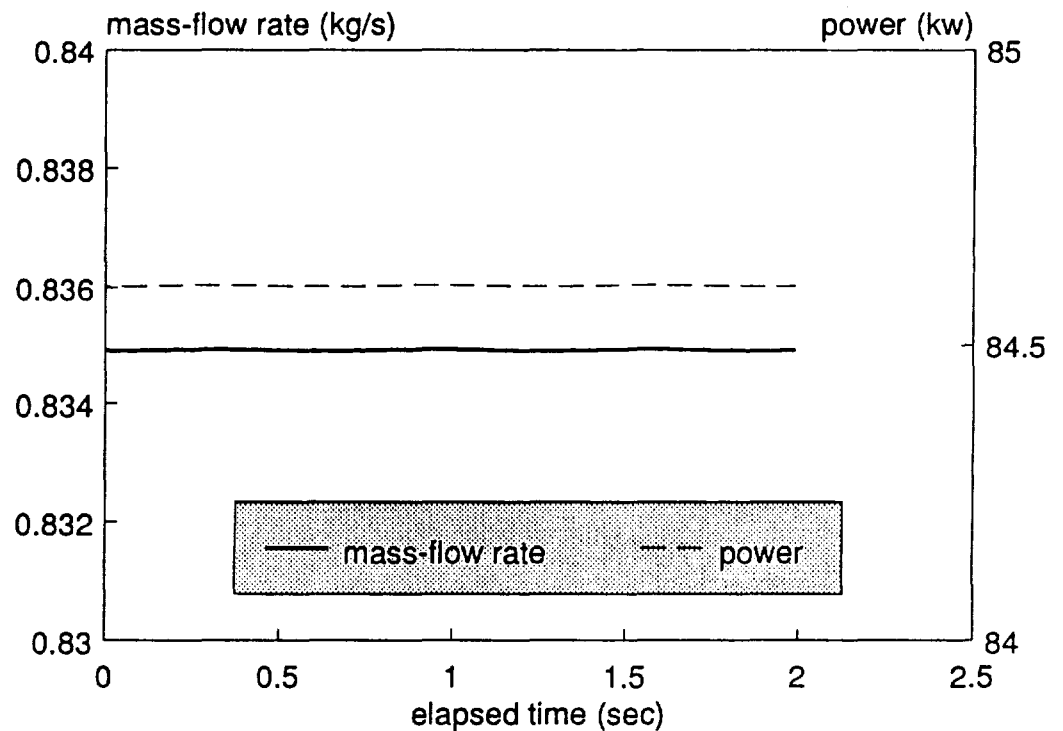
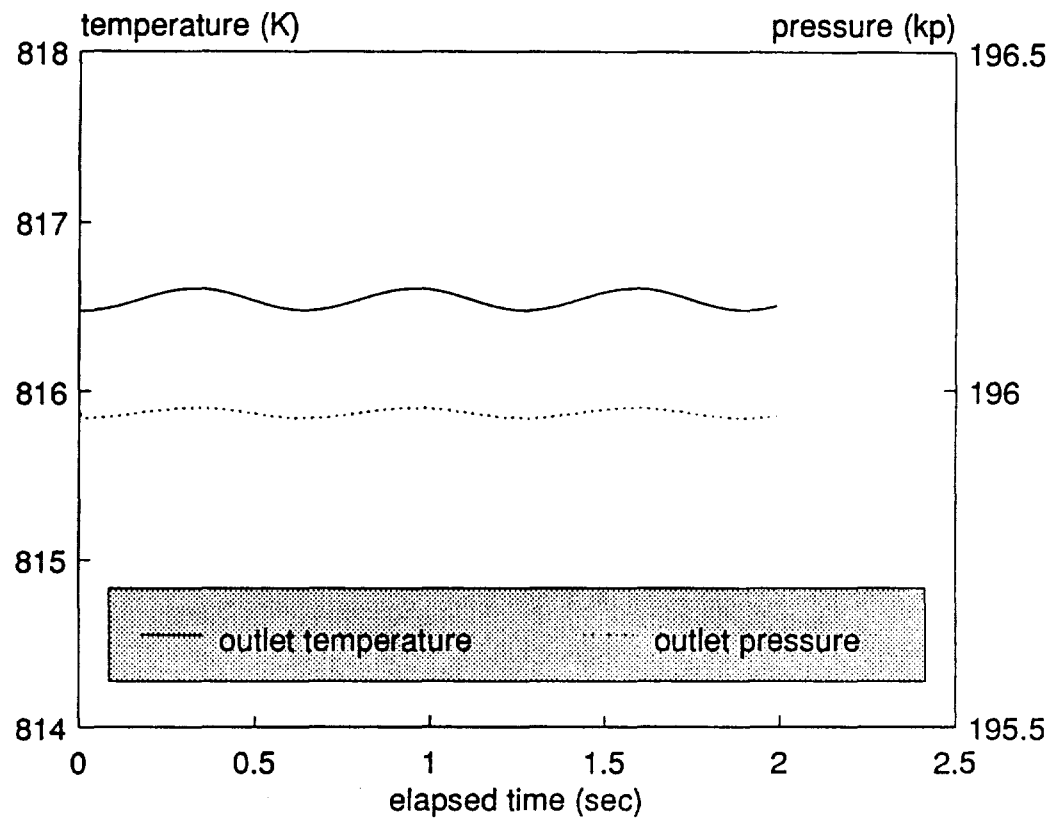


Fig. 4.33 Response of turbine outlet parameters (to sinusoidal salt temp.)



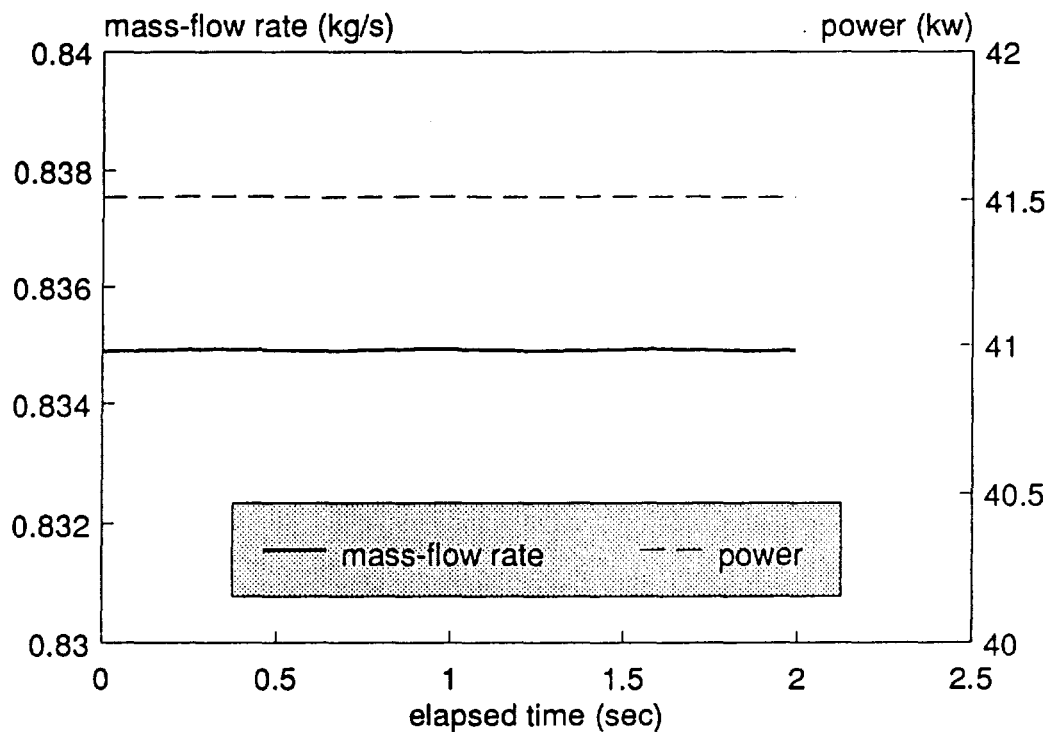
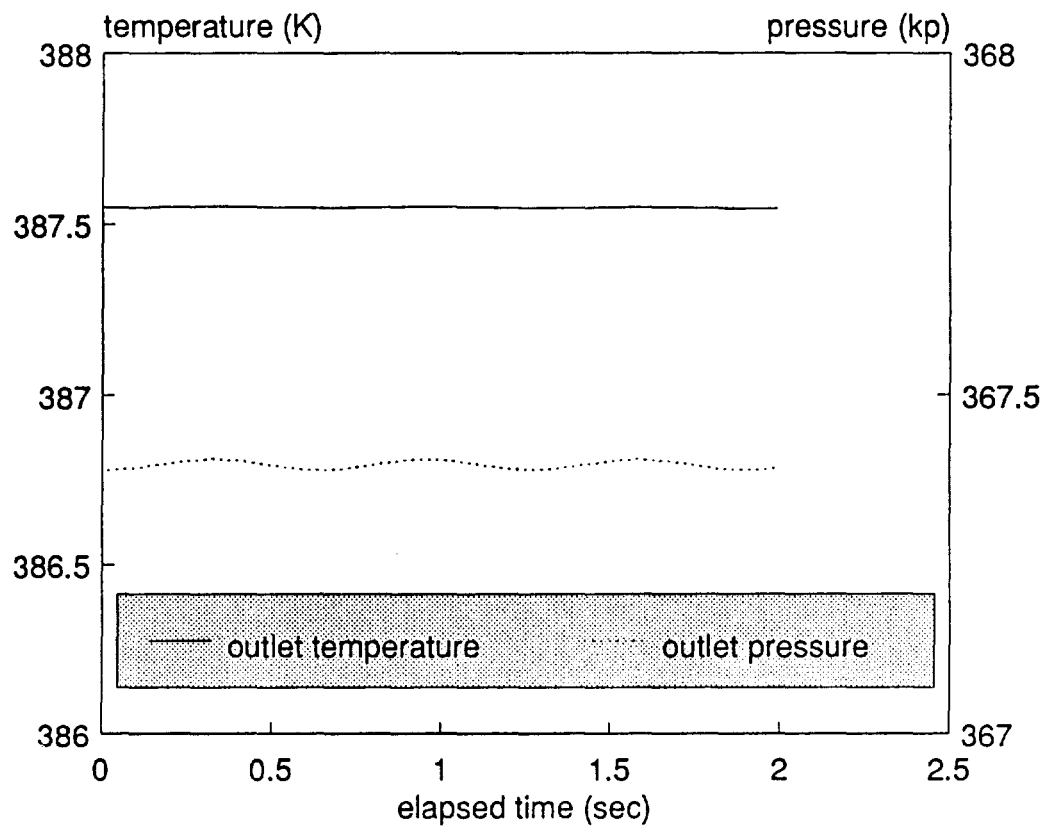


Fig. 4.34 Response of compressor outlet parameters (to sinusoidal salt temp.)

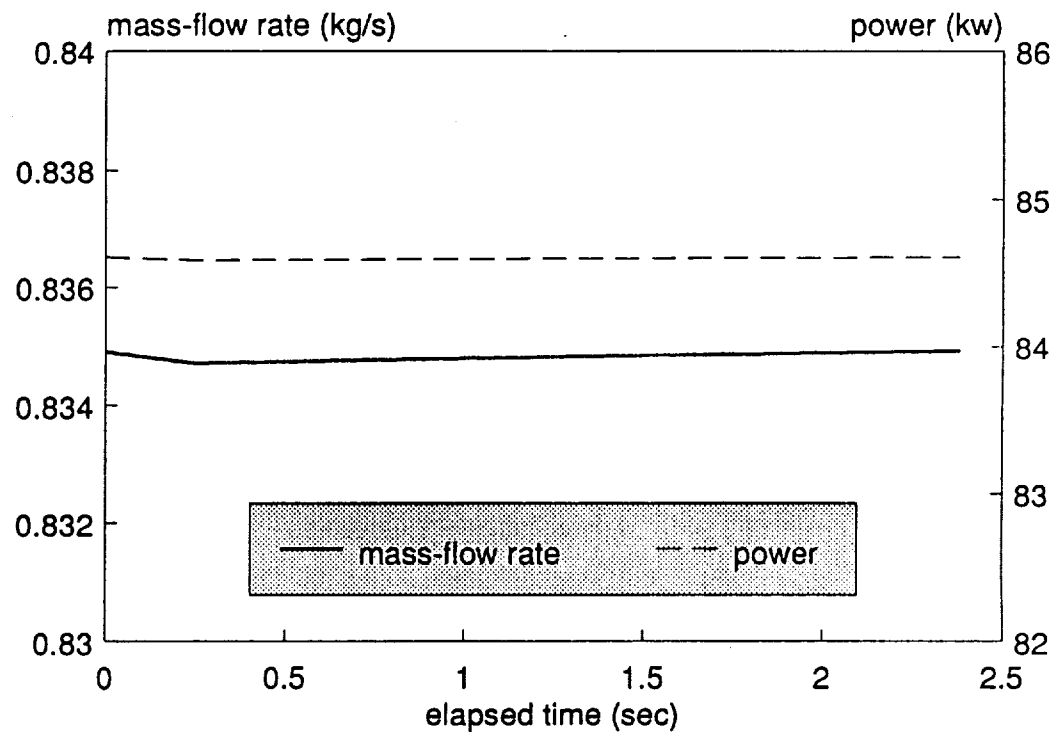
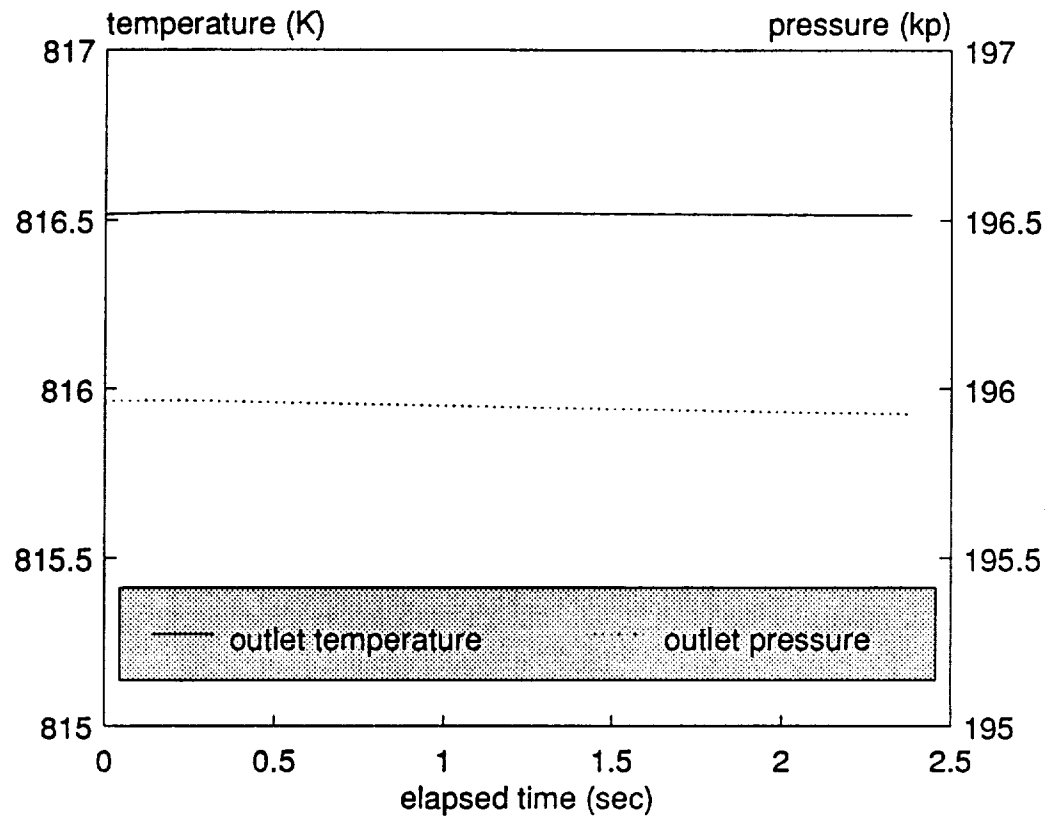


Fig. 4.38 Response of turbine outlet parameters (to ramp of output power)

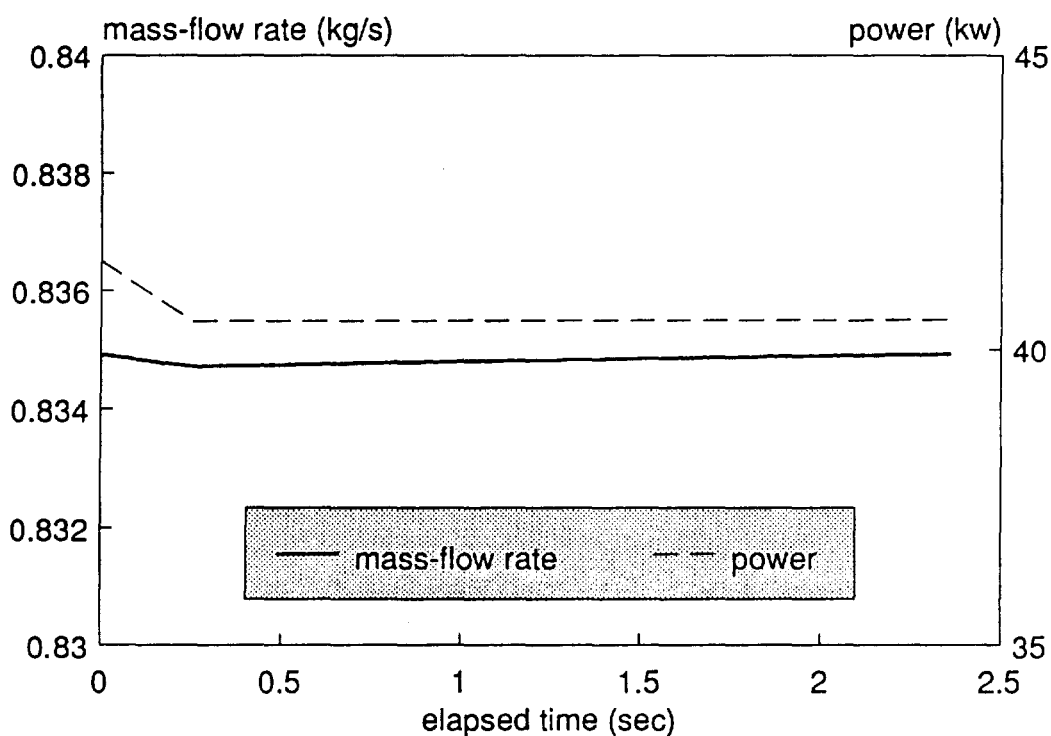
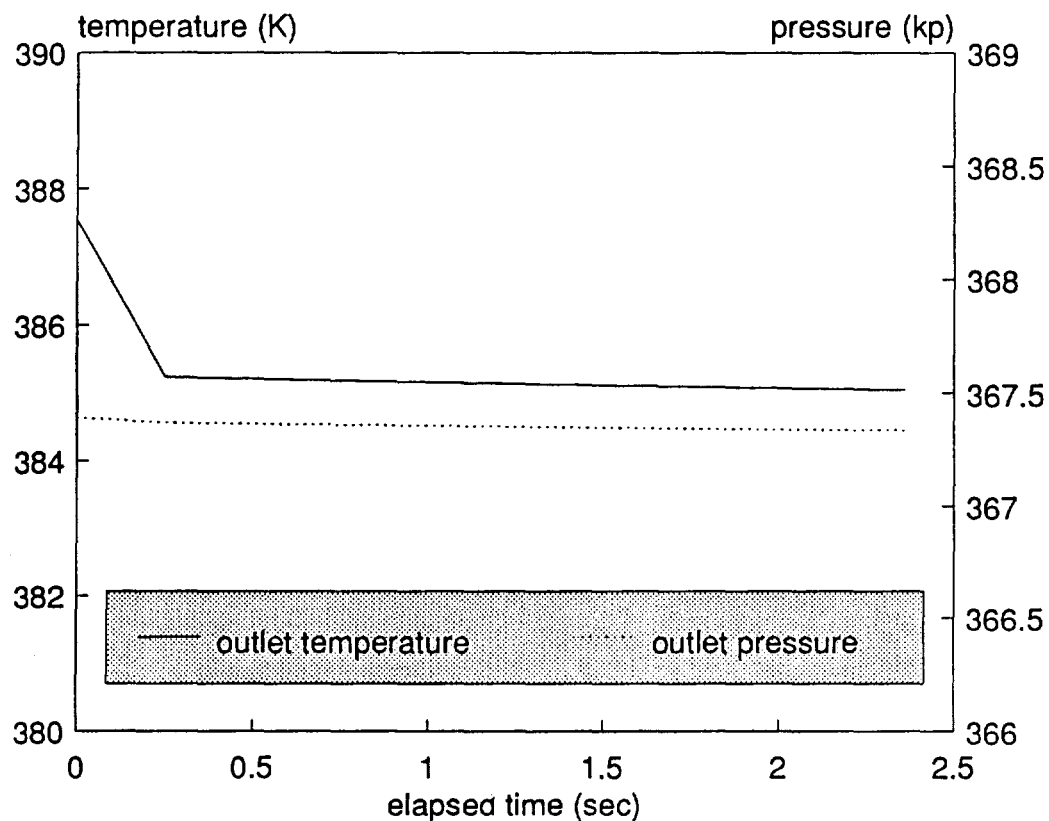


Fig. 4.39 Response of compressor outlet parameters (to ramp of output power)

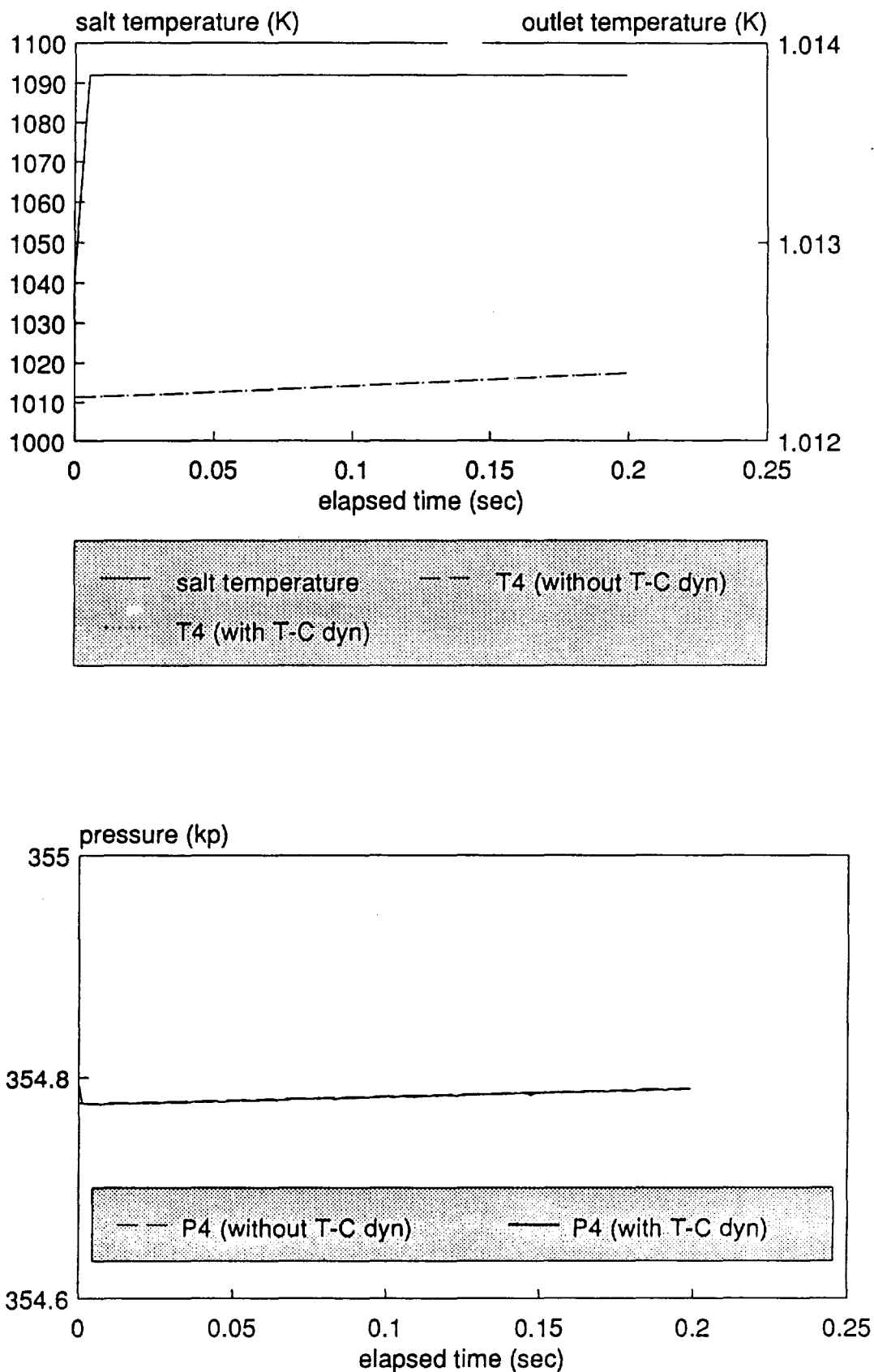


Fig. 4.44 Response of receiver outlet parameters (to ramp of salt temperature) (time step = 0.000025 (sec))

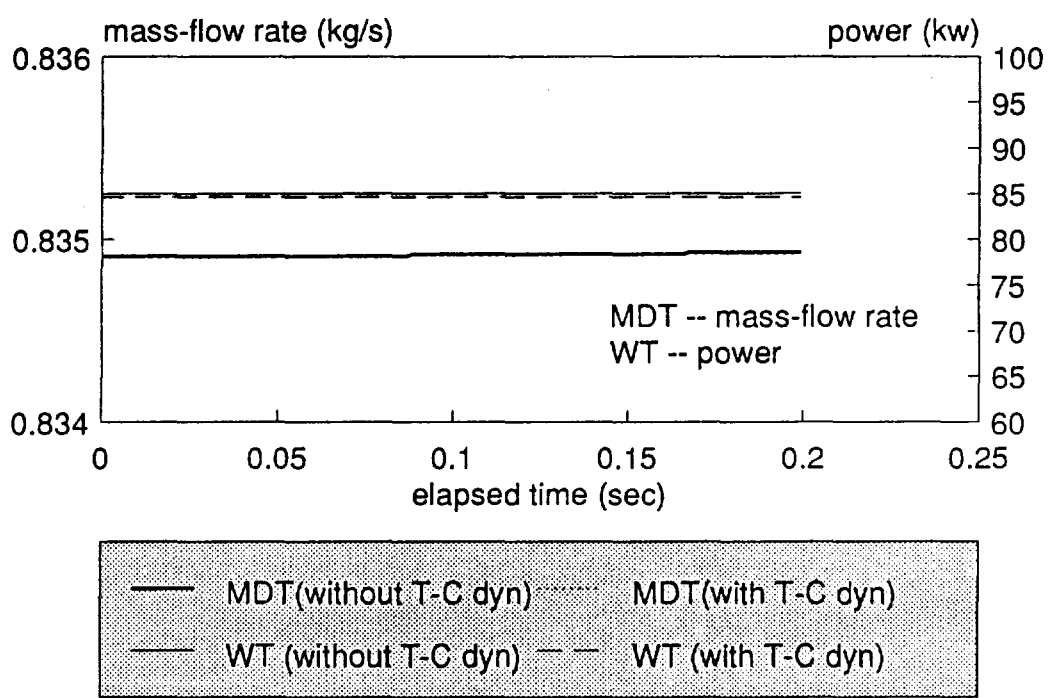
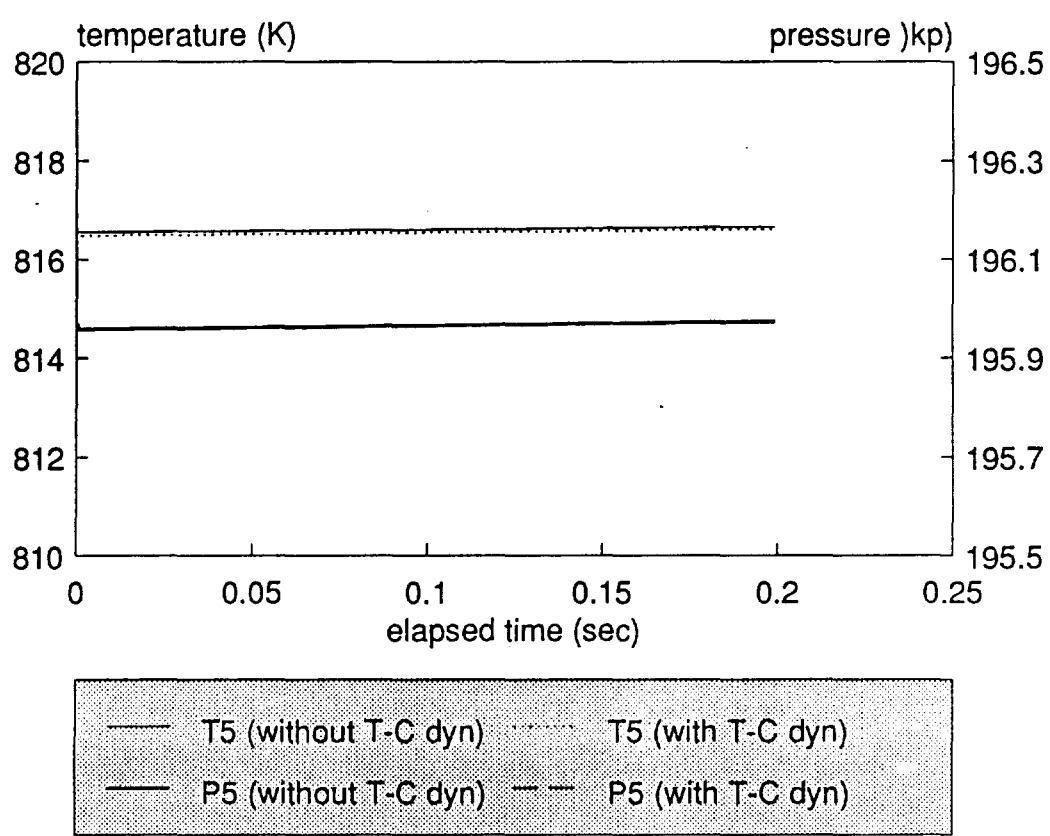


Fig. 4.45 Response of the turbine outlet parameters (to ramp of salt temperature) (time step = 0.000025 (sec))

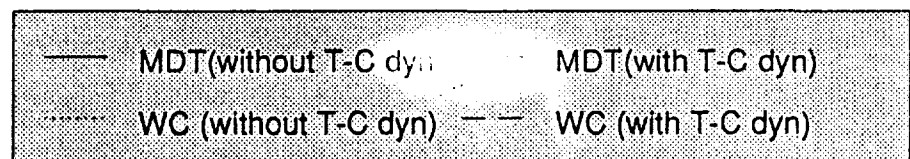
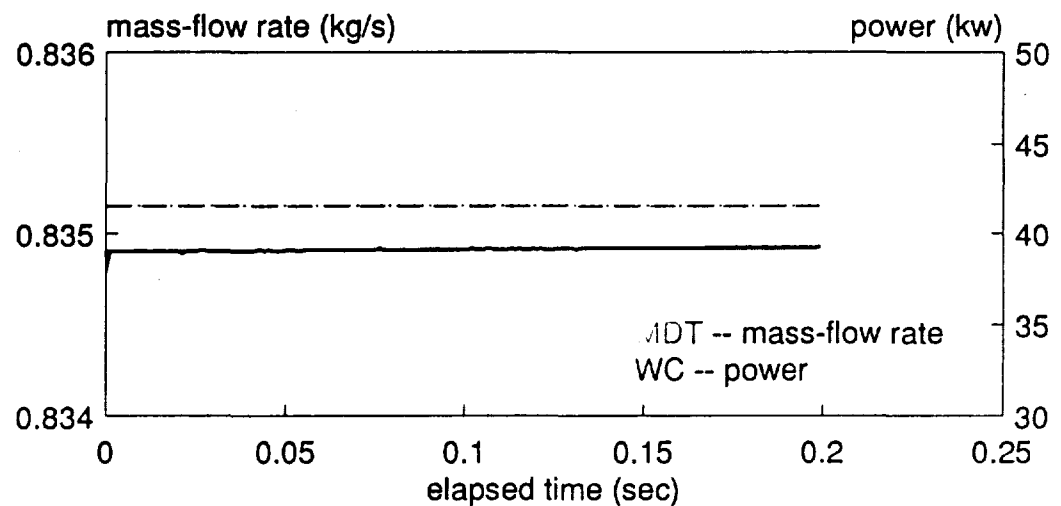
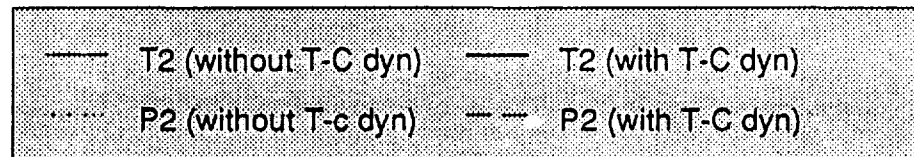
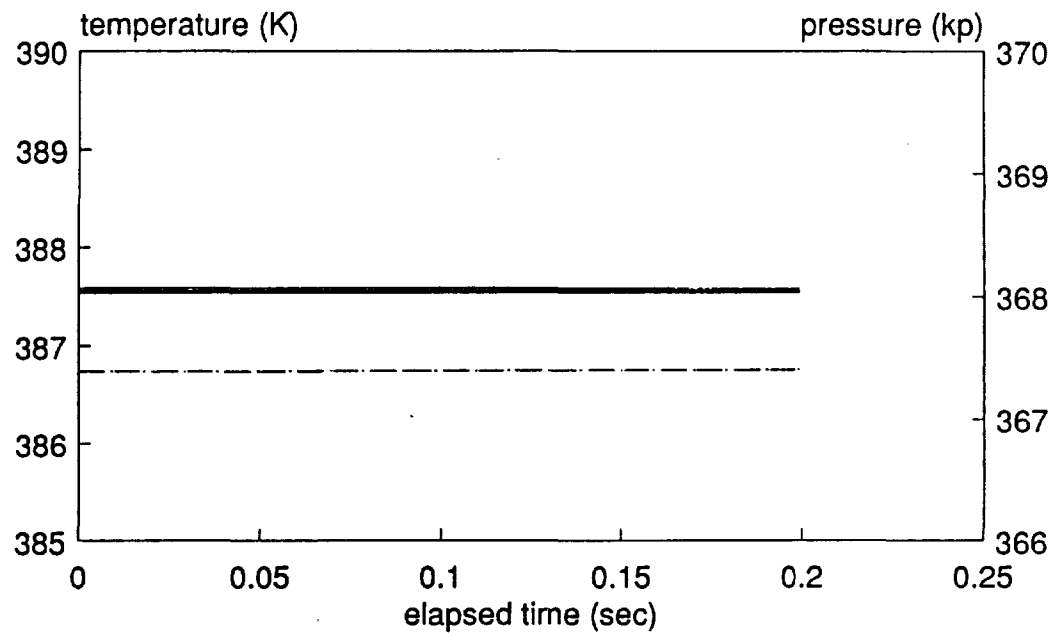


Fig. 4.46 Response of compressor outlet parameters (to ramp of salt temperature) (time step = 0.000025 (sec))

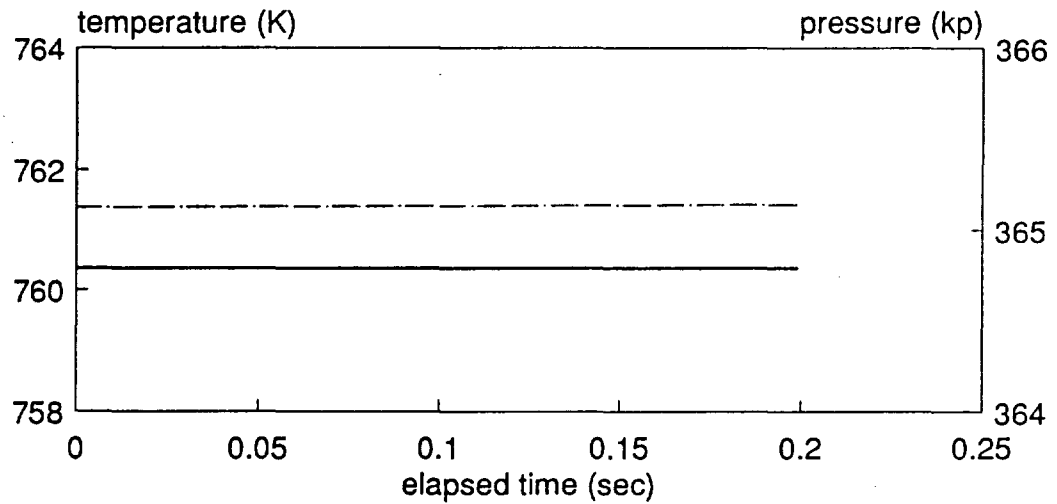
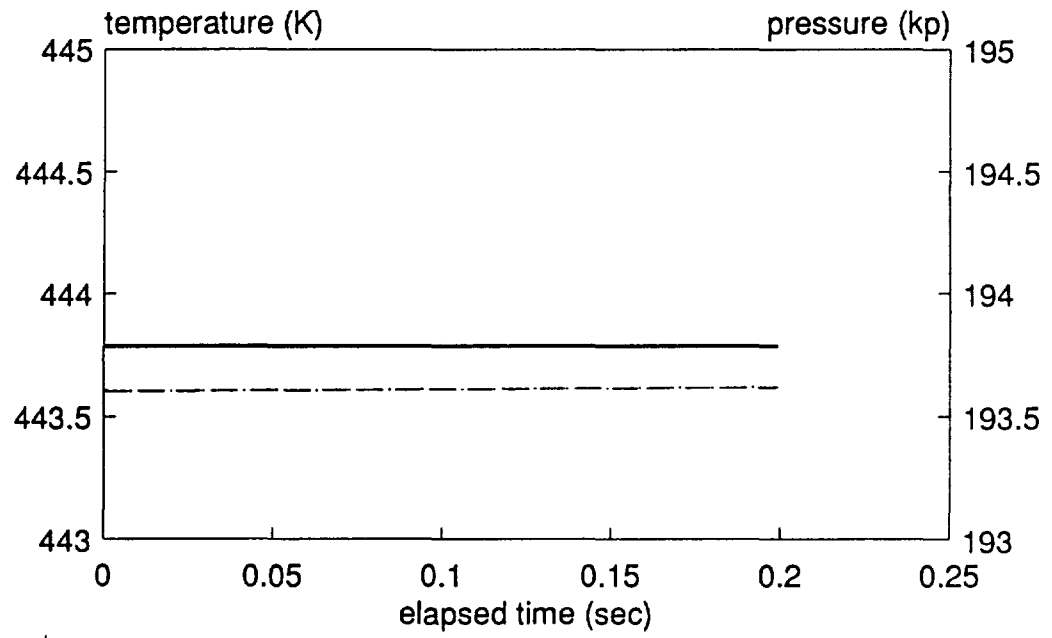


Fig. 4.47 Response of recuperator outlet parameters (to ramp of salt temperature) (time step = 0.000025 (sec))

- EASY5 was: - a time sink, not a time saver  
- not suitable for iterative looping

If mandated for use in total system model (to match electrical system), it is recommended that entire thermodynamic model be introduced as a single FORTRAN block.

- Considerable effort expended, and time wasted, in guessing hardware geometry and performance.
- Negative consequence of "emergency" mode at start-up and cancellation of support prior to scheduled completion.



- 
- Successfully developed models of components of Solar Dynamic Power Generation System.
    - Turbomachinery
      - Quasi-Steady (immediate response), Full Dynamic
      - Identified suitability according to driving transient
    - Heat Exchangers
      - Steady, Dynamic
    - Other Components (pumps, pipes, manifolds, etc.)
    - Tested for sensitivity to assumptions and to analyst selected parameters
  - Successfully integrated components into system model using conservation of mass as system constraint.
    - Tested predictions against simple transients
      - (step, double-step, etc.)
    - Analyzed transients of interest (orbital fluctuations, failures)